# Seventh Oregon Climate Assessment



Dominique Bachelet

## Oregon Climate Change Research Institute

OCCRI

# Acknowledgments

# Authors

Greyson Adams, Schatz Energy Center, California State Polytechnic University, Humboldt
Glenn Ahrens, Oregon State University
Jay Austin, Environmental Law Institute
Dominique Bachelet, Oregon State University
Michael Barnett, Rutgers University
John A. Barth, Oregon State University
Tina Beavers, Oregon State University
Brianna Beechler, Oregon State University
Ralph Bloemers, Green Oregon
Hilary Boudet, Oregon State University
Jacob J. Bukoski, Oregon State University
Jeff Burright, Oregon Department of Land Conservation and Development
Olivia Z. Cameron, Oregon State University
Sarah Cameron, Oregon State University
Daniel A. Cayan, Scripps Institution of Oceanography
Taylor Chapple, Oregon State University
Aubryn Cooperman, National Renewable Energy Laboratory
Andrea Copping, Pacific Northwest National Laboratory
Christopher Daly, Oregon State University
Loren Davis, Oregon State University
Travis Douville, Pacific Northwest National Laboratory
Kelsey A. Emard, Oregon State University
Erica Escajeda, Schatz Energy Center, California State Polytechnic University, Humboldt
Hayley Farr, Pacific Northwest National Laboratory
Nathan Fillmann, Oregon State University
Erica Fleishman, Oregon State University
Shawn Hazboun, Oregon State University
Sarah Henkel, Oregon State University, Pacific Marine Energy Center
Scott Heppell, Oregon State University
Selina Heppell, Oregon State University
Nancy Hiner, Oregon State University
Annie Hommel, Oregon State University
Elizabeth G. Hyde, Oregon State University
Arne Jacobson, Schatz Energy Center, California State Polytechnic University, Humboldt
Matthew Koszuta, Oregon State University
Sharon Kramer, Schatz Energy Center, California State Polytechnic University, Humboldt
Stephanie Kruse, Oregon Department of Energy
David J. Lewis, Oregon State University
Brad Ling, Principle Power
Paul C. Loikith, Portland State University
Danica L. Lombardozzi, National Center for Atmospheric Research
Rachel Lookadoo, University of Nebraska Medical Center
Dan Loomis, Portland General Electric
Kyle Newton, Oregon State University

Karina Nielsen, Oregon State University, Oregon Sea Grant
Mariah O'Brien, Oregon Health & Science University
Larry W. O'Neill, Oregon State University
Rajat Panwar, Oregon State University
Collin Peterson, Oregon State University
David W. Pierce, Scripps Institution of Oceanography
Kaus Raghukumar, Integral Consulting
Gabriel Rivera, Oregon State University
Bryson Robertson, Oregon State University, Pacific Marine Energy Center
Todd Rounsaville, U.S. Department of Agriculture–Agricultural Research Service
David E. Rupp, Oregon State University
Mark Schulze, Oregon State University
Mark Severy, Pacific Northwest National Laboratory
Jason Sierman, Oregon Department of Energy
Nick Siler, Oregon State University
Joni Sliger, Oregon Department of Energy
James Sterns, Oregon State University
Elizabeth Tomasino, Oregon State University
Rose Una, Oregon State University
Yuhan Wang, Oregon State University
Will R. Wieder, National Center for Atmospheric Research
Kurt Williams, Oregon State University

# Table of Contents

Established and emerging understanding of observed and projected climate change in Oregon, and knowledge of the opportunities and risks that climate change poses to natural and human systems, may inform actions such as equitable mitigation of climate-related natural hazards and implementation of Oregon's Climate Change Adaptation Framework.

### State of Climate Science

**Temperature and precipitation.** Oregon's annual average temperature increased by 2.2°F per century since 1895. Without considerable reductions in greenhouse gas emissions, annual temperature in Oregon is projected to increase by at least 5°F by 2074 and 7.6°F by 2100, with the greatest seasonal increases in summer. Precipitation is projected to increase during winter and decrease during summer, and the intensity of heavy winter precipitation events is projected to increase. Furthermore, the proportion of precipitation falling as rain rather than snow is expected to increase. Increases in extreme temperatures contributed to recent revisions of the national Plant Hardiness Zone Map.

**Effects of the El Niño–Southern Oscillation on Oregon's climate.** From 1951–2023, La Niña years, regardless of strength, generally were cooler than El Niño years. Statewide, La Niña years were more likely than most El Niño years to be wetter than average, but precipitation and peak runoff were greatest during years with Very Strong El Niño events. Although seasonal temperature forecasts associated with El Niño–Southern Oscillation events are reasonably accurate for the Pacific Northwest, precipitation forecasts tend to be less reliable.

### Climate-Related Natural Hazards

**Floods.** Models suggest that total annual precipitation will increase by 0–10 percent in Oregon by the middle of the twenty-first century, but with drier summers in western Oregon. Projected extreme wet-day precipitation increases throughout the century, especially in winter and in southeastern Oregon. In western Oregon and the Willamette Valley, the largest projected increases in extreme daily precipitation occur in autumn. Over the period 1950–2100, snowfall is projected to decrease by at least 50 percent across Oregon, with decreases of over 65 percent in the Cascades ecoregion.

**Winter storms.** Much of the response of freezing rain to climate change can be explained by two factors: a decrease in the frequency of near-surface air temperatures below 32°F and an increase in the frequency of air temperatures above 32°F aloft. The net effect of these factors in a given location depends on the location's initial temperature. In the northern Willamette Basin, the future frequency of freezing rain is projected to increase in initially colder locations and decrease in initially warmer locations. Projections suggest that easterly winds through the Columbia River Gorge may strengthen during winter, even as the Willamette Basin becomes warmer. Therefore, ice accretion on some surfaces in the region may increase during freezing rain events.

**Droughts.** During 18 of the years from 1999–2023, Oregon's precipitation was below average. The average temperature was warmer than normal in 21 of those years, which contributed to higher rates of evapotranspiration and more-frequent drought. Drought risk likely will increase over the twenty-first century on the western slopes of the Cascade Range and the southern Coast Range, decrease in the Deschutes and John Day basins in north-central Oregon, and change little elsewhere. Drought risk during summer is likely to increase statewide.

### Adaptation Sectors

**Economy.** In Oregon, Washington, and California, increasing wildfire exposure reduces timberland prices relative to those that would be applicable without a change in wildfire risk. Such an impact is consistent with landowners' perception that wildfire risk is increasing. A warmer and drier climate also depresses timberland prices due to higher risk of drought stress.

Economic losses from a major smoke event in Oregon are likely to be highly localized and industry-specific given the unequal distribution of wildfire smoke and economic activity and the unequal effects of smoke among industries. Quantitative estimates suggest that a major smoke event will reduce the state's per annum Gross Domestic Product by at least $1 billion, or about one-third of one percent.

Compounded or cascading losses from multiple independent or interacting events within the same year will result in greater economic effects, as will accounting for health effects of smoke.

**Natural systems.** Oregon's forests have considerable potential for carbon storage. Models suggest that given the carbon sequestration potential of reforestation in Oregon could reach 2.9 million metric tons of $CO_2$ by 2030 and 15.7 million metric tons by 2050. The latter represents 12 percent of Oregon's statewide 2030 carbon sequestration goal and 7 percent of the 2050 goal. The total modeled reforestation, which accounts for a number of ecological, logistic, and social constraints, would expand tree cover on approximately 940,000 acres, or 0.6 percent of Oregon's land base.

**Built environment.** Offshore winds on the U.S. West Coast represent one of the most energetic and consistent renewable energy resources in the nation. Harnessing these winds is a possibly viable technological pathway to meet decarbonization goals. Floating offshore wind energy is in a period of rapid global research, development, and deployment. Proposed lease areas in Oregon are in far deeper ocean waters than previously attempted for offshore wind, which leads to uncertainty for many government, community, tribal, and industry parties. Any potential development of floating offshore wind energy is far more likely to succeed with collaborative and capacity-generating engagement among diverse interested and affected parties.

Trees ameliorate urban heat and have other public health benefits. Nevertheless, establishing and maintaining trees in cities is challenged by difficult growing conditions, the partnerships necessary to sustain urban trees, and perceptions that the disadvantages of trees outweigh the benefits. Collaboration between health and environmental professionals on tree planting guidelines may increase the likelihood that urban trees thrive and provide diverse societal goods and services.

**Public health.** Projections of wildfire smoke and population in Oregon from 2046–2051 suggest that the number of cases of short-term health outcomes attributable to smoke are likely to increase considerably relative to 2005–2009 among all adults, and especially among older adults. The increase in adverse outcomes was associated with substantial increases in economic losses and lost quality-of-life. Drought also is associated with many negative health outcomes, from water and food insecurity to poor air quality. Moreover, drought conditions are correlated with increased rates of mental health issues, including anxiety, depression, and suicide. Promotion of accessible mental health care and support services for impacted populations, particularly in rural and agricultural communities, contributes to effective drought preparedness and mitigation.

Infectious diseases in Oregon's wild and domestic animals continue to evolve as climate changes. Human population growth and expansion into wildlands further increase the risk that the ranges of some vectors will increase and that novel pathogens will be transmitted into humans from species that previously were not in close proximity to people.

**Social systems.** As the effects of climate change are increasingly felt across Oregon and nationwide, demands on the legal system have increased. Climate change cases address mitigation, adaptation, and impacts. The legal theories pursued by plaintiffs include federal and state constitutional, statutory, regulatory, and common-law claims, often several in a single suit. Oregon's land-use planning system, which encourages dense housing and mass transit, local implementation, and adjudication by the Land Use Board of Appeals, is a potentially useful framework for adapting to climate change and resolving disputes.

Efforts to prevent losses of structures to wildfires often focus on vegetation clearing. However, wind-driven wildfires can spot over substantial distances. The design and maintenance of a structure and the immediate five feet around it can substantially reduce the probability that it will ignite, and may encourage insurance providers to continue coverage or write new policies in areas where wildfire risk is high.

Oregon vineyards are being affected by heat waves, especially early in the growing season, and by smoke exposure. Nevertheless, the increase in temperatures in Oregon over the past 125 years benefited wine grape production. There may be a threshold of climate change beyond which growers are unable to adapt, but so far research is keeping pace with the effects of climate change on vineyards in Oregon.

The Seventh Oregon Climate Assessment is available at https://doi.org/10.5399/osu/1181 and blogs.oregonstate.edu/occri/oregon-climate-assessments.

# Introduction

Consistent with its charge under Oregon House Bill 3543, the Oregon Climate Change Research Institute (OCCRI) conducts a biennial assessment of the state of climate change science, including biological, physical, and social science, as it relates to Oregon and the likely effects of climate change on Oregon. This seventh Oregon Climate Assessment, which builds on the previous assessments, is structured with the goal of supporting the state's mitigation planning for natural hazards and implementation of the Oregon Climate Change Adaptation Framework.

The first and second sections of this assessment, *State of Climate Science* and *Climate-Related Natural Hazards*, reflect sustained appraisal by OCCRI and its collaborators of observed trends and future projections of temperature, precipitation, and other major climate variables. Previous insights about projected changes in Oregon's climate, such as warmer temperatures, particularly in summer; wetter winters and drier summers; and an increase in the frequency, duration, and severity of drought; remain consistent. Extreme cold temperatures during winter are the most significant environmental factor for predicting the survival of perennial plants and winter annual crops. As explained in *State of Climate Science*, increases in extreme cold temperatures, improvements in climate mapping over the past decade, and increases in the availability of weather data contributed to revision and updating of the U.S. Department of Agriculture Plant Hardiness Zone Map, the agricultural and horticultural industries' standard for selecting regionally adapted plants. *State of Climate Science* continues by examining the effects of the El Niño–Southern Oscillation (ENSO) on Oregon's weather, climate, and hydrology. It also explores the current capability of weather forecast models to predict winter climate in Oregon on the basis of climate during the preceding autumn given different ENSO conditions. Precipitation effects of El Niño are not simply the reverse of those during La Niña.

*Climate-Related Natural Hazards* delves into the projected effects of climate change on precipitation in Oregon, which can affect flood risk, and freezing rain and ice accretion in the northern Willamette Valley. This section also reviews historical drought occurrences in Oregon and presents drought projections for the state during the twenty-first century. Models suggest that total annual precipitation in Oregon may increase by 0–10 percent by mid-century, but with seasonal variation that includes 5–15 percent drier summers in western Oregon. Projections indicate that if global emissions of carbon dioxide do not decrease rapidly and appreciably, precipitation across the Pacific Northwest on extremely wet days will increase by about 7 percent by mid-century. Over the period 1950–2100, snowfall is projected to decrease by no less than 50 percent in any part of Oregon, with decreases of over 65 percent in the Cascades ecoregion and over 85 percent in western Oregon. The proportion of precipitation falling as rain is projected to increase by 30–50 percent over much of southeastern Oregon and 3–10 percent in western and coastal Oregon.

Two simultaneous conditions are necessary for freezing rain to occur: near-surface air temperatures that are below freezing and air temperatures aloft that are above freezing. As climate changes, the frequency of the former is projected to decrease, and the frequency of the latter is projected to increase. The net effect of these opposing factors depends on the initial temperature of a given location. In Oregon's northern Willamette Basin, the frequency of freezing rain is projected to increase in initially colder locations and decrease in initially warmer locations. Models indicate that in the future, easterly winds through the Columbia River Gorge will strengthen during winter and become more likely to enable freezing rain locally, even as the Willamette Basin becomes warmer. Exposure to stronger winds during freezing rain, especially easterly winds, leads to additional ice accretion on cables and other structures from the increased horizontal transport of water droplets.

During 18 of the 24 water years from 1999 through 2023, Oregon's water year precipitation was below average. The average temperature in Oregon was also warmer than normal in 21 of the last 24 water years, which contributed to higher rates of evapotranspiration and more-frequent drought. Statewide, Oregon experienced relatively little drought, and primarily drought of low intensity, from water years 1939 through 1976. The trend to a drier regime after 2000 coincides with widespread, prolonged drought across the western United States during this period. Projections suggest that drought risk likely will increase over the twenty-first century on the western slopes of the Cascade Range and the southern Coast Range, decrease in the Deschutes and John Day basins in north-central Oregon, and change little elsewhere. However, due to a shift in the seasonal distribution of precipitation, drought risk during summer is likely to increase statewide.

The third section of this assessment addresses five of the six sectors within which Oregon's 2021 Climate Change Adaptation Framework aggregates vulnerabilities and strategic responses: economy, natural systems, built environment and infrastructure, public health, and social systems. Two of the contributions related to the economy emphasize the consequences of wildfire exposure and wildfire smoke. Across Oregon, Washington, and California from 2004 through 2020, increasing wildfire exposure of privately owned timberland, as measured by the number of large wildfires that overlapped a parcel, the number of large wildfires that burned within 9.3 miles of the parcel, and whether the parcel was within 9.3 miles of an extremely large wildfire, reduced timberland prices relative to those that would be applicable without a change in wildfire risk. Moreover, a warmer and drier climate depressed timberland prices due to higher risk of drought stress. Estimates illustrate that a major smoke event similar to those that Oregon residents have experienced in recent years is expected to lead to localized and industry-specific economic losses in the state. The Oregon industries most susceptible to economic losses due to wildfire smoke events represent approximately 40 percent of total employment, 31 percent of labor income, and 33 percent of total economic output per year for the state. A major smoke event may reduce the state's per annum Gross Domestic Product by at least $1 billion, or about one-third of one percent.

This assessment also discusses how businesses, including those in Oregon, are responding to and seeking to mitigate climate change. Oregon has the third highest number of B Corporations in the United States, and a greater number of B Corporation-certified wineries than any other state or country. These corporations are certified as upholding high standards of social and environmental performance, accountability, and transparency. Many corporations are motivated at least in part by the business case for sustainability: the calculation that environmentally positive practices advance companies' self-interest in multiple ways, ultimately leading to improved profitability.

The section on natural systems highlights the potential role of trees in enhancing carbon sequestration in Oregon. Forestation includes both reforestation (restoring tree cover on previously forested lands) and afforestation (establishing tree cover on non-forested lands); reforestation tends to be favored over afforestation. Models identified an upper bound of carbon dioxide sequestration from forestation by 2050 that is equivalent to 60 percent of Oregon's statewide 2050 carbon sequestration goal. Although actual carbon sequestration will be constrained by social, physical, financial, logistical, and technical factors, analyses suggest that forestation could play a substantial role in achieving Oregon's climate-change mitigation goals on natural and working lands. Additionally, the section demonstrates how data contributed by community observers to Oregon Season Tracker have advanced understanding of variation and trends in phenology, or seasonal events in the life cycle of plants and animals.

As detailed in the section on the built environment, the potential development of floating offshore wind energy off the coast of Oregon has prompted a range of responses, opinions, questions, and concerns from diverse interested and affected parties. The assessment explains why floating offshore wind is being pursued off west coast of the United States, describes the infrastructure being considered, and examines potential interactions of this infrastructure with the ocean environment and coastal human communities. Furthermore, it explores public perceptions, energy and environmental justice, and community benefit plans related to floating offshore wind. Assessment materials on the built environment also investigate trade-offs of planting trees in urban and suburban areas. Trees can alleviate heat and other adverse health outcomes that disproportionately affect cities, particularly in underserved neighborhoods. However, establishing and maintaining trees in cities is challenged by difficult growing conditions, the partnerships necessary to sustain those trees, and perceptions that the disadvantages of trees outweigh the benefits.

Contributions related to public health in this assessment examine the potential effects of climate change on transmission of zoonotic diseases and of climate-related natural hazards on human health and healthcare costs. The compounded effects of climate change and land use influence not only the distributions of pathogens that can cause disease in humans but the extent to which wild and domesticated animals and humans are exposed to those pathogens. New research presented in the public health section projects the cumulative number of health events associated with a range of short-term health outcomes attributable to wildfire smoke, quantifying impacts in economic terms and as quality-of-life loss. The projections were conducted under different scenarios of air quality and population size and age structure. Many of the projections reflect outcomes across the populations of all adults and older adults. The assessment also summarizes emerging understanding of the breadth of effects of drought on physical and mental health.

This assessment demonstrates some of the diverse ways in which contemporary society is responding to climate change. For example, the legal system in Oregon and the United States increasingly is regarded as a potential mechanism to reduce greenhouse gas emissions into the atmosphere, adapt to the present or anticipated effects of climate change, and remedy realized harms related to climate change. At the same time, artists are using the power of stories to disseminate science on causes and effects of wildfires and encourage people to prevent losses of lives and property when wildfires occur. Actions in the immediate area around homes can reduce the risk of ignition appreciably and may forestall insurance retreat.

Links between social systems and other adaptation sectors are evident in responses of Oregon's farmers and wine industry to climate variability and change. Requests from farmers in the Willamette Valley for projections of particular climate variables and data on adaptive farm practices are informing the next generation of Earth system models by atmospheric researchers. The increase in maximum and minimum temperatures in Oregon over the past 125 years benefited wine grape production in the state, although production sometimes was hampered by weather extremes and wildfire smoke. There may be a threshold of climate change beyond which growers are unable to adapt, but so far research is keeping pace with the effects of climate change on vineyards.

Both the Climate Change Adaptation Framework and this assessment recognize that the myriad interactions and feedbacks among natural and human systems are complex and can be difficult to differentiate. An iterative assessment process can indicate the extent to which natural hazards may affect adaptation sectors, and inform selection of actions to maximize livelihoods and well-being.

# Trends in Climate and Advances in Climate Science

## Observed and Projected Trends in Climate

Oregon is becoming warmer and, despite relatively stable long-term precipitation totals, more prone to drought. Oregon's annual average temperature increased at a rate of 2.2°F (1.2°C) per century from 1895–2023 (NCEI 2024). Oregon's temperatures are projected to continue increasing at the annual level (Figure 1, Table 1) and in all seasons, particularly summer (Table 1).

Climate projections in this assessment largely are based on outputs from global climate models that were included in the sixth phase of the Climate Model Intercomparison Project (CMIP6; Eyring et al. 2016) and subsequently downscaled. CMIP6 is the climate modeling foundation for the sixth assessment report of the Intergovernmental Panel on Climate Change (IPCC; 2021), and represents the most current understanding of Earth's climate. The scenarios that drove the CMIP6 models represent global radiative forcing levels paired with assumptions, referenced as shared socioeconomic pathways (SSPs) (O'Neill et al. 2016), about future global population, technological, and economic growth by 2100. Radiative forcing is the total amount of energy retained in the atmosphere after absorption of incoming solar radiation, which is affected by the reflectivity of Earth's surface, and emission of outgoing long-wave radiation, which is affected by the concentrations of heat-trapping or greenhouse gases. The radiative forcings in the scenarios we reference in this chapter and assessment are 4.5, 7.0, and 8.5 watts per square meter (W m$^{-2}$) by 2100,
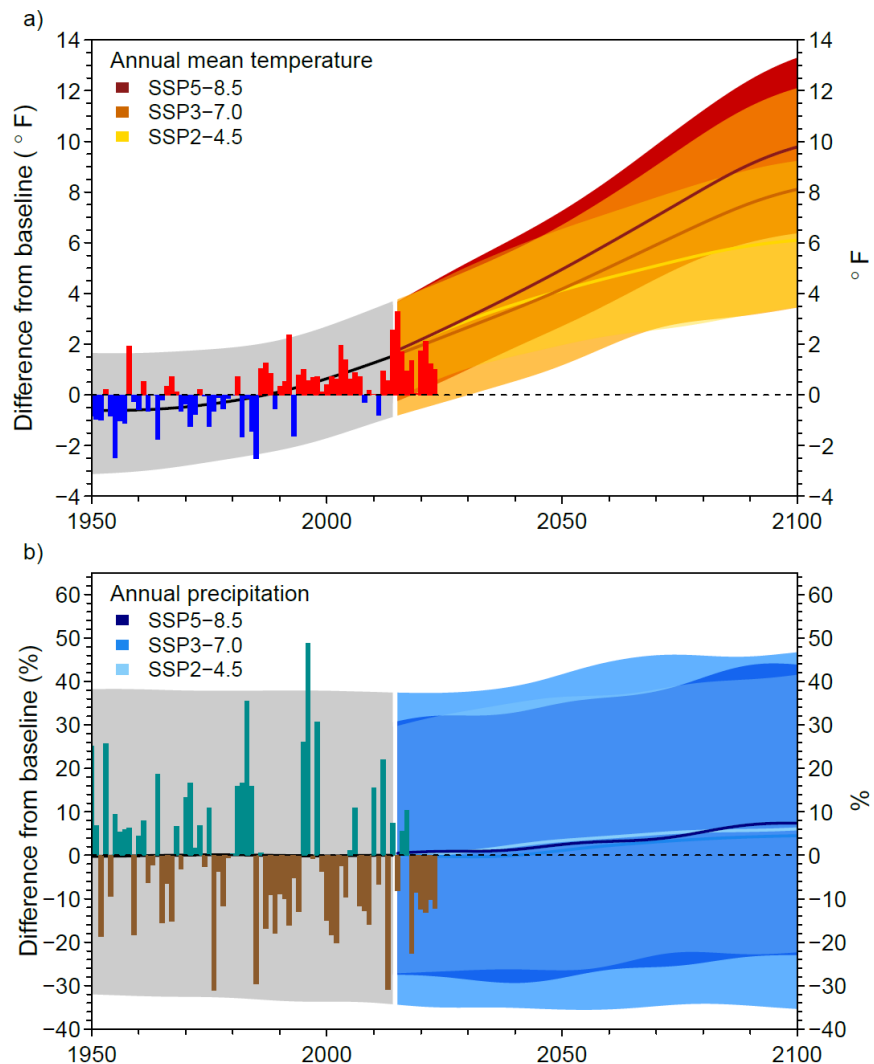


**Figure 1.** Observed and projected changes in Oregon's average annual (a) temperature and (b) precipitation relative to 1950–2014 (baseline) under three shared socioeconomic pathways (SSPs). Colored bars are observed values from the National Centers for Environmental Information. Solid lines are the mean values of simulations from 7–11 downscaled climate models for the years 1950–2100. Shading indicates the range in values from all models. The mean and range were smoothed to emphasize long-term variability.

respectively. The social and economic assumptions in the scenarios are continuation of historical social and economic trends, with moderate challenges to mitigation and adaptation (SSP2); conflicts among regions and substantial challenges to mitigation and adaptation (SSP3); and dependence on fossil fuels with substantial challenges to mitigation, but minor challenges to adaptation (SSP5) (O'Neill et al. 2016).

When paired with radiative forcing levels, the SSPs produce trajectories of greenhouse gas emissions that result in different degrees of warming by 2100. SSP2–4.5 assumes that carbon dioxide emissions plateau and then gradually decline by mid-century. Under SSP3–7.0, carbon dioxide emissions double by 2100, and SSP5–8.5 assumes that carbon dioxide emissions double by 2050.

Another concept relevant to understanding projections of future climate is the equilibrium climate sensitivity (ECS), an estimate of the temperature response to carbon dioxide concentrations that have doubled, and remained at that doubled level, after stabilization of temperature over hundreds or thousands of years. On the basis of observations, paleoclimate data, and other evidence, the ECS of Earth was assessed to be within 2.5–4.0°C (4.5–7.2°F) (66 percent likelihood) or 2.0–5.0°C (3.6–9.0°F) (90 percent likelihood) (Forster et al. 2021). The scientific community typically evaluates climate model outputs on the basis of how close they are to this assessed range of ECS. Some climate models are more sensitive than others: they produce greater warming given the same concentration of greenhouse gases.

The range of ECS among all CMIP6 models is 1.8–5.6°C (3.2–10.0°F). In about one-fifth of the CMIP6 models, sometimes referenced as *hot models*, ECS was above 5°C (9°F) (Hausfather et al. 2022). Cloud feedbacks and cloud-aerosol interactions most likely are the primary contributors to the higher sensitivities (Meehl et al. 2020, Zelinka et al. 2020). Although there is a five percent likelihood that Earth's ECS could be above 5°C, the CMIP6 climate models with ECS >5°C overestimate observed warming. There are cases in which inclusion of these hot models in climate projections is warranted. For example, a few of the hot models effectively represent observed hydroclimate across the western United States (Lybarger et al. 2024). Nevertheless, when using ouputs of individual CMIP6 climate models or interpreting published results that were based on CMIP6 climate models, the models' climate sensitivity and their skill in simulating past climate is central to evaluation of reliability (Tokarska et al. 2020, Hausfather et al. 2022).

Depending on the scenario, Oregon's annual average temperature is projected to increase by 2.6–3.0°F (1.4–1.7°C) by 2044, 4.6–5.9°F (2.6–3.3°C) by 2074, and 5.9–9.1°F (3.3–5.1°C) by 2100 (Table 1, Figure 1). Temperatures in summer are projected to increase more than those in any other season: 3.4–3.5°F (1.9–2.0°C) by 2044, 5.2–7.0°F (2.9–3.9°C) by 2074, and 6.7–10.9°F (3.8–6.1°C) by 2100 (Table 1). The slightly higher annual and seasonal projections under SSP2–4.5 than SSP3–7.0 for the 2015–2044 period likely reflects that the former were based on a smaller suite of climate models and ensemble members.

Oregon's annual precipitation varies considerably among years, and has not changed significantly over the observational record (increase of about 0.08 in. [0.20 cm] per century from 1895–2023) (NCEI 2024). At the state level, annual average precipitation is expected to increase by about four to six percent by the late twenty-first century, with wide variability and uncertainty in the projections (Figure 1, Table 2). However, a focus on annual precipitation can mask changes in the type, timing, and intensity of precipitation, which often have greater impacts on social and natural systems than annual totals. For example, some statistically significant increases in heavy precipitation have been documented in Oregon (Dalton et al. 2017), and projections suggest that the intensity of heavy

| SSP | 2015–2044 | | | 2045–2074 | | | 2074–2100 | | |
|---|---|---|---|---|---|---|---|---|---|
| | 2–4.5 | 3–7.0 | 5–8.5 | 2–4.5 | 3–7.0 | 5–8.5 | 2–4.5 | 3–7.0 | 5–8.5 |
| Annual | 2.9 (2.2, 4.4) | 2.6 (1.5, 3.5) | 3.0 (2.0, 4.5) | 4.6 (3.2, 6.6) | 5.0 (3.6, 6.4) | 5.9 (4.3, 7.7) | 5.9 (3.8, 8.6) | 7.6 (5.6, 9.8) | 9.1 (6.3, 11.9) |
| Winter | 2.7 (1.4, 3.6) | 2.3 (0.7, 3.5) | 2.9 (1.7, 4.7) | 4.5 (3,0, 7.3) | 4.5 (2.5, 6.5) | 5.6 (3.7, 8.6) | 6.0 (3.8, 8.5) | 6.7 (4.1, 9.2) | 8.5 (6.8, 11.4) |
| Spring | 2.5 (1.5, 4.6) | 2.1 (1.3, 2.9) | 2.5 (1.3, 4.0) | 3.8 (2.0, 5.9) | 4 (2.6, 5.5) | 4.9 (3.4, 6.9) | 4.9 (3.1, 6.9) | 6.0 (4.1, 8) | 7.3 (5.6, 9.6) |
| Summer | 3.4 (2.4, 4.8) | 3.4 (2.1, 4.7) | 3.5 (2.3, 5.1) | 5.2 (3.5, 7.5) | 6.2 (4.4, 8.4) | 7.0 (4.6, 9.9) | 6.7 (3.9, 10.1) | 9.6 (6.5, 12.8) | 10.9 (6.8, 15.7) |
| Autumn | 3.0 (1.9, 4.8) | 2.7 (1.4, 3.7) | 3.2 (1.8, 5.0) | 4.9 (3.1, 7.1) | 5.2 (3.7, 6.9) | 6.2 (4.5, 8.2) | 6.0 (3.7, 8.8) | 8.0 (6.1, 10.8) | 9.6 (6.0, 13.0) |

**Table 1.** Projected future changes in mean annual and seasonal temperature (°F) in Oregon from the historical baseline (1950–2014) to three periods of time under three shared socioeconomic pathways (SSPs). Values are the average of 18 ensemble members from 8 global climate models (SSP 2–4.5), 52 ensemble members from 11 global climate models (SSP 3–7.0) and 18 ensemble members from 7 global climate models (SSP 5–8.5). Values in parentheses are the 5th to 95th percentile range across those models. Winter includes December, January, and February; spring includes March, April, and May; summer includes June, July, and August; and autumn includes September, October, and November.

| SSP | 2015–2044 | | | 2045–2074 | | | 2074–2100 | | |
|---|---|---|---|---|---|---|---|---|---|
| | 2–4.5 | 3–7.0 | 5–8.5 | 2–4.5 | 3–7.0 | 5–8.5 | 2–4.5 | 3–7.0 | 5–8.5 |
| Annual | 0.9 (-3.3, 6.2) | -0.5 (-6.9, 5.6) | 0.6 (-6.4, 5.9) | 3.9 (-4.4, 15.1) | 2.3 (-3.4, 7.6) | 3.6 (-4.7, 11.3) | 6.2 (1.1, 13.6) | 4.3 (-3.1, 12.5) | 6.6 (-1.1, 16.4) |
| Winter | 4.1 (-5.7, 13.1) | 2.5 (-8.7, 13.5) | 3.2 (-11.4, 16) | 8.2 (-1.6, 28.2) | 7.1 (-3.1, 22.1) | 8.8 (-9.3, 25) | 10 (-3.4, 21.5) | 9.5 (-1.4, 25) | 12.7 (-3.7, 35.5) |
| Spring | 1.2 (-5.8, 8.7) | -0.5 (-10.3, 9) | 1.8 (-7.6, 8.1) | 3.3 (-7.6, 9.7) | 1.1 (-6.2, 9.1) | 3.0 (-4.9, 17.3) | 5.6 (-10.8, 25.6) | 2.6 (-8.9, 13.8) | 4.0 (-12.8, 18.1) |
| Summer | -6.2 (-18.8, 3.2) | -8.5 (-22.9, 7) | -8.1 (-25.3, 11) | -5.8 (-19.5, 3.2) | -8.9 (-34.3, 8.8) | -6.8 (-21.8, 10.2) | -3.9 (-26.4, 17.6) | -6.6 (-41.5, 33.9) | -9.2 (-27.1, 23.7) |
| Autumn | -2.2 (-12.3, 8.0) | -2.7 (-12.3, 7.9) | -1.9 (-12.1, 14.4) | 0.9 (-15.7, 12.6) | -0.7 (-13.9, 15.5) | -1.0 (-16.3, 18.7) | 4.2 (-13.7, 26.9) | 1.2 (-14.3, 25.3) | 4.5 (-14.2, 26.3) |

**Table 2.** Projected future changes in total annual and seasonal precipitation (percentages) in Oregon from the historical baseline (1950–2014) to three periods of time under three shared socioeconomic pathways (SSPs). Values are the average of 18 ensemble members from 8 global climate models (SSP 2–4.5), 52 ensemble members from 11 global climate models (SSP 3–7.0) and 18 ensemble members from 7 global climate models (SSP 5–8.5). Values in parentheses are the 5th to 95th percentile range across those models. Winter includes December, January, and February; spring includes March, April, and May; summer includes June, July, and August; and autumn includes September, October, and November.

precipitation events will continue to increase during the twenty-first century. Additionally, regardless of SSP and time period, average statewide summer precipitation is projected to decrease (Table 2).

**Extreme Heat Events**

It is uncertain whether mean and extreme daily maximum temperatures are increasing in parallel, or whether the trend in extremes is steeper than the trend in means. There are several reasons why extreme maximum daily temperature may increase at a faster rate than mean daily maximum temperature. For example, as summer precipitation over the Pacific Northwest decreases, drying of the land surface weakens the moderating influence of evaporation on temperature and increases temperature variability (Rupp et al. 2017, Zhang et al. 2023). A wider distribution of summer temperatures can enable heat extremes to increase faster than mean temperature. However, where the land surface already is relatively dry, and the absolute projected decrease in precipitation is

small, the modeled effect on temperature also is small (Rupp et al. 2017, Bercos-Hickey et al. 2022). Climate change also may affect the rate of change in maximum temperature through dynamical changes, or changes in atmospheric circulation patterns that can alter the frequency, amplitude, or duration of the regional high-pressure anomalies called ridges or heat domes (Horton et al. 2015).

In late June, 2021, an extreme heat wave across the Pacific Northwest of the United States and Canada threatened public health, disrupted economic activity, and strained the capacity of infrastructure and social services. The June 2021 heat wave often has been referenced as a heat dome in popular and some scientific fora. The meteorological features that contributed to this heat wave were consistent with a heat dome as defined by the American Meteorological Society: an exceptionally hot air mass that develops when high pressure aloft prevents warm air below from rising, thereby trapping the warm air in a manner similar to a dome (AMS 2024). However, not all heat waves are caused by heat domes, and not all heat domes cause heat waves. For example, heat domes commonly are associated with blocking patterns (AMS 2024). In the Pacific Northwest, blocking patterns tend to be more frequent during winter than summer, and typically are not associated with anomalously high heat during winter. Therefore, we refer to the event as a heat wave, and encourage differentiation between the manifestation of an atmospheric phenomenon (heat wave) and the mechanism that sometimes causes such phenomena (heat dome).

We examined observational data from 113 long-term weather stations in Washington, Oregon, and western Idaho, with data records that began before 1955, that are archived in the Global Historical Climatology Network daily database (Menne et al. 2012). These observations
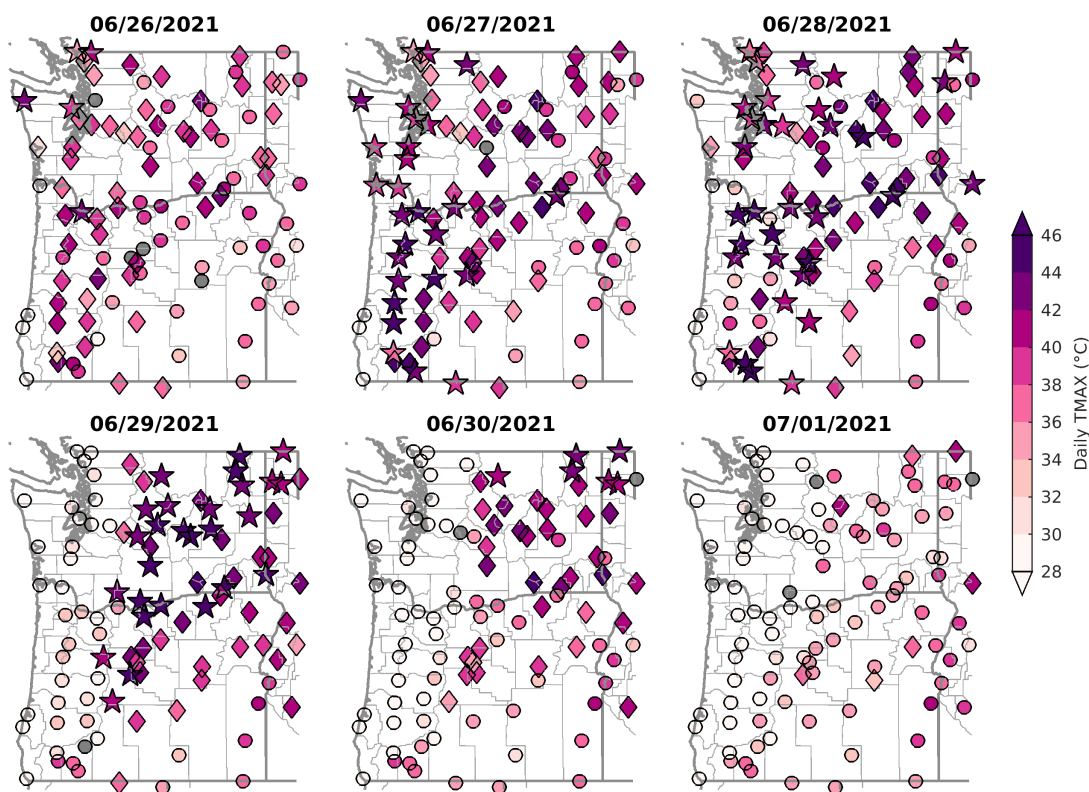


**Figure 2.** Daily maximum near-surface air temperatures during each day of the June 2021 heat wave at 113 weather stations with data records that began before 1955. All-time records at each station were determined relative to 25 June 2021 for their periods of record, and were not updated during the heat wave. Data from the Global Historical Climatology Network daily (GHCNd) database (Menne et al. 2012).
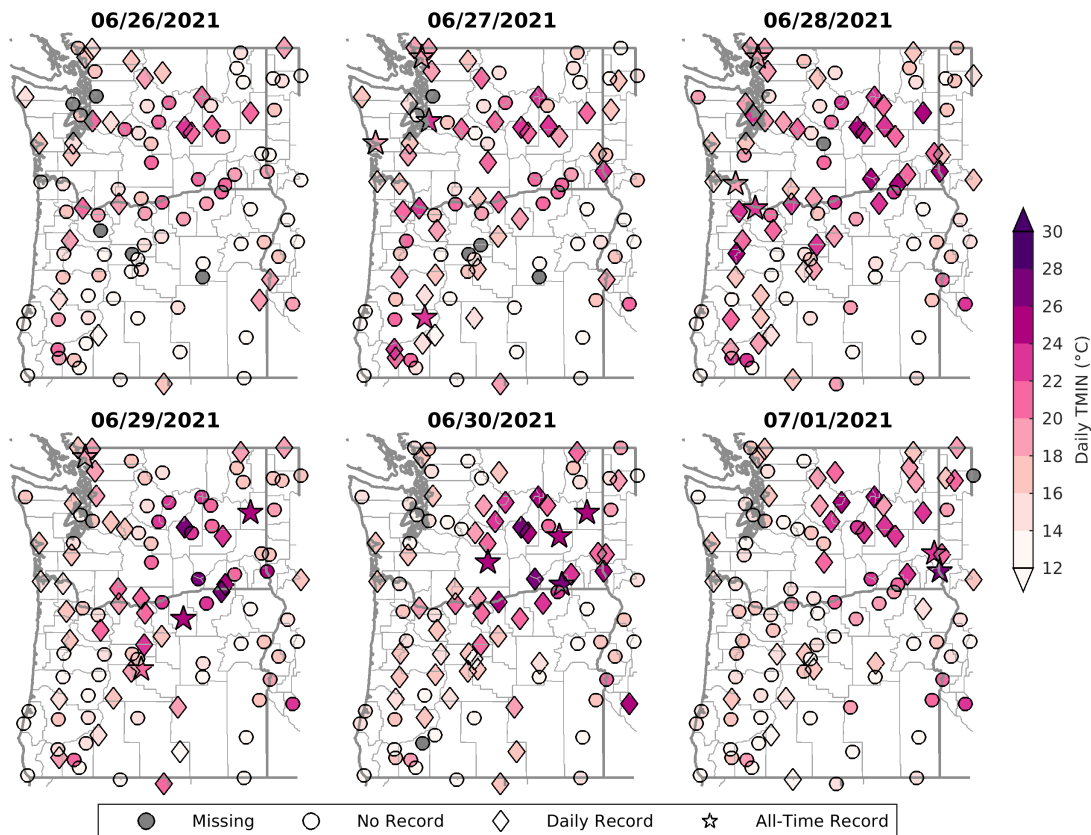
**Figure 3.** Maximum daily minimum near-surface air temperatures during each day of the June 2021 heat wave at 113 weather stations with data records that began before 1955. All-time records at each station were determined relative to 25 June 2021 for their periods of record, and were not updated during the heat wave. Data from the Global Historical Climatology Network daily (GHCNd) database (Menne et al. 2012).

indicated that the heat wave began on 26 June in Washington and western Oregon, where 48 daily records and five all-time records were broken. Over the next two days, many more daily and all-time record maximum temperatures at stations in western Washington and Oregon were broken. Prior to the event, the highest temperature recorded at Portland International Airport was 107.1°F (41.7°C), set on 30 July 1965. During the 2021 heat wave, Portland set all-time records on three consecutive days: 108.3°F (42.4°C) on 26 June, 111.9°F (44.4°C) on 27 June, and 116.1°F (46.7°C) on 28 June. On 29 June, a strong marine layer dramatically cooled western Washington and Oregon, and the heat wave mainly centered east of the Cascade Range. On the same day, the all-time maximum temperature record in Washington was broken at Hanford, which reached 120.0°F (48.9°C) (Miller and Bair 2022), and the all-time maximum temperature record in Oregon, 118.9°F (48.3°C), was tied at both Pelton Dam and Moody Farms (Vescio and Bair 2022). The heat wave ended on 1 July. During the six days from 26 June through 1 July, 350 of 666 possible daily maximum temperature records (52.6 percent) at 133 stations (Figure 2) were tied or broken. During those days, 116 all-time daily maximum temperature records (17.4 percent of possible observations) were tied or broken.

Many warm daily minimum temperature records also were tied or broken during the heat wave (Figure 3). At the 113 stations over the six-day heat wave, 664 daily minimum temperature observations were possible. Of these observations, 18 all-time high minimum temperature records (2.7 percent) and 286 daily records (43.1 percent) were tied or broken.

## Recent Advances in Climate Science

As illustrated above, projected changes in precipitation have greater uncertainty than changes in temperature. Accordingly, two chapters in this assessment address variability and projected climate change-driven changes in Oregon's precipitation, and one chapter addresses historical and projected trends in drought across the state.

*Impacts of the El Niño-Southern Oscillation (ENSO) on Oregon's Weather and Climate* evaluates how the El Niño-Southern Oscillation (ENSO), one of the world's most monitored and studied climate phenomena, affects Oregon's water year temperature, precipitation, snowpack, streamflow, and reservoir storage. We also explore the current capability of weather forecast models to predict winter climate in Oregon on the basis of climate during the preceding autumn, given different phases and strengths of ENSO.

*Projected Changes in Oregon Precipitation* examines projected future changes in precipitation and the proportions of precipitation falling as rain and snow in Oregon and across the Pacific Northwest from 2025–2100, with a non-exclusive emphasis on model-projected changes by mid-century (2045–2074) under SSP 3-7.0. Models suggest that total annual precipitation is likely to increase by 0–10 percent in Oregon by mid-century, but with seasonal variation that includes drier summers, especially in western Oregon. Projected extreme wet-day precipitation increases during the century, particularly in winter. Over the full time period of analysis (1950–2100), snowfall is projected to decrease by no less than 50 percent in any part of Oregon. At the same time, the proportion of precipitation falling as rain increases by 30–50 percent over much of southeastern Oregon and by 3–10 percent in western and coastal Oregon.

*Oregon Drought History and Twenty-First Century Projections* presents historical drought occurrences at the state, regional, and county levels. During 18 of the 24 water years from 1999 through 2023, Oregon's water year precipitation was below average. The average temperature in Oregon also was warmer than normal in 21 of the last 24 water years, which contributed to higher rates of evapotranspiration and more-frequent drought. Drought projections for Oregon on the basis of downscaled climate model simulations for the twenty-first century suggest that the effects of increasing carbon dioxide concentrations on plant physiology (some plants will use less water as those concentrations increase; Yang et al. 2019) only partially will offset the increase in atmospheric dryness due to warmer temperatures. Results suggest that drought risk likely will increase over the twenty-first century on the western slopes of the Cascade Range and the southern Coast Range, decrease in the Deschutes and John Day basins in north-central Oregon, and change little elsewhere. However, due to a shift in the seasonal distribution of precipitation, drought risk during summer is likely to increase statewide.

## Literature Cited

AMS (American Meteorological Society). 2024. Glossary of meteorology: heat dome. glossarytest. ametsoc.net/wiki/Heat_dome. Accessed 18 July 2024.

Bercos-Hickey, E., T.A. O'Brien, M.F. Wehner, L. Zhang, C.M. Patricola, H. Huang, and M.D. Risser. 2022. Anthropogenic contributions to the 2021 Pacific Northwest heatwave. Geophysical Research Letters 49:e2022GL099396. https://doi.org/10.1029/2022GL099396.

Dalton, M.M., K.D. Dello, L. Hawkins, P.W. Mote, and D.E. Rupp. 2017. Third Oregon climate assessment report. Oregon Climate Change Research Institute, Oregon State University, Corvallis, Oregon. https://doi.org/10.5399/osu/1158.

Eyring, V., S. Bony, G.A. Meehl, C.A. Senior, B. Stevens, R.J. Stouffer, and K.E. Taylor. 2016.

Overview of the Coupled Model Intercomparison Project Phase 6 (CMIP6) experimental design and organization. Geoscientific Model Development 9:1937–1958.

Hausfather, Z., K. Marvel, G.A. Schmidt, J.W. Nielsen-Gammon, and M. Zelinka. 2022. Climate simulations: recognize the 'hot model' problem. Nature 605:26–29.

Horton, D.E., N.C. Johnson, D. Singh, D.L. Swain, B. Rajaratnam, and N.S. Diffenbaugh. 2015. Contribution of changes in atmospheric circulation patterns to extreme temperature trends. Nature 522:465–469.

IPCC (Intergovernmental Panel on Climate Change). 2021. Summary for policymakers. In V. Masson-Delmotte et al., editors. Climate change 2021: the physical science basis. Contribution of Working Group I to the Sixth Assessment Report of the Intergovernmental Panel on Climate Change. Cambridge University Press, Cambridge, UK and New York, USA.

Lybarger, N.D., A. Smith, A.J. Newman, E.D. Gutmann, A.W. Wood, C.D. Frans, M.D. Warner, and J.R. Arnold. 2024. Improving Earth system model selection methodologies for projecting hydroclimatic change: case study in the Pacific Northwest. Journal of Geophysical Research: Atmospheres 129:e2023JD039774. https://doi.org/10.1029/2023JD039774.

Meehl, G.A., C.A. Senior, V. Eyring, G. Flato, J.-F. Lamarque, R.J. Stouffer, K.E. Taylor, and M. Schlund. 2020. Context for interpreting equilibrium climate sensitivity and transient climate response from the CMIP6 Earth system models. Science Advances 6:eaba1981. https://doi.org/10.1126/sciadv.aba1981.

Menne, M.J., I. Durre, B. Korzeniewski, S. McNeill, K. Thomas, X. Yin, S. Anthony, R. Ray, R.S. Vose, B.E. Gleason, and T.G. Houston. 2012. Global Historical Climatology Network daily (GHCNd), Version 3.31-upd-2024062518. NOAA National Climatic Data Center. https://doi.org/10.7289/V5D21VHZ. Accessed June 2024.

Miller, R.J., and A. Bair. 3 February 2022. New value for Washington maximum temperature record at Hanford, WA. Memorandum. State Climate Extremes Committee. National Weather Service. www.ncei.noaa.gov/monitoring-content/extremes/scec/reports/20220210-Washington-Maximum-Temperature.pdf.

NCEI (National Centers for Environmental Information). 2024. Climate at a glance: state-wide time series. National Oceanic and Atmospheric Administration. www.ncei.noaa.gov/access/monitoring/climate-at-a-glance/statewide/time-series.

O'Neill, B.C., et al. 2016. The Scenario Model Intercomparison Project (ScenarioMIP) for CMIP6. Geoscientific Model Development 9:3461–3482.

Rupp, D.E., S. Li, P.W. Mote, K.M. Shell, N. Massey, S.N. Sparrow, D.C.H. Wallom, and M.R. Allen. 2017. Seasonal spatial patterns of projected anthropogenic warming in complex terrain: a modeling study of the western US. Climate Dynamics 48:2191–2213.

Tokarska, K.B., M.B. Stolpe, S. Sippel, E.M. Fischer, C.J. Smith, F. Lehner, and R. Knutti. 2020. Past warming trend constrains future warming in CMIP6 models. Science Advances 6:eaaz9549. https://doi.org/10.1126/sciadv.aaz9549.

Vescio, M. D., and A. Bair. 1 February 2022. Oregon all time maximum temperature record tied at Pelton Dam, OR and Moody Farms, OR. Memorandum. State Climate Extremes Committee. National Weather Service. www.ncei.noaa.gov/monitoring-content/extremes/scec/reports/20220210-Oregon-Maximum-Temperature.pdf.

Yang, Y., M.L. Roderick, S. Zhang, T.R. McVicar, and R.J. Donohue. 2019. Hydrologic implications of vegetation response to elevated $CO_2$ in climate projections. Nature Climate Change 9:44–48.

Zelinka, M.D., T.A. Myers, D.T. McCoy, S. Po-Chedley, M.P. Caldwell, P. Ceppi, S.A. Klein, and K.E. Taylor. 2020. Causes of higher climate sensitivity in CMIP6 models. Geophysical Research Letters 47:e2019GL085782. https://doi.org/10.1029/2019GL085782.

Zhang, X., T. Zhou, W. Zhang, L. Ren, J. Jiang, S. Hu, M. Zuo, L. Zhang, and W. Man. 2023. Increased impact of heat domes on 2021-like heat extremes in North America under global warming. Nature Communications 14:1690. https://doi.org/10.1038/s41467-023-37309-y.

# Changes in the 2023 U.S. Department of Agriculture Plant Hardiness Map

Christopher Daly and Todd Rounsaville

Extreme cold temperatures during winter are the most significant environmental factors for predicting the survival of perennial plants and winter annual crops. Determining the appropriate geographical range for crops and landscape plants is critical for producers, farmers, and home gardeners who seek to cultivate long-lived, healthy, and high-yielding plants. The U.S. Department of Agriculture (USDA) Plant Hardiness Zone Map (PHZM; Figure 1) classifies plant growing zones on the basis of the average annual extreme minimum temperature. Each of the 13 zones, from zone 1 (coldest) to zone 13 (warmest), covers a 10-degree Fahrenheit (F) range. Each zone is subdivided into two 5-degree F half-zones, which are designated as a and b. Temperatures currently are calculated as 30-year averages of the extreme minimum temperature recorded annually (the plant hardiness statistic).
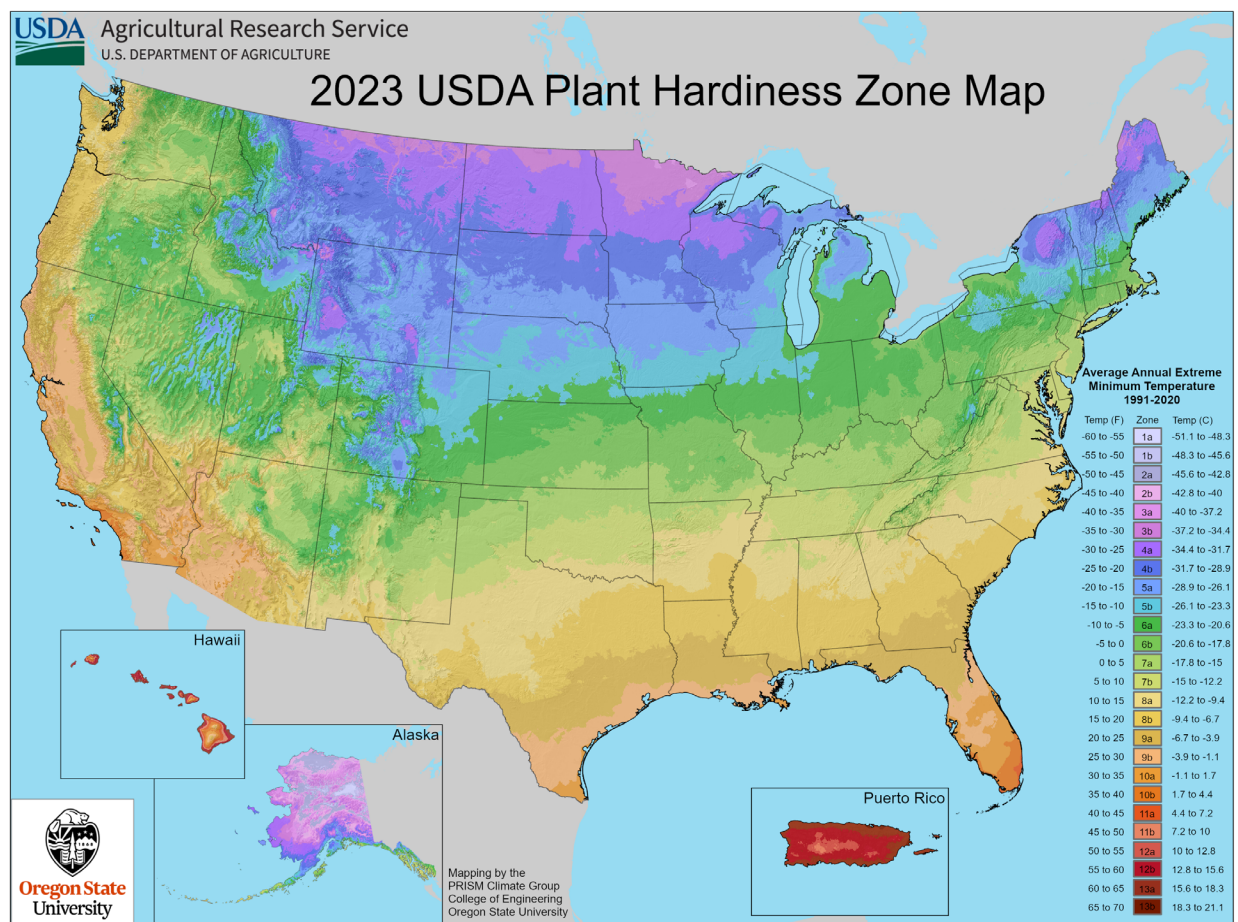


**Figure 1.** The 2023 USDA Plant Hardiness Zone Map for the United States and Puerto Rico.

The agricultural and horticultural industries have adopted the USDA Plant Hardiness Zones as their standard for selecting regionally adapted plants. Beginning with plant breeders and evaluators, hardiness zones are tested and documented for individual species or varieties of plants. The associations between zones and suitability of plants for those winter conditions are communicated by commercial growers in catalogs, marketing materials, and plant labels. Consumers such as farmers
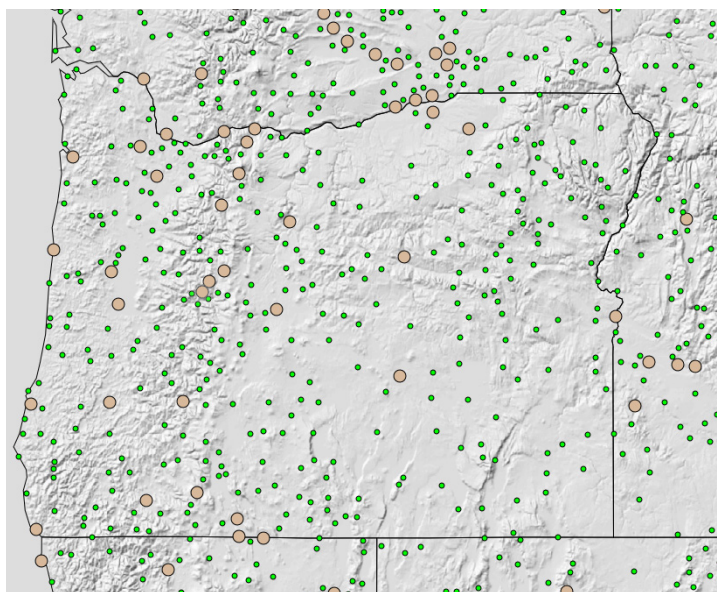
**Figure 2.** Locations of stations in Oregon and neighboring states used in the development of the 2023 Plant Hardiness Zone Map. Large circles indicate clusters of stations.

and home gardeners then consult the PHZM to determine the hardiness zone for their location, and purchase plants that are suited to their local conditions. Thus, the PHZM serves as a risk management tool, presenting historical minimum-temperature data in a standardized format that expresses the probability that a plant will survive the most extreme cold temperatures at a given location.

Although plant cold-hardiness maps have been in use since the late 1920s, and the first USDA map was released in 1960, the 2012 PHZM was the first to reflect standardized data modeling through the PRISM climate mapping system developed by the PRISM Climate Group at Oregon State
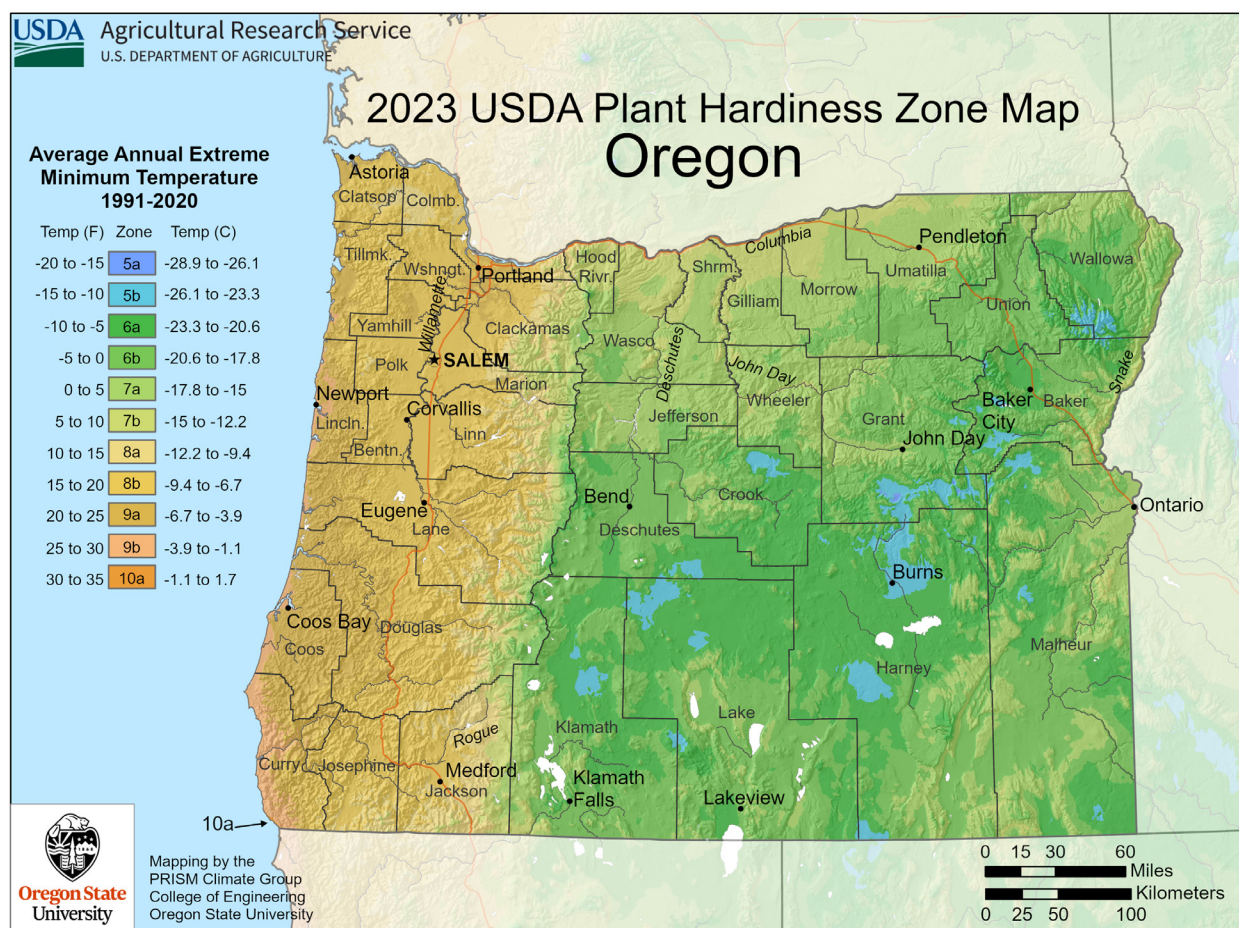


**Figure 3.** The 2023 USDA Plant Hardiness Zone Map for Oregon.

University, and to be presented in fully digital form. The 2012 PHZM was based on data from 1976–2005. The release of 1991–2020 U.S. Climate Normals data in 2021 presented an opportunity to revise and update the PHZM by analyzing 15 years of more-recent temperature data (2006–2020) and removing 15 earlier years (1976–1990) from the record, while incorporating data from 68 percent more weather stations and improvements to mapping techniques.
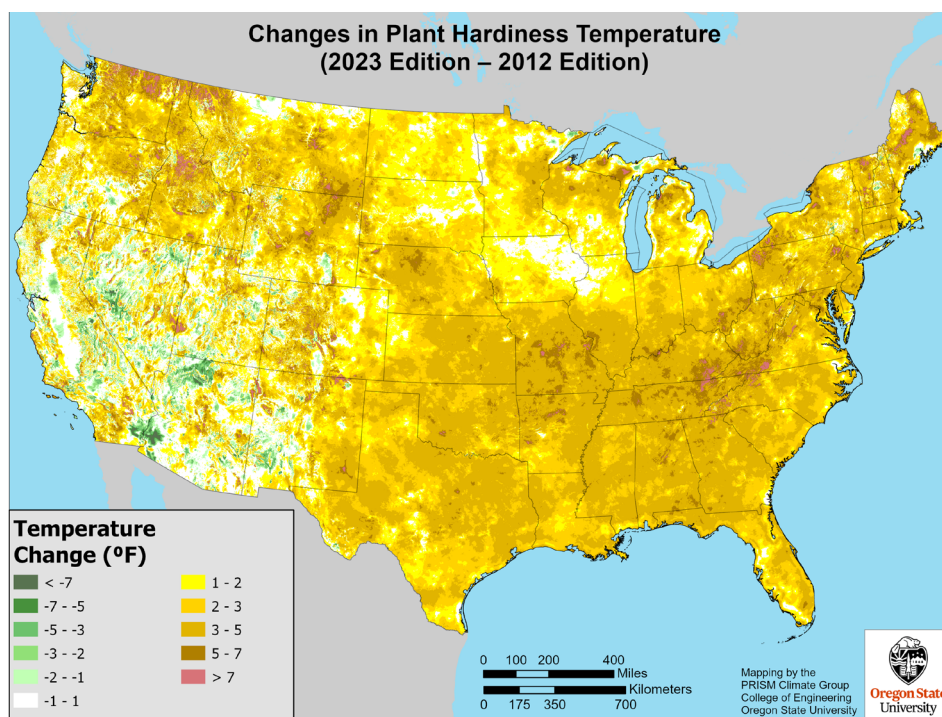


**Figure 4.** Changes in the plant hardiness temperature statistic in the conterminous United States between the 2012 Plant Hardiness Zone Map (1976–2005 averaging period) and the 2023 Plant Hardiness Zone Map (1991–2020 averaging period).

The 2023 PHZM incorporated data from 13,625 weather stations from national, regional, and state networks. In Oregon (Figure 2), data sources included stations from the National Weather Service Cooperative Observer Program (COOP), Automated Surface Observing System (ASOS), and Weather Bureau–Army–Navy (WBAN); USDA Natural Resources Conservation Service Snow Telemetry (SNOTEL); USDA Forest Service and Bureau of Land Management Remote Automatic Weather Stations (RAWS); Bureau of Reclamation AgriMet; Washington State University AgWeatherNet; and Oregon State University H.J. Andrews Experimental Forest. The greatest number of stations that contributed to the 2023 map are within the COOP network. These stations are operated primarily by volunteer observers, and most are located in human-inhabited areas that can be accessed daily. The SNOTEL automated network is designed to observe conditions in the snow zones of the western United States and provided data for high-elevation regions. The RAWS automated network mainly focuses on fire-weather conditions at elevations between those of the COOP and SNOTEL stations. AgriMet and AgWeatherNet automated stations provided data from agricultural regions of the Pacific Northwest. The H.J. Andrews Experimental Forest, on the western slopes of the central Oregon Cascade Range, provided data at fine spatial resolution in this topographically complex region.

Within Oregon (Figure 3), the 2023 PHZM indicates two distinct climate regimes, a colder regime east of the Cascade Range and a milder regime to the west of the Cascade Range. Areas east of the Cascade Range are shielded from moist, mild air from the Pacific Ocean but are exposed to potential Arctic air outbreaks from Alaska and Canada that penetrate west of the Rocky Mountains. Most of the coldest areas (zone 5; -10° to -20°F) are located in valley bottoms where cold, dense air can pool and persist during the coldest nights of winter. Extreme minimum temperatures are somewhat

warmer above the cold pools but decrease again at higher elevations. Extremely cold air rarely penetrates west of the Cascade Range. Instead, winter conditions are dominated by frequent storms and onshore air flow from the relatively warm Pacific Ocean, and hardiness zones are dictated by proximity to the coastline. Most of the Willamette Valley is within zone 8 (10° to 20°F), whereas coastal areas are typically in zone 9 (20° to 30°F). A small area of zone 10a (30° to 35°F) lies on the far southwest coast of Oregon.

Comparing the 2023 PHZM with the 2012 map indicates that, when averaged across the country, the average extreme minimum temperature has increased by 2.5°F (Figure 4). As a result, approximately half of the United States was reclassified into a warmer Plant Hardiness half-zone (Figure 5). The zone change map, although preferred by most users, can be misleading. Changes in the plant hardiness statistic are continuous values (Figure 4), but the key question most users ask is whether their zone has changed (Figure 5). Many locations at the colder end of the half-zone range did not warm enough to move into the next warmer half-zone, whereas numerous locations at the warmer end of the half-zone range, which warmed by a similar amount, moved into a warmer half-zone.

Changes between the 2012 and 2023 PHZMs varied widely across Oregon (Figures 6, 7). Minimum temperatures in low elevation areas east of the Cascade Range and in the central and southern Willamette Valley changed little. Substantial warming in high elevation areas in northeastern Oregon in the PHZM does not reflect climate change per se, but rather improvements in mapping over the past decade that produced more-accurate estimates of temperatures in these data-sparse areas.
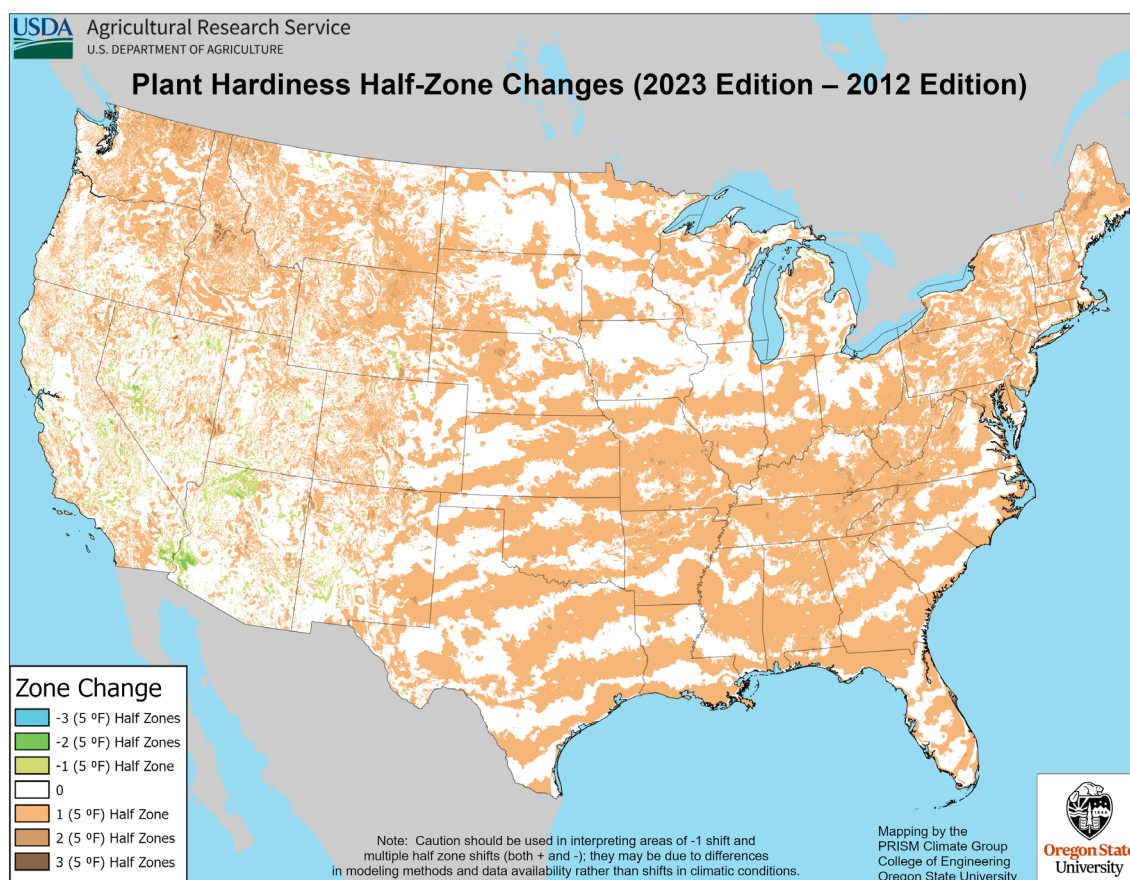


**Figure 5.** Five-degree half-zone changes in the conterminous United States between the 2012 Plant Hardiness Zone Map (1976–2005 averaging period) and the 2023 map (1991–2020 averaging period).
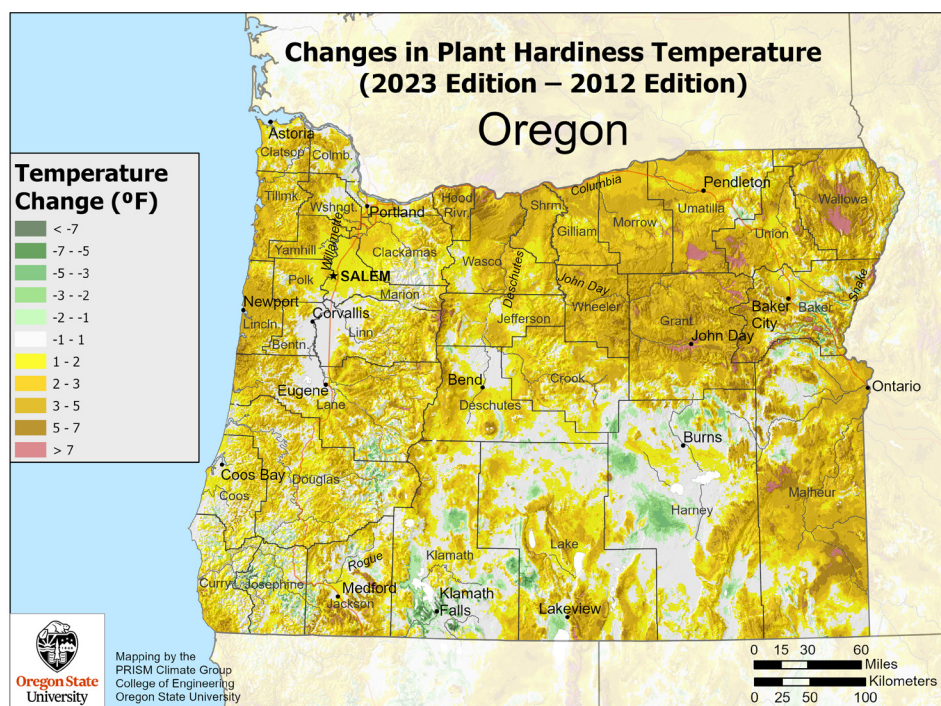
**Figure 6.** Changes in the plant hardiness temperature statistic in Oregon between the 2012 Plant Hardiness Zone Map (1976–2005 averaging period) and the 2023 Plant Hardiness Zone Map (1991–2020 averaging period).

Apparent local areas of cooling are likely a result of additional station data and improved modeling of cold air pools.

Changes in minimum temperature across the Pacific Northwest between the 2012 and 2023 maps also varied regionally (Figure 8). As in Oregon, considerable warming at high elevations in northern Washington and central Idaho reflects improvements in mapping.

The plant hardiness statistic, defined as the single coldest daily minimum temperature of the year, is inherently volatile from year to year. Therefore, comparing the 2023 PHZM with the 2012 PHZM does not provide a complete picture of longer-term trends and variation in the plant hardiness statistic. Some stations in Oregon have recorded daily temperature data since 1950, which allows for examination of the plant hardiness statistic over a longer duration (Figure 9). Annual extreme minimum temperature at most of these locations is cyclical, with slight cooling in the 1980s, warming in the 2000s, and cooling in the most recent years. These cycles are superimposed on a long-term warming trend that may be a climate change signal but is difficult to attribute with certainty due to the volatility of the statistic.

The variability of the plant hardiness statistic differs across Oregon. The Willamette Valley is in zone 8 on average, but annual variations may yield conditions similar to those in zone 7 or 9. Astoria, although coastal, is susceptible to cold air outbreaks through the Columbia Gorge, which can drop plant hardiness temperatures well below the local average. Stations in interior Oregon have greater year-to-year variability: any given year could be several zones above or below its 30-year average.

What do these changes mean for gardening in Oregon? The 2023 PHZM documents what happened during the period 1991–2020. Therefore, any changes have already been felt in gardens across the state. It is unlikely that Oregon gardeners will radically alter the perennials they grow on the basis of the new map, especially given the microclimatic variation in many gardens that is not accounted for in the PHZM, from sunny south-facing walls where plants rated for warmer zones may thrive, to cold depressions in deep shade where the same plants may struggle. However, the PHZM provides an updated and quantitative standard by which risk can be assessed. Because the

PHZM is based on a long-term average, the volatility of the plant hardiness statistic becomes relevant when planting varieties at zone boundaries; a perennial rated for a warmer zone may do well for a few years, but then be damaged or killed by an unusually severe Arctic air outbreak.

The PHZM provides information on only one statistic, the mean extreme annual minimum temperature. It does not provide information on the frequency, timing, or duration of winter cold events. Additionally, many factors other than minimum temperature, such as light, soil moisture, humidity, and snow cover, influence plant survival. Details on these factors and
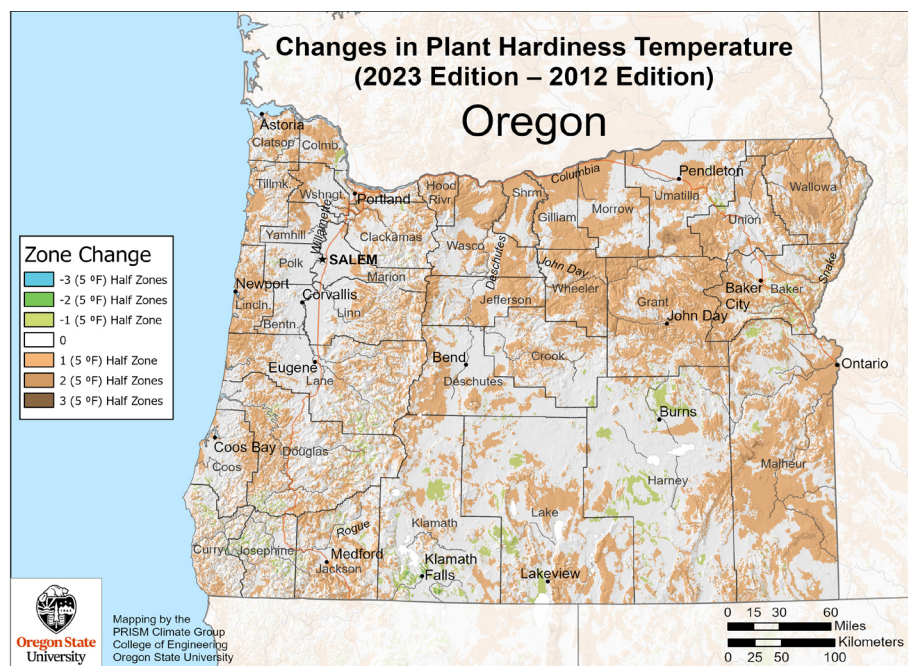


**Figure 7.** Five-degree half-zone changes in Oregon between the 2012 Plant Hardiness Zone Map (1976–2005 averaging period) and the 2023 Plant Hardiness Zone Map (1991–2020 averaging period).

other considerations for use of the PHZM are at planthardiness. ars.usda.gov. Technical details on the creation of the 2012 map and its potential uses as a risk management tool are available from prism.oregonstate. edu/documents/ pubs/2012jamc_ plantHardiness_ daly.pdf and prism. oregonstate.edu/ documents/pubs/ 2012horttech_ hortApps_ widrlechner.pdf.
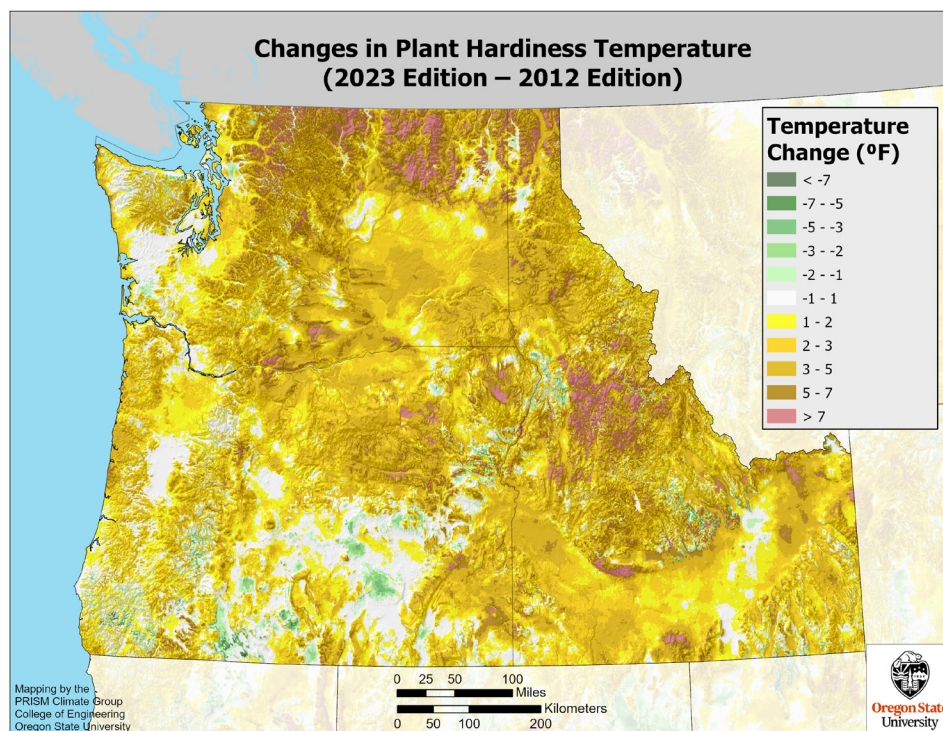


**Figure 8.** Changes in the plant hardiness statistic in the Pacific Northwest between the 2012 Plant Hardiness Zone Map (1976–2005 averaging period) and the 2023 Plant Hardiness Zone Map (1991–2020 averaging period).
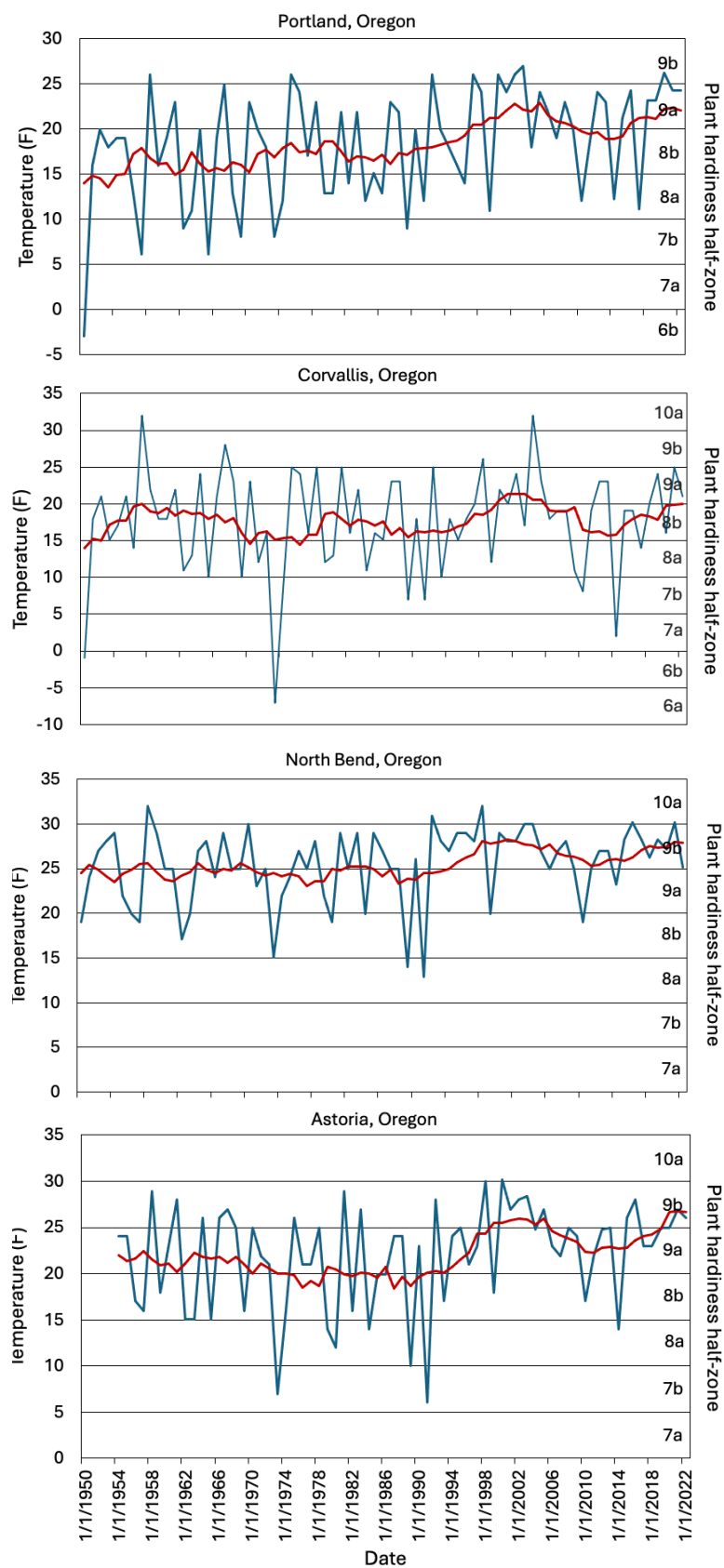
**Figure 9.** Time series of the plant hardiness statistic at (a) Portland, (b) Corvallis, (c) North Bend, (d) Astoria, (e) Redmond, (f) Baker City, and (g) Boise, Idaho, 1950–2022. Red lines indicate the 10-year moving average.

Redmond, Oregon

Baker City, Oregon

Boise, Idaho
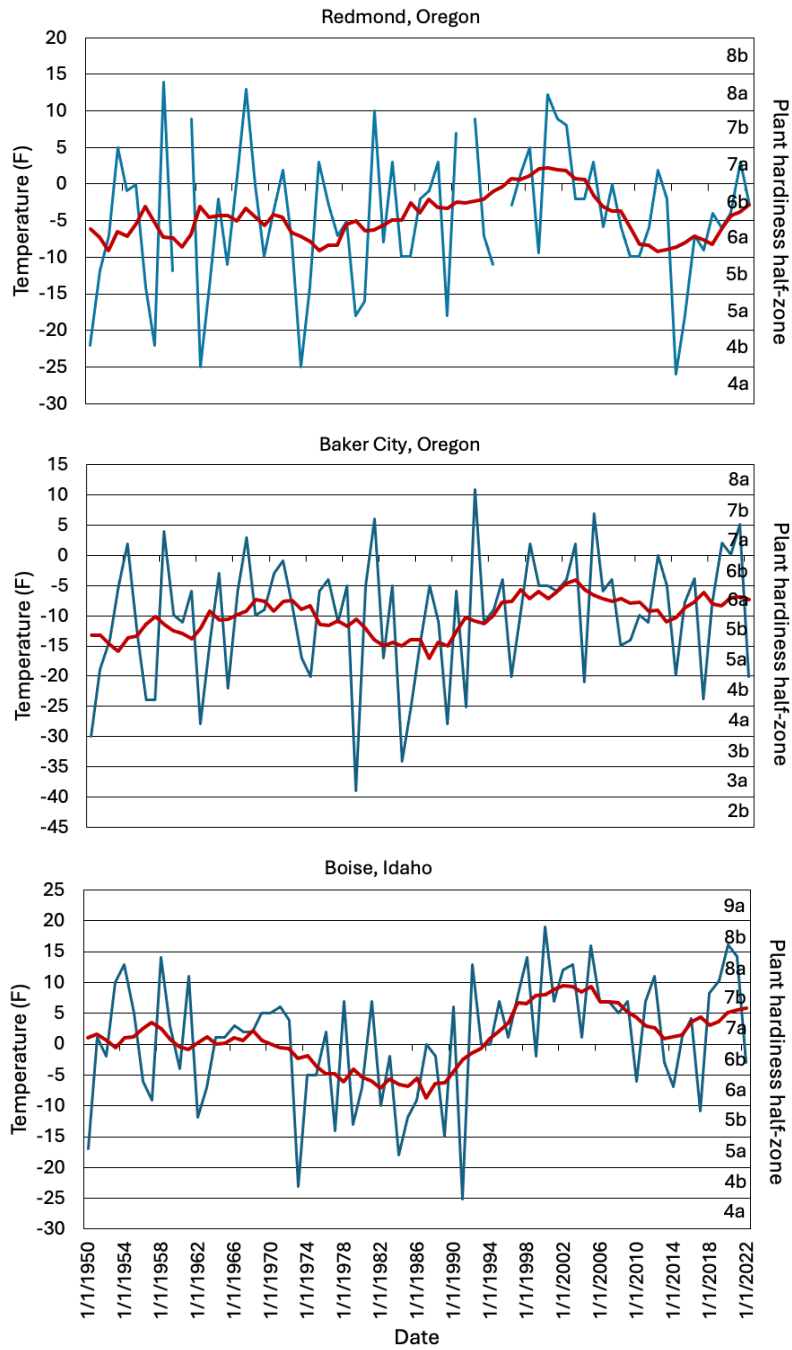
# Impacts of the El Niño–Southern Oscillation (ENSO) on Oregon's Weather and Climate

Larry W. O'Neill, Rose Una, Gabriel Rivera, Nathan Fillmann, David E. Rupp, and Nick Siler

## Introduction to the El Niño–Southern Oscillation

The El Niño–Southern Oscillation (ENSO) is one of the world's most monitored and studied climate phenomena due to its substantial impact on weather and on human and natural systems. ENSO is a natural fluctuation of ocean temperature near the equator in the Pacific Ocean that strongly affects global weather patterns and seasonal climate. Although ENSO's effects on seasonal climate are not always consistent, it is one of the few useful signals for forecasting seasonal climate of many regions one or two seasons in advance. In this chapter, we examine the effects of ENSO on Oregon's weather, climate, and hydrology. We also explore the current capability of weather forecast models to predict winter climate in Oregon on the basis of climate during the preceding autumn given different ENSO conditions.

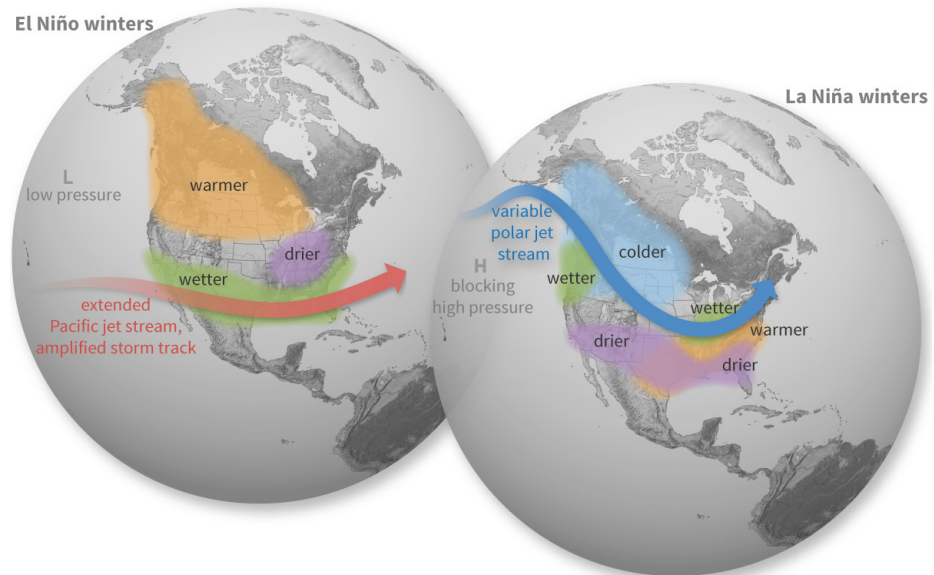ENSO has three primary phases: El Niño, La Niña, and ENSO-Neutral. Surface water in the equatorial Pacific Ocean is much warmer than normal during an El Niño, much cooler than normal during a La Niña, and near normal during ENSO-Neutral. The geographic extent of oceanic warming or cooling varies, but often affects most of the equatorial Pacific Ocean. El Niño events typically last less than a year, whereas La Niña can persist for up to three years. These events occur irregularly, with intervals from two to seven years. In most cases, the transition between ENSO phases occurs between May and September. Ocean temperature anomalies associated with changing ENSO phases can initiate changes in weather in the tropics that affect the path and intensity of the jet stream and storm tracks in the mid-latitudes of both hemispheres. This remote linkage is often referred to as a teleconnection. The response of mid-latitude weather to El Niño or La Niña is most apparent during autumn and winter. Because the Northern Hemisphere jet stream and storm track often pass through Oregon, deviations in the jet stream caused by ENSO can impact water-dependent systems in the state, including snowpack, streamflows, soil moisture, fuel moisture, and shallow groundwater, with cascading effects on human and natural systems.

During the last four years, severe drought, record-high temperatures, highly variable winter snowpack, and other climatic extremes reinvigorated interest in the relevance of ENSO for accurately predicting seasonal climate across the Pacific Northwest, especially with respect to drought conditions. Since 1950, the earliest year for which reliable records exist, there were three instances in which La Niña occurred during three consecutive years. The most recent was 2021–2023. A Strong El Niño (ocean temperatures that are considerably warmer than normal; see next section) developed in autumn 2023, and dissipated in spring 2024. As of late October 2024, the majority of forecasts favor development of La Niña. The magnitude of change in ocean temperature between the 2022–2023 Weak La Niña and the 2023–2024 Strong El Niño was one of the greatest associated with an ENSO phase transition within a single year since at least 1950.

The stereotypical impact of El Niño and La Niña on global weather patterns is illustrated by a widely used graphic developed by the National Oceanic and Atmospheric Administration (NOAA) (Figure 1). The rule of thumb is that on average, weather conditions in the Pacific Northwest are warm and dry during El Niño events and cool and wet during La Niña events. General expectations of temperature and precipitation anomalies in the southwestern United States are the opposite. For instance, California tends to be cool and wet during El Niño events and warm and dry during La

Niña events (Figure 1). Because Oregon is located at the transition between the Pacific Northwest and U.S. Southwest, outcomes of ENSO on the state's weather and climate can deviate considerably from this rule of thumb. Previous research also recognizes that these weather and climate outcomes in the Pacific Northwest are not universal, particularly during El Niño events,



**Figure 1.** Typical winter weather patterns and anomalies associated with El Niño and La Niña events. Source: NOAA Climate Prediction Center.

but can depend on the strength of El Niño or La Niña as measured by the magnitude of the ocean temperature anomaly along the equatorial Pacific Ocean (Hoerling et al. 1997, Khan et al. 2006, Fleming et al. 2007, Fleming and Dahlke 2014).

Although connections between ENSO and global weather patterns often are statistically significant, subtle differences between ENSO events and variability in atmospheric circulation independent of ENSO can result in outcomes much different from the rule of thumb on a case-by-case basis, particularly over relatively small regions such as the Pacific Northwest. Additionally, other patterns of variability in the coupled ocean-atmosphere system, such as the Pacific Decadal Oscillation, Arctic Oscillation, and Pacific-North American teleconnection pattern, can interact with ENSO to generate changes in weather patterns inconsistent with the general rule.

Current state-of-the-art global weather prediction systems do not support accurate forecasts of individual weather events more than about five to ten days in advance. ENSO provides some insight on likely seasonal temperature and precipitation anomalies about three to six months in advance, providing important clues about how seasonal weather patterns may affect, for example, water supply and snowpack. The effects of ENSO on seasonal weather variability have motivated intensive efforts to develop more-accurate predictive capabilities. Even so, extending the predictability of ENSO to global patterns of precipitation and surface air temperature is challenging.

Despite intensive research to improve seasonal weather and climate predictability, the connection between ENSO and climate change remains elusive (Cai et al. 2021). It is unclear whether the frequency or intensity of ENSO events; global teleconnections that influence precipitation, snowpack, and temperature; or the effects of ENSO on weather and climate in the Pacific Northwest will shift during the twenty-first century.

## ENSO Categorization

The strength and phase of ENSO fundamentally characterize anomalies of the near-surface ocean temperature around the equator in the Pacific Ocean. As we detail in this chapter, the strength of

these anomalies correlates with the impact of ENSO on Pacific Northwest weather and climate. A close surrogate of the near-surface ocean temperature, the sea surface temperature, is routinely measured by a network of satellites, ships, and buoys. The main operational index used to categorize ENSO by the NOAA Climate Prediction Center, the Oceanic Niño Index (ONI), is based on deviations of the average sea surface temperature across a large area of the eastern equatorial Pacific Ocean (referred to as the Niño-3.4 region) over rolling three-month periods from its most recent 30-year average value (NOAA 2024a,b) (Table 1). The 30-year average sea surface temperatures on which anomalies are based are updated every five years to account for the longer-term oceanic warming trend, which is due mainly to climate change. ONI values above +0.5°C are categorized as El Niño events, whereas ONI values below -0.5°C are categorized as La Niña events. Events with an ONI between these values are categorized as ENSO-Neutral. The ONI time series began in 1950 (Figure 2) and is updated every month. Sea surface temperatures used to compute the ONI for operational monitoring are derived from the Extended Reconstructed Sea Surface Temperature (ERSST; Huang et al. 2017).

| ENSO phase and strength | Range of ONI values |
|---|---|
| Very Strong El Niño | ≥2.0°C |
| Strong El Niño | 1.5 to 1.9°C |
| Moderate El Niño | 1.0 to 1.4°C |
| Weak El Niño | 0.5 to 0.9°C |
| ENSO-Neutral | -0.5 to 0.5°C |
| Weak La Niña | -0.9 to -0.5°C |
| Moderate La Niña | -1.4 to -1.0°C |
| Strong La Niña | -1.9 to -1.5°C |
| Very Strong La Niña | ≤-2.0°C |

**Table 1.** Categorization of the El Niño-Southern Oscillation (ENSO) phase and strength on the basis of the Oceanic Niño Index (ONI) value.

In this chapter, we use the ONI to characterize the historical influence of ENSO phase on Oregon's water year temperature, precipitation, snowpack, streamflow, and reservoir storage. We examined these influences during two time periods: 1951 through 2023, for which temperature and precipitation data are available, and 1981 through 2023, for which snowpack, streamflow, and reservoir storage data are available.

Water years are defined as the 12-month period from 1 October through 30 September. Water year 2024, for instance, corresponds to the period 1 October 2023 through 30 September 2024. We categorized the ENSO phase for each water year on the basis of monthly ONI values that met one of the ENSO phase criteria (Table 1) for at least three consecutive



**Figure 2.** Time series of the monthly Oceanic Niño Index (ONI) since 1950. Data source: NOAA Climate Prediction Center.

30

months during the 12-month period from 1 July through 30 June, which usually is the period during which an ENSO event materializes and reaches its peak intensity (Trenberth 1997). For instance, a Strong El Niño corresponds to a period in which the monthly ONI for at least three consecutive months from July through June is between 1.5 and 1.9°C. Although three Very Strong El Niños occurred since 1950, there have been no Very Strong La Niñas (Table 2). There are only a few Strong or Very Strong events in the contemporary observational record, at least since 1950, so knowledge of the effects of these events on Oregon's seasonal weather patterns is limited.

| Strong La Niña | Moderate La Niña | Weak La Niña | ENSO-Neutral | Weak El Niño | Moderate El Niño | Strong El Niño | Very Strong El Niño |
|---|---|---|---|---|---|---|---|
| 1974 | 1956 | 1951 | 1957 | 1953 | 1952 | 1958 | 1983 |
| 1976 | 1971 | 1955 | 1960 | 1954 | 1964 | 1966 | 1998 |
| 1989 | 1996 | 1965 | 1961 | 1959 | 1969 | 1973 | 2016 |
| 1999 | 2012 | 1967 | 1962 | 1970 | 1987 | 1988 | |
| 2000 | 2021 | 1968 | 1963 | 1977 | 1995 | 1992 | |
| 2008 | 2022 | 1972 | 1979 | 1978 | 2003 | | |
| 2011 | | 1975 | 1981 | 1980 | 2010 | | |
| | | 1984 | 1982 | 2005 | | | |
| | | 1985 | 1986 | 2007 | | | |
| | | 2001 | 1990 | 2015 | | | |
| | | 2006 | 1992 | 2019 | | | |
| | | 2009 | 1993 | 2020 | | | |
| | | 2017 | 1994 | | | | |
| | | 2018 | 1997 | | | | |
| | | 2023 | 2002 | | | | |
| | | | 2004 | | | | |
| | | | 2013 | | | | |
| | | | 2014 | | | | |

**Table 2.** ENSO categorization for water years 1951–2023 on the basis of the Oceanic Niño Index (ONI). For instance, ENSO during water year 2011 is characterized as a Strong La Niña because the monthly ONI for at least three consecutive months from July 2010 through June 2011 was between -1.5 and -1.9°C.

In the peer-reviewed literature, indices other than the ONI are sometimes used to characterize the ENSO phase and its intensity (Trenberth and Stepaniak 2001, Hanley et al. 2003, Kennedy et al. 2009, Karnauskas 2013, van Oldenborgh et al. 2021). These other indices account for spatial shifts in ocean temperature anomalies along the equator and other factors that potentially affect mid-latitude weather. There is no scientific consensus on which of these indices best captures changes in weather far from the equator that are associated with different ENSO phases. Nearly all ENSO indices suggest similar impacts on Oregon's weather and climate.

## Historical Variability of Oregon's Weather and Hydrology Associated with ENSO Phase and Strength

This section summarizes the wide range of effects of ENSO on Oregon's weather and short-term climate patterns on the basis of historical observations of temperature, precipitation, snowpack, streamflow, and reservoir storage.

### Temperature

To analyze responses of mean surface air temperature to ENSO phase and strength, we used monthly values from the PRISM Climate Group, which provides gridded air temperature over the contiguous United States and is based on observational weather station data and statistical interpolation between stations (Daly et al. 1994, Daly et al. 2008) (Figure 3). Oregon's annual average temperature from 1950 through 2023 was 47.4°F, and varied substantially across the state due to differences in elevation and proximity to the Pacific Ocean.

As discussed in a previous chapter, Oregon's statewide average temperature has increased by roughly 3°F since the early twentieth century due to anthropogenic climate change. Recent ENSO events

## Mean Annual Temperature
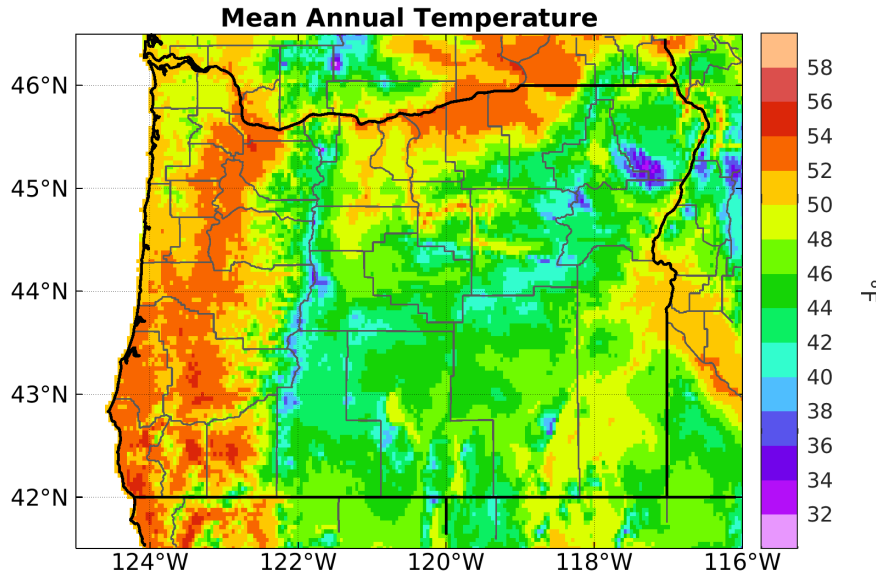


**Figure 3.** Average annual surface air temperature over calendar years 1950 through 2023. Data from the PRISM Climate Group.

are much warmer than earlier events, which confounds determination of the expected air temperature anomalies due solely to ENSO. To account for this warming trend and more clearly identify the effects of ENSO variability on temperature, we subtracted a linear trend in annual average temperature from 1950 through 2023 from the average temperature at each location. This method yields temperature anomalies without the temporal linear trend; we used these data in our analyses.

The statewide annual average temperature can vary by several degrees within each ENSO category (Figure 4). Median and mean temperatures over the water year generally increase from Strong La Niña to Very Strong El Niño. Irrespective of strength, temperatures during La Niña years generally are cooler than those during El Niño years (Figure 4). Additionally, on average, the magnitude of the temperature anomalies roughly varies with the strength of the ENSO event: Strong La Niña events are the coolest and Very Strong El Niño events are the warmest. Annual temperatures were above average during 11 (39 percent) of the 28 La Niña years since the 1951 water year, 17 (63 percent) of the 27 El Niño years, and 10 (56 percent) of the

## Detrended Temperature Anomalies
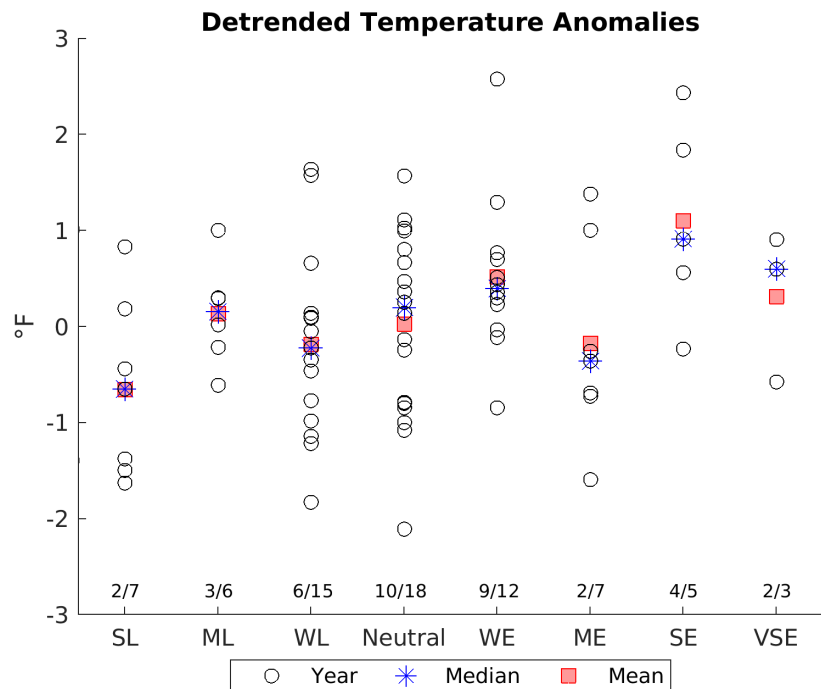


**Figure 4.** Statewide air temperature anomalies averaged for each water year 1951–2023, categorized by ENSO phase and strength. SL, Strong La Niña; ML, Moderate La Niña; WL, Weak La Niña; Neutral, ENSO-Neutral; WE, Weak El Niño; ME, Moderate El Niño; SE, Strong El Niño; VSE, Very Strong El Niño. Anomalies were computed from a linear regression detrending of 1951–2023 monthly temperature data. Median and mean temperature anomalies corresponding to each ENSO phase and strength were computed for the applicable water years (Table 2). Fractions above the x-axis indicate the number of years, of the total per phase and strength, in which the average detrended temperature anomaly was greater than normal. Data from the PRISM Climate Group.

18 ENSO-Neutral years (Figure 4). The temperature response to ENSO is typically greatest from October through March.

Although temperatures during La Niña and El Niño phases were generally cooler and warmer, respectively, than the statewide averages, the extent to which ENSO phase and strength correlated with above- or below-average temperature varied spatially (Figure 5). Across the majority of Oregon, water year average temperatures usually were below average during Strong and Weak La Niña events and above average during Strong and Weak El Niño events. Temperatures during Moderate La Niña and El Niño events were outliers: eastern Oregon was consistently warmer than average during Moderate La Niña events and most of Oregon was cooler than average during Moderate El Niño events. In northern Oregon, average temperatures during the three Very Strong El Niño events were warmer than average, whereas in southern Oregon, temperatures were warmer than average during one of the three Very Strong El Niño events. The lower temperatures in southern Oregon may be related to the consistent cooling effect of El Niño events in California and the Southwest (Figure 1).

Even with some exceptions, El Niño years are likely to be warmer than average and La Niña years are likely to be cooler than average across much of Oregon. A



**Figure 5.** Number of water years per ENSO phase and strength (color shading) during which temperatures in Oregon were warmer than the annual average detrended temperature anomalies. The numbers in parentheses are the number of water years per ENSO phase and strength from 1951 through 2023 (see Table 1). Data from the PRISM Climate Group.

caveat is that our use of detrended temperatures reduces the influence of warming associated with climate change that is unrelated to ENSO-induced temperature anomalies. Temperatures during all ENSO phases are about 3°F warmer now than since the year 1900 (Cai et al. 2021), and this trend will continue until greenhouse gas concentrations begin to decrease.
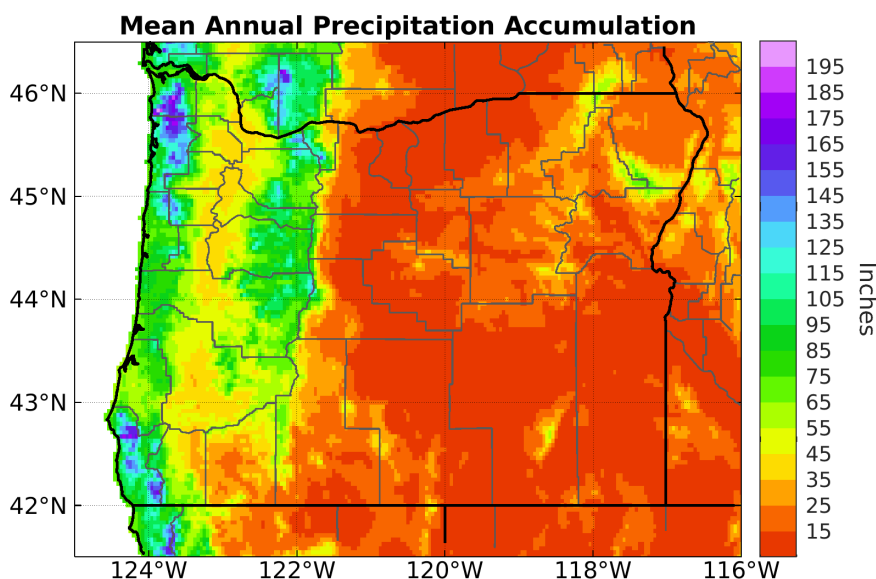
## Precipitation

To analyze responses of precipitation to ENSO phase and strength, we used monthly values of precipitation from the PRISM Climate Group. Average annual precipitation differs strongly west and east of the Cascade Range (Figure 6). Storm systems moving east into the Pacific Northwest deposit large amounts of precipitation on the Coast Range and Cascade Range, where annual average precipitation exceeds 100 inches. Precipitation in the Willamette Valley and central Oregon is much less than in surrounding areas because most precipitation falls on the upwind mountains, leaving a rain shadow. Most of central and eastern Oregon is semi-arid or arid, and receives less than 15 inches of precipitation per year. Exceptions are the Steens Mountains in southeastern Oregon and the Wallowa Mountains in northeastern Oregon, which receive



**Figure 6.** Average annual precipitation across calendar years 1950–2023. Data from the PRISM Climate Group.

more than 50 inches of precipitation per year. The statewide annual average precipitation from 1950 through 2023 was 35.31 inches. As noted in the chapter *Trends in Climate*, the trend in annual precipitation in Oregon during the twentieth century was not statistically significant.

Similar to temperature, the annual statewide average precipitation varied roughly as a function of ENSO phase and strength, with the exception of Very Strong El Niño events (Figure 7). La Niña events were more likely than El Niño events to be wetter than average. On average, annual precipitation during Strong La Niña events was about 7 inches (20 percent) greater than during El Niño events. However, average precipitation was greatest, nearly 39 inches, during all three Very Strong El Niño events (1983, 1998, and 2016).

A somewhat less clear picture emerges when considering the proportion of water years that are wetter than normal statewide. Since the 1951 water year, precipitation was above average during 15 (54 percent) of 28 La Niña years, 7 (39 percent) of 18 ENSO-Neutral years, and 13 (48 percent) of 27 El Niño years. Excluding the Very Strong El Niño years, precipitation in Oregon generally is above normal during La Niña and below normal during El Niño. In some other parts of the western United States, Very Strong El Niños are not the driest ENSO phase (Hoerling et al. 1997, Fleming et al. 2007); this phenomenon is not well known or understood.

## Statewide Water Year Accumulated Precipitation



**Figure 7.** Statewide accumulated precipitation for each water year from 1951 through 2023, categorized by ENSO phase and strength. SL, Strong La Niña; ML, Moderate La Niña; WL, Weak La Niña; Neutral, ENSO-Neutral; WE, Weak El Niño; ME, Moderate El Niño; SE, Strong El Niño; VSE, Very Strong El Niño. Fractions indicate the number of years, of the total per phase and strength, that were wetter than average. Data from the PRISM Climate Group.

In addition to this discrepancy of wetter than expected Very Strong El Niños, there is a noticeable statewide divide in precipitation expected during each ENSO phase and strength (Figure 8). In much of western and northern Oregon, Strong and Moderate La Niñas typically were wetter than normal, whereas precipitation in southern and southeastern Oregon was normal or less than normal. Weak El Niño, Weak La Niña, and ENSO-Neutral events often were drier than normal throughout most the state, although precipitation in southeastern and north-central Oregon was above normal during Weak and Moderate El Niño events. Strong El Niño events tended to be the driest, with one in five such events since 1951 coinciding with above-average precipitation across most of the state. During the three Very Strong El Niño events, precipitation over most of the state was above average. Although precipitation was above average during Strong La Niña events across a majority of the state, it was below normal in much of north-central and southeast Oregon.

Based on observations alone, it remains challenging to determine if the unusually wet years linked to Very Strong El Niño events are merely coincidental—only three such events have been recorded. One approach to assess the consistent impact of ENSO on precipitation is to use high-quality numerical weather model simulations for the Pacific Northwest. By running each simulation with varied large-scale atmospheric circulation conditions, the model offers a more comprehensive depiction of precipitation association with ENSO phases than possible solely with observations (see Rupp et al. 2022 for more details). We used observed sea surface temperature to run 100 high-quality numerical weather model simulations of the western United States from 1 October through 31 March for each of the water years 1988–2017. Each run included a different set of large-scale atmospheric circulation conditions, which yielded a more robust indication of the dependence of precipitation on ENSO category than can be obtained with observations alone.

Similar to observations, these model simulations indicated that Strong La Niña events tend to be the wettest ENSO phase and Strong El Niño events the driest (Figure 9), with the magnitude of the precipitation anomaly dependent on the strength of the ENSO phase. Again similar to observations, precipitation during Very Strong El Niños deviated from this pattern, resulting in precipitation anomalies that were significantly wetter than normal and comparable to those during

Strong La Niñas. Additionally, these model simulations indicated that the apparent discrepancies in precipitation anomalies during years with Moderate El Niños and Moderate La Niñas seen in observations (Figures 7, 8) are likely due to small sample sizes or other factors.

These model simulations also demonstrated relatively diverse precipitation anomalies within each ENSO category (Figure 9). For instance, the most common outcome of Moderate La Niña simulations was above-normal precipitation. However, a few simulations yielded either less or much more precipitation than normal. The wide range of outcomes for all ENSO categories again reflects that ENSO is not the only influence on winter precipitation.



**Figure 8.** Number of water years per ENSO type (shading) in which annual precipitation was greater than the average across the 1991–2020 water years. The numbers in parentheses are the number of water years per ENSO phase and strength from 1951 through 2023 (Table 1). Data from the PRISM Climate Group.

## Mountain Snowpack

The condition of the winter mountain snowpack is a strong and reliable indicator of spring and summer water supply conditions in snowmelt-dominated basins in Oregon and throughout the western United States (e.g., Safeeq et al. 2013, Leibowitz et al. 2014). Given that temperature and precipitation vary considerably across the range of ENSO categories, we evaluated whether the magnitude of snowpack and the timing of its melt also vary among ENSO categories.

The U.S. Department of Agriculture's Natural Resources Conservation Service operates a network of snow telemetry (SNOTEL) stations across the western United States. There are currently 82 SNOTEL stations in Oregon (Figure 10), most of which are at elevations between 3000 and 6500 feet. These automated stations continuously measure the water content of the snowpack. The primary snowpack metric, snow water equivalent (SWE), corresponds to the depth of liquid water (in inches) of the melted snow. Accordingly, SWE effectively quantifies the amount of water within snowpack, eliminating the need to consider variation in snow density when evaluating other types of snowpack observations, such as snow depth.

We analyzed SWE for water years 1981–2023 with data from the Natural Resources Conservation Service. The product we used averages all SNOTEL SWE observations within each of 12 basins and across the state (Figure 10). Because basins do not follow political boundaries, the basin averages include some data from SNOTEL stations in Washington, Idaho, Nevada, and California. The statewide average SWE only includes stations within Oregon.



**Figure 9.** Relative frequency of simulated precipitation anomalies, averaged across Oregon, from 1 October through 31 March for water years 1988-2017. Water years are ordered from Very Strong El Niño (top) to Strong La Niña (bottom) using an ENSO index similar to the ONI called the Niño-3 index (NINO3). Light and dark gray shading indicates the 5th – 95th and 25th-75th percentile ranges, and vertical gray lines indicate the median precipitation anomaly for each water year. Further details in Rupp et al. (2022).

A primary metric for quantifying snowpack amount is the peak annual SWE, the maximum SWE recorded within a water year. In all drainage basins in Oregon, peak annual SWE historically occurred in early spring (early March to early April) (Figure 11), which is typical across most of the western United States. Because snowpack provides a natural reservoir for water storage during the winter, peak annual SWE is a strong indicator of summer water supply and streamflows in snowmelt-dominated basins in the Pacific Northwest.

The timing of snowmelt in spring and early summer is also an important consideration related to the seasonal snowpack. Early melting of the snowpack can lead to reduced water supply and

streamflows in late summer, when water is needed the most. Historically, the snowpack within the elevation range of the SNOTEL stations usually melted fully between mid-May and early July in Oregon.

The statewide average peak SWE during La Niña years, about 18 inches, was 50 percent greater than during El Niño years and 20 percent greater than the 1981–2023 mean (Figure 11). From 1981–2023, SWE in Oregon was



**Figure 10.** The NRCS basin subdivisions entirely or partially in Oregon in which SNOTEL stations (blue circles) collect data on snow water equivalent (SWE). Data from the Natural Resources Conservation Service.

above average in 11 of 17 La Niña years, 6 of 12 ENSO-Neutral years, and 3 of 12 El Niño years. Overall, La Niña years favor a larger statewide snowpack than ENSO-Neutral and El Niño years.

In each basin, the relation between peak annual SWE and ENSO phase was mostly consistent with the statewide averages (Figure 11). Departures from average peak SWE generally were largest in basins in north and northwestern Oregon and smallest in south and southeastern Oregon. The greatest difference between La Niña and El Niño years, nearly 200 percent, was in the Willamette basin, which includes much of the north and central Oregon Cascade Range. The smallest difference between La Niña and El Niño years was in the Lake County–Goose Lake basin in south-central Oregon. In all basins, and throughout the snow season, the average SWE during ENSO-Neutral years was close to the long-term average.

At the levels of the state and individual basins, neither the start of the snow season nor the date of peak annual SWE differed substantially between La Niña and El Niño years (Figure 11). However, in the Willamette and Hood–Sandy–Lower Deschutes basins, SWE in December and January accumulated more slowly during El Niño than La Niña or ENSO-Neutral years. In these basins, the slow accumulation early in the season can provide an early warning of impending snow drought later in the season. Snow droughts are recognized when snowpack or SWE is below average for a given point in the water year, and generally leads to low summer streamflows and limited water supply.

In all basins, irrespective of ENSO phase and strength, the peak annual SWE occurred around 1 April (Figure 11). In most basins, the timing of complete snowmelt differed considerably among ENSO phases: snowmelt was several weeks earlier during El Niño than La Niña or ENSO-Neutral years except in the Lake County–Goose Lake, Harney, and Owyhee basins in south-central and southeastern Oregon, where snowmelt during La Niña years was earlier than during El Niño years.

While La Niña years generally favor more mountain snow compared to El Niño years, the relationship between peak annual SWE and ENSO phase strength is less consistent (Figure 12). For
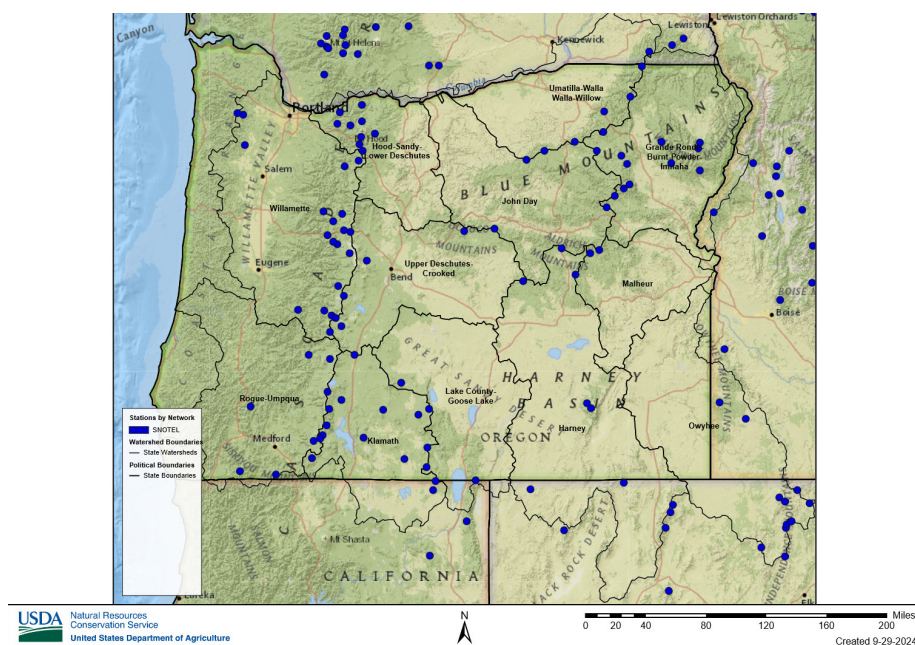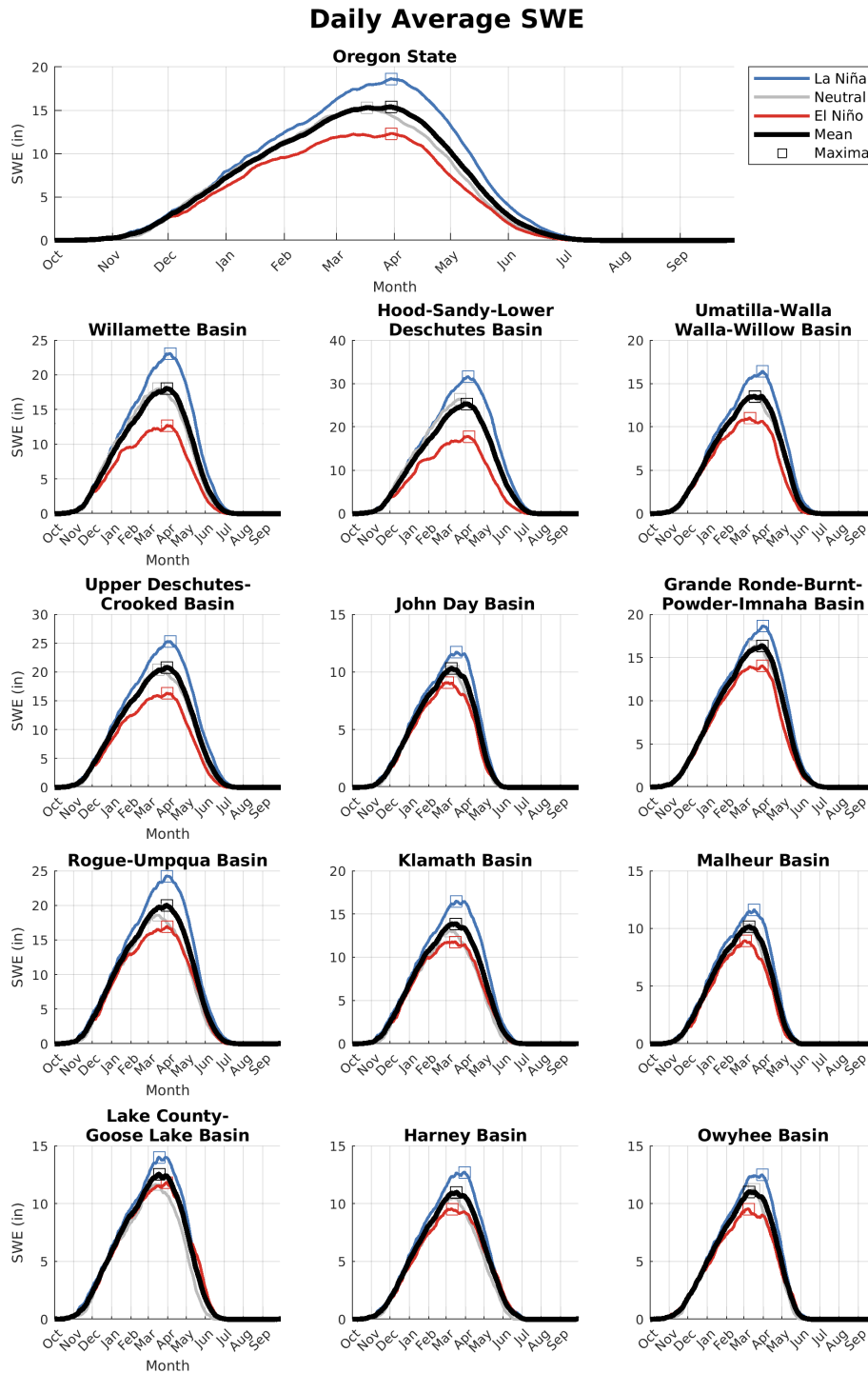
**Figure 11.** Statewide and basin-level time series of daily mean snow water equivalent (SWE) throughout water years from 1981 through 2023 that corresponded to La Niña (blue curves), ENSO-Neutral (gray curves), and El Niño (red curves) phases, and for all years (black curves). The average SWE curves for ENSO-Neutral years (gray) are close to those for all years (black) and therefore are difficult to distinguish.

example, statewide average SWE during Very Strong El Niño years was similar to that of Weak La Niña years and was similar to Strong La Niña years. In specific basins, such as Lake County–Goose Lake, Harney, John Day, and Owyhee, peak annual SWE during Very Strong El Niño years matched or exceeded the peak SWE observed during Strong La Niña years. Additionally, peak SWE during Moderate and Weak La Niña years generally was higher than during Moderate and Strong El Niño years.

Overall, the magnitude of peak mountain snowpack averaged statewide for a given year varies on the basis of ENSO phase and strength (Figure 13). Peak SWE was above average in 6 of 8 Weak La Niña years, 6 of 12 ENSO-Neutral years, and all 5 Strong La Niña years. Nevertheless, peak SWE was not above average in any of the four Moderate La Niña years. As El Niño strength increased from weak to strong, median and mean statewide maximum SWE generally decreased. However, maximum SWE during the three Very Strong El Niño years was considerably

greater than during the two Strong El Niño years. Maximum SWE during the Very Strong El Niño years was more similar to the above-average SWE during ENSO-Neutral, Weak La Niña, and Strong La Niña years than to SWE during weaker El Niño years. The progression of median and mean maximum SWE during the water year (Figure 13) is consistent with understanding that in Oregon, La Niña years are relatively cool and wet, and more conducive to lasting snowpack, than all but the strongest El Niño years. Very Strong El Niño years have produced some of the highest maximum SWEs on record (Jin et al. 2006).

This variability highlights the complexity of SWE dependence on the strength of ENSO phases, indicating that other factors, such as regional atmospheric patterns, storm tracks, and intra-seasonal variability, contribute significantly to annual SWE outcomes. For instance, variations in moisture transport during ENSO events, such as atmospheric rivers or shifts in the jet stream, may amplify or mitigate SWE anomalies, depending on local geography and elevation. Moreover, climate change could be adding further unpredictability to SWE responses across
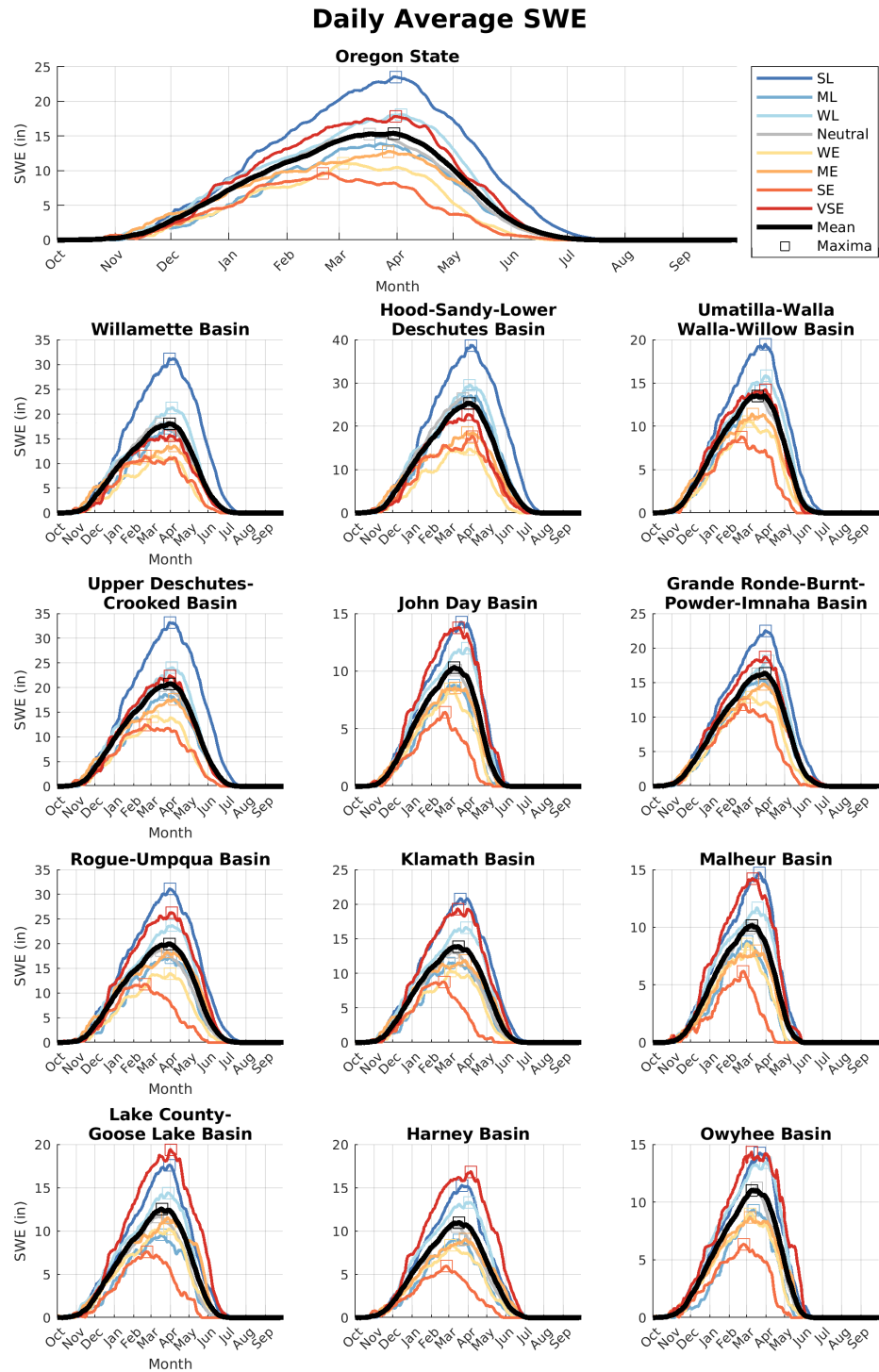


**Figure 12.** Statewide and basin-level time series of daily average snow water equivalent (SWE) throughout water years from 1981–2023. SL, Strong La Niña; ML, Moderate La Niña; WL, Weak La Niña; Neutral, ENSO-Neutral; WE, Weak El Niño; ME, Moderate El Niño; SE, Strong El Niño; VSE, Very Strong El Niño.

40
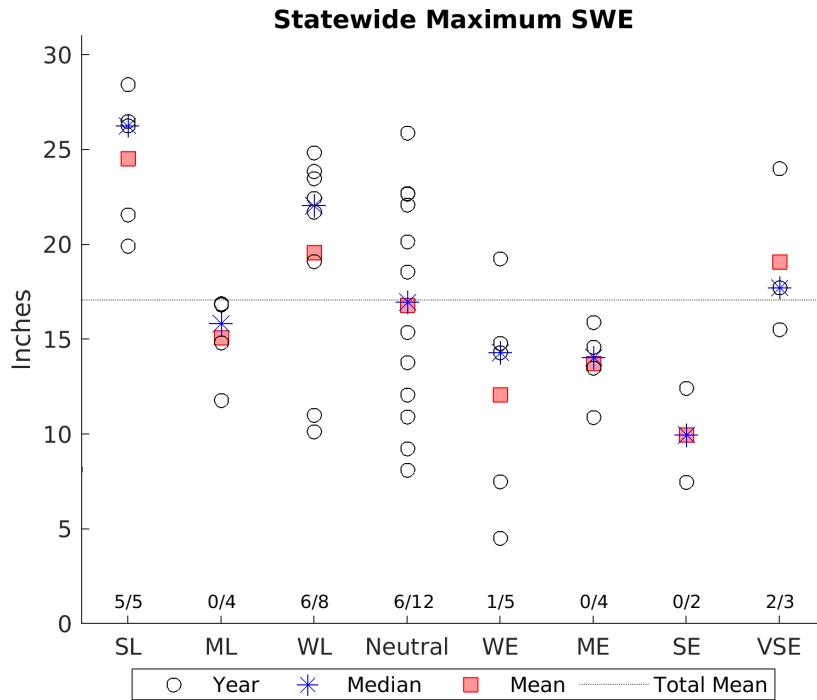
**Figure 13.** Statewide average peak annual snow water equivalent (SWE) for each water year from 1981 through 2023, categorized by ENSO phase and strength. SL, Strong La Niña; ML, Moderate La Niña; WL, Weak La Niña; Neutral, ENSO-Neutral; WE, Weak El Niño; ME, Moderate El Niño; SE, Strong El Niño; VSE, Very Strong El Niño. Fractions above the x-axis labels indicate the number of years, of the total per category, in which peak annual SWE was equal to or greater than average.

ENSO phases. Understanding these dynamics is critical for water resource management and forecasting in regions where winter snowpack is a primary water source.

**Streamflow**

Given the influence of ENSO on temperature, precipitation, and snowpack, it is reasonable to hypothesize that ENSO also affects streamflow: the movement of water in streams, rivers, and other channels. Streamflow is often measured as the volume of water flowing through the main channel of a stream or river at a given time. A network of gages measures streamflow on many of Oregon's streams and rivers. Here, we used streamflow data from the U.S. Geological Survey and Oregon Water Resources Department.

Daily streamflow values in many locations are highly variable due to rapid, precipitation-induced changes in water volumes and steep topography. Additionally, streamflow volumes typically increase in proportion with drainage basin area, making it difficult to combine streamflow measurements from numerous gages. Variability in streamflow in time and space complicates identification of consistent differences in streamflow among ENSO phases. Therefore, we analyzed a related quantity, surface runoff. Surface runoff is more directly related to the amount of precipitation and SWE upstream of stream gages than streamflow volume, and for this reason allows more insight into seasonal water supply within a basin. We also analyzed differences in the magnitude of daily peak flows among ENSO phases to assess whether potential flood conditions varied among those phases.

*Surface Runoff*

We defined surface runoff as the daily-averaged flow volume observed at the U.S. Geological Survey streamflow gages within a hydrologic unit code (HUC) 6 watershed (Figure 14), normalized by the surface area of the drainage basin upstream of the gage. The units of runoff used here are inches, and can be interpreted as the depth of water that would flow past the basin's stream gages if the water was distributed uniformly across the basin.

ENSO phase and strength affects surface runoff consistent with what is expected given the precipitation and SWE responses discussed above (Figure 15). Peak runoff during Very Strong El

Niño years was equal to or greater than that during La Niña years. The timing of peak runoff in a given basin depends on whether its primary runoff source is rain or snow; runoff peaks earlier in rain-dominated basins. In most basins, the timing of peak runoff did not vary much among ENSO phases or strengths, although the magnitude generally did. Exceptions were the Middle Columbia, Deschutes, and Klamath basins, where peak runoff during Very Strong El Niño years occurred unusually late in March.

In the northern Oregon basins, runoff decreased earlier during all El Niño years relative to La Niña years (Figure 15). Further south, runoff during Very Strong El Niño years was similar to that during La Niña years, and was higher and more sustained than during El Niño years of other strengths. Runoff during Very Strong El Niño years in the southernmost



**Figure 14.** The 12 hydrologic unit code (HUC) 6 drainage basins used in this streamflow analysis that are contained within or overlap Oregon.

basins (Klamath, Oregon Closed Basins, and Middle Snake–Boise) was higher than during years of any other ENSO phase and strength, even La Niña, during most of the year. Runoff rate decreases more slowly as peak runoff increases. Therefore, runoff in the southernmost basins during Very Strong El Niño years remained higher than during La Niña years throughout spring and summer.

We calculated cumulative basin runoff (Figure 16) by summing basin runoff (Figure 15) as the water year progressed. Cumulative runoff better reflects cumulative water-year precipitation throughout the upstream basin. The magnitude of cumulative runoff during years of all La Niña strengths and Very Strong El Niño years was greater than during weaker El Niño and ENSO-Neutral years. Cumulative runoff in the northern basins was greater in La Niña than in Very Strong El Niño years for the majority of the year or the entire year. However, in the southern basins, cumulative runoff during Very Strong El Niño years was greater than during La Niña years. The exception was the Deschutes Basin, where cumulative runoff during Very Strong El Niño and Strong La Niña years was roughly equal throughout the year. The greatest difference in cumulative runoff between Very Strong El Niño years and La Niña years was in the southernmost basins. Consistent with the high peak runoff during Very Strong El Niño years in the latter basins (Figure 15), cumulative runoff from February through June increased most rapidly during Very Strong El Niño years. Therefore, by the end of the water year, cumulative runoff was greatest during Very Strong El Niño years. The rate of cumulative runoff throughout the year varied among basins, but within basins, the streamflow runoff evolution throughout the year was similar among ENSO phases and strengths.

*High Flow Events*

In addition to affecting the volume of water that flows through each basin, variation in ENSO phase can affect the frequency of exceptionally high streamflows and potential flood events. We analyzed
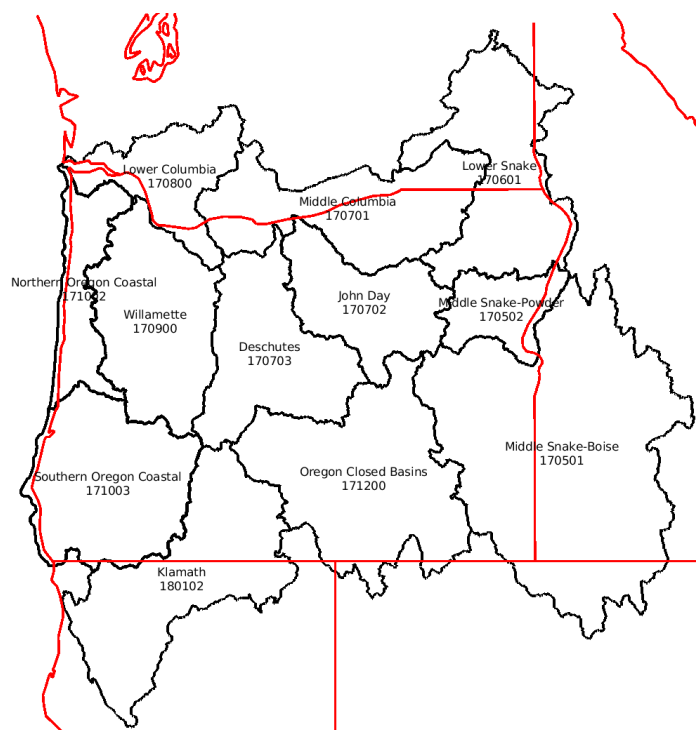
## Basin Runoff
### Flow per Month Normalized by Basin Area
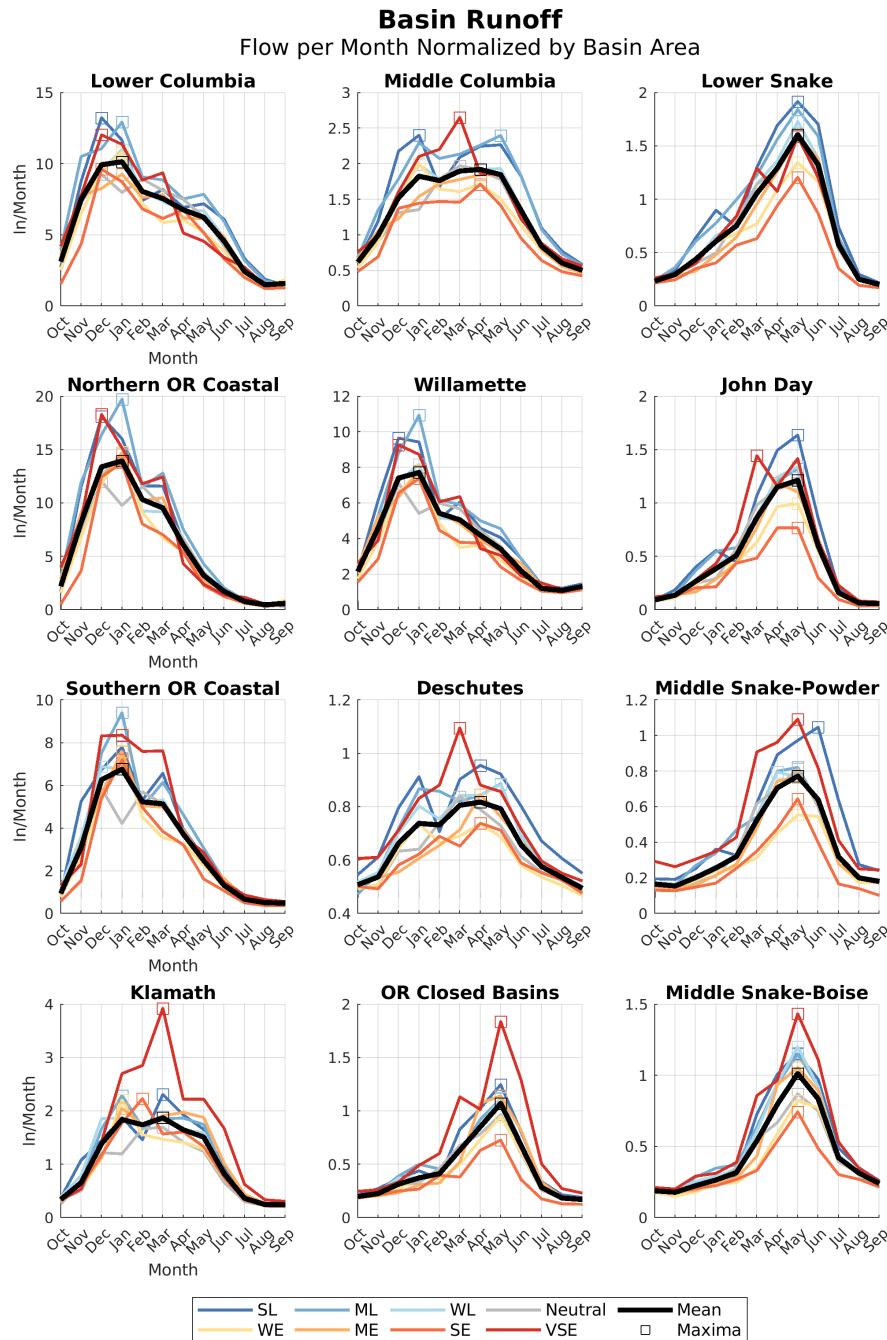


**Figure 15.** Time series of surface runoff in each hydrologic unit code (HUC) 6 drainage basin in Oregon (Figure 14). SL, Strong La Niña; ML, Moderate La Niña; WL, Weak La Niña; Neutral, ENSO-Neutral; WE, Weak El Niño; ME, Moderate El Niño; SE, Strong El Niño; VSE, Very Strong El Niño. Data from the U.S. Geological Survey.

the average number of high flow days per water year, where high flow days are defined as those on which daily streamflow values were equal to or greater than the 95th percentile for a given gage throughout each water year, as a function of ENSO phase. We used daily reference streamflow data from the second version of the U.S. Geological Survey's Geospatial Attributes of Gages for Evaluating Streamflow (GAGES-II; Falcone et al. 2010) network and the Oregon Water Resources Department. Reference gages are located in watersheds with minimal upstream flow regulation or disturbance relative to non-reference gages. We used data from 95 GAGES-II gages and 45 Oregon Water Resources Department gages for which complete data from water years 1951–2023 were available in Oregon, and averaged the number of high flow days for all these gages to create a statewide average.

On average, more high flow days occurred during La Niña years than during Weak, Moderate, and Strong El Niño and ENSO-Neutral years (Figure 17). The greatest number of high streamflow days occurred during January (3.2 days) and May (2.9 days) of Moderate La Niña years and December (3.1 days) of Strong La Niña years. The similarity in precipitation and SWE between Very Strong El Niño and Moderate and Strong La Niña years is reflected by the number of high flow days during Very Strong El Niño years: 2.9 days in December, 2.6 in March, and 2.1

in May. The average number of high flow days during March was greater during Very Strong El Niño years than years of any other ENSO phase and strength. From December through March and in May, the number of high flow days during Very Strong El Niño years was greater than during El Niño years of other strengths. Although the number of high flow days during La Niña years was consistently greater than during El Niño years, the risks associated with high streamflow tended to be high during the first half of water years that coincided with Very Strong El Niños.

## Reservoir Storage

Oregon's reservoirs operate to satisfy domestic and irrigation water demand, prevent floods, produce hydropower, provide recreation, and control flow volume and water temperature to support downstream ecosystems. To optimize these



**Figure 16.** Cumulative runoff in each hydrologic unit code (HUC) 6 drainage basin in Oregon (Figure 14), normalized by basin area. SL, Strong La Niña; ML, Moderate La Niña; WL, Weak La Niña; Neutral, ENSO-Neutral; WE, Weak El Niño; ME, Moderate El Niño; SE, Strong El Niño; VSE, Very Strong El Niño. Data from the U.S. Geological Survey.

objectives, reservoir operators must decide how to best use inflows from variable precipitation and snowpack. Given the effect of ENSO on precipitation, snowpack, and streamflow, we investigated how ENSO affected Oregon's historical water storage.

We selected 16 reservoirs on the basis of their large rated storage capacity and geographic distribution (Figure 18). Either the U.S. Army Corps of Engineers or the U.S. Bureau of
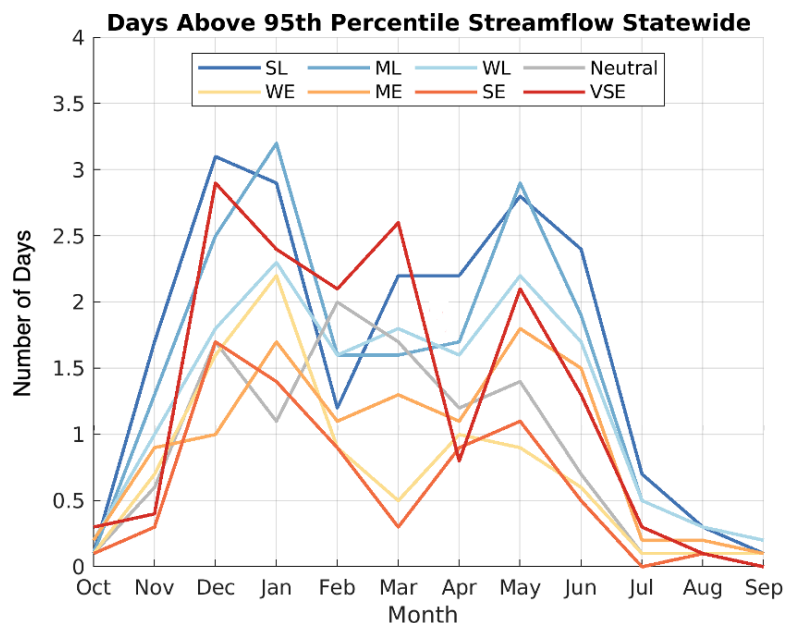
**Figure 17.** Average number of days per month on which daily streamflow at individual gages in Oregon that met or exceeded the 95th percentile of daily flow volume. SL, Strong La Niña; ML, Moderate La Niña; WL, Weak La Niña; Neutral, ENSO-Neutral; WE, Weak El Niño; ME, Moderate El Niño; SE, Strong El Niño; VSE, Very Strong El Niño. Streamflow data from the U.S. Geological Survey GAGES-II dataset and the Oregon Water Resources Department.

Reclamation operates each reservoir. We obtained data on daily storage on the first of each month for water years 1981–2023 from the Natural Resources Conservation Service. Here, we present results associated with La Niña, ENSO-Neutral, El Niño (excluding Very Strong), and Very Strong El Niño years; further classification by ENSO intensity yielded little additional insight.

Generally, Oregon experiences cold, wet winters and early springs and warm, dry summers. Consequently, water storage at all reservoirs peaks at the end of the wet season, roughly between April and June. At some reservoirs, minimum storage occurs at the end of the dry season in October. At others, the minimum typically occurs during mid-winter. In the latter cases, the lag in timing of minimum storage reflects either the need for adequate capacity for flood control throughout the wet season or the natural timing of inflow from spring snowmelt.

ENSO phase had no clear bearing on average reservoir storage or the timing of refill and drawdown in the Willamette Basin in northwestern Oregon (Figure 18). A minor exception was Lookout Point reservoir, where average storage during El Niño years (excluding Very Strong) was about 15 percent less than during all other years. At most other reservoirs outside of northwestern Oregon, the relation between storage and ENSO phase was consistent with that expected by the effects of ENSO phases and strengths on precipitation, snowpack, and streamflow: reservoir storage was greatest during La Niña and Very Strong El Niño years (Figure 18). Additionally, reservoir storage during Very Strong El Niño years was greater than during La Niña years in the eight reservoirs in southern and eastern Oregon.

## Predictability of Oregon's Seasons via ENSO

### Introduction

Because the western United States receives most of its annual precipitation during winter, seasonal temperature and precipitation outlooks—released each autumn for the upcoming winter by NOAA's Climate Prediction Center—often generate tremendous interest among parties including farmers, water resource managers, the ski industry, and the public at large. These forecasts are based in part on simulations performed with weather forecast models from the North American Multi-Model Ensemble (NMME), all of which couple a conventional atmospheric model (such as those used for weather prediction) with a dynamic ocean model. In principle, the
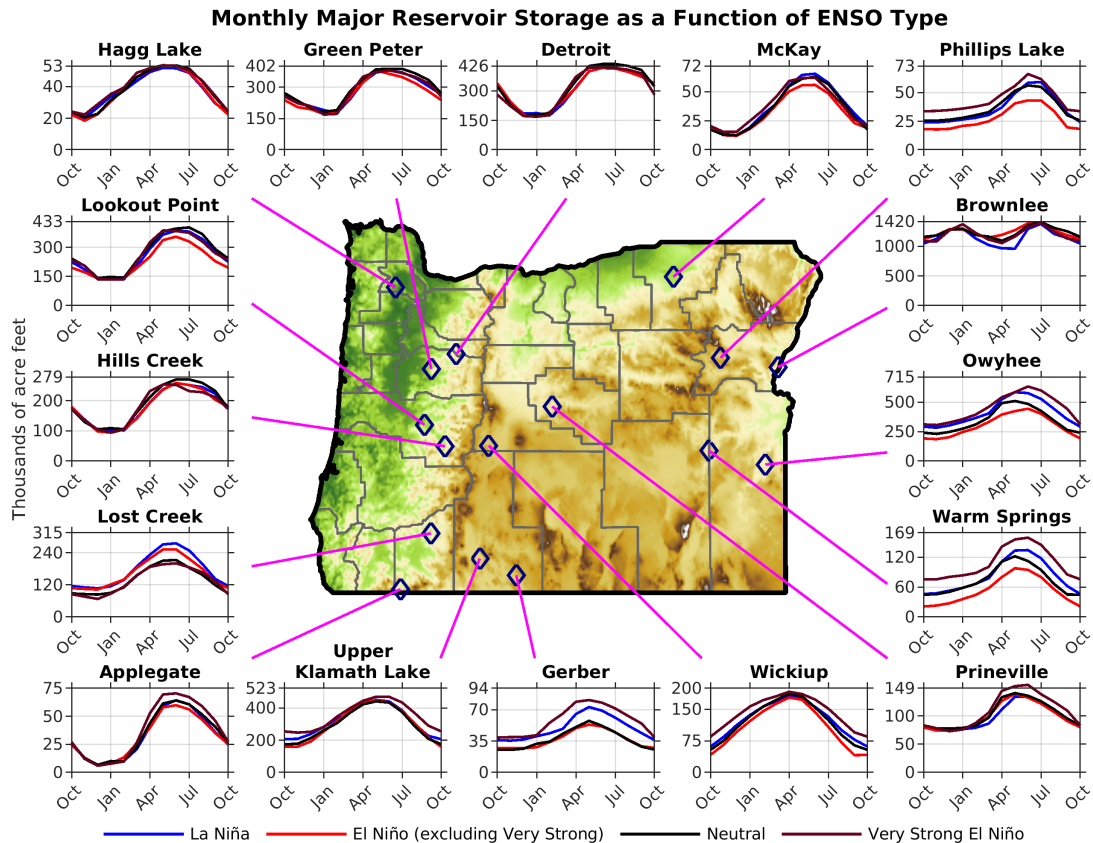
**Figure 18.** Evolution of water storage during the water year in 16 selected major reservoirs throughout Oregon as a function of ENSO phase. Values represent average storage on the first of each month. The maximum number on each y-axis represents the reservoir's capacity. Data from the U.S. Department of Agriculture Natural Resources Conservation Service.

coupling of the models should allow the simulations to accurately represent coupled ocean-atmosphere phenomena such as ENSO, which is the primary predictor of seasonal climate in the western United States. Indeed, most of these models skillfully predict winter temperatures across much of the region (Figure 19). However, the models' predictions of precipitation are much less skillful (Figure 19). This is especially true in the Pacific Northwest, where none of the eight models used in the Climate Prediction Center outlooks, when initiated with starting conditions observed in November (initialized in November), suggested a significant correlation with observed precipitation from December through March.

There are at least two possible reasons why the seasonal forecast models do not accurately predict winter precipitation in the Pacific Northwest. First, the models may not accurately predict the evolution of sea surface temperature anomalies in the region associated with ENSO (along the equator in the Pacific Ocean), which have a strong influence on winter weather in Pacific Northwest. Second, even if the models accurately predict sea surface temperatures associated with ENSO, they may not accurately represent the remote atmospheric response to these temperatures. We evaluate each of these hypotheses below.

### Data and Methods

We obtained outputs of seasonal forecast models from the North American Multi-Model Ensemble (NMME), which is maintained by the Columbia Climate School Research Institute. These models

# NMME Model Accuracy
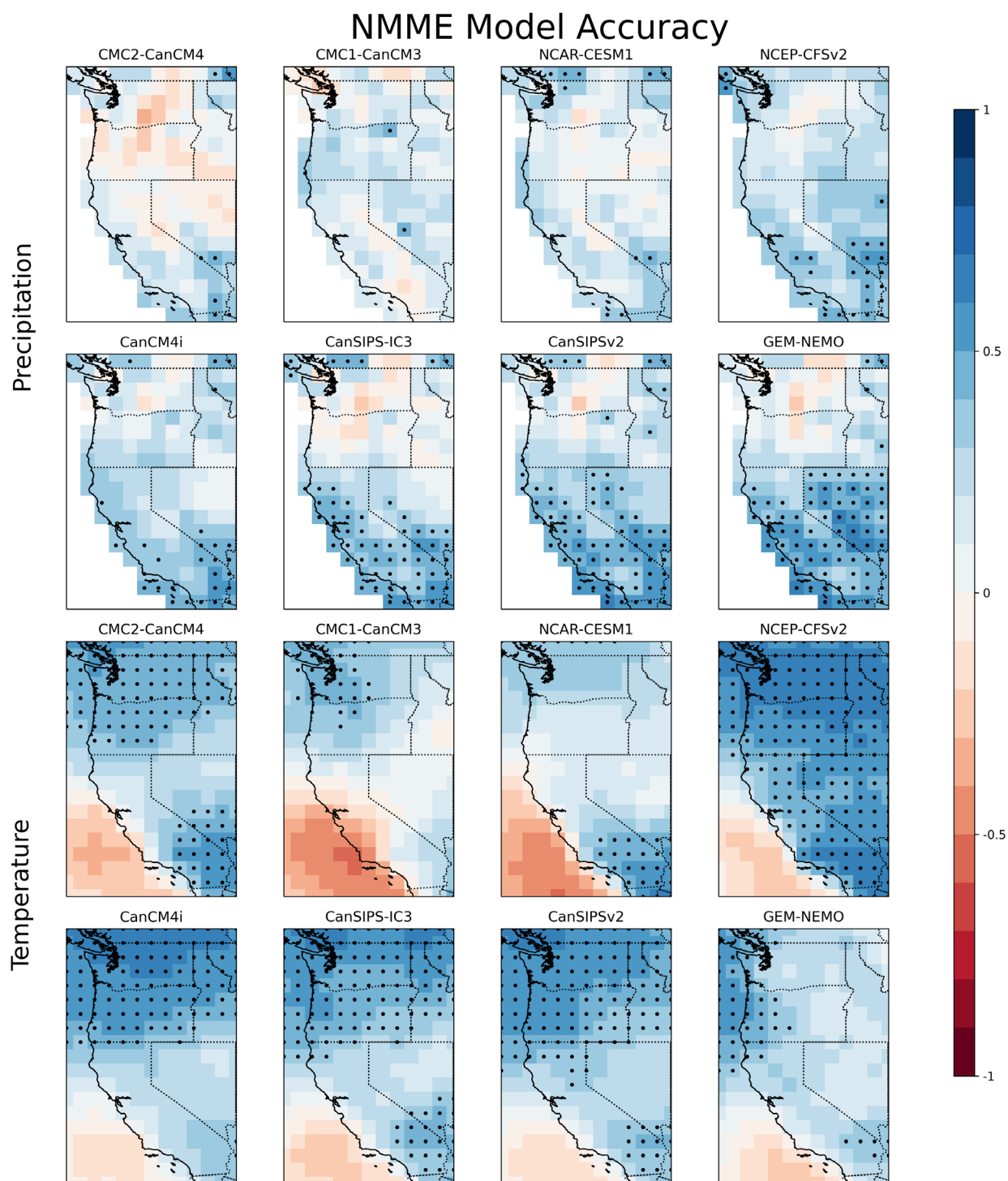


**Figure 19.** Correlation coefficients (shading) between observed winter (December–March) precipitation (top two rows) or average temperature (bottom two rows) during 30 consecutive water years beginning in 1982–1983 and the ensemble-mean winter precipitation or temperature predicted by the North American Multi-Model Ensemble (NMME) seasonal forecast models initialized with conditions observed in November. Stippling indicates a statistically significant positive correlation at the 95 percent confidence level.

yield predictions of both the atmosphere and ocean, including sea surface temperature. We focused on hindcast simulations initialized each November from 1982 through 2011 and run through the following winter (December–March). This configuration allows investigation of the accuracy of winter forecasts for each year that are issued in late autumn. We analyzed output from eight models, all of which have 1-degree grid spacing: CanCM4i, CanSIPS-IC3, CanSIPSv2, CMC1-CanCM3, CMC2-CanCM4, NCAR-CESM1, NCEP-CFSv2, and GEM-NEMO. Ensembles of 10–20 simulations were run with each model for every winter from 1982–1983 through 2011–2012, and for some models through 2019–2020. For each model and ensemble member, we analyzed interannual variability in predicted winter sea surface temperature, air temperature, and precipitation, and compared the predicted values to observations over the same time period.

The NMME predictions of sea surface temperature are compared with observations obtained from the NOAA Extended Reconstructed Sea Surface Temperature version 5 (Huang et al. 2017), which has a grid spacing of 2 degrees. Our source of temperature observations was the ERA5 reanalysis, which has a grid spacing of 0.25 degree. We obtained precipitation observations from NOAA's Gridded Precipitation Reconstruction over Land, which has a grid spacing of 1 degree. To enable direct comparison between the model output and observations, we applied bilinear interpolation to regrid the finer-resolution data to the coarser-resolution grid for each climate variable.

**Results**

We first evaluated the ability of the forecast models to predict the sea surface temperature anomalies associated with ENSO. Predictions of all models and ensemble members were strongly correlated with observed sea surface temperatures in the Niño 3.4 region (Figure 20), with correlation coefficients from 0.85 (CMC2-CanCM4) to 0.91 (NCEP-CFSv2 and GEM-NEMO). Therefore, errors in predictions of sea surface temperature likely are not the primary cause of the models' inability to predict winter precipitation.

Given that the greatest impacts of ENSO on climate in Oregon coincided with Strong La Niña, Strong El Niño, and Very Strong El Niño years, we compared the responses of temperature and precipitation to these events in observations an in the seasonal forecast models. Observations indicated that winter temperatures during Strong La Niña years generally have been cooler than average in the Pacific Northwest, whereas temperatures during Strong and Very Strong El Niño winters have been warmer than average (Figure 21). The models accurately reflected these observations in the Pacific Northwest, although they were less consistent with observations over much of California, especially during Strong El Niño years (Figure 21).

Observed precipitation had a nonlinear response to ENSO variability. Precipitation in the Pacific Northwest was below average during Strong El Niño years, but much greater than average during Very Strong El Niño years (Figure 21). However, models did not predict a nonlinear response of precipitation to ENSO variability. Instead, the models predicted a similar direction, albeit different magnitude, of precipitation anomalies during both Strong and Very Strong El Niño years (Figure 21, second column).

To assess whether random weather variability might account for the differences between models and observations (Figure 21), we plotted the mean temperature and precipitation anomalies averaged over Oregon during Strong La Niña, Strong El Niño, and Very Strong El Niño years. We compared the observed anomalies to the predictions from each seasonal forecast model. To isolate the role of random weather variability, we also compared observations to a 100-member ensemble

of atmosphere-only simulations with sea surface temperatures that matched historical observations. Because all members of these ensembles were run with the same model configuration and sea surface temperatures, the variation in temperature and precipitation anomalies across the ensemble can only reflect random weather variability unrelated to ENSO.

Observations and models generally indicated that the



**Figure 20.** Correlation between modeled mean monthly sea surface temperature (SST) and observed monthly values during winter (December through March) within the Niño 3.4 region for eight models (x-axis) from the North American Multi-Model Ensemble.

temperature anomaly is negative or near zero during Strong La Niña years, weakly positive during Strong El Niño years, and more strongly positive during Very Strong El Niño years (Figure 22). The mean modeled temperature anomaly for each ENSO category fell within the range of uncertainty of the observations, reinforcing the above inference that the models realistically represent the observed temperature response to ENSO variability in Oregon.

Observations suggested that the response of precipitation to Strong and Very Strong El Niño events is highly uncertain (Figure 23), reflecting both the small number of historical events within each category and the variance in precipitation observed among those events. As a result, the precipitation anomalies simulated by the models were well within the observational range of uncertainty, and it is possible that the models accurately represent the true response of precipitation to these events. However, modeled and observed mean precipitation were noticeably different, with models generally predicting more precipitation than observed during Strong El Niño years and less precipitation than observed during Very Strong El Niño years. Therefore, although random weather variability may obscure the true precipitation response to sea surface temperature variability in the observational record, we cannot rule out the influence of model bias. Whether random weather variability or model bias plays a larger role will likely become clearer as more data accrue from future Strong and Very Strong El Niño years.

**Synopsis**

The North American Multi-Model Ensemble seasonal forecast models, which are widely used to inform seasonal forecasts of temperature and precipitation issued by the NOAA Climate Prediction
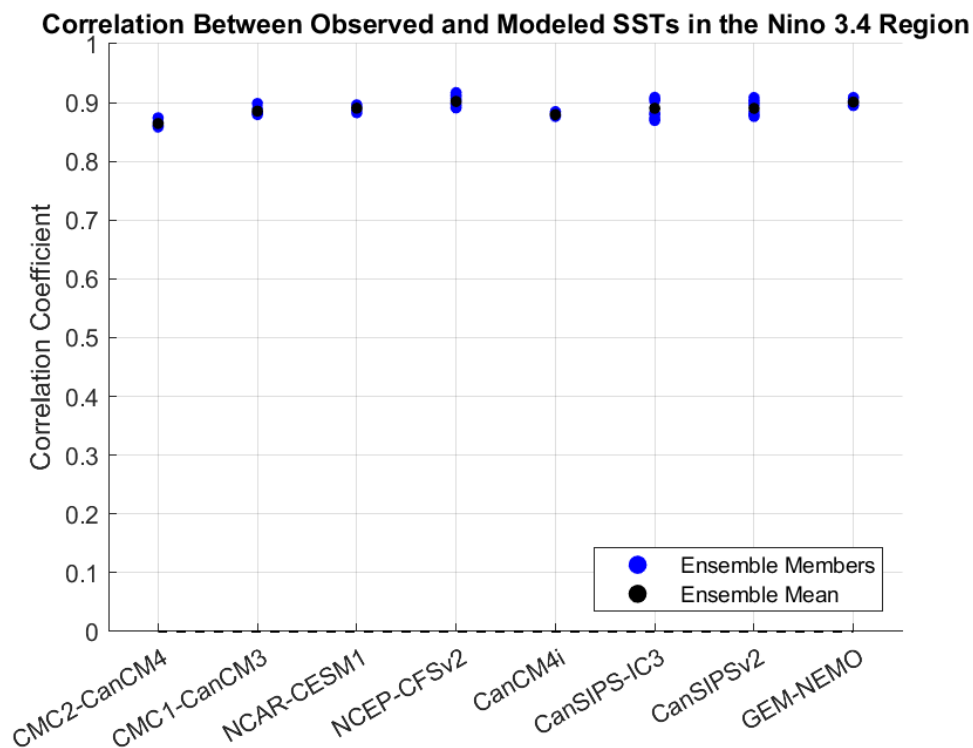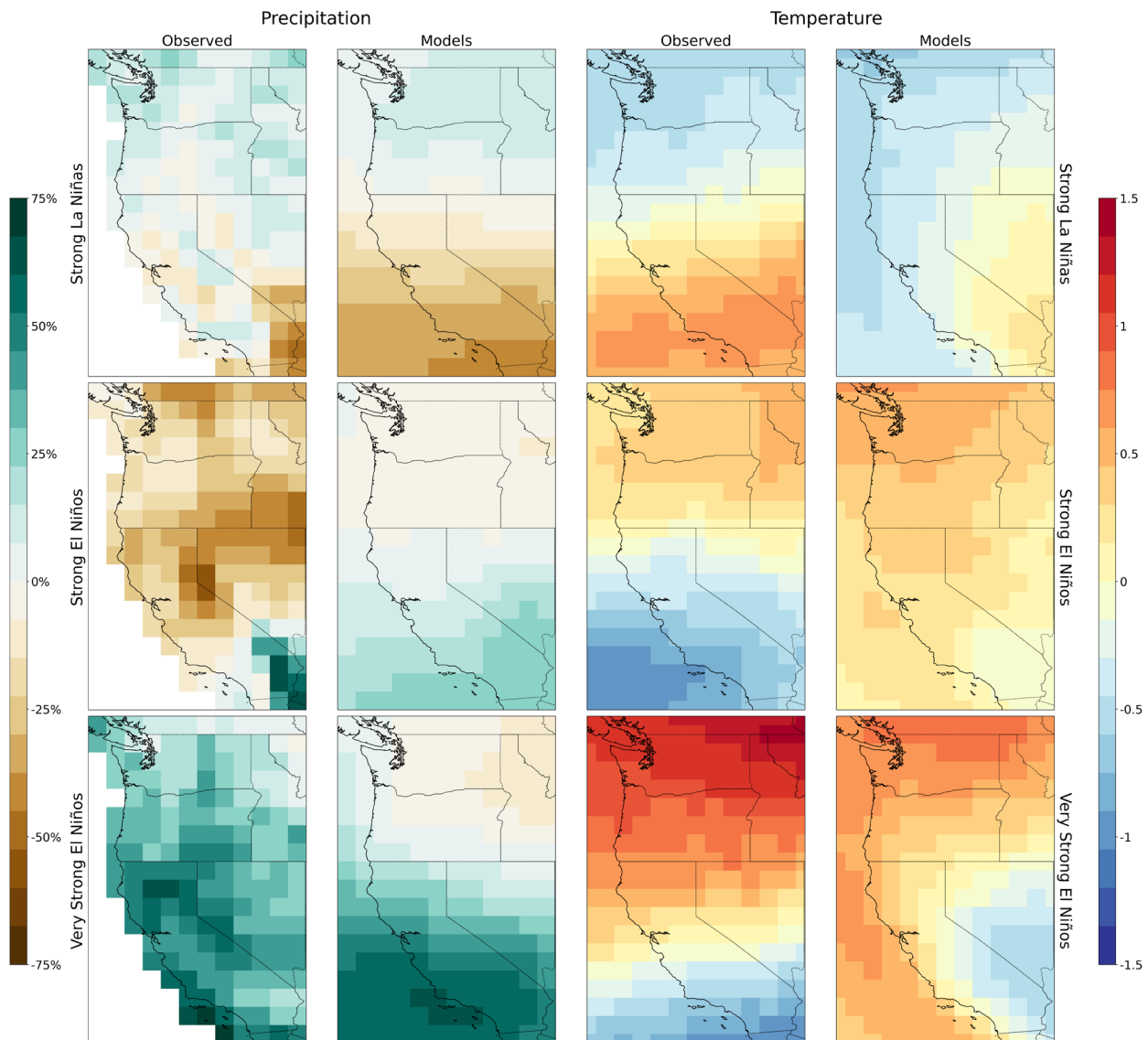
**Figure 21.** Winter (December–March) mean anomalies in observed precipitation (column 1), modeled precipitation (column 2), observed temperature (column 3), and modeled temperature (column 4) during all Strong La Niña years (row 1), Strong El Niño years (row 2), and Very Strong El Niño years (row 3). The anomalies were computed during all winters in each ENSO category from 1982 through 2016, averaged over all models and ensemble members. Precipitation anomalies are calculated as percentage departure from the 1982–2011 mean and temperature anomalies as departures from the 1982–2011 mean (°C).

Center, skillfully predicted winter temperature but not winter precipitation in the Pacific Northwest. These errors in the models' precipitation forecasts do not seem to be driven by inaccurate predictions of sea surface temperatures associated with ENSO variability. Rather, they likely reflect some combination of random weather variability, which is inherently unpredictable at seasonal extents, and model biases in the response of precipitation to Strong and Very Strong El Niño events. Because the number of Strong and Very Strong El Niño events in the observational record is small, it is not possible to quantify the relative contributions of random weather variability and model biases. Even if model bias plays no role, however, the models' predictions of winter precipitation across the Pacific Northwest appear to be unreliable.
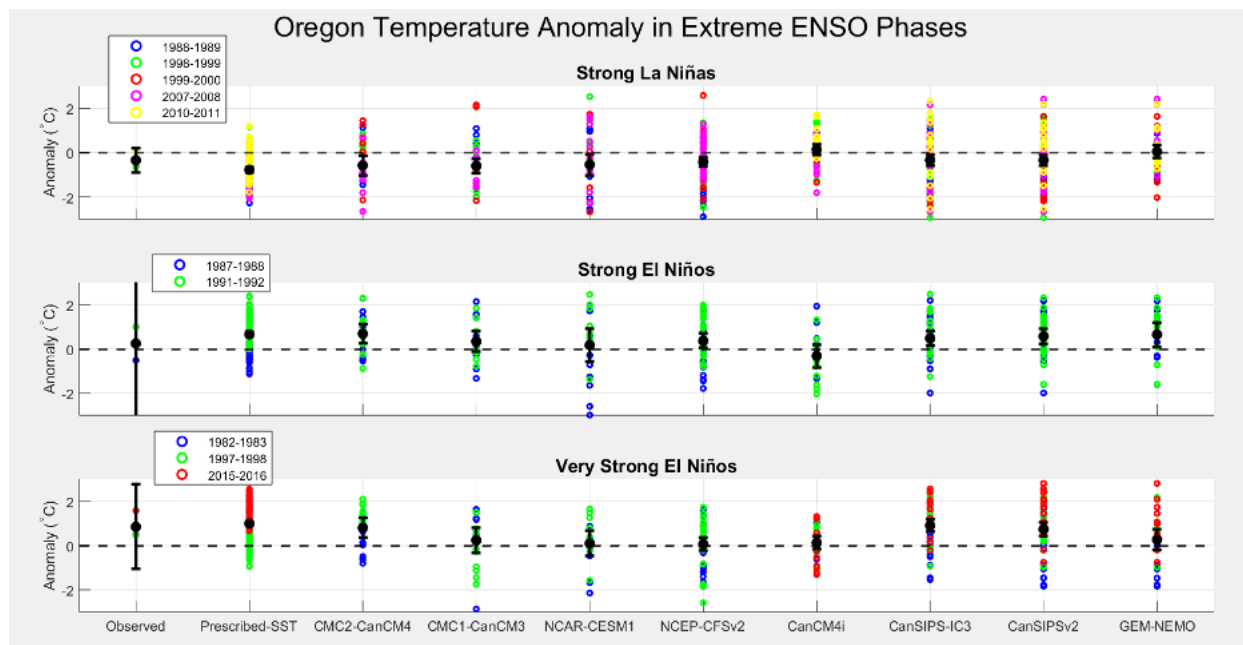
**Figure 22.** Oregon statewide winter (December–March) mean monthly temperature anomalies averaged over all Strong La Niña, Strong El Niño, and Very Strong El Niño events from 1982–2011 in observations and model simulations initialized in November. Prescribed-SST values reflect an ensemble of atmosphere-only simulations with sea surface temperatures that matched historical observations. Individual ensemble members are represented by colored dots and means by black dots. Anomalies are calculated as departures from the 1982–2011 mean. Error bars represent the 95 percent confidence interval of the mean across years and ensemble members.
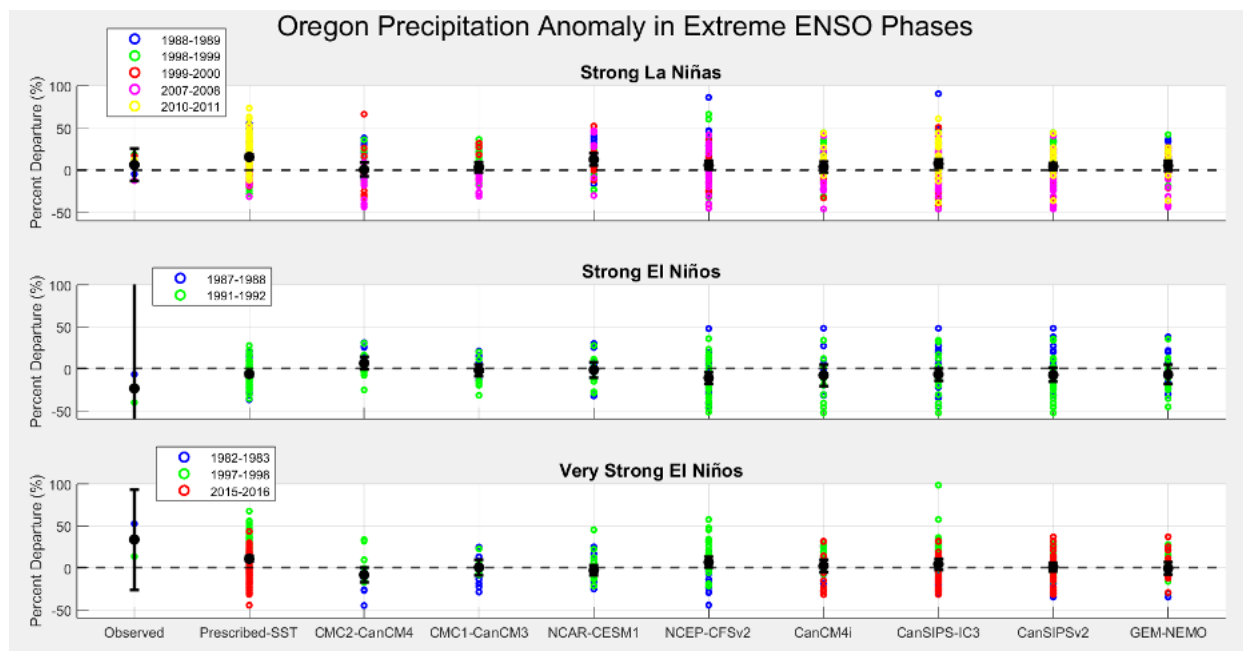


**Figure 23.** Oregon statewide winter (December–March) mean monthly precipitation anomalies averaged over all Strong La Niña, Strong El Niño, and Very Strong El Niño events from 1982–2011 in observations and model simulations initialized in November. Prescribed-SST values reflect an ensemble of atmosphere-only simulations with sea surface temperatures that matched historical observations. Individual ensemble members are represented by colored dots and means by black dots. Anomalies are calculated as departures from the 1982–2011 mean. Error bars represent the 95 percent confidence interval of the mean across years and ensemble members.

51

## Summary

On average, conditions in Oregon are relatively cool and wet during La Niña years and warm and dry during El Niño years (Table 3). Nevertheless, the precipitation and hydrological effects of El Niño are not simply the reverse of those during La Niña. For example, during the three Very Strong El Niño events since 1950, snow water equivalent, streamflow, and reservoir storage across Oregon, especially in southern and eastern Oregon, were above average. Hydrological conditions during Very Strong El Niño years were as wet as those observed during an average Strong La Niña year.

| ENSO phase and strength | Number of water years above average | | |
|---|---|---|---|
| | Temperature | Precipitation | Peak annual snow water equivalent |
| Very Strong El Niño | 2 of 3 | 3 of 3 | 2 of 3 |
| Strong El Niño | 4 of 5 | 1 of 5 | 0 of 2 |
| Moderate El Niño | 2 of 7 | 3 of 7 | 0 of 4 |
| Weak El Niño | 9 of 12 | 6 of 12 | 1 of 5 |
| ENSO-Neutral | 10 of 18 | 7 of 18 | 6 of 12 |
| Weak La Niña | 6 of 15 | 7 of 15 | 6 of 8 |
| Moderate La Niña | 3 of 6 | 3 of 6 | 0 of 4 |
| Strong La Niña | 2 of 7 | 5 of 7 | 5 of 5 |

**Table 3.** Number of water years within each ENSO phase and strength in which average statewide precipitation, temperature, and peak annual snow water equivalent was above average. Precipitation and temperature include water years 1951 through 2023. Snow water equivalent includes water years 1981 through 2023.

Statewide precipitation, snow water equivalent, streamflow, and reservoir storage in the Pacific Northwest generally decrease from Strong La Niña to ENSO-Neutral to Strong El Niño conditions, but increase significantly during Very Strong El Niño events. Although this hydroclimatic pattern has been noted in previous studies (e.g., Hoerling et al. 1997, Khan et al. 2006, Fleming et al. 2007, Fleming and Dahlke 2014), it remains under-recognized by both the research community and the public.

The mechanisms driving this asymmetric response are not yet fully understood. However, our analysis suggests that it is not appropriate to assume that hydroclimatic impacts during Very Strong El Niño events will mirror those of weaker El Niño years. Additionally, although seasonal temperature forecasts associated with ENSO events are reasonably accurate for the Pacific Northwest, precipitation forecasts tend to be less reliable.

## Literature Cited

Cai, W., et al. 2021. Changing El Niño–Southern Oscillation in a warming climate. Nature Reviews Earth and Environment 2:628–644.

Daly, C., M. Halbleib, J.I. Smith, W.P. Gibson, M.K. Doggett, G H. Taylor, J. Curtis, and P.A. Pasteris. 2008. Physiographically-sensitive mapping of temperature and precipitation across the conterminous United States. International Journal of Climatology 2815:2031–2064.

Daly, C., R.P. Neilson, and D.L. Phillips. 1994. A statistical-topographic model for mapping climatological precipitation over mountainous terrain. Journal of Applied Meteorology 33:140–158.

Falcone, J.A., D.S. Vogt, and C.D. Moser. 2010. GAGES-II: Geospatial Attributes of Gages for Evaluating Streamflow. U.S. Geological Survey. https://doi.org/10.3133/sir20105174.

Fleming, S.W., and H.E. Dahlke. 2014. Parabolic northern-hemisphere river flow teleconnection to El Niño-Southern Oscillation and the Arctic Oscillation. Environmental Research Letters

9:104007. https://doi.org/10.1088/1748-9326/9/10/104007.

Fleming, S.W., P.H. Whitfield, R.D. Moore, and E.J. Quilty. 2007. Regime-dependent streamflow sensitivities to Pacific climate modes across the Georgia-Puget transboundary ecoregion. Hydrological Processes 21:3264–3287.

Hanley, D.E., M.A. Bourassa, J.J. O'Brien, S.R. Smith, and ER. Spade. 2003. A quantitative evaluation of ENSO indices. Journal of Climate 16:1249–1258.

Hoerling, M.P., A. Kumar, and M. Zhong. 1997. El Niño, La Niña, and the nonlinearity of their teleconnections. Journal of Climate 10:1769–1786.

Huang, B., P.W. Thorne, V.F. Banzon, T. Boyer, G. Chepurin, J.H. Lawrimore, M.J. Menne, T.M. Smith, R.S. Vose, and H-M. Zhang. 2017. Extended reconstructed sea surface temperature, version 5 (ERSSTv5): upgrades, validations, and intercomparisons. Journal of Climate 30:8179–8205.

Jin, J., N.L. Miller, S. Sorooshian, and X. Gao. 2006. Relationship between atmospheric circulation and snowpack in the western USA. Hydrological Processes 20:753–767.

Karnauskas, K.B. 2013. Can we distinguish canonical El Niño from Modoki? Geophysical Research Letters 40:5246–5251.

Khan, S., A.R. Ganguly, S. Bandyopadhyay, S. Saigal, D.J. Erickson, V. Protopopescu, and G. Ostrouchov. 2006. Nonlinear statistics reveals stronger ties between ENSO and the tropical hydrological cycle. Geophysical Research Letters 33:L24402. https://doi.org/10.1029/2006GL027941.

Leibowitz, S.G., R.L. Comeleo, P.J. Wigington, Jr., C.P. Weaver, P.E. Morefield, E.A. Sproles, and J.L. Ebersole. 2014. Hydrologic landscape classification evaluates streamflow vulnerability to climate change in Oregon, USA. Hydrology and Earth System Sciences 18:3367–3392.

NOAA (National Oceanic and Atmospheric Administration). 2024a. Niño regions. www.cpc.ncep.noaa.gov/products/analysis_monitoring/ensostuff/nino_regions.shtml. Accessed 15 April 2024.

NOAA (National Oceanic and Atmospheric Administration). 2024b. Cold and warm episodes by season. origin.cpc.ncep.noaa.gov/products/analysis_monitoring/ensostuff/ONI_v5.php. Accessed 15 April 2024.

Omernik, J.M. 1987. Ecoregions of the conterminous United States. Map (scale 1:7,500,000). Annals of the Association of American Geographers 77:118–125.

Rupp, D.E., L.R. Hawkins, S. Li, M. Koszuta, and N. Siler. 2022. Spatial patterns of extreme precipitation and their changes under ~2°C global warming: a large-ensemble study of the western USA. Climate Dynamics 59:2363–2379.

Safeeq, M., G.E. Grant, S.L. Lewis, and C.L. Tague. 2013. Coupling snowpack and groundwater dynamics to interpret historical streamflow trends in the western United States. Hydrological Processes 27:655–668.

Trenberth, K.E. 1997. The definition of El Niño. Bulletin of the American Meteorological Society 78:2771–2778.

Trenberth, K.E., and D.P. Stepaniak. 2001. Indices of El Niño evolution. Journal of Climate 14:1697–1701.

van Oldenborgh, G.J., H. Hendon, T. Stockdale, M. L'Heureux, E.C. de Perez, R. Singh, and M. van Aalst. 2021. Defining El Niño indices in a warming climate. Environmental Research Letters 16:044003. https://doi.org/10.1088/1748-9326/abe9ed.

# Projected Changes in Oregon Precipitation

David W. Pierce and Daniel A. Cayan

## Introduction

Precipitation worldwide is being altered by anthropogenic climate change. The fact that greenhouse gases, particularly carbon dioxide released by the combustion of fossil fuels, reduce the ability of longwave radiation to cool Earth's surface by emission to space has been understood for well over a century (Arrhenius 1896).

We projected future changes in precipitation across the northwestern United States, with a focus on Oregon, as a result of human-caused climate change. The fundamental data underpinning these projections are results from global climate models that were included in the sixth phase of the Climate Model Intercomparison Project (CMIP6; Eyring et al. 2016). The CMIP6 global climate models are produced and run by scientists from 49 institutions worldwide and represent the best estimations available of how future emissions of greenhouses gases and aerosols and changes in land use will affect global to continental climate.

The CMIP6 global climate models are run under a variety of scenarios of future greenhouse gas emissions, aerosol emissions, land use changes, and population, technological, and economic growth; these scenarios are termed shared socioeconomic pathways (SSPs) (O'Neill et al. 2014, 2016; Riahi et al. 2017). We considered three SSPs: 2–4.5, 3–7.0, and 5–8.5. SSP 2–4.5 assumes moderate reductions in emissions, continuation of historical social and economic trends, and moderate challenges to mitigation and adaptation. SSP 3–7.0 assumes a doubling of carbon dioxide emissions by 2100, conflicts among regions, and substantial challenges to mitigation and adaptation. SSP 5–8.5 assumes that carbon dioxide emissions double by 2050 with substantial challenges to mitigation, but minor challenges to adaptation. We projected precipitation during four periods: historical (1950–2014), early twenty-first century (2015–2044), mid-twenty-first century (2045–2074), and late twenty-first century (2075–2100).

The spacing of grid cells in the CMIP6 global climate models is relatively coarse, typically in the range of 70 to 200 km (43 to 124 mi.). Therefore, the models are unable to resolve many topographic features that affect local climate. In Oregon, these features include the Coast Range, Willamette Valley, and Cascade Range. For this reason, we did not use the global climate model data directly, but rather used global climate model data that were statistically downscaled to a 1/16th degree latitude-longitude grid (nominally 6 km [3.7 mi.]) by the LOCA2 method (Pierce et al. 2014, 2015, 2023). The LOCA2 data cover the period 1950–2100, and the CMIP6 historical period ends in 2014. Hence, we set the historical period for our analyses as 1950–2014.

The LOCA2 statistical downscaling method uses historically observed relations between weather and climate at coarse (50–1000 km [31–621 mi.]) and fine (6 km) resolution to regionalize the global climate model results (in this case, to the Pacific Northwest). Downscaling adds the effects of local topography to the original global climate model results, which is necessary to accurately represent climate in regions with complex terrain. LOCA2 precipitation was trained on the station-based observational data of Pierce et al. (2021). Below, we refer to those training data as observations.

The impacts of climate change on ecosystems, society, and the economy are felt primarily at the extremes. Our analysis therefore emphasized projected changes in extreme precipitation. Additionally, water supply in the Pacific Northwest strongly depends on whether winter precipitation

falls as rain or snow. Accordingly, our secondary emphasis was the temperature at which winter precipitation is projected to fall in the future.

**Model Selection**

Although the full LOCA2 archive includes 27 global climate models, not all are equally skilled at reproducing observed weather and climate over the western United States. To select models for these analyses, we followed the guidance of Krantz et al. (2021), who evaluated approximately 30 CMIP6 global climate models with respect to their ability to realistically capture major weather processes that affect the west coast of the United States and surface mean annual and seasonal climate and variability over the greater California region, including western Nevada and southern Oregon. Although this region does not include northern Oregon, many of the weather processes that determine the climate of Oregon are the same as those that affect northern California. Furthermore, our previous evaluations of global climate models to understand regional climate change taught us that the main objective of selecting global climate models is to eliminate the models that have consistently poor performance across a wide variety of metrics and regions.

The best-performing models have different sets of trade-offs with respect to various performance metrics. The process-based metrics included measures of Northern Hemisphere blocking (high pressure systems that block the west-to-east movement of mid-latitude weather systems), offshore wind shear, the El Niño-Southern Oscillation, and vertically integrated column water vapor, sea level pressure, and zonal wind on days with extreme precipitation. The surface climate and variability metrics included seasonal means of temperature and precipitation, the standard deviation of temperature and precipitation averaged over one-, five-, and ten-year intervals, the amplitude and phase of the annual harmonic of temperature and precipitation (used to evaluate the seasonal cycle), and the standard deviation of monthly values of temperature and precipitation in January and July, used to evaluate subseasonal variability. More details on the metrics and methods for evaluating the metrics are in Krantz et al. (2021).

We included 11 global climate models in our analyses (Table 1). Although we largely based our selection of models on the results of the evaluation in Krantz et al. (2021), we did not include EC-Earth3, a model that performed

| Model | Institution | Number of ensemble members for each SSP |
|---|---|---|
| ACCESS-CM2 | Commonwealth Scientific and Industrial Research Organisation (CSIRO), Australia | 3, 3, 3 |
| CEMS2-LENS | National Center for Atmospheric Research, Boulder, Colorado, USA | 0, 10, 0 |
| CNRM-ESM2-1 | Centre National de Recherches Meteorologiques, France | 1, 1, 1 |
| EC-Earth3-Veg | European consortium of national meteorological services and research institutes, European Union | 5, 4, 4 |
| FGOALS-g3 | Chinese Academy of Sciences, Beijing, China | 3, 4, 3 |
| GFDL-ESM4 | Geophysical Fluid Dynamics Laboratory, Princeton, New Jersey, USA | 1, 1, 1 |
| IPSL-CM6A-LR | Institut Pierre-Simon Laplace, France | 5, 10, 4 |
| MIROC6 | Division of Climate System Research, Atmosphere and Ocean Research Institute, The University of Tokyo, Japan | 3, 3, 5 |
| MPI-ESM1-2-HR | Max Planck Institute for Meteorology, Hamburg, Germany | 2, 10, 2 |
| MRI-ESM2-0 | Meteorological Research Institute, Tsukuba, Ibaraki, Japan | 1, 5, 1 |
| TaiESM1 | Research Center for Environmental Changes, Academia Sinica, Nankang, Taipei, Taiwan | 1, 1, 0 |

**Table 1.** Global climate models used in these analyses, their originating institutions, and the number of ensemble members available for shared socioeconomic pathways (SSPs) 2–4.5, 3–7.0, and 5–8.5, respectively.

well but is similar to EC-Earth3-Veg in its representation of closely related physical processes. The models also are in general agreement with, although not identical to, ranks of global climate models in an evaluation aimed at hydroclimate applications in the Pacific Northwest (Lybarger et al. 2024). Eight of our 11 models were in the upper half of Lybarger et al.'s (2024) performance rankings.

Many of the models have multiple ensemble members. The number of ensemble members mainly is determined by available computer resources rather than by model quality. Ensemble members can be used to examine the effects of natural internal climate variability. However, because natural climate variability was not our focus, we primarily evaluated the multi-model ensemble average (MMEA) of the models and ensemble members. The MMEA represents climate processes better than any single global climate model (e.g., Pierce et al. 2009). To calculate the MMEA, we first averaged across the ensemble members of each model, then averaged across all models. This method avoids over-representing models that have many ensemble members.

## Regional Averaging

Some of our results are presented as averages across the U.S. level III ecoregions (Omernik 1987) in Oregon (Figure 1). Ecoregions are areas in which abiotic and biotic environmental attributes, such as climate, hydrology, vegetation, and land use, generally are similar. They are intended to provide a basis for research and management that is ecologically meaningful, particularly in contrast to political boundaries.

## Mean Precipitation Changes

Projected changes in mean precipitation provide context for analyses of extreme precipitation and relative proportions of rain



**Figure 1.** Level III U.S. ecoregions within Oregon overlaid on the 6 km LOCA2 grid.

and snow. Precipitation in Oregon is characterized by wet winters and dry summers, with notable regional variability. Over the historical period (1950–2014), the Coast Range and Cascade Range received much more precipitation than eastern, especially southeastern, Oregon (Figure 2). Annual precipitation in the Willamette Valley was intermediate between that in the wet coastal areas and Cascade Range and the dry interior.

Given SSP 3–7.0, the MMEA projected an annual increase in precipitation of 0–10 percent by 2045–2074 (Figure 3). However, the magnitude of change varies among seasons. Summer precipitation is projected to decrease by 15–20 percent along much of Oregon's coast and the Columbia River Gorge. A decrease in summer precipitation is consistent among model projections of precipitation changes during other periods in the twenty-first century and across SSPs. The summer drying signal strengthens over time and with stronger anthropogenic climate forcing (higher SSPs).

**Figure 2.** Annual and seasonal multi-model ensemble average precipitation over the historical period (1950–2014). DJF, December, January, and February (winter); MAM, March, April, and May (spring); JJA, June, July, and August (summer); SON, September, October, and November (autumn).



**Figure 3.** Annual and seasonal multi-model ensemble average projected change in precipitation between the historical period (1950–2014) and the mid-twenty-first century (2045–2074) given shared socioeconomic pathway 3–7.0. DJF, December, January, and February (winter); MAM, March, April, and May (spring); JJA, June, July, and August (summer); SON, September, October, and November (autumn).

57

Historically, over 65 percent of winter days in the coastal Pacific Northwest and Cascade Range were wet (≥0.5 mm/day) (Figure 4). Over much of Oregon, especially east of the Cascade Range and in the Columbia Plateau, less than 15 percent of summer days were wet. Projections suggest a 0–6 percent decrease in the proportion of wet days in summer, and negligible changes during other seasons. Projected decreases in summer precipitation (Figure 3) and the proportion of wet days during summer (Figure 4) roughly coincide, although the greatest reductions in the former and latter are in the Olympic Peninsula and central and eastern Washington, respectively. These changes, and the fact that the projected reduction in precipitation is stronger than that of proportion of wet days, suggest that reductions in mean summer precipitation are not solely a result of fewer wet days.
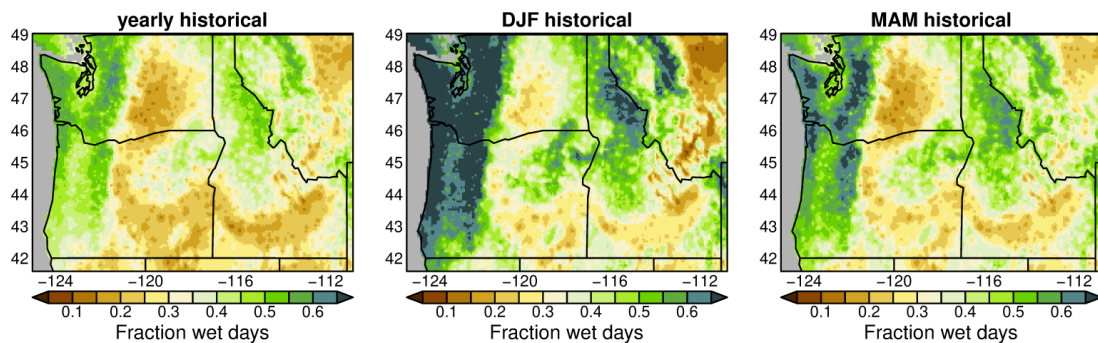


**Figure 4a.** Annual and seasonal multi-model ensemble average proportion of wet days (precipitation ≥0.5 mm/day) over the historical period (1950–2014).
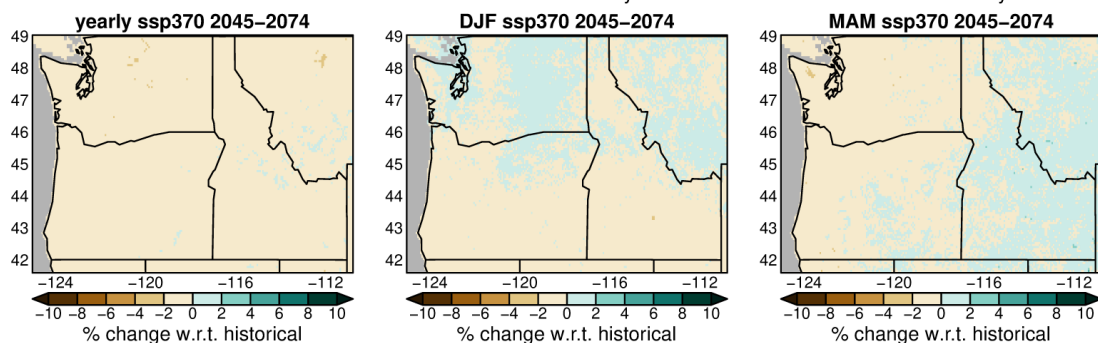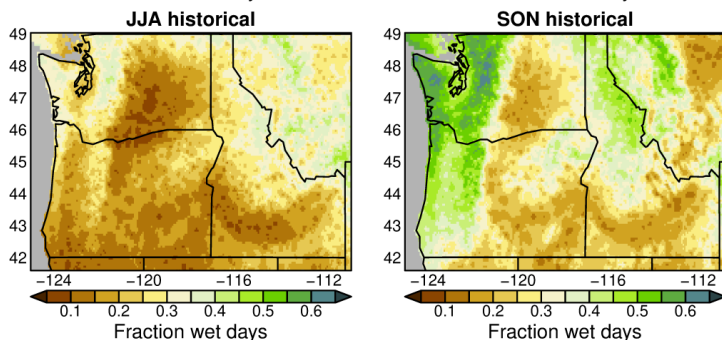
**Figure 4b.** Annual and seasonal multi-model ensemble average change in the proportion of wet days between 1950–2014 and 2045–2074 given shared socioeconomic pathway (SSP) 3–7.0. DJF, December, January, February; MAM, March, April, May; JJA, June, July, August; SON, September, October, November.
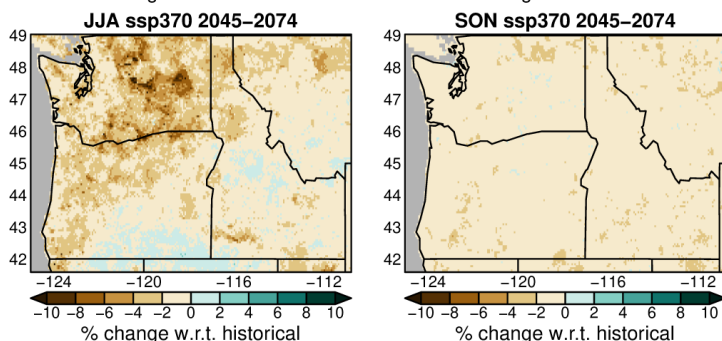
Although seasons traditionally are employed in meteorological analyses, seasonal averages do not capture all aspects of the projected monthly changes in precipitation. Therefore, we also examined MMEA-projected changes in monthly mean regional precipitation (Figure 5). By the mid-twenty-first century, assuming SSP 3–7.0, precipitation in the Willamette Valley, Columbia Plateau, Blue Mountains, and Coast Range is projected to decrease in September but increase in November. Projected decreases in precipitation extend from April through September in western and northwestern Oregon, and into November in the Klamath Mountains and Cascades.
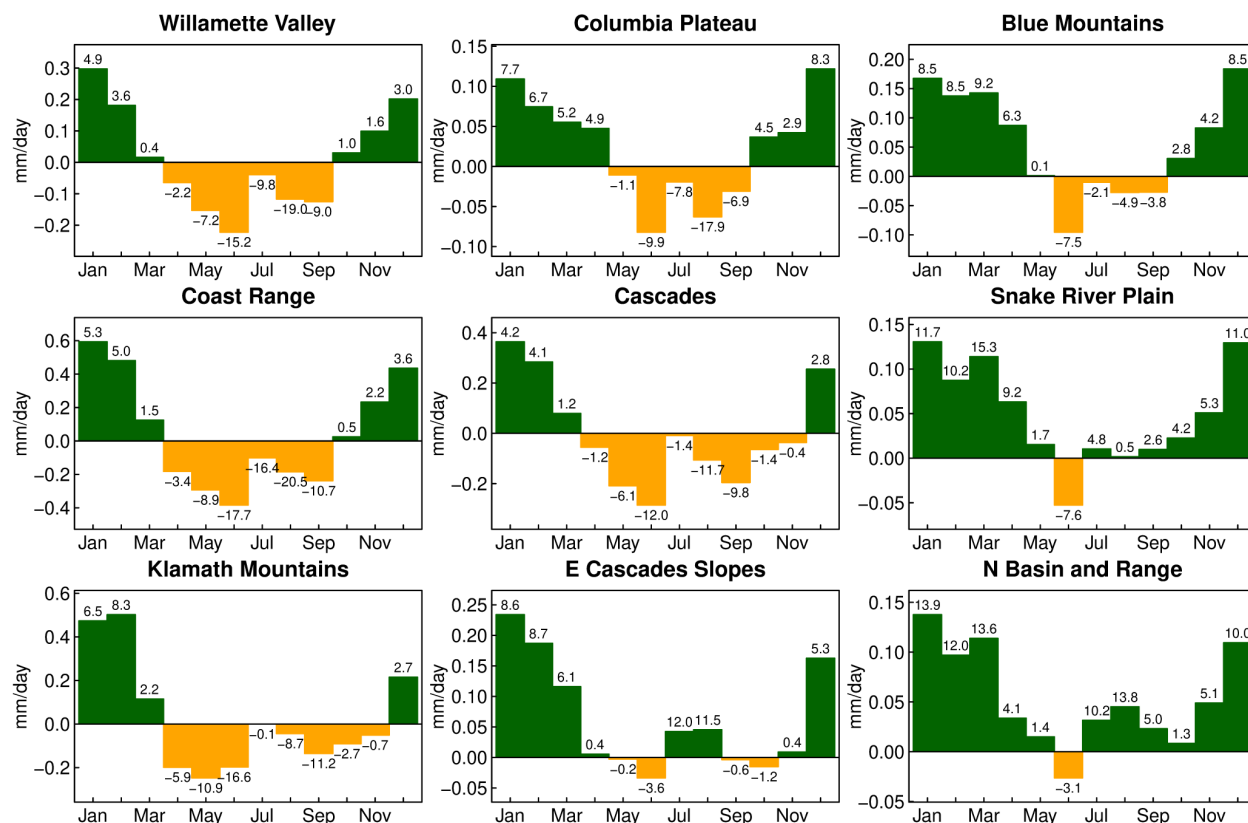


**Figure 5.** Multi-model ensemble average projected changes in monthly mean precipitation between the historical period (1950–2014) and the mid-twenty-first century (2045–2074), given shared socioeconomic pathway 3–7.0, in Oregon's level III ecoregions (Figure 1). Numbers on the bars are changes in percent.

## Projected Changes in Extreme Precipitation

During the historical period (1950–2014), the highest values of wet day (≥0.5 mm/day) precipitation at the 95th, 99th, and 99.9th percentiles occurred in meteorological autumn (September, October, and November) and winter (December, January, and February), and the lowest values occurred in spring (March, April, and May) and summer (June, July, and August) (Figure 6). Geographically, the highest values were in the Olympic Peninsula and in southern coastal Oregon.

Nearly all MMEA-projected annual changes in extreme wet day precipitation (99th percentile), regardless of time period and SSP, are increases. The changes range from a few percent to more than 20 percent wetter on those extremely wet days (Figure 7). By the mid-twenty-first century (2045–2074) and beyond, all projected annual changes in extreme precipitation are increases. This is consistent with the general thermodynamic expectations of
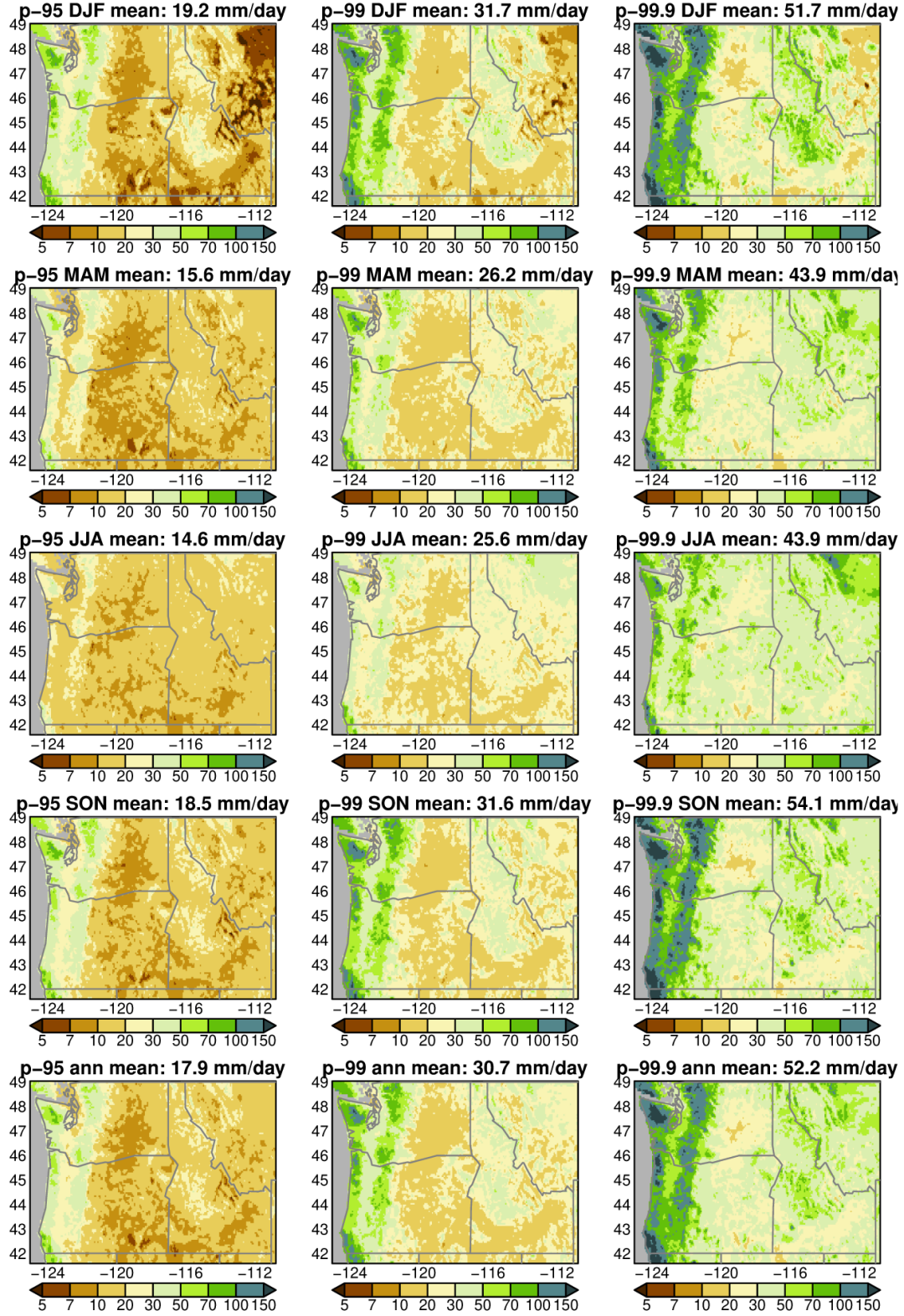
**Figure 6.** Historical (1950-2014) observed 95th (left column), 99th (middle column), and 99.9th (right column) percentiles of wet day (≥0.5 mm) seasonal and annual (ann) precipitation. Values in panel titles are means over the geographic domain. DJF, December, January, and February (winter); MAM, March, April, and May (spring); JJA, June, July, and August (summer); SON, September, October, and November (autumn).

anthropogenic climate change. Warmer air temperatures lead to an increase in the saturation vapor pressure of water vapor in the atmosphere, yielding an increase in the amount of water available to precipitate onto Earth (e.g., Westra et al. 2014, Kroner et al. 2017, Norris et al. 2019, Harp and Horton 2022). By the middle of the century under SSP 3–7.0, the annual average increase in precipitation over the Pacific Northwest is about 7.3 percent. For all three SSPs, the projected increase in extreme precipitation becomes larger throughout the twenty-first century (Figure 7).
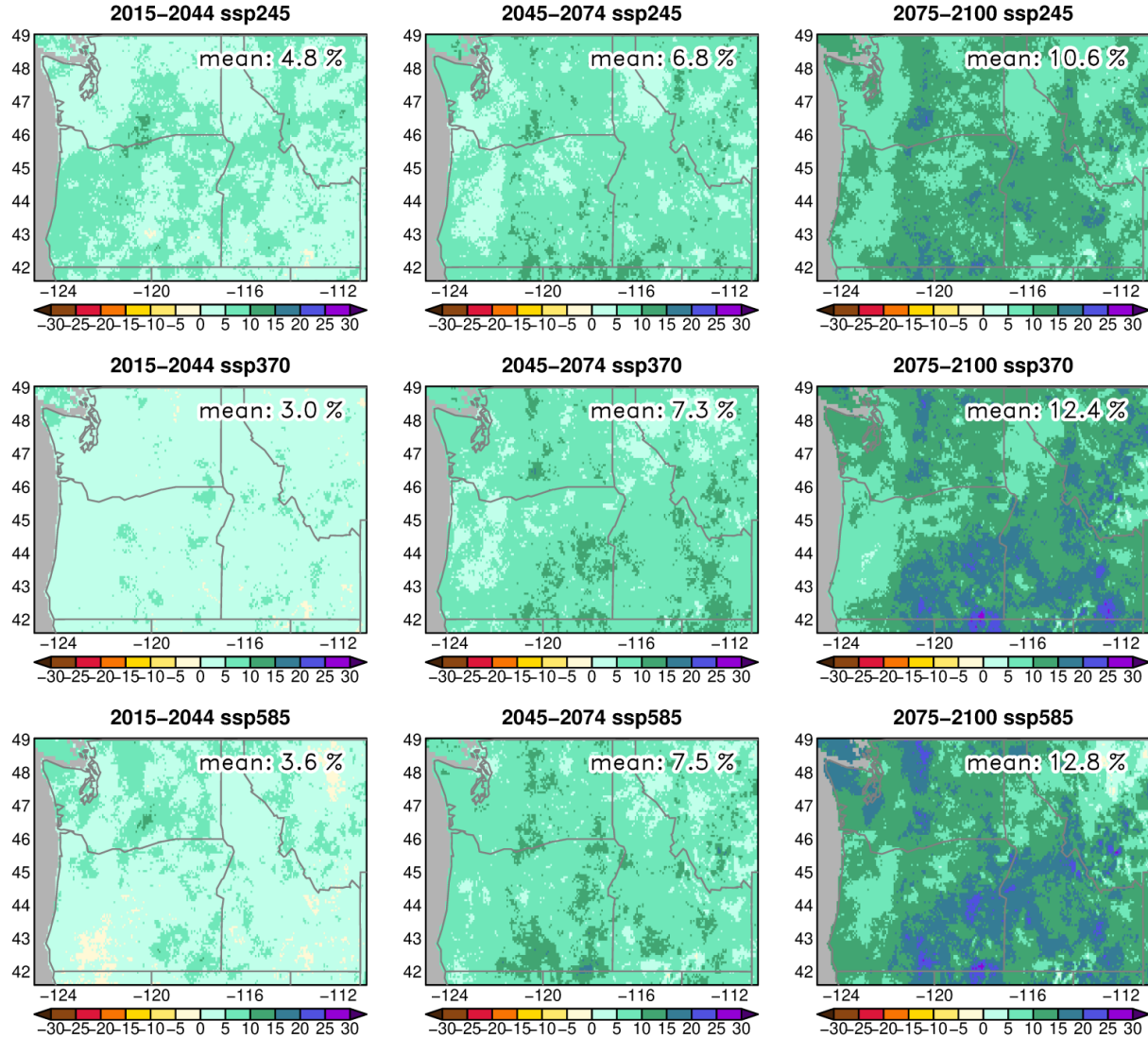


**Figure 7.** Multi-model ensemble average percentage change in precipitation at the 99th percentile of wet days between the historical period (1950–2014) and three periods during the twenty-first century (columns) given three shared socioeconomic pathways (SSPs) (rows). Means over the geographic domain are in the upper right of each panel.

The MMEA represents climate processes more effectively than any individual model, but model variability can be better understood by examining the range of projected changes across the models. Individual models suggest decreases in annual, extreme (99th percentile) wet-day precipitation early in the century, although the MMEA and interquartile range are positive (Figure 8), and the MMEA projections increase as the century progresses. Nevertheless, some models indicate increases in
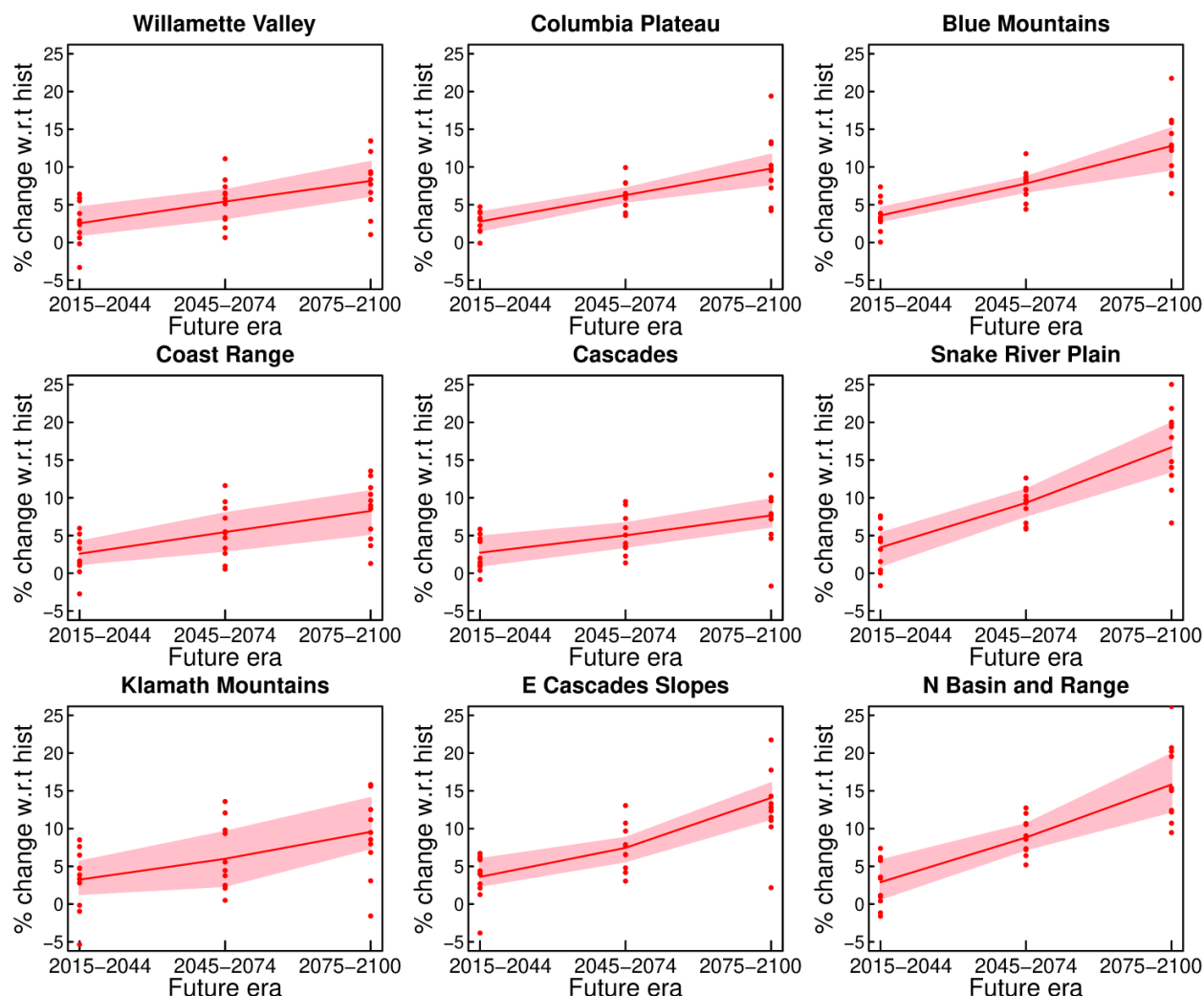
**Figure 8.** Projected change in precipitation (percentage) at the 99th percentile of wet days between the historical period (1950–2014) and three periods during the twenty-first century, given shared socioeconomic pathway 3–7.0, in Oregon's level III ecoregions (Figure 1). Lines represent the multi-model ensemble average. The red envelope indicates the interquartile range across the 11 models. Dots represent results from each model.

precipitation that are substantially higher than indicated by the MMEA. The future precipitation extremes projected for any given location, such as Salem, Eugene, or Bend, reflect two factors. The first, driven by anthropogenic climate change, is a systematic tendency toward increases in precipitation extremes for known physical reasons, primarily an increase in atmospheric water vapor as temperatures warm. The second factor is annual, natural variation in weather and climate: for example, some winters are wetter than others, heavy storms may pass north or south of a particular city, and so forth.

Similar to projected changes in mean precipitation (Figure 3), projected changes in the 99th percentile of wet day precipitation by mid-century under SSP 3–7.0 have a distinct seasonal cycle, with the lowest values in summer (Figure 9). Across the geographic domain, average increases are 9 percent in winter (December, January, and February) and 8.8 percent in autumn (September, October, and November). In Oregon, the largest and second-largest increases also are projected to occur in winter and autumn, respectively. Projected changes in summer across the Pacific Northwest
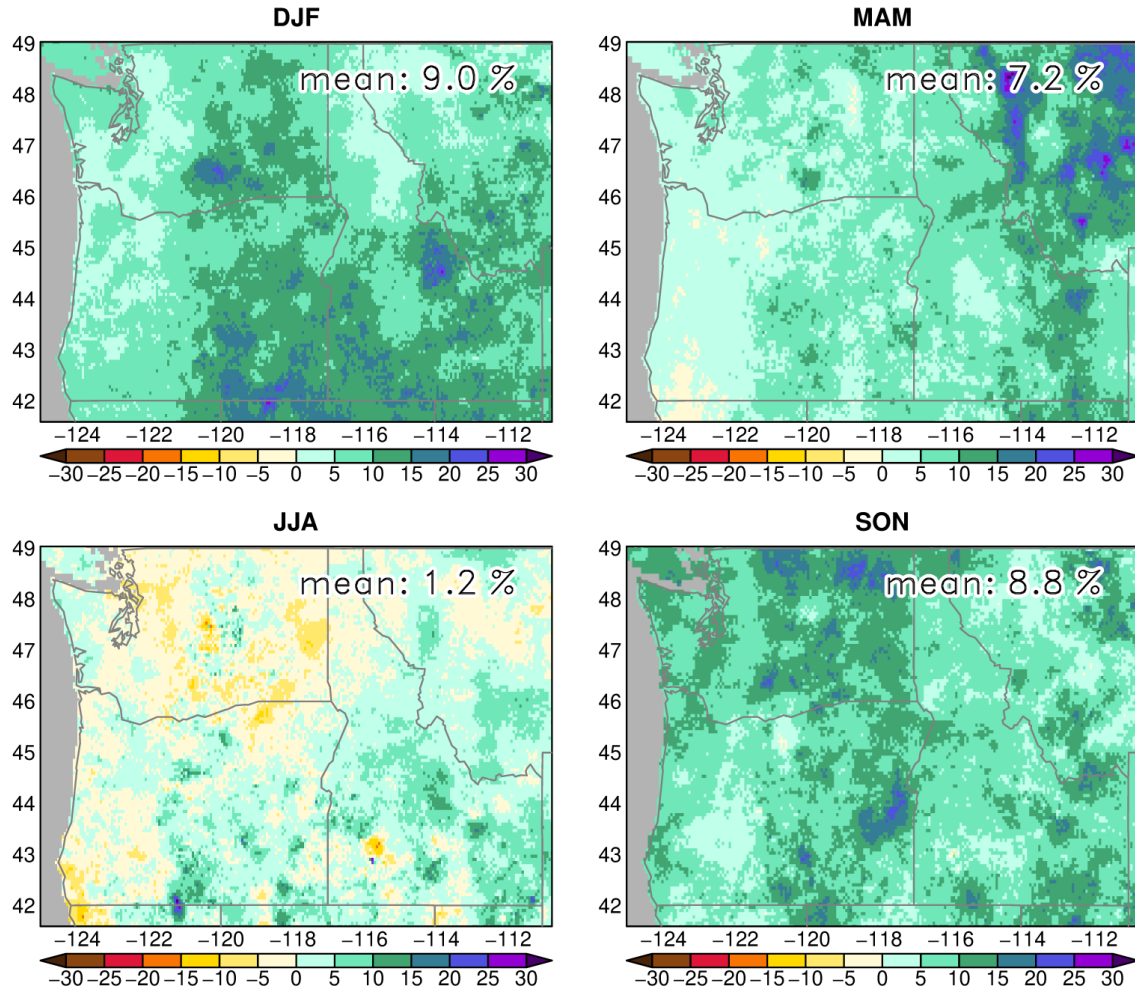
**Figure 9.** Multi-model ensemble average change in seasonal precipitation (percentage) at the 99th percentile of wet days between the historical period (1950–2014) and the mid-twenty-first century (2045–2074) given shared socioeconomic pathway 3–7.0. DJF, December, January, and February (winter); MAM, March, April, and May (spring); JJA, June, July, and August (summer); SON, September, October, and November (autumn). Means over the geographic domain are in the upper right of each panel.

and in Oregon are weak, just over one percent averaged over the geographic domain, with the lowest values (weakly negative) in coastal Oregon, especially in the south.

During the late twenty-first century (2075–2100), the projected magnitude of 99th percentile wet day precipitation continues to increase in winter, spring, and autumn (Figure 10), especially in winter in southeastern Oregon. By contrast, changes in summer remain modest.

In autumn, winter, and spring, projected extreme precipitation across Oregon tends to increase the most at the highest extremes (99.9th percentile) (Figure 11). The largest increases are in autumn and winter. Autumn increases tend to be the greatest in northwestern Oregon, and winter increases the greatest in southeastern Oregon. Summer changes are more variable, although in western and northwestern Oregon, precipitation tends to decrease most markedly at the 90th percentile and less so at higher percentiles. In southeastern Oregon, projected changes in summer precipitation are modest, and the extremes tend to decrease at the highest percentiles.

Projected increases in the most extreme percentiles of precipitation are consistent across the ecoregions of Oregon with the highest population densities, especially the Willamette Valley. The
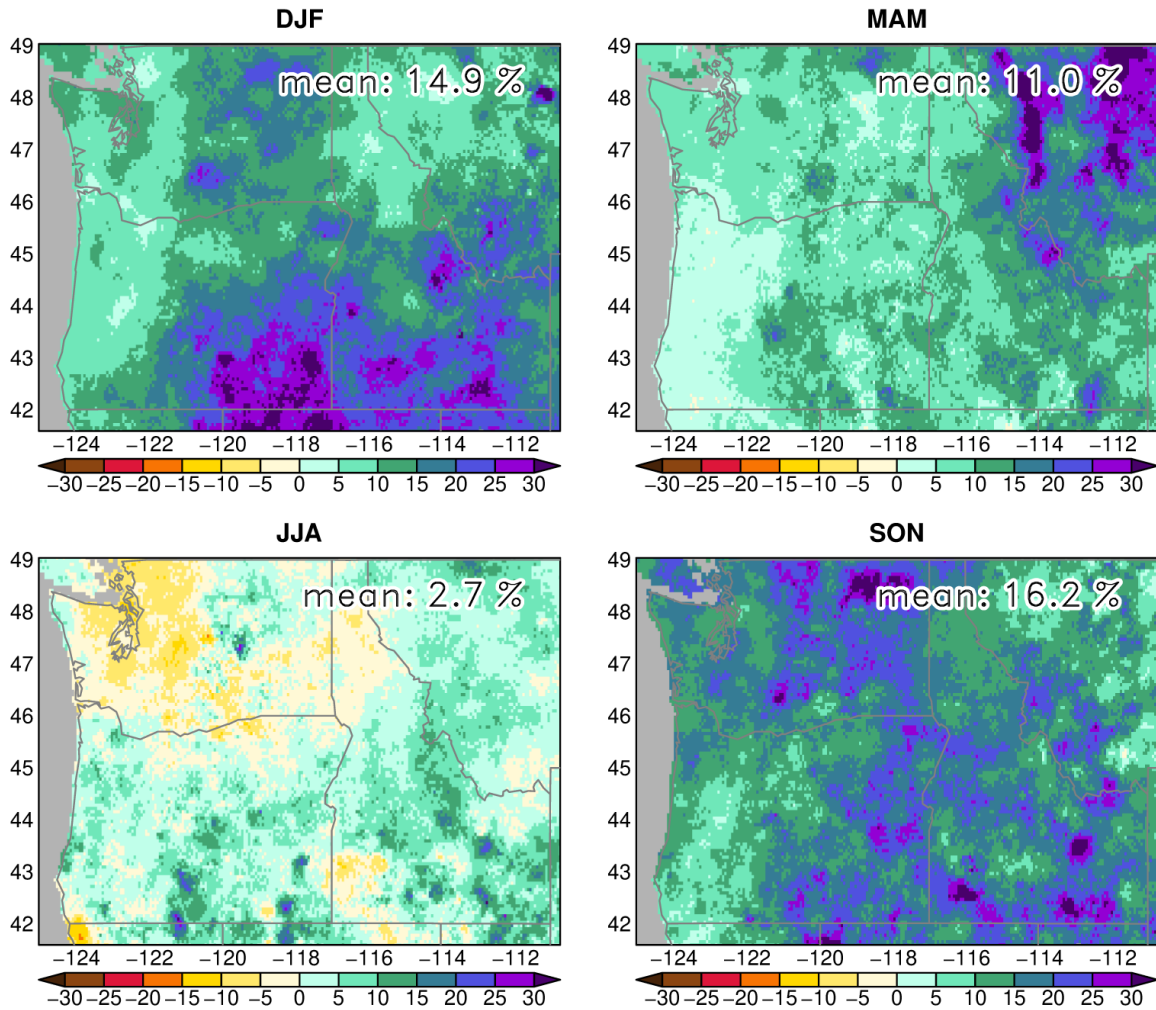
**Figure 10.** Multi-model ensemble average change in seasonal precipitation (percentage) at the 99th percentile of wet days between the historical period (1950–2014) and the late twenty-first century (2075–2100) given shared socioeconomic pathway 3–7.0. DJF, December, January, and February (winter); MAM, March, April, and May (spring); JJA, June, July, and August (summer); SON, September, October, and November (autumn). Means over the geographic domain are in the upper right of each panel.

greatest increases are in autumn (nearly 20 percent) and winter, which are already the wettest seasons in the Willamette Valley. These changes are likely to increase flooding risks.

We examined precipitation values at even higher extremes on the basis of return values (also called return periods) of daily precipitation over periods of a decade to a century (Figure 12). Return values correspond to probabilities: a 10-year return value also can be interpreted as a ten percent probability of occurrence in a given year, whereas a 50-year return value can be interpreted as a two percent probability of occurrence in a given year. We computed return values with annual block maxima and L-moments (Hosking 1990). This estimator is robust and relatively quick to compute, which is advantageous for application across numerous global climate models. 100-year return values of daily precipitation reached about 100 mm (3.9 in.) in the Willamette Valley, and over 350 mm (13.8 in.) on the Olympic Peninsula and parts of Oregon's southeastern coast.

The MMEA projected that extreme return values, from the wettest day in a decade to the wettest day in a century, will increase in all regions (Figure 13). Within Oregon, increases in the 100-year return

value by the mid-twenty-first century range from 11 to 20 percent. Increases generally become larger during the century except in the Willamette Valley and Columbia Plateau, where there is little change. Elsewhere in Oregon, late-century changes become quite substantial, with many 100-year return values more than 20 percent greater than historical values.
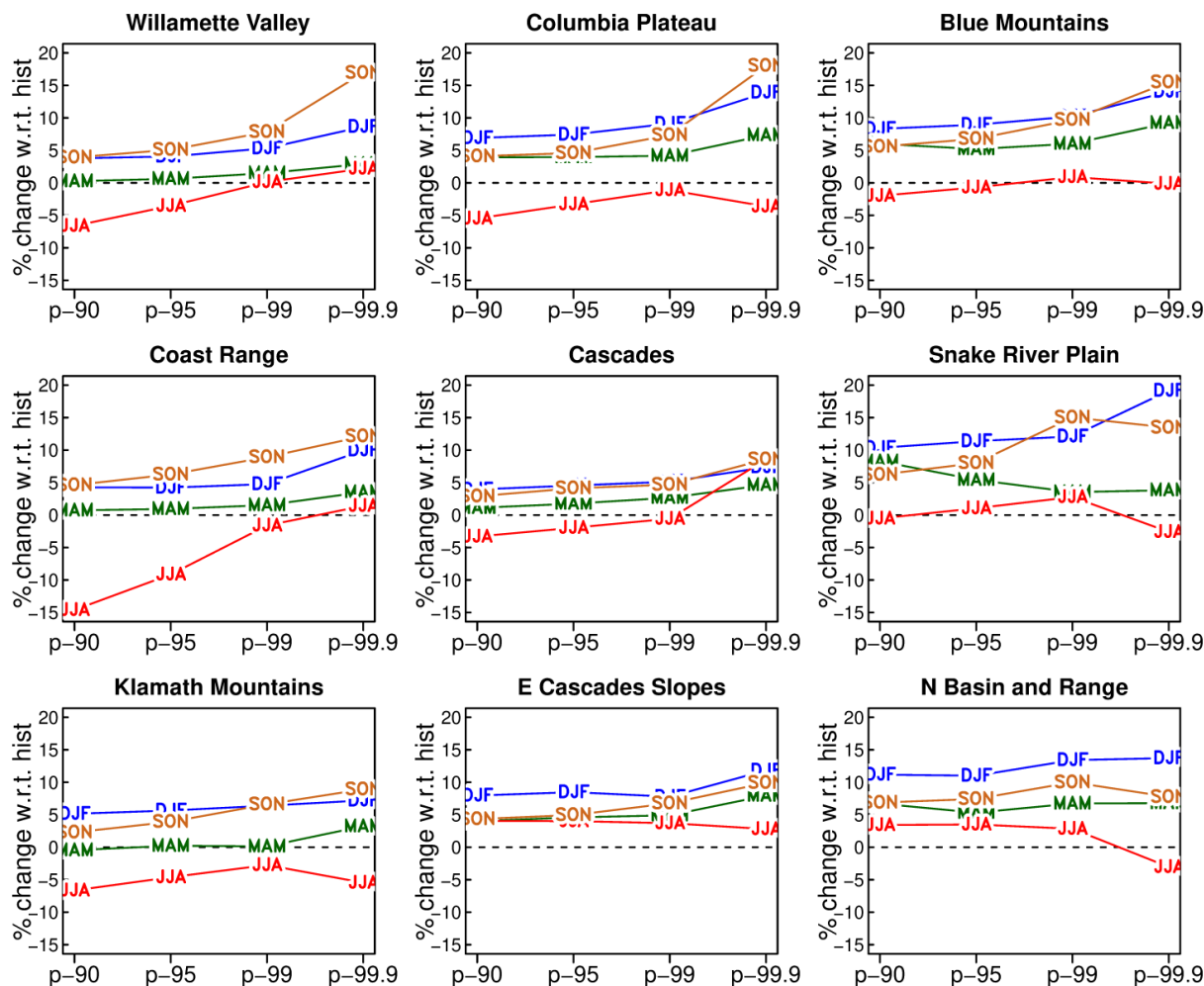


**Figure 11.** Multi-model ensemble average projected changes (percentage) in extreme precipitation between the historical period (1950–2014) and the mid-twenty-first century, given shared socioeconomic pathway 3–7.0, as a function of percentile of wet day precipitation, season, and level III ecoregion (Figure 1). DJF, December, January, and February (winter); MAM, March, April, and May (spring); JJA, June, July, and August (summer); SON, September, October, and November (autumn).

## Snow to Rain Transition

Diverse human and natural systems are affected by the proportions of precipitation that fall as rain and snow. Snow acts as a large, natural reservoir of water that accumulates during winter and is released slowly during spring and summer. Lack of snow in winter increases the likelihood of hydrological or agricultural drought during the following spring and summer. Rather than estimating snow depth, we estimated the water content of the snow that falls (the snow water equivalent, SWE). For example, if 10 cm of snow falls on a given day and that snow contains 1 cm of water, the SWE snowfall is 1 cm.

**Figure 12.** Return values (mm/day) of daily wet-day precipitation from observations over the historical period (1950–2014). Values in panel titles are the means over the geographic domain.
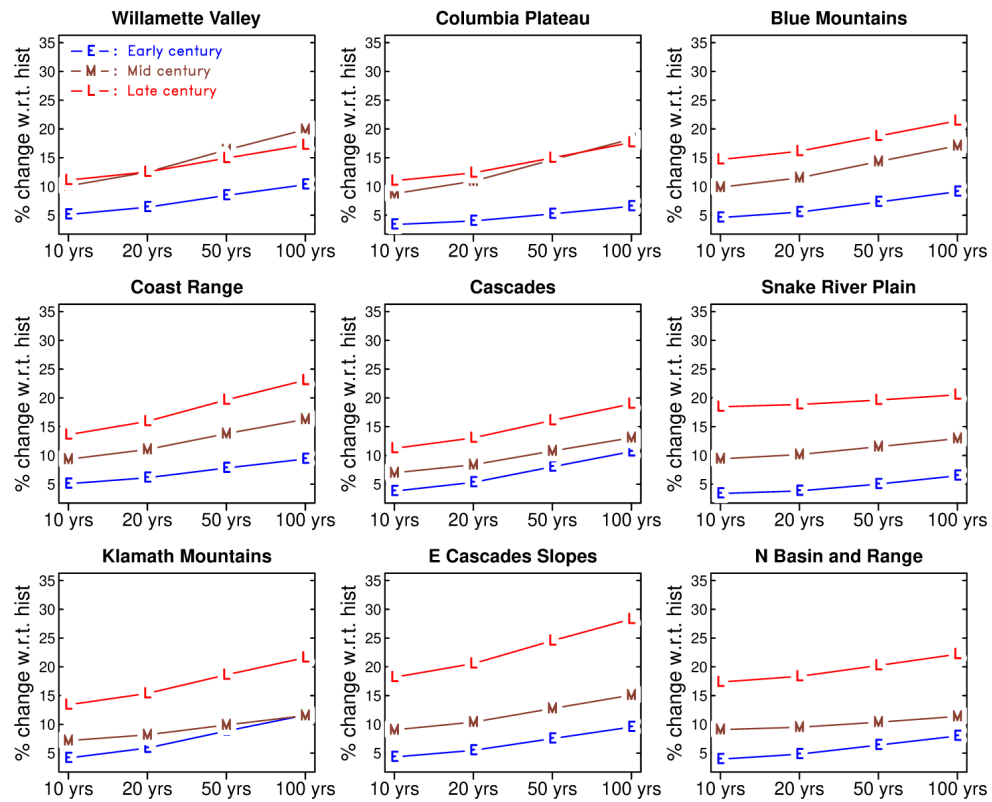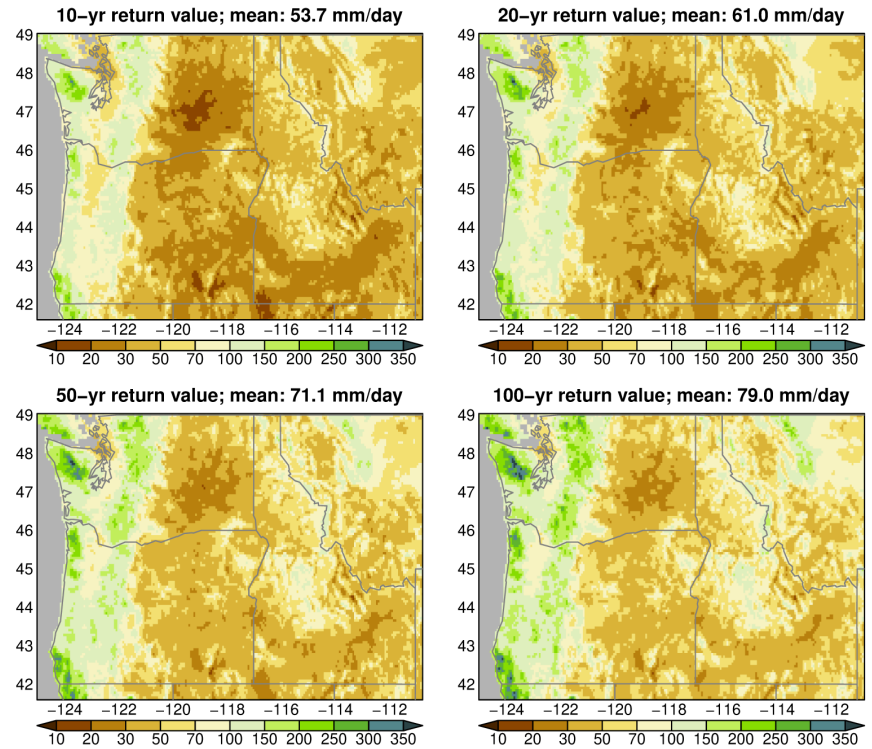


**Figure 13.** Multi-model ensemble average projected changes (percentage) in return values of wet-day precipitation by the early twenty-first century (2014–2044, E), mid-twenty-first century (2045–2074, M), and late twenty-first century (2075–2100, L). Changes calculated relative to 1950–2014 given shared socioeconomic pathway 3–7.0.

We estimated SWE snowfall (mm/day) from daily minimum temperature (Tmin), maximum temperature (Tmax), and average temperature (Tavg) [Tavg = 0.5*(Tmin + Tmax)] and total precipitation (P, mm/day) (Figure 14). Our SWE snowfall algorithm is based on that used in the Variable Infiltration Capacity hydrological model (Liang et al. 1994) and Mountain Microclimate Simulation Model (MTCLIM) (Hungerford et al. 1989), which determine whether total precipitation inputs to the Variable Infiltration Capacity model are interpreted as rain or snow.

During the historical period (1950–2014), seasonal mean total precipitation, rainfall, and SWE snowfall peaked in winter (Figure 15). We omitted summer from this analysis because snowfall is rare in Pacific Northwest during summer. The largest SWE snowfall values in Oregon were in the Cascade Range in winter, although snowfall in the Cascade Range also was prevalent in spring and autumn.

The percentage of precipitation that historically fell as snow in the coastal Pacific Northwest, and is projected to fall as snow from 2044–2074, was low during all seasons, typically less than 10 percent (Figure 16). In interior Idaho, by contrast, over 95 percent of winter precipitation was snow. The highest snow percentages in Oregon were in the Cascade Range and Blue Mountains, where more than 50 percent of winter precipitation may fall as snow. By mid-century, SWE snowfall across much of the state is projected to decrease by 10–25 percent during winter, and 5–20 percent annually.

The projected future change in the proportion of precipitation falling as snow in the Willamette Valley and Coast Range was lower in the TaiESM1 model than in any other model (Figure 17). However, the historical proportion of snow in these regions is low, so small changes in absolute SWE snowfall can equate to large changes in the proportion of snow. In other regions, the range of projected changes in the proportion of precipitation falling as snow is lower. The extent to which weather is variable means that even a perfect model of Earth would include a range of projected future changes in climate; climate is probabilistic, not deterministic. For example, consider the projected change in percentage precipitation falling as snow in the Cascades ecoregion by the mid-twenty-first century (2045–2074) (Figure 17). The 11 models suggest that the mid-century reduction in proportion of SWE snowfall due to climate change is about 45 percent (the value indicated by the MMEA line), and that natural climate variability can alter this percentage by about 10 percent in either direction (interquartile range).

Absolute snowfall (SWE) is another way to evaluate changes in precipitation type. In Oregon, the largest annual changes in absolute snowfall between the historical period and mid-century are in

Let Tmin, Tmax, Tavg be daily minimum, maximum, and average temperature; Let P and S be the total precipitation and (snow water equivalent) snowfall rates; Let $T_f$ be freezing temperature (0°C)

Tmax < $T_f$? → S = P

Tmin > $T_f$? → S = 0

Tavg < -0.5C? → S = P

Tavg > 0.5C? → S = 0

$F = (Tavg – (-0.5C)) / (0.5C – (-0.5C))$
$S = F * P$
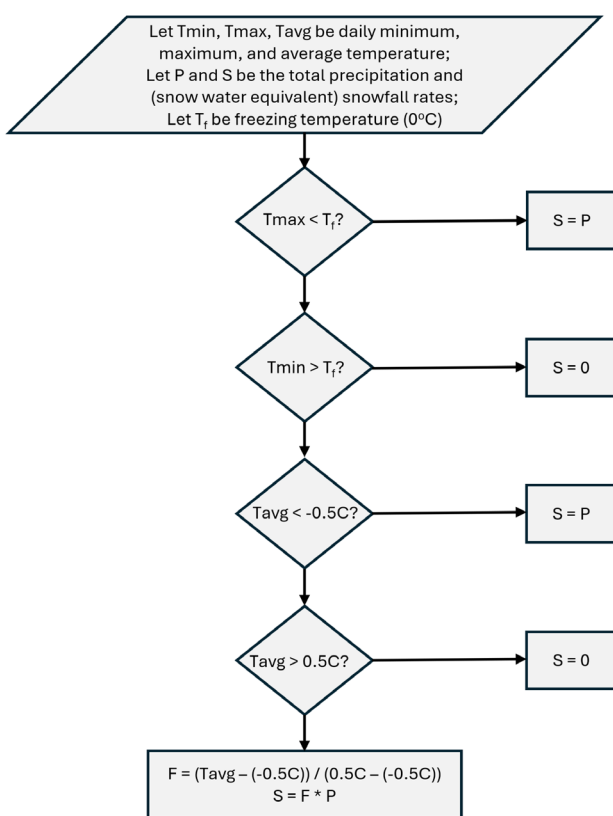
**Figure 14.** Process for estimating the daily snow water equivalent (SWE) snowfall rate, S, from daily minimum, maximum, and average temperature (Tmin, Tmax, Tavg) and precipitation (P).
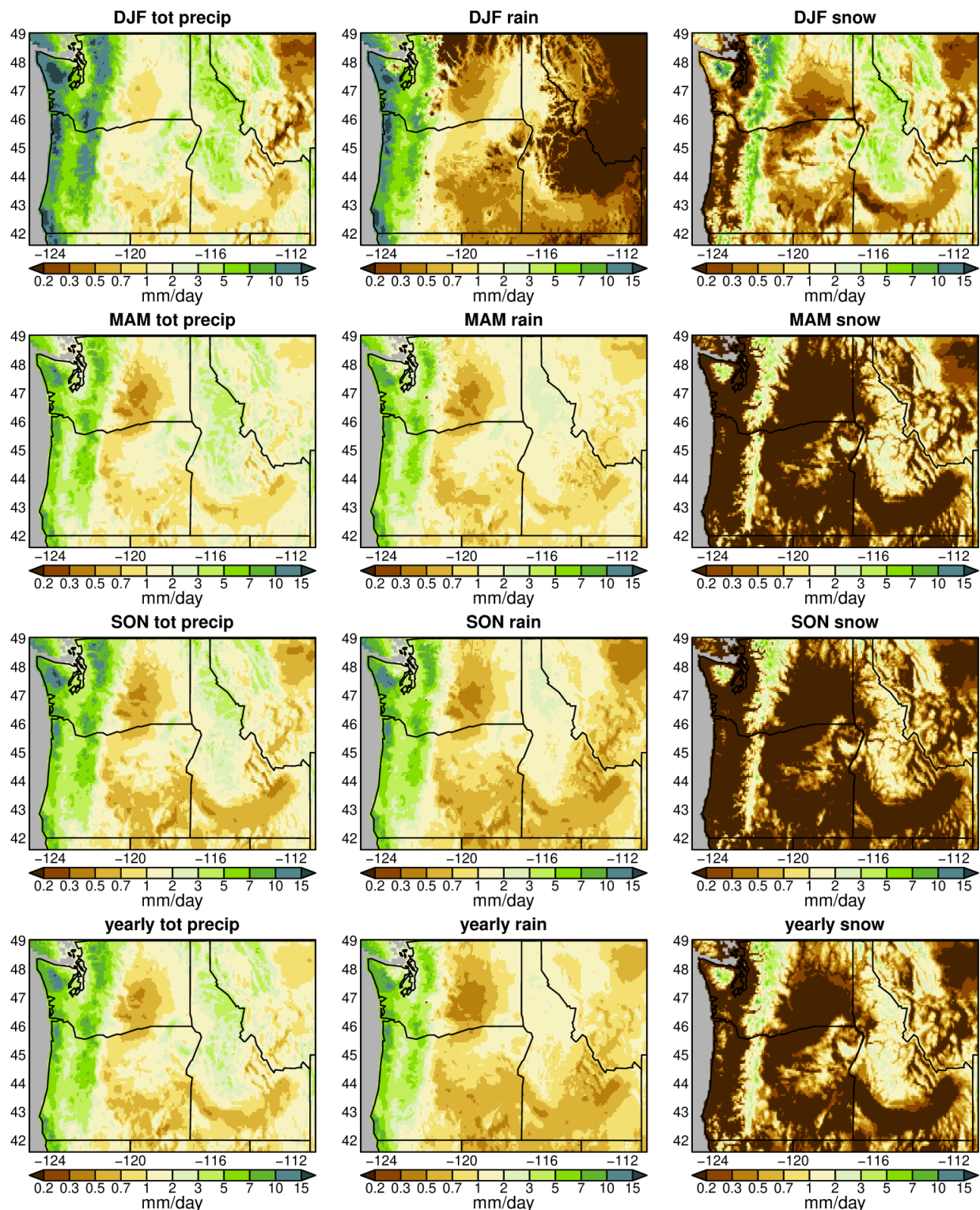
**Figure 15.** Seasonal and annual mean precipitation during the historical period (1950–2014). Left column: total precipitation (rain and snow). Middle column: amount of precipitation that fell as rain. Right column: amount of precipitation that fell as snow (snow water equivalent). DJF, December, January, and February (winter); MAM, March, April, and May (spring); SON, September, October, and November (autumn). Summer is omitted given the rarity of snow across the Pacific Northwest during that season.
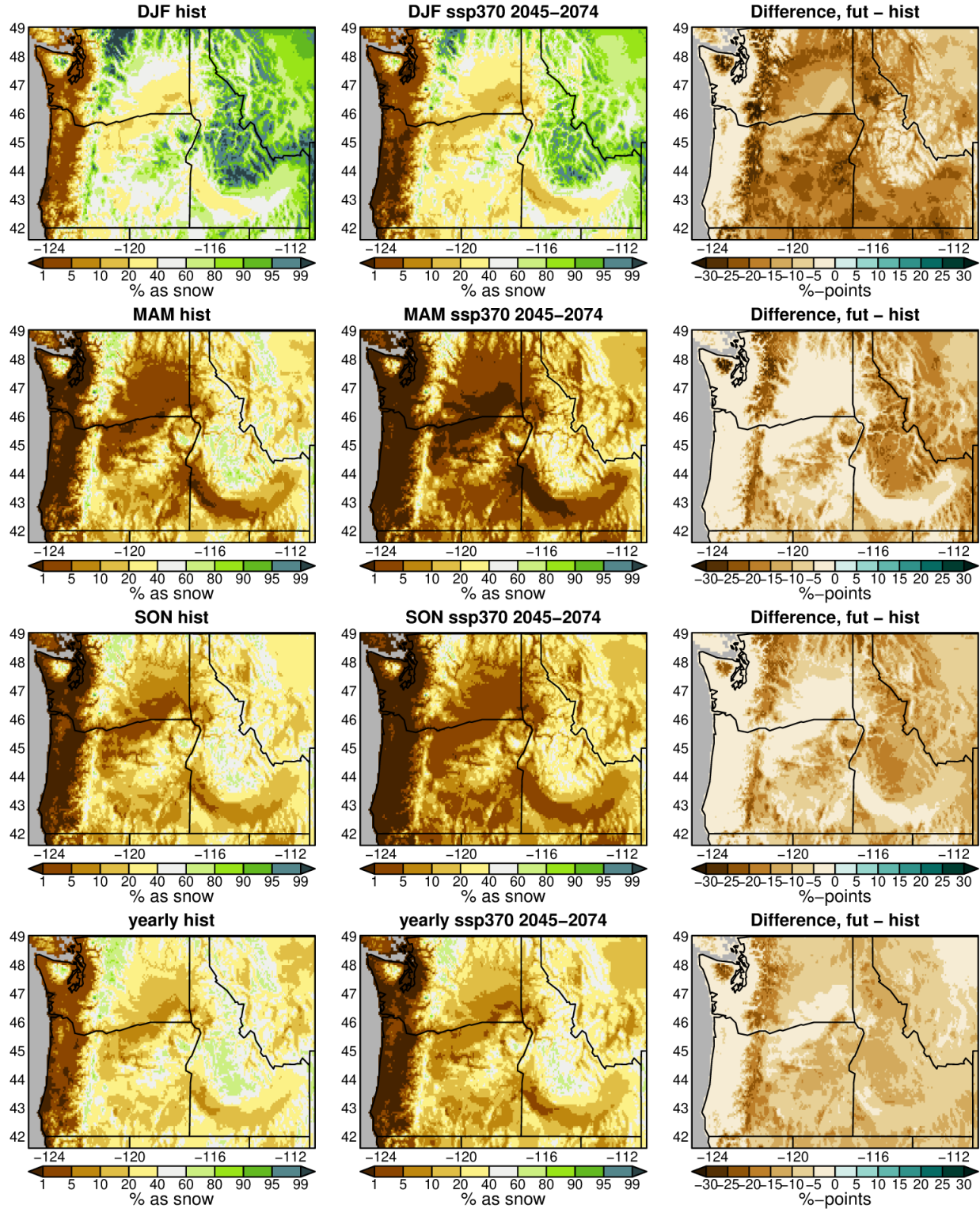
**Figure 16.** Historical (1950–2014) (left column) and projected mid-twenty-first century (2045–2074) (middle column) percentage of precipitation that falls as snow (measured as snow water equivalent), and difference (percentage change) between the historical period and mid-century (right column). Projections assume shared socioeconomic pathway (SSP) 3–7.0. DJF, December, January, and February (winter); MAM, March, April, and May (spring); SON, September, October, and November (autumn).

69
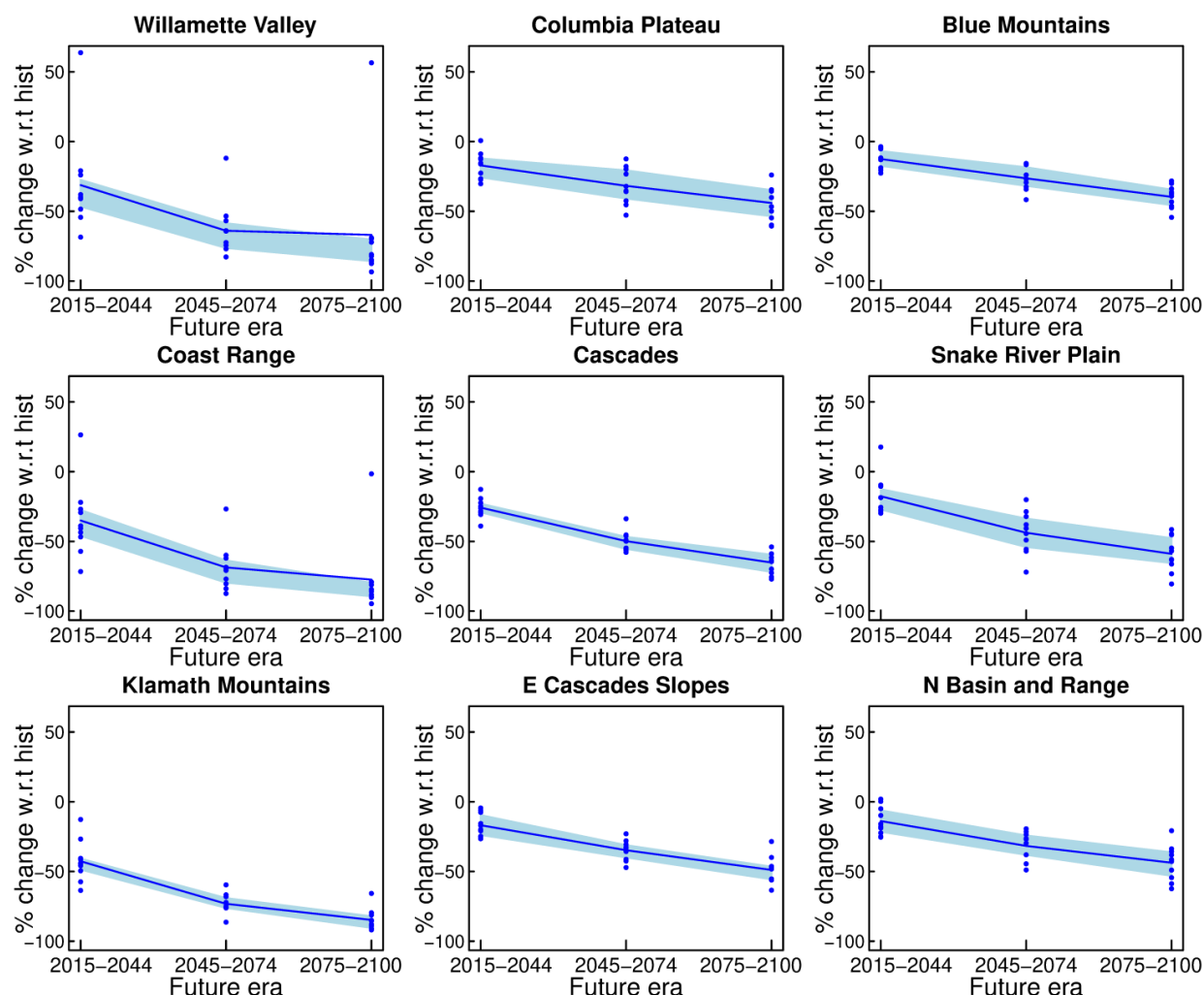
**Figure 17.** Projected change in the percentage of precipitation falling as snow (snow water equivalent) between the historical period (1950–2014) and three periods during the twenty-first century, given shared socioeconomic pathway 3–7.0, in Oregon's level III ecoregions (Figure 1). Lines represent the multi-model ensemble average. The blue envelope indicates the interquartile range across the 11 models. Dots represent results from each model.

winter in the Cascade Range, where decreases in SWE of 2–3 mm/day are common (Figure 18). These changes represent relative decreases in SWE of 20–60 percent. The largest relative seasonal changes in absolute snowfall occur during spring, with decreases exceeding 80 percent in western Oregon, albeit snow rarely falls in this region. Projected changes during autumn are similar to those during spring. Winter SWE snowfall is projected to decrease by mid-century across most of the geographic domain, in many regions by 40 percent or more. In parts of the northern Cascade Range and Rocky Mountains in Idaho and Montana, however, SWE snowfall is projected to increase.

The complement to snowfall changes is rainfall changes. The largest projected changes in absolute rainfall by the mid-twenty-first century are in winter, particularly in the Cascade Range and Olympic Peninsula (Figure 19). Relative changes between the historical period and the mid-century reach 400 percent in Washington and 200 percent in the Cascade Range and Blue Mountains in Oregon. Changes in spring, autumn, and annual precipitation are notable. Annual rainfall is projected to increase by 10 to 50 percent in much of the Cascade Range and eastern Oregon.
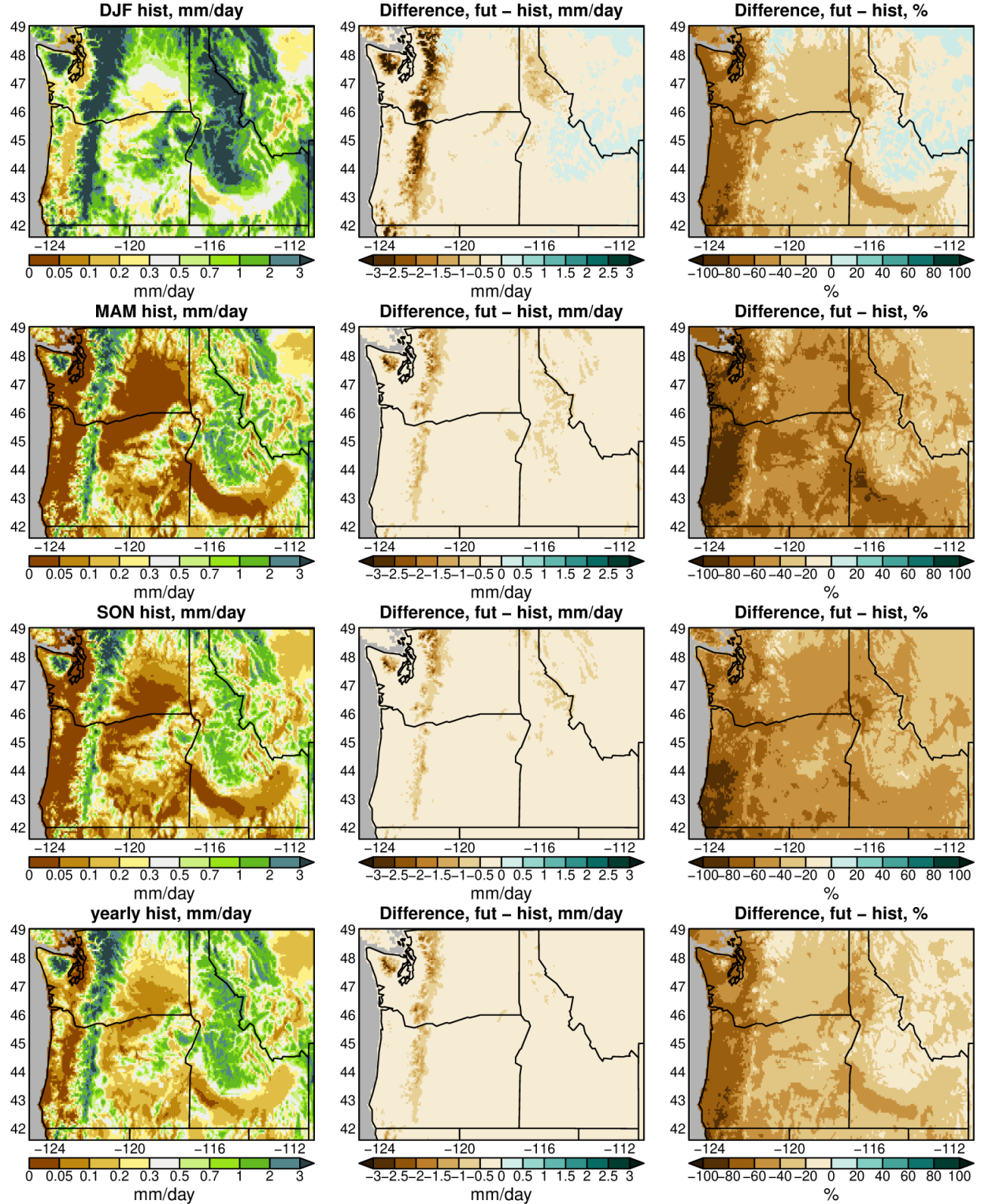
**Figure 18.** Left column: historical (1950–2014) seasonal and annual snow water equivalent. Middle column: multi-model ensemble average projected absolute change in snow water equivalent between the historical period and the mid-twenty-first century (2045–2074) given shared socioeconomic pathway 3–7.0. Right column: multi-model ensemble average projected percentage change in snow water equivalent between the historical period and the mid-twenty-first century. DJF, December, January, and February (winter); MAM, March, April, and May (spring); SON, September, October, and November (autumn).
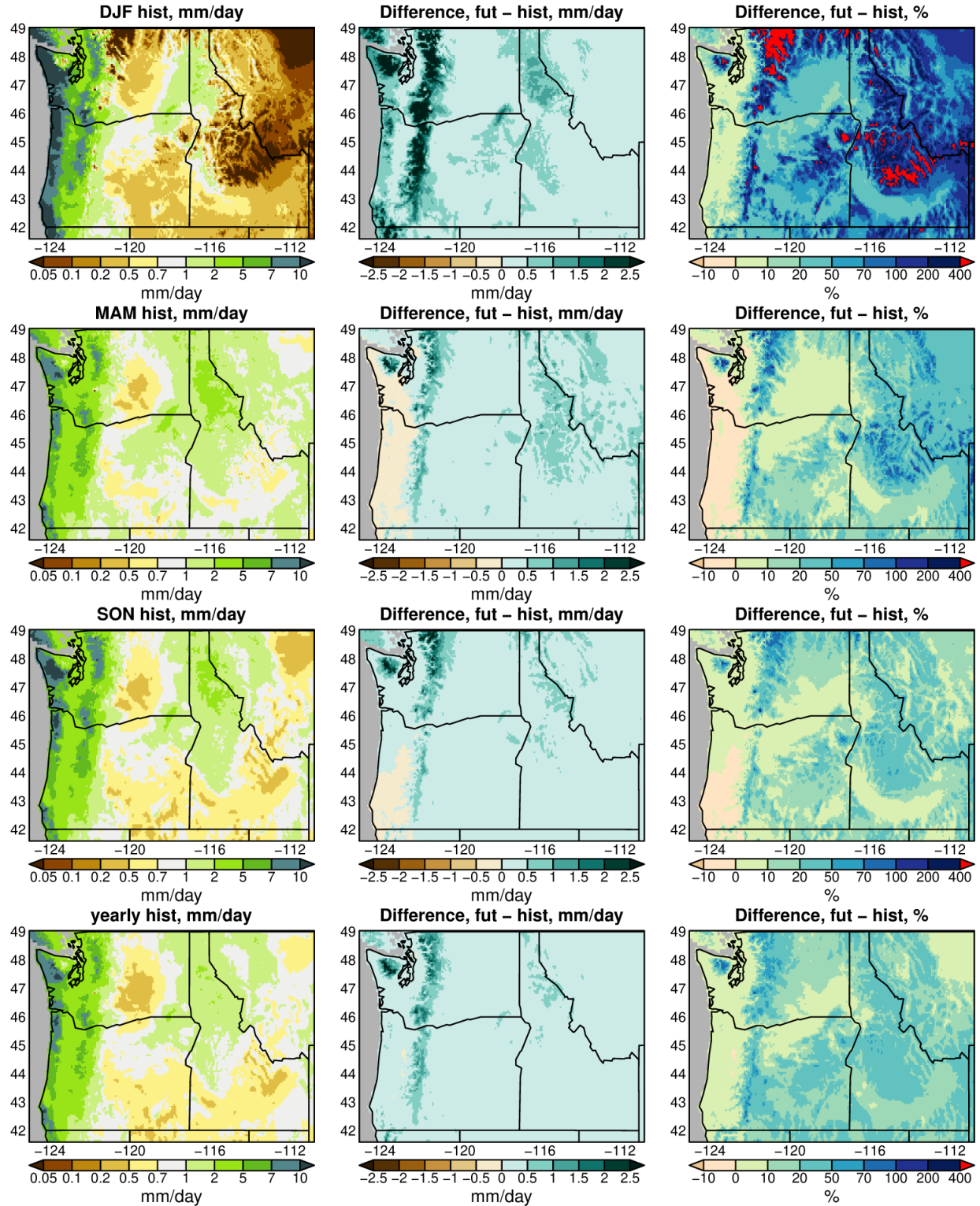
**Figure 19.** Left column: historical (1950–2014) seasonal and annual rainfall. Middle column: multi-model ensemble average projected changes in rainfall between the historical period and the mid-twenty-first century (2045–2074) given shared socioeconomic pathway 3–7.0. Right column: multi-model ensemble average projected change (percentage) between the historical period and the mid-twenty-first century. DJF, December, January, and February (winter); MAM, March, April, and May (spring); SON, September, October, and November (autumn).

Projected precipitation amounts during the most extreme precipitation events increase across Oregon, with more pronounced increases as the century progresses (Figure 13). At the same time, the amount of precipitation falling as rain increases in much of the state (Figure 19). This leads to the question of whether the rate of increase in extreme rainfall events is greater than the rate of increase in extreme total precipitation.

In western and coastal Oregon, there is little difference between return values of total precipitation and rainfall alone (Figure 20) given that SWE is low in those regions (Figure 16). The largest projected increases in rainfall are in the Cascades and Eastern Cascades Slopes and Foothills, where the change from snow to rain is an appreciable percentage (Figure 18) and absolute amount of total precipitation. In these ecoregions, the 10-year return value of rainfall increases considerably more than that of total precipitation (11 percent rainfall versus 7 percent total precipitation in the Cascades, and 14 percent versus 9 percent in the Eastern Cascades Slopes and Foothills). Smaller increases in rainfall relative to total precipitation are projected in the Blue Mountains and Northern Basin and Range. The projected future increases in total precipitation and rainfall at the longest return values we considered, 100 years, are marginally different. This suggests that some of the
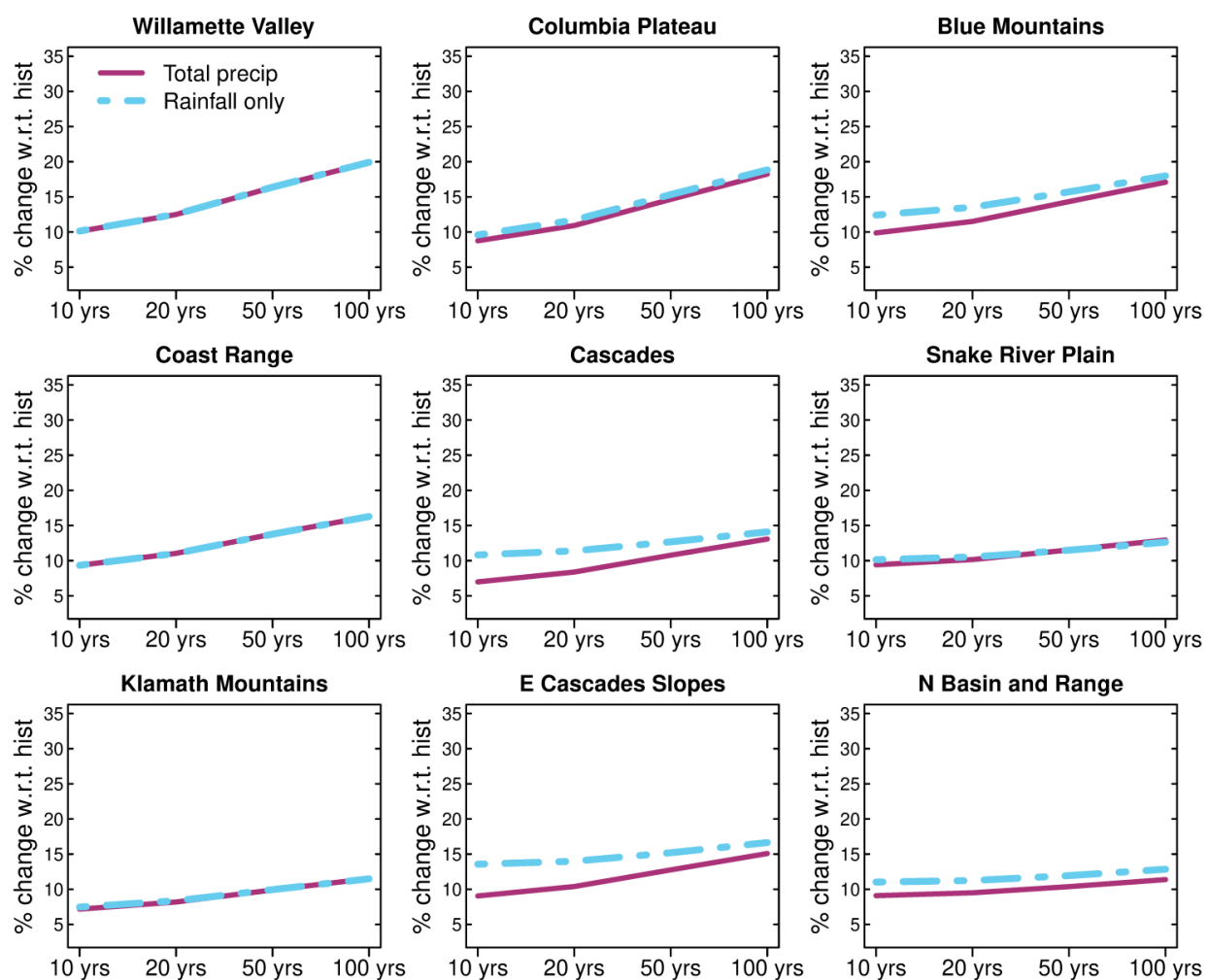


**Figure 20.** Multi-model ensemble average projected changes in return values of wet-day precipitation (snow and rain) and rainfall between the historical period (1950–2014) and the mid-twenty-first century (2045–2074), given shared socioeconomic pathway 3–7.0, in Oregon's level III ecoregions (Figure 1).

heaviest storms, as measured by production of precipitation, historically produced snow, and these storms likely will continue to be cold enough to produce snow by mid-century.

All ecoregions are projected to lose at least half of their SWE snowfall from 1950–2100 (Figure 21). Changes in the amounts of precipitation falling as snow and rain are greatest in the Cascades and Eastern Cascades Slopes and Foothills. From the 1950s to the 2090s, given SSP 3–7.0, 68 percent of SWE snowfall in the Cascades and 65 percent in the Eastern Cascade Slopes and Foothills will be lost. Projected increases in rainfall are also considerable in many regions, such as 30–50 percent over much of southeastern Oregon. Although the greatest percentages in loss of SWE snowfall are projected in near the coast (Coast Range, Willamette Valley, and Klamath Mountains), absolute snowfall in those ecoregions is low compared to that in the Cascade Range. Accordingly, the loss of SWE snowfall does not lead to appreciable increases in yearly averaged rainfall.
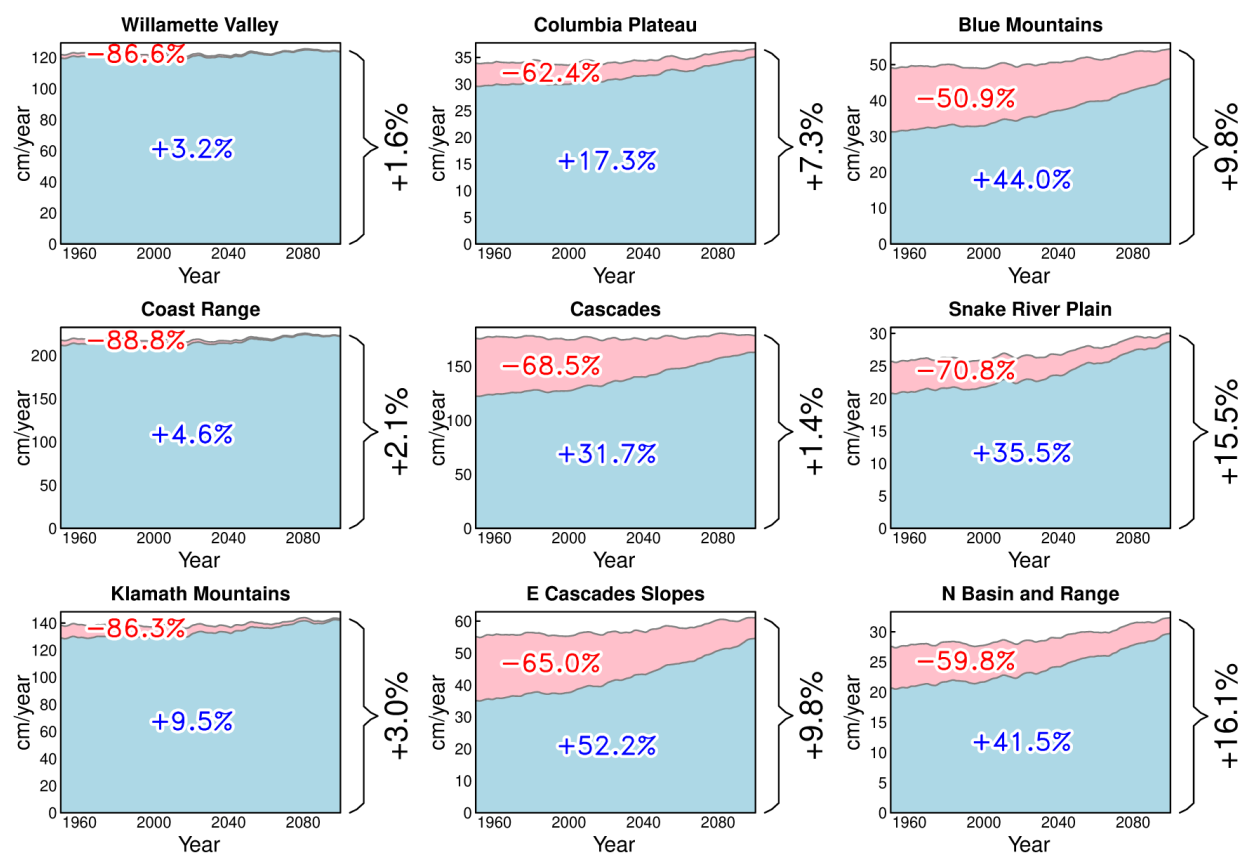


**Figure 21.** Multi-model ensemble average projected annual total rainfall (blue), snow water equivalent snowfall (pink), and total precipitation in Oregon's level III ecoregions (Figure 1) from 1950 through 2100 under shared socioeconomic pathway 3–7.0. Changes from the first (1950–1959) to the last (2091–2100) decade of the record are indicated by percentages. To reduce natural internal variability and clarify the underlying trends, we applied a third order Butterworth low-pass filter with cutoff of 0.1 cycles/year to the time series.

## Uncertainty and Variability

There are three main sources of uncertainty and variability in climate projections. The first, scenario uncertainty, is uncertainty in future human behavior, particularly the volume of greenhouse gases that are emitted by human activity. The second, model uncertainty, is differences in how climate

models depict the physical processes that produce the climate. The third, internal climate variability, is natural variability in climate and weather. Examples include the path of a particular storm, occurrence of a dry summer in a given region, or the phase of the El Niño-Southern Oscillation.

The primary cause of variation in climate projections at the global level is the model projection or forecast lead time (Hawkins and Sutton 2009). By the end of the twenty-first century, the effect of greenhouse gas emissions on climate becomes so large that scenario uncertainty swamps model uncertainty and internal climate variability.

At lead times of about 15–45 years, model uncertainty dominates uncertainty in climate projections. This is one of the motivations for selecting models that skillfully simulate climate in the region of interest when concentrating on mid-century climate projections. Model uncertainty is the secondary source of uncertainty in global climate projections from the middle to the end of the twenty-first century. Therefore, it is worthwhile to continue improving the quality of climate models.

Internal climate variability, including the initial state of Earth's climate system and the detailed evolution of weather events and natural climate fluctuations, is the main factor in climate projection uncertainty at lead times of 0 to 15 years. Climate projections over these relatively short periods are sometimes referred to as decadal climate forecasts. These forecasts have attracted considerable scientific interest due to their utility.

At the spatial extent of regions (e.g., Pacific Northwest) or states (Oregon), other sources of uncertainty are relevant, particularly with respect to precipitation extremes. By definition, extremes are rare, so there is considerable sampling uncertainty in estimating the true return value given a limited data record. Furthermore, an extreme precipitation event with an estimated 10-year return value is unlikely to occur in any given decade; actual precipitation during a given decade could be greater or less than what was projected on the basis of long-term statistics. Natural variability also means that a major storm could affect a particular town but not a neighboring town, so there can be considerable spatial variation in the occurrence of extremes. Even within small areas, topographic features such as hills can cause local variation in microclimate that leads to local differences in precipitation amounts from the same storm. Given these sources of uncertainty in climate projections, we emphasize that systematic changes from greenhouse gas emissions, aerosols, land use changes, and other factors will have a discernible effect on future climate. The actual future experienced at any particular location will reflect both the changes that arise from human-caused climate change and random, unpredictable fluctuations that reflect natural climate variability.

## Summary

We examined projected future changes in precipitation and the proportions of precipitation falling as rain and snow in Oregon and across the Pacific Northwest as a result of anthropogenic climate change. We selected 11 global climate models for analysis on the basis of their ability to realistically simulate key weather processes and historically observed climatology and variability over the region. We then used statistically downscaled and bias-corrected data to examine model-projected future changes in precipitation. The period of analysis is 1950–2100, although we focused on model-projected changes by mid-century (2045–2074). We considered three scenarios of greenhouse gas and aerosol emissions, land use changes, and population, technological, and economic growth; we emphasized an intermediate scenario, shared socioeconomic pathway (SSP) 3–7.0.

Models tend weakly toward higher total annual precipitation (0–10 percent) in Oregon by mid-century, but with seasonal variation that includes drier summers (5–15 percent) in western Oregon.

Projected extreme wet-day precipitation increases progressively as the century advances, with geographic domain-average projected increases of about 7 percent by mid-century under SSP 3–7.0 for the 99th percentile wet day. In Oregon, these changes are greatest in winter, particularly in southeastern Oregon, and continue to increase toward the end of the century. In western Oregon and the Willamette Valley, the largest projected increases in extreme daily precipitation occur in autumn, with values approaching 10 percent for the 99th percentile and 20 percent for the 99.9th percentile by mid-century.

In Oregon, the proportion of annual total precipitation that falls as snow is projected to decrease by 10–20 percent from the Cascades ecoregion and to the east by mid-century. The largest decreases, 40–80 percent across much of the state, are in spring. As a result, rainfall is projected to increase by mid-century, with annual average increases of 10–20 percent over much of the state from the Cascades ecoregion eastward.

Over the full time period of analysis (1950–2100), snowfall is projected to decrease by no less than 50 percent in any part of Oregon, with decreases of 65 percent or more in the Cascades and Eastern Cascades Slope and Foothills ecoregions and over 85 percent in western Oregon. At the same time, the proportion of precipitation falling as rain is projected to increase by 30–50 percent over much of southeastern Oregon and by 3–10 percent in western and coastal Oregon given the limited historical snowfall in those regions.

## Appendix

Appendix A includes two additional future periods, early twenty-first century (2015–2044) and late twenty-first century (2075–2100); and two additional shared socioeconomic pathways (SSPs), 2–4.5 and 5–8.5; associated with the results represented in chapter figures 3, 4, 5, 8, 9, 13, 16, 17, 18, 19, 20, and 21.

## Acknowledgments

## Literature Cited

Arrhenius, S. 1896. On the influence of carbonic acid in the air upon the temperature of the ground. The London, Edinburgh, and Dublin Philosophical Magazine and Journal Science 41:8.

Eyring, V., S. Bony, G.A. Meehl, C.A. Senior, B. Stevens, R.J. Stouffer, and K.E. Taylor. 2016. Overview of the Coupled Model Intercomparison Project Phase 6 (CMIP6) experimental design and organization. Geoscientific Model Development 9:1937–1958.

Harp, R.D., and D.E. Horton. 2022. Observed changes in daily precipitation intensity in the United States. Geophysical Research Letters 49:e2022GL099955. https://doi.org/10.1029/2022GL099955.

Hawkins, E., and R. Sutton. 2009. The potential to narrow uncertainty in regional climate

predictions. Bulletin of the American Meteorological Society 90:1095–1108.

Hosking, J.R. 1990: L-moment—analysis and estimation of distributions using linear-combinations of order-statistics. Journal of the Royal Statistical Society: Series B (Methodological) 52:105–124.

Hungerford, R.D., R.R. Nemani, S.W. Running, and J.C. Coughlan. 1989. MTCLIM: a mountain microclimate simulation model. Research Paper INT-RP-414. Department of Agriculture, Forest Service, Intermountain Research Station, Ogden, Utah. https://doi.org/10.2737/INT-RP-414.

Krantz, W., D.W. Pierce, N. Goldenson, and D.R. Cayan. 2021. Memorandum on evaluating global climate models for studying regional climate change in California. www.energy.ca.gov/sites/default/files/2022-09/20220907_CDAWG_MemoEvaluating_GCMs_EPC-20-006_Nov2021-ADA.pdf.

Kroner, N., S. Kotlarski, E. Fischer, D. Luthi, E. Zubler, and C. Schar. 2017. Separating climate change signals into thermodynamic, lapse-rate and circulation effects: theory and application to the European summer climate. Climate Dynamics 48:3425–3440.

Lee, H., and J. Romero, editors. 2023. Summary for policymakers. Pages 35–115 in Climate change 2023: synthesis report. Contribution of Working Groups I, II and III to the Sixth Assessment Report of the Intergovernmental Panel on Climate Change. IPCC, Geneva, Switzerland. https://doi.org/10.59327/IPCC/AR6-9789291691647.

Liang, X., D.P. Lettenmaier, E.F. Wood, and S.J. Burges. 1994. A simple hydrologically based model of land-surface water and energy fluxes for general-circulation models. Journal of Geophysical Research: Atmospheres 99:14415–14428.

Lybarger, N.D., A. Smith, A.J. Newman, E.D. Gutmann, A.W. Wood, C.D. Frans, M.D. Warner, and J.R. Arnold. 2024. Improving Earth system model selection methodologies for projecting hydroclimatic change: case study in the Pacific Northwest. Journal of Geophysical Research: Atmospheres 129:e2023JD039774. https://doi.org/10.1029/2023JD039774.

Norris, J., G. Chen, and J.D. Neelin. 2019. Thermodynamic versus dynamic controls on extreme precipitation in a warming climate from the Community Earth System Model Large Ensemble. Journal of Climate 32:1025–1045.

O'Neill, B.C., E. Kriegler, K. Riahi, K.L. Ebi, S. Hallegatte, T.R. Carter, R. Mathur, and D.P. van Vuuren. 2014. A new scenario framework for climate change research: the concept of shared socioeconomic pathways. Climatic Change 122:387–400.

O'Neill, B.C., et al. 2016. The Scenario Model Intercomparison Project (ScenarioMIP) for CMIP6. Geoscientific Model Development 9:3461–3482.

Omernik, J. Ecoregions of the conterminous United States. Map (scale 1:7,500,000). Annals of the Association of American Geographers 77:118–125.

Pierce, D.W., T.P. Barnett, B.D. Santer, and P.J. Gleckler. 2009. Selecting global climate models for regional climate change studies. Proceedings of the National Academy of Sciences 106:8441–8446.

Pierce, D.W., D.R. Cayan, D.R. Feldman, and M.D. Risser. 2023. Future increases in North American extreme precipitation in CMIP6 downscaled with LOCA. Journal of Hydrometeorology 24:951–975.

Pierce, D.W., D.R. Cayan, and B.L. Thrasher. 2014. Statistical downscaling using localized constructed analogs (LOCA). Journal of Hydrometeorology 15:2558–2585.

Pierce, D.W., D.R. Cayan, E.P. Maurer, J.T. Abatzoglou, and K.C. Hegewisch. 2015. Improved bias correction techniques for hydrological simulations of climate change. Journal of Hydrometeorology 16:2421–2442.

Pierce, D.W., L. Su, D.R. Cayan, M.D. Risser, B. Livneh, and D.P. Lettenmaier. 2021. An extreme-preserving long-term gridded daily precipitation dataset for the conterminous United States. Journal of Hydrometeorology 22:1883–1895.

Riahi, K., et al. 2017. The Shared Socioeconomic Pathways and their energy, land use, and greenhouse gas emissions implications: an overview. Global Environmental Change 42:153–168.

Westra, S., H.J. Fowler, J.P. Evans, L.V. Alexander, P. Berg, F. Johnson, E.J. Kendon, G. Lenderink, and N.M. Roberts. 2014. Future changes to the intensity and frequency of short-duration extreme rainfall. Reviews of Geophysics 52:522–555.

# Projections of Freezing Rain and Ice Accretion in the Northern Willamette Basin, Oregon

David E. Rupp, Larry W. O'Neill, Erica Fleishman, Paul C. Loikith, and Dan Loomis

## Introduction

Ice accretion from freezing rain can damage power and communication lines, housing, and other infrastructure; disrupt and endanger air and ground transportation (Changnon 2003, Houston and Changnon 2007); and harm plants and animals. Within the conterminous United States, freezing rain occurs most often in the Northeast, eastern Appalachia, the Midwest, and the Pacific Northwest (Changnon 2003, Cortinas et al. 2004). Data collected from a small number of weather stations at lower elevations in the Willamette Basin, Oregon, indicate that during the latter half of the twentieth century, freezing rain occurred in the basin on an average of one or two days per year (Changnon 2003, Cortinas et al. 2004, Groisman et al. 2016) and five to ten hours per year (Bernstein 2000, Robbins and Cortinas 2002). Although freezing rain intensities tend to be low, persistent freezing rain can lead to heavy ice accretion (McCray et al. 2019). From 1979 through 2016, four weather stations in the Willamette Basin recorded at least two freezing rain events of 18 or more hours, and Portland International Airport (PDX) recorded ten such events. Among 579 weather stations across the United States and Canada, only one, in British Columbia, recorded a greater number of freezing rain events of 18 hours or longer than PDX (McCray et al. 2019).

Freezing rain conditions can develop when precipitation falls on an above-freezing layer of air that lies above a subfreezing layer at the surface. During precipitation, falling ice particles may melt in the warm layer, become super-cooled liquid droplets in the subfreezing layer, and freeze on contact with a frozen surface. In the Pacific Northwest, such conditions most often occur in and around the Portland, Oregon, metropolitan area when strong easterly winds, or gap winds, emanate from the Columbia River Gorge (Gorge) during winter. Easterly gap winds drain colder, denser air from the Intermountain West into western Oregon and Washington. This air flows west through the Gorge along the surface and, if winds are strong enough, fans southward into the Willamette Basin toward Salem and Eugene. When near-surface air temperatures in the Willamette Basin are below freezing and moist, above-freezing maritime air moves over the basin from the west or southwest, freezing rain can occur (Sharp and Mass 2004). If the subfreezing, low-altitude gap winds are sustained, freezing rain can persist long enough for large amounts of ice to accumulate on exposed surfaces.

Anthropogenic climate change can increase or decrease or the frequency of freezing rain. The divergent responses can occur because the change in the frequency of freezing rain in a warming climate is driven largely by two opposing factors: a decreasing frequency of the requisite near-surface subfreezing conditions and an increasing frequency of the requisite above-freezing conditions aloft. A simple model (Figure 1) illustrates how the interaction of these two factors can lead to either large decreases or large increases in freezing rain frequency. In a hypothetical, initially cold climate, a uniform 2°C warming increases the frequency of freezing rain (Figure 1a), whereas in an initially warmer climate (Figure 1c), the same amount of warming decreases the frequency of freezing rain. A greater increase in air temperature aloft relative to that near the surface can either accelerate the rate of increase in freezing rain frequency (Figure 1a) or slow the rate of decrease in freezing rain frequency (Figure 1c) over time. Projections suggest that over western Oregon and Washington, temperatures aloft generally will warm more than near-surface temperatures during winter, when freezing rain is more likely (Rupp et al. 2017).
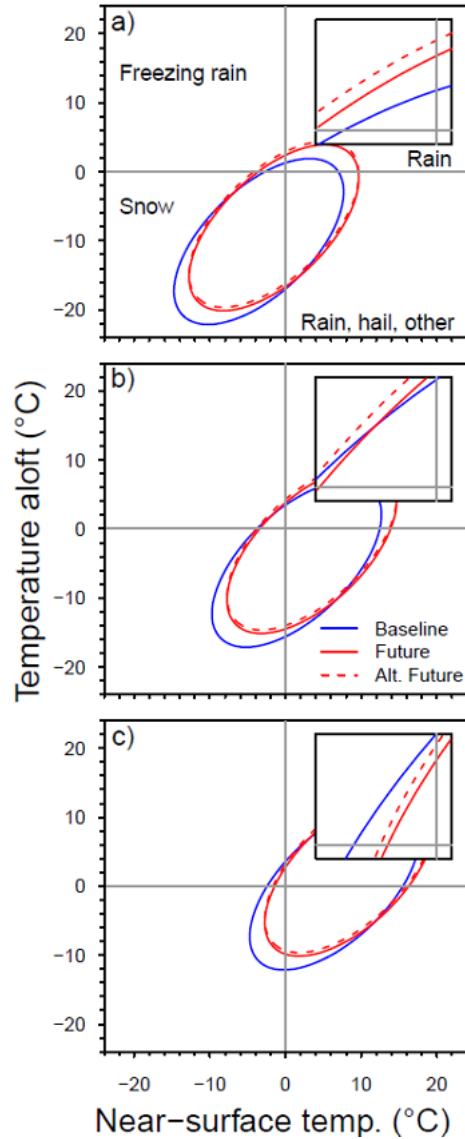
**Figure 1.** Hypothetical response of freezing rain frequency to a warming climate. The regions bounded by the ellipses represent the joint range of near-surface temperature (temp.) and temperature aloft during precipitation above a fixed intensity in a historical baseline period (blue line) and two future periods (solid and dashed red lines). Precipitation becomes freezing rain when near-surface temperatures are below 0°C and temperatures aloft are above 0°C (upper left quadrant). The inset plot magnifies the region near 0°C. Assuming negligible change in the frequency of precipitation, uniformly warming the vertical temperature profile by 2°C (solid red line) can lead to (a) an increase, (b) no change, or (c) a decrease in the frequency of freezing rain if the initial baseline climate is relatively (a) cold, (b) less cold, or (c) warm, respectively. Increasing the near-surface temperature by 2°C and the temperature aloft by 2.5°C (dashed red line) results in a (a and b) more positive and (c) less negative change in frequency compared to the uniformly warmed temperature profile. Source: Rupp et al. 2024.

The frequency of freezing rain is projected to increase over most of Canada and decrease over the southeastern and south-central United States (Cheng et al. 2007, 2011; Lambert and Hansen 2011; Klima and Morgan 2015; Jeong et al. 2018, 2019; McCray et al. 2022). Both increases and decreases in the frequency of freezing rain are projected across the Intermountain West (Jeong et al. 2019, McCray et al. 2022). Projections consistently suggest that near the U.S. Pacific Coast, the frequency of freezing rain mainly will decline (Jeong et al. 2018, McCray et al. 2022). However, future changes in the magnitude or frequency of extreme freezing rain events are less certain. Therefore, we aimed to characterize the spatial distribution of freezing rain and ice accretion across the northern Willamette Basin (Figure 2) during the recent past and to project how freezing rain and ice accretion in the region will respond to climate change.

## Methods

To characterize the spatial distribution of freezing rain and ice loads across the northern Willamette Basin during the recent past, we examined how gap winds influence where freezing rain occurs and simulated where ice will accumulate on power and communication lines. To project how freezing rain and ice accretion in the region will respond to climate change, we simulated ice accretion from freezing rain over the northern Willamette Basin.

We acquired observations of freezing precipitation during the water years 2001–2013 (October 2000–September 2013) from Automated Surface Observing Systems (ASOS) stations at PDX, Salem/McNary Municipal Airport (SLE), Portland–Hillsboro Airport, McMinnville Municipal Airport, Scappoose Industrial Airpark, Portland-Troutdale Airport, Aurora State Airport, and Pearson Airpark, Vancouver. We treated reports of both freezing rain and freezing drizzle as freezing rain, although the number of freezing rain records is far greater. We acquired observations of hourly wind speed and direction from PDX and SLE.

We acquired gridded (~4-km resolution) historical daily minimum temperature and daily precipitation from the PRISM Climate Group (Daly et al. 2008, 2021). We used PRISM data to identify potential biases in the simulated climate.

We used two sets of dynamically downscaled climate model simulations. The first was produced by the National Center for Atmospheric Research with the Weather Research and Forecasting model run at a grid spacing of 4×4 km (Rasmussen and Liu 2017) (Figure 3a). We refer to
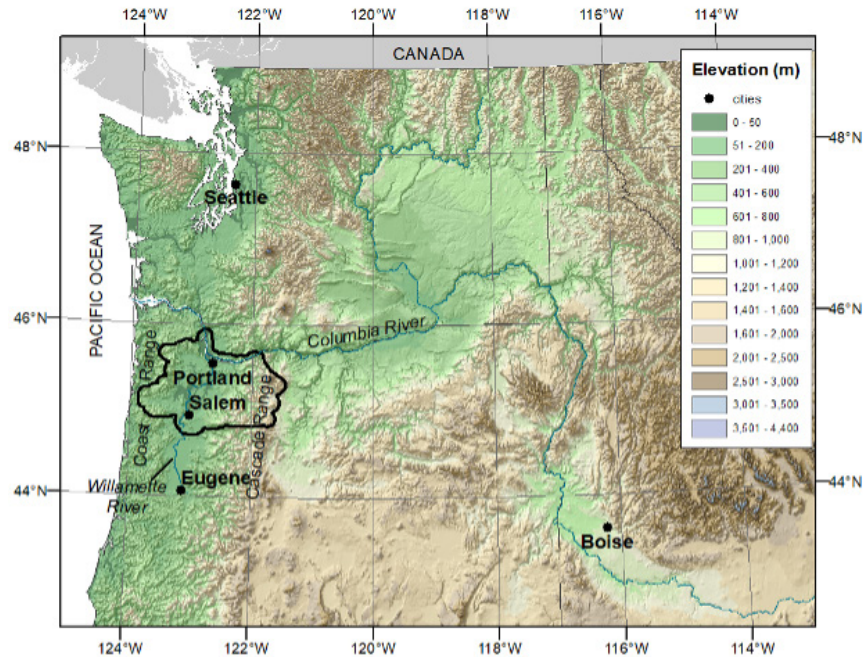


**Figure 2.** Topography of the northwestern United States. The heavy black line indicates the boundary of the study area, which coincides with the service territory of Portland General Electric. Source: Rupp et al. 2024.
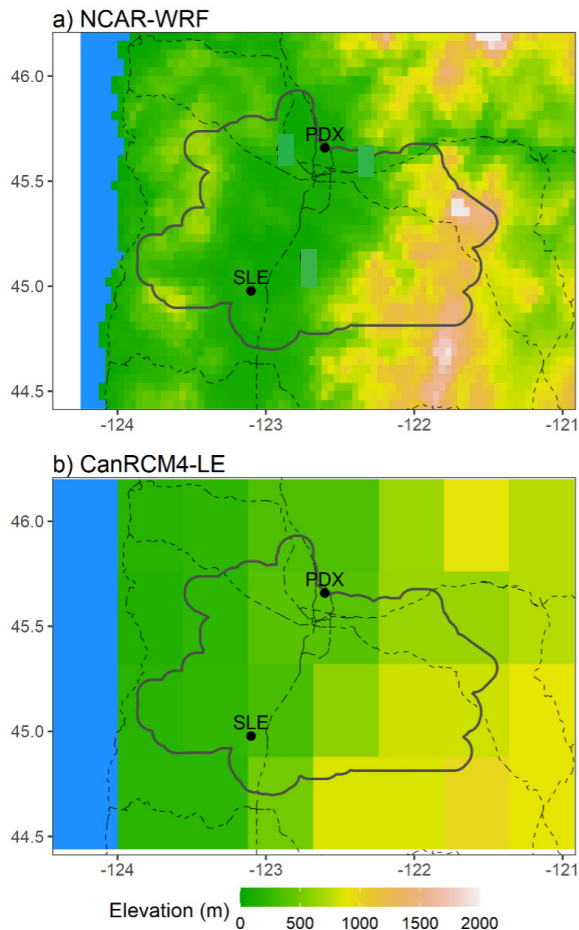


these data as NCAR-WRF. NCAR-WRF includes two simulations (Liu et al. 2017). The first, the control (CTRL) run, is a 13-year (2001–2013 water years) simulation that approximates actual historical weather events. The second, the pseudo-global warming (PGW) run, simulates how historical events might differ if they occurred during the years 2071–2100 under Representative Concentration Pathway (RCP) 8.5 (Meinshausen et al. 2011), which assumes emissions of greenhouse gases continue increasing throughout the twenty-first century. RCP 8.5's relatively large anthropogenic forcing helps to differentiate the regional climate response to climate change from natural variability in the climate system.

**Figure 3.** Surface elevation in and around the study area (heavy gray outline) as represented by (a) the National Center for Atmospheric Research's Weather Research and Forecasting model (NCAR-WRF) with 4×4 km grid spacing and (b) the Canadian Region Climate Model Version 4 Large Ensemble (CanRCM4-LE) with 0.44×0.44º latitude and longitude grid spacing. Dashed lines indicate Interstate and U.S. highways. Points labeled PDX and SLE indicate the locations of the Automated Surface Observing System stations at Portland International and Salem/McNary Municipal airports, respectively. Source: Rupp et al. 2024.

The second set of climate model outputs is the Canadian Regional Climate Model Version 4 Large Ensemble (CanRCM4-LE), which has a grid spacing of about 0.44×0.44° latitude/longitude, or 50×50 km (Figure 3b). CanRCM4-LE consists of an ensemble of 50 simulations, each covering the years 1950–2099 (Scinocca et al. 2016, Jeong et al. 2019). Values of climate variables after 2005 also assumed RCP 8.5.

From each set of model simulations, we acquired outputs of precipitation, near-surface (2-m) air temperature, surface pressure, 10-m zonal (*u*) and meridional (*v*) wind components, and vertical temperature profiles (air temperature versus air pressure). Because some data were missing from the NCAR-WRF PGW run, we excluded January through March 2005 from both the CTRL and PGW runs from our analysis of freezing rain. Because gap winds strongly affect local freezing rain conditions, we compared 10-m winds measured at PDX and SLE with winds simulated by NCAR-WRF in the grid cells with centroids closest to those two stations.

Neither NCAR-WRF nor CanRMC4-LE distinguish freezing rain from other types of precipitation. Therefore, we used the method of Bourgouin (2000) to estimate when precipitation was freezing rain on the basis of the simulated vertical temperature profile. We classified precipitation as either freezing rain or non-freezing rain at three-hour intervals, which corresponded to the finest temporal resolution available for most variables across the model output.

We used the method of Jones (1998) to calculate ice accretion on horizontal cylinders (an approximation of suspended utility cables). Jones (1998) accounted for the role of wind in transporting water droplets to vertically exposed surfaces. We defined an ice event as a period of uninterrupted presence of ice >0.254 mm (0.01 in.) thick. We chose this 0.254 mm threshold because precipitation accumulations below 0.254 mm are typically not measured but reported as a trace amount. We assumed that an ice event began in the first 3-hour period during which the ice thickness exceeded 0.254 mm. Following Jeong et al. (2019), we also assumed that new ice could accumulate on existing ice without melting while the 2-m air temperature was below 1°C. We assumed that ice on the radial surface disappeared completely and instantaneously when the 2-m air temperature exceeded 1°C. Because the temporal resolution of the data is three hours, the minimum duration of an event also was three hours.

## Results

*Comparison of Simulated and Observed Freezing Rain and Winds*

There are few observations against which to evaluate simulated ice accretion. Standardized observations of ice loads from freezing rain on power lines and other structures are rare (Changnon and Creech 2003) and were not available for the study area. Therefore, to evaluate model performance, we focused on the frequency of freezing rain and near-surface wind velocities during freezing rain.

It is difficult to assess the accuracy of modeled freezing rain by directly comparing modeled values to station observations because of vast differences in the spatial and temporal resolution of the model simulations and observational data. As an alternative, we examined the mean annual number of days with freezing rain as a function of elevation. At similar elevations, the observed number of days with freezing rain at the ASOS stations fell within the range of values simulated by NCAR-WRF, although the ASOS values tended to be near the low end of the range. In general, the relation between elevation and the mean annual number of days with freezing rain was positive in NCAR-

WRF, although other factors contributed to the variability in freezing rain across the study area. Because there were few observations across the basin, we could not validate NCAR-WRF's higher frequencies of freezing rain.

Across the study area, including high elevations, consistent with Liu et al. (2017), we found that the NCAR-WRF simulations reproduced the mean annual number of subfreezing days well but simulated too few days with precipitation and tended to generate winds that were weaker than observed, especially easterly winds that accompany freezing rain. However, NCAR-WRF's simulated and the observed freezing rain frequencies were similar at airports, indicating other systematic errors in the simulations may have compensated for the bias in precipitation. In contrast, CanRCM4-LE simulated too few days per year with freezing rain: 0.10 to 0.36 days at elevations below 600 m.

At PDX during freezing rain, observed winds were predominantly east-by-southeasterly, with the strongest winds coming from the east (Figure 4). In contrast, during other periods, the greatest percentage of observed wind directions was northwesterly (300° and 330°), although some strong winds arrived from the south and south-by-southwest. These wind patterns for freezing rain and other weather conditions, although with notably fewer southeasterly winds, also were apparent in the NCAR-WRF simulations. Again, NCAR-WRF tended to generate winds that were weaker than observed, especially easterly winds that accompany freezing rain.

At SLE, observed winds tended to be relatively weak and northerly (between 315° and 45°) during freezing rain, but southerly during all weather conditions (Figure 4). NCAR-WRF also generated
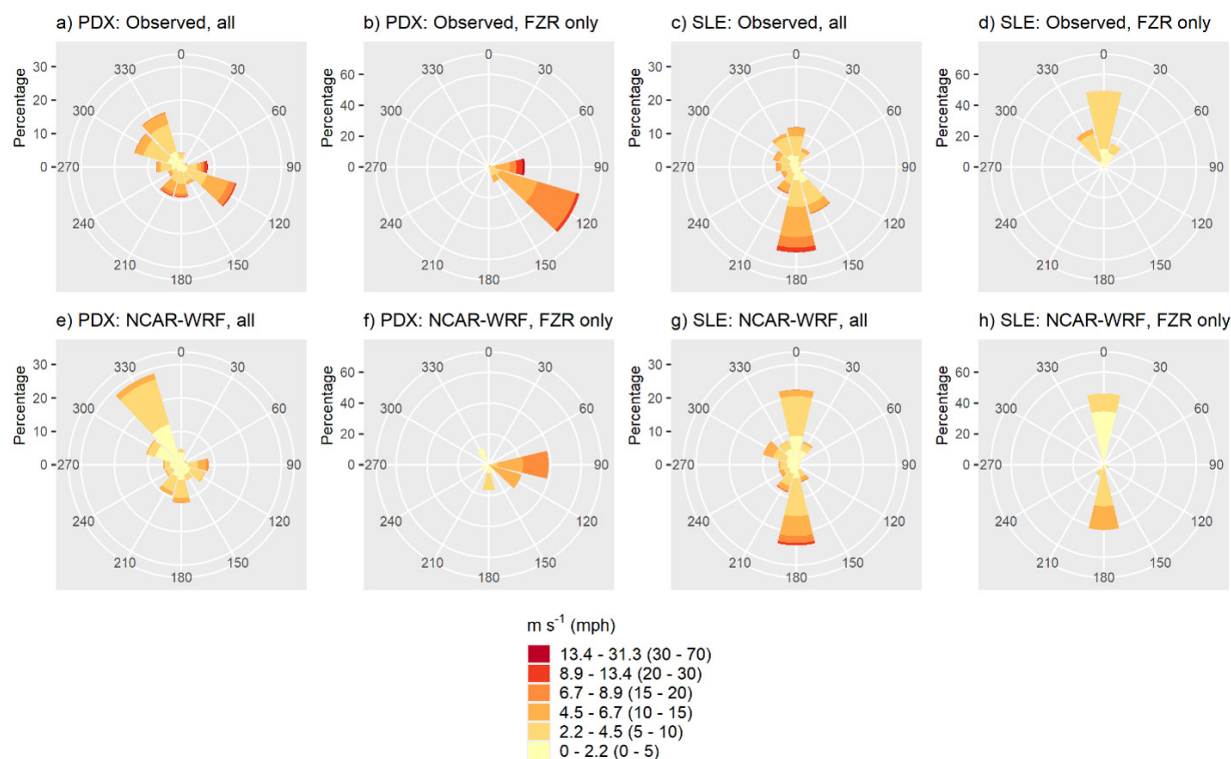


**Figure 4.** Wind roses for observed and simulated (NCAR-WRF) winds at Portland International Airport (PDX) and Salem/McNary Municipal Airport (SLE) during water years 2001–2013 for all weather conditions (all) and freezing rain (FZR) conditions only. The radial axis scale is different for all weather conditions and freezing rain conditions. Source: Rupp et al. 2024.

weak winds during freezing rain, with a roughly equal percentage of northerly and southerly winds. This directional distribution of observed winds at SLE is due to its location within the center of the north-south oriented Willamette Valley.

CanRCM4-LE also simulated distinct differences in wind patterns between periods with and without freezing rain (Figure 5). Within the study area, nearly all CanRCM4-LE freezing rain events were accompanied by easterly winds. The dominant direction of winds during other periods was much more diverse, from southerly to westerly. A direct model pixel-to-station comparison is not informative because CanRCM4-LE cannot simulate the topographic influence on 10-m wind direction at the ASOS stations.

*Projections of Freezing Rain and Radial Ice Accretion*

**NCAR-WRF.** The CTRL run most often produced freezing rain intensities >0.254 mm 3-hr$^{-1}$ on the eastern exposures of the Coast Range and Cascade Range, including the ridges that extend northwest from the mainly north-south oriented Cascade Range (Figure 6a). The valley floor generally had the fewest hours with freezing rain. Higher-intensity freezing rain tended to occur in the same areas that received the greatest number of hours of freezing rain.



**Figure 5.** Wind roses for 10-m winds during (a, c) all weather conditions and (b, d) freezing rain (FZR) conditions for a model pixel in the (a, d) northeastern and (c, d) south-central part of the study area as simulated by CanRCM4-LE for the water years 1971–2020. The radial axis scale is different for all weather conditions and freezing rain conditions. Source: Rupp et al. 2024.

The number of hours with freezing rain intensity >0.254 mm 3-hr$^{-1}$ was lower in the PGW run than in the CTRL run at nearly all locations. The number of hours decreased by at least 75 percent across 45 percent of the study area (Figure 6b,c). Of the few locations with an increased number of hours of freezing rain, most were in the Cascade Range. Across the Willamette Basin study area, the number of hours with freezing rain intensity >0.254 mm 3-hr$^{-1}$ decreased by 66 percent from 2001–2013 to 2071–2100.

At higher intensities of freezing rain, the number of hours of freezing rain increased across relatively more of the study area; the increases were less limited to the Cascade Range and included parts of the valley floor and the eastern slopes of the Coast Range. Above freezing rain intensities of 10 mm (0.4 in.) 3-hr$^{-1}$, the number of hours with freezing rain increased by 22 percent from 2001–2013 to 2071–2100 across the study area.

The CTRL run most often produced radial ice accretions thicker than a trace (0.254 mm) in the same locations where it produced the most freezing rain (Figure 7a). However, areas more directly downwind from the Gorge tended to accumulate more ice than other locations at which the number of hours with freezing rain was similar (Figure 8a). Areas most exposed to gap winds also

**Figure 6.** Total number of hours during which **freezing rain intensity** exceeded 0.254 mm 3-hr$^{-1}$ from October 2000—September 2013 in the (a) NCAR-WRF control (CTRL) and (b) pseudo-global warming (PGW) runs, and (c) the relative difference between those runs. Dashed lines indicate Interstate and U.S. highways. Source: Rupp et al. 2024.
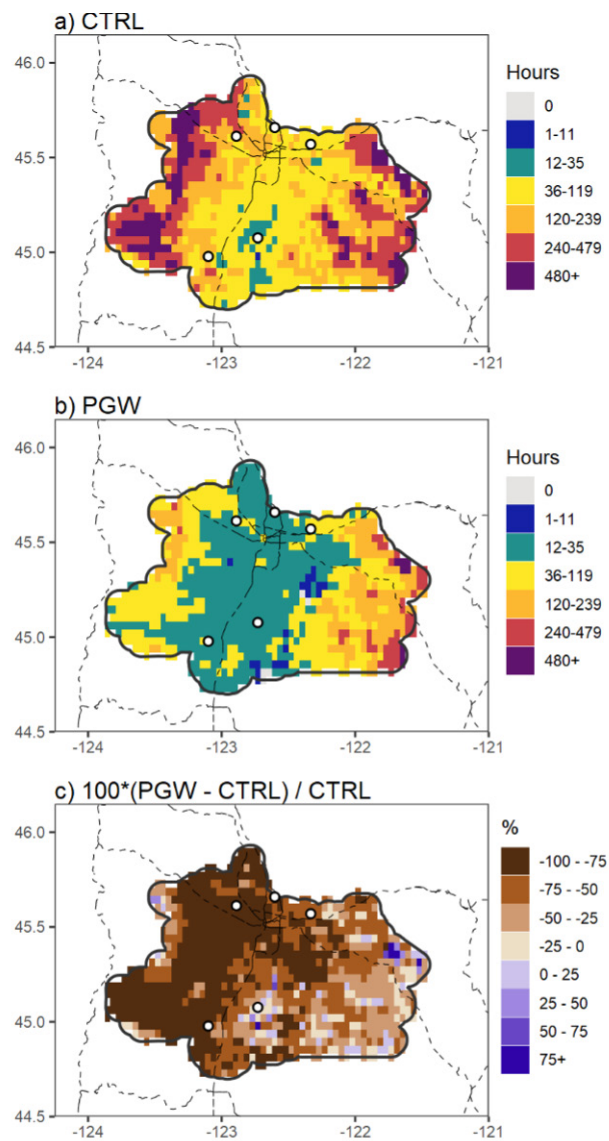
**Figure 7.** Total number of hours during which **simulated radial ice thickness** exceeded 0.254 mm from October 2000—September 2013 in the (a) NCAR-WRF control (CTRL) and (b) pseudo-global warming (PGW) runs, and (c) the relative difference between those runs. Dashed lines indicate Interstate and U.S. highways. Source: Rupp et al. 2024.

accumulated some of the largest amounts of ice; most of the area with ice thicknesses >10 mm was limited to a band extending from the Gorge westward through the eastern Portland area.

The relative changes from the CTRL to the PGW run in the number of hours with ice thicker than a trace largely reflected the changes in number of hours of freezing rain across the study area, with decreases in the number of hours of ice over a large majority of the study area (Figure 9b,c). At the regional level, the number of hours with ice thicker than a trace decreased by 65 percent from 2001–2013 to 2071–2100.

As ice became thick, increases in the number of hours of ice were more widespread across the study area (Figure 8c). Most of the increase in hours with ice thickness >10 mm occurred in a band from
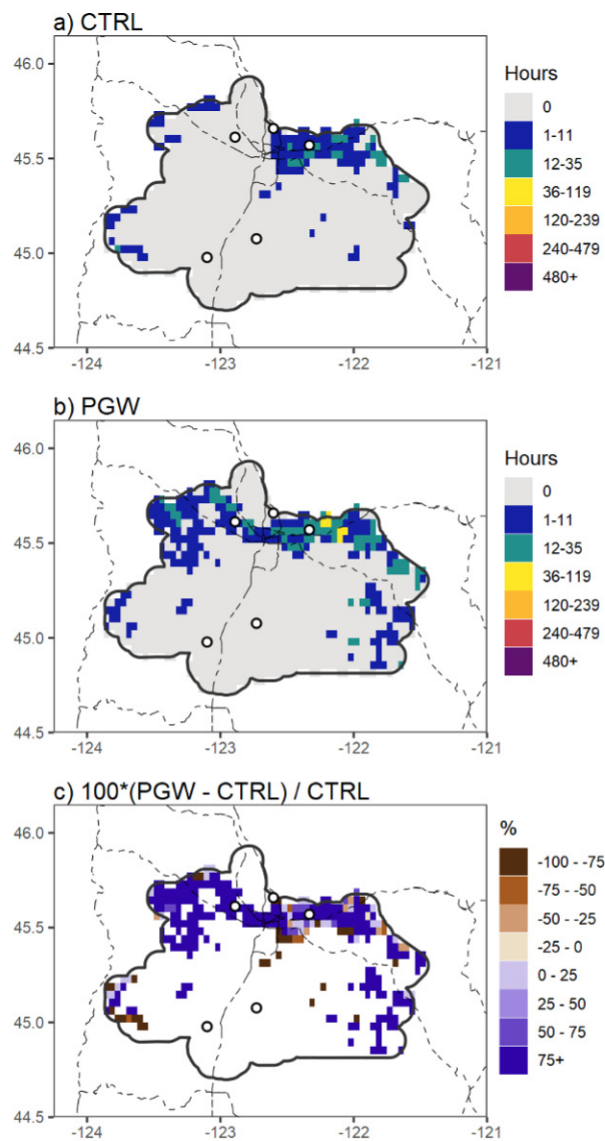
**Figure 8.** Total number of hours during which simulated radial ice thickness exceeded 10 mm from October 2000–September 2013 in the (a) NCAR-WRF control (CTRL) and (b) pseudo-global warming (PGW) runs, and (c) the relative difference between the CTRL and PGW runs. Dashed lines indicate Interstate and U.S. highways. Source: Rupp et al. 2024.

the Gorge to the Coast Range (Figure 8b,c). The number of hours of ice thickness >10 mm was 2.5 times greater in the PGW run than in the CTRL run.

Only a few simulated storms produced ice thickness >10 mm. In the CTRL run, the storm with by far the greatest ice accretion occurred from 5–8 January 2004. Ice thickness exceeded 10 mm across 8 percent of the study area and was thickest in the eastern Portland metropolitan area and east toward the Gorge, on the northeast side of Mt. Hood, and in several locations along the Coast Range (Figure 9a). Ice thicker than at least a trace accumulated across all but the southeastern study area. At the pixel closest to PDX, ice accumulated for 15 hours. The PGW run for the same dates yielded higher maximum ice accumulation than the CTRL run, with ice thickness >10 mm over 16 percent of the study area (Figure 9b).

In the Portland metropolitan area, the actual storm that occurred from 5–8 January 2004 delivered over 25.4 mm (1 in.) of freezing rain in some locations and wind gusts exceeding 31 m s$^{-1}$ (70 mph), and led to the closure of Portland International Airport for two days for the first time in its history (Nelson 2004). PDX reported freezing rain on 6 and 7 January 2004.

The second largest amount of radial ice accretion in the CTRL run occurred from 17–20 December 2005, with 4 percent of the study area accumulating >10 mm of ice. The magnitude and spatial extent of this storm were similar between the CTRL and PGW runs.

A series of winter storms in December 2008 had the second-greatest ice accretion in the PGW run, although relatively little ice accreted in the CTRL run during the same period (Figure 9c,d). In the CTRL run, these storms yielded ice thickness >10 mm across less than 1 percent of the study area (Figure 9c). By contrast, in the PGW run, the storms led to ice thickness >10 mm across 11 percent of the study area (Figure 8d). The difference between the runs likely reflects that some of the precipitation that fell as snow in the CTRL run fell as freezing rain in the PGW run. In reality, three successive storms in December 2008 led to major disruptions of travel and electricity supply because of snow accumulation. Snow accumulation was greatest from 20–22 December, followed by thawing and refreezing, and probably freezing rain (Le Comte 2009, Williams 2018).
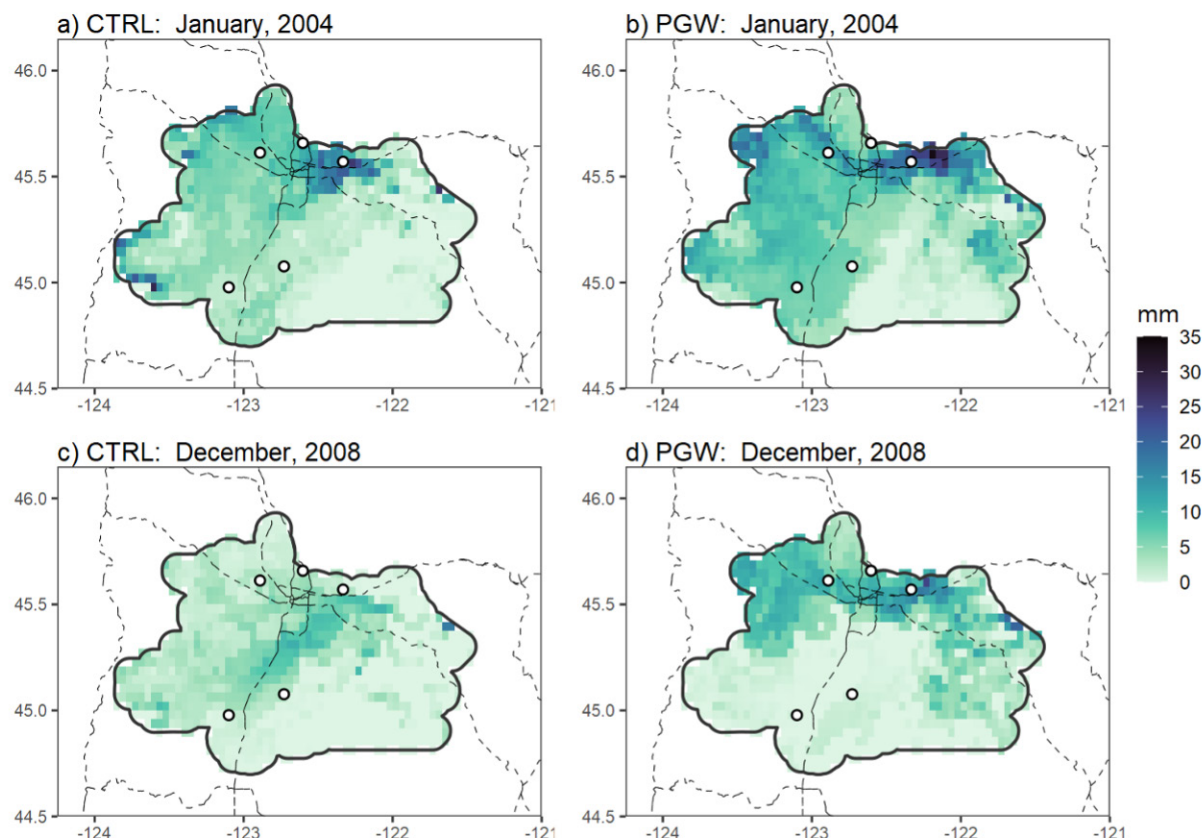
**Figure 9.** Maximum radial ice thickness during (a, b) 5–8 January 2004 and (c, d) 13–31 December 2008 as simulated in the (a, c) NCAR-WRF control (CTRL) and (b, d) pseudo-global warming (PGW) runs. Dashed lines indicate Interstate and U.S. highways. Source: Rupp et al. 2024.

**CanRCM4-LE.** CanRCM4-LE simulated a wide range of number of hours of freezing rain across the study area, from as few as 4 hr decade$^{-1}$ to as many as 53 hr decade$^{-1}$, with average freezing rain intensity $>0.254$ mm 3-hr$^{-1}$ during a baseline period (water years 1951–2000). Freezing rain tended to occur more often in areas with a colder climate (Figure 10a,b).

Changes in the number of hours of freezing rain from a baseline to a future period (water years 2050–2099) ranged from negative to positive across the study area (Figure 10c). At freezing rain intensities $>0.254$ mm 3-hr$^{-1}$, the number of hours increased by 5–40 percent in the colder half of the study area and decreased by 8–39 percent in the warmer half. At higher freezing rain intensities ($>2.54$ mm 3-hr$^{-1}$), the number of hours of freezing rain increased in only the coldest 25 percent of the study area.

The patterns of accretion of ice greater than a trace (0.254 mm) and freezing rain were similar: ice accreted more often in colder areas (Figure 11a), and the number of hours with at least a trace of ice increased from the baseline to the future period over the colder half of the study area (Figure 11c).

Above progressively thicker ice thresholds, the area in which the number of hours with ice increased grew to encompass the colder 88 percent of the study area (Figure 11c). Net changes in the number of hours of ice over the entire study area were positive, and the increases became greater as ice became thicker. For example, the number of hours increased by 57 percent and 204 percent for ice thicker than 2.54 mm and 10 mm, respectively.
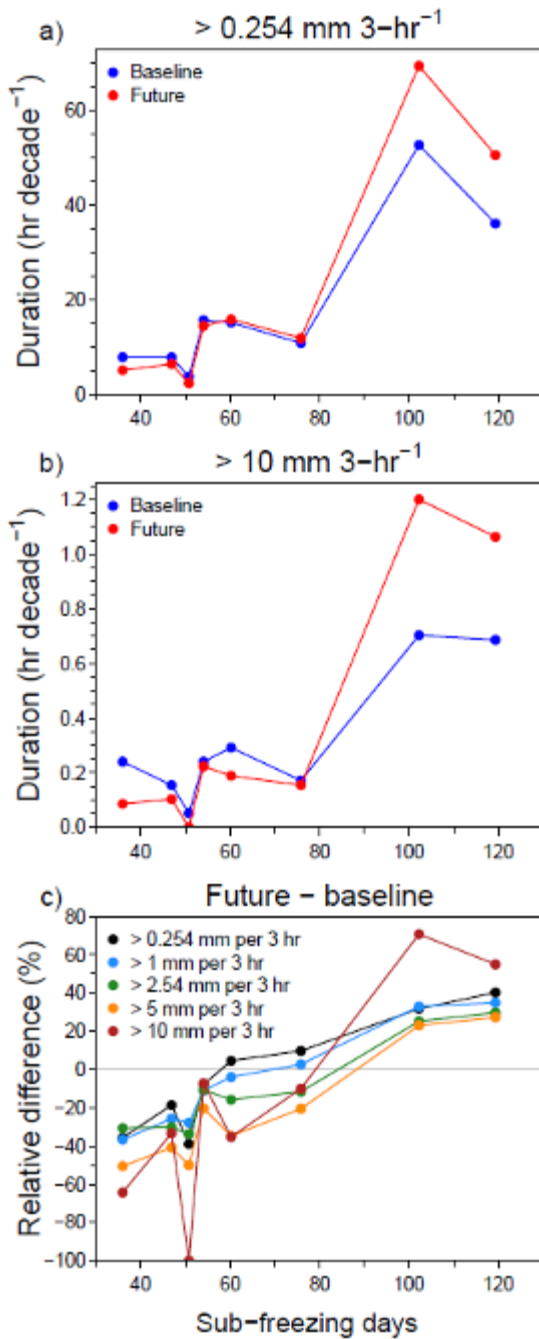
**Figure 10.** Baseline (water years 1951-2000) and future (water years 2050–2099) average duration (hr decade$^{-1}$) during which CanRCM4-LE simulated **freezing rain intensity** above (a) 0.254 mm 3-hr$^{-1}$ and (b) 10 mm 3-hr$^{-1}$ versus the baseline mean annual number of days with daily minimum 2-m temperature below 0°C, and (c) the relative difference between the future and baseline periods in the duration of intensities exceeding 0.254–10 mm 3-hr$^{-1}$. Only the eight pixels within the study area are shown. Source: Rupp et al. 2024.
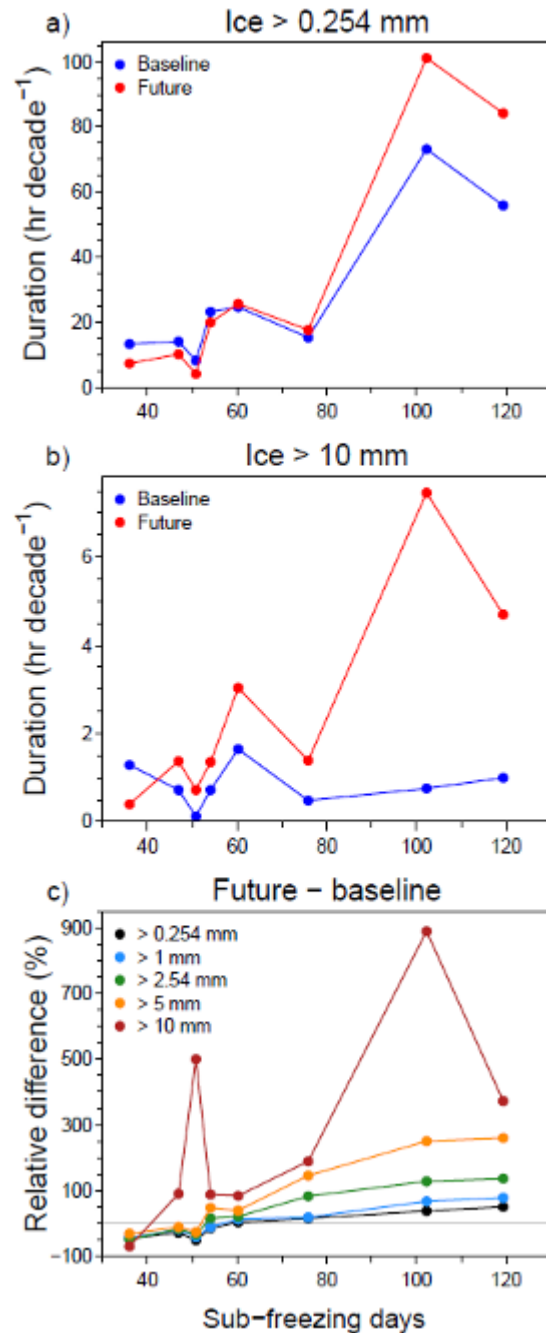
**Figure 11.** Baseline (water years 1951–2000) and future (water years 2050–2099) average duration (hr decade$^{-1}$) during which CanRCM4-LE simulated **radial ice** thicker than (a) 0.254 mm and (b) 10 mm versus the baseline mean annual number of days with daily minimum 2-m temperature below 0°C, and (c) the relative difference between the future and baseline periods in the duration of ice thicker than 0.254–10 mm. Only the eight pixels within the study area are shown. Source: Rupp et al. 2024.

**Discussion**

*Drivers of Changes in Freezing Rain and Ice Accretion*

As noted above, in a warming climate, the change in the frequency of freezing rain is driven largely by two opposing factors: a decreasing frequency of the requisite near-surface conditions and an increasing frequency of the requisite conditions aloft. The net effect is that in a location that is becoming warmer, but has a sufficiently cold baseline climate, the frequency of freezing rain initially will increase, then reach a threshold beyond which it decreases. Consistent with this effect, the number of hours of freezing rain in both NCAR-WRF (Figure 6c) and CanRCM4-LE (Figure 10c) generally increased in cooler baseline climates and decreased in warmer baseline climates.

However, this simple response to warming (e.g., Figure 1) does not explain all of the spatial variability in projected changes in future freezing rain frequency, particularly in NCAR-WRF. Although the number of hours of freezing rain >0.254 mm 3-hr$^{-1}$ decreased considerably in most of the warmer and lower elevation areas and decreased slightly or increased in cooler areas such as the crest of the Coast Range and much of the Cascade Range, smaller decreases or even increases occurred in some low-elevation areas (Figure 6c).

Changes in winds can also affect where and when freezing rain occurs and the rate at which water droplets are transported to vertically exposed frozen surfaces. In NCAR-WRF, gap winds exiting the Gorge were stronger during freezing rain in the PGW run than in the CTRL run. Further west, the stronger gap winds resulted in a greater frequency and intensity of easterly winds. Further south in the Willamette Basin, northerly winds were stronger and more frequent, presumably influenced by the stronger gap winds. Over the study area and irrespective of direction, winds speeds <4.5 m s$^{-1}$ occurred 15 percent less often, whereas the frequency of winds >4.5 m s$^{-1}$ more than doubled. The winds in CanRCM4-LE also were more easterly during freezing rain in the future than in the baseline period and were stronger: the frequency of winds <4.5 m s$^{-1}$ decreased by 19 percent, whereas the frequency of winds >4.5 m s$^{-1}$ increased by 10 percent.

Strong gap winds, more than weak gap winds, contribute to creating and maintaining favorable conditions for freezing rain. Stronger gap winds can more readily produce subfreezing near-surface conditions below a westerly intrusion of warmer (>0°C) marine air, made yet warmer by global warming. Stronger gap winds also can expand the area of freezing rain conditions by pushing cold air further west and south into the Willamette Basin. By increasing the duration of subfreezing near-surface conditions, stronger gap winds can cause ice to persist longer. Across the study area, NCAR-WRF simulated a 24 percent increase (from 9.2 to 11.3 hours) in the mean duration of ice events between the CTRL and PGW runs, and CanRCM4-LE simulated a 30 percent increase (8.8 to 11.4 hours) in the mean duration of ice events between the baseline and future periods.

The direct cause of the stronger easterly wind during freezing rain in future projections is likely a stronger pressure gradient across the Cascade Range. However, climate models do not suggest that this pressure gradient, nor easterly winds, will become stronger in general. Instead, weaker easterly winds are less likely to cool basin temperatures below freezing, and stronger gradients will be necessary for freezing rain to occur. As a result, weak-wind freezing rain events will become less frequent while strong-wind freezing rain events will become relatively (if not absolutely) more common. Moreover, temperatures east of the Cascade Range will become warmer on average, so only the more extreme precursor conditions will bring sufficiently cold air and sufficiently high mesoscale pressures to the Columbia Basin.

A change in the distribution of precipitation intensity also can change the frequency of freezing rain. The frequency of precipitation events is not projected to change appreciably in response to increases in temperature, but an increase in the relative proportion of precipitation events with high intensities is anticipated globally (Allen and Ingram 2002, O'Gorman 2015) and in Oregon (Rupp et al. 2022, *Projected Changes in Oregon Precipitation*, this volume). However, it is not apparent that the frequency of high-intensity freezing rain events will increase given that freezing rain occurs within a relatively narrow range of temperatures, and this range will not change much in a warmer climate.

Projected changes in the frequency distribution of freezing rain intensities were inconsistent between NCAR-WRF and CanRCM4-LE. Freezing rain intensities tended to be higher in the NCAR-WRF PGW run than in the CTRL run. For example, the relative frequency of freezing rain intensities >2.54 mm 3-hr$^{-1}$ was 60 percent greater in the PGW run than in the CTRL run, whereas the frequency of intensities ≤2.54 mm 3-hr$^{-1}$ was relatively lower. CanRCM4-LE, however, had the opposite pattern: the relative frequency of freezing rain intensities >2.54 mm 3-hr$^{-1}$ was 9 percent lower in the future whereas intensities ≤2.54 mm 3-hr$^{-1}$ were relatively more common. Differences in experimental design or climate model resolution may underlie this inconsistency.

*Limitations*

The ability to accurately simulate freezing rain and ice accretion in complex terrain requires models with high horizontal and vertical resolution. Although the Gorge is reasonably well resolved in NCAR-WRF at 4×4 km, running a different weather model over a range of resolutions suggested that a grid cell size smaller than 1.4×1.4 km is required for air to flow fully through the Gorge without passing over the Cascade Range during gap wind events (Sharp and Mass 2002). Accordingly, we suspect that the speed of the gap winds simulated by NCAR-WRF is unrealistically low and therefore that our analysis underestimates their role in the development of freezing rain and ice accumulation. At the much coarser resolution of CanRCM4-LE, the Gorge is represented by a wide, high-elevation pass that does not drain the Columbia Basin cold-air pool (Sharp and Mass 2002). This simulated pass still allows easterly flow from the east side of the Cascade Range into the northern Willamette Basin. However, an improperly resolved basin along with the lower vertical resolution of the modeled atmosphere means that results of CanRCM4-LE should be interpreted as a response to global warming over a larger extent that lacks fine-resolution geography relevant to the Willamette Basin. The results of CanRCM4-LE are not an estimate of how the response across larger areas interacts with local features, such as the Columbia Gorge, to affect future freezing rain.

Uncertainty also arises from the methods used to calculate freezing rain and radial ice accretion. Several methods exist for diagnosing freezing rain and calculating ice accretion on cylinders, although we limited our study to one method for each because of resource constraints. We suggest that further work include a sensitivity analysis of multiple methods for diagnosing freezing rain and simulating ice accretion under projected changes in climate.

**Conclusions**

Much of the response of freezing rain to global warming can be explained by two opposing factors: a decrease in the frequency of the requisite subfreezing (<0°C) near-surface air temperature and an increase in the frequency of the requisite above-freezing (>0°C) air temperature aloft. The net effect of these opposing factors depends on the initial temperature of a given location. The frequency of freezing rain will increase in initially colder locations and decrease in initially warmer locations.

In the future, intensified gap winds are more likely to establish the necessary vertical temperature profile for freezing rain, even as the Willamette Basin becomes warmer. Therefore, future freezing rain events are expected to be accompanied by stronger easterly winds. Exposure to stronger winds, especially easterly winds, leads to additional radial ice accretion on cables and other structures from the increased horizontal transport of water droplets. Stronger low-level easterly gap winds through the Columbia River Gorge can also maintain subfreezing near-surface temperatures for a longer period during which freezing rain can occur and ice can accumulate and persist. The consistency of projected stronger easterly winds from both higher and lower resolution models implies that stronger easterly winds during future freezing rain is not limited to the gap winds but is a regional, if not more widespread, result of global warming.

## Acknowledgments

## Literature Cited

Allen, M.R., and W.J. Ingram. 2002. Constraints on future changes in climate and the hydrologic cycle. Nature 419:228–232.

Bernstein, B.C. 2000 Regional and local influences on freezing drizzle, freezing rain, and ice pellet events. Weather and Forecasting 15:485–508.

Bourgouin, P. 2000. A method to determine precipitation types. Weather and Forecasting 15:583–592.

Changnon, S.A. 2003. Characteristics of ice storms in the United States. Journal of Applied Meteorology and Climatology 42:630–639.

Changnon, S.A., and T.G. Creech. 2003. Sources of data on freezing rain and resulting damages. Journal of Applied Meteorology and Climatology 42:1514–1518.

Cheng, C.S., H. Auld, G. Li, J. Klaassen, and Q. Li. 2007. Possible impacts of climate change on freezing rain in south-central Canada using downscaled future climate scenarios. Natural Hazards and Earth System Sciences 7:71–87.

Cheng, C.S., G. Li, and H. Auld. 2011. Possible impacts of climate change on freezing rain using downscaled future climate scenarios: updated for eastern Canada. Atmosphere-Ocean 49:8–21.

Cortinas, J.V., Jr., B.C. Bernstein, C.C. Robbins, and J.W. Strapp. 2004. An analysis of freezing rain, freezing drizzle, and ice pellets across the United States and Canada: 1976–90. Weather and Forecasting 19:377–390.

Daly, C., M. Halbleib, J.I. Smith, W.P. Gibson, M.K. Doggett, G.H. Taylor, J. Curtis, and P.P. Pasteris. 2008. Physiographically sensitive mapping of climatological temperature and precipitation across the conterminous United States. International Journal of Climatology 28:2031–2064.

Daly, C., et al. 2021. Challenges in observation-based mapping of daily precipitation across the conterminous United States. Journal of Atmospheric and Oceanic Technology 38:1979–1992.

Groisman, P.Y., O.N. Bulygina, X. Yin, R.S. Vose, S.K. Gulev, I. Hanssen-Bauer, and E. Førland. 2016. Recent changes in the frequency of freezing precipitation in North America and Northern Eurasia. Environmental Research Letters 11:045007. https://doi.org/10.1088/1748-9326/11/4/045007.

Houston, T.G., and S.A. Changnon. 2007. Freezing rain events: a major weather hazard in the conterminous US. Natural Hazards 40:485–494.

Jeong, D.I., A.J. Cannon, and X. Zhang. 2019. Projected changes to extreme freezing precipitation and design ice loads over North America based on a large ensemble of Canadian regional climate model simulations. Natural Hazards and Earth System Sciences 19:857–872.

Jeong, D.I., L. Sushama, M.J.F. Vieira, and K.A. Koenig. 2018. Projected changes to extreme ice loads for overhead transmission lines across Canada. Sustainable Cities and Society 39:639–649.

Jones, K.F. 1998. A simple model for freezing rain ice loads. Atmospheric Research 46:87–97.

Klima, K., and M.G. Morgan. 2015. Ice storm frequencies in a warmer climate. Climatic Change 133:209–222.

Lambert, S.J., and B.K. Hansen. 2011. Simulated changes in the freezing rain climatology of North America under global warming using a coupled climate model. Atmosphere-Ocean 49:289–295.

Le Comte, D. 2009. U.S. weather highlights 2008: winter wins. Weatherwise 62:14–21.

Liu, C., et al. 2017. Continental-scale convection-permitting modeling of the current and future climate of North America. Climate Dynamics 49:71–95.

McCray, C.D., E.H. Atallah, and J.R. Gyakum. 2019. Long-duration freezing rain events over North America: regional climatology and thermodynamic evolution. Weather and Forecasting 34:665–681.

McCray, C.D., D. Paquin, J.M. Thériault, and É. Bresson. 2022. A multi-algorithm analysis of projected changes to freezing rain over North America in an ensemble of regional climate model simulations. Journal of Geophysical Research: Atmospheres 127:e2022JD036935. https://doi.org/10.1029/2022JD036935.

Meinshausen, M., et al. 2011. The RCP greenhouse gas concentrations and their extensions from 1765 to 2300. Climatic Change 109:213. https://doi.org/10.1007/s10584-011-0156-z.

Nelson. M. 2004. Portland's January 2004 snow / ice storm—the failure of mesoscale models. American Meteorological Society, New Orleans, Louisiana.

O'Gorman, P.A. 2015. Precipitation extremes under climate change. Current Climate Change Reports 1:49–59.

Rasmussen, R., and C. Liu. 2017. High resolution WRF simulations of the current and future climate of North America. Research Data Archive, National Center for Atmospheric Research, Computational and Information Systems Laboratory, Boulder, Colorado.

Robbins, C.C., and J.V. Cortinas. 2002. Local and synoptic environments associated with freezing rain in the contiguous United States. Weather and Forecasting 17:47–65.

Rupp, D.E., L.R. Hawkins, S. Li, M. Koszuta, and N. Siler. 2022. Spatial patterns of extreme precipitation and their changes under ~ 2 °C global warming: a large-ensemble study of the western USA. Climate Dynamics 59:2363–2379.

Rupp, D.E., S. Li, P.W. Mote, K.M. Shell, N. Massey, S.N. Sparrow, D.C.H. Wallom, and M.R. Allen. 2017. Seasonal spatial patterns of projected anthropogenic warming in complex terrain: a modeling study of the western US. Climate Dynamics 48:2191–2213.

Rupp, D.E., L.W. O'Neill, E. Fleishman, P.C. Loikith, and D. Loomis. 2024. Response of gap wind-driven freezing rain and ice accretion to global warming. Climate Dynamics 62:807–827.

Scinocca, J.F., V.V. Kharin, Y. Jiao, M.W. Qian, M. Lazare, L. Solheim, G.M. Flato, S. Biner, M. Desgagne, and B. Dugas. 2016. Coordinated global and regional climate modeling. Journal of Climate 29:17–35.

Sharp, J., and C.F. Mass. 2002. Columbia Gorge gap flow: insights from observational analysis and ultra-high-resolution simulation. Bulletin of the American Meteorological Society 83:1757–1762.

Sharp. J., and C.F. Mass. 2004. Columbia Gorge Gap winds: their climatological influence and synoptic evolution. Weather and Forecasting 19:970–992.

Williams, K. 11 December 2018. 10 years later: the 2008 blizzard that walloped Portland (photos). The Oregonian/OregonLive. www.oregonlive.com/news/erry-2018/12/0e131ca88d8678/10-years-later-the-2008-blizza.html.

# Oregon Drought History and Twenty-First Century Projections

Larry W. O'Neill, Matthew Koszuta, Nick Siler, and Erica Fleishman

## Introduction

There are many conceptual and quantitative definitions of drought (Wilhite and Glantz 1985, Rasmussen et al. 1993), some of which are objective and some of which are subjective. The simplest definition of drought is insufficient water to meet demand (Redmond 2002, Swann 2018). However, the precise definition of drought depends on the location and context. Meteorological drought traditionally has been defined just by lack of precipitation, but is better defined as evaporative demand that exceeds precipitation over a prolonged period. Hydrological drought occurs when extended periods of meteorological drought affect surface water supply or soil moisture, and is most consequential for society when water supply does not meet human demand. Meteorological and hydrological drought are driven by physical factors and do not describe impacts on humans or ecosystems. Several other types of drought are defined on the basis of their effects on particular components of human and natural systems. For example, agricultural drought occurs when lack of surface or subsurface water supply adversely affects agricultural production.

Another noteworthy type of drought is flash drought. Flash droughts, which occasionally occur throughout Oregon (Pendergrass et al. 2020, Otkin et al. 2022), are characterized by rapid-onset periods of elevated surface temperatures, low relative humidities, precipitation deficits, and rapid declines in soil moisture. These conditions often occur in Oregon during heat waves in late spring and summer, and the adverse impacts of flash drought can emerge in as little as a week (Mo and Lettenmaier 2015, Rupp et al. 2017).

The conceptual definition of drought is insufficient to define drought severity in operational or research applications. Drought severity is a metric that incorporates both drought duration and intensity relative to historical conditions at a given location. Therefore, the dependence of drought severity and extent on variability in historical weather, climate, and soil moisture is a major consideration in classifying drought. This dependence has led to the use of long-term meteorological observations, mainly precipitation and temperature, to estimate surface water balances and, in turn, drought severity and extent. Additional long-term measurements of streamflow, snow water equivalent (the amount of water contained in the snowpack), and soil moisture content augment assessment of drought severity with information on availability of surface water. These physical indicators of drought are used for a variety of purposes, including operational drought assessment and research on drought variability due to climate variability and change.

In North America, operational drought is assessed through weekly updates of the U.S. Drought Monitor (Svoboda et al. 2002) and monthly updates of the North American Drought Monitor (Lawrimore et al. 2002). Both drought monitors synthesize multiple physical indicators of drought severity, extent, and duration into a classification of current drought conditions. Most of the indicators are meteorological or hydrological (e.g., precipitation, snow water equivalent, streamflow, soil moisture, shallow groundwater, and evapotranspiration). Drought is classified through a confluence of indicators, an approach in which assignment to a given drought class is supported by multiple indicators. For instance, determination of a drought class in a particular area may be supported by concurrent observations of unusually low precipitation, streamflows, and soil moisture and unusually high evaporation. The result is a national map of drought severity that differentiates short-term drought (duration typically less than six months) from long-term drought (duration

typically greater than six months). The U.S. Drought Monitor's classification is among the criteria for consideration of administrative drought declarations, such as emergency drought declarations issued at the county level by the governor of Oregon or drought declarations issued by the U.S. Department of Agriculture to trigger financial relief and crop insurance programs for agricultural and livestock producers. Administrative drought declarations are based not only on the existence of drought, but its social and economic impacts. These impacts may include shortages of water for municipal use, irrigation, livestock rearing, and other social and economic priorities. Although social and economic impacts are commonly considered in administrative drought declarations, they are not formally considered in the U.S. Drought Monitor drought depiction.

Here, we review historical drought occurrences in Oregon on the basis of common meteorological and hydrological drought indices used in operational monitoring and research applications. We also present drought projections for Oregon on the basis of downscaled climate model simulations for the twenty-first century.

## Defining Drought

Conceptual definitions of drought, although useful, cannot fully describe the duration and intensity of drought. Diverse physical indices have been used to quantify drought. The indices that describe meteorological drought are based on standard meteorological observations, mainly precipitation and temperature, or an estimate of evaporative water loss. Streamflow observations are also used to assess hydrological drought at the watershed level, and observations of snow water equivalent are used in snowmelt-dominated basins. Drought indices that are based on meteorological observations are intended to represent simplified balances between precipitation input and evaporative losses, whereas those that use streamflow and snowpack observations aim to represent water availability.

Three drought indices commonly are used to quantify drought severity and extent in the western United States, especially Oregon. The Standardized Precipitation Index (SPI) quantifies precipitation deficits and surpluses over multiple temporal extents that reflect the availability of water while accounting for differences in regional climate (McKee et al. 1993, Edwards and McKee 1997). The SPI skillfully determines drought in northwest Oregon that is caused by precipitation deficits (Keyantash and Dracup 2002). The SPI calculation fits long-term precipitation records to a probability distribution and then transforms the values into a Gaussian (or normal) distribution with zero mean and unit variance. This method allows precipitation departures from the mean value to be compared across seasons at a given location or across regions with different climates. For instance, January precipitation that is one inch below normal has a much different effect on people living near coastal Newport (which receives about 80 inches of precipitation per year) than inland near Bend or Burns (which receive less than 15 inches of precipitation per year). Positive SPI values indicate greater than mean precipitation over the period of interest, whereas negative values indicate less than mean precipitation over the period of interest.

The U.S. Drought Monitor's drought classes are based in part on ranges of SPI values that align with the expected frequency of drought occurrence. The least severe drought class, moderate drought (D1), corresponds to an SPI of -0.8 to -1.29, and is expected to occur, on average, ten percent of the time. Severe drought (D2) corresponds to an SPI of -1.3 to -1.59, and is expected to occur five percent of the time. Extreme drought (D3) corresponds to an SPI of -1.6 to -1.99, and is expected to occur three percent of the time. The class corresponding to the most intense drought, exceptional drought (D4), corresponds to an SPI less than -2, and is expected to occur less than two percent of

the time. Accordingly, drought (D1–D4) is expected to occur at a given location in approximately 20 percent of time periods. A classification of abnormally dry (D0) is not a formal drought designation. It corresponds to an SPI of -0.5 to -0.79, and is expected to occur ten percent of the time.

However effectively the SPI captures water input from precipitation, it does not account for variation in evaporative losses or runoff. Therefore, the SPI does not account for the supply and demand concept of surface water availability. Neglecting these losses can lead to miscategorization of drought conditions, particularly in climates with well-defined wet and dry seasons, such as those experienced in Oregon, and in climates driven by unusually high evaporation.

The dimensionless Standardized Precipitation-Evapotranspiration Index (SPEI; Vicente-Serrano et al. 2010) improves on the SPI by incorporating estimates of surface evaporative loss, thereby providing a more accurate measure of variations in surface water availability. The SPEI is a primary metric used operationally to assess the existence and severity of meteorological and hydrological drought, especially in the western United States. The SPEI compares the net water balance between precipitation and potential evapotranspiration (evapotranspiration from a large area with uniform vegetation and unlimited soil water) between a recent and a historical period of time (Vicente-Serrano et al. 2010). The SPEI allows for evaluation of drought severity in different locations and time periods, identification of different drought types (Ahmadalipour et al. 2017), and consideration of the role of evapotranspiration in drought. SPEI over the preceding 12 months (SPEI12) is a reliable predictor of annual streamflow in the Pacific Northwest in rainfall-dominated watersheds (Abatzoglou et al. 2014, Peña-Gallardo et al. 2019) and of water levels in lakes and reservoirs (McEvoy et al. 2012). Consequently, the SPEI at extents from 3 to 24 months is a key indicator of drought severity and extent in the U.S. Drought Monitor for Oregon.

Calculation of the SPEI is similar to calculation of the SPI, but is based on the difference (D) between precipitation (P) and potential evapotranspiration (PET). Few direct observations of PET are available to compute SPEI. As a result, numerous approximations have been developed to estimate PET. Similar to the SPI calculation, monthly average D is fit to a probability distribution function, then transformed to a normal distribution (Hosking 1990, Beguería et al. 2014) in a manner that allows for comparison of drought across time and space. The same ranges of SPEI and SPI values correspond to the same U.S. Drought Monitor classes (D0–D4). Given the sparseness of direct PET observations, approximate evapotranspiration estimates (described below) have been developed to use available weather data.

The Standardized Streamflow Index (SSI) is often used to depict streamflow-based hydrological drought from stream gage data, particularly in research (e.g., Modarres 2007, Vicente-Serrano et al. 2012). The SSI is computed in the same manner as the SPI, with the same probability distribution and transformation, but from observations of monthly streamflow rather than precipitation.

## Data

Data selection affects definitions of drought severity and extent on the basis of drought indices. Among the considerations in selecting data are the need for long-duration historical records, the available variables, and the spatial and temporal resolutions of the data. With these considerations in mind, we used two sources of atmospheric data, PRISM and the ERA5-Land reanalysis, to assess meteorological drought. We also used two sources of streamflow data to assess hydrological drought, the second version of the U.S. Geological Survey Geospatial Attributes of Gages for Evaluating Streamflow (GAGES-II) and the Oregon Water Resources Department stream gages.

**Meteorological Observations**

*PRISM Monthly Precipitation and Temperature*

The PRISM Climate Mapping Program (Daly et al. 1994) produces and disseminates detailed, high-quality spatial climate data. PRISM uses surface meteorological observations from weather stations and a digital elevation model to generate gridded estimates of monthly precipitation and temperature from January 1895 to present at a fine spatial grid spacing of 4 km. The gridded climate data fields are continually updated to map climate variables across all regions, topographic features, and associated climates, such as high mountains, rain shadows, temperature inversions, coastal regions, and associated complex mesoscale climate processes. The PRISM data are among the best estimates of precipitation and temperature in the highly variable terrain of the western United States.

Within Oregon, the density of stations from which PRISM is constructed is greatest in western Oregon and relatively sparse in much of central and eastern Oregon. One consequence of the difference in station density is higher uncertainties in the PRISM climate fields in data-sparse regions. Therefore, in Oregon, these uncertainties are most prevalent near steep elevational gradients in the state's numerous mountain ranges, particularly in central and eastern Oregon.

The PRISM climate analysis is updated regularly as more observations become available. PRISM temperature and precipitation fields are provisional for six months, and potentially considerable changes can be expected for up to two years. Therefore, values of drought indices derived from PRISM data since November 2022 should be considered preliminary.

*ERA5-Land Hourly Surface Meteorological Analyse*s

The ERA5-Land product (Muñoz-Sabater et al. 2021) extends the primary reanalysis product, ERA5, from the European Centre for Medium-Range Weather Forecasts. The ERA5-Land reanalysis blends a global weather model system with weather observations over an extended historical period to estimate atmospheric fields over all land on Earth. Although ERA5-Land uses some observational data to improve the models' representation of the atmosphere, PRISM uses many more observations of precipitation and surface air temperature. ERA5-Land has a horizontal grid spacing of 0.1° latitude and longitude (about 9 km grid spacing) and provides data for every hour from 1950 to present.

The primary reason we used ERA5-Land to construct Oregon's drought history is that it supports computation of evapotranspiration with a relatively sophisticated and accurate method, described further below, whereas PRISM does not. ERA5-Land includes all components needed to estimate the surface energy balance from which evapotranspiration is derived: 2-m air temperature, 2-m relative humidity, 10-m wind speed, net surface radiation, surface skin temperature, and surface soil moisture. It also incorporates a land surface model that allows soil moisture and infiltration to vary on the basis of realistic physical processes, which leads to a realistic estimate of evapotranspiration.

**Streamflow Observations**

*U.S. Geological Survey GAGES-II Streamflow Data*

Version II of the Geospatial Attributes of Gages for Evaluating Streamflow (GAGES-II) network (Falcone 2011) (Figure 1) includes reference and non-reference gages maintained by the U.S. Geological Survey that have measured streamflow for at least 20 years. Data from some gages are
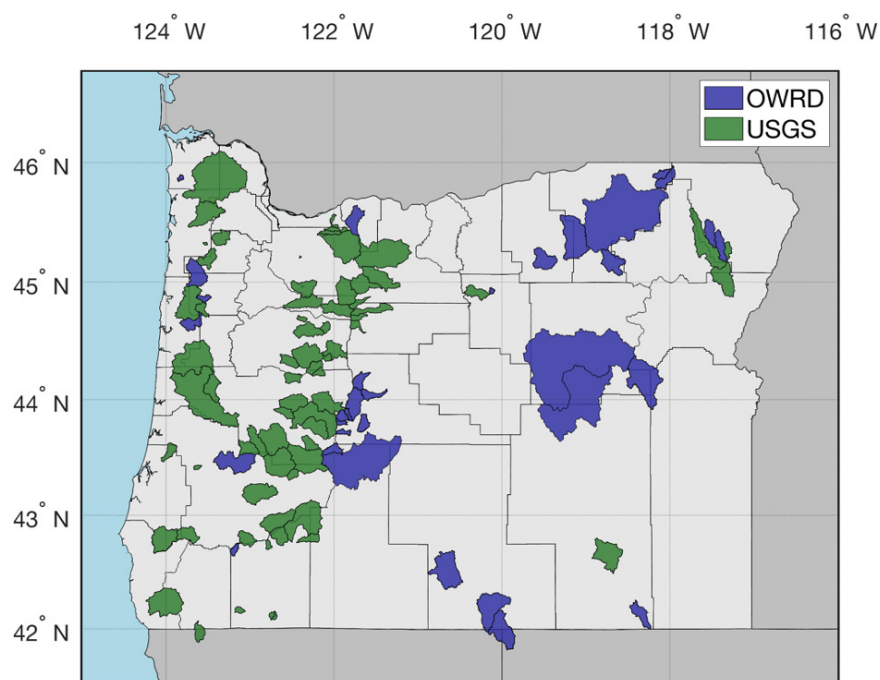
**Figure 1.** Boundaries of watersheds that encompass the stream gages in the GAGES-II network (operated by the U.S. Geological Survey [USGS]) and the Oregon Water Resources Department (OWRD) network.

discontinuous or do not extend past the 2009 water year. A water year encompasses 1 October through 30 September and references the year in which it ends; for instance, water year 2023 began on 1 October 2022 and ended on 30 September 2023. Reference gages, from which we obtained the data in this chapter, are located in watersheds with minimal upstream flow regulation or disturbance relative to non-reference gages. Accordingly, the reference gages used here are the best available for studying long-term regional climate and hydrological drought.

*Oregon Water Resources Department Streamflow Data*

The Oregon Water Resources Department (OWRD) maintains a separate network of stream gages in watersheds throughout the state (Figure 1) that are used to supplement data from the GAGES-II reference gages, particularly in data-sparse regions. The OWRD used a method similar to that of GAGES-II to classify reference stations. The density of reference gages in eastern Oregon fills some gaps in the spatial coverage of the GAGES-II network.

**Projections of Future Climate**

Our projections of future climate are based on output from an ensemble of regional climate model simulations performed through the North American Coordinated Regional Downscaling Experiment (NA-CORDEX; Mearns et al. 2017). These simulations have a horizontal grid spacing of 25 km and were applied to multiple regional climate models. The boundary conditions of the regional climate models were derived from diverse coupled global climate model simulations that prescribed a near-continuation of current levels of greenhouse gas emissions through the year 2100 according to the Representative Concentration Pathway 8.5 emissions scenario. We included seven combinations of global and regional climate models in our analyses: GFDL-ESM2M + WRF, GFDL-ESM2M + RegCM4, MPI-ESM-LR + RegCM4, MPI-ESM-LR + CRCM5-UQAM, MPI-ESM-MR + CRCM5-UQAM, CanESM2 + CanRCM4, and CanESM2 + CRCM5-UQAM.

**Estimation of Potential Evapotranspiration**

When possible, we used a standard method of estimating potential evapotranspiration (PET) from the Penman-Monteith equation, which depends not only on near-surface air temperature but on relative humidity, wind speed, net surface radiation, and surface vegetation. These variables

are available from ERA5-Land. We followed the standard practice of using a reference ground cover type in the Penman-Monteith equation that was adopted by the United Nations Food and Agriculture Organization (FAO) in its Irrigation and Drainage Paper No. 56 (FAO-56 PM; Allen et al. 1998). We modified the surface evaporative resistance to account for reduced transpiration by plants as carbon dioxide ($CO_2$) concentrations increase over the next century (Swann et al. 2016, Yang et al. 2019). This adaptive response of plants can inhibit PET and hence affect drought determination. We call this method of calculating PET the *$CO_2$-aware Penman-Monteith*.

A second method of estimating PET simplifies the Penman-Monteith equation to allows its estimation strictly from air temperature, facilitating PET estimates from both PRISM and ERA5-Land. For this method, we used the Thornthwaite equation (Thornthwaite 1948), which depends only on near-surface air temperature (typically 2 m above ground). Although the Thornthwaite equation produces reasonably accurate estimates of variability in PET in the historical record at monthly resolution, it typically overestimates PET and therefore future probability of drought when projected air temperatures exceed the historical values used to calibrate the model (Vicente-Serrano et al. 2010, Hoerling et al. 2012). Nevertheless, the Thornthwaite method is used for operational drought monitoring with the SPEI in many applications that are based on historical data (e.g., from information provided by the WestWide Drought Tracker [wrcc.dri.edu/wwdt/; Abatzoglou et al. 2017] or the Climate Toolbox [climatetoolbox.org]).

## Comparison of Meteorological Drought Depictions from PRISM and ERA5-LAND

Including both PRISM and ERA5-Land reanalysis products in our analyses allowed us to compare distinct representations of the severity and extent of historical droughts. Linear trends in annual mean precipitation, near-surface (2-m) air temperature, and potential evapotranspiration (PET) anomalies from 1950–2022 that were based on PRISM data and defined relative to the 1950–1999 mean were statistically significant at the 95 percent confidence level. Annual mean precipitation decreased by 0.5 inches per decade (dec$^{-1}$), temperature increased by 0.4°F dec$^{-1}$, and PET increased by 0.2 dec$^{-1}$ (Figure 2). Linear trends
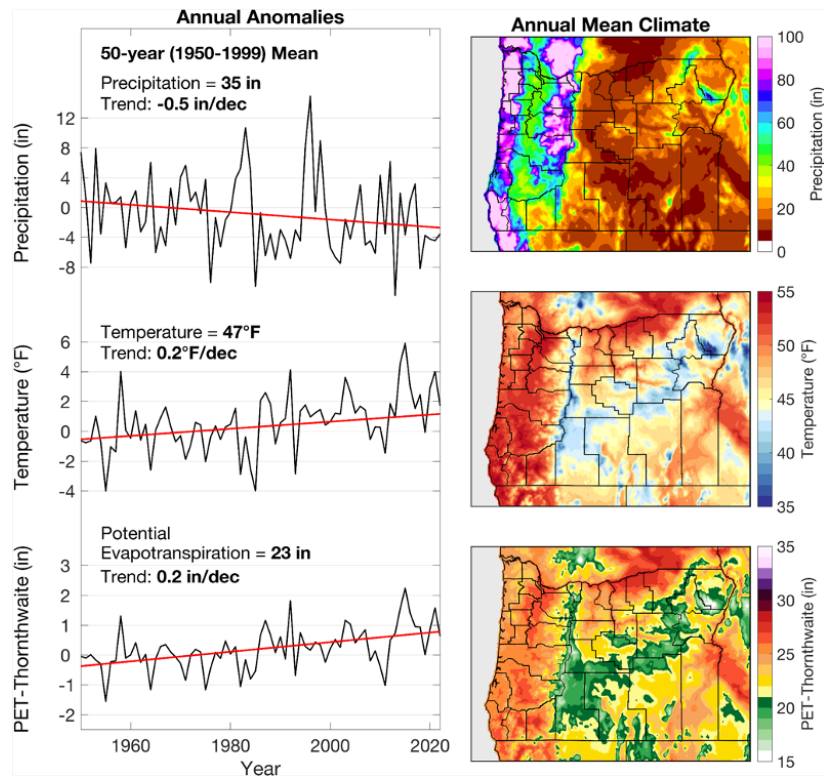


**Figure 2.** Data derived from PRISM. (Left) Time series of annual anomalies of (top to bottom) precipitation, temperature, and potential evapotranspiration (PET) as calculated with the Thornthwaite equation. Anomalies are the departure from the 1950–1999 mean. Linear trends were significant above the 95 percent confidence level. (Right) Annual mean (top to bottom) precipitation, temperature, and PET as calculated with the Thornthwaite equation for the period 1950–2022.
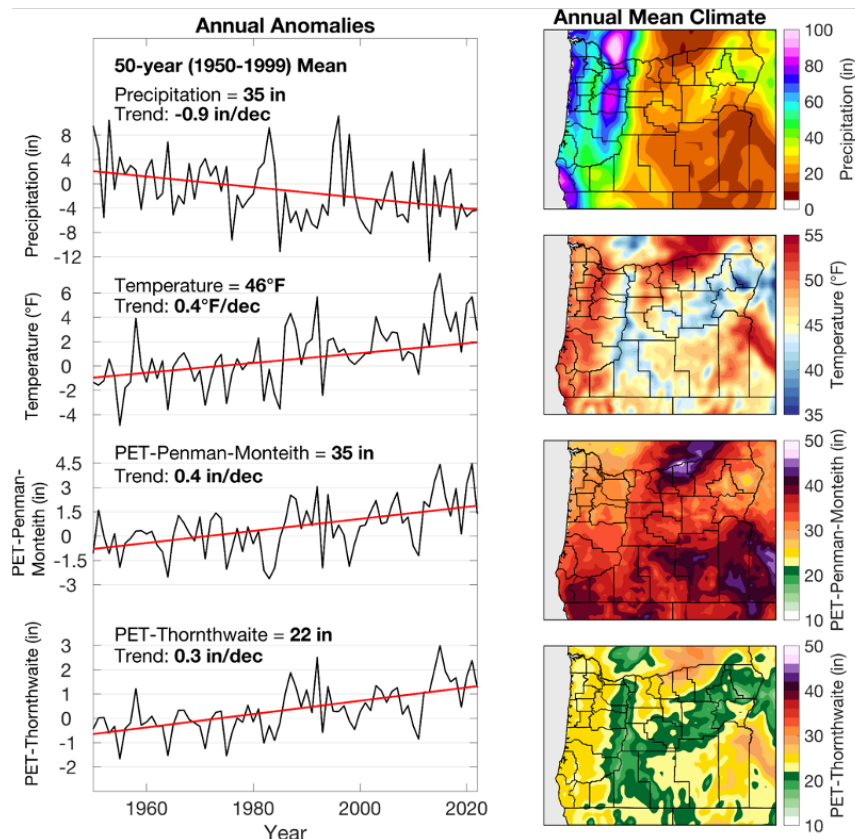
**Figure 3.** Data derived from ERA5-Land. (Left) Time series of annual anomalies of (top to bottom) precipitation, temperature, and potential evapotranspiration (PET) as calculated with the $CO_2$-aware Penman-Monteith and Thornthwaite equations. Anomalies are departures from the 1950–1999 mean. Dec, decade. Linear trends were significant at the 95 percent confidence level. (Right) Annual mean (top to bottom) precipitation, temperature, and PET as calculated with the $CO_2$-aware Penman-Monteith and Thornthwaite equations for the period 1950–2022.

in annual mean precipitation, temperature, and PET that were based on data from the ERA5-Land reanalysis also were statistically significant (Figure 3). The latter trends were somewhat greater than those based on PRISM, but the signs and statistical significance of the trends derived from the two sources of data did not differ. However, the slope of the linear trend derived from ERA5-Land was nearly double that derived from PRISM (Figures 2, 3). The differences between PRISM and ERA5-Land are most apparent before 1980, where PRISM indicates about five to ten percent less annual precipitation than does ERA5-Land (Figure 4). The differences likely reflect the relatively coarse spatial resolution of the ERA5-Land precipitation data, which may not adequately resolve the steep elevational gradients characteristic of Oregon's mountain ranges. Despite these differences, the two estimates of statewide annual precipitation from 1950–2022 were highly correlated (0.97).

Monthly mean precipitation values from PRISM and ERA5-Land were highly correlated (*R*>0.95 for all months), which suggests that drought indices derived from either source are quite similar. The spatial correlations between monthly PRISM and ERA5-Land data (*R*=0.69–0.92) were highest in winter and lowest in summer. The lower correlations in summer may be due in part to the inability of the coarser-resolution ERA5-Land reanalysis to accurately represent precipitation from summer convection, but this shortcoming mainly affects the characterization of the intensity of drought and not the temporal distribution of drought.

## Relations Between Meteorological Drought Indices and Streamflow Indices

We investigated the historical relation between drought and streamflow to identify the drought index and temporal extent that best characterizes the co-occurrence of meteorological and hydrological drought statewide. Doing so allowed us to analyze a small subset of drought indicators and time scales in the past and in future projections that are most societally relevant. Building on the analysis

by Abatzoglou et al.
(2014), we examined
the relation between the
standardized streamflow
index (SSI) and the SPI
and SPEI over a range
of temporal extents
to determine the best
predictors of hydrological
drought within watersheds.



**Figure 4.** Annual water year precipitation in Oregon as estimated from PRISM and ERA5-Land data. The correlation between the estimates is 0.97.

The coefficient of
determination (i.e., the
squared correlation
coefficient, $R^2$) represents the proportion of variance in the water year Standardized Streamflow Index (SSIWY) that is explained by a given drought index and time scale. Values close to one indicate that the drought index is a good proxy for interannual streamflow variability. Although both the ERA5-Land SPI and SPEI were highly correlated with the SSI ($R^2 > 0.7$) across all months and temporal durations, the strongest correlations were at durations of 6–12 months (long enough to capture most of the wet season) and over periods beginning in October and ending in spring or summer (in phase with the wet season) (Figure 5). The SPI explained slightly more variance in the SSI than either the Thornthwaite or Penman-Monteith versions of the SPEI, indicating that annual streamflow variability, and hence possible hydrological drought, is somewhat more strongly influenced by precipitation than by potential evapotranspiration. Nevertheless, the correlations between $SSI_{WY}$ and either SPI or SPEI were similar, suggesting that both the SPI and SPEI, when computed over the water year, are reasonable proxies for interannual streamflow variability, and thus reasonable metrics of hydrological drought. Hereafter, we refer to the 12-month SPI and SPEI, computed for each water year, as SPI12 and SPEI12, respectively.



**Figure 5.** Mean coefficient of determination ($R^2$) between meteorological drought indices (SPI and SPEI) from ERA5-Land and the standardized streamflow index ($SSI_{WY}$) as functions of month (y axis) and temporal extent in months (x axis).

We calculated the coefficient of determination between the water year SPI12 ending in September and the $SSI_{WY}$

for each watershed upstream of the USGS and OWRD reference gages. Although $R^2$ values generally exceeded 0.8 in western Oregon, they tended to be weaker east of the Cascade Range crest ($0.5 < R^2 < 0.75$) (Figure 6). The reasons for the longitudinal gradient are not clear, but we speculate that it reflects a stronger influence of groundwater sources and sinks on annual streamflows in watersheds in eastern Oregon. Alternatively, actual



**Figure 6.** $R^2$ between the ERA5-Land-derived 12-month Standardized Precipitation Index (SPI) ending in September and the water year Standardized Streamflow Index (SSI$_{WY}$) for watersheds monitored by the USGS and OWRD reference gages (Figure 1).

evapotranspiration may not be accurately represented by PET in central or eastern Oregon. Whatever the cause, this gradient implies that the SPI12 may be a more reliable proxy for interannual streamflow variability in watersheds west of the Cascade crest than in those east of the Cascade crest. Even so, the differences between the SPI12 and SPEI12 are relatively modest. Therefore, for simplicity, we present results that are based on the SPEI12 in the remainder of the chapter.

## Drought History

We provide two perspectives on Oregon's drought history. The first is a statewide characterization that provides the simplest summary of drought conditions across the state. This summary is incomplete because historical drought varied considerable across the state, particularly east and west of the Cascade Range. To account for this gradient, we summarize the drought history of each of Oregon's 36 counties.

Drought classes were assigned on the basis of the criteria used by the U.S. Drought Monitor. For a region to qualify as experiencing drought, the SPEI12 value must be less than or equal to -0.8, corresponding to the moderate drought category (D1) in the U.S. Drought Monitor. Regions with SPEI12 values between -0.5 and -0.8 are classified as abnormally dry (D0) but are not considered to be in a state of drought.

### State-level Drought History

During 18 of the 24 water years from 1999 through 2023, Oregon's water year precipitation was below average (Figure 7). Since 1896, the five water years with the lowest precipitation statewide, in order of increasing precipitation, were 1977, 1924, 2001, 1994, and 2020. The water years of 2001 and 2020 thus were ranked as the third and fifth driest on record, respectively. The average
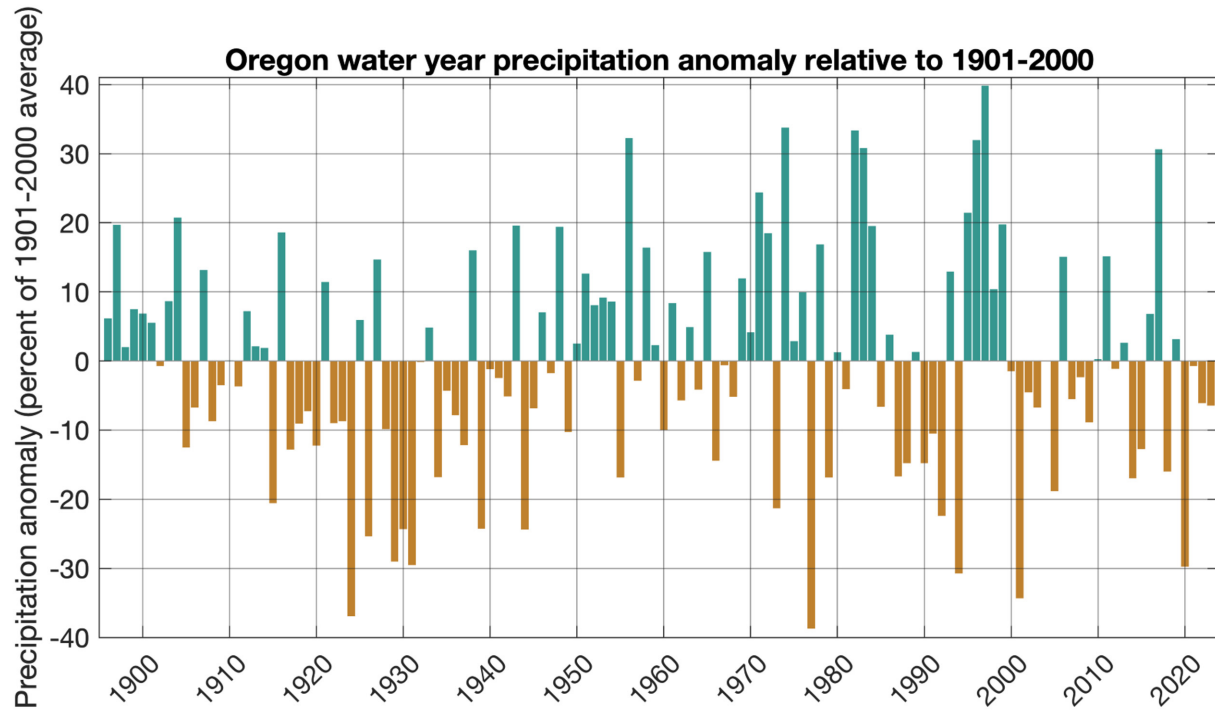
**Figure 7.** Total water year precipitation anomaly, expressed as percentage of the 1901–2000 statewide average of 35.32", averaged across Oregon for each water year from 1896 through 2023. Data from the PRISM Climate Group.
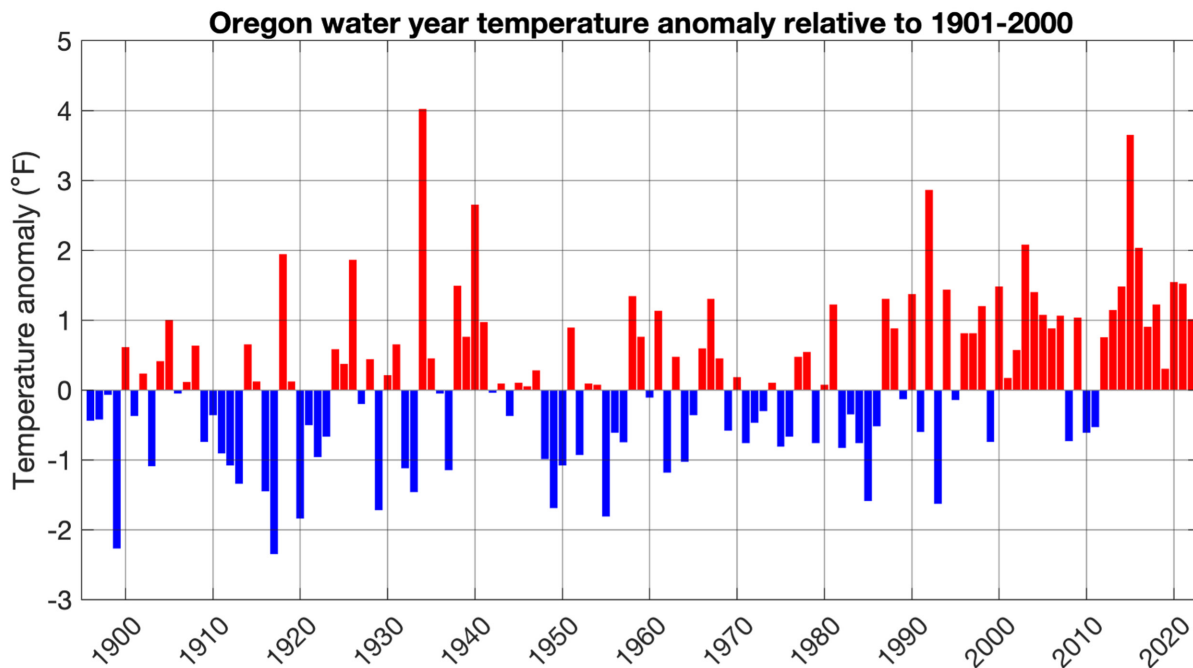


**Figure 8.** Average temperature anomaly in Oregon for each water year from 1896 through 2023. Data from the PRISM Climate Group.

temperature in Oregon was also warmer than normal in 21 of the last 24 water years (Figure 8), which contributed to higher rates of evapotranspiration and more-frequent drought.

The lowest precipitation during a single water year was in 1977, following an exceptionally dry winter (Dickson 1977). Precipitation was highest during water year 1998. Below-average annual precipitation was common in the 1920s and 1930s. Multiple moderately to extremely wet years occurred during the early 1980s and late 1990s and were at least partially associated with water years that coincided with a Very Strong El Niño (1983 and 1998).

On the basis of the relation between drought and streamflow, we chose the SPEI12 drought index to classify drought severity. A classification based on SPI12 yielded a similar drought depiction. As noted above, SPEI12 accounts not only for precipitation but for potential evapotranspiration. We evaluated state and county-level drought classification with SPEI12 for each county in Oregon. Correlations between drought and streamflow indices in some watersheds were slightly higher over shorter periods of time, but use of a single metric that encompassed the water year retained major drought periods while simplifying presentation. We chose the 12-month period to coincide with each water year represented in the monthly PRISM data (1896–2023). The background colors in
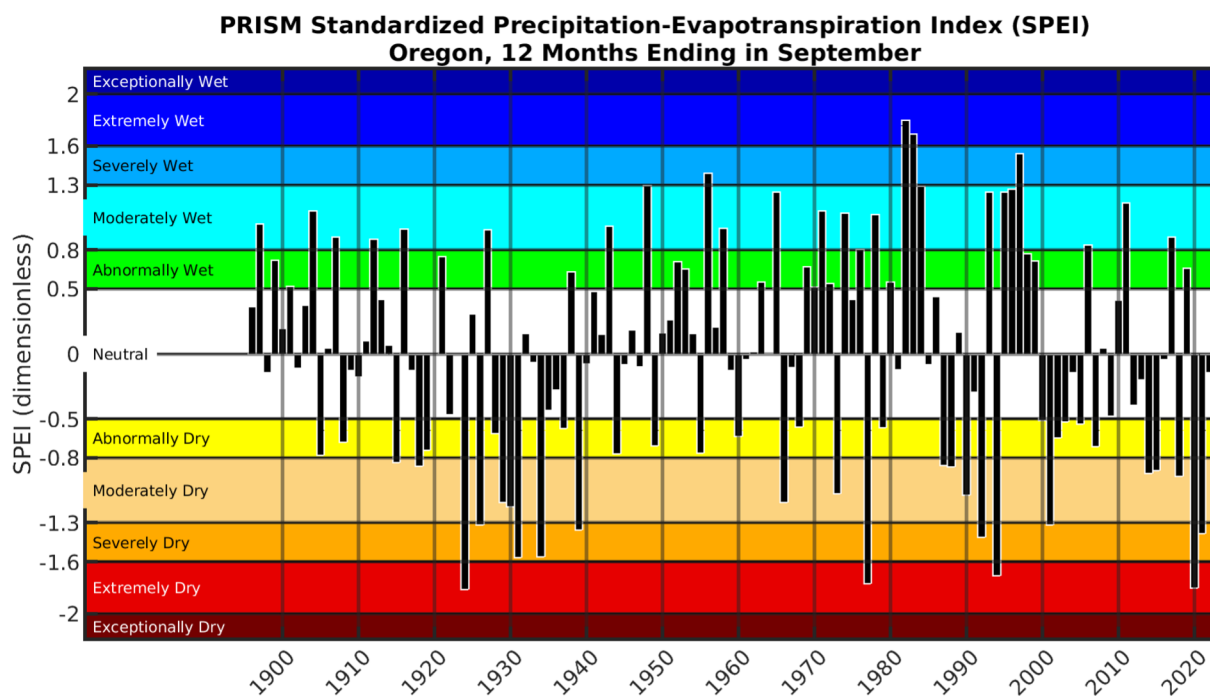


**Figure 9.** PRISM-derived SPEI12 in Oregon for each water year from 1896 through 2023. Abnormally dry and drought classes of moderate, severe, extreme, and exceptional drought are consistent with the classification used in the U.S. Drought Monitor as summarized in the introduction.

the SPEI12 time series (Figure 9) correspond to drought classes as represented by the U.S. Drought Monitor and wet conditions as represented by the Climate Toolbox's U.S. Water Watcher tool (climatetoolbox.org/tool/Historical-Water-Watcher).

We computed the statewide average SPEI12 by averaging the SPEI computed for all grid cells within Oregon. The SPEI12 indicated four periods of intense drought in Oregon: 1924–1938, 1977, 1987–1993, and 2000–2022. The 1977 drought, although the most exceptional of all single-year droughts according to the SPEI12, was preceded by three water years that were wetter than normal (1974–

1976), and was followed by a moderately wet water year (1978). The drought period of 2020–2021 is unique in its inclusion of consecutive years in which the SPEI12 indicated severe and extreme drought, intensities that had not occurred consecutively since records began in 1895. Two multiple-year wet periods since 1950 are clear from SPEI12: 1982–1984 and 1995–1999. Both encompassed a Very Strong El Niño (1982–1983 and 1997–1998). Average precipitation across the state during the only other Very Strong El Niño (2015–2016) was slightly lower than normal (Figure 7).

The SPEI12 from ERA5-Land produced a comparable drought timeline for Oregon, identifying the five most severe drought years, ranked by severity, as 1994, 1977, 1992, 2021, and 2020 (Figure 10). Like the PRISM SPEI12, the ERA5-Land SPEI12 showed that the water years 2020 and
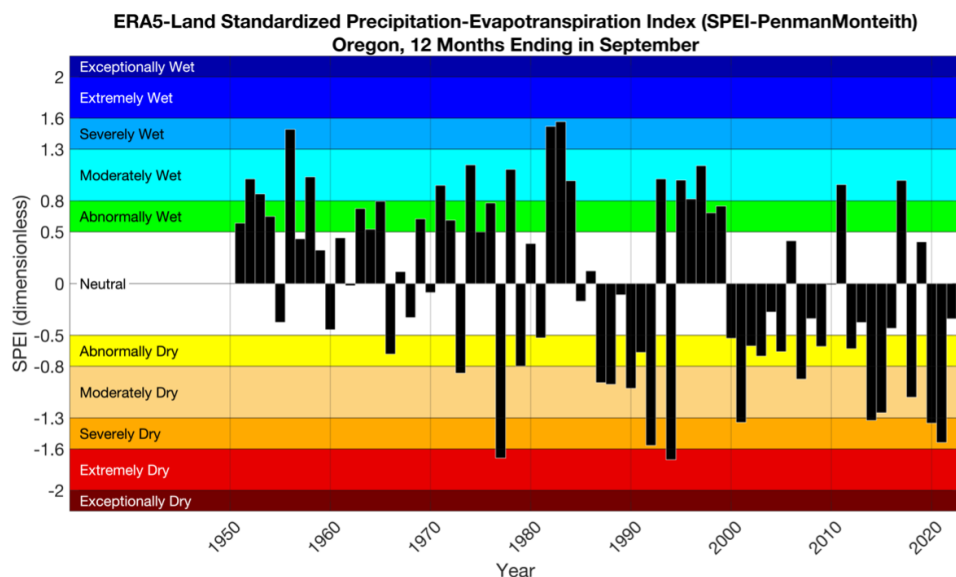


**Figure 10.** SPEI12 in Oregon, calculated from ERA5-Land data and the $CO_2$-aware Penman-Monteith equation for potential evapotranspiration, for water years since 1951.

2021 marked the first occurrence of consecutive years of severe drought (D2) in the historical record. The only distinction is that PRISM classified water year 2020 as extreme drought (D3), whereas ERA5-Land categorized it as severe drought (D2).

PRISM data indicate that drought events were relatively uncommon in Oregon from 1939 through 1976. Similarly, the SPEI12 derived from ERA5-Land reflects this trend but identifies 1966 as an abnormally dry year and 1973 as a year with moderate drought conditions (Figure 10). We conclude that statewide, Oregon experienced relatively little drought, and primarily drought of low intensity, from water years 1939 through 1976. These trends, which suggest a shift from a relatively wet regime from about 1950 through 1980 (with some notable exceptions, e.g., 1977) to a drier regime after 2000, coincide with what has been referred to as a megadrought in the western United States (Williams et al. 2020, 2022).

## Regional and County-level Drought History

The statewide assessment is a useful summary of drought history in Oregon, but does not reflect important regional variations in drought severity and extent. Oregon is a large state with diverse climate regions and water resources, and environmental conditions can vary substantially from north to south or on either side of the Cascade and Coast Ranges, leading to considerable variability in drought classification. We accounted for regional variability in this drought history by classifying drought at the county level and grouping Oregon's 36 counties into six geographic regions, Northwest, Southwest, Northcentral, Southcentral, Northeast, and Northwest (Figure 11). Although climate among counties within each region tends to be similar over time, the fact that the Oregon state drought declaration process is initiated at the county level led us to develop a county-

level drought history. We focused on drought periods at the regional and county levels since 1950 because station data that underly the PRISM data prior to 1950 are relatively sparse and uncertain.

We identified drought periods in each region and county, outlining major drought episodes and how these differed from the statewide conditions described above. We classified historical drought at the state, regional, and county levels with the water year SPEI12 since 1950 (Figure 12). For simplicity, we only present the PRISM-derived SPEI12 with evapotranspiration computed by the Thornthwaite equation. Drought classification that was based on the SPEI12 derived from ERA5-Land and the $CO_2$-aware Penman-Monteith equation differed relatively little, at least during the historical period.
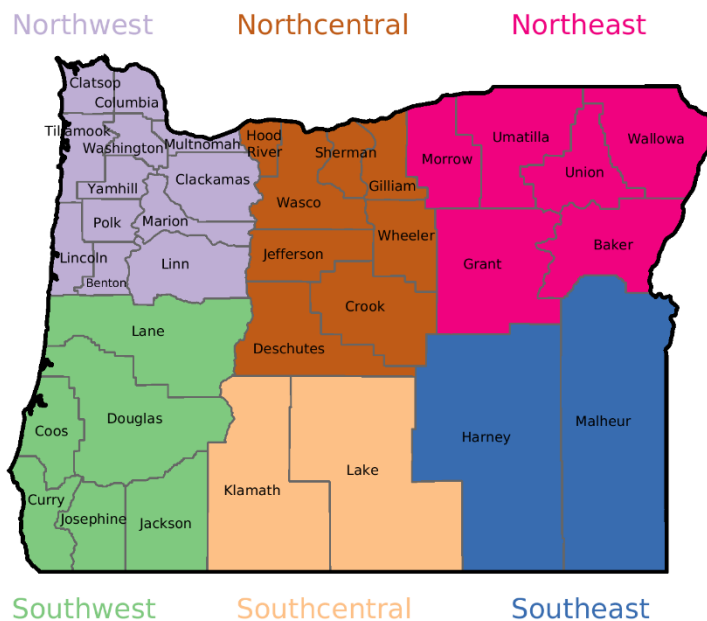


**Figure 11.** Oregon's 36 counties grouped into six regions for this drought history.

*Northeast Region*

Droughts in Northeast Oregon occurred during the water years of 1955 (~D2), 1965 (D2-D4), 1973 (D1-D3), 1977 (D3-D4), 1987-1988 (D1-D2), 1990 (~D1), 1992 (D1-D3), 1994 (D1-D3), 2001 (D1-D3), 2004 (D1-D3), 2006 (~D1), and 2020–2021 (~D1). Drought in Morrow County tended to be more intense than in surrounding counties during the last decade. The apparent difference in the regional and county-level drought intensity may reflect low station density.

*Southeast Region*

Droughts in Southeast Oregon occurred during the water years of 1954–1955 (D1), 1965 (D3-D4), 1977 (D3), 1988 (D1-D2), 1990 (~D2), 1992 (D1), 1994 (D2), 2002 (D2), 2006 (D2), 2012 (D1-D2), 2014 (D1), 2018 (D1), and 2020-2021 (D1-D2). The 1965 and 1977 droughts were the most intense in this region since 1950.

*Northcentral Region*

Droughts in Northcentral Oregon occurred during the water years of 1955 (~D2), 1960 (~D1), 1963 (D1-D3), 1965 (~D1), 1967 (~D1), 1973 (D2-D3), 1977 (D2-D4), 1994 (D1-D4), 2001–2002 (~D1-D3), 2004 (D1-D4), 2018 (~D1), and 2020–2021 (~D2-D3). Drought classifications in Hood River County were distinct from those in other counties in the region.

The 1955, 1960, and 1963 droughts in Northcentral Oregon were not apparent across all regions of Oregon. During 1965, drought also affected the Northeast, Southeast, and possibly the Southcentral regions. The water year 2020 and 2021 drought was most intense in the Northcentral and Southcentral regions of Oregon, with D3 drought experienced in both years.
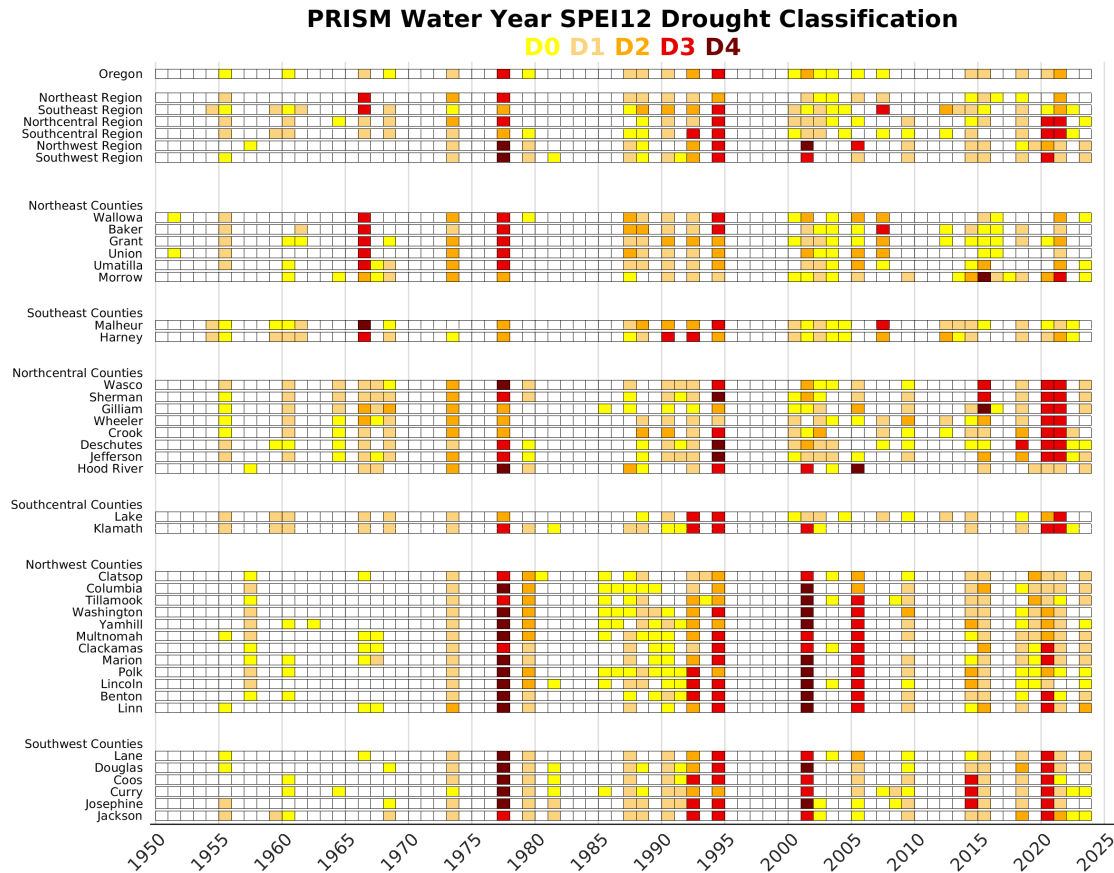
**Figure 12.** Drought classification based on the PRISM-derived SPEI12 for each water year at state, regional, and county levels. Non-white tile colors correspond to the U.S. Drought Monitor dryness classes according to the color-scale in the title: D0, abnormally dry; D1, moderate drought; D2, severe drought; D3, extreme drought; and D4, exceptional drought. White tiles indicate either neutral or wet hydrological conditions.

## Southcentral Region

Droughts in Southwest Oregon occurred during the water years of 1955 (D2-D3), 1959 (D1), 1967 (D1), 1977 (D2-D3), 1992 (D1-D2), 1994 (D2-D3), 2001 (D1-D3), 2020 (D3), and 2021 (D2-D3).

## Northwest Region

Droughts in Northwest Oregon occurred during the water years of 1973 (~D1), 1977 (~D4), 1979 (~D2), 1993 (~D2), 1994 (D2-D3), 2001 (D3-D4), 2005 (~D3), 2009 (~D1), 2014–2015 (~D1), and 2019–2021 (D1-D3). From 1950 through 1973, the Northwest region was essentially drought-free. The 2001 drought was confined to western Oregon, including the Southwest region, and the 2005 drought was confined to the Northwest region.

## Southwest Region

We identified droughts in southwest Oregon during the water years of 1955, 1973, 1977 (D4), 1979 (D1), 1986 (D1), 1990 (~D1), 1992 (~D1), 1994 (D3-D4), 2001 (D4), 2014 (D1-D3), 2018 (D1), 2020 (D3-D4), and 2021 (~D1)

# Projections of Future Drought

Projections of future drought usually are based on one of two types of analysis (Hrachowitz and Clark 2017). The first, sometimes called the bottom-up approach, directly simulates changes in streamflow and soil moisture on the basis of Earth system models forced with projected greenhouse gas concentrations. Earth system models include atmospheric and ocean models that are similar to those in traditional global climate models, but incorporate an interactive land-surface model that allows vegetation, surface albedo, and soil moisture to respond dynamically to changes in climate and greenhouse gas concentrations. Earth system model simulations generally predict that over the twenty-first century, streamflow and root-zone soil moisture in Oregon will decrease in summer, increase in winter, and have a similar annual mean (Lai et al. 2023, Zhou et al. 2023). However, the ~100-km horizontal resolution of most Earth system model simulations is too coarse to resolve the modulating effects of Oregon's mountains and coastline on the state's climate and hydrology.

A second method of projecting drought is to calculate the indices used to assess historical drought conditions, but with meteorological variables derived from climate model simulations rather than historical observations or reanalysis. This type of analysis does not require an interactive land-surface model, and therefore can be performed with output from any standard climate model. There are three major caveats to this second method.

First, most global climate models have the same resolution limitations as Earth system models. We attempted to mitigate this limitation by restricting our analysis to an ensemble of regional climate model simulations (NA-CORDEX) with horizontal resolutions of 25 km (Mearns et al. 2017). Although this resolution is too coarse to capture the sharpest climate gradients in the Coast Range and Cascade Range, it is a substantial improvement over standard global models in which these mountain ranges are unresolved.

Second, accurate calculation of indices that incorporate PET, such as SPEI, requires accounting for changes in plant physiology driven by rising $CO_2$ concentrations. If these changes are not incorporated into the PET calculation, the indices will exaggerate the increase in aridification and drought risk as climate changes (Lemordant et al. 2018, Yang et al. 2019, Scheff et al. 2022). To address this issue, we calculated the SPEI with a version of the Penman-Monteith equation that accounts for rising $CO_2$ concentrations (Yang et al. 2019).

Third, $CO_2$-aware drought indices such as the SPEI are better predictors of long-term changes in root-zone soil moisture than of streamflow (Yang et al. 2019, Scheff et al. 2022). This is because the ratio of runoff to precipitation (the runoff ratio) is highly sensitive to changes in the temporal characteristics of precipitation, which might include shifts in the seasonal cycle and changes in the relative frequency of extreme versus moderate precipitation events (Scheff et al. 2022). Such changes are widely expected with projected climate change, but their hydrologic impacts are not well captured by any drought index, including those that account for rising $CO_2$ concentrations.

The seven-member NA-CORDEX simulations from 1950 through 2099 projected statistically significant (two-tailed Student's $t$-test, 95 percent confidence level) increases in statewide precipitation and PET (Figures 13, 14). Annual mean precipitation increased by 0.27 inches per decade (Figure 13). PET estimated with the $CO_2$-aware Penman-Monteith equation increased by 0.25 inches per decade (Figure 14), which can be expected to largely offset the projected increase in precipitation. Because of the increase in PET, the $CO_2$-aware Penman-Monteith equation did not project a statistically significant change in SPEI12 (Figure 15).
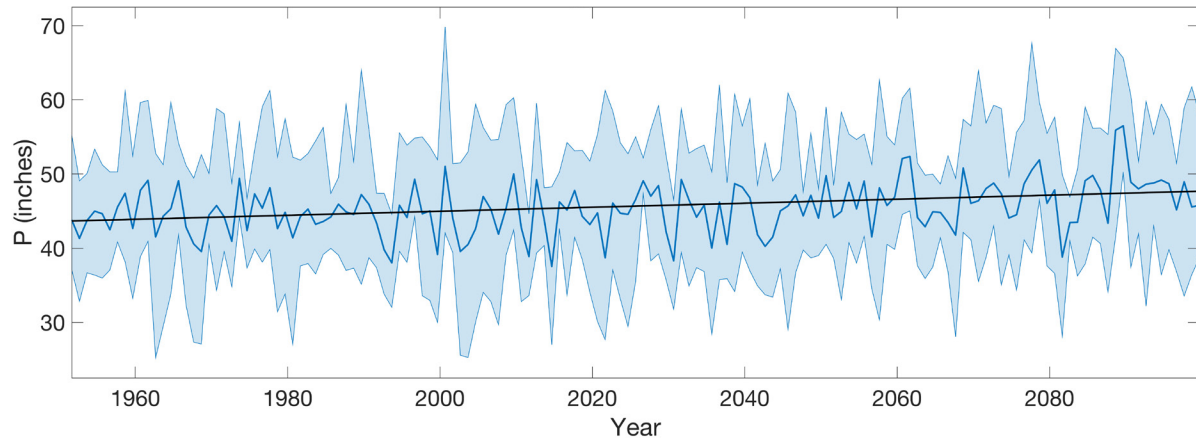
**Figure 13.** Oregon statewide water year precipitation (P) in the seven-member NA-CORDEX-22i ensemble from 1950–2099. The solid blue line represents the ensemble mean and the blue shading represents the ensemble range. The linear trend (solid black line) is +0.27 inches per decade and statistically significant.
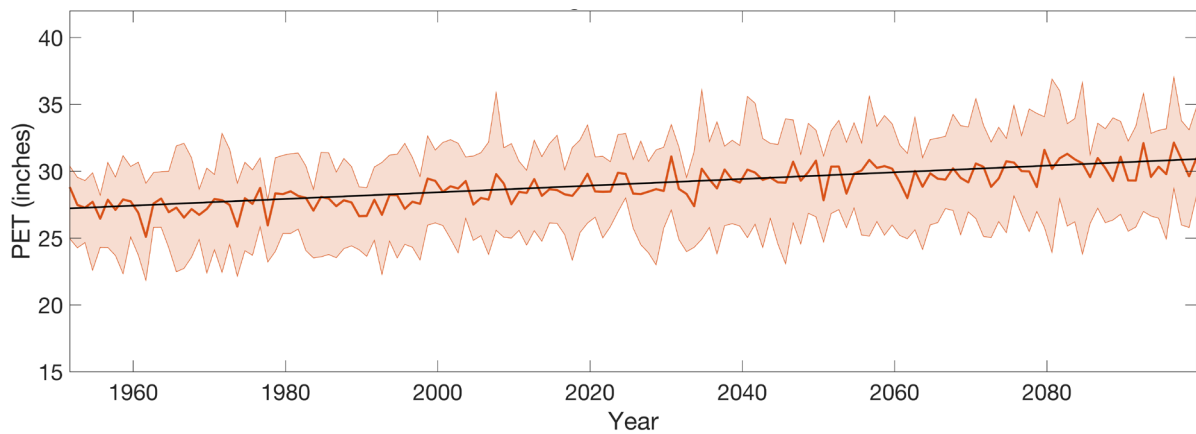


**Figure 14.** Oregon statewide water year potential evapotranspiration (PET), estimated with the $CO_2$-aware Penman-Monteith equation, in the seven-member NA-CORDEX-22i ensemble from 1950–2099. The solid red line represents the ensemble mean and shading represents the ensemble range. The linear trend (solid black line) is +0.25 inches per decade and statistically significant.
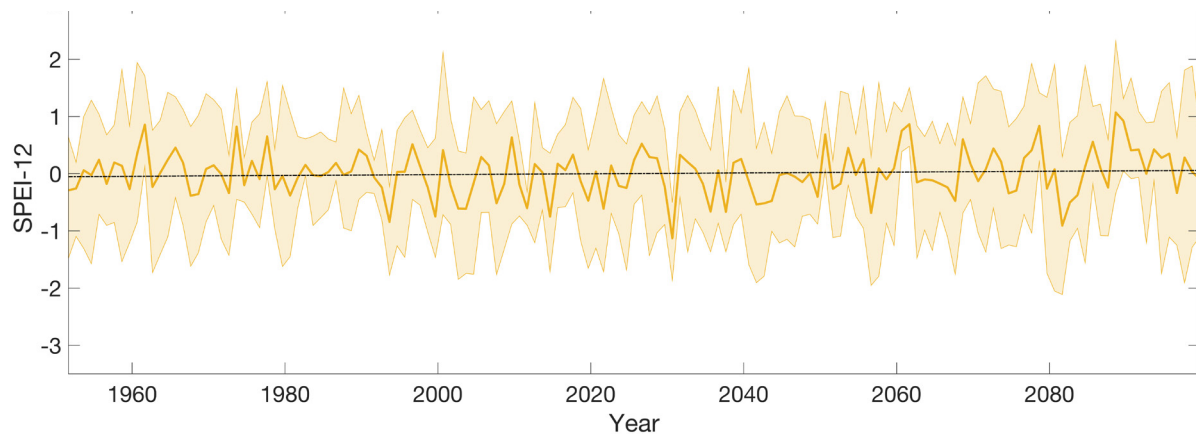


**Figure 15.** Oregon statewide water year SPEI12, estimated with the $CO_2$-aware Penman-Monteith equation, based on precipitation and PET projections from the seven-member NA-CORDEX-22i ensemble from 1950–2099. The solid yellow line represents the ensemble mean and shading represents the ensemble range. The linear trend (solid black line) of +0.0073 per decade is not statistically significant.

Precipitation

PET (CO2-aware Penman-Monteith)

inches per decade

0.6

0.3

0

-0.3

-0.6
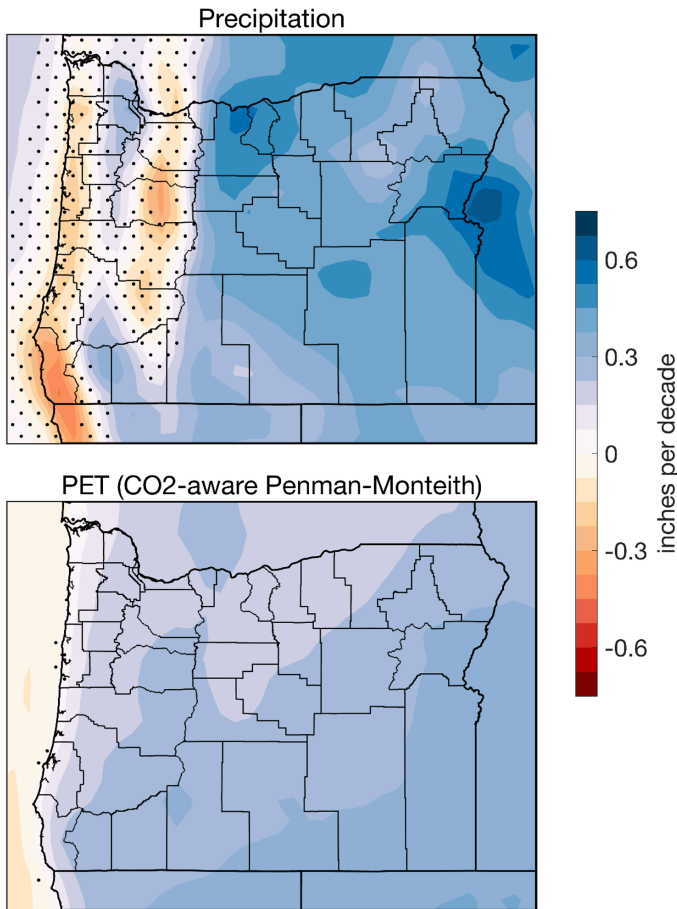
**Figure 16.** Linear trends in water year precipitation (top) and potential evapotranspiration (PET) (bottom) from 1950–2099 in the ensemble mean of the NA-CORDEX simulations. Stippling indicates that trends were not statistically significant at the 95 percent confidence level.

Regional projections are more complex, with considerable variability in both the magnitude and sign of the trends (Figure 16). Most increases in precipitation were projected to occur east of the Cascade Range, where the average trends exceeded 0.3 inches per decade. Significantly positive trends occurred west of the Cascade Range in the Rogue Valley and northern Willamette Valley. In contrast, a decrease in precipitation was projected for much of the west slopes of the Cascade and Coast Ranges, but the negative trends were statistically significant only in the southwestern corner of the state (Curry County) and in parts of eastern Linn and Marion Counties near Detroit Lake. Regional trends in PET were less variable, with significant increases projected across the state (Figure 16).

The spatial trends in SPEI12 (Figure 17) and precipitation (Figure 16) were similar, but offset by the relatively spatially uniform increase in PET. PET computed from the $CO_2$-aware Penman-Monteith equation yielded a significant decrease only along the western slopes of the Cascade and Coast Ranges, with

a significant increase in the lower Deschutes basin in north-central Oregon; changes elsewhere were not statistically significant.

Even in regions where trends in the SPEI12 were positive, changes in the seasonal cycle of precipitation may increase drought risk during parts of the year. Precipitation across most of the state likely will increase during winter and spring but decrease during summer, particularly in western Oregon. Increases in PET also will be greatest during summer, resulting in a significant statewide decrease in



SPEI12 (CO2-aware Penman-Monteith)

Drought Trend (per decade)

0.1

0.06

0.02

-0.02

-0.06

-0.1
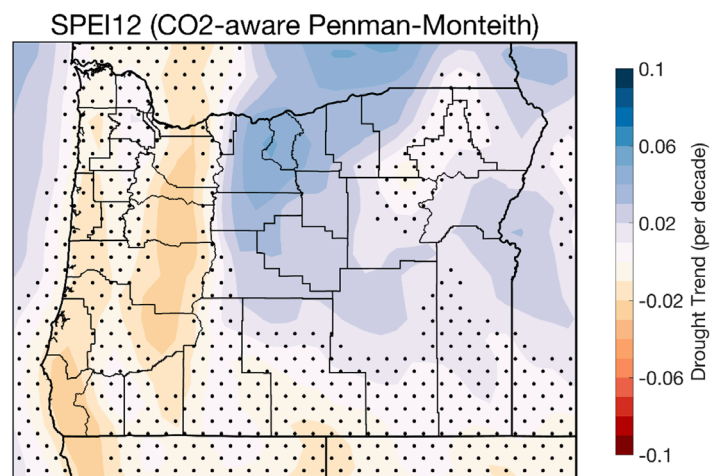
**Figure 17.** Linear trends in SPEI12 from 1950 through 2099 in the ensemble mean of the NA-CORDEX simulations. Stippling indicates that trends were not statistically significant at the 95 percent confidence level.
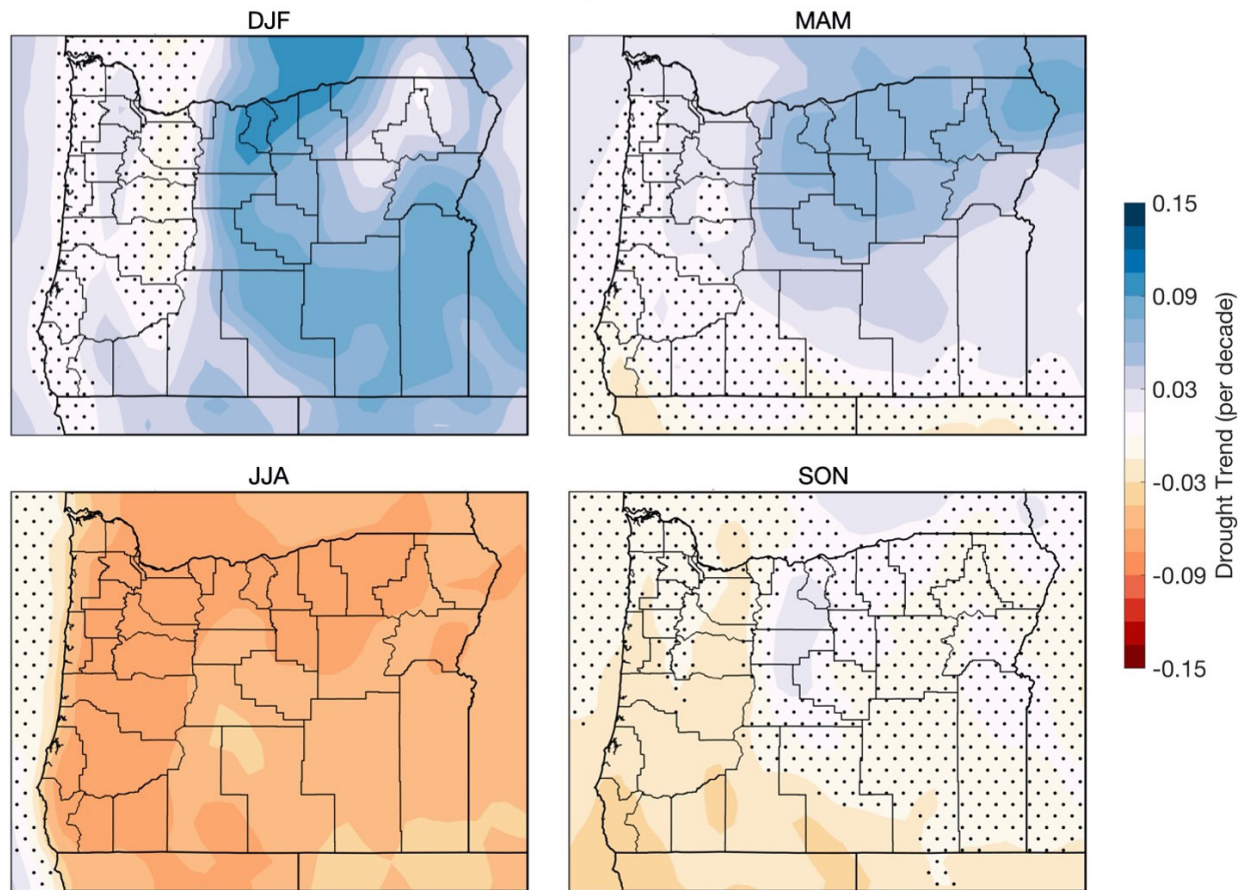
**Figure 18.** Linear trends in SPEI3 by season from 1950 through 2099 in the ensemble mean of the NA-CORDEX simulations. PET was calculated with the $CO_2$-aware Penman-Monteith equation. Stippling indicates that trends were not statistically significant at the 95 percent confidence level. DJF, December, January, and February (winter); MAM, March, April, and May (spring); JJA, June, July, and August (summer); SON, September, October, and November (autumn).

the 3-month SPEI (SPEI3; Figure 18) and increased incidence of short-term drought during the growing season, in which water demand is greatest.

In summary, whereas the NA-CORDEX simulations indicate that precipitation likely will increase across much of the state during the twenty-first century, the increase is most likely to occur east of the Cascade Range. Projected changes in precipitation in western Oregon are more uncertain. In contrast, PET is projected to increase across the state, with the effects of increasing $CO_2$ concentrations on plant physiology only partially offsetting the increase in vapor pressure deficit due to warmer temperatures. If SPEI12 is interpreted as a proxy for root-zone soil moisture, then these results suggest that drought risk likely will increase over the twenty-first century on the western slopes of the Cascade Range and the southern Coast Range, decrease in the Deschutes and John Day basins in north-central Oregon, and change little elsewhere. However, due to a shift in the seasonal distribution of precipitation, drought risk during summer is likely to increase statewide.

**Literature Cited**

Abatzoglou, J.T., R. Barbero, J.W. Wolf, and Z.A. Holden. 2014. Tracking interannual streamflow variability with drought indices in the U.S. Pacific Northwest. Journal of Hydrometeorology

15:1900–1912.

Abatzoglou, J.T., D.J. McEvoy, and K.T. Redmond. 2017. The West Wide Drought Tracker: drought monitoring at fine spatial scales. Bulletin of the American Meteorological Society 98:1815–1820.

Ahmadalipour, A., H. Moradkhani, and M. Svoboda. 2017. Centennial drought outlook over the CONUS using NASA-NEX downscaled climate ensemble. International Journal of Climatology 37:2477–2491.

Allen, R.G., L.S. Pereira, D. Raes, and M. Smith. 1998. Crop evapotranspiration: guidelines for computing crop water requirements. FAO Irrigation and Drainage Paper 56. www.fao.org/3/X0490E/X0490E00.htm.

Beguería, S., S.M. Vicente-Serrano, F. Reig, and B. Latorre. 2014. Standardized precipitation evapotranspiration index (SPEI) revisited: parameter fitting, evapotranspiration models, tools, datasets and drought monitoring. International Journal of Climatology 34:3001–3023.

Daly, C., R.P. Neilson, and D.L. Phillips. 1994. A statistical-topographic model for mapping climatological precipitation over mountainous terrain. Journal of Applied Meteorology 33:140–158.

Dickson, R.R. 1977. Weather and circulation of February 1977: widespread drought. Monthly Weather Review 105:684–689.

Edwards, D.C., and T.B. McKee. 1997. Characteristics of 20th century drought in the United States at multiple time scales. Department of Atmospheric Science, Colorado State University, Fort Collins, Colorado. Mountain Scholar. http://hdl.handle.net/10217/170176.

Falcone, J., 2011. GAGES-II: Geospatial Attributes of Gages for Evaluating Streamflow. U.S. Geological Survey data release. https://doi.org/10.5066/P96CPHOT.

Hoerling, M.P., J.K. Eischeid, X-W. Quan, H.F. Diaz, R.S. Webb, R.M. Dole, and D.R. Easterling. 2012. Is a transition to semipermanent drought conditions imminent in the U.S. Great Plains? Journal of Climate 25:8380–8386.

Hosking, J.R.M. 1990. L-Moments: analysis and estimation of distributions using linear combinations of order statistics. Journal of the Royal Statistical Society Series B 52:105–124.

Hrachowitz, M., and M.P. Clark. 2017. Hess opinions: the complementary merits of competing modelling philosophies in hydrology. Hydrology and Earth System Sciences 21:3953–3973.

Keyantash, J., and J.A. Dracup. 2002. The quantification of drought: an evaluation of drought indices. Bulletin of the American Meteorological Society 83:1167–1180.

Lai, E.N., L. Wang-Erlandsson, V. Virkki, M. Porkka, and R.J. van der Ent. 2023. Root zone soil moisture in over 25% of global land permanently beyond pre-industrial variability as early as 2050. Hydrology and Earth System Sciences 27:3999–4018.

Lawrimore, J., et al. 2002. Beginning a new era of drought monitoring across North America. Bulletin of the American Meteorological Society 83:1191–1192.

Lemordant L., P. Gentine, A.L.S. Swann, B.I. Cook, and J. Scheff. 2018. Critical impact of vegetation physiology on the continental hydrologic cycle in response to increasing $CO_2$. Proceedings of the National Academy of Sciences 115:4093–4098.

McEvoy, D.J., J.L. Huntington, J.T. Abatzoglou, and L.M. Edwards. 2012. An evaluation of multiscalar drought indices in Nevada and eastern California. Earth Interactions 16:18. https://doi.org/10.1175/2012EI000447.1.

McKee, T.B., N.J. Doesken, and J. Kleist. 1993. The relationship of drought frequency and duration to time scales. Pages 179–184 in Eighth Conference on Applied Climatology, American Meteorological Society, Anaheim, California. www.droughtmanagement.info/literature/

AMS_Relationship_Drought_Frequency_Duration_Time_Scales_1993.pdf

Mearns, L.O., et al. 2017. The NA-CORDEX dataset, version 1.0. NCAR Climate Data Gateway, Boulder, Colorado. https://doi.org/10.5065/D6SJ1JCH. Accessed 16 April 2023.

Mo, K.C., and D.P. Lettenmaier. 2015. Heat wave flash droughts in decline. Geophysical Research Letters 42:2823–2829.

Modarres, R. 2007. Streamflow drought time series forecasting. Stochastic Environmental Research and Risk Assessment 21:223–233.

Muñoz-Sabater, J., et al. 2021. ERA5-Land: a state-of-the-art global reanalysis dataset for land applications. Earth System Science Data 13:4349–4383.

Otkin, J.A., et al. 2022. Getting ahead of flash drought: from early warning to early action. Bulletin of the American Meteorological Society 103:E2188–E2202. https://doi.org/10.1175/BAMS-D-21-0288.1.

Pendergrass, A.G., et al. 2020. Flash droughts present a new challenge for subseasonal-to-seasonal prediction. Nature Climate Change 10:191–199.

Peña-Gallardo, M., S.M. Vicente-Serrano, J. Hannaford, J. Lorenzo-Lacruz, M. Svoboda, F. Domínguez-Castro, M. Maneta, M. Tomas-Burguera, and A. Kenawy. 2019. Complex influences of meteorological drought time-scales on hydrological droughts in natural basins of the contiguous United States. Journal of Hydrology 568:611–625.

Rasmussen, E.M., R.E. Dickinson, J.E. Kutzbach, and M.K. Cleveland. 1993. Climatology. Pages 2.1–2.4 in D.R. Maidment, editor. Handbook of hydrology. McGraw-Hill, New York.

Redmond, K.T. 2002. The depiction of drought: a commentary. Bulletin of the American Meteorological Society 83:1443–1147.

Rupp, D.E., S. Li, P.W. Mote, K.M. Shell, N. Massey, S.N. Sparrow, D.C.H. Wallom, and M.R. Allen. 2017. Seasonal spatial patterns of projected anthropogenic warming in complex terrain: a modeling study of the western US. Climate Dynamics 48:2191–2213.

Scheff, J., S. Coats, and M.M. Laguë. 2022. Why do the global warming responses of land-surface models and climatic dryness metrics disagree? Earth's Future 10:e2022EF002814. https://doi.org/10.1029/2022EF002814.

Svoboda, M., et al. 2002. The Drought Monitor. Bulletin of the American Meteorological Society 83:1181–1190.

Swann, A.L.S. 2018. Plants and drought in a changing climate. Current Climate Change Reports 4:192–201.

Swann, A.LS., F.M. Hoffman, C.D. Koven, and J.T. Randerson. 2016. Plant responses to increasing $CO_2$ reduce estimates of climate impacts on drought severity. Proceedings of the National Academy of Sciences 113:10019–10024.

Thornthwaite, C.W. 1948. An approach toward a rational classification of climate. Geography Review 38:55–94.

Vicente-Serrano, S.M., S. Beguería, and J.L. López-Moreno. 2010. A multi-scalar drought index sensitive to global warming: the standardized precipitation evapotranspiration index. Journal of Climate 23:1696–1718.

Vicente-Serrano, S.M., J.I. López-Moreno, S. Beguería, J. Lorenzo-Lacruz, C. Azorin-Molina, and E. Morán-Tejeda. 2012. Accurate computation of a streamflow drought index. Journal of Hydrologic Engineering 17:318–332.

Wilhite, D.A., and M.H. Glantz. 1985. Understanding the drought phenomenon: the role of definitions. Water International 10:111–120.

Williams, A.P., B.I. Cook, and J.E. Smerdon. 2022. Rapid intensification of the emerging

southwestern North American megadrought in 2020–2021. Nature Climate Change 12:232–234.

Williams, A.P., E.R. Cook, J.E. Smerdon, B.I. Cook, J.T. Abatzoglou, K. Bolles, S.H. Baek, A.M. Badger, and B. Livneh. 2020. Large contribution from anthropogenic warming to an emerging North American megadrought. Science 368:314–318.

Yang, Y., M.L. Roderick, S. Zhang, T.R. McVicar, and R.J. Donohue. 2019. Hydrologic implications of vegetation response to elevated $CO_2$ in climate projections. Nature Climate Change 9:44–48.

Zhou, S., B. Yu, B.R. Lintner, K.L. Findell, and Y. Zhang. 2023. Projected increase in global runoff dominated by land surface changes. Nature Climate Change 13:442–449.

# Economy

Global, national, and local economies are strongly affected by climate variability and change, yet it is virtually impossible to credibly estimate the full breadth of economic effects of these phenomena (Dundas et al. 2023). As emphasized in previous Oregon Climate Assessments, not only are economic sectors and relevant climate variables extraordinarily diverse, but primary data are limited and human behavior rarely has been considered in projections of the economic effects of climate change. Gradually, however, economic assessment methods and data sources are improving (Dundas et al. 2023), particularly when assessment focuses on a well-defined sector or climate event. Evidence of how individuals, companies, and governments are responding to trends in climate or extreme events also is accruing. The three contributions in this section illustrate the latter points.

Two contributions focus on economic ramifications of wildfires. Wang and Lewis quantified how local drought stress and changes in wildfire risk, or landowners' perceptions of risk, affected the market price of privately owned timberland across Oregon, Washington, and California. They discovered that the bulk of the economic costs resulted from changing expectations of wildfire risk. Yet they also noted substantial variation in price over time, and effects of national and global economic fluctuations on local timberland prices.

Sterns and Beavers estimated the potential economic effects of a major wildfire smoke event on 22 industries that from 2015 through 2021 represented 40.5 percent of total employment, 31.3 percent of labor income, and 32.9 percent of total economic output per year in Oregon. They are frank about the uncertainties created by constrained climate, environmental, and economic data; use of proxies for missing data; and necessary assumptions about relative exposure and vulnerability of particular economic sectors. Additionally, Sterns and Beavers recognized the potential for compounded or cascading losses from multiple wildfires or wildfires and other extreme events. They found that the economic losses from a major smoke event are likely to be highly localized and industry-specific given the unequal distribution of smoke and economic activity in space and time.

Panwar and Barnett examined businesses' motivations and actions related to investments in mitigation of or adaptation to climate change. Precise estimation of firms' climate change programs is inhibited by the fact that many companies do not differentiate among climate change, biological diversity, pollution, and sustainability. In response to the question whether voluntary corporate efforts to address climate change are effective, they explained why "The honest answer is that we don't know." Nevertheless, Oregon businesses demonstrably are capitalizing on state regulations to become regional, national, and global leaders in sustainable practices.

## Literature Cited

Dundas, S.J., S. Capalbo, and J. Sterns. 2023. The economic implications of climate change for Oregon. Pages 134–157 in Fleishman, E., editor. Sixth Oregon climate assessment. Oregon Climate Change Research Institute, Oregon State University, Corvallis, Oregon. https://doi.org/10.5399/osu/1161.

# Wildfire Impacts on the Economic Value of Privately Owned Timberland

Yuhan Wang and David J. Lewis

## Introduction

The twenty-first century began with a sharp increase in the annual area burned by wildfires in the United States. According to the 2020 U.S. Forest Service Resource Planning Act Assessment, the average annual area burned in wildfires in the United States more than doubled after the year 2000, and is projected to continue increasing in the future (Costanza et al. 2023). Wildfire can generate numerous economic impacts, such as costs to human health from smoke exposure (Burke et al. 2021), damages to housing structures and other property (Dale 2010), and government response expenditures that can exceed $2 billion per year (Bayham et al. 2022). However, an unanswered question is how increasing wildfire risk is affecting the economic value of key natural assets such as land and water, also known as natural capital.

Across Oregon and the western United States, forests represent a nationally important stock of natural capital, the economic value of which is becoming more exposed to risk from wildfire. These forests include privately owned timberland, a subset of western forests that produces most of the region's timber. Because private timberland is actively bought and sold in competitive land markets, the transaction price of timberland reflects how buyers and sellers value forested land. Economic theory indicates that the market value of timberland should reflect the land's ability to produce timber over time, which depends on many factors such as climate, soil quality, and local and global timber market conditions (Amacher et al. 2009). Because the threat of wildfire generates risk to the future productivity of timberland, theory also suggests that risk should be reflected in the price of timberland (Reed 1984). Consider two identical parcels of timberland, A and B. If wildfire risk increases suddenly on parcel A but not on parcel B, then parcel A's future ability to produce timber becomes less certain than that of parcel B. Therefore, buyers and sellers in a competitive market will bid down the price of parcel A relative to parcel B consistent with their perception of risk.

We used quantitative empirical economic methods, or econometrics, to examine how spatially variable changes in wildfire risk have affected the market price of private timberland. We studied over 9,000 individual timberland transactions across Oregon, Washington, and California from 2004 through 2020 to understand how participants in timberland markets perceive wildfire risk and incorporate it into prices. Although wildfire occurrence has increased substantially in some areas east of the Cascade Range and in southern Oregon, wildfire occurrence in other regions, especially the Coast Range of Oregon and Washington, has changed little. By linking the location and timing of timberland transactions with dates of known wildfires and maps of their perimeters, we are able to quantify how locally changing wildfire risk affects the market price of timberland that is exposed to this risk. The results provide evidence that the economic value of timberlands across Oregon, Washington, and California is being affected by wildfire risk.

## Trends in Western Wildfires and Exposure of Private Timberland

The boundaries of wildfires larger than 1,000 acres (405 ha) have been consistently mapped by the U.S. Geological Survey's Monitoring Trends in Burn Severity (MTBS) program since 1984 (Figure 1a,b). While wildfires have always occurred in the Pacific states, the area burned was much greater after the year 2000, which is consistent with national trends (Costanza et al. 2023).
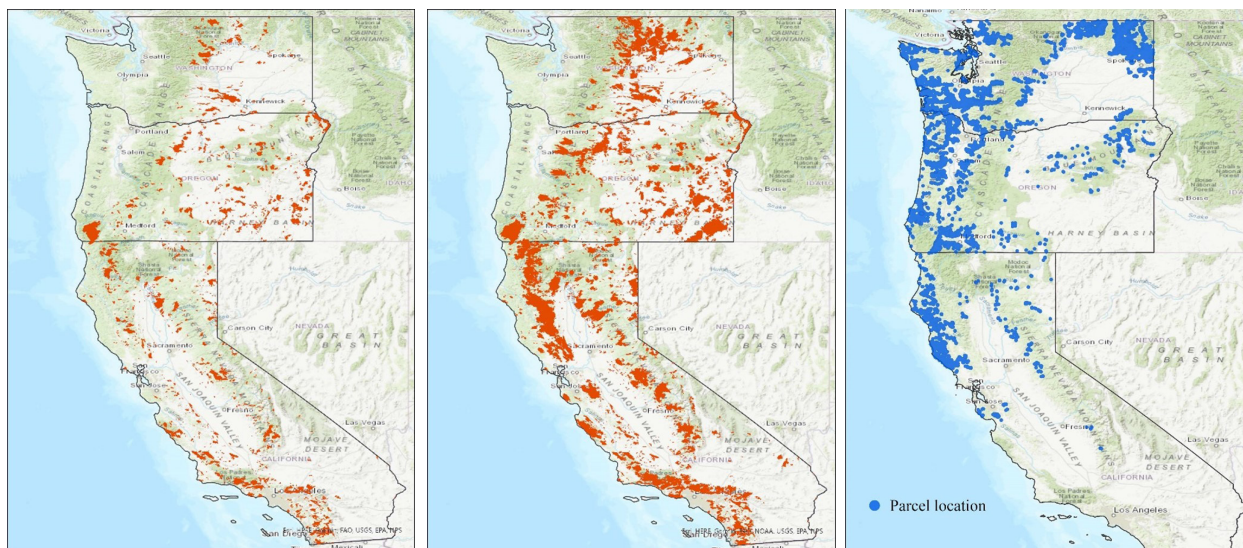
**Figure 1.** (a, left) Locations of large (>1000 acres) wildfires in Washington, Oregon, and California, 1984–2003. (b, center) Locations of large wildfires, 2001–2020. (c, right) Locations of sales of privately owned timberland, 2004–2020. Source: Wang and Lewis 2024, published under the Creative Commons license https://creativecommons.org/licenses/by/4.0/.

Private timberland is concentrated in western Oregon and Washington, northeastern Washington, and northwestern coastal California. We examined transaction data on sales of privately owned timberland from 2004 through 2020 and data on the location (Figure 1c) and size of wildfires during the preceding 20 years. Much of the forested land in the Cascade Range and Sierra Nevada is public and managed by federal agencies, especially the U.S. Forest Service and Bureau of Land Management. We did not include public lands in our data because they are rarely sold. Exposure of private timberland to large wildfires varies considerably, with timberland near the coast much less exposed (Figure 1).

We computed three metrics of wildfire exposure for each privately owned timberland parcel in our data during the 20 years prior to sale: the number of large wildfires that overlapped the parcel, the number of large wildfires that burned within 15 km (9.3 mi.) of the parcel perimeter, and whether an extremely large wildfire (12,355 acres [5,000 ha] or larger; Barbero et al. 2015) was within 15 km of the parcel perimeter. Average values of the three metrics were higher for parcels sold in 2021 (affected by wildfires from 2001–2020) than for parcels sold in 2004 (affected by wildfires from 1984–2003). About 2 percent of the timberland parcels coincided with one large wildfire from 1984–2003, and none of the parcels was burned by more than one large wildfire. In contrast, about 5.6 percent of parcels were overlapped by one large wildfire from 2001–2020, and 0.8 percent were burned by more than one large wildfire. The average number of large wildfires per decade that were within 15 km of a parcel increased from 0.39 to 0.72, and the percentage of parcels within 15 km of extremely large wildfires increased from 12 to 36 percent. In 2023, as a consequence of the increasing wildfire risk, the state of Oregon dropped its long-standing and unique private insurance for wildfire suppression expenses due to rising premiums and deductibles.

## Changes in Economic Value of Private Timberland

Increasing risk of wildfire can affect the economic value of timberland in at least two ways. First, forest parcels that are burned sell for less because they have fewer standing trees of commercial or

non-market (e.g., recreational) value. Second, if current and potential landowners expect wildfire to become more frequent, then prices should fall the most in places with the largest increases in wildfire risk, even if parcels have not burned prior to sale.

We estimated how the prices of over 9,000 timberland parcels sold at different points in time responded to the three wildfire exposure metrics described above. We evaluated whether climate (drought status), biophysical variables (elevation, slope, soil quality), geography (proximity to urban areas and roads), and economic factors that change over time and affect all parcels equally (interest rates) affected timberland values. We accounted for additional geographic factors that are difficult to measure (e.g., other productivity or risk measures) by calculating the difference between a land parcel's price and the long-term (2004–2020) average price in that parcel's county; in econometrics, it is common to account for geographic factors as fixed effects, which we defined at the county level. The fixed effects accounted for all other geographic factors that affect timberland values and do not change over time. Thus, the method estimates how local and time-varying wildfire exposure affects what people pay for timberland parcels after controlling for climate, biophysical variables, geography, and economic factors.

We found that increasing wildfire exposure, as measured by any of our three metrics, reduces timberland prices relative to those that would be applicable without a change in wildfire risk. Because timberland values are depressed simply by proximity to large wildfires, even if the parcel does not burn, we interpret such a negative price impact as being consistent with landowners' perception that wildfire risk is increasing.

We also found that a warmer and drier climate, measured as vapor pressure deficit, depresses timberland prices due to higher risk of drought stress. Furthermore, the price of a timberland parcel decreases as elevation, average slope, distance from the nearest road, and distance from the nearest urban center increase and as distance to the nearest publicly owned forest decreases. Prices varied considerably over time, and were lower in the years following the 2008–2009 recession than in most of the other years from 2004 through 2020.

To examine the magnitude of the price impacts of wildfires, we used the estimates from the econometric model to estimate how forest prices were affected by changes in drought stress and the number of large and extremely large wildfires (overlapping with the parcel or within 15 km of the parcel) between the years 1984–2003 and 2001–2020.

Forest prices were reduced by 1.04 percent by increasing drought stress and an additional 8.78 percent (9.82 percent total) by increases in the number of wildfires. The majority of these impacts arise from wildfires that burn near (within 15 km), but not on, private timberland. Thus, the bulk of the economic costs from wildfires on private timberlands come from changing expectations of wildfire risk. The changes in price should not be interpreted as decreases over time, but as decreases attributable to changes in drought stress and wildfires. These combined effects have led to $11.2 billion in lost economic value of private timberland in Oregon, Washington, and California. Economists refer to such losses in economic value as damages.

We examined regional variation in the timberland price impacts of changes in drought stress and the number of large wildfires (Figure 2). The largest percentage impact of number of wildfires on forest price was in California (-13.7 percent), and the smallest was in western Washington (-5 percent). The changing wildfire risk has depressed the economic value of privately owned Oregon forests by 7.7 percent west of the Cascade Range and by 6 percent east of the Cascade Range.
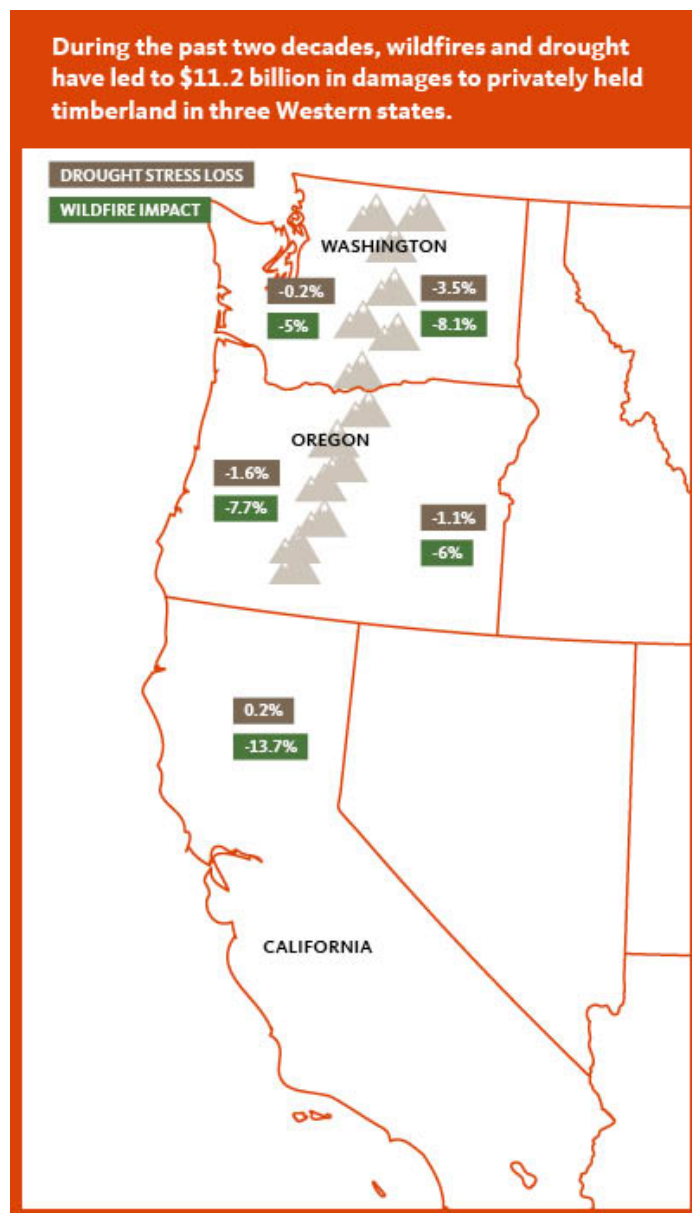
**Figure 2.** Regional variation in the estimated economic effect of drought stress and wildfires on the value of privately owned timberland. Courtesy of Oliver Day, Oregon State University.

Climate change is the strongest driver of the increase in frequency of large wildfires in the western United States (Abatzoglou and Williams 2016) and of the increase in regional drought stress (Zhuang et al. 2021). Therefore, the majority of the $11.2 billion in lost economic value to private forests that we estimate to have come from drought stress and the number of large wildfires can be interpreted as an economic cost of recent changes in climate. Furthermore, the majority of the lost economic value from large wildfires was caused by apparent changes in landowners' expectations of fire frequency or size. Thus, our study indicates that the economic value of timberland, a form of natural capital, in Oregon and along the West Coast is greatly affected by risks to the production value of those lands. The loss of economic value to timberland from climate-related changes in wildfire and drought stress adds to other economic evidence of climate damages, including damages to croplands (Diffenbaugh et al. 2021), slower growth of agricultural productivity (Ortiz-Bobea et al. 2021), increases in global economic inequality (Diffenbaugh and Burke 2019), flood damages (Davenport et al. 2021), property value losses from sea level rise (Bernstein et al. 2019), and human health impacts of wildfire smoke (Burke et al. 2021).

**Authors' Note:** A peer-reviewed article on this subject with more technical detail is available at https://doi.org/10.1016/j.jeem.2023.102894.

## Literature Cited

Abatzoglou, J.T., and A.P. Williams. 2016. Impact of anthropogenic climate change on wildfire across western US forests. Proceedings of the National Academy of Sciences 113:11770–11775.

Amacher, G.S., M. Ollikainen, and E. Koskela. 2009. Economics of forest resources. MIT Press,

Cambridge, Massachusetts.

Barbero, R., J.T. Abatzoglou, N.K. Larkin, C.A. Kolden, and B. Stocks. 2015. Climate change presents increased potential for very large fires in the contiguous United States. International Journal of Wildland Fire 24:892–899.

Bayham, J., J.K. Yoder, P.A. Champ, and D.E. Calkin. 2022. The economics of wildfire in the United States. Annual Review of Resource Economics 14:379–401.

Bernstein, A., M.T. Gustafson, and R. Lewis. 2019. Disaster on the horizon: the price effect of sea level rise. Journal of Financial Economics 134:253–272.

Burke, M., A. Driscoll, S. Heft-Neal, J. Xue, J. Burney, and M. Wara. 2021. The changing risk and burden of wildfire in the United States. Proceedings of the National Academy of Sciences 118:e2011048118. https://doi.org/10.1073/pnas.2011048118.

Costanza, J.K., et al. 2023. Disturbances to forests and rangelands. Pages 5-1–5–55 in Future of America's forest and rangelands: Forest Service 2020 Resources Planning Act assessment. General Technical Report WO-102. U.S. Department of Agriculture, Forest Service, Washington, D.C. https://doi.org/10.2737/WO-GTR-102-Chap5.

Dale, L. 2010. The true cost of wildfires in the western US. Western Forestry Leadership Coalition. https://doi.org/10.7916/c490-r123.

Davenport, F.V., M. Burke, and N.S. Diffenbaugh. 2021. Contribution of historical precipitation change to US flood damages. Proceedings of the National Academy of Sciences 118:e2017524118. https://doi.org/10.1073/pnas.2017524118.

Diffenbaugh, N.S., and M. Burke. 2019. Global warming has increased global economic inequality. Proceedings of the National Academy of Sciences 116:9808–9813.

Diffenbaugh, N.S., F.V. Davenport, and M. Burke. 2021. Historical warming has increased US crop insurance losses. Environmental Research Letters 16:084025. https://doi.org/10.1088/1748-9326/ac1223.

Ortiz-Bobea, A., T.R. Ault, C.M. Carrillo, R.G. Chambers, and D.B. Lobell. 2021. Anthropogenic climate change has slowed global agricultural productivity growth. Nature Climate Change 11:306–312.

Reed, W.J. 1984. The effects of the risk of fire on the optimal rotation of a forest. Journal of Environmental Economics and Management 11:180–190.

Wang, Y., and D.J. Lewis. 2024. Wildfires and climate change have lowered the economic value of western US forests by altering risk expectations. Journal of Environmental Economics and Management 123:102894. https://doi.org/10.1016/j.jeem.2023.102894.

Zhuang, Y., R. Fu, B.D. Santer, R.E. Dickinson, and A. Hall. 2021. Quantifying contributions of natural variability and anthropogenic forcings on increased fire weather risk over the western United States. Proceedings of the National Academy of Sciences 118:e2111875118. https://doi.org/10.1073/pnas.2111875118.

# Potential Economic Impacts of a Major Wildfire Smoke Event in Oregon

James Sterns and Tina Beavers

## Introduction

One of the greatest challenges to analyzing the potential economic effects of a wildfire smoke event is compiling relevant data. Smoke events have direct economic effects, such as business closures and canceled events, and indirect effects, such as reductions in employees' take-home pay and, in turn, the money they can spend on household needs. Smoke events also have induced effects, or continuing reductions in economic activity that ripple through the economy, such as lower revenues for grocery stores and retail hardware outlets because their would-be customers have less take-home pay to spend and hence make fewer purchases at these stores.

Either quantitative or qualitative methods can be used to estimate direct effects. Quantitative methods require primary data, collected via interviews or surveys, that document recollections and aggregate financial records about the impacts of an event. Collecting data via these methods can require considerable time and money. Qualitative methods extract data from records of past events, such as news articles and industry reports. When available, these data can be used to establish baseline estimates of the types and magnitudes of direct economic losses.

Modeling is necessary to determine the magnitude of indirect and induced effects. For example, input-output models capture the cascading effects of a shock to an economic system. These models quantify the interactions of firms, industries, and social institutions within a local economy. As firms purchase, create, or add value to inputs, and then sell outputs to other firms or to consumers, the consumers both generate demand for products and function as employees whose labor is an input to the firms.

## Methods

We used Impact Analysis and Planning (IMPLAN n.d., Mulkey and Hodges 2000) to estimate the economic impacts of a hypothetical major wildfire smoke event in Oregon. IMPLAN is an input-output model and software initially developed by the U.S. Forest Service in cooperation with the Federal Emergency Management Agency and the Bureau of Land Management. Since 1993, IMPLAN has been managed as a private company, which now compiles and integrates economic data from the U.S. Department of Commerce, U.S. Bureau of Labor Statistics, and other federal and state government agencies. Data are synthesized and organized into 546 productive sectors similar to those in the North American Industry Classification System (www.census.gov/naics/), the standard used by federal statistical agencies in the United States, Canada, and Mexico to classify businesses. Data are collated at the levels of sectors and counties, and can be aggregated. Data for each sector include inputs and outputs, industrial performance, productivity, unit labor costs, and employment. IMPLAN supports estimation of the effects of changes in demand for one sector on all other sectors within a given geographic area.

IMPLAN is used to evaluate the positive or negative economic impacts of what is referred to in the software as events, such as opening of a new public facility, closure of a factory, or a flood. Information about a given event is necessary to parameterize the model to estimate the economic sectors most likely to be affected and the magnitude of those effects. Examples of IMPLAN studies include estimates of potential economic impacts of changes to the Conservation Reserve Program

(Campiche et al. 2011) and of the economic impact of the U.S. Department of Agriculture's Supplemental Nutrition Assistance Program (Paynter et al. 2014).

Our IMPLAN analysis required assumptions about the major sectors of Oregon's state economy that are most susceptible to direct effects of wildfire smoke and the magnitudes of those direct effects. We used news articles, peer-reviewed journal articles, and research reports from government and non-governmental agencies about the effects of wildfire smoke as primary sources of that information. To identify news articles, we searched the online databases Lexis-Nexis and America's News (NewsBank) for articles from 2015 through 2023 that reported economic consequences of wildfire smoke.

After identifying Oregon industries that likely are most susceptible to wildfire smoke, we queried the IMPLAN database to evaluate and rank the economic contribution of these industries to the state's economy. We excluded industries that contributed relatively small percentages of direct economic output given our assumption that these industries would have marginal indirect effects and negligible induced effects. The IMPLAN data disaggregate economic activity by industry code to the county level, allowing for estimates of economic activity of each industry in each county (although IMPLAN has its own internal system of 546 industry codes, which we matched to the NAICS codes). These county data are archived within IMPLAN annually, allowing for comparisons of economic output for each industry code in each county in each year.

The U.S. Environmental Protection Agency (EPA) monitors and archives daily values of the Air Quality Index for specific locations throughout the United States. We queried the data to identify days with poor air quality (unhealthy for sensitive groups or worse) for 23 Oregon counties in which air quality monitors collected data. We calculated the number of days with poor air quality during eight years, 2015 through 2022. We excluded the 13 Oregon counties without air quality monitoring data from our analysis. As a consequence, our analysis likely underestimates the economic impacts of a hypothetical smoke event on Oregon's economy.

We then estimated the magnitude of economic impact of a smoke event on the total output of each of the retained industries. We based these estimates on our synthesis from the literature review. If the review yielded little to no information about a particular industry, we relied on inferences about impacts on related industries. As demonstrated in other IMPLAN studies, proxies for missing data are sometimes necessary (e.g., Serhat and Ramaswamy 2021). Hence, our results reflect the supposition that at the county level, a normal level of daily economic activity for a given industry (the default value in the IMPLAN model) will be reduced by a given percentage on each smoke day. We summed this daily impact over the average duration of smoke events in each county.

**Results**

*Synthesis of News Articles*

Most news articles focused on event cancellation and related loss of tourism, lost opportunities for outdoor recreation, and effects on farm and agricultural production (Appendix B). For example, in 2015, the cost of smoke-related cancellation of a sold-out performance at the Oregon Shakespeare Festival in Ashland was estimated at $65,000. Annual attendance at the festival in 2014 exceeded 100,000, and festival attendance has been a major contributor to the estimated $500 million in annual revenue generated by the tourism industry in Jackson County, Oregon (the county that includes Ashland) (Anonymous 2015). The cost of cancelling nine outdoor Oregon Shakespeare

Festival performances at one venue in September and October 2017 was estimated at $400,000, with associated reductions in the number of ticket renewals for the 2018 season (Morgan 2017). Cancellation of more than 26 outdoor performances from July through September 2018 led to a loss to the festival of $2 million and reduced local revenue from tourism (Flaccus 2018).

The Sisters Folk Festival is another example of economic losses as a result of wildfire smoke. In 2014, about 3,700 people attended the festival and spent about $1.2 million in Sisters, Oregon (Spurr 2017). In 2017, the festival was canceled because of smoke-related unhealthy air quality. In June and July 2019, transient room taxes on overnight stays in the city were 21 percent and 12 percent greater, respectively, than in the corresponding months in 2017, and transient room taxes in August 2018 were 36 percent greater than in 2017 (Spurr 2019).

Smoke-related cancellation of concerts at outdoor amphitheaters in Bend, Oregon, in 2021 and 2023 led to loss of money not only by the venues but by hotels, restaurants, bars, shops, and museums (Anonymous 2021, Kohn 2022, Land 2023). Moreover, anecdotal reports suggested that wildfire smoke in Oregon decreased demand for outdoor recreation such as rafting (Moriarty 2017, Wastradowski 2019), cycling (Fisicaro and Wieber 2017, Moriarty 2017), and running (Visser 2018), adversely affecting businesses that support such activities.

Wildfire smoke disproportionately affects businesses with outdoor operations, such as construction and agriculture. During some smoke events or on some days, outdoor activities are delayed (Rogoway and Theen 2018), but it is not uncommon that workers and businesses must choose between health and income (Goldberg 2020). In other cases, construction and other operations cease and airlines cancel flights (Rogoway 2020). In 2018, damage to Oregon-grown wine grapes from wildfire smoke led a customer in California to cancel contracts for about 2000 tons of grapes (Alberty 2019), corresponding to a market value of about $4 million. Wildfire smoke in 2020 reportedly was a major contributor to a 29 percent decrease in grape production in Oregon from 2019 to 2020, and wildfires across the United States in 2020 caused $3.7 billion in losses to the national wine industry (Beck 2022). It was suggested that winemakers were reluctant to purchase grapes from vineyards exposed to wildfire smoke because they were uncertain whether the resulting wine would be tainted (Madhusoodanan 2021).

*Synthesis of Peer-reviewed Articles and Other Research Reports*

Similar to the news articles, peer-reviewed journal articles and other research reports focused on economic effects such as loss of tourism, diminished labor productivity, and negative effects on farm and agricultural production. For example, monthly data from 1993 through 2015 on visits to national parks in Utah indicated that annual visitation losses were 0.5–1.5 percent during a typical fire season, resulting in an estimated regional economic loss of $2.7–4.5 million (Kim and Jakus 2019). A survey of members of the Kootenay Rockies Tourism Association (British Columbia, Canada) estimated that wildfire and its consequences caused an estimated total sales revenue loss of $38.4 million in 2017, and a reduction in payroll costs of $2.7 million over an average four-week period of disruption (Peak Solutions Consulting 2018). Analysis of data on use of more than 1,000 campsites in the western United States from 2008 through 2017, and concurrent, daily satellite data on wildfire and smoke, led to the conclusion that wildfires and smoke increased campsite cancellation rates, but overall smoke effects were small (Gellman et al. 2022).

As further illustrations, an examination of loss in labor productivity attributed to wildfires estimated that for each day of smoke, labor-force quarterly per capita earnings are reduced by about 0.1

percent, and concluded that wildfire smoke reduced earnings in terms of U.S. annual labor income by an average of $125 billion (in 2018 dollars) per year from 2007 through 2019 (Borgschulte et al. 2022). A study of the effects of air pollution on productivity of workers at a pear packing plant in California (Chang et al. 2016) also is relevant given that the size of particulate matter was comparable to particulate matter commonly detected in wildfire smoke. Increases in air pollution reduced worker productivity by approximately 6 percent of workers' average hourly earnings (Chang et al. 2015).

With respect to agricultural production, a survey of beef and dairy cattle, sheep, and goat producers in California, Nevada, and Oregon documented a range of losses attributed to wildfire smoke. These losses included livestock with elevated rates of pneumonia, poor weight gain, reduced conception rates, decreased milk production, lower birth weights, increased abortion rates, and unexplained deaths (O'Hare et al. 2021). Modeling of the determinants of total costs of 54 wildfires in 2004 through 2006 on coastal agricultural land in Greece estimated that economic losses from each wildfire ranged from €30,000 to 600,000 (Stougiannidou and Zafeiriou 2021).

*Estimated Economic Impacts of a Smoke Event*

An analysis of wildfire smoke's impact on labor markets identified 20 industries, each corresponding to a 2-digit NAICS industry code, that likely would be most vulnerable (Borgschulte et al. 2022). Similarly, research on populations vulnerable to wildfire smoke exposure identified frontline workers as active in 13 industries (Lappe and Vargo 2022). The initial set of 2-digit NAICS industries that we selected as most susceptible to impacts of wildfire smoke events in Oregon were agriculture (11), manufacturing (31–33), retail (45), transportation (48), real estate and rental (53), administrative and support services (56), healthcare (62), arts, entertainment and recreation (71), accommodation and food service (72), and other services (81). To refine the set of impacted industries, we reviewed the 3-digit industries within each of these 2-digit categories, yielding 46 3-digit industries that we believe are most susceptible to wildfire smoke events.

We included 22 of the 46 industries in our final analysis (Table 1). Our simplification was motivated by the trade-off between inclusion of a greater number of industries and

| 2017 NAICS 3-digit code | Industry |
|---|---|
| 111 | Crop production |
| 112 | Animal production and aquaculture |
| 115 | Support activities for agriculture and forestry |
| 230 | Construction |
| 445 | Food and beverage stores |
| 446 | Health and personal care stores |
| 447 | Gasoline stations |
| 451 | Sporting goods, hobby, musical instrument and book stores |
| 452 | General merchandise stores |
| 481 | Air transportation |
| 485 | Transit and ground passenger transportation |
| 487 | Scenic and sightseeing transportation |
| 488 | Support activities for transportation |
| 532 | Rental and leasing services |
| 561 | Travel arrangements, services to buildings, landscaping services |
| 711 | Performing arts, spectator sports, and related industries |
| 712 | Museums, historical sites, and similar institutions |
| 713 | Amusement, gambling, and recreation industries |
| 721 | Accommodations |
| 722 | Food service and drinking places |
| 811 | Repair and maintenance (car washes) |
| 812 | Personal and laundry services |

**Table 1.** Industries included in analysis of potential economic impacts of a wildfire smoke event in Oregon. NAICS, North American Industry Classification System.

124

computational time and, again, our assumption that the excluded industries would have marginal indirect effects and negligible induced effects. Collectively and averaged over 2015 through 2021, the 22 industries that we retained represent 40.5 percent of total employment, 31.3 percent of labor income, and 32.9 percent of total economic output per year for Oregon.

Over the eight years of our analysis, major wildfire smoke events occurred in 2015, 2017, 2018, 2020, and 2021 (Table 2). The average number of days of poor air quality varied considerably among years and among counties with smoke sensors. Jackson and Klamath counties averaged 20 or more days with poor air quality. The number of days of poor air quality also was relatively high in Lane (16), Josephine (15), and Deschutes, and Lake counties (11 each).

| County | County seat | 2015 | 2016 | 2017 | 2018 | 2019 | 2020 | 2021 | 2022 | Average |
|---|---|---|---|---|---|---|---|---|---|---|
| Baker | Baker City | 10 | 0 | 6 | 2 | 0 | 7 | 5 | 1 | 4 |
| Benton | Corvallis | 2 | 0 | 2 | 2 | 0 | 11 | 0 | 0 | 2 |
| Clackamas | Oregon City | 4 | 1 | 12 | 6 | 1 | 9 | 1 | 0 | 4 |
| Columbia | Saint Helens | 1 | 0 | 4 | 4 | 0 | 9 | 0 | 0 | 2 |
| Crook | Prineville | 8 | 1 | 16 | 7 | 1 | 7 | 9 | 0 | 6 |
| Deschutes | Bend | 6 | 0 | 28 | 14 | 5 | 14 | 20 | 1 | 11 |
| Douglas | Roseburg | 1 | 0 | 7 | 2 | 0 | 10 | 5 | 0 | 3 |
| Grant | Canyon City | 9 | 0 | 12 | 3 | 1 | 7 | 10 | 0 | 5 |
| Harney | Burns | 3 | 1 | 8 | 6 | 5 | 11 | 9 | 0 | 5 |
| Jackson | Medford | 29 | 0 | 31 | 42 | 7 | 15 | 35 | 0 | 20 |
| Jefferson | Madras | 4 | no data | 9 | 6 | 2 | 11 | 6 | 0 | 5 |
| Josephine | Grants Pass | 6 | 0 | 21 | 39 | 5 | 26 | 19 | 2 | 15 |
| Klamath | Klamath Falls | 13 | 0 | 26 | 40 | 6 | 46 | 50 | 1 | 23 |
| Lake | Lakeview | 3 | 2 | 18 | 22 | 1 | 18 | 23 | 0 | 11 |
| Lane | Eugene | 15 | 1 | 30 | 8 | 8 | 14 | 20 | 31 | 16 |
| Linn | Albany | 5 | 0 | 9 | 5 | 2 | 11 | 1 | 0 | 4 |
| Marion | Salem | 3 | 0 | 9 | 6 | 0 | 11 | 0 | 0 | 4 |
| Multnomah | Portland | 2 | 1 | 6 | 9 | 0 | 9 | 1 | 0 | 4 |
| Umatilla | Pendleton | 9 | 1 | 12 | 8 | 1 | 8 | 8 | 0 | 6 |
| Union | La Grande | 11 | 0 | 11 | 6 | 0 | 9 | 7 | 0 | 6 |
| Wallowa | Enterprise | 9 | 0 | 9 | 2 | 1 | 7 | 10 | 0 | 5 |
| Wasco | The Dalles | 2 | 0 | 16 | 5 | 0 | 3 | 2 | 0 | 4 |
| Washington | Hillsboro | 2 | 0 | 12 | 7 | 1 | 10 | 0 | 0 | 4 |
| Average among counties | | 7 | 0 | 14 | 11 | 2 | 12 | 10 | 2 | |

**Table 2.** Annual number of days with poor air quality (unhealthy for sensitive groups or worse) for the 23 counties in Oregon with U.S. Environmental Protection Agency (EPA) monitors. Source: www.epa.gov/outdoor-air-quality-data/air-quality-index-daily-values-report.

To complete the IMPLAN analysis, we estimated the magnitude of economic impact of a smoke event on the total output of each of the 22 industries (Table 1). We based these estimates on our synthesis of information from the literature review. If the review yielded little to no information about a particular industry, we relied on inferences about impacts on related industries (Appendix B). Again, as demonstrated in other IMPLAN studies, proxies for missing data are sometimes necessary (e.g., Serhat and Ramaswamy 2021). Hence, our results reflect the supposition that at the county level, a normal level of daily economic activity for a given industry (the default value in the IMPLAN model) will be reduced by a given percentage on each smoke day.

Our estimated reductions in the normal level of daily economic activity for a given industry on each day with poor air quality ranged from 0 to 60 percent (Table 3).

| IMPLAN industry category | NAICS 3-digit codes | Reduction (percentage) |
|---|---|---|
| Agriculture | 111, 112, 115 | 3 |
| Construction | 230 | 60 |
| Retailing | 445, 446, 447, 451, 452 | 3 |
| Transportation | 481, 485, 487, 488 | 5 |
| Rentals | 532 | 5 |
| Travel arrangements | 561 | 3 |
| Services to buildings | 561 | 3 |
| Landscaping services | 561 | 3 |
| Tourism—amusement | 711, 712, 713 | 5 |
| Tourism—accommodations | 721 | 5 |
| Food service, drinking places | 722 | 5 |
| Repair and maintenance | 811 | 0 |
| Personal care services | 812 | 5 |

**Table 3.** Daily percentage reduction in county-level economic output in Oregon due to a major smoke event.

Summing the estimated daily impact over the average duration of smoke events in each county (Table 2) yielded an estimate of the direct, indirect, and induced economic impacts of an event (Table 4).

When taken as absolute values, these estimates of economic loss appear to be substantial. To more clearly calibrate the interpretation of these model estimates, we calculated annual, statewide values of economic activity and the percentage reduction in annual economic activity per economic indicator (Table 5).

## Discussion

In the absence of readily available quantitative data to measure the economic impacts of recent wildfire smoke events, we used the IMPLAN input-output model to estimate

| Impact | Employment (number of jobs) | Labor income (dollars) | Value added (dollars) | Output (dollars) |
|---|---|---|---|---|
| Direct | 3,638 | 293,575,121 | 452,005,317 | 1,102,241,6312 |
| Indirect | 2,151 | 155,381,224 | 252,308,023 | 430,353,448 |
| Induced | 2,192 | 150,048,541 | 226,101,392 | 368,762,440 |
| Total | 7,981 | 599,004,886 | 930,414,732 | 1,901,357,520 |

**Table 4.** IMPLAN model estimates of economic loss as a consequence of a hypothetical major smoke event in 23 of Oregon's 36 counties.

impacts of a hypothetical smoke event similar to those that Oregon residents have experienced in recent years. A major smoke event will lead to economic losses in the state, but those losses are likely to be highly localized and industry-specific because the intensity and duration of wildfire smoke events are unlikely to be equally distributed across the state, economic activity is unequally distributed across the state, and smoke events will have disparate impacts across industries. Only some industries will face significant risks of losses, especially those dependent on outdoor work or activities. The Oregon industries

| Economic indicator | Estimated loss | Aggregated annual value, as calculated by IMPLAN | Estimated percentage reduction in activity |
|---|---|---|---|
| Employment, number of jobs[1] | 7,981 | 2,494,460 | 0.32 |
| Labor income[2] | $599,005,000 | $175,996,321,000 | 0.34 |
| Value-added economic activity[3] | $930,415,000 | $273,437,380,000 | 0.34 |
| Output[4] | $1,901,358,000 | $482,344,131,000 | 0.39 |

[1]Includes full-time, part-time, and seasonal work, and self-employed individuals.
[2]Includes all forms of employee compensation (e.g., wages, salaries, benefits, payroll taxes) and proprietor income (e.g., payments received by self-employed and unincorporated business owners, and current-production income of sole proprietorships, partnerships, and tax-exempt cooperatives).
[3]IMPLAN estimate of Oregon's Gross Domestic Product.
[4]Includes both value-added economic activity and the value of intermediate inputs.

**Table 5.** Estimated percentage loss of annual statewide economic activity in Oregon resulting from a hypothetical major smoke event in 23 of the state's 36 counties.

most susceptible to economic losses due to wildfire smoke events represent approximately 40 percent of total employment, 31 percent of labor income, and 33 percent of total economic output per year for the state. We estimated that a major smoke event will reduce the state's per annum Gross Domestic Product by at least $1 billion, or about one-third of one percent.

We acknowledge that we estimated economic loss from a single, distinct wildfire smoke event. We did not address potential compounded or cascading losses from multiple independent or interacting events within the same year. For example, a single smoke event leads to cancellation of some economic activity, but often activities only are delayed. Multiple smoke events would likely compound losses because activities are more likely to be canceled. Furthermore, our estimates almost certainly undervalue the economic impacts of wildfire smoke events. As noted above, our analysis only included 23 of Oregon's 36 counties. Additionally, we did not estimate the cost of long-term negative health outcomes such as diminished quality of life due to acute or chronic health conditions resulting from or exacerbated by smoke exposure. Some of those effects are estimated in *Scenarios of Wildfire Smoke Exposure, Health Impacts, and Associated Costs in Oregon* (this volume).

## Appendix

Appendix B documents the literature from which we estimated industry-specific economic impacts of wildfire smoke.

## Literature Cited

Alberty, M. 24 May 2019. Oregon vineyards, hazelnut farmers included in federal disaster relief package. The Oregonian. www.oregonlive.com/wine/2019/05/oregon-vineyards-hazelnut-farmers-included-in-federal-disaster-relief-package.html.

Anonymous. 24 August 2015. Wildfire smoke and outdoor theater don't mix. Klamath Falls Herald and News. www.heraldandnews.com/news/northwest/wildfire-smoke-and-outdoor-theater-dont-mix/article_27c97f83-ffd5-5b20-b973-5d23ef2ac8f7.html.

Anonymous. 6 September 2021. Labor Day weekend a bust as wildfire smoke creates hazardous air quality. Central Oregon Daily News. www.centraloregondaily.com/archives/central-oregon-daily/labor-day-weekend-a-bust-as-wildfire-smoke-creates-hazardous-air-quality/article_b672f362-02a8-5030-835f-04f6d617f516.html.

Beck, L. 27 June 2022. As wildfires take over the West, Oregon winemakers adapt. The New Lede. www.thenewlede.org/2022/06/as-wildfires-take-over-the-west-oregon-winemakers-adapt/.

Borgschulte, M., D. Molitor, and E.Y. Zou. 2022. Air pollution and the labor market: evidence from wildfire smoke. The Review of Economics and Statistics 106:1558–1575.

Campiche, J., M. Dicks, D. Shideler, and A. Dickson. 2011. Potential economic impacts of the managed haying and grazing provision of the Conservation Reserve Program. Journal of Agricultural and Resource Economics 36:573–593.

Chang, T., J.G. Zivin, T. Gross, and M. Neidell. 2016. Particulate pollution and the productivity of pear packers. American Economic Journal: Economic Policy 8:141–169.

Fisicaro, K., and A. Wieber. 6 September 2017. Smoke break not likely to last. The Bulletin. www.bendbulletin.com/localstate/smoke-break-not-likely-to-last/article_90738a35-cf08-500e-8265-cbf67705360d.html.

Flaccus, G. 25 September 2018. Wildfire smoke costs famed Oregon Shakespeare Festival. Associated Press. apnews.com/article/413a6a87eb68414fb2052c16041c505f.

Gellman, J., M. Walls, and M. Wibbenmeyer. 2022. Wildfire, smoke, and outdoor recreation in the

western United States. Forest Policy and Economics 134:102619. https://doi.org/10.1016/j. forpol.2021.102619.

Goldberg, J. 21 September 2020. Oregon farmworkers face 'awful choice' as wildfire smoke plagues harvest. The Oregonian. www.oregonlive.com/wildfires/2020/09/oregon-farmworkers-face-awful-choice-as-wildfire-smoke-plagues-harvest.html.

IMPLAN. n.d. Where it all started. implan.com/history/. Accessed July 2023.

Kim, M-K., and P.M. Jakus. 2019. Wildfire, national park visitation, and changes in regional economic activity. Journal of Outdoor Recreation and Tourism 26:34–42.

Kohn, M. 7 January 2022. Wildfire smoke an increasing problem in Central Oregon. The Bulletin. www.bendbulletin.com/localstate/wildfire-smoke-an-increasing-problem-in-central-oregon/article_4facd8ee-700b-11ec-b465-1761d822621a.html.

Land, J.A. 21 August 2023. 2 concerts in Bend canceled due to wildfire smoke. Oregon Public Broadcasting. www.opb.org/article/2023/08/21/wildfire-smoke-bend-oregon-concerts-canceled/.

Lappe, B., and J. Vargo. 2022. Disruptions from wildfire smoke: vulnerabilities in local economies and disadvantaged communities in the U.S. Federal Reserve Bank of San Francisco. Community Development Research Brief 2022-06. https://doi.org/10.24148/cdrb2022-06.

Madhusoodanan, J. 13 September 2021. Wildfire smoke ruins taste of some wines. The Washington Post. www.washingtonpost.com/health/wildfires-smoke-wine-taste/2021/09/10/ce4cd4ec-1007-11ec-bc8a-8d9a5b534194_story.html.

Morgan, N. 23 September 2017. Local businesses lament losses from smoke. Mail Tribune. infoweb-newsbank-com.oregonstate.idm.oclc.org/apps/news/document-view?p=AMNEWS&docref=news/1671ECCB03AC98F8.

Moriarty, L. 5 September 2017. Wildfire smoke is taking a toll on Oregon's tourist economy. Jefferson Public Radio. www.ijpr.org/business-and-labor/2017-09-05/wildfire-smoke-is-taking-a-toll-on-oregons-tourist-economy.

Mulkey, D., and A. Hodges. 2000. Using IMPLAN to assess local economic impacts. University of Florida, Florida Cooperative Extension Service, Institute of Food and Agricultural Sciences Extension, Gainesville, Florida. ufdcimages.uflib.ufl.edu/UF/00/08/96/07/00001/using-implan.pdf.

O'Hara, K.C., J. Ranches, L.M. Roche, T.K. Schohr, R.C. Busch, and G.U. Maier. 2021. Impacts from wildfires on livestock health and production: producer perspectives. Animals 11:3230. https://doi.org/10.3390/ani11113230.

Paynter, S.R., G.J. Jolley, and A.J. Nousaine. 2014. Policy implications of projecting the multiplier effects of social safety net programs using IMPLAN: reevaluating the economic impact of the Supplemental Nutrition Assistance Program. State & Local Government Review 46:28–45.

Peak Solutions Consulting. 2018. Economic impact of 2017 wildfires on tourism in the Kootenay Rockies tourism region. Kootenay Rockies Tourism Association, Kimberley, British Columbia. www.krtourism.ca/wp-content/uploads/2018/10/Wildfire-Recovery-Survey-2018.pdf.

Rogoway, M. 21 September 2020. Oregon wildfire smoke shuts down outdoor work for many, but 'there are some people who may not have a choice.' The Oregonian. www.oregonlive.com/business/2020/09/oregon-wildfire-smoke-shuts-down-outdoor-work-for-many-but-there-are-some-people-who-may-not-have-a-choice.html.

Rogoway, M., and A. Theen. 22 August 2018. Smoke creates headaches, uncertainty for Oregon

workers and businesses. The Oregonian. www.oregonlive.com/business/2018/08/smoke_creates_headaches_uncert.html.

Serhat, A., and K. Ramaswamy. 2021. Issues facing the Californian fruit sector. Choices 36(2):1–8. www.jstor.org/stable/27098589.

Spurr, K. 14 September 2017. Sisters tries to bounce back after tough year. The Bulletin. www.bendbulletin.com/localstate/sisters-tries-to-bounce-back-after-tough-year/article_5bcd036f-945e-5ef9-a85b-6eff8409a23a.html.

Spurr, K. 6 September 2019. Sisters revels in wildfire smoke-free summer. East Oregonian. www.eastoregonian.com/news/state/sisters-revels-in-wildfire-smoke-free-summer/article_50572e8e-d0b7-11e9-bb2c-cf928da24034.html.

Stougiannidou, D., and E. Zafeiriou. 2022. Wildfire economic impact assessment: an empirical model-based investigation for Greek agriculture. Modeling Earth Systems and Environment 8:3357–3371.

Visser, B. 4 December 2018. Hood to smoke. The Astorian. www.dailyastorian.com/news/local/hood-to-smoke/article_5f6edffc-dfa2-5d19-844a-dbd2711da358.html.

Wastradowski, M. 20 September 2019. Tourism organizations reckon with wildfire. REI Uncommon Path. www.rei.com/blog/news/tourism-organizations-reckon-with-wildfire.

# Business and Climate Change

Rajat Panwar and Michael Barnett

Businesses (also called firms, companies, corporations, and business organizations) have a central but conflicted role in the global discourse on climate change. Sometimes they are portrayed as villains, with the media highlighting industries responsible for a disproportionate share of greenhouse gas emissions and denouncing profit-driven firms for focusing on economic growth without due regard for its environmental toll (e.g., Riley 2017). At other times, businesses are hailed as heroes, with the media publicizing business-led innovations such as renewable energy sources, carbon capture technology, and sustainable products and services that show promise for mitigating climate change (e.g., Gelles 2024). This duality underscores the complex position businesses hold in the effort to limit climate change: businesses are a central cause of climate change, yet their resources and resourcefulness make them indispensable to its mitigation (Wright and Nyberg 2017).

Recognizing their vital role, businesses have shown significant interest in mitigating climate change. The majority of prominent corporations have staff dedicated to climate initiatives and actively communicate these efforts to shareholders, stakeholders, and the general public (Figure 1) (Harris 2023). Nearly half of the Fortune 500 companies have committed to at least one major climate initiative, such as the Science-Based Targets Initiative, Clean Energy Buyers



**Figure 1.** Oregon-based Tillamook Creamery aims for net zero greenhouse gas emissions by 2050 and has an interim target of a 30 percent reduction by 2030. Photograph by Gary Halvorson, Oregon State Archives.

Association, Carbon Disclosure Project, or Climate Group's RE100 (Miller 2023). However, the ways in which firms address climate change vary and can be difficult to track. Many companies do not differentiate among climate change, biological diversity, pollution, and sustainability, using these terms interchangeably. Accordingly, corporate initiatives focused on climate change can be indistinguishable from the broader portfolio of corporate environmental management or so-called greening activities, making it infeasible to assess firms' climate change mitigation efforts precisely.

Academics also are quite interested in the relationship between business and climate change (Li 2024, Vurbano et al. 2024). As with firms, this large and ever-growing body of scholarship often blurs the distinction between mitigating climate change and more general corporate greening and efficiency efforts. Due to its spread across a tangle of overlapping constructs such as corporate greening, sustainable business, and corporate sustainability, mapping the boundaries of the academic literature on business and climate change is increasingly onerous.

The most prominent research domains of relevance to business and climate change include sustainability reporting and disclosures, sustainable business models, sustainable production, sustainable supply chains, green human resource management, sustainable finance and investment, sustainable entrepreneurship, and environmental or sustainable marketing (Renwick et al. 2013, Pinkse and Groot 2015, White et al. 2019, Bocken and Geradts 2020, Christensen 2021, Kouhizadeh et al. 2021, Yu et al. 2021, Edmans and Kacperczyk 2022) (Figure 2). In addition to these core areas, research has emerged at the interface of business and market-driven soft policies (Cashore et al. 2004, Buchanan and Barnett 2022). This work covers a wide range of topics, including but not limited to third-party certification, eco-labeling, the circular economy, the sharing economy, the bioeconomy, and net-zero emission targets. Studies in this vast sphere examine how businesses navigate market-driven policy environments, engage with stakeholders, and manage reputational risks.



**Figure 2.** Oregon Tilth provides organic certification services for operations that produce crops and livestock or handle organic products.

More recently, scholarly attention has shifted toward the development and application of tools that enable businesses to measure and manage their environmental impacts (Hauschild 2018). These tools include environmental impact assessment, life cycle analysis, and methods such as carbon footprint analysis, natural capital accounting, and biodiversity impact assessment. Such tools are crucial for translating environmental sustainability goals into actionable business strategies and for holding businesses accountable for their environmental performance. Moreover, the literature increasingly explores interdisciplinary and cross-sectoral themes, such as the integration of technology (e.g., artificial intelligence and blockchain) into sustainability practices, the role of cultural and institutional contexts in shaping sustainable business behavior, and the emergence of hybrid organizations (such as B Corporations, companies that are certified as upholding high standards of social and environmental performance, accountability, and transparency) that blend profit-making with social and environmental missions (Stubbs 2017). These new areas highlight the dynamics and evolution of the field in response to scientific, political, and social change.

As the academic literature has grown, one question has remained central: Why should companies behave in environmentally responsible ways? This question underpins and drives the discipline of sustainable business. In the United States, regulatory requirements such as the Clean Air Act, Clean Water Act, Toxic Substances Control Act, and Resource Conservation and Recovery Act compel firms to behave in more environmentally sustainable ways. Sustainable business, however, emphasizes voluntary actions that go beyond regulatory compliance. An extensive body of literature has revealed a spectrum of corporate motivations for voluntary environmental initiatives. Some firms are driven purely by a sense of social and environmental responsibility, whereas others view initiatives to address climate change as sound investments because consumers, employees, investors, and other stakeholders value corporate environmental initiatives and patronize companies

with strong environmental commitments (Schaltegger et al. 2019). In such cases, climate action is driven by what is commonly termed the business case for sustainability—the calculation that environmentally positive practices advance companies' self-interest in multiple ways, ultimately leading to improved profitability. Thousands of scientific articles have explored and debated the circumstances under which such a business case can be made (Busch et al. 2024). There is general agreement that firms can profit from a range of voluntary environmental initiatives.

**Business Case for Voluntary Corporate Environmental Initiatives**

Corporate environmental initiatives offer several tangible benefits to companies (Fisher-Vanden et al. 2011). One of the primary advantages is cost savings (Kurapatskie and Darnall 2013). By improving energy efficiency, reducing waste, and utilizing renewable resources (Figure 3), corporations can lower operating costs considerably (in the sustainable business literature, waste reduction and waste elimination refer to resource efficiency, implying reduced extraction and processing of materials and, ultimately, lower emissions). For instance, investments in energy-efficient technologies, such as light-emitting diode (LED) lighting or more efficient machinery, reduce electricity consumption and lead to lower utility bills. Additionally, shifting towards renewable energy sources such as solar or wind can stabilize long-term costs, protecting corporations from fluctuations in fossil fuel prices.

Another key benefit of corporate environmental initiatives is enhanced brand reputation (Opoku et al. 2023). Consumers are increasingly aware of and concerned about climate change, and they often favor companies that demonstrate environmental responsibility. Corporations that minimize emissions are more likely to attract ecologically conscious customers, which can drive sales and customer loyalty (Godefroit-Winkel et al. 2022). For example, brands



**Figure 3.** Wind turbines overlook a canola field south of Hermiston, Oregon. Photograph by Gary Halvorson, Oregon State Archives.

such as Patagonia and Unilever strengthened their market positions by emphasizing sustainability in their business models, gaining a competitive edge over companies that have been slower to act on climate-change issues.

Moreover, climate initiatives help companies mitigate risk. The effects of climate change, from extreme weather events to resource scarcity, pose direct threats to business operations. Companies that proactively take steps to reduce their carbon footprint are better positioned to form alliances with other businesses and stakeholders (Rondinelli and London 2003, Lin and Darnall 2015), which helps them reduce operational and reputational risks (Cai et al. 2016) and enhance supply-chain resiliency (Ullah et al. 2022). Additionally, as governments around the world increasingly impose regulations and taxes on carbon emissions, companies that have already begun transitioning to

low-carbon operations are likely to face fewer regulatory hurdles and financial penalties. Corporate environmental initiatives can enable companies to preempt public regulation (Malhotra et al. 2019).



**Figure 4.** Solar-powered charging station for electric vehicles.

Corporate climate initiatives facilitate access to new markets (Jacobs et al. 2010) and investment opportunities (Eccles et al. 2014). As the demand for green technologies and sustainable products grows, companies that adopt these technologies and products early can tap into emerging markets. For instance, companies can meet the growing demand for electric vehicles (Figure 4), development of renewable energy, and sustainable packaging. Many global investors prioritize environmental, social, and governance (ESG) criteria in their investment decisions, although political backlash against such investments has erupted in some U.S. states in recent years. Companies that demonstrate leadership in climate action are more likely to attract capital from institutional investors and fund managers who are focusing on sustainable portfolios (Friede et al. 2015, Chen and Xie 2022).

Employee engagement and retention is another advantage of corporate climate initiatives (Umrani et al. 2022). Workers today, particularly younger generations, are more likely to seek employment with companies whose practices align with their personal values, which can include a commitment to climate action. By establishing sustainability initiatives, corporations not only attract top talent but improve employee morale and productivity. A workforce that feels part of a larger mission is typically more engaged and motivated, which can lead to lower turnover rates (Backhaus et al. 2002).

Corporate climate initiatives also foster innovation (Nidmolu et al. 2009). Reducing environmental impact often forces corporations to rethink their processes, products, and services, prompting advances that can differentiate them from competitors (Sharma and Vredenburg 1998, Demirel and Kesidou 2019). A focus on sustainability can drive research and development, resulting in creation of new technologies or business models that improve environmental and financial performance.

In sum, voluntary corporate climate initiatives can yield a range of benefits including cost savings, risk mitigation, enhanced reputation, market opportunities, and employee engagement. These initiatives help corporations meet some environmental goals and can position them for long-term success in today's sustainability-driven business context (Busch et al. 2024). Thus, the business case is often the primary driver of voluntary actions toward climate change mitigation, although small businesses frequently stand out as exceptions, driven more by a desire to make a positive impact (Panwar et al. 2017).

Often asked is whether voluntary corporate efforts to address climate change are effective. The honest answer is that we don't know. These efforts have undoubtedly improved energy and resource efficiency, spurred the development of products with lower life-cycle emissions, and raised consumer awareness about such products. However, critics argue that these initiatives have

largely fueled green consumerism rather than fostered sustainable consumption (Akenji 2014). Market-driven policy frameworks, such as the circular economy, bioeconomy, and net-zero targets, have similarly created conditions for sustainable investments. Yet their effectiveness in mitigating climate change remains unclear, even at scale. Compounding this uncertainty, many companies struggle to align their business models with these policy frameworks (Hopkinson et al. 2018, Panwar and Niesten 2022, Pinkse et al. 2024). Some have rolled back their climate commitments in the face of economic or political pressures (Bryan and Mooney 2024). Even when such initiatives are fully implemented, no empirical evidence or simulations demonstrate that they have, or can, contribute substantively to climate change mitigation. On the contrary, some scholars argue that corporate-led efforts may hinder mitigation efforts by delaying or deterring regulatory interventions that could prove more effective (Barnett et al. 2021).

What we do know is that substantive corporate climate actions are most likely to emerge under strong regulatory frameworks (Aragon-Correa et al. 2020, Zhang et al. 2022) and institutional pressures, including monitoring by consumers, nongovernmental organizations, and investors. However, companies' capacity to implement meaningful actions is often compromised in the context of global operations (Murcia et al. 2021). Therefore, some scholars argue that fundamental economic transformations, such as localization, deglobalization (Bu et al. 2017, Chaurasia et al. 2024), or even degrowth (intentionally shrinking the economy) (Hickel 2020), are essential for climate change mitigation. Amidst these broader debates, business scholarship has predominantly focused on advancing climate initiatives within the existing economic system, largely overlooking the critical question of whether these system-constrained initiatives mitigate climate change.

Given the above challenges, the importance of localized corporate responses to climate change cannot be overstated. However, such geographically focused research also remains scant. For example, the response of Oregon-based businesses to climate change has received little attention in academic literature although Oregon offers a rich research context given the number of climate-change mitigation initiatives implemented by its local businesses and strong supporting regulations. These topics are explored in greater detail below.

## Voluntary Corporate Environmental Initiatives by Oregon-based Companies

Oregon is home to several of the world's most prominent companies, including Nike, Intel, Columbia Sportswear, Daimler Trucks North America, and Lithia Motors. These global companies play a major role in the state's economy, particularly in industries such as sportswear, technology, transportation, and manufacturing. Their corporate communications consistently express concern about the environmental impact of their operations and highlight the actions they are taking to mitigate that impact (Box 1, 2).

Not only global corporations but many Oregon-based businesses that serve local, regional, and national markets have undertaken substantial environmental initiatives. B Corp PDX (www.blocalpdx. com), a regional network of certified B Corporations in Portland, Oregon, exemplifies this trend. Oregon has the third highest number of B Corporations in the United States (139, following California and New York), and a greater number of B Corporation-certified wineries than any other state or country (Grand Canyon University 2021, Oregon Wine Board 2024). Among the B Corporations, Tillamook Creamery's climate strategy, which aims for net zero greenhouse gas emissions by 2050 and an interim target of a 30 percent reduction by 2030, is particularly ambitious (Box 3).

Oregon-based businesses are also creating low-emission products and processes. For instance, Freres Lumber, a family-owned company in Lyons, Oregon, has developed mass plywood panels, an addition to mass timber products that arguably has lower greenhouse gas emissions than alternative building materials (Churkina et al. 2020,

> ### Box 2: Intel's Sustainability Strategy
>
> To address climate change, we collectively need to take immediate action through systems change, technological innovation, and global collaboration. At Intel, we've significantly invested in reducing our manufacturing environmental footprint for more than 20 years, raising the bar on our own efforts and leveraging our experience and international influence to drive change through collaboration with customers, competitors, and peers across industries.
>
> To drive our own environmental footprint to the lowest possible levels, we've set ambitious goals. In manufacturing we aim to achieve net-zero greenhouse gas (GHG) emissions for scopes 1 and 2 by 2040 as well as net-positive water and zero waste to landfills by 2030. For our products, our objective is to increase the energy efficiency of client and server microprocessors tenfold by 2030. Finally, we expanded our commitment to net-zero GHG emissions and set a goal to achieve net-zero upstream Scope 3 GHG emissions by 2050.
>
> We remain committed to doing our part and are proud to be a leading contributor to the larger collective effort that focuses on making positive change happen to move us all toward more- sustainable computing and a more sustainable future.
>
> We are making noteworthy progress toward our environmental goals by focusing on sustainability in several key semiconductor manufacturing areas—electricity, water, waste, our value chain, and alternative green chemistry solutions. Discover the actions we've taken and progress we've made in each of these areas as we drive toward our larger goal of achieving carbon-neutral computing to address climate change.
>
> As AI investment and adoption surges almost universally, the role of AI in driving sustainable transformation remains an area of huge opportunity. Our Sustainable Intelligence Index examines the trends and progress of organizations across all stages of the AI adoption journey, sectors, and regions as they aim to drive sustainable AI adoption for tech zero and tech positive aims.
>
> *Source: www.intel.com/content/www/us/en/environment/ sustainability.html. Accessed 20 September 2024.*

Liang et al. 2021). Skip Technology, a Portland-based startup, is developing a liquid battery that does not require rare earth mining and has large and long-duration (4 to 100 or more hours) stationary energy storage. The company, which has received a U.S. National Science Foundation Small Business Innovative Research award, claims that a single battery can power 35 homes for 10 hours. Puyallup Tribal Enterprises, the Puyallup Tribe's economic development arm, is the lead investor in Skip Technology. Similar examples are common across various sectors of the economy. For instance, HILOS, a Portland-based company, supports the design and manufacture of zero-waste shoes with

circular design practices, and ARIS Hydronics has created the world's first modular combi heat pump system. Combi systems, which heat both water and space, are much more energy-efficient than traditional systems. As another illustration, Photon Marine builds electric outboard motor systems to reduce the carbon footprint of commercial boat fleets.

Decarbonizing the energy production system is essential for reducing emissions of greenhouse gases from business operations. In 2023, approximately 62 percent of Oregon's energy was generated by renewable sources, including hydropower, wind, and solar power (EIA 2024). Ongoing projects aim to further increase this share. For instance, NextEra Energy's proposed Wheatridge Renewable Power Facility in Umatilla and Morrow counties will provide 300 megawatts of wind capacity, 50 megawatts of solar power, and 30 megawatts of battery storage—enough to power around 100,000 households. The Powerize Northwest Consortium, a coalition of public, private, and community organizations, focuses on strengthening Oregon's leadership in smart grid infrastructure, energy storage, research, commercialization, and workforce development. The Clean Tech Manufacturing Task Force, which is co-convened by Governor Kotek, Senator Wyden, and Daimler Truck North America's Chief Executive Officer John O'Leary, seeks to accelerate Oregon's transition to a clean energy economy. By addressing barriers and making targeted recommendations, the task force envisions Oregon as a clean technology hub, enabling businesses to significantly decarbonize their operations and establish global leadership in sustainable practices. Additionally, nonpartisan nonprofits such as Oregon Business for Climate mobilize industry support and business leadership to advance climate policies in the state.

Oregon-based businesses are demonstrating climate leadership in some unexpected yet critical sectors, too. For example, Northwest Permanente's climate action plan is pioneering a path for the healthcare industry to address climate change in a holistic manner (Box 4).

**Regulations Guiding Oregon's Corporate Environmental Initiatives**

Oregon's environmental regulatory framework, one of the most comprehensive in the United States, is designed to address environmental sustainability, pollution, climate change, and social equity.

Corporations operating in Oregon are subject to numerous regulations that promote environmentally responsible practices. The state has adopted stringent standards that encourage the use of clean energy, waste reduction, water conservation, and the mitigation of greenhouse gas emissions.

The Oregon Department of Environmental Quality is the primary regulatory agency overseeing environmental compliance in the state. Created in 1969, the Department is responsible for implementing state and federal environmental laws, including those related to air and water quality, waste management, hazardous materials, and toxic substances. Businesses engaged in activities that could affect the environment must obtain three types of permits: air quality, water quality, and hazardous waste management. The Office of Greenhouse Gas Programs spearheads the Department of Environmental Quality's efforts to minimize Oregon's contribution to global greenhouse gas emissions by creating and implementing policies, strategies, and programs aimed at significant reductions. The four existing Department programs, Greenhouse Gas Reporting, Clean Fuels, Climate Protection, and Third Party Verification, collectively focus on monitoring and reducing emissions and ensuring that further reductions are both effective and equitable.

The Greenhouse Gas Reporting Program mandates that dominant sources of emissions, such as large stationary facilities

> **Box 4: Northwest Permanente's Climate Action Plan**
>
> To date, relatively few physicians in this country are taking a stand on climate - and few if any major medical groups. Yet, the World Health Care organization (WHO) has estimated that approximately 250,000 deaths annually between 2030 and 2050 could be due to the impacts of climate change . . . .
>
> Northwest Permanente has chosen to make this issue our issue, and we are proud to share with you our Climate Action Plan, which takes into account a number of steps to limit our carbon footprint while adapting our business for success in a world beset by climate change. Not only do we see climate change as a health emergency, but as the first physician-owned medical group in the world to become a certified B Corp, we value the triple bottom of line of people, planet, and profit and our business is modeled on this commitment.
>
> The key tenets of our Climate Action Plan are as follows:
>
> - Ensure that the most vulnerable populations in our communities have a leading voice in planning for climate interventions
> - Minimize our greenhouse gas (GHG) footprint and offset the carbon our core business createss
> - Work with our business partners and vendors to insist on climate-smart facilities and operations
> - Ensure the health of our supply chains by supporting local and regional purchasing and creating redundancies in our procurement practices
> - Adapt our medical model to anticipate changing disease burdens our communities will face in the coming years secondary to climate impacts
> - Work with our business partners to create back-up plans for insurance failures
> - Make the case for climate-smart business as a strategy for financial solvency amidst growing uncertainty
> - Take a leading stance as a medical group on the need for climate action
>
> *Source: northwest.permanente.org/blog/confronting-climate-change-northwest-permanentes-climate-action-plan. Accessed 19 November 2024.*

and suppliers of liquid fuel, natural gas, propane, and electricity, report their greenhouse gas emissions and related data. This information is collected, audited, and published annually. Beginning in 2022, the reports of certain major emitters must be verified by a third party. In 2021, the Oregon Legislature passed the Clean Energy Targets bill, setting ambitious goals for reducing greenhouse gas emissions from electricity sold in Oregon. The bill mandates that Portland General Electric, PacifiCorp, and Electricity Service Suppliers cut emissions to 80 percent below baseline levels by 2030, 90 percent by 2035, and 100 percent by 2040 and every year thereafter. Baseline levels are

defined as the average annual greenhouse gas emissions from 2010, 2011, and 2012 associated with the electricity sold to retail consumers. The Oregon Department of Environmental Quality, in partnership with the Public Utility Commission, is responsible for implementing the program. The Department's key duties are collecting emissions data, calculating baseline levels, and determining the reductions required to meet the targets established by the legislation.

Around 35–40 percent of Oregon's greenhouse gas emissions is attributed to the transportation sector. The Clean Fuels Program, established in 2016, is Oregon's primary policy for reducing greenhouse gas emissions from transportation fuels. The program aims to limit the carbon emitted by fuels used in the state, targeting a 10 percent reduction by 2025, 20 percent by 2030, and 37 percent by 2035. According to the Oregon Department of Environmental Quality, biofuel production has increased, and biofuels are being produced more cleanly and in higher volumes. The shift to biofuels, electricity, and other renewable fuels has reduced tailpipe pollution, which may improve public health, particularly for historically overburdened communities (DEQ 2024). The program operates via a credit and deficit system, creating an incentive for businesses to supply low-carbon fuels while generating credits for compliance. Oregon's transition to cleaner transportation fuels has spurred $200 million in annual investment without raising fuel prices substantially, and renewable options such as biodiesel, renewable diesel, electricity, and renewable natural gas have become viable alternatives to fossil fuels (DEQ 2024). The program complements other state initiatives, including the Zero Emission Vehicle regulations, ensuring that Oregon's transportation sector increasingly relies on low- or zero-carbon fuels. Since its implementation, the program has avoided use of over 1.5 billion gallons of petroleum-based fuels and prevented emissions of 6.8 million metric tons of greenhouse gases (DEQ 2024).

In 2021, Oregon launched its Climate Protection Program, a regulation with far-reaching implications for fossil fuel companies that at the time of its passage was considered to be one of the strongest climate action programs in the United States. The program established a cap-and-reduce approach to greenhouse gas emissions, focusing on suppliers of fossil fuels and large stationary sources, such as factories and power plants. The program targeted a 50 percent reduction in carbon emissions by 2035 and a 90 percent reduction by 2050. Corporations that fall under the regulation must report their emissions annually and comply with the declining cap on allowed emissions. However, a group of fossil fuel companies sued to block the program, and in 2023 an appeals court ruled the program invalid on the grounds that Oregon did not follow Clean Air Act rules when implementing the program. The Oregon Department of Environmental Quality initiated a rulemaking process to reinstate the program. In November 2024, the Environmental Quality Commission, which oversees the department, unanimously approved the program, maintaining its original emissions reduction targets and timelines. The program will apply to fossil fuel companies and major natural gas users, including manufacturers of cement, fertilizer, gypsum, and paper.

The Third Party Verification Program was developed in 2020 to bolster the Greenhouse Gas Reporting and Clean Fuels Programs by requiring companies to submit data verified by an independent third party. The program aims to enhance data reliability and ensure that businesses in Oregon accurately calculate emissions while meeting Department of Environmental Quality reporting requirements. As the Greenhouse Gas Reporting and Clean Fuels Programs evolve, the amount of data collected will continue to expand in scope, detail, and information content. Verification mainly applies to large facilities and suppliers that report emissions of 25,000 metric tons of carbon dioxide equivalent ($MTCO_2e$) or more for the previous calendar year.

Additionally, Oregon has enacted several pieces of legislation aimed at promoting recycling and reducing or preventing industrial waste. At its core, waste prevention minimizes the use of materials, which can help reduce greenhouse gas emissions at every phase of a material's life cycle, including resource extraction, production, transportation, and final management (such as recycling or disposal). Oregon has long been a leader in waste reduction and recycling. The Oregon Recycling Act of 1983 made recycling of certain materials mandatory, and the state continues to expand its waste management regulations. For example, proposed changes to the recycling program under the 2022 Plastic Pollution and Recycling Modernization Act would require producers and manufacturers of packaged goods, paper products, and food service ware to contribute financially to updating Oregon's recycling infrastructure and to share responsibility for making Oregon's recycling collection and processing system more effective (Circular Action Alliance 2024). These companies will provide funding through a producer responsibility organization that will administer an extended producer responsibility program on the companies' behalf. In most cases, the responsible producer is the owner of the brand under which the packaged or paper item is marketed. Compliance with the program revisions is required by 1 July 2025. In 2024, the Oregon legislature passed the Right to Repair Bill, which requires cellular telephone and appliance companies to provide parts to consumers who wish to repair their devices, reducing the need for new purchases and thus preventing further greenhouse gas emissions. The Oregon E-Cycles program, which will launch on 1 January 2026, will be one of the first statewide electronics recycling programs in the nation.

## Looking Ahead

Businesses are both a leading cause of climate change and key to its mitigation. In Oregon, many companies acknowledge environmental sustainability and climate change as fundamental concerns, taking steps toward mitigation. Smaller companies and niche start-ups are also contributing to a vibrant sustainable business ecosystem. The regulatory framework is robust and evolving. However, corporate resistance to environmental regulations persists. This resistance appears through litigation, such as challenges to the Climate Protection Program, and lobbying efforts. For example, Amazon reportedly lobbied against a bill regulating emissions from energy-intensive data centers (O'Donovan 2023), while Apple opposed the right-to-repair bill, lobbying against banning parts pairing in Oregon (Garden 2024). Public sentiment strongly supports action. A 2000s survey by the Oregon Department of Environmental Quality found that 68 percent of Oregonians favored stricter environmental regulations (Carlough 2004). Today, as the impacts of climate change become more visible, societal expectations for corporate sustainability have likely intensified. Simultaneously, the global investment climate has grown more favorable for sustainability-focused businesses, presenting opportunities for Oregon firms.

Oregon businesses can leverage the state's regulatory environment to innovate and lead in sustainable practices, positioning themselves as national and global leaders. Policymakers, too, have a chance to drive progress by aligning regulations and investment strategies. Academic institutions, meanwhile, can serve as catalysts. By prioritizing education and research on climate change, they not only can bolster Oregon's sustainable economy but respond to rising expectations from accreditation bodies (e.g., Association to Advance Collegiate Schools of Business or AACSB), students, and business media (e.g., *Financial Times*, *Wall Street Journal*), who increasingly call for climate-related curriculum enhancements.

## Literature Cited

Akenji, L. 2014. Consumer scapegoatism and limits to green consumerism. Journal of Cleaner Production 63:13–23.

Aragòn-Correa, J.A., A. Marcus, and D. Vogel. 2020. The effects of mandatory and voluntary regulatory pressures on firms' environmental strategies: a review and recommendations for future research. Academy of Management Annals 14:339–365.

Backhaus, K.B., B.A. Stone, and K. Heiner. 2002. Exploring the relationship between corporate social performance and employer attractiveness. Business & Society 41:292–318.

Barnett, M., B. Cashore, I. Henriques, B. Husted, R. Panwar, and J. Pinkse. 2021. Reorient the business case for corporate sustainability. Stanford Social Innovation Review summer 2021:35–39.

Barnett, M.L., I. Henriques, and B.W. Husted. 2020. Beyond good intentions: designing CSR initiatives for greater social impact. Journal of Management 46:937–964.

Bocken, N.M., and T.H. Geradts. 2020. Barriers and drivers to sustainable business model innovation: organization design and dynamic capabilities. Long Range Planning 53:101950. https://doi.org/10.1016/j.lrp.2019.101950.

Bryan, K., and A. Mooney. 24 June 2024. Why top companies are starting to back away from green targets. Financial Review. www.afr.com/policy/energy-and-climate/why-companies-are-starting-to-back-away-from-green-targets-20240624-p5jo5n.

Bu, M., C.-T. Lin, and B. Zhang. 2017. Globalization and climate change: new empirical panel data evidence. Pages 201–220 in B.C. Lin and S. Zheng, editors. Environmental Economics and Sustainability. John Wiley and Sons, West Sussex, United Kingdom.

Buchanan, S., and M.L. Barnett. 2022. Inside the velvet glove: sustaining private regulatory institutions through hollowing and fortifying. Organization Science 33:2159–2186.

Burbano, V.C., M.A. Delmas, and M.J. Cobo. 2024. The past and future of corporate sustainability research. Organization & Environment 37:133–158.

Busch, T., et al. 2024. Moving beyond "the" business case: how to make corporate sustainability work. Business Strategy & the Environment 33:776–787.

Cai, L., J. Cui, and H. Jo. 2016. Corporate environmental responsibility and firm risk. Journal of Business Ethics 139:563–594.

Carlough, L. 2004. General deterrence of environmental violation: a peek into the mind of the regulated public. Oregon Department of Environmental Quality, Portland, Oregon. www.oregon.gov/deq/FilterDocs/DeterrenceReport.pdf.

Cashore, B.W., G. Auld, and D. Newsom. 2004. Governing through markets: forest certification and the emergence of non-state authority. Yale University Press, New Haven, Connecticut.

Chaurasia, S., R.K. Pati, S.S. Padhi, and S. Gavirneni. 2024. Is localization better than globalization for sustainability? Evidence from the nutraceuticals industry for managing malnutrition in India. International Journal of Production Economics 268:109106. https://doi.org/10.1016/j.ijpe.2023.109106.

Chen, Z., and G. Xie. 2022. ESG disclosure and financial performance: moderating role of ESG investors. International Review of Financial Analysis 83:102291. https://doi.org/10.1016/j.irfa.2022.102291.

Christensen, H.B., L. Hail, and C. Leuz. 2021. Mandatory CSR and sustainability reporting: economic analysis and literature review. Review of Accounting Studies 26:1176–1248.

Churkina, G., A. Organschi, C.P.O. Reyer, A. Ruff, K. Vinke, Z. Liu, B.K. Reck, T.E. Graedel, and H.J. Schellnhuber. 2020. Buildings as a global carbon sink. Nature Sustainability 3:269–276.

Circular Action Alliance. 31 March 2024. Oregon Program Plan (2025–2027). www.oregon.gov/deq/recycling/Documents/CAAProposedRMAplan.pdf.

Demirel, P., and E. Kesidou. 2019. Sustainability-oriented capabilities for eco-innovation: meeting the regulatory, technology, and market demands. Business Strategy and the Environment 28:847–857.

DEQ (Oregon Department of Environmental Quality). 2024. Oregon Clean Fuels Program. www.oregon.gov/deq/ghgp/cfp/pages/default.aspx. Accessed October 2024.

Eccles, R.G., I. Ioannou, and G. Serafeim. 2014. The impact of corporate sustainability on organizational processes and performance. Management Science 60:2835–2857.

Edmans, A., and M. Kacperczyk. 2022. Sustainable finance. Review of Finance 26:1309–1313.

EIA (U.S. Energy Information Administration). 18 April 2024. Oregon state profile and energy estimates. www.eia.gov/state/analysis.php?sid=OR#:~:text=In%202023%2C%20renewable%20energy%20resources,in%2Dstate%20electricity%20net%20generation. Accessed November 2024.

Fisher-Vanden, K., and K.S. Thorburn. 2011. Voluntary corporate environmental initiatives and shareholder wealth. Journal of Environmental Economics and Management 62:430–445.

Friede, G., T. Busch, and A. Bassen. 2015. ESG and financial performance: aggregated evidence from more than 2000 empirical studies. Journal of Sustainable Finance & Investment 5:210–233.

Garden, L. 3 April 2024, updated 24 July 2024. Apple loses with Oregon's new right-to-repair law. Trellis. trellis.net/article/apple-loses-oregons-new-right-repair-law/.

Gelles, D. 1 April 2024. The new climate tech. The New York Times. www.nytimes.com/2024/04/01/briefing/climate-technology-carbon-capture.html.

Godefroit-Winkel, D., M. Schill, and F. Diop-Sall. 2022. Does environmental corporate social responsibility increase consumer loyalty? International Journal of Retail & Distribution Management 50:417–436.

Grand Canyon University. 12 October 2021. An analysis of B Corporations by U.S. state. www.gcu.edu/blog/gcu-experience/analysis-b-corporations-us-state.

Harris, D. 21 July 2023. 99% of the S&P 500 is reporting on ESG and 65% are obtaining ESG assurance. BDO USA. www.bdo.com/insights/sustainability-and-esg/99-of-the-s-p-500-is-reporting-on-esg-and-65-are-obtaining-esg-assurance.

Hauschild, M.Z. 2018. Introduction to LCA methodology. Pages 59–66 in M. Hauschild, R. Rosenbaum, and S. Olsen, editors. Life Cycle Assessment. Springer, Cham, Switzerland. https://doi.org/10.1007/978-3-319-56475-3_6.

Hickel, J. 2020. Less is more: how degrowth will save the world. Windmill Books, London, United Kingdom.

Hopkinson, P., M. Zils, P. Hawkins, and S. Roper. 2018. Managing a complex global circular economy business model: opportunities and challenges. California Management Review 60:71–94.

Jacobs, B.W., V.R. Singhal, and R. Subramanian. 2010. An empirical investigation of environmental performance and the market value of the firm. Journal of Operations Management 28:430–441.

Kouhizadeh, M., S. Saberi, and J. Sarkis. 2021. Blockchain technology and the sustainable supply chain: theoretically exploring adoption barriers. International Journal of Production Economics 231:107831. https://doi.org/10.1016/j.ijpe.2020.107831.

Kurapatskie, B., and N. Darnall. 2013. Which corporate sustainability activities are associated with

greater financial payoffs? Business Strategy and the Environment 22:49–61.

Li, X. 2024. Physical climate change exposure and firms' adaptation strategy. Strategic Management Journal, in press. https://doi.org/10.1002/smj.3674.

Liang, S., H. Gu, and R. Bergman. 2021. Environmental life-cycle assessment and life-cycle cost analysis of a high-rise mass timber building: a case study in Pacific Northwestern United States. Sustainability 13:7831. https://doi.org/10.3390/su13147831.

Lin, H., and N. Darnall. 2015. Strategic alliance formation and structural configuration. Journal of Business Ethics 127:549–564.

Malhotra, N., B. Monin, and M. Tomz. 2019. Does private regulation preempt public regulation? American Political Science Review 113:19–37.

Miller, Z. 17 October 2023. Nearly half of Fortune 500 companies engaged in major climate initiatives. David Gardiner and Associates. www.dgardiner.com/fortune-500-climate-initiatives-2023.

Murcia, M.J., R. Panwar, and J. Tarzijan. 2021. Socially responsible firms outsource less. Business & Society 60:1507–1545.

Nidumolu, R., C.K. Prahalad, and M.R. Rangaswami. 2009. Why sustainability is now the key driver of innovation. Harvard Business Review 87(9):56–64.

O'Donovan, C. 4 April 2023. Amazon, despite climate pledge, fought to kill emissions bill in Oregon. The Washington Post. www.washingtonpost.com/technology/2023/04/04/amazon-climate-energy-fuel-oregon/.

Opoku, R.A., S. Adomako, and M.D. Tran. 2023. Improving brand performance through environmental reputation: the roles of ethical behavior and brand satisfaction. Industrial Marketing Management 108:165–177.

Oregon Wine Board. 2024. Did you know Oregon has the most B Corp wineries in the world? www.oregonwine.org/blog/did-you-know-oregon-has-the-most-b-corp-wineries-in-the-world/. Accessed Novemember 2024.

Panwar, R., and E. Niesten. 2022. Jump-starting, diffusing, and sustaining the circular economy. Business Strategy and the Environment 31:2637–2640

Panwar, R., E. Nybakk, E. Hansen, and J. Pinkse. 2017. Does the business case matter? The effect of a perceived business case on small firms' social engagement. Journal of Business Ethics 144:597–608.

Pinkse, J., P. Demirel, and A. Marino. 2024. Unlocking innovation for net zero: constraints, enablers, and firm-level transition strategies. Industry and Innovation 31:16–41.

Pinkse, J., and K. Groot. 2015. Sustainable entrepreneurship and corporate political activity: overcoming market barriers in the clean energy sector. Entrepreneurship Theory and Practice 39:633–654.

Renwick, D.W., T. Redman, and S. Maguire. 2013. Green human resource management: a review and research agenda. International Journal of Management Reviews 15:1-14.

Riley, T. 10 July 2017. Just 100 companies responsible for 71% of global emissions, study says. The Guardian. www.theguardian.com/sustainable-business/2017/jul/10/100-fossil-fuel-companies-investors-responsible-71-global-emissions-cdp-study-climate-change.

Rondinelli, D.A., and T. London. 2003. How corporations and environmental groups cooperate: assessing cross-sector alliances and collaborations. Academy of Management Perspectives 17:61–76.

Schaltegger, S., J. Hörisch, and R.E. Freeman. 2019. Business cases for sustainability: a stakeholder theory perspective. Organization & Environment 32:191–212.

Sharma, S., and H. Vredenburg. 1998. Proactive corporate environmental strategy and the development of competitively valuable organizational capabilities. Strategic Management Journal 19:729–753.

Stubbs, W. 2017. Sustainable entrepreneurship and B corps. Business Strategy and the Environment 26:331–344.

Ullah, M., M. Zahid, S.M.A. Rizvi, Q.G.M. Qureshi, and F. Ali. 2022. Do green supply chain management practices improve organizational resilience during the COVID-19 crisis? A survival analysis of global firms. Economics Letters 219:110802. https://doi.org/10.1016/j.econlet.2022.110802.

Umrani, W.A., N.A. Channa, U. Ahmed, J. Syed, M.H. Pahi, and T. Ramayah. 2022. The laws of attraction: role of green human resources, culture and environmental performance in the hospitality sector. International Journal of Hospitality Management 103:103222. https://doi.org/10.1016/j.ijhm.2022.103222.

Wright, C., and D. Nyberg. 2017. An inconvenient truth: how organizations translate climate change into business as usual. Academy of Management Journal 60:1633–1661.

White, K., R. Habib, and D.J. Hardisty. 2019. How to SHIFT consumer behaviors to be more sustainable: a literature review and guiding framework. Journal of Marketing 83:22–49.

Yu, Z., A. Razzaq, A. Rehman, A. Shah, K. Jameel, and R.S. Mor. 2021. Disruption in global supply chain and socio-economic shocks: a lesson from COVID-19 for sustainable production and consumption. Operations Management Research 15:233–248.

Zhang, W., Q. Luo, and S. Liu. 2022. Is government regulation a push for corporate environmental performance? Evidence from China. Economic Analysis and Policy 74:105–121.

# Carbon Sequestration Potential from Afforestation and Reforestation in Oregon

Jacob J. Bukoski

## Introduction

Nearly half of Oregon is forested, with the variety of forest types reflecting the state's diverse climate, topography, and geology. Favorable conditions for growth in the coastal and wet montane areas of the state (Figure 1) produce some of the highest forest carbon stock densities in the world (Smithwick et al. 2002, Kauffman et al. 2020). Recognizing this large potential for carbon storage in Oregon's forests, strategies such as forest conservation, improved forest management, and forestation (expansion of tree cover) have been proposed to meet the state's goals for climate change mitigation.

Oregon's goals and strategies for climate change mitigation on natural and working (harvested or farmed) lands have been proposed by the Oregon Climate Action Commission (OCAC; formerly the Oregon Global Warming Commission). For example, OCAC's Oregon Climate Action Roadmap to 2030 recommends goals for carbon sequestration in natural and working lands that are separate from and in addition to sector-based emission reduction goals (Macdonald et al. 2023). OCAC recommended a goal of sequestering "at least an additional 5 million metric tons of $CO_2e$ [carbon dioxide equivalent] per year in natural and working lands by 2030, and at least 9.5 million metric tons of $CO_2e$ per year by 2050 relative to a 2010–2019 activity-based business-as-usual net [carbon] sequestration baseline" (Macdonald et al. 2021). This sequestration is expected to occur across ecosystems, including forests, tidal and non-tidal wetlands, and shrublands.

Forestation is an important approach to enhancing carbon sequestration (Nave et al. 2019) and includes both reforestation (restoring tree cover on previously forested lands) and afforestation (establishing tree cover on non-forested lands). Distinguishing between these two is essential for



**Figure 1.** The West Fork of the Wallowa River along Chief Joseph Trail in the Wallowa Mountains south of Wallowa Lake, Wallowa County, Oregon. Photograph by Gary Halvorson, Oregon State Archives.

understanding whether tree planting can help meet Oregon's climate goals, as changes in land cover and land use influence whether these actions contribute additional carbon sequestration beyond the state's baseline. Reforestation tends to be favored over afforestation, which converts land cover and affects biological diversity and non-carbon ecosystem services (Veldman et al. 2015, Bond et al. 2019). For example, converting shrublands to forests can increase carbon sequestration, but reduces the amount of habitat for species that depend on shrublands, while expanding habitat for woodland- and forest-associated species. Despite these trade-offs, some conversion of land cover may be needed to meet Oregon's ambitious goals for enhanced carbon sequestration.

Here, I examine the carbon sequestration potential of forestation in Oregon. I build on the foundational work of others who assessed select forestation strategies in Oregon (Law et al. 2018, Cook-Patton et al. 2020, Graves et al. 2020), but largely did not investigate interventions that would result in trade-offs in species' habitats and ecosystem services. By providing additional transparency and addressing options such as afforestation of shrublands, I expand understanding of forestation's potential for meeting Oregon's climate goals on natural and working lands. First, I review forestation strategies that have been proposed for the state and evaluate whether each will add to Oregon's baseline carbon sequestration. Second, I use spatial modeling to estimate the potential for carbon sequestration across a variety of land cover types and jurisdictions. Third, I discuss logistical, biological, and social limitations, such as widely held views on where tree cover should be expanded, to achieving this potential carbon sequestration. Although I focus on potential for climate change mitigation, I recognize that policies, programs, and investments in forestation also must consider impacts on local human communities, economic costs and benefits, social and political feasibility, and biological diversity.

## Proposed Strategies for Forestation Within Oregon

Forestation strategies proposed for Oregon range from planting trees in urban settings to reforesting areas burned by wildfire. The concept of additionality—"relative to a 2010–2019 activity-based business-as-usual baseline"—is foundational to the Oregon Climate Action Commission's proposed climate change mitigation goals. The additionality principle requires interventions to reduce emissions or enhance $CO_2$ sequestration beyond what would have happened in the absence of the intervention, and is typically assessed with financial, legal, and common-practice criteria. As a simple example, replanting harvested stands on an industrial forest is rarely additional, because Oregon's Forest Practices Act requires the landowner to reforest the land. Even without this legislation, an industrial forest owner's business depends on wood harvest, and they likely would replant the harvested area regardless of climate change mitigation goals. Conversely, a statewide program that encourages owners of non-forested lands to plant trees may be considered additional given that the landowners are unlikely to afforest these areas without such incentives.

With respect to Oregon's climate change mitigation goals, I consider additionality not only at a project level, but also at the statewide level at which progress toward the goals is being assessed. That is, what are the baseline trends in forest carbon sequestration across different land uses in the state, and what interventions would contribute meaningful, additional $CO_2$ sequestration to the state's baseline? One needs to understand trends in forest carbon sequestration across different land cover types to evaluate these questions. In the following, I discuss the additionality of Oregon's most prominent forestation strategies.

### Reforestation Following Wildfire

Reforestation of burned areas following wildfire is among the most referenced climate change mitigation strategies for Oregon (Law et al. 2018, Graves et al. 2020, Macdonald et al. 2021). The number, size, and frequency of wildfires in Oregon's forests are projected to increase (Reilly et al. 2017, Halofsky et al. 2020), with varied effects on forests' current and potential future carbon stocks. Although wildfires tend to have limited effects on standing carbon stocks regardless of severity, severity can have much more pronounced impacts on distribution of carbon across ecosystem pools (e.g., standing trees vs. downed woody debris) and future rates of carbon sequestration (Maestrini et al. 2017, Miesel et al. 2018, Hemes et al. 2023).

In many instances, low- and moderate-severity wildfires result in a slight and short-term reduction of on-site carbon stocks and carbon sequestration rates (Miesel et al. 2018). Even stand-replacing, high-severity wildfires tend to have limited effects on total carbon stocks, with stand-replacing fires in Oregon driving losses of approximately 10 percent of aboveground carbon stocks (Kauffman et al. 2019). Rather than immediate loss of ecosystem carbon, high-severity wildfires shift carbon from live wood to dead wood pools, impacting ecosystem recovery and future carbon sequestration. Carbon fluxes after wildfires depend on the rates of downed wood decomposition and forest regrowth (Figure 2). The loss of carbon sequestration capacity in mature forests impacted by high-severity wildfire can be substantial. In California, for example, high severity wildfires resulted in the foregone sequestration of 9.9 million metric tons of $CO_2$ per year from 1998–2018 (Hemes et al. 2023), which is roughly 8 percent of $CO_2$ emissions from wildfires on forestlands in the United States in 2022 (EPA 2024). No comparable estimate has been made for Oregon. However, a similar trend in loss of baseline carbon sequestration may be occurring in forests across the state, particularly those in which the extent and severity of wildfire is increasing.



**Figure 2.** Live and standing dead trees following mixed-severity wildfire. Photograph by Erica Fleishman.

Reforestation following wildfire is therefore important for maintaining baseline carbon sequestration levels but is unlikely to provide additional sequestration. Industrial landowners typically harvest burned trees and are required to reforest these lands, suggesting that wildfire on industrial lands does not lead to additional carbon sequestration. Reforestation of burned federal lands is only required within areas that are actively managed for timber supply, and financial and personnel constraints largely preclude federal forest managers from widespread reforestation of areas not used for timber harvest (Stevens-Rumann and Morgan 2019). As wildfire extent increases, geographic prioritization of active reforestation is needed (Dobrowski et al. 2024). For example, many areas will naturally regenerate following wildfire and are therefore low priorities for active reforestation (Hemes et al. 2023). In other instances, active reforestation may be necessary due to novel climatic conditions, repeated disturbances, or competition from non-native invasive species; predicting when and where such processes will occur is difficult (Odion et al. 2010).

*Increasing Tree Density*

Rncreasing the density of trees to the desired level for a given site is a prominent strategy for expanding tree cover within Oregon (Macdonald et al. 2021). Although increasing stocking or enrichment planting following wildfire is a form of increasing tree density, I solely refer to unburned areas here. For landowners engaged in productive forestry, Oregon's Forest Practices Act mandates a certain level of stocking following harvesting of a stand (ODF 2024). Forest producers usually set their own stocking levels based on site quality and preferred silvicultural practices, which in many

cases may include tree densities that exceed the state's requirements. Given that forest producers are likely to maintain stocking levels that maximize profit (thus maximizing growth on a given site), increasing the density of trees in these forests is unlikely to substantially contribute to additional carbon sequestration.

In stands with partial tree cover and no mandate to increase stocking, adding trees could sequester carbon beyond a baseline. For example, owners of woodlands in the Willamette Valley could potentially plant more trees to increase carbon sequestration potential. Furthermore, agricultural landscapes or areas that were historically forested could be planted with trees (Sprenkle-Hyppolite et al. 2024). In many instances, increasing stocking may induce an ecosystem type conversion, raising the need to consider social and ecological impacts such as maintenance of pasture or other agricultural lands, species composition or viability, and aesthetic values. Given its broad applicability across land use and land cover types, adding trees likely has substantial potential for additional carbon sequestration.

*Restoration of Forest Cover in Riparian Areas*

Reforestation of riparian areas has also been suggested as a forestation strategy (Macdonald et al. 2021) with considerable potential for carbon sequestration (Graves et al. 2020). In eastern Oregon, livestock grazing has historically been the dominant driver of loss and degradation of riparian zones (Kauffman et al. 2022, 2023). Native riparian vegetation across Oregon is varied and includes native sedges, grasses, forbs, and shrubs in addition to trees (Kauffman et al. 2022). Expanding forest cover in riparian areas will require not only addressing drivers of degradation, but identification of areas that are appropriate for planting of woody and non-woody vegetation.

Reforestation of riparian areas tends to have existing, widespread support through state-level policies and incentive programs, although much of this support is targeted toward goals such as increasing floodplain connectivity, water quality and provisioning, and the amount and quality of fish habitat. Because riparian reforestation programs already exist within Oregon, carbon sequestration additional to Oregon's baseline would need to extend beyond the impact of these efforts. Current rates of riparian reforestation have been estimated at 1,713 ha (4,233 acres) per year in interior Oregon and 683 ha (1,688 acres) per year in coastal and western Oregon (Graves et al. 2020). The total area available for riparian reforestation has been estimated at about 76,000 ha east of the Cascade Range and 125,000 ha west of the Cascade Range (Graves et al. 2020), suggesting substantial room to increase rates of riparian reforestation and associated carbon sequestration.

*Expanding Urban Tree Cover*

Urban areas are not included within Oregon's climate change mitigation goals for natural and working lands (Macdonald et al. 2021, 2023). Nevertheless, expanding tree cover in urban areas is a priority for the state. Expanding urban tree cover is promoted primarily to address social, economic, and environmental inequities (see *Trade-offs in Planting Trees in Urban and Suburban Areas*, this volume). For example, integration of trees into urban areas can lower extreme maximum temperatures, which can reduce energy consumption (and costs) for adjacent buildings. Urban trees also improve air quality, facilitate stormwater management by reducing runoff and soil erosion, and provide mental and physical health benefits for residents (O'Brien et al. 2022). In many cities, low-income communities have less tree cover than higher-income areas, leading urban forestry efforts to prioritize adding trees in underserved neighborhoods (Schell et al. 2020, McDonald et al. 2024).

Expansion of urban tree cover can contribute to many of Oregon's goals, but widespread adoption faces barriers. For example, Oregon's zoning for urban growth may drive competition for urban spaces in which trees could be planted. Moreover, maintenance of urban trees over the long term can be costly and difficult. For example, the interaction of weakened trees and disturbances such as ice storms can cause extensive property damage. To overcome these challenges, state agencies are seeking funding to increase the extent of urban forestry programs. The Urban and Community Forestry Program of the Oregon Department of Forestry recently received $26.6 million from the Inflation Reduction Act to support urban forestry within the state (ODF 2023). Of this total, $10 million is devoted to Oregon's nine federally recognized tribes and $12.5 million will be available to all eligible urban entities. The funds are directed towards projects and challenges that have been identified by the communities themselves and may not always be used to expand urban tree cover. Nevertheless, the influx of financial support is likely to expand urban tree cover and associated carbon sequestration.

## Estimates of Carbon Sequestration Potential from Forestation in Oregon

Prior studies of carbon sequestration from expanded forestation in Oregon were limited to certain strategies. For example, Law and colleagues (2018) examined afforestation of irrigated grass crops, afforestation of non-forested areas within current forest boundaries, and reforestation of areas with tree mortality from harvest, wildfire, and beetles. Similarly, Graves and colleagues (2020) focused on reforestation of riparian areas and wildfire-burned federal lands. Here, I estimate carbon sequestration associated with forestation across all land cover types.

*Methods*

I used spatially explicit data to identify potential candidate areas for forestation; modeled the vegetation association most likely to occur in each area; mapped nonlinear carbon accumulation curves to these areas; and applied ecological, logistical, and social constraints to understand where carbon sequestration from forestation is most feasible. I resampled all raster data to match the 30 m resolution of the National Land Cover Dataset (Dewitz 2023).

To identify areas in Oregon that may be appropriate for expansion of tree cover, I used a national map of forestable areas (Cook-



**Figure 3.** Treefall created a break in the dense canopy of a coastal forest in Oregon. Photograph by Erica Fleishman.

Patton et al. 2020). The map identifies areas that historically supported forests with at least 25 percent canopy cover (Figure 3). I intersected this map of forestable areas with the National Land Cover Dataset (Dewitz 2023) and a map of tree canopy cover from 2021 (GTAC 2022) to identify

current land cover and exclude areas that may be inappropriate for forestation: open water, perennial ice and snow, low to high intensity developed areas, cultivated crops, woody wetlands, emergent herbaceous wetlands, and areas with greater than 50 percent tree canopy cover. I assumed that reforestation was feasible in deciduous, evergreen, and mixed forests, and afforestation was feasible in developed open space, barren areas, shrub or scrub, grass or herbaceous, and pasture or hay land cover types.

Next, I built a probabilistic model of the forest type most likely to establish in each area if it was to be reforested or afforested. The U.S. Forest Service classifies current forests across the country via plant association zones (PAZs) (Ruefenacht et al. 2008). To allow for afforestation, I mapped the most likely PAZ across all non-forested areas of Oregon. I extracted both PAZ types from currently forested areas and 64 climatic, topographic, and edaphic covariates that partially determine the location of PAZs (Lamarque et al. 2010, Danielson and Gesch 2011, Kriticos et al. 2012, Hengl et al. 2017, Karlsson et al. 2017, Fick and Hijmans 2017, Abatzoglou et al. 2018, Trabucco and Zomer 2019). I then entered these data into a probabilistic random forest classifier that predicted the likelihood of each PAZ across Oregon. The highest-probability PAZ for each pixel is an estimate of the forest type most likely to establish in that location. I produced the most likely PAZ estimates at 1 km resolution but resampled them to 30 m resolution to match the other spatial data.

| Reclassified jurisdiction | U.S. Protected Areas Database land ownership or jurisdiction types |
|---|---|
| U.S. Forest Service | U.S. Forest Service |
| U.S. Bureau of Land Management | U.S. Bureau of Land Management |
| U.S. Fish and Wildlife Service | U.S. Fish and Wildlife Service |
| Other federal | National Park Service, Department of Defense, Army Corps of Engineers, Natural Resources Conservation Service, Bureau of Reclamation, other or unknown federal lands |
| Tribal | Tribal lands |
| State | State land board, department of land, fish and wildlife, department of natural resources, park and recreation, department of conservation, other or unknown state lands |
| Local | City, county, regional agency, regional water district, other or unknown local lands |
| Private | Privately owned |
| Other | Non-governmental organizations, jointly managed, unknown |

**Table 1.** Jurisdictions used in the analysis of carbon sequestration potential. Land ownership and jurisdiction were extracted from the U.S. Protected Areas Database. All areas for which land ownership or jurisdiction was not specified in the U.S. Protected Areas Database were assumed to be privately owned.

To model the carbon sequestration potential of each PAZ, I used recent models of carbon accumulation in aboveground and belowground biomass within 19 forest types in the Pacific Northwest (Chisholm and Gray 2024), including all dominant types in Oregon. The models were parameterized with U.S. Forest Inventory and Analysis program data and fitted to the Chapman-Richards growth function, which accounts for temporal variation in carbon stock accumulation rates as forests develop (Bukoski et al. 2022, Busch et al. 2024). The parameters can be localized with stand-level data on mean annual increment (average annual growth volume per acre) and maximum canopy cover. Because I did not have spatial data on the latter variables across Oregon, I used median values for each forest type reported in the supplementary information of Chisholm and Gray (2024). I linked these state-level growth functions for each forest type to the most likely PAZ in each forestable pixel and projected carbon accumulation across time. To account for existing biomass in partially forested areas, I adjusted the future carbon sequestration proportional to the canopy cover in 2021 (GTAC 2022).

The actual carbon sequestration that can be achieved by expanding tree cover is much lower than the biophysical potential due to logistical, ecological, and social constraints. I therefore applied a series of such constraints. First, given that reforestation of forest burned by wildfires would not be additional to Oregon's climate-change mitigation goals, I used the Monitoring Trends in Burn Severity data (USGS 2021) to remove burned areas from consideration. I also removed areas on federal lands that are further than 1 km from a road (U.S. Census Bureau 2021) because the expense of transporting seedlings and equipment over rough terrain may prohibit active reforestation (Dobrowski et al. 2024). Next, I removed areas that may be too arid to support expansion of tree cover. Projecting future aridity is complex and involves assumptions about future climate outcomes, which was beyond the scope of this analysis. Instead, I used the 50th quantile (median) of annual precipitation (Fick and Hijmans 2017) for each PAZ type as a proxy of areas that may be poorly suited for forestation. Within the remaining areas available for tree cover expansion, I examined the carbon potential that may be socially acceptable as a function of whether expansion of tree cover would require land-cover conversion (afforestation).

After applying the above constraints, I summarized the data by land ownership and management jurisdiction, recognizing that the design of forestation policies and programs will vary among owners or managers of the targeted lands. I obtained data on ownership and jurisdiction from the U.S. Protected Areas Database (USGS 2024). I grouped these jurisdictions into nine classes: U.S. Forest Service, U.S. Bureau of Land Management, U.S. Fish and Wildlife Service, other federal, tribal, state, local, private, and other (Table 1). I report all carbon sequestration estimates in million metric tons of $CO_2$ and compare these values against Oregon's stated goals for annual carbon sequestration in 2030 and 2050.

## Results

I identified an upper bound of 26.7 million metric tons of $CO_2$ sequestration from forestation by 2030, or sequestration of 5.3 million metric tons of $CO_2$ per year (Table 2). This would be equivalent to 106 percent of Oregon's goal for enhanced carbon sequestration in natural and working lands by 2030. By 2050, unconstrained forestation could sequester a maximum of 142.6 million metric tons of $CO_2$, or 5.7 million metric tons of $CO_2$ per year. This represents 60 percent of Oregon's statewide 2050 carbon sequestration goal. The modeled forestation would occur across more than 3.3 million ha (8.2 million acres) of eight land cover types (Table 2, Figure 4). Roughly 68 percent of the modeled carbon sequestration potential by 2050 is classified as afforestation, whereas 32 percent would occur through reforestation. The total modeled forestation would expand tree cover on approximately 14.5 percent of Oregon's land base.

*Carbon Sequestration Potential Under Ecological and Logistical Constraints*

The above estimates indicate the maximum, unconstrained potential carbon sequestration. However, it is unrealistic that 14.5 percent of the state is available, or appropriate, for expansion of tree cover. For example, the analysis suggested that more than half of lands currently used for livestock grazing and hay production may be available. This is highly unlikely to be socially or economically feasible given the role of these land uses for Oregon's rural economies.

After applying logistical constraints (excluding areas burned by wildfire and federal lands further than 1 km from roads) and ecological constraints (excluding areas that receive less than the 50th percentile of annual precipitation for each PAZ), the area available for forestation was reduced to

| Type of forestation | Land cover type | Statewide extent (ha) | Forestable extent | | Carbon sequestration (million metric tons CO$_2$) | |
|---|---|---|---|---|---|---|
| | | | ha | percentage | By 2030 | By 2050 |
| | | | | | | |
| Afforestation | Shrub/scrub | 8,294,567 | 1,285,252 | 15.5 | 10,394,228 | 51,790,739 |
| | Grass/herbaceous | 4,244,769 | 542,604 | 12.8 | 4,812,077 | 24,218,860 |
| | Pasture/hay | 791,961 | 405,620 | 51.2 | 3,514,749 | 19,281,439 |
| | Developed open space | 388,665 | 118,921 | 30.6 | 909,431 | 5,081,353 |
| | Barren | 163,165 | 5,682 | 3.5 | 41,220 | 340,992 |
| | **Total** | 13,883,127 | 2,358,079 | 17.0 | 19,671,705 | 100,713,383 |
| | | | | | | |
| Reforestation | Evergreen forest | 8,357,951 | 928,801 | 11.1 | 6,852,310 | 40,746,377 |
| | Mixed forest | 579,351 | 20,252 | 3.5 | 117,020 | 816,048 |
| | Deciduous forest | 61,689 | 8,214 | 13.3 | 51,849 | 326,101 |
| | **Total** | 8,998,991 | 957,267 | 13.0 | 7,021,179 | 41,888,526 |
| | | | | | | |
| | **Total** | 22,882,118 | 3,315,348 | 14.5 | 26,692,884 | 142,601,909 |

**Table 2.** Carbon sequestration potential in aboveground and belowground biomass across land cover types in Oregon.

1.2 million ha, or roughly 4.8 percent of Oregon's land base. These constraints reduced carbon sequestration potential by approximately two-thirds, to 9.6 million metric tons of CO$_2$ by 2030 (1.9 million metric tons per year) and 48.7 million metric tons by 2050 (1.9 million metric tons per year) (Table 3). Sixty-nine percent of the 2030 potential and 68 percent of the 2050 potential is considered afforestation.

Assessing social constraints on forestation is more challenging. Potential areas for afforestation are typically excluded from tree planting assessments to safeguard species in non-forested ecosystems, agricultural production, and competing demands on land from other societal goals, such as
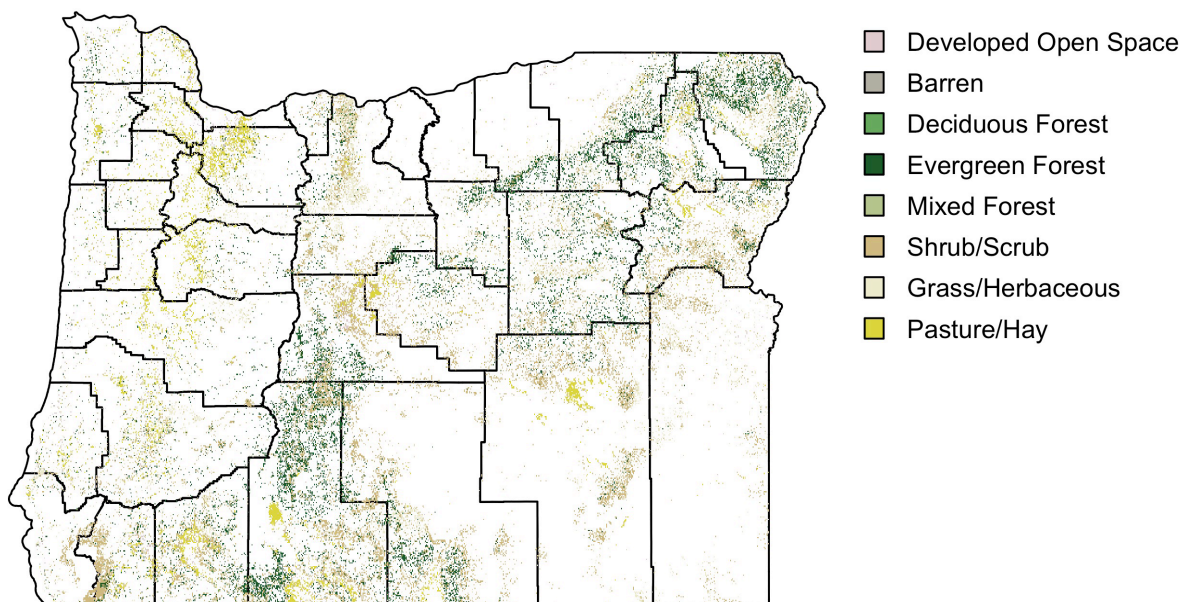


Figure 4. Areas identified as potentially forestable in Oregon and their current land cover type.

construction of housing. However, afforestation provides substantially more carbon sequestration potential than reforestation in our analysis. If we remove all afforestation from our estimates, the remaining reforestation would sequester approximately 2.9 million metric tons of $CO_2$ by 2030 and 15.7 million metric tons of $CO_2$ by 2050 (Table 3), meeting just 12 percent of Oregon's 2030 goal (0.58 million metric tons of $CO_2$ per year) and 7 percent of the 2050 goal (0.63 million metric tons of $CO_2$ per year).

| Type of forestation | Land cover type | Statewide extent (ha) | Forestable extent | | Carbon sequestration (million metric tons CO2) | |
|---|---|---|---|---|---|---|
| | | | ha | percentage | By 2030 | By 2050 |
| | | | | | | |
| Afforestation | Shrub/scrub | 8,294,567 | 442,501 | 5.3 | 2,936,729 | 14,946,217 |
| | Grass/herbaceous | 4,244,769 | 212,511 | 5.0 | 1,846,270 | 8,635,651 |
| | Pasture/hay | 791,961 | 168,093 | 21.2 | 1,514,850 | 7,462,578 |
| | Developed open space | 388,665 | 44,974 | 11.6 | 355,256 | 1,860,549 |
| | Barren | 163,165 | 1,900 | 1.2 | 13,667 | 112,654 |
| **Total** | | 13,883,127 | 869,979 | 6.3 | 6,666,772 | 33,017,648 |
| | | | | | | |
| Reforestation | Evergreen forest | 8,357,951 | 364,785 | 4.4 | 2,818,015 | 15,068,941 |
| | Mixed forest | 579,351 | 10,833 | 1.9 | 61,589 | 427,361 |
| | Deciduous forest | 61,689 | 4,207 | 6.8 | 26,101 | 164,392 |
| **Total** | | 8,998,991 | 379,824 | 4.2 | 2,905,705 | 15,660,694 |
| | | | | | | |
| **Total** | | 22,882,118 | 1,249,804 | 5.5 | 9,572,477 | 48,678,342 |

**Table 3.** Constrained carbon sequestration potential across land cover types in Oregon.

*Distribution of Carbon Sequestration Potential Across Jurisdictions*

More than 90 percent of the total constrained carbon sequestration (including both afforestation and reforestation) falls within three jurisdiction types: private (61.8 percent), U.S. Forest Service (24.5 percent), and Bureau of Land Management (5.7 percent) (Figure 5). These three jurisdictions equate to a potential of 8.7 and 44.8 million metric tons of $CO_2$ sequestered by 2030 and 2050, respectively. Within these jurisdictions, the opportunities for tree cover expansion are primarily in areas classified as evergreen forest or shrub/scrub, but there is also substantial opportunity for forestation of privately owned pasture/hay and grass/herbaceous lands.

**Discussion**

The analysis presented here provides a transparent and comprehensive estimate of potential carbon sequestration from expanding tree cover across all land cover types in Oregon. I built on the work of others (Law et al. 2018, Cook-Patton et al. 2020, Graves et al. 2020) by initially exploring all biophysically possible options for expanding forest cover and then applying selected logistical, ecological, and social constraints. I identified roughly 1.2 million ha of land with potential to support additional tree cover. The total estimated carbon sequestration from constrained reforestation and afforestation would meet 38 percent of Oregon's goal of sequestering an additional 5 million metric tons of $CO_2e$ per year by 2030, and 21 percent of the goal of sequestering an additional 9.5 million

metric tons of $CO_2$e by 2050 (Table 4). The results suggest that forestation could play a significant role in achieving Oregon's climate-change mitigation goals on natural and working lands.

My estimates of annual $CO_2$ sequestration rates in 2030 and 2050 align well with the estimates of Graves and colleagues (2021) but are notably lower than those of Cook-Patton et al. (2021) and Law et al. (2018) (Table 5). Cook-Patton and colleagues used U.S. Forest Service stocking tables to estimate carbon sequestration in forest biomass (averaged over the first 30 years of growth) and a mean annual rate of carbon sequestration in soils. After adjusting their estimate to remove soil carbon sequestration, their estimated annual rate is still five times higher than mine. I lack details of their analysis and cannot fully explain the difference, but variation



**Figure 5.** Carbon sequestration potential from forestation by jurisdiction and existing land cover type across Oregon. The light green bars correspond to million metric tons of $CO_2$ sequestered by 2030 and the dark green bars correspond to million metric tons of $CO_2$ sequestered by 2050.

in our carbon accumulation models may partially explain the discrepancy. For example, my carbon accumulation models include forest types with low carbon density, such as juniper (*Juniperus* spp.) and open-canopy Oregon white oak (*Quercus garryana*) woodlands. These forest types represent 23 percent of the forestable lands in my analysis and have low carbon sequestration potential per the Chisholm and Gray (2024) models. Additionally, my use of nonlinear growth functions, which have lower rates of carbon accumulation at younger ages, could partially explain the differences.

I also lack Law et al.'s (2018) estimates of total areas available for reforestation and afforestation, which precludes me from understanding what drives the differences in estimates (Table 5). However, it is worth noting that they used process-based modeling (Community Land Model 4.5) rather than

| Climate-change mitigation goal | Carbon sequestration potential from reforestation | Carbon sequestration potential from afforestation |
|---|---|---|
| By 2030, sequester additional 5 million metric tons of $CO_2e$ per year in natural and working lands relative to a 2010-2019 baseline | 0.58 million metrics tons $CO_2$ per year in 2030 | 1.33 million metric tons $CO_2$ per year in 2030 |
| By 2050, sequester an additional 9.5 million metric tons of $CO_2e$ per year in natural and working lands relative to a 2010-2019 baseline | 0.63 million metric tons $CO_2$ per year in 2050 | 1.32 million metric tons $CO_2$ per year in 2050 |

**Table 4.** Carbon sequestration potential compared to the Oregon Climate Action Commission's goals for climate change mitigation in natural and working lands. The carbon sequestration estimates incorporate major logistical, ecological, and social constraints.

empirical modeling, and the different modeling structure may partially explain the differences. Their model included physiological parameters for 10 major tree species, and it estimated growth with inputs of climate and atmospheric carbon dioxide concentrations at 4 km resolution. Differences between their estimates and others could have been driven by varying extents of forestable areas, rates of carbon accumulation, or enhanced growth projections due to future climatic and carbon dioxide conditions.

## Carbon Sequestration Potential from Forestation in Oregon

Although forestation may represent a substantial opportunity for the state, my sequestration estimates assume immediate expansion of tree cover across all 1.2 million ha (about 3 million acres). Of course, immediate establishment of trees on roughly 5 percent of Oregon's land base is impossible. Actual carbon sequestration also will be constrained by the physical, financial, logistical, and technical resources necessary to operationalize widespread expansion of tree cover (Fargione et al. 2021, Dobrowski et al. 2024). I lacked data necessary to estimate the baseline rate of forest expansion across all possible land cover types and jurisdictions and therefore did not apply these additional constraints. Nevertheless, approximate estimates and coarse assumptions can demonstrate the magnitude of these challenges.

| Statewide extent (ha) | Maximum extent (ha) | Sequestration (million metric tons $CO_2$/yr) | | |
|---|---|---|---|---|
| | | 2030 | 2050 | 2100 |
| **Graves et al. 2021** | | | | |
| Reforestation of post-wildfire federal lands | - | 0.12 (0.07-0.22) | 0.24 (0.15-0.45) | - |
| Reforestation of riparian areas | 202,415 | 0.31 (0.14-1.47) | 0.83 (0.21-1.86) | - |
| **Law et al. 2018** | | | | |
| Reforestation of lands with tree mortality from harvest, fire, and beetles | - | 25.8[a] | 35.8 | 14.62 |
| Afforestation within current forest boundaries | - | 8.06[a] | 11.1 | 4.36 |
| Irrigated grass crops | 127,000 | | | |
| **Cook-Patton et al. 2021** | | | | |
| Reforestation of biological corridors, floodplains, marginal croplands, grassy areas, pasture, shrub, streamside buffers, and urban open spaces | 1,869,000 | - | 21.12 | - |
| **This assessment (with constraints)** | | | | |
| Afforestation of shrub/scrub, grass/herbaceous, pasture/hay, developed open space, and barren lands | 867,588 | 1.33 | 1.32 | - |
| Reforestation of current forest lands with less than 50 percent canopy cover | 367,388 | 0.58 | 0.63 | - |

**Table 5.** Estimated carbon sequestration potential from afforestation and reforestation across Oregon. Numbers in parentheses are 90 percent confidence intervals. a: estimates for the year 2035.

Expansion of tree cover is constrained at many stages: project planning (including finances), seed collection, seed storage, seedling production, outplanting, and monitoring (Fargione et al. 2021, Kildisheva et al. 2023, Dobrowski et al. 2024). Apart from coarse estimates of seedling production, there are no data on capacity levels for most of these activities. The U.S. Forest Service National Center for Reforestation, Nurseries, and Genetic Resources' annual reports on nursery production of forest seedlings has become the de facto means of estimating reforestation capacity (Pike et al. 2023). In 2022, for example, Oregon's nurseries produced 81.5 million seedlings, more than any other western state (Christiansen et al. 2023, Pike et al. 2023). The same report used two methods to translate this seedling estimate into extent of planted areas. First, they multiplied the seedling production capacity by the average planting density (865 stems/ha), derived from Forest Inventory and Analysis data. Second, they used the Forest Inventory and Analysis program's estimates of planted area. For Oregon, the first and second methods estimated 94,278 and 47,894 ha, respectively. I cannot explain the difference in the two estimates, but export of seedlings to other states (e.g., California, which produces roughly two-thirds fewer seedlings than Oregon) is plausible.

Most of the 47,894 ha of current reforestation estimated by the Forest Inventory and Analysis program—83 percent of seedlings—is likely the maintenance of industrial forests, whereas the remainder likely represents post-wildfire reforestation. Both would represent non-additional carbon sequestration. Therefore, carbon sequestration beyond the baseline would require expanded capacity across all stages of the reforestation pipeline (Fargione et al. 2021). Even an immediate doubling of reforestation capacity, with an additional ~80,000 seedlings and about 50,000 ha of reforestation per year, would meet just 4 percent of the potential 1.2 million ha of forestable areas.

I recommend four future lines of research to elucidate the potential for expanded tree cover to contribute to Oregon's climate-change mitigation goals. First, improve estimates of baseline rates of reforestation and afforestation and realistically estimate how quickly these rates can be increased. Second, identify social and economic barriers to integrating trees into non-forest ecosystems. Third, improve carbon modeling by accounting for spatial variation in carbon accumulation across the state and impacts on existing soil organic carbon, which can be substantial in grasslands, shrublands, wetlands, riparian zones, and coastal areas, including tidal forests. Fourth, identify areas where reforestation may exacerbate climate-related hazards (e.g., aridification or wildfire) or is socially undesirable. For example, the results presented here could be overlaid on Oregon's Statewide Wildfire Hazard Map, released in early 2025. Doing so could help identify areas where expanded tree cover may bring additional hazard and risk to human communities

Expansion of tree cover across Oregon represents a potentially significant opportunity for achieving the state's climate-change mitigation goals on natural and working lands. However, realistic pathways for operationalizing this potential have not yet been identified. Moreover, forestation strategies such as replanting areas where trees burned are likely to only maintain baseline carbon sequestration levels rather than sequester additional carbon. In addition to building on current forestation policies and programs, it may be wise to consider other strategies (e.g., improved forest management) with potential for additional carbon sequestration, such as reducing harvest or extending rotation lengths (Law et al. 2018, Graves et al. 2020, Shanley et al. 2024).

## Acknowledgments

## Literature Cited

Abatzoglou, J.T., S.Z. Dobrowski, S.A. Parks, and K.C. Hegewisch. 2018. TerraClimate, a high-resolution global dataset of monthly climate and climatic water balance from 1958–2015. Scientific Data 5:170191. https://doi.org/10.1038/sdata.2017.191.

Bond, W.J., N. Stevens, G.F. Midgley, and C.E.R. Lehmann. 2019. The trouble with trees: afforestation plans for Africa. Trends in Ecology & Evolution 34:963–965.

Bukoski, J.J., S.C. Cook-Patton, C. Melikov, H. Ban, J.L. Chen, E.D. Goldman, N.L. Harris, and M.D. Potts. 2022. Rates and drivers of aboveground carbon accumulation in global monoculture plantation forests. Nature Communications 13:4206. https://doi.org/10.1038/s41467-022-31380-7.

Busch, J., J.J. Bukoski, S.C. Cook-Patton, B. Griscom, D. Kaczan, M.D. Potts, Y. Yi, and J.R. Vincent. 2024. Cost-effectiveness of natural forest regeneration and plantations for climate mitigation. Nature Climate Change 14:996–1002.

Chisholm, P.J., and A.N. Gray. 2024. Forest carbon sequestration on the west coast, USA: role of species, productivity, and stockability. PLoS ONE 19:e0302823. https://doi.org/10.1371/journal.pone.0302823.

Christiansen, A., J.D. Putney, M. Bennett, and G. Ahrens. 2023. Reforestation in Oregon. Tree Planters' Notes 66(2):4–27.

Cook-Patton, S.C., et al. 2020. Lower cost and more feasible options to restore forest cover in the contiguous United States for climate mitigation. One Earth 3:739–752.

Danielson, J.J., and D.B. Gesch. 2011. Global multi-resolution terrain elevation data 2010 (GMTED2010). Open-file report 2011-1073. https://doi.org/10.3133/ofr20111073.

Dewitz, J. 2023. National Land Cover Database (NLCD) 2021 products. U.S. Geological Survey. https://doi.org/10.5066/P9JZ7AO3.

Dobrowski, S.Z., et al. 2024. 'Mind the gap'—reforestation needs vs. reforestation capacity in the western United States. Frontiers in Forests and Global Change 7:1402124. https://doi.org/10.3389/ffgc.2024.1402124.

EPA (U.S. Environmental Protection Agency). 2024. Inventory of U.S. greenhouse gas emissions and sinks: 1990–2022. EPA 30-D-24-001. www.epa.gov/ghgemissions/draft-inventory-us-greenhouse-gas-emissions-and-sinks-1990-2022.

Fargione, J., et al. 2021. Challenges to the reforestation pipeline in the United States. Frontiers in Forests and Global Change 4:629198. https://doi.org/10.3389/ffgc.2021.629198.

Fick, S.E., and R.J. Hijmans. 2017. WorldClim 2: new 1-km spatial resolution climate surfaces for global land areas. International Journal of Climatology 37:4302–4315.

Graves, R.A., R.D. Haugo, A. Holz, M. Nielsen-Pincus, A. Jones, B. Kellogg, C. Macdonald, K. Popper, and M. Schindel. 2020. Potential greenhouse gas reductions from natural climate solutions in Oregon, USA. PLoS ONE 15:e0230424. https://doi.org/10.1371/journal.pone.0230424.

GTAC (U.S. Forest Service Geospatial Technology and Applications Center). 2022. Tree canopy cover, 2021. data.fs.usda.gov/geodata/rastergateway/treecanopycover/.

Halofsky, J.E., D.L. Peterson, and B.J. Harvey. 2020, December 1. Changing wildfire, changing forests: the effects of climate change on fire regimes and vegetation in the Pacific Northwest, USA. Fire Ecology 16:4. https://doi.org/10.1186/s42408-019-0062-8.

Hemes, K.S., C.A. Norlen, J.A. Wang, M.L. Goulden, and C.B. Field. 2023. The magnitude and pace of photosynthetic recovery after wildfire in California ecosystems. Proceedings of the National Academy of Sciences 120:e2201954120. https://doi.org/10.1073/

pnas.2201954120.

Hengl, T., et al. 2017. SoilGrids250m: global gridded soil information based on machine learning. PLoS ONE 12:e0169748. https://doi.org/10.1371/journal.pone.0169748.

Karlsson, K.-G., et al. 2017. CLARA-A2: CM SAF cLoud, Albedo and surface RAdiation dataset from AVHRR data—Edition 2. Satellite Application Facility on Climate Monitoring. https://doi.org/10.5676/EUM_SAF_CM/CLARA_AVHRR/V002.

Kauffman, J.B., R.L. Beschta, P.M. Lacy, and M. Liverman. 2023. Forum: climate, ecological, and social costs of livestock grazing on western public lands. Environmental Management 72:699–704.

Kauffman, J.B., G. Coleman, N. Otting, D. Lytjen, D. Nagy, and R.L. Beschta. 2022. Riparian vegetation composition and diversity shows resilience following cessation of livestock grazing in northeastern Oregon, USA. PLoS ONE 17:e0250136. https://doi.org/10.1371/journal.pone.0250136.

Kauffman, J.B., L.M. Ellsworth, D.M. Bell, S. Acker, and J. Kertis. 2019. Forest structure and biomass reflects the variable effects of fire and land use 15 and 29 years following fire in the western Cascades, Oregon. Forest Ecology and Management 453:117570. https://doi.org/10.1016/j.foreco.2019.117570.

Kauffman, J.B., L. Giovanonni, J. Kelly, N. Dunstan, A. Borde, H. Diefenderfer, C. Cornu, C. Janousek, J. Apple, and L. Brophy. 2020. Total ecosystem carbon stocks at the marine-terrestrial interface: blue carbon of the Pacific Northwest Coast, United States. Global Change Biology 26:5679–5692.

Kildisheva, O., S. Hobbs, S. Dobrowski, J. Sloan, N. Shaw, and M. Aghai. 2023. Got seeds? Strengthening the reforestation pipeline in the Western United States. Tree Planters' Notes 66(1):4–17.

Kriticos, D.J., B.L. Webber, A. Leriche, N. Ota, I. Macadam, J. Bathols, and J.K. Scott. 2012. CliMond: global high-resolution historical and future scenario climate surfaces for bioclimatic modelling. Methods in Ecology and Evolution 3:53–64.

Lamarque, J.F., et al. 2010. Historical (1850–2000) gridded anthropogenic and biomass burning emissions of reactive gases and aerosols: methodology and application. Atmospheric Chemistry and Physics 10:7017–7039.

Law, B.E., T.W. Hudiburg, L.T. Berner, J.J. Kent, P.C. Buotte, and M.E. Harmon. 2018. Land use strategies to mitigate climate change in carbon dense temperate forests. Proceedings of the National Academy of Sciences 115:3663–3668.

Macdonald, C., M. Buchanan, A. Hatch, and A. Strawn. 2021. Natural and working lands proposal. www.oregon.gov/lcd/Commission/Documents/2021-11_Item-10_OGWC_Attachment-A_Natural-and-Working-Lands-Carbon-Sequestration-and-Storage-Proposal-OGWC.pdf.

Macdonald, C., A. Zelenka, and Z. Baker. 2023. Oregon climate action roadmap to 2030: Commission recommendations. climate.oregon.gov/tighger.

Maestrini, B., E.C. Alvey, M.D. Hurteau, H. Safford, and J.R. Miesel. 2017. Fire severity alters the distribution of pyrogenic carbon stocks across ecosystem pools in a Californian mixed-conifer forest. Journal of Geophysical Research: Biogeosciences 122:2338–2355.

McDonald, R.I., T. Biswas, T.C. Chakraborty, T. Kroeger, S.C. Cook-Patton, and J.E. Fargione. 2024. Current inequality and future potential of US urban tree cover for reducing heat-related health impacts. npj Urban Sustainability 4:18. https://doi.org/10.1038/s42949-024-00150-3.

Miesel, J., A. Reiner, C. Ewell, B. Maestrini, and M. Dickinson. 2018. Quantifying changes in total and pyrogenic carbon stocks across fire severity gradients using active wildfire incidents.

Frontiers in Earth Science 6:41. https://doi.org/10.3389/feart.2018.00041.

Nave, L.E., B.F. Walters, K.L. Hofmeister, C.H. Perry, U. Mishra, G.M. Domke, and C.W. Swanston. 2019. The role of reforestation in carbon sequestration. New Forests 50:115–137.

O'Brien, L.E., R.E. Urbanek, and J.D. Gregory. 1 September 2022. Ecological functions and human benefits of urban forests. Urban Forestry and Urban Greening 75:122707. https://doi.org/10.1016/j.ufug.2022.127707.

ODF (Oregon Department of Forestry). 2023. Growing equity: urban and community forestry subaward programs. www.oregon.gov/odf/forestbenefits/Pages/ucf-subaward-programs.aspx.

ODF (Oregon Department of Forestry). 2024. Forest Practice Administrative Rules and the Oregon Forest Practices Act. www.oregon.gov/odf/working/pages/fpa.aspx.

Odion, D.C., M.A. Moritz, and D.A. DellaSala. 2010. Alternative community states maintained by fire in the Klamath Mountains, USA. Journal of Ecology 98:96–105.

Oregon Global Warming Commission. 2023. Biennial report to the Oregon Legislature: 2023. static1.squarespace.com/static/59c554e0f09ca40655ea6eb0/t/64275b98de28d74ea4a96dc3/1680300956035/2023-Legislative-Report.pdf.

Pike, C.C., D.L. Haase, S. Enebak, A. Abrahams, E. Bowersock, L. Mackey, Z. Ma, and J. Warren. 2023. Forest nursery seedling production in the United States–fiscal year 2022. Tree Planters' Notes 66(2):73–80.

Reilly, M.J., C.J. Dunn, G.W. Meigs, T.A. Spies, R.E. Kennedy, J.D. Bailey, and K. Briggs. 2017. Contemporary patterns of fire extent and severity in forests of the Pacific Northwest, USA (1985–2010). Ecosphere 8:e01695. https://doi.org/10.1002/ecs2.1695.

Ruefenacht, B., M. Finco, M. Nelson, R. Czaplewski, E. Helmer, J. Blackard, G. Holden, A. Lister, D. Salajanu, D. Weyermann, and K. Winterberger. 2008. Conterminous U.S. and Alaska forest type mapping using Forest Inventory and Analysis data. Photogrammetric Engineering & Remote Sensing 74:1379–1388.

Schell, C.J., K. Dyson, T.L. Fuentes, S. Des Roches, N.C. Harris, D.S. Miller, C.A. Woelfle-Erskine, and M.R. Lambert. 2020. The ecological and evolutionary consequences of systemic racism in urban environments. Science 369:1446. https://doi.org/10.1126/science.aay4497.

Shanley, C.S., R.A. Graves, C.R. Drever, M. Schindel, J.C. Robertson, M.J. Case, and T. Biswas. 2024. Mapping forest-based natural climate solutions. Communications Earth and Environment 5:502. https://doi.org/10.1038/s43247-024-01678-z..

Smithwick, E.A.H., M.E. Harmon, S.M. Remillard, S.A. Acker, and J.E. Franklin. 2002. Potential upper bounds of carbon stores in forests of the Pacific Northwest. Ecological Applications 12:1303–1317.

Sprenkle-Hyppolite, S., B. Griscom, V. Griffey, E. Munshi, and M. Chapman. 2024. Maximizing tree carbon in croplands and grazing lands while sustaining yields. Carbon Balance and Management 19:23. https://doi.org/10.1186/s13021-024-00268-y

Stevens-Rumann, C.S., and P. Morgan. 2019. Tree regeneration following wildfires in the western US: a review. Fire Ecology 15:15. https://doi.org/10.1186/s42408-019-0032-1.

Trabucco, A., and R. Zomer. 2019. Global Aridity Index and Potential Evapotranspiration (ET0) climate database v2. https://doi.org/10.6084/m9.figshare.7504448.v3.

U.S. Census Bureau. 2021. 2021 TIGER/Line shapefiles: roads. www.census.gov/cgi-bin/geo/shapefiles/index.php?year=2021&layergroup=Roads.

USGS (U.S. Geological Survey). 2021. Monitoring Trends in Burn Severity thematic burn severity mosaic (ver. 10.0). www.usgs.gov/data/monitoring-trends-burn-severity-thematic-burn-

severity-mosaic-ver-100-october-2024.

USGS (U.S. Geological Survey). 2024. Protected Areas Database of the United States (PAD-US) 4. U.S. Geological Survey data release. https://doi.org/10.5066/P96WBCHS.

Veldman, J.W., G.E. Overbeck, D. Negreiros, G. Mahy, S. Le Stradic, G.W. Fernandes, G. Durigan, E. Buisson, F.E. Putz, and W.J. Bond. 2015. Tyranny of trees in grassy biomes. Science 347:484–485.

# Connecting Climate and Community Science through Oregon Season Tracker

Sarah Cameron, Mark Schulze, and Glenn Ahrens

As detailed in the sixth Oregon Climate Assessment, weather and climate mapping systems nationwide increasingly are capitalizing on the expertise and generosity of members of the public, or community observers, who measure precipitation in areas without formal observation stations. These data contribute to development of 30-year climate normals, updates to Plant Hardiness Zone maps (see *Changes in the 2023 U.S. Department of Agriculture Plant Hardiness Map*, this volume), and numerous other resources that support diverse economic, recreational, and scientific sectors. Community observations also are a rich resource for assessing variation and trends in phenology, or seasonal events in the life cycle of plants and animals, that largely reflect variability and trends in weather and climate.

## Development of Oregon Season Tracker

Oregon Season Tracker, a project of Oregon State University, engages community observers in collecting, recording, and reporting data on precipitation, plant phenology, or both. Participants provide robust data for research while drawing their own inferences about environmental change. Through collaborative community science, Oregon Season Tracker connects natural resource managers, educators, researchers, and others members of the public. The initiative was launched in 2014 by Oregon State University Extension and the H.J. Andrews Experimental Forest, a member of the U.S. National Science Foundation's Long-Term Ecological Research Program, to develop collaborative climate change research and educational activities (Figure 1). The goal of the tracker is to expand awareness, knowledge, and understanding of climate variability and climate science among community members.

Oregon Season Tracker enables participants to place their local knowledge and observations in a regional and long-term context, improving



**Figure 1.** Volunteers practice plant phenology protocols at the H.J. Andrews Experimental Forest. Photograph by Jody Einerson.

understanding of organisms' adaptations to weather and climate across diverse Oregon landscapes. Volunteers participate by monitoring manual rain gauges daily or observing the phenological events (phenophases) of native plant species selected by program staff. Observers may collect data immediately outside their homes or in woodlands, farms, schools, or other areas of interest. Participation and training are free, although those collecting data on precipitation are required to purchase a program-approved gauge (about $40–50) that meets National Weather Service standards.

A network of collaborators supports the Oregon Season Tracker program with coordination, research, and data collection and management. Oregon State University Extension is the Oregon Season Tracker's coordinating partner. Extension in Oregon and nationwide has a long and successful history of interpreting and applying science to the benefit of local landowners, managers, and residents. Climate change brings new challenges and information needs to natural resource-based communities, and requires new approaches to communication, as society seeks to mitigate and adapt to climate change.

The H.J. Andrews Experimental Forest has been a partner in Oregon Season Tracker since the program's inception. The 6,475-hectare (16,000-acre) research forest is administered cooperatively by Oregon State University, the U.S. Forest Service's Pacific Northwest Research Station, and the Willamette National Forest. Oregon Season Tracker expands the scope and clarity of results from research conducted at the Experimental Forest by making data available from many dispersed, rural areas that currently are not well represented in regional climate models and weather predictions. Oregon Season Tracker volunteers are encouraged to monitor local vine maple (*Acer circinatum*), the focal species of the program (Figure 2), to supplement ongoing research on the species at the Experimental Forest. In the absence of vine maple, western Oregon volunteers monitor bigleaf maple (*Acer macrophyllum*), black cottonwood (*Populus trichocarpa*), common snowberry (*Symphoricarpos albus*), Douglas-fir (*Pseudotsuga menziesii*), Oregon white oak (*Quercus garryana*), Pacific ninebark (*Physocarpus capitatus*), or ponderosa (valley) pine (*Pinus ponderosa*). Additional Eastern Oregon species include antelope bitterbrush (*Purshia tridentata*), big sagebrush (*Artemisia tridentata*), rabbitbrush (*Chrysothamnus* spp., *Ericameria* spp., *Lorandersonia* spp.), and quaking aspen (*Populus tremuloides*).



**Figure 2.** Open flowers phenophase on a vine maple, the focal species of Oregon Season Tracker. Photograph by Declan O'Hara.

To centralize data collection and management, Oregon Season Tracker works with two national organizations, the Community Collaborative Rain, Hail, and Snow Network (CoCoRaHS) and the USA National Phenology Network (USA–NPN). CoCoRaHS, operated by the Colorado Climate Center, began as a local community project following a flash flood in 1997. It now has over 26,000 active observers in all state, territories, and provinces in the United States and Canada (Daly and Newman 2023). The National Phenology Network collects, organizes, and shares phenological data, information, and forecasts to support decision making, scientific discovery, and wide understanding of phenology. Since 1999, it has operated Nature's Notebook, which monitors the phenology of plants and animals across the country. Partnership with CoCoRaHS and the National Phenology Network allows Oregon Season Tracker to centralize and provide open access to data, which in turn expands the research power of the program and allows training materials to be shared.

In the 10 years since Oregon Season Tracker was initiated, over 500 volunteers in 21 counties have been trained in the program protocols. Many volunteers are actively engaged in ongoing Extension programs including Master Gardener, Oregon Naturalist, and Land Stewards. Participants include formal and informal educators employed by local schools and nature centers. Training sessions initially were held in-person in cooperation with county Extension agents. Most training is now conducted online, with skill-building sessions designed to reinforce



**Figure 3.** Master Gardeners in Jackson County, Oregon, monitor a rain gauge in their native plant garden. Photograph by Grace Florjancic.

training outcomes and refresh the expertise of active volunteers. We estimate that 200 volunteers currently monitor precipitation and 35 monitor plant phenology, although the number fluctuates by season and year. Although the flexibility of program participation is appealing to prospective volunteers, it can complicate tracking the number of active observers at a given point in time.

## Applications of Oregon Season Tracker Data

Data collected through Oregon Season Tracker have many applications, in part due to the project's partners. Via collaborations with CoCoRaHS on collection of precipitation data and USA–NPN on collection of plant phenology data, data from Oregon Season Tracker volunteers contribute to ongoing local and national research.

CoCoRaHS and the USA–NPN offer open-source data with a wide range of practical applications for research and management. Data visualization tools provided by these partners have user-friendly interfaces that enable the public to engage with the data as well. Precipitation data compiled by CoCoRaHS are used by the National Weather Service; meteorologists; hydrologists; emergency managers; city utilities responsible for water supply, water conservation, and storm water; insurance adjusters; the U.S. Department of Agriculture; engineers; mosquito control districts; ranchers and farmers; teachers; and students (CoCoRaHS n.d.). USA–NPN phenology data also are widely used among researchers and decision makers affiliated with entities including the National Park Service, U.S. Fish & Wildlife Service, USDA Forest Service, National Ecological Observatory Network, and Indigenous Phenology Network (USA–NPN n.d.). More than 170 peer-reviewed scientific publications and 45 graduate theses have used USA–NPN data since the program began in 1999.

Precipitation data collected by Oregon Season Tracker also contribute to the work of Oregon State University's PRISM Climate Group, the source of the most widely used spatial climate data in the United States. PRISM simulates how weather and climate vary spatially as a function of Earth's topography (Daly and Newman 2023). The PRISM climate mapping system regularly incorporates information from thousands of community observers. The most comprehensive community science

network contributing to PRISM is the Oregon Season Tracker's partner in precipitation monitoring, CoCoRaHS. PRISM provides monthly (1895–present) and daily (1981–present) time series of variables including precipitation, temperature, dew point, vapor pressure deficit, and solar radiation at 800 m and 4 km resolution (Daly et al. 2021, Rupp et al. 2022). Additionally, the PRISM Climate Group revised and updated the most recent version of the USDA Plant Hardiness Zone maps, released in November 2023 (see *Changes in the 2023 U.S. Department of Agriculture Plant Hardiness Map*, this volume). The updated zones are based in part on average extreme minimum temperature as reflected in PRISM's 1991–2020 U.S. Climate Normals, and cover all 50 states and Puerto Rico.

At the local level, the Oregon Season Tracker collaborative illustrates the power of combining geographically extensive community science with site-specific long-term study. Researchers at the H.J. Andrews Experimental Forest have been studying climate and plant phenology in the Lookout Creek Basin since the 1950s and 1970s, respectively. This research foundation enables detailed spatial modeling of variation in microclimate in forested mountains and investigation of the effects of regional climate change on environmental conditions at scales relevant to forest species (Daly et al. 2007, 2010; Frey et al. 2016; Rupp et al. 2020, 2021; Wolf et al. 2021).

**A Closer Look at Phenology Research**

Many species are highly sensitive to variation in climate and microclimate across space and time (Frey et al. 2016, Betts et al. 2018, Schmidt 2019, Finn et al. 2022). For example, budburst dates for a given plant species can vary by up to 60 days within the 6,400-hectare (15,815 acre) Lookout Creek basin, and by up to 80 days between years for an individual plant (Ward et al. 2018). In warm winters with low snowpack, an increasingly common circumstance, the expected variation in budbreak across elevational gradients is muted or nonexistent (Ward et al. 2018). Combining spatial models of microclimate and predictive models of budbreak makes it possible to model phenology accurately within the H.J. Andrews Experimental Forest (Ward 2018, Taylor et al. 2019), but modeling phenology across a larger region is difficult.

A comparison of the performance of phenology models that were based on data from the H.J. Andrews Experimental Forest and other long-term ecological research (LTER) sites versus those based on distributed USA–NPN (including Oregon Season Tracker) observations indicated that models based on LTER data excelled when predicting phenology in the areas from which the data were collected, but the USA–NPN-based models were better able to predict phenology across the large areas in which those observations were made (Taylor et al. 2019). Both local and regional data and models are needed to fully understand how climate variability and change is impacting fundamental life history processes and ecological interactions.

Phenological information has been important in understanding and responding to major disturbances and weather events in Oregon in recent years. Factors that affect the pace of tree regeneration following wildfire include cone production in the year of the fire, timing of the fire in relation to cone maturity, and cone production by surviving trees in subsequent years. Seed production by the mast-seeding conifer species that dominate Oregon forests is highly variable from year to year (Figure 4), and failure of cone crops tends to be synchronized across large geographic areas. Therefore, seed availability for natural regeneration and seedling production can vary by orders of magnitude from one fire to the next within a given area. Seed and seedling limitation was an impediment to restoration efforts after the historic Labor Day fires in 2020. Forest susceptibility to weather extremes can be influenced by the phenological stages of forest organisms at the time

**Figure 4.** Ripe Douglas-fir cones with recent seed drop. Photograph by Brad Withrow-Robinson.

of the extreme event. Thus, a better understanding of potential shifts in phenology can improve prediction of natural regeneration after disturbance, or suggest the necessity for intervention.

Another extreme example, the June 2021 heat wave in the Pacific Northwest, occurred at the peak of the growing season and prior to full development and hardening of new foliage and buds. Spatial patterns of canopy needle scorch were related to phenological variation across the region, with higher levels of canopy scorch in areas where needle and bud development of the dominant canopy species were not as advanced as in other areas with similar maximum air temperatures during the record-breaking heat wave (Still et al. 2022, Sibley et al. unpublished manuscript). The timing of this heat wave, and a less-severe heat wave relatively early in the 2015 growing season, resulted in early cessation of tree-diameter growth, which reduced annual forest productivity (Ford et al. 2017, Harrington et al. 2023). Similarly, atmospheric heat and drought stress can be strong predictors of latewood formation and annual tree growth (Jarecke et al. 2023, 2024). An increase in the number and magnitude of atmospheric stress events, as is expected as climate change accelerates, may have substantial impacts on forest productivity and condition.

As extreme weather events become more common, winter snowpack declines, and summer heat and drought stress increase, regional climate drivers will influence local environmental conditions and ecological processes in complex ways. Collaborative community science has the potential to fill in gaps in knowledge and predictive ability as society attempts to adapt to global climate change at the local level.

## Literature Cited

Betts, M.G., B. Phalan, S.J.K. Frey, J.S. Rousseau, and Z. Yang. 2018. Old-growth forests buffer climate-sensitive bird populations from warming. Diversity and Distributions 24:439–447.

CoCoRaHS (Community Collaborative Rain, Hail, and Snow Network). n.d. About us. www.cocorahs.org/.

Daly, C., D.R. Conklin, and M.H. Unsworth. 2010 Local atmospheric decoupling in complex topography alters climate change impacts. International Journal of Climatology 30:1857–1864.

Daly, C., J.W. Smith, J.I. Smith, and R.B. McKane. 2007. High-resolution spatial modeling of daily weather elements for a catchment in the Oregon Cascade Mountains, United States. Journal of Applied Meteorology and Climatology 46:1565–1586.

Daly, C., et al. 2021. Challenges in observation-based mapping of daily precipitation across the

conterminous United States. Journal of Atmospheric and Oceanic Technology 38:1979–1992.

Finn, D.S., S.L. Johnson, W.J. Gerth, I. Arismendi, and J.L. Li. 2022. Spatiotemporal patterns of emergence phenology reveal complex species-specific responses to temperature in aquatic insects. Diversity and Distributions 28:1524–1541.

Ford, K.R., C.A. Harrington, S. Bansal, P.G. Gould, and J.B. St. Clair. 2017. Will changes in phenology track climate change? A study of growth initiation timing on coast Douglas-fir. Global Change Biology 23:3348–3362.

Frey, S.J.K., A.S. Hadley, and M.G. Betts. 2016. Microclimate predicts within-season distribution dynamics of montane forest birds. Diversity and Distributions 22:944–959.

Frey, S.J.K., A.S. Hadley, S.L. Johnson, M. Schulze, J.A. Jones, and M.G. Betts. 2016. Spatial models reveal the microclimatic buffering capacity of old-growth forests. Science Advances 24:9. https://doi.org/10.1126/sciadv.1501392.

Harrington, C.A., P.J. Gould, and R. Cronn. 2023. Site and provenance interact to influence seasonal diameter growth of *Pseudotsuga menziesii*. Frontiers in Forests and Global Change 6:1173707. https://doi.org/10.3389/ffgc.2023.1173707.

Jarecke, K.M., K.D. Bladon, F.C. Meinzer, and S.M. Wondzell. 2024. Impact of rainfall and vapor pressure deficit on latewood growth and water stress in Douglas-fir in a Mediterranean climate. Forest Ecology and Management 551:121529. https://doi.org/10.1016/j.foreco.2023.121529.

Jarecke, K.M., L.R. Hawkins, K.D. Bladon, and S.M. Wondzell. 2023. Carbon uptake by Douglas-fir is more sensitive to increased temperature and vapor pressure deficit than reduced rainfall in the western Cascade Mountains, Oregon, USA. Agricultural and Forest Meteorology 329:109267. https://doi.org/10.1016/j.agrformet.2022.109267.

Rupp, D.E., C. Daly, M.K. Doggett, J.I. Smith, and B. Steinberg. 2022. Mapping an observation-based global irradiance climatology across the conterminous United States. Journal of Applied Meteorology and Climatology 61:857–876.

Rupp, D.E., S.L. Shafer, C. Daly, J. Jones, and S.J.K. Frey. 2020. Temperature gradients and inversions in a forested Cascade Range basin: synoptic-to local-scale controls. Journal of Geophysical Research: Atmospheres 125:23. https://doi.org/10.1029/2020JD032686.

Rupp, D.E., S.L. Shafer, C. Daly, J.A. Jones, and C.W. Higgins. 2021. Influence of anthropogenic greenhouse gases on the propensity for nocturnal cold-air drainage. Theoretical and Applied Climatology 146:231–241.

Schmidt, S.A. 2019. Buzzing Bolbomyiidae and air temperature monitoring methods: investigating long-term ecological data from the H.J. Andrews Experimental Forest. M.S. Thesis, Oregon State University, Corvallis, Oregon.

Still, C.J., et al. 2023. Causes of widespread foliar damage from the June 2021 Pacific Northwest heat dome: more heat than drought. Tree Physiology 43:203–209.

Taylor, S.D., J.M. Meiners, K. Riemer, M.C. Orr, and E.P. White. 2019. Comparison of large-scale citizen science data and long-term study data for phenology modeling. Ecology 100:ecy.2568. https://doi.org/10.1002/ecy.2568.

USA–NPN (USA National Phenology Network). (n.d.) Learn about our partners. www.usanpn.org/community#national-partners.

Ward, S.E. 2018. Microclimate and phenology at the H.J. Andrews Experimental Forest. M.S. Thesis, University of Oregon, Eugene, Oregon.

Ward, S.E., M. Schulze, and B. Roy. 2018. A long-term perspective on microclimate and spring

plant phenology in the Western Cascades. Ecosphere 9:e02451. https://doi.org/10.1002/ecs2.2451.

Wolf, C., D.M. Bell, H. Kim, M.P. Nelson, M. Schulze, and M.G. Betts. 2021. Temporal consistency of undercanopy thermal refugia in old-growth forest. Agricultural and Forest Meteorology 307:108520. https://doi.org/10.1016/j.agrformet.2021.108520.

# Floating Offshore Wind Energy Infrastructure

Karina Nielsen and Bryson Robertson, Editors

## Introduction

*The Rationale for Development of Floating Offshore Wind Energy Along the U.S. West Coast*

Karina Nielsen and Bryson Robertson

The policy goal of limiting climate change by decarbonizing and electrifying the energy sector is driving rapid development and innovation of offshore wind energy technologies, including floating offshore wind. The U.S. West Coast is an attractive location for development of offshore wind energy because of its strong and reliable offshore winds (Figure 1).
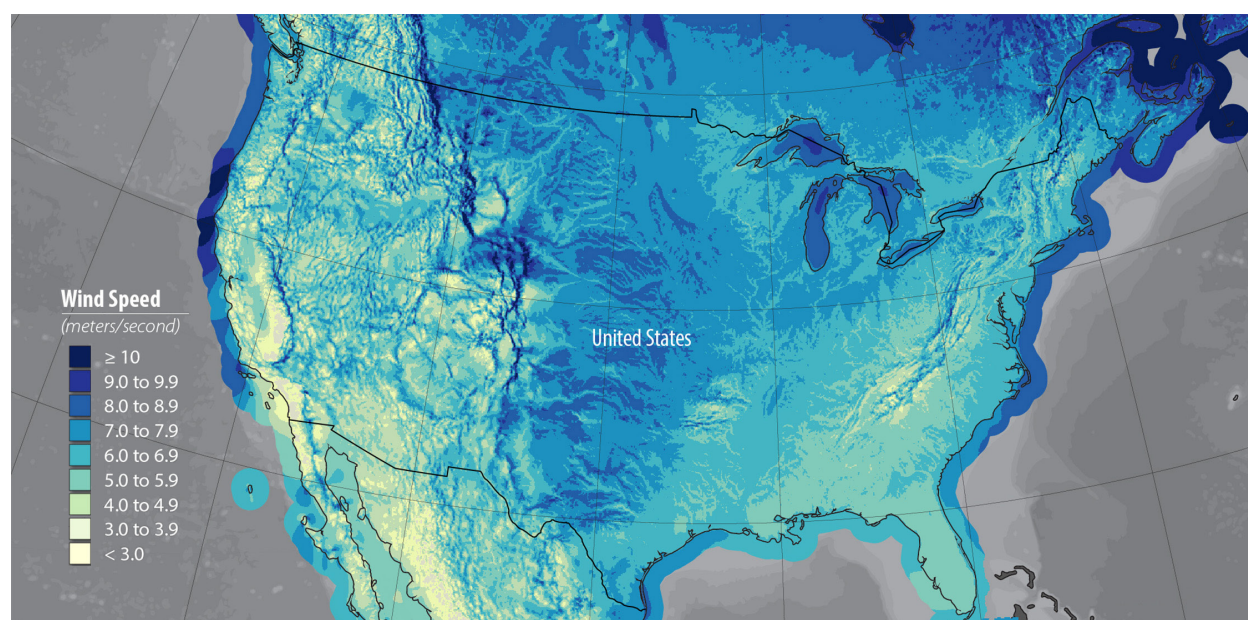


**Figure 1.** Annual average wind speed at 100 m (328 ft.) above the surface of the contiguous United States and the adjacent 50 nautical mi. (57.5 mi.; 92.6 km). Modified from a figure produced by the National Renewable Energy Laboratory (www.nrel.gov/gis/assets/images/wtk-100-north-america-50-nm-01.jpg).

Accessing these winds, which are over ocean waters much deeper than 60 m (197 ft.), will require the use of floating offshore wind (FOSW) energy instead of fixed-bottom technologies (Figures 2, 3). Wind turbines deployed at sea are classified as either fixed-bottom or floating. Fixed-bottom offshore wind turbines are attached to foundations that are rigidly affixed to the seafloor. In contrast, floating offshore wind turbines are attached to floating foundations that are held in place by mooring lines connected to anchors on the seafloor.

As of 2024, the four FOSW arrays in operation worldwide are off the coasts of Scotland, Portugal, and Norway (173.5 MW of generating capacity). The arrays are WindFloat Atlantic (8 MW; Windfloat Atlantic n.d.), Hywind Scotland (30 MW; Equinor n.d. a), Kincardine Offshore Wind Farm (47.5 MW; Principle Power n.d.), and Hywind Tampen (88 MW; Equinor n.d. c). They are from 15 to 140 km (8 to 76 nautical mi.) offshore at depths of 60 to 300 m (197 to 984 ft.) and represented 0.2 percent of global offshore wind generating capacity in 2023. The cumulative generating capacity of all offshore wind installations in 2023, most of which are in Europe and Asia (GWEC 2024) and use fixed-bottom technologies (Figure 3), was 75,200 MW (72.5 GW).

**Figure 2.** General locations off the coast and within lakes of the United States where water depth (maximum 1300 m [4265 ft.]) and wind speeds are sufficient for installation of fixed-bottom (yellow) and floating (blue) wind energy turbines. Image does not consider potential siting constraints. Modified from a graphic by Philipp Beiter, National Renewable Energy Laboratory.

Although no FOSW arrays currently operate in U.S. federal waters, in 2022 the Bureau of Ocean Energy Management sold the first five U.S. leases for FOSW along the West Coast near Humboldt Bay and Morro Bay, California (BOEM n.d. a). Since then, the Bureau of Ocean Energy Management engaged with federal, state, and local agencies and tribal governments through the Oregon Intergovernmental Renewable Energy Task Force to identify additional lease areas off the coast of Oregon.

The Bureau of Ocean Energy Management planned to hold an auction to sell two more lease areas in U.S. federal waters near Coos Bay and Brookings, Oregon (BOEM n.d. b), in October 2024. However, on 27 September 2024, the Bureau of Ocean Energy Management postponed the lease auction due to insufficient bidder interest (BOEM 2024). Simultaneously, Governor Kotek withdrew Oregon from the Oregon Intergovernmental Renewable Energy Task Force. In a letter to the Bureau, the Governor cited the need to complete the Oregon Offshore Wind Energy Roadmap before a lease sale; concerns of tribes, sectors, and the public; the risks that a failed lease process would pose to Oregon's developing supply chain industry; and potential risks to offshore ecosystems; while also stating her confidence "that offshore wind holds exciting promise to be part of our nation's clean energy future" (Kotek 2024). The Bureau of Ocean Energy Management intends to continue working with federal, state, and local agencies and tribal governments and to support the state-led offshore wind energy roadmap process, as directed by Oregon House Bill 4080 (passed in 2024), to determine opportunities for a future lease sale.

The potential development of FOSW off the coast of Oregon has prompted a range of responses, opinions, questions, and concerns from Oregonians and tribes (Informal Offshore Wind Work

Group 2024). In this chapter, we explore why FOSW is being pursued off the U.S. West Coast, describe the floating offshore infrastructure being considered, and examine potential interactions of this infrastructure with the ocean environment and coastal human communities. The scope of our exploration includes the at-sea infrastructure, supporting port infrastructure, and shore-based transmission stations. The many other infrastructure topics that are beyond the scope of this chapter include inland transmission, storage, supply chain, manufacturing, procurement, and the vessels needed to support deployment. Our discussion of environmental interactions with FOSW infrastructure focuses on wind-driven upwelling, underwater sound, electromagnetic fields, entanglement hazards, and fishes. The chapter also explores public perceptions, energy and environmental justice, and community benefit plans related to FOSW. Environmental and societal topics that also were beyond the scope of this chapter include potential effects of FOSW on birds, bats, marine mammals, fisheries, tribal cultural resources, and tribal federal trust and treaty rights.
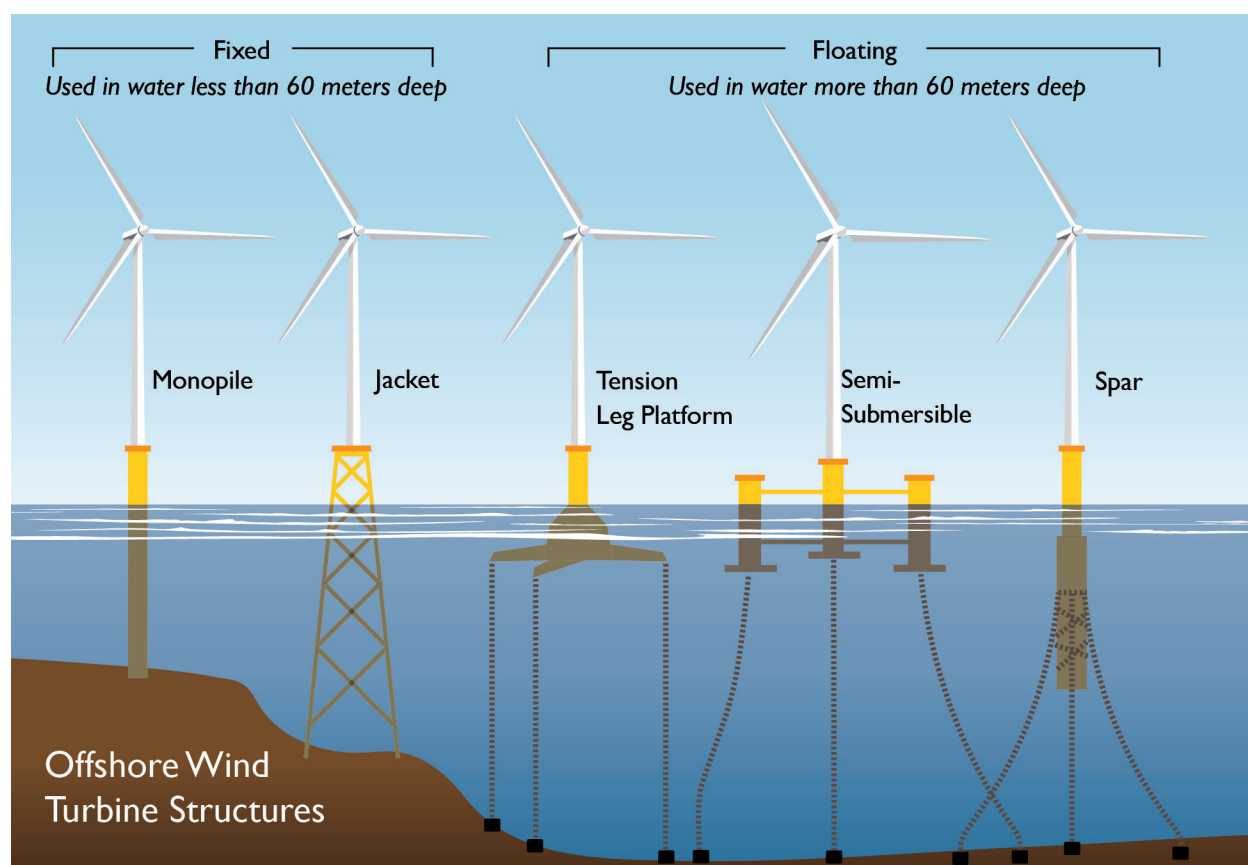


**Figure 3.** Fixed-bottom and floating offshore structures for wind turbines. Graphic by Allison Walkingshaw.

## International and National Efforts to Limit Climate Change

Several substantive international, national, and state-level policies are contributing to actions and innovations to decarbonize the energy sector and reduce greenhouse gas emissions with the goal of limiting climate change. The United States is a party to the Paris Agreement, an international treaty to limit climate change that was adopted in 2015 (UNFCCC n.d. a). Members of the Paris Agreement were required to submit a national climate action plan, also known as a Nationally Determined Contribution (UNFCCC n.d. b), in 2020, and must update the plan every five years. In its first submission, the United States set an economy-wide target of reducing its net greenhouse gas

emissions by 50–52 percent below 2005 levels by 2030 (United States 2021). In setting this target, the United States described taking an all-of-government and sector-by-sector approach to reducing greenhouse gas emissions by decarbonizing the energy sector, increasing carbon sink capacity and reducing greenhouse gas emissions from natural and agricultural systems, and reducing emissions of greenhouse gases other than carbon dioxide.

Achieving its energy sector decarbonization goal will require the United States to rapidly deploy solar and wind technologies while reducing the percentage of energy derived from fossil fuels and increasing the percentage of electricity produced by non-carbon emitting sources to at least 75 percent by 2030 (NASEM 2021). The International Energy Agency's Net-Zero Roadmap further clarifies that rapid deployment of commercially available technologies and widespread use of technologies that are not commercialized yet will be required to reach the net zero carbon goal by 2050 (IEA 2021). About 45 percent of the reduction in carbon dioxide emissions necessary by 2050 relies on extant technologies that need to be commercialized.

In 2021, the White House issued Executive Order 14008, which directed the Secretary of the Interior and other relevant federal administrators and agencies to increase renewable energy production on public lands and offshore waters. The executive order included a goal of doubling "offshore wind by 2030 while ensuring robust protection for our lands, waters, and biodiversity and creating good jobs." Offshore wind energy is a relatively mature wind technology, and the United States has set ambitious and aggressive goals to advance and deploy wind energy in support of energy sector decarbonization. In 2021, the White House set the goal of deploying 30 GW of offshore wind by 2030 (The White House 2021), and in 2022, it added another 15 GW to its floating offshore wind energy goal for 2035 (The White House 2022).

The U.S. federal government made an unprecedented commitment to and investment in the modernization and decarbonization of the U.S. energy system through the Infrastructure Investment and Jobs Act of 2021 (House Bill 3684; commonly called the Bipartisan Infrastructure Law) and Inflation Reduction Act of 2022 (House Bill 5376). The Congressional Budget Office estimated that total support for the climate and clean energy programs, tax credits, and other incentives authorized through the two acts will exceed $430 billion from 2022 through 2031 (Steinberg et al. 2023).

The Inflation Reduction Act includes multiple provisions related to offshore wind leasing, transmission planning, and tax credits (CRS 2022). One of the provisions set a new limit on the Bureau of Ocean Energy Management's authority to issue offshore wind leases through 2032: it may not issue a lease for offshore wind development unless it has also offered at least 60 million acres (93,750 mi$^2$ or 242,800 km$^2$) for oil and gas leasing on the outer continental shelf during the previous year. Given this constraint, and the 2024 postponement of the planned lease sale by the Bureau of Ocean Energy Management, the next opportunity for a lease sale off the Oregon coast will occur in 2026. 2026 is the year after the next proposed offshore oil and gas lease sale on the Bureau's leasing schedule for the outer continental shelf. The combination of these provisions, the administration's goals for offshore wind energy, and the substantial federal investments and provisions approved by Congress has been driving the rapid and constrained timeline for the Bureau of Ocean Energy Management to complete its planned offshore wind lease auctions.

The White House also projects that its policies to develop a U.S. offshore wind industry will deliver social and economic benefits including jobs, domestic manufacturing and supply chains, and improvements in port infrastructure, and will contribute to addressing historical inequities in energy development (Biden 2023, Ocean Policy Committee 2023). A study of the social and economic

effects of European offshore wind energy arrays developed since 2010 indicated that the economic benefits of the local offshore construction stage were substantially overestimated due to imported labor and skills (Glasson et al. 2022). Other economic benefits over the offshore wind lifecycle, including onshore construction and, especially, the 20–25 years of the operation and management stage, were underestimated (Glasson et al. 2022). The data on social effects were much more limited; the overall impact on well-being was positive, but effects on aspects of social capital were less positive (Glasson et al. 2022). Although it is too soon to analyze the economic benefits of offshore wind array development in the United States, land-based wind energy installations in the country have meaningful employment and earnings impacts that extend beyond the construction phase (Gilbert et al. 2024). Earnings and employment among workers who were male, Black, or without a high school or college degree were higher within 32 km (20 mi.) of a project (Gilbert et al. 2024). However, the increases in spending and investment were lower than is typical of other industries.

Several technical value propositions support the development of offshore wind energy. These include the ability of offshore wind turbines to generate large amounts of reliable power. Because no mountains or buildings obstruct wind flow over water, wind speeds tend to be higher and more consistent, and wind less turbulent, over water than on land (Wilson and Zimmerman 2023). Additionally, many areas suitable for offshore wind energy arrays tend to have stronger winds in the afternoon and evening than in the morning (although this diurnal effect diminishes farther offshore). Therefore, offshore wind arrays continue generating power in the evening and in winter, when solar energy generation decreases. This characteristic of offshore wind aligns with daily power demand cycles and can complement other variable or intermittent renewable energy sources, such as solar and land-based wind.

As the energy sector is decarbonized, the percentage of variable or intermittent renewables in the energy sector portfolio, also referenced as their penetration, will increase. For energy and electricity demand to be met reliably and consistently, the increasing penetration of renewables must be complemented by a suite of baseload and dispatchable energy sources and energy storage. Baseload generation has a consistent power output and its production does not increase or decrease over short periods of time. Examples of baseload generators include coal-fired generators and nuclear facilities. Production by a dispatchable energy source can be increased or decreased on demand to adjust the power output supplied to the electrical grid. Examples of non-variable dispatchable generators include natural gas generators and hydroelectric, hydrogen-generated, and some geothermal power sources, albeit the dispatchability of hydropower depends on the amount of water stored behind the dam. Furthermore, hydropower is vulnerable to climate change given evolving operational restrictions related to riverine ecosystems and projected future extreme storms, droughts, and asynchronous timing of changes in supply and demand (Kao et al. 2022). As penetration of wind and solar energy sources increases and use of baseload coal declines, use of dispatchable natural gas is increasing to fill the gap (EIA 2023). Interest in expanding nuclear energy capacity to meet energy needs is also growing (Mandler 2024, Plumer 2024, Sierra 2024). Other sources of clean energy and energy storage lag in coming to market.

An emerging and substantive concern is that the demand for energy is increasing faster than previously projected. Five-year growth projections almost doubled, from 2.6 to 4.7 percent, between 2022 and 2023 (Wilson and Zimmerman 2023). New data centers (including cryptocurrency and artificial intelligence) and industrial facilities (primarily semiconductors, batteries, and automotive, but also hydrogen) are two of the main drivers of this sudden growth in energy load (Wilson and Zimmerman 2023). Building and transportation electrification (e.g., heat pumps, electric

vehicle chargers) are also increasing demand over longer periods of time, but are less volatile. The combination of demand increases, decarbonization targets, and a limited number of new low-carbon technologies for energy generation creates uncertainty in the future of Oregon's electricity sector.

## Oregon's Energy Sources

In 2021, nearly half of the electricity that supplied Oregon's demand was generated via the combustion of fossil fuels (Table 1). Natural gas accounted for the largest percentage of fossil fuels (24.5 percent), followed by coal (21.8 percent) (ODOE 2022). Hydropower, wind, and nuclear generated 38.4, 9.3, and 3.1 percent of Oregon's electricity, respectively. There is a cost to generating electricity regardless of the energy source, but not all sources of energy incur costs. Most forms of renewable energy, such as wind and sun, are free and abundant. Therefore, the costs of electricity generated from most renewable sources are relatively stable. By contrast, fossil fuels must be mined, processed, and transported. As a result, they have a cost and their availability can be constrained, causing the costs of electricity generated from fossil fuels to be more variable than the costs of electricity generated from renewables. Costs of electricity generated from fossil fuels can also be volatile and high if and when supply-chain constraints cause fossil fuels to become scarce. Another, non-monetary cost of fossil fuels is the greenhouse gases they emit when combusted.

| Resource | Percentage | Millions of MWh |
|---|---|---|
| Hydropower | 38.4 | 22.10 |
| Natural gas | 24.5 | 14.07 |
| Coal | 21.8 | 12.55 |
| Wind | 9.3 | 5.37 |
| Nuclear | 3.1 | 1.76 |
| Solar | 1.7 | 0.98 |
| Biomass | 0.6 | 0.35 |
| Other non-biogenic | 0.1 | 0.08 |
| Biogas | 0.1 | 0.07 |
| Geothermal | 0.1 | 0.06 |
| Petroleum | 0.1 | 0.05 |
| Other biogenic | 0.1 | 0.04 |
| Waste | 0.1 | 0.03 |

**Table 1.** Oregon electricity resource mix for investor- and consumer-owned electric utilities serving Oregon in 2021. MWh, megawatt-hours. Source: www.oregon.gov/energy/energy-oregon/pages/electricity-mix-in-oregon.aspx.

Oregon's clean electricity law (House Bill 2021), passed in 2021, requires that Oregon's two largest investor-owned utilities, Portland General Electric and PacifiCorp, and the state's electricity service suppliers reduce the greenhouse gas emissions from the electricity they use to meet Oregon demand by 80 percent below the baseline by 2030, 95 percent by 2035, and 100 percent by 2040.

In 2021, via House Bill 3375, the Oregon Legislature set a state goal to plan for the development of up to 3 GW of floating offshore wind within the federal waters off the Oregon coast by 2030, but it has neither set a state deployment target nor mandated or created specific incentives for procurement of floating offshore wind by Oregon utilities. The 2022 Floating Offshore Wind Study by the Oregon Department of Energy (as charged by the legislature in House Bill 3375) concluded, "Achieving Oregon's economy-wide decarbonization and clean electricity policies will require developing a tremendous scale of new renewable generation projects." Land-based wind and solar renewable resources remain the lowest cost and fastest growing renewable energy resources in Oregon, as other renewable generation technologies are not yet commercially mature, scalable, and deployable.

FOSW offers many advantages and challenges. Key benefits identified by the Oregon Department of Energy reflect national findings and include the reliably strong and consistent winds off the Oregon coast, FOSW's complementarity to other renewables, its potential to offset land-use impacts related to the development of onshore renewable energy sources, and its potential to enhance

power system reliability, local energy resilience, and economic development, especially for coastal communities. The major challenges include concerns about adverse effects on coastal communities, existing industries, and the environment and cultural resources; siting and permitting approvals; technology readiness and costs of commercial-scale deployment; upgrades to port infrastructure needed to support initial construction and ongoing operations and maintenance; necessary improvements to transmission infrastructure; and commitments to procure the power.

In contrast to California and other regions of the United States, the Pacific Northwest (Idaho, Montana, Oregon, and Washington, as defined by the 1980 Pacific Northwest Electric Power Planning and Conservation Act [Senate Bill 885]) does not have a centralized and independent regional transmission provider or a centralized power market. Instead, the many transmission and power providers in the Pacific Northwest each conduct their own local transmission and power planning and generally contract bilaterally for transmission and power services. In other regions, Regional Transmission Organizations and Independent System Operators provide centralized transmission planning and operate centralized power markets, both of which help to optimize power and transmission planning and procurement to serve regional loads more efficiently and cost effectively. Additionally, unlike several East Coast states, neither Oregon nor California has created specific incentives for offshore wind or mandated its procurement through state policies, such as a state-wide power purchase agreement or offshore wind renewable energy certificates, to support explicit offshore wind procurement goals. To realize gigawatt-scale FOSW development to serve Pacific Northwest customers, Pacific Northwest utilities would likely need to collaborate with each other or cooperate with utilities outside the region to plan and commit to the necessary procurement agreements and transmission infrastructure investments (Sierman et al. 2022).

*West Coast Energy Policies and Strategies*

Jason Sierman, Joni Sliger, and Stephanie Kruse

The states of Oregon, Washington, and California have mid-twenty-first century goals for economy-wide decarbonization and 100 percent clean electricity. As of 2021, the populations of Oregon, Washington, and California were 4.3, 7.7, and 39.2 million, respectively. California's large population, associated demand for energy, and clean energy and climate policies are currently the primary motivations for pursuing development of floating offshore wind (FOSW) along the West Coast.

California Assembly Bill 525, passed during the 2021–2022 legislative session, directed the California Energy Commission to establish state policy targets for FOSW development and produce a government-wide strategic plan to help meet those targets. In 2022, the California Energy Commission established a state target of developing 2 to 5 GW of FOSW by 2030 and 25 GW by 2045. California has also committed to making the port and transmission infrastructure investments that are prerequisites to deploying several gigawatts of FOSW projects. California's actions have significant effects on the opportunities and challenges for deploying FOSW anywhere along the West Coast, including ocean areas adjacent to Oregon and Washington.

**Oregon Clean Energy and Climate Policies**

To reduce emissions of greenhouse gases and mitigate climate change and its effects, Oregon has enacted some of the most aggressive economy-wide decarbonization and renewable and clean energy goals in the nation. These include several major bills passed by the legislature in 2007 (House Bill 3543), 2016 (Senate Bill 1547), and 2021 (House Bill 2021) and Executive Order No. 20-40,

issued by Governor Kate Brown in 2020. House Bill 3543 established Oregon's goal of reducing greenhouse gas emissions to 75 percent below 1990 levels by 2050. Senate Bill 1547 increased Oregon's Renewable Portfolio Standard, requiring Oregon's largest consumer-owned utilities to achieve 25 percent renewables by 2025 and its largest investor-owned utilities to achieve 50 percent renewables by 2040. Senate Bill 1547 also requires investor-owned utilities to remove coal power costs from rates by 2030. House Bill 2021 requires Oregon's two largest investor-owned utilities and its electricity service suppliers to provide 100 percent non-greenhouse gas-emitting electricity by 2040. Executive Order 20-40 called for the state to reduce its greenhouse gas emissions by at least 80 percent below 1990 levels by 2050. The latter mandate led to the Oregon Department of Environmental Quality's ongoing rulemaking to establish the state's Climate Protection Program, which proposes to require a 50 percent reduction in greenhouse gas emissions from fossil fuels used in Oregon by 2035 and a 90 percent reduction by 2050.

## Oregon Offshore Wind Policies

The Oregon Legislature passed bills regarding FOSW in 2021 (House Bill 3375) and 2024 (House Bill 4080). House Bill 4080 directs the Oregon Department of Land Conservation and Development to lead engagement with and gather input from diverse interested parties, tribes, communities, and state agencies to develop a state offshore wind roadmap that supports public engagement; coastal communities; new economic opportunities and sustained existing economies; a local, trained, housed and equitable FOSW workforce; protection of tribal cultural and archaeological resources, viewsheds, and other tribal interests; protection of the environment and marine species; and achievement of state energy and climate policies, including energy diversity, reliability, and resilience of state and regional energy systems. A report on the roadmap and related standards must be submitted to the Oregon Legislature by 1 September 2025.

House Bill 4080 also includes three state policies. The first supports engagement among developers, stakeholders, and communities. The second supports the interconnection of FOSW projects in ways that promote reliability and resilience of Oregon's power grid. The third supports economic diversification and quality workmanship in the development and operation of FOSW and port infrastructure projects by requiring and defining strong labor standards.

House Bill 3375 directed the Oregon Department of Energy to study and report on the benefits and challenges of integrating up to 3 GW of FOSW into Oregon's power grid by 2030. This study and the report were completed in 2022. The bill also set two state policy goals for offshore wind: a goal to plan for the development of up to 3 GW of FOSW within the federal waters off the Oregon coast by 2030, and a goal that the planning be conducted in a manner that maximizes benefits to Oregon while minimizing conflicts among FOSW projects, the ocean ecosystem, and ocean users. The former goal is not an explicit deployment target and does not designate an entity to procure the power. House Bill 3375 does not direct the state (or any state agency) to conduct the strategic planning necessary to mobilize the capital investments required to deploy FOSW at a gigawatt scale. Nor does it mandate or create incentives for procurement of FOSW by Oregon utilities. Given this context, the first planning goal has not been interpreted as a minimum or maximum bound on potential FOSW development off Oregon's coast.

In response to the two state policy goals for FOSW planning, the Oregon Department of Energy added offshore wind-related data into its development of the Oregon Renewable Energy Siting Assessment mapping tool. The Oregon Department of Energy also submitted comments to the

Bureau of Ocean Energy Management supporting the bureau's identification of ocean areas capable of accommodating up to 3 GW of FOSW development and participated in several studies exploring the potential transmission infrastructure necessary to connect gigawatts of FOSW to the regional power grid.

**Oregon's Energy Strategy**

As directed by House Bill 3630 (pased in 2023), the Oregon Department of Energy is developing a comprehensive state energy strategy that identifies optimized pathways to achieving the state's energy policy objectives. The department has reached out to tribes and engaged with the public, data holders, and other state agencies to ensure that the strategy is informed by Oregon-specific data and the real-world experiences of Oregonians, communities, businesses, and industry. Development of the strategy is ongoing and will be completed by 1 November 2025.

In summer 2024, the Oregon Department of Energy began to quantitatively model and assess the ability of candidate clean electricity technologies, including FOSW, to contribute to reliably and affordably meeting state and regional demands for clean electricity. The modeling will include scenarios that explore different pathways to meet Oregon's energy policy objectives by considering and evaluating different risks and uncertainties, such as constraints to interstate transmission. The analysis will examine resource development, cost, and other effects associated with different potential futures. Complementary technical analyses will assess how each scenario could affect jobs, household energy costs, and public health. The next phase of the Oregon Energy Strategy process will draw on the results of the modeling and technical analyses to inform policy recommendations.

*Jurisdictional Boundaries, Regulations, and Permits*

Jeff Burright

The regulatory and permitting process associated with an offshore wind project is complex, involving multiple entities at multiple levels of government. Components of the project, such as shoreside support facilities, navigation channel modifications, transmission infrastructure improvements, and the offshore installation itself, generally are distinct permit actions that may require separate but interdependent permitting processes.

Numerous federal, state, and local permits, authorizations, and consultations are required before an offshore wind project installation is allowed to proceed (Table 2). The primary authorizations for a project in federal waters are a Construction and Operations Plan from the Bureau of Ocean Energy Management and a permit issued by the U.S. Army Corps of Engineers under the Clean Water Act and Rivers and Harbors Act. These federal authorizations also trigger the need for an assessment of environmental impacts under the National Environmental Policy Act of 1969 and state federal consistency review under the Coastal Zone Management Act of 1972.

Under the Coastal Zone Management Act, federally approved state coastal programs have the authority to review federal actions (including federal licenses and permits for offshore wind) that may affect coastal resources and uses with respect to the actions' consistency with state enforceable policies. In Oregon, these policies are drawn from existing state statutes and rules, the 19 Statewide Planning Goals, and the local embodiment of the goals in city and county plans and codes.

Oregon's review authority has been approved by the National Oceanic and Atmospheric Administration's Office for Coastal Management to extend into a portion of federal jurisdictional

| Authority | Agency | Application | Format of decision | Purpose |
|---|---|---|---|---|
| **Federal regulatory** | Bureau of Ocean Energy Management | Construction and operations plan | Approval to develop | Approve a use of the Outer Continental Shelf to produce energy |
| | U.S. Army Corps of Engineers | §404 (Clean Water Act) | Permit | Regulate discharges to waters of the United States and permit construction of structures in or over any navigable water of the United States |
| | | §10 (Rivers and Harbors Act) | Permit | |
| **Federal consultation** | National Oceanic and Atmospheric Administration; National Marine Fisheries Service | Magnuson-Stevens Fishery Conservation and Management Act; Marine Mammal Protection Act | Biological opinion | Conserve essential habitat for federally managed fishes; protect marine mammals |
| | U.S. Fish and Wildlife Service | Endangered Species Act consultation | Biological opinion | Ensure that the action shall not jeopardize listed species or designated critical habitat |
| | U.S. Army Corps of Engineers | National Historic Preservation Act §106 Consultation | Report | Protect historical properties and archaeological resources |
| **Subject to federal consistency review** | | | | |
| **Federal authority delegated to the state** | Department of Environmental Quality | § 401 Clean Water Act beneficial use | § 401 certification | Protect water quality standards |
| | Department of Land Conservation and Development, Oregon Coastal Management Program | Consistency certification and necessary information | Federal consistency | Ensure that federal licenses and permits are fully consistent with state enforceable policies |
| **State agency regulatory authority** | Department of State Lands | Removal-fill | Permit | Protect wetlands and waters for home, commercial, wildlife habitat, public navigation, fishing, and recreational uses |
| | | Proprietary lease | Lease | Manage state submerged and submersible lands in the public trust |
| | Oregon Parks and Recreation Department | Ocean shore | Permit | Approve ocean shore alterations and protect the free and uninterrupted use of ocean shores |
| | Oregon Parks and Recreation Department-State Historic Preservation Office | Archaeological resources | Permit | Protect historical properties and archaeological resources |
| **State consultation** | Oregon Department of Fish and Wildlife | | Consultation | Optimally manage fishes caught for human consumption; protect wildlife |
| | Oregon Department of Energy | | Consultation | |
| **Local government** | City or county | Permit (conditional use) | Land use | Ensure that shoreside portions of projects are consistent with Oregon Statewide Planning Goals |

**Table 1.** Regulatory overview of an offshore wind energy installation.

waters for marine renewable energy projects, recognizing that a project in federal waters has reasonably foreseeable effects on state coastal resources and uses. The review authority for marine renewable energy projects (defined by a Geographic Location Description, one of which Oregon maintains for renewable energy projects; DCLD n.d.) extends to approximately 32–80 km (20–50 mi.) offshore and is delineated by the 500-fathom (914.4 m or 3000 ft.) depth contour. The portions of projects within state jurisdiction, such as those related to water quality, uses of the seafloor,

effects on the ocean shore, and effects on estuaries, shorelands, and uplands within local jurisdiction, also are subject to permits and authorizations.

The Oregon Department of Land Conservation and Development is the lead state agency for these federal consistency reviews. The Oregon Coastal Management Program within the Department of Land Conservation and Development coordinates with other local, state, and federal agencies and consults with tribal nations in the review of any proposed project. This networked program, which is federally approved under the Coastal Zone Management Act, includes the authorities, policies, and subject-matter expertise of 11 state agencies, 8 counties, and 33 cities in the coastal zone. The program incorporates over 3,000 enforceable policies that apply to federal actions with coastal effects. At the conclusion of the review, the Coastal Management Program may concur that the activity is consistent, concur with conditions, or object on the grounds that the activity is inconsistent with the state's enforceable policies. If a review of a federally permitted project results in an objection, the federal agency will not issue the permit to the applicant. The applicant may appeal an objection to the U.S. Secretary of Commerce.

Offshore wind projects require the development of offshore transmission infrastructure that crosses state waters, port infrastructure, and onshore transmission infrastructure that connects the project to Oregon's onshore grid. Each of these infrastructure developments requires permitting reviews from local, state, and federal authorities. Federal consistency review also applies to development activities within state waters, such as routing subsea transmission cables and onshore connection infrastructure. Any alteration to Oregon's shoreline, estuaries, wetlands, or navigation channels to facilitate the deployment of offshore wind projects also is subject to federal consistency review.

The full permitting process for an offshore wind project may take years of coordinated effort, with a high burden of information. The construction, installation, and decades of operation of floating offshore wind in Oregon are novel uses in a region that prioritizes protection of its living renewable ocean resources. Uncertainties about the individual and cumulative effects of development on natural, economic, and social systems are of great concern to potentially affected communities.

## Floating Offshore Wind Energy Infrastructure, Transmission, and Ports

*Floating Offshore Wind Infrastructure*

Bryson Robertson and Travis Douville

Offshore wind systems are generally classified as fixed-bottom or floating (Figure 3). Most global offshore wind deployments are fixed-bottom, whereas those off the U.S. West Coast will be floating. Fixed-bottom offshore wind turbines are attached to foundations that are rigidly affixed to the seafloor through an embedment monopile or a jacket foundation. The installation machinery and structural members of fixed-bottom systems require water depths less than about 60 m (200 ft.). The ocean floor along the U.S. West Coast is much deeper, and therefore cannot support fixed-bottom systems. For example, the current Oregon wind energy areas have water depths of 600 m (1970 ft.) to 1300 m (4265 ft.).

A floating offshore wind (FOSW) system has four major subsystems: the turbine subsystem, which includes the rotor blades, hub, nacelle, and tower; floating platform subsystem; mooring and anchoring subsystem, and balance of plant, which includes the grid connection, cables, and electrical components (Figure 4).
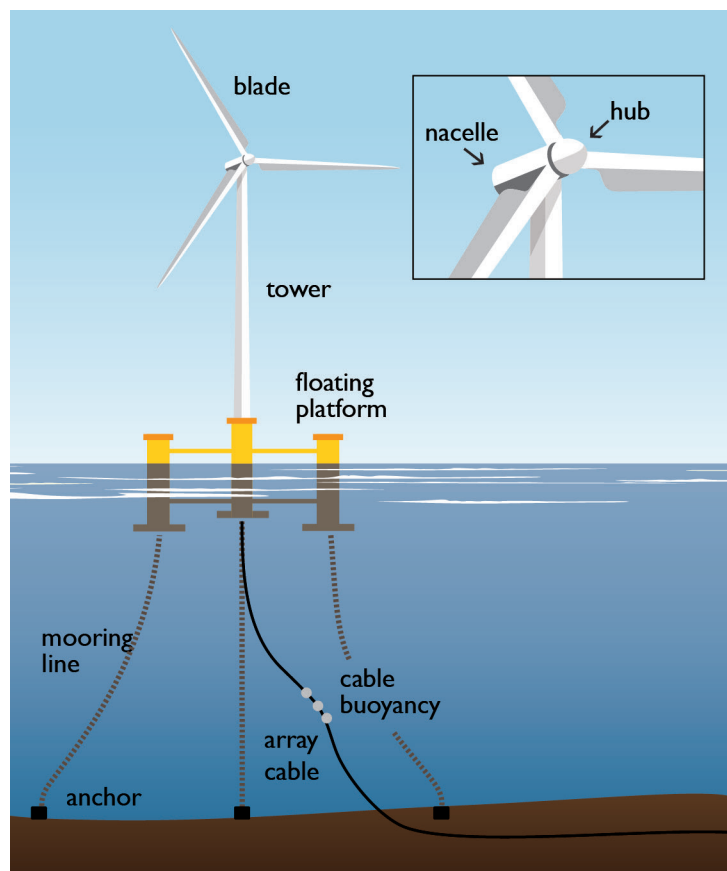
## Wind Turbine Subsystem

The wind turbine rotor blades, hub, and nacelle (which houses the generators, converters, transformers, controllers, and potentially gearboxes) harness ocean winds to create lift on the blades. This lift creates the forces necessary for rotation of the hub to drive the generator within the nacelle and create electrical power. Although land-based and offshore wind turbines are substantially similar, offshore blades, hubs, and nacelles are significantly larger than those on land.

The comparatively large size of offshore rotor blades is driven by higher and more consistent wind speeds and lower turbulence and boundary layer effects offshore, the ability to transport larger blades by sea than on land, continuous improvements in the composite materials from which the blades are constructed, and the ability to increase the capacity factor (a metric that indicates the efficiency of the system) and reduce overall costs of energy by maximizing the energy produced at each turbine. Major offshore wind turbine components are manufactured by international companies such as Vestas, Siemens Gamesa, and General Electric. The diameter of a Vestus 15 MW offshore wind turbine, which is often cited as a potential system for Oregon, is 236 m (774 ft.). This diameter results in a rotor swept area (the area enclosed by rotation of the rotor blades) of 44,000 m$^2$ (430,556 ft.$^2$). Each blade of the turbine is more than 100 m (328 ft.) long and the hub is about 150 m (492 ft.) above sea level (Vestas 2024).



**Figure 4.** Components of a floating offshore wind system. Graphic by Allison Walkingshaw.

The blade, hub, and nacelle subsystems are actively controlled to improve power production within a load envelope that is consistent with the operational and service plans for the FOSW array. Based on wind direction and speed sensor input, the turbine controller activates motors that drive yaw rings to enable constant positioning of the rotor to receive the desired amount of wind energy for power conversion while maintaining acceptable structural loads through the blades, hub, drivetrain, and tower. When the rotor is yawed into the prevailing wind, the turbine controller pitches blades into and out of the wind through hydraulic actuation and large pitch bearings.

A master power plant controller communicates with the turbine controllers to guide the array's active and reactive power output, maintain performance through grid disturbances, and potentially establish grid voltage and frequency. Siemens generators use direct drive technology, which does

not require a gearbox, and thereby avoids the associated losses and maintenance, but requires a heavy and costly low-speed generator. In contrast, current Vestas and General Electric generators include gearboxes that translate the low rotational speed of the rotor into the higher rotational speeds needed for a much smaller, high-speed electrical generator. Permanent magnet generators coupled with four-quadrant electrical converters enable the machines to match electrical output to characteristics at the plant substation with the point of connection to the main electrical grid (detailed below). Transformers in the nacelle or tower convert low voltage power at the generator (typically less than 1 kilovolt) to the medium voltage of the collector system.

Towers are composed of cylindrical, rolled-steel cone sections that are bolted together with internal flanges. Although base sections may have large diameters and therefore are difficult to ship by land, the modular nature of tower subcomponents simplifies the shipping of components to port. Tower sections can be manufactured to precise standards of original equipment manufacturers by a greater number of suppliers and in more locations around the world than other turbine components. Original equipment manufacturers commonly leverage this greater diversity in the supply chain to save costs on a given project.

**Floating Platforms**

FOSW facilities along the U.S. West Coast will be constructed in deeper waters than conventional fixed-bottom offshore wind arrays along the U.S. East Coast and in Europe. Wind turbines in water depths up to 60 m (200 ft.) typically have fixed foundations. In contrast, wind turbines on the West Coast will be in waters with depths of about 600–1300 m (1970–4265 ft.), necessitating the use of floating platforms and robust mooring systems to maintain the turbines' position while operating. The floating platform provides a stable foundation or virtual ground onto which the turbine tower is mounted. The tower must be structurally sufficient to bear the dynamic motion and weight of the nacelle, blades, and hub; resilient to vibrations and oscillatory flow from system operation; and lightweight enough to maintain hydrodynamic stability of the entire floating platform.

A wide variety of floating platforms has been developed, with many more concepts in development at lower technology readiness levels. The fundamental objectives of the platform are to float the weight of the tower, blades, hub, and nacelle; maintain hydrodynamic stability in variable sea states; and allow for efficient and robust turbine aerodynamics by keeping the platform stable in all six degrees of freedom. The most common platform designs are the tension leg platform, semi-submersible, and spar buoy (Figure 3).

A tension leg platform is a vertically moored system: mooring lines extend vertically downward from the platform to the sea floor. The platform's excess buoyancy is counteracted by the mooring lines to maintain the platform's position below the surface. As discussed below, the need to counteract the excess buoyancy and associated forces can create significant design constraints for the mooring and anchoring system. The tension leg platform system is stable in heave (upward and downward) and rotational motion (pitch and roll), yet often requires bespoke mooring and anchor systems. The semi-submersible system generally features three or four shallow draft columns that are connected by a lattice or similar structure to maintain the relative position and structural integrity of the column locations. In most cases, each column has a large, flat heave plate on its lower (deeper) end. The heave plate creates additional hydrodynamic damping and viscous drag to help stabilize the platform. Additionally, many semi-submersible platforms have active ballasting systems and can pump water between columns to maintain stability under different wind and wave conditions.

Semi-submersible platforms are relatively stable in isolation from their mooring system, but the area between construction ports and offshore turbines must be deep and wide. The Principle Power WindFloat design, described below, is an illustrative example of a semi-submersible platform.

The spar buoy is a simple structure. Its one major cylindrical spar is stabilized by ballasting the hollow core with water or other weight. However, construction of that cylinder requires deep port and navigation channels. For example, the spar buoys for the 6 MW turbines installed at Hywind Scotland penetrate about 80 m (262 ft.) below the surface (Equinor n.d. b). Spar buoys are generally towed to the project location in a position parallel to the water surface and then ballasted until the platform becomes vertically oriented. This process eliminates the opportunity to install turbines, blades, and nacelles in ports with shallow or medium water depths.

## Anchors and Mooring Lines

Moving downward through the floating offshore wind system, the next subsystems are the mooring and anchoring subsystems. Each platform is anchored to the sea floor by mooring lines, and platforms are connected by electric power cables suspended in the water column.

The mooring and anchoring systems' objective is to keep the floating platform in a specific location or, in the case of a tension leg platform system, to provide a reaction force to the excess buoyancy. A wide range of mooring and anchoring systems are possible, and selection depends heavily on the platform, operational water depths, meteorological and physical oceanographic conditions, and seafloor and sediment composition. Mooring lines are generally composed of synthetic lines, sections of chain, and mid-water column or surface floats that have high strength-to-weight ratios.

The seafloor and sedimentary conditions strongly affect what anchors are feasible. Most anchors can be classified as embedment, suction, gravity, or pile systems. If the sediment allows embedment, or penetration, then a drag embedment, micro-pile, or suction bucket anchor may be effective. For example, to create a suction bucket anchor, giant upside-down steel buckets are sunk directly onto the seabed. A suction pump then removes the water and air from inside the bucket, which creates negative pressure inside the bucket and drives the foundation down into the seabed. If the seafloor sediment is much firmer (more consolidated), then gravity foundations or pile anchors might be more appropriate. The massive weight of gravity anchors provides a reaction mass or force for the mooring systems, whereas pile anchors are drilled into the seafloor and create a rigid connection between the seafloor and the mooring system.

*Balance of Plant and Electrical Transmission*

Travis Douville

Balance of plant generally refers to all the other, mainly electrical, components of the floating offshore wind (FOSW) system, including the collector system, substations, and export cables (Figure 5). Numerous technological components in addition to the individual turbine, platform, and moorings systems are required to complete the power plant and are critical to its operation. After alternating current (AC) power is transformed to medium voltage in the nacelle or tower, it is transmitted on a collector system of AC electrical cables typically rated between 66 and 132 kV. These cables usually run from one turbine to another three to five turbines on an electrical feeder line before they connect to the plant substation. On the shore-side of the substation connection, the design of these balance of plant systems is classified as high voltage alternating current (HVAC) or high voltage direct current (HVDC).

Most land-based wind energy projects use HVAC substations and overhead cables to their points of interconnection to the bulk utility electricity system. However, some FOSW systems are sufficiently far from points of interconnection that they require more-efficient HVDC transmission. Although HVDC cables are more expensive than HVAC cables per unit length, they lose less electricity and avoid the need for reactive power compensation equipment. For these reasons, there is a break-even distance between HVAC and HVDC cable costs. A comparison of the costs of offshore
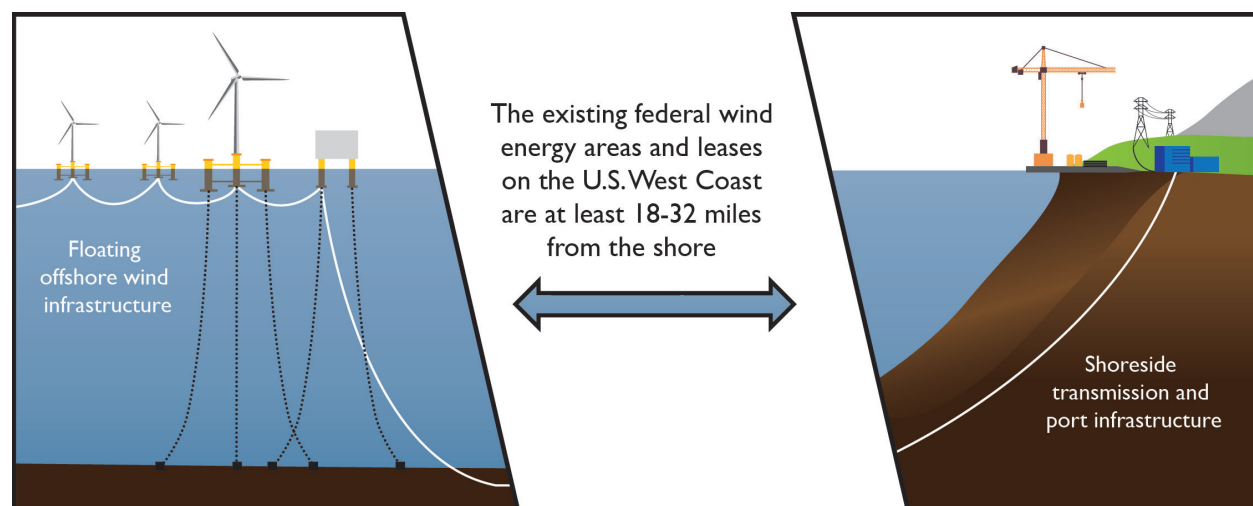


**Figure 5.** Floating offshore wind energy infrastructure, balance of plant, and electrical transmission systems. The closest point of the wind energy and lease areas established by the Bureau of Ocean Energy Management on the West Coast range from 29–51 km (18–32 mi.) offshore. Graphic by Allison Walkinshaw. Accurately scaled visual simulations of the coastal viewshed under a range of meteorological conditions, with and without hypothetical offshore wind arrays, from six key observation points in Oregon are available at www.boem.gov/renewable-energy/state-activities/oregon-offshore-wind-visual-simulation.

transmission technologies suggested that beyond 100 km (62 mi.), the costs of HVDC are lower than those of HVAC (Beiter et al. 2016). Another analysis indicated that beyond 186 km (116 mi.), the cost of 320 kV HVDC fell below that of 220 kV HVAC (Larsson 2021). As plant size increases, HVDC may be cheaper even at shorter distances (DNV 2022).

The collector system cables of HVAC systems terminate in an offshore AC substation near the turbines (Figure 6). On the west coast of the United States, these substations must float given the water depths in the vicinity of the lease areas and high-quality winds (Figures 3, 5). In the AC substations, voltage again is increased to that of the export cable, which is rated for long-distance transmission (export cables are currently expected to be rated at 230 kV or 400 kV). The export cable connects to land under the beach and terminates in an onshore AC substation. Onshore, the voltage again may be adjusted to meet the needs of the onshore grid (transmission system). HVAC transmission over land, whether above-ground or underground, links the onshore AC substation to the point of interconnection with the transmission system, which is approved on a project-by-project basis by the grid system operator.

Four types of floating substations, semi-submersible, spar, tension leg platform, and barge, are under development for FOSW. The turbine platforms and mooring and anchoring systems of these substations are similar to those of offshore wind turbines. A key difference between turbine and substation platforms is the weight that must be supported. The components of the substation that are above the water's surface can be 2000–4500 metric tons (MT) heavier than the wind turbines.
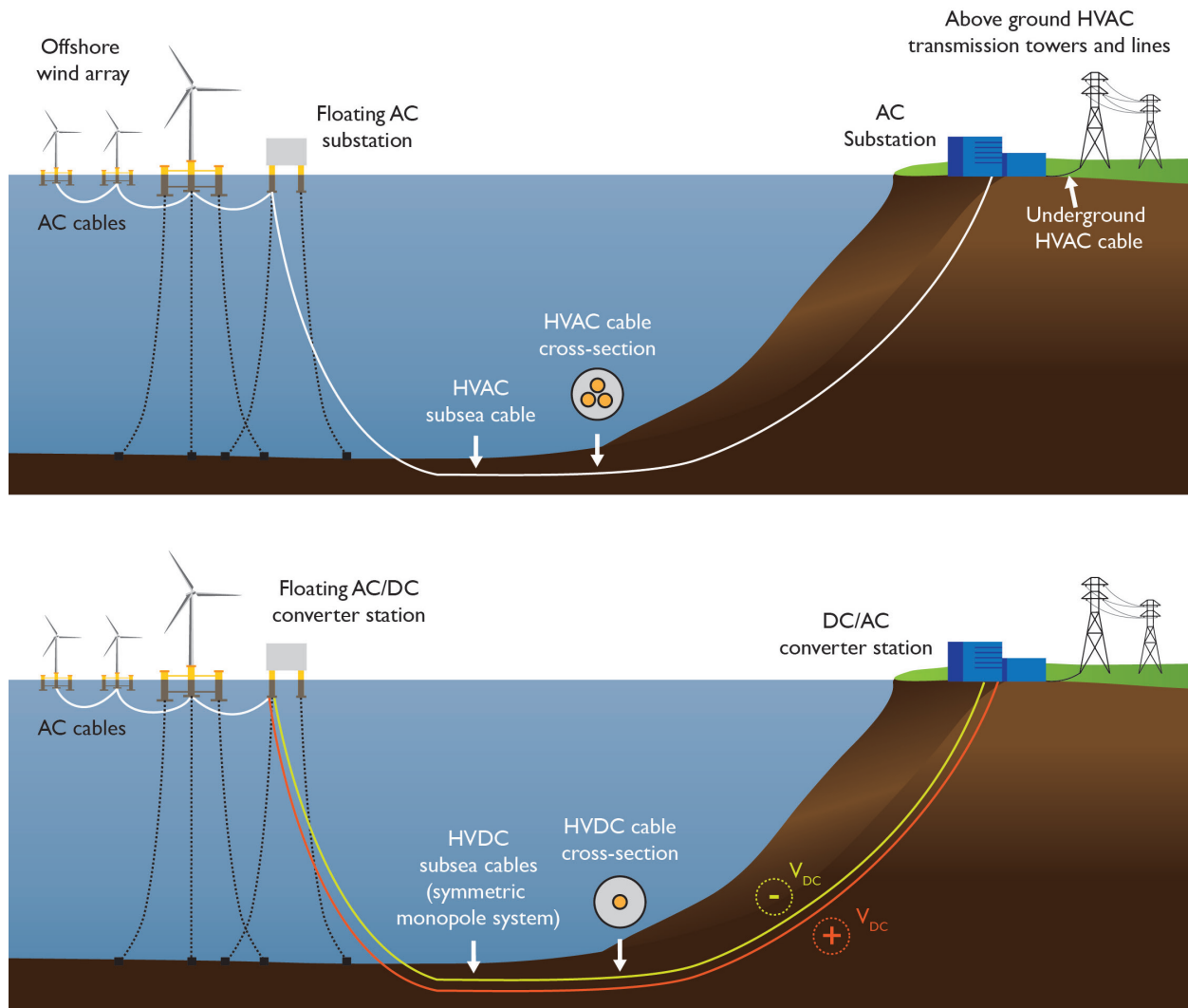
**Figure 6.** High voltage alternating current (HVAC) (top) and direct current (HVDC) (bottom) subsea transmission systems depicted from the floating offshore wind array to the point of interconnection with the land-based grid transmission system. HVAC subsea cables carry three-phase AC power via a tri-core of conductors (see Figure 7) and are more economical for shorter transmission distances (see text). HVDC subsea cable systems can have different configurations (asymmetric monopole, symmetric monopole [shown in figure], or bipole) and use single core subsea cables to carry direct current (see Figure 7). HVDC subsea cables are more cost effective over longer transmission distances.

The above-water components also have lower centers of gravity, which affects their stability and could require platform and mooring designs different than those of floating turbines. Additionally, the substation platforms must accommodate multiple subsea cable connections and the motion between cables and the platform (DNV 2022).

Borrowing from decades of work in the oil and gas industry, floating AC substation designs are under development by major vendors such as Hitachi, General Electric, and BW Ideol (Huang et al. 2023, Buljan 2024, GE Vernova 2024). The following three designs have been publicized, and others are underway. Ideol and Atlantique Offshore Energy's Damping Pool design traps sea water within an inner ring to dampen dynamic movements of the substation. The design is modular (in 200–300 MW segments) and can scale to 1000 MW (Richard 2019). Semco Maritime, ISC Consulting Engineers, and Technip Energies have introduced a three-column design with 400 MW capacity that

weighs 6,500-7,500 tons (Semco Maritime 2022, Huang et al. 2023). Siaipem and Siemens Energy plan a 500 MW floating substation with a semisubmersible structure (Chadderdon 2022).

The HVAC export cables that leave the floating substation are typically three-core extruded cross-linked polyethylene (XLPE) and qualified up to 400 kV (Figure 7). However, current commercially available cables do not bend or move as would be necessary for FOSW arrays. The depth of the water along the West Coast necessitates vertical cables that run from the floating platforms through the water column to the seafloor. These vertical sections of cable, like the mooring cables, will move as the floating turbine moves. Design and testing to accommodate these movements has not yet been completed at the 230 kV or 400 kV rating.
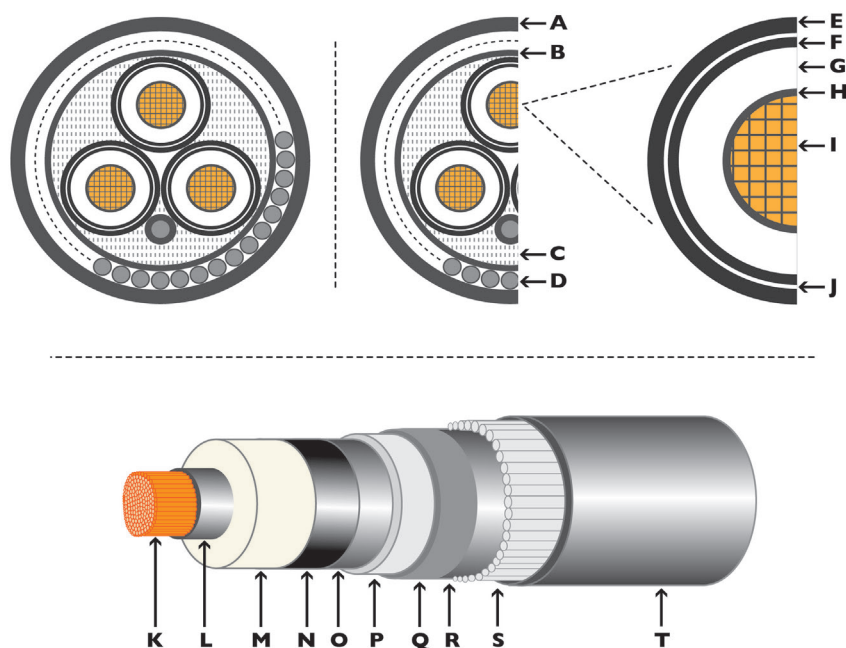


**Figure 7.** High voltage alternating current (HVAC) (top) and direct current (HVDC) (bottom) subsea cables. Subsea cables may also incorporate optical fiber for data transmission. **HVAC cable components:** Polypropylene yarn serving (A) and polypropylene yarn bedding (B) protect the steel armoring that helps prevent against magnetic field losses (D). Polypropylene yarn filler (C) surrounds the three copper conducting cores that carry three-phase HVAC power (I). The spaces between the copper wires within the conducting core are filled with a swellable tape to limit migration of water along the cable and minimize the repair length should the cable become physically damaged on the seafloor. The copper wires are encased in a conductor shield (H), a layer of cross-linked polyethylene (XLPE) insultation (G), an insulation shield (F), a metallic (lead) shield that prevents intrusion of water (J), and an anticorrosion polyethylene shield (E). **HVDC cable components:** The single copper or aluminum conducting core (K) is surrounded by an inner semi-conduction layer (L), XLPE insulation (M), outer semiconducting layer (N), swellable tape (O), and a metallic (lead) sheath (P). These are surrounded by a polypropylene inner sheath (Q). The outermost sheath of polypropylene yarn (T) and the polypropylene bedding (R) protects the armoring layer (S). Graphic by Allison Walkingshaw, adapted from Sumitomo Electric (global-sei.com/power-cable-business/products/submarinecable/) (HVAC) and Anatolia Technologies (anatoliacom.com/extruded-dc-up-to-525-kv) (HVDC).

Like most fixed-bottom offshore wind arrays, FOSW uses HVAC transmission. However, HVDC designs for offshore wind plants soon will be operational. The first such project in the United States, Sunrise Wind (924 MW, fixed-bottom, with a 161 km [100 mi.] HVDC export cable into Long Island), is projected to be operational in 2025 (Sunrise Wind 2021). Tennet, a German transmission system operator, is planning projects with a modular 2 GW HVDC design (Tennet n.d.). On the West Coast, initial electrical transmission connections, particularly those closer to coastal points of FOSW interconnection, such as the Morro Bay leases, are expected to proceed with HVAC cables. However, HVDC systems may be necessary to reach more remote FOSW arrays off the Oregon and California coasts in the 2030s.

For interconnections exceeding one GW or export cables longer than about 161 km (100 mi.), HVDC technology is often

# Case Study: Principle Power Semi-submersible Platform

Bradley Ling

Principle Power's WindFloat® semi-submersible floating foundation has a track record of pre-commercial deployments in Europe. Nine WindFloat units have been deployed in Portugal and Scotland with wind turbine generators up to 9.5 MW, and three more are under construction in France. The WindFloat is designed to be compatible with any commercial wind turbine generator.

The WindFloat is a triangular, semi-submersible, column-stabilized offshore platform that uses water plane stiffness to counteract large, wind-induced overturning moments. Damping heave plates at the bottom of each column provide additional hydrodynamic inertia by increasing the volume of displaced water and adding viscous damping to the system in roll, pitch, and heave motions. The platform also includes a closed-loop hull trim, or ballasting, system that moves water ballast among the three columns to counteract variable thrust loads on the blades, hub, and nacelle that result from changes in the average wind speed and direction and to minimize loads and optimize power production. The WindFloat is in its fourth generation and is fully modular to enable different execution plans.

The WindFloat has two variants, both steel semi-submersibles (Figure 8). The WindFloat T has columns suitable for tubular construction. The WindFloat F has columns and pontoons suitable for flat panel construction.
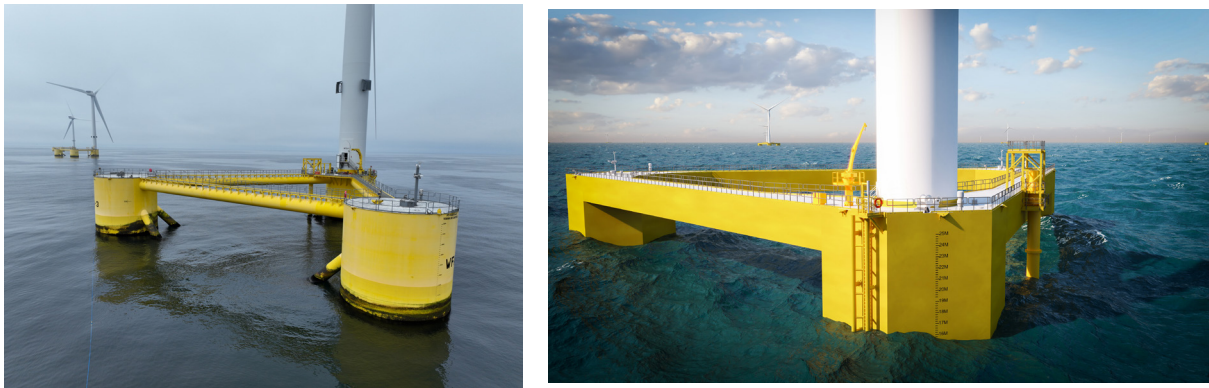


**Figure 8.** WindFloat T (left) and WindFloat F (right) offshore platforms. Photograph of the WindFloat Atlantic project courtesy of Principle Power and Ocean Winds.

With two variants, the platform can be tailored to local supply chain capabilities and project constraints. For example, the tubular design may be preferable in the U.S. Gulf of Mexico due to the local supply chain's ability to fabricate tubular structures similar to jackets used in the oil and gas sector. The tubular design also may be better suited to water depths greater than 11–13 m (36–43 ft.). Due to the relatively low effort required for its final assembly, this variant also may be more favorable for projects where components are fabricated at different locations and the platform is fabricated at a relatively small site.

Alternatively, for the U.S. West Coast, the flat panel design may be less expensive for new, purpose-built facilities capable of automated, indoor manufacturing of large, stiffened panel components. The flat panel design may be preferable for sites with more restrictive draft constraints (<8–10 m [26–33 ft.]) at the quay (loading platform) where the wind turbine and tower are integrated with the floating foundation. This variant may also be less expensive when fabrication is centralized at a shipyard or other large site with permanent equipment and a stable workforce that can run the final assembly process.

The WindFloat principal dimensions (column diameter, column spacing, and column height) are adjusted to meet specific project meteorological and oceanographic conditions and generator and logistical constraints. Platforms have been deployed around the world in meteorological and oceanographic conditions similar to those off the Oregon coast.

Mooring systems for the WindFloat vary across project sites. The relatively deep water in the proposed Oregon lease areas (>200 m [656 ft.]) would likely require a semi-taut or taut mooring design in which a long, synthetic rope in the water column is connected to a shorter chain that is attached to the anchor. An anchor that can resist vertical loading, such as a suction pile, probably would be most suitable, although the final selection of anchor type will depend on the seabed sediment type and other geological attributes.

Depending on how the wind turbine is integrated and how the platform is fabricated for a specific project, the generator, hub, blades, and tower can be integrated with the floating foundation at the location of the

platform's final assembly and launch or at a separate location (Figure 9). Integration should occur as close to the project site as possible to minimize weather-related risks and delays in platform assembly. The integration operation has the most demanding port infrastructure requirements. Methods of integrating the wind turbine components and platform include use of a shore-based crane, a crane and temporary buoyancy aids to reduce platform draft, a crane with the platform grounded to integrate the generator on the platform while it floats alongside quay, or a jack-up vessel equipped with a crane either alongside quay or in a sheltered environment (Figure 9). Once fully integrated, the system is towed to the project site, where it is attached to the mooring lines and inter-array electrical connection cable.



**Figure 9.** Integration of wind turbine components with a crane (tower [left], nacelle [middle], and blade [right]). Photograph of the WindFloat Atlantic project courtesy of Principle Power and Ocean Winds.

advantageous. After the AC power is collected at the plant, it is sent through HVAC to HVDC converter stations (Figure 6). These stations also must float. From the stations, HVDC export cables carry power at high voltages, typically 320–525 kV, to the landing point. The export cable terminates in an onshore HVDC converter station, where the power is prepared for connection to the bulk energy system at the point of interconnection to the transmission system. The interconnection has been approved by the transmission system operator.

Voltage source converters, a relatively new technology that allows full directional flow and control of power quality (voltage and frequency signals), connection of high-capacity power flows to weak grids, and the ability to establish grids after a disruption, commonly are used to convert AC power to DC or vice versa. These converters are well suited to the multiple-terminal direct current systems that are likely to emerge in the future. HVDC export cables are designed for asymmetric monopole, symmetric monopole (Figure 6), or bipole systems. They usually are single core conductors with extruded XPLE, mass-impregnated paper, or paper-polypropylene laminated insulators (Figure 7). XPLE insulators are less susceptible to leakage than the two latter types of insulators, and therefore are the most common for offshore applications.

At 320 kV and when arranged in a symmetric monopole configuration, HVDC subsea cables can transmit 1300 MW of power. At 525 kV and when arranged in a bipole configuration, they can transmit 2000 MW of power. Unlike AC lines, DC lines do not have a theoretical power transmission length limit. However, technology risks are associated with DC transmission, including an unstable supply chain and limited supply of DC circuit breakers. The DC circuit breakers will be necessary to isolate faults in the case of networked transmission.

The four major types of FOSW systems are undergoing rapid and global innovation and development. Floating offshore wind arrays have not yet been built in the United States, but are in early planning phases in California and the Gulf of Maine. Commercial projects (those with a minimum capacity of 50 MW) are under development in South Korea (Ocean Winds n.d.) and France (Offshore 2024). Development is based heavily on the experience of the offshore oil and gas industry in deep water and from European and East Coast deployments of fixed bottom offshore wind systems. Building floating offshore wind on the West Coast will require adapting the experience from other regions and industries to the demanding wave and depth conditions of the coastal Pacific Ocean. As early FOSW projects mature, information about their system performance and manufacturability can be used to design projects and build a West Coast supply chain.

*Offshore Wind Port Requirements*

Aubryn Cooperman

Ports and vessels enable the transportation of equipment, materials, and people to and from an offshore wind site or among suppliers, and allow for the construction of floating offshore wind (FOSW) systems. Different vessels, port sites, and port types can support offshore wind projects. Vessels used to deploy offshore infrastructure and transportation of components, parts, and people must comply with the Jones Act (Merchant Marine Act of 1920 [Section 27]). Within the United States, there are few Jones Act-compliant options for vessels that can support FOSW in Oregon.

Ports can be classified as staging and integration, manufacturing, or operations and maintenance. At staging and integration ports, the largest ports, all wind turbine components are integrated with floating platforms before being towed to an offshore site (Figure 10). Staging and integration ports are primarily used during the installation phase of a project but may also serve as a base for heavy maintenance after a wind array becomes operational. The size

| Port location | Capabilities | | | Notes |
|---|---|---|---|---|
| | S&I | MF | O&M | |
| Hammond Boat Basin | | | X | U.S. Army Corps of Engineers maintains channel. Not much space available. |
| Warrenton | | X | X | Water depth can accommodate barges |
| Astoria | | | X | Not much land available. Adequate water depth for operations and maintenance vessels. |
| Wauna | | | | Currently in use, no land available |
| Port of Columbia County | | X | | Industrial land, deep-draft access, multiple sites |
| Port of Portland | | X | | Multiple sites |
| Nehalem | | | | No maintained channel |
| Tillamook Bay at Garibaldi | | | X | 4.5 m (18 ft.) deep, crew transfer vessel only for operations and maintenance, not as close to wind energy areas |
| Depoe Bay | | | | Entrance channel not adequate for operations and maintenance |
| Yaquina River/ Toledo/Newport | | X | X | U.S. Army Corps of Engineers maintains channel. A maximum of 16 ha (40 acres) may be available. |
| Waldport | | | | No maintained channel |
| Siuslaw River at Florence | | | | No land available |
| Umpqua River at Reedsport | | X | X | Shallow water depth in channel |
| Coos Bay | X | X | X | Best option, but airport and dredging create challenges |
| Bandon | | | X | Coquille River depth is 4 m (13 ft.). Crew transfer vehicle only for operations and maintenance site. |
| Port Orford | | | | No protected harbor |
| Rogue River (Gold Beach) | | | X | Crew transfer vessel only due to channel depth |
| Brookings Harbor at Chetco | | | X | Crew transfer vessel only due to channel depth |

**Table 3.** Oregon port capabilities for offshore wind. Green, yellow, and red indicate good, moderate, and unlikely candidate sites, respectively. S&I, staging and integration; MF, manufacturing and fabrication; O&M = operations and maintenance. Adapted from Shields et al. 2023.

**Figure 10.** Floating offshore wind turbines at assembly ports. Top: Floating wind turbine (9.5 MW) for Scotland's Kincardine Offshore Wind project at a port in The Netherlands. Bottom: Floating platform for an 8.4 MW Floating wind turbine for Portugal's WindFloat Atlantic project along a quay in Spain (for scale, note the figure in red coveralls at the top right side of the floating platform). Photographs courtesy of Principle Power.

and weight of the offshore wind components staged at these ports lead to demanding specifications for facilities (Porter and Phillips 2016, Trowbridge et al. 2022, Lim and Trowbridge 2023, Shields et al. 2023). Requirements include high bearing-capacity wharves long enough to accommodate FOSW platforms and vessels transporting large components; space for component storage, including mid- to high bearing capacity upland areas and sheltered harbor areas for wet storage of floating components; heavy-lift cranes and load-handling equipment such as self-propelled modular transporters (as noted in the Principle Power case study); navigation channels and berths with sufficient depth and width for FOSW systems and large vessels (a key challenge in Oregon); and at least 305 m (1000 ft.) of clearance above navigation channels to allow passage of fully integrated floating wind systems.

Manufacturing or fabrication ports host factories and facilities for assembly of major offshore wind energy components and subsystems. Many of these components are too large for transportation over land, so they must be manufactured at a port with access to a navigable waterway. There may be more flexibility in the requirements for manufacturing ports than for staging and integration ports. For example, manufacturing ports can be located farther from offshore wind installations and, depending on the type of component (e.g., blades, nacelles, towers) they produce, may not require a channel depth, width, or air clearance as great as that needed for a fully assembled floating wind system.

Operations and maintenance ports serve offshore wind arrays throughout their operational life. Typical onshore facilities include offices for operational monitoring and management, space for vessel provisions, warehouses for storage of spare parts, and workshops for repairing small components. Berth requirements depend on the type of vessels used for day-to-day maintenance of the wind array. Crew transfer vessels are typically used when travel time to the operations and maintenance port is within two hours, allowing for daily return to port (ACP 2023). Service

operations vessels, which are likely to be used for larger or more distant wind arrays, require larger berths and a deeper channel than crew transfer vessels.

Existing ports on the U.S. West Coast could serve as each type of FOSW port (Shields et al. 2023; Table 3). The Port of Coos Bay, which has engaged in initial scoping activities related to offshore wind (Trowbridge et al. 2022), is the only good candidate for staging and integration. Several ports along the Columbia River and the Pacific coast are potential candidates for manufacturing and fabrication. A greater number of ports can support operations and maintenance, although several would be limited to crew transfer vessels rather than the larger service operations vessels.

## Floating Offshore Wind Infrastructure and the Environment

### *State of the Science*

#### Andrea Copping and Hayley Farr

Understanding of the potential environmental effects of floating offshore wind (FOSW) energy is limited. Research and monitoring at Hywind Scotland and Kincardine (Scotland), Hywind Tampen (Norway), Principle Power Windfloat Atlantic (Portugal), and smaller demonstration projects are just beginning to build the evidence base. However, data from coastal development, land-based wind, fixed offshore wind, wave and tidal energy, and other industries provide some insights into FOSW's potential environmental effects, monitoring priorities, and strategies for mitigating undesirable effects (Copping and Hemery 2020, Farr et al. 2021, Maxwell et al. 2022, Rezaei et al. 2023).

The potential environmental effects of FOSW, like those of other offshore renewables, can be examined with a stressor-receptor framework (Boehlert and Gill 2015). Stressors are the parts of a FOSW array (e.g., turbines, cables) or its lifecycle (e.g., operational sound, vessel traffic) that may cause harm or stress to receptors, such as marine animals, their habitats, and ecological processes. Diverse potential stressor-receptor interactions, or risks, are associated with offshore wind energy's siting, construction, operations and maintenance, and decommissioning (SEER 2022). Below we summarize some of the common concerns and key risks.

**Ecosystem Dynamics.** Like many offshore industries, FOSW development can change coastal, benthic, and pelagic ecosystems. For example, the installation of anchors, cables, and scour protection can disturb or alter benthic systems. However, these effects are often localized and may be temporary. Throughout their lifecycle, floating offshore wind turbine substructures, moorings, and anchors may act as artificial reefs, potentially increasing the species richness and abundance of some marine fishes and other taxonomic groups while increasing the size or quality of foraging and sheltering areas for others (Hemery 2020, SEER 2022; see *Effects on Fishes*, this chapter). There is some concern that the development of large FOSW arrays affects ocean dynamics, such as coastal upwelling, by reducing wind energy at the surface (Raghukumar et al. 2023; see *Wind-driven Upwelling*, this chapter).

**Underwater Sound.** Underwater sound is generated throughout the lifecycle of a floating offshore wind array. Construction sound associated with vessel traffic, mooring and anchor installation, and cable burial is localized and temporary, but may disrupt some communication, navigation, or other uses of acoustic signals by marine mammals or fishes (SEER 2022). During operations, sound and vibrations from FOSW turbines are transmitted via the turbine, substructure, and moorings. Acoustic data from Hywind Scotland and Kincardine suggest that operational sound from floating wind turbines is similar to sound from fixed-bottom wind turbines, which does not typically exceed

background sound levels and is considered to be a low risk (Burns et al. 2022, Risch et al. 2023) (see *Underwater Sound*, this chapter).

**Entanglement and Collisions with Vessels.** Although accidental entanglement in fishing gear is a major threat to marine animals, the likelihood of entanglement with FOSW moorings and cables is extremely low (Benjamins et al. 2014, Garavelli 2020, SEER 2022). These structures have large diameters and are spaced far apart; marine animals generally have the sensory capacity to avoid these potential hazards. There is little to no evidence that marine animals might become entangled by debris caught on offshore wind moorings and cables (but see *Secondary Entanglement Hazards*, this chapter). Collision of marine mammals and sea turtles with wind array construction and maintenance vessels is another concern. These risks are generally mitigated by use of onboard protected-species observers, reducing vessel speeds, and route restrictions (SEER 2022).

**Electromagnetic Fields.** Electromagnetic fields are generated around power export cables on the seafloor, inter-array cables draped between floating turbines, and offshore substations that service floating offshore wind platforms. Depending on the amount of power transmitted, electromagnetic fields may affect the behavior of some crustaceans (e.g., crabs, lobsters) and elasmobranchs (e.g., sharks, skates, rays). The effects of anthropogenic electromagnetic fields on marine animals appear to be minor (Gill and Desender 2020, 2023; Hutchison et al. 2020b; SEER 2022) (see *Electromagnetic Fields*, this chapter).

**Effects on Birds and Bats.** Risks of FOSW developments to birds and bats include disturbance from construction activities, displacement from habitat or migration routes, and collision with turbine blades. Depending on the wind array's location, layout, and other characteristics, some bird species may be attracted to or avoid the array. Bat activity may be lower offshore than on land. Animals that are attracted to either land-based or offshore wind turbines may be susceptible to injury or death.

As with all major new technological developments, additional research and monitoring are needed to better understand the likelihood and magnitude of the range of risks from FOSW arrays and potential cumulative effects of FOSW and other human activities.

*Effects on the Physical Environment of the Coastal Ocean*

**Wind-Driven Upwelling**

John A. Barth and Kaustubha Raghukumar

Winds blowing along coastal regions can move seawater up (upwelling) or down (downwelling), which can deliver or remove nutrient-rich water that feeds a rich ecosystem. Wind-driven upwelling is responsible for much of the primary productivity in the California Current, which is one of the world's most productive ocean ecosystems (Figure 11). The California Current extends southward from British Columbia, Canada, to Baja California, Mexico, delivering cool, nutrient-rich waters to the west coast of North America. The extraction of wind energy by an offshore wind array can reduce wind speeds downwind of the array, which in turn can affect local or regional wind-driven upwelling, nutrient delivery, and ecosystem dynamics. Here we review the possible effects of floating offshore wind arrays on coastal upwelling.

Oregon's coastal waters are strongly influenced by southward, upwelling-favorable winds in spring, summer, and early autumn, and by intermittent storms with strong northward winds in late autumn and winter (Huyer 1983). The upwelling season runs from April or May through mid-October.

A typical southward wind event lasts two to five days and reaches about 20 knots (10 m s$^{-1}$) in strength. The force that moves surface waters and results in upwelling is the stress generated by the interaction of the wind with the surface of the sea. Stress is a measure of force tangential to a surface. It is expressed in units of newtons (N) per square meter (m$^2$) of surface area (N m$^{-2}$). A 20 knot (10.3 m s$^{-1}$) wind blowing over the surface of the sea surface generates a stress of 0.18 N m$^{-2}$. This stress moves surface waters offshore in a process called Ekman transport (in this example, the transport is 1.8 m$^2$ s$^{-1}$). The Bakun upwelling index can be related to this quantity by multiplying by one in the form 100 m per 100 m of coastline in the along-coast direction: in this case, 180 m$^3$ s$^{-1}$ per 100-m-coastline. To balance mass, water upwells from below to replace the surface water driven offshore by wind. If this upwelling is distributed over the continental shelf out to, for example, 18 km offshore (9.7 nautical mi.), the deeper water upwells to the surface at a vertical velocity of 0.0001 m per second (1 x 10$^{-4}$ m s$^{-1}$). This is an extremely low vertical velocity that cannot be measured directly with a current meter, but when summed over a day, results in about 8.6 m of upwelling for a 20-knot wind. This upwelling amount can be verified by tracking the depth of standard oceanographic features of water temperature (isotherms), salinity (isohalines) or, most appropriately, density (isopycnals).



**Figure 11.** Schematic of upwelling processes near an eastern ocean boundary. Coastal upwelling occurs in a 10–20 km coastal band and curl-driven upwelling over a larger offshore area (from Raghukumar et al. 2022).

Two- to five-day periods of upwelling winds are separated by weak winds (wind relaxations) or even northward downwelling winds during summer (downwelling-favorable winds force surface water downward). The upwelling supplies nutrients from depths of the ocean without sunlight to the sunlit surface waters, fueling the growth of photosynthetic phytoplankton and a productive food web that includes zooplankton (krill), small fishes (forage fish), larger fishes (e.g., rockfish [*Sebastes* spp.], hake [*Merluccius productus*], salmon [*Salmo* spp. and *Oncorhynchus* spp.]), seabirds, marine mammals, and humans.

The southward, upwelling-favorable winds off the Oregon coast vary from north to south. Off the northern and central Oregon coast, southward summer winds averaged over all upwelling, relaxation, and downwelling events are relatively weak, with an average alongshore wind speed of about 6.4 knots (3.3 m s$^{-1}$; stress of 0.02 N m$^{-2}$). To the south and offshore of Cape Blanco in southern Oregon, both the average and individual wind events increase alongshore wind speeds, reaching average values of 12.8 knots (6.6 m s$^{-1}$; stress of 0.08 N m$^{-2}$) (Samelson et al. 2002). Orographic intensification—a process in which an atmospheric flow near the surface is compressed

by tall mountains and hence accelerates —of the winds near Cape Blanco may be responsible for this variation. Winds of more than 30 knots near Cape Blanco during summer are not uncommon, and generated interest in offshore generation of electricity from wind.

Another form of upwelling, curl-driven upwelling, occurs at the edges of these strong winds off Cape Blanco. Curl-driven upwelling refers to a process in which horizontal differences in wind speed drive horizontal differences in the amount of surface Ekman transport and hence upwelling and downwelling to conserve mass. Curl-driven upwelling here can be of the same magnitude as direct, coastal upwelling farther south in the California Current (Pickett and Paduan 2003), for example near the offshore wind array areas off Humboldt and Morro Bay, California. The wind curl near Cape Blanco contributes to the separation of the southward coastal upwelling jet in this region (Barth et al. 2000, Castelao and Barth 2006), a process that fluxes nutrient- and species-rich coastal waters offshore and south, contributing to the productivity in the northern California Current.

In the region of Heceta Bank off the Oregon coast, where the width of the continental shelf doubles from about 30 km (18.6 mi.) to over 60 km (37.3 mi.), there is another contribution to upwelling that is not directly due to the wind (Barth et al. 2005). A strong (0.5–1 m s$^{-1}$) southward coastal upwelling jet sweeps around the contours of Heceta Bank in a counterclockwise half-circle. This strong curving of the flow introduces a centrifugal force that is balanced by additional upwelling. The additional upwelling makes the waters over Heceta Bank colder, saltier, more nutrient rich, and consequently more productive than the continental shelf waters to the north and south (Barth et al. 2005).

Some have questioned the ramifications for upwelling off Oregon if offshore wind development extracts energy from the southward, upwelling-favorable winds. Models projected that wind speeds will decrease by about 10 percent, or 1 m s$^{-1}$, in a typical 10 m s$^{-1}$ (20 knots) upwelling event given energy extraction by a wind array of about 150–500 turbines, each designed to extract 10 MW of power and spaced 1.8 km (1 nautical mi.) apart (Raghukumar et al. 2023). Such an array would yield 1.5–5 GW of wind energy capacity; the lower end of this range is comparable to the approximately 1 to 2 GW estimates for the Oregon lease areas. The decrease in winds can extend up to 150 km (81 nautical mi.) downwind of the wind energy areas (Raghukumar et al. 2023). Because upwelling is balanced by offshore surface Ekman transport, this 1 m s$^{-1}$ decrease results in a decrease in upwelling speeds of about 1.6 m day$^{-1}$, a reduction of about 18 percent. For a 5 m s$^{-1}$ (10 knot) wind, the corresponding decrease in upwelling speed is 0.4 m day$^{-1}$, again about 18 percent. These simple estimates agree with the model outputs (Raghuhumar et al. 2023).

Research on the potential upwelling effects of floating offshore wind to date has included only models of physical circulation (Raghukumar et al. 2023). These models suggested that the region of reduced wind speeds in the lee of a wind array leads to about a 10 percent reduction in the total amount of coastal upwelling when summed across the wind array region. Furthermore, the wind array induces a curl-driven downwelling on the inshore side of the wind array and equally sized, curl-driven upwelling on the offshore side of the wind array. Evaluation of the effects of modified upwelling circulation on nutrient delivery and lower trophic level responses in the California Current is ongoing. Separately, modeling and observations of the effects of the wind turbine structures on upper-ocean circulation, for example wake effects and mixing, are also needed.

Wind energy extraction by fixed-bottom foundations has been well-studied in the North Sea (Broström 2008, Daewel et al. 2022), and formation of upwelling and downwelling regions in the lee (downwind) of a wind array has been documented (Floeter et al. 2022). However, these results are

not applicable to potential offshore wind arrays on the west coast of the United States because these latter arrays likely will be floating and attached to the sea floor by mooring lines and anchors, not fixed-bottom foundations (steel piles or lattice structures fixed to the sea floor).

Any long-term changes in upwelling due to wind energy extraction will be complicated and potentially difficult to detect. A useful metric for assessing wind-driven upwelling is the sum of the upwelling and downwelling at a particular location over the entire upwelling season, called cumulative upwelling (Barth et al. 2007). The result is effectively the strength of the marine growing season, and is expressed in wind stress days, or N m$^{-2}$ days. As an example, cumulative upwelling off central Oregon, estimated from winds measured at NOAA's Newport, Oregon, Coastal-Marine Automated Network station (NWP03) (Large and Pond 1981), averaged 3.0 wind stress (N m$^{-2}$) days, with annual variability of 1–3 wind stress (N m$^{-2}$) days and a standard deviation of 0.8 wind stress (N m$^{-2}$) day (Barth et al. 2024). The annual variability results from differences in the timing and strength of the atmospheric North Pacific high pressure system and adjacent continental low pressure system. The southward, upwelling-favorable summer wind flows between these two pressure systems (Huyer 1983). The annual variability exceeds the estimated 18 percent decrease in cumulative wind stress (N m$^{-2}$) days due to offshore wind energy extraction, which will complicate detection of any changes in wind-driven upwelling due to offshore wind energy extraction. Long-term studies that are initiated before offshore wind array operations begin and are sustained for multiple years during operations will be necessary to document any such changes.

In the Cape Blanco region and off the southern Oregon coast, the strong, southward, upwelling-favorable winds during summer often exceed 10 m s$^{-1}$, the maximum wind speed for the most efficient extraction of wind energy (Song et al. 2020). Therefore, the approximately ten percent reduction in wind speed due to offshore wind energy extraction can be offset by winds that exceed 11 m s$^{-1}$. Furthermore, wind in excess of 11 m s$^{-1}$ will continue to contribute to wind-driven upwelling and will not be reduced through extraction of energy by turbines.

Any decrease in upwelling due to offshore wind energy extraction also may be offset by an increase in alongshore, upwelling-favorable winds that is projected as climate changes (Bakun 1990). In theory, the difference in temperature between the land and the sea will increase because the ocean will warm less than the adjacent land. The resulting increase in the onshore-offshore atmospheric pressure gradient will result in an increase in southward, upwelling-favorable winds. In some places in the northern California Current, trends in direct wind measurements are consistent with this hypothesis (e.g., García-Reyes and Largier 2010). For example, there is a significant increasing trend in cumulative summer upwelling off Newport (Barth et al. 2024). The number of days on which the maximum temperature at Portland International Airport (Station OR6751, mesonet.agron.iastate.edu) exceeded 90°F increased over the last 25 years at a rate of 0.18±0.06 days per year (Barth et al. 2024). As land temperatures increase, so does the onshore-offshore atmospheric pressure gradient. The cumulative upwelling is also increasing at a rate of 0.03±0.02 N m$^{-2}$ days per year. At these rates, it would take 10–20 years to offset a 10–20 percent reduction by offshore wind energy extraction.

## Underwater Sound

Kaustubha Raghukumar

Underwater sound from offshore wind turbines can occur during all phases of development (construction, operations, and decommissioning), and can encompass both continuous and impulsive sound (Figure 12).
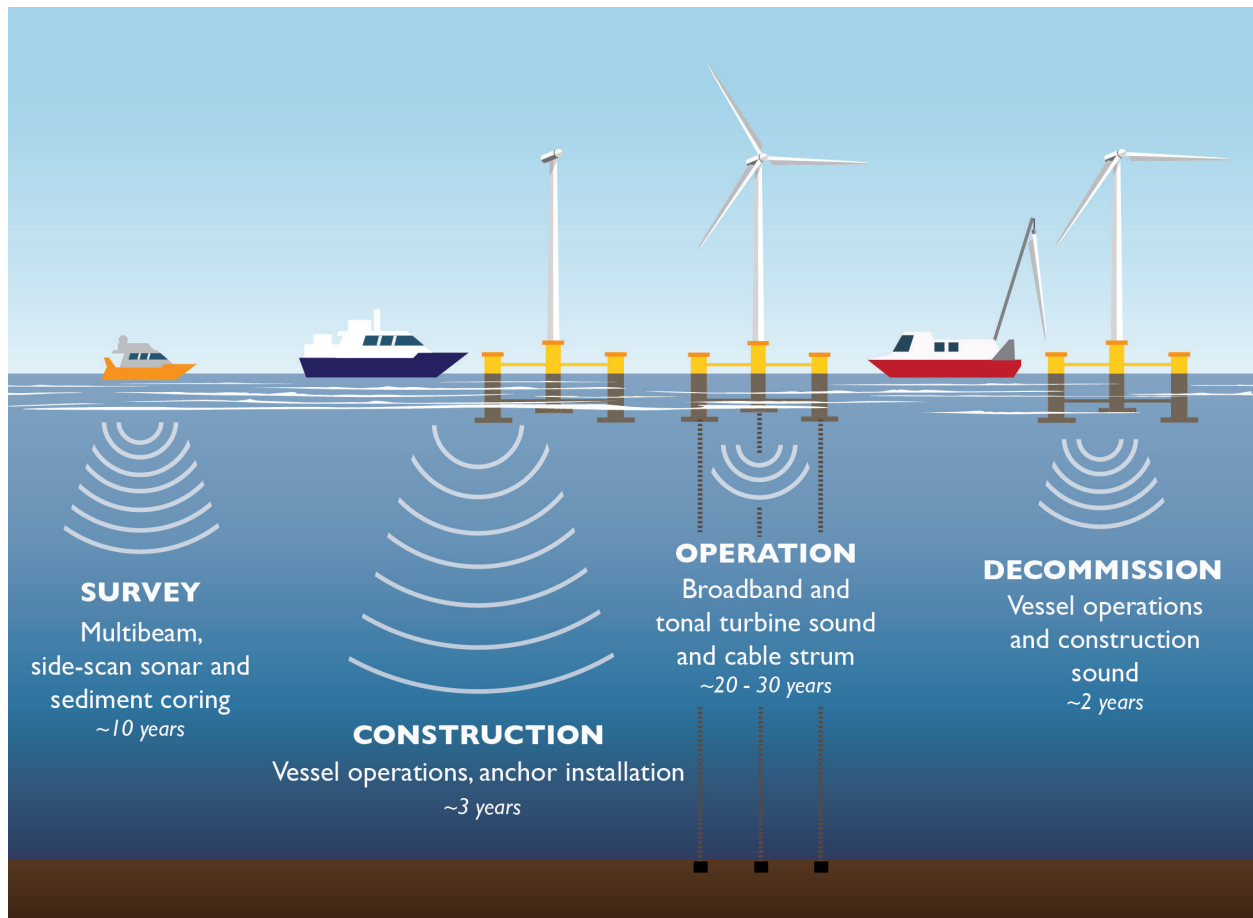
**Figure 12.** Acoustic life of an offshore wind array. Development phases include site surveys, construction, operation, and decommission. Graphic by Allison Walkingshaw, adapted from Mooney et al. 2020.

Underwater sound and its transmission, or acoustics, during offshore wind array construction can be generated by vessel activity in support of construction (continuous sound) and by impulsive or vibratory pile driving during installation of monopiles or jacketed foundations (for fixed-bottom foundations) or anchors for installation of tension leg platforms. Operational sound from offshore wind arrays is typically associated with the vibration of the superstructure (blades, tower, and platform) and resulting radiation of underwater sound. Decommissioning of offshore wind arrays can result in generation of underwater sound by the removal of foundations and vessel activity.

Marine mammals experience sound as pressure; fishes and invertebrates sense particle acceleration associated with the propagation of an acoustic wave, whereas benthic animals can sense seabed vibrations. Although percussive pile-driving in shallow water (fixed foundations) can generate high levels of sound that can cause behavioral responses in marine animals, analogous effects of floating offshore wind installations have not been observed or measured. Pile driving for floating offshore wind platforms will be related to anchor installation for tension leg platforms. However, unlike fixed-bottom foundations, these piles will not span the water column and are more likely to use a deep-water vibratory hammer for installation into the seabed, resulting in lower sound levels than impulsive pile-driving.

Effects of loud, impulsive sound on marine mammals can include temporary and permanent threshold shifts (hearing loss), masking (e.g., interference with communication, navigation, or detection of predators and prey), and behavioral changes (Madsen et al. 2001, Thompson et al.

2010, NMFS 2018, NRC 2003). Radiated sound from impulsive and vibratory pile-driving during installation of fixed bottom wind turbines is the best-understood source of sound from these structures. Some measurements have been made of operational sound from fixed platforms. Underwater sound from floating offshore installations is among the least studied of all sources of sound from offshore operations.

Sound levels associated with floating installations may be lower than those associated with fixed-bottom turbines. Pile-driving of water-column spanning piles will not occur in deep water, and is likely to be limited to installation of anchors for tension lines. Quieter alternative installation methods, such as suction buckets or gravity installations, likely will be mature by the time the first offshore wind arrays on the U.S. West Coast are installed. In suction bucket foundations, giant upside-down steel buckets are sunk directly onto the seabed. A suction pump then removes the water and air from inside the bucket, creating negative pressure inside the bucket and driving the foundation down into the seabed. Gravity foundations are concrete and filled with water and sand, sinking the base so it sits firmly on a layer of gravel that has been prepared on the seabed.

Operational sound from floating offshore wind arrays is likely to be different than that from fixed-bottom foundations. The presence of multiple mooring lines associated with each turbine structure can result in mooring sound via cable strum, which is absent in fixed-bottom turbines. A study of two Scottish wind arrays (Risch et al. 2023) found that, unlike in fixed structures, the occurrence of impulsive mooring-related sound scaled with wind speeds for floating turbine structures. Whether mooring sound levels from U.S. West Coast installations will exceed regulatory thresholds for temporary threshold shifts is uncertain.

The acoustic output from offshore wind arrays can be ameliorated to minimize impacts on marine animals and the surrounding environment. Bubble curtains or sound abatement systems sometimes are employed to reduce the sound generated during the construction phase. Single or double bubble curtains create a wall of rising bubbles around the construction site. The impedance mismatch between the bubbles and surrounding water dampens underwater sound exposure levels by up to 20 dB (Bellmann et al. 2020). Other sound abatement systems include in-pipe acoustic dampening devices or cofferdams (typically limited to shallow water pile installation), which are enclosures built around the pile-driving area that reduce the sound that is transmitted into the surrounding water. It is recognized that depending on the acoustic output, specific deep water acoustic mitigation measures may need to be developed or appropriately adapted from shallow water techniques. Additionally, during construction phases, passive acoustic monitoring or visual monitoring is used to detect marine mammals near construction sites. If mammals are detected, construction activities may be delayed or halted temporarily to avoid causing harm. Construction activities may be scheduled outside of breeding or migratory periods to reduce potential impacts on taxonomic groups such as whales or dolphins. If necessary, operational noise from cable strum could be reduced by use of jacketed cables.

Once operational, offshore wind turbines generate lower levels of sound than during construction. Operational sounds primarily are produced by the rotation of blades and internal machinery, and from cable strum due to the presence of water-column spanning tension lines. Mitigation strategies for operational sound may include designing turbines with quieter gears and bearings and use of jacketed tension lines. Some sound also is expected from decommissioning activities such as vessel activity and anchor removal. This sound could be similar to those generated during the construction phase, but without pile driving.

**Secondary Entanglement Hazards**

Greyson Adams, Erica Escajeda, Arne Jacobson, Sharon Kramer, and Mark Severy

Entanglement in fishing gear and other debris is a well-documented cause of injury and mortality of marine mammals, sea turtles, and other marine animals. Entanglement is characterized as primary, secondary, or tertiary. Direct entanglement with mooring lines and cables associated with marine energy infrastructure, including offshore wind systems, is known as primary entanglement. Secondary entanglement occurs when an animal becomes entangled in floating debris caught on the mooring lines and cables associated with a floating offshore wind (FOSW) system. Tertiary entanglement occurs when an animal that is already entangled in gear or debris becomes ensnared on undersea cables and lines. Because floating offshore wind systems are a relatively new technology with few deployments, the risk of entanglement with floating offshore wind platforms, mooring lines, or anchors is not yet fully understood. No cases of entanglement have been documented in relation to FOSW.

Offshore wind facilities on the U.S. West Coast are expected to operate in deeper waters than conventional fixed-bottom offshore wind arrays along the U.S. East Coast and in Europe. Wind turbines on the U.S. West Coast will be in water with depths ranging from about 550 m (1804 ft.) to 1300 m (4265 ft.) necessitating the use of floating platforms and robust mooring systems to maintain their position while operating. Each wind turbine platform will be anchored to the sea floor by mooring lines, and platforms will be connected to each other by electric power cables suspended in the water column. Although these mooring lines and electrical cables themselves are not expected to create a significant entanglement risk for most species (Benjamins et al. 2014), there is concern that derelict fishing gear and other debris may wrap around the lines and cables, creating a secondary entanglement hazard.

Many types of marine debris can entangle marine life, including lost fishing gear. Modern fishing gear is often made of durable synthetic materials that do not biodegrade (Macfadyen et al. 2009), and therefore can remain a hazard for years after they are lost or discarded. A global analysis of 5,440 documented instances of entanglement in lost fishing gear by marine mammals, sea turtles, sharks, and rays indicated that 55 percent of the entanglements were with fishing nets, 35 percent with monofilament lines, and about 10 percent with lines associated with traps and pots, rope of unknown origin, and other sources (Stelfox et al. 2016).

Some marine animals are more susceptible to entanglement than others. Seventy percent of documented entanglement events affected marine mammals, 27 percent affected sea turtles, and 2 percent affected sharks and rays (Stelfox et al. 2016). Juveniles of all species are at higher risk of entanglement than adults due to their inexperience and curiosity and, in the case of sea turtles, their inability to avoid obstacles (Benjamins et al. 2014, Duncan et al. 2017). Body size, flexibility while swimming, behavior, and ability to detect objects in the water affect the degree of risk (Benjamins et al. 2014). Among marine mammals, baleen whales are considered to be the most susceptible to entanglement due to their foraging and feeding behavior, limited ability to detect obstacles immediately in front of them, and large body size (Benjamins et al. 2014, Maxwell et al. 2022). In contrast, porpoises, dolphins, and toothed whales have smaller body sizes and can use echolocation (reflection of sound waves) to detect objects in their path, which helps them avoid entanglement. That said, toothed whales can still become entangled given that some hazards are difficult to detect,

especially when an animal is distracted (e.g., while foraging; Benjamins et al. 2014). Sea lions and seals may be somewhat more vulnerable to entanglement than toothed whales because of their smaller body size and their interest in unfamiliar objects (Cawthorn 1985, Yoshida and Baba 1985).

Floating offshore wind infrastructure on the U.S. West Coast will create novel vertical structure in deep waters. Mooring lines, electrical cables, floating platforms, and other FOSW system elements are likely to support communities of invertebrates, such as barnacles, mussels, anemones, and corals. These invertebrates will attract fishes, which may then attract marine mammals and other larger-bodied species. If lost fishing gear or other debris becomes entangled in the cables and lines, animals foraging around the infrastructure may be at higher risk of entanglement.

Although no FOSW facilities currently are installed on the U.S. West Coast, research is underway to identify potential strategies for reducing the risk of secondary entanglement. A California Energy Commission-funded study led by researchers at the Schatz Energy Research Center at California State Polytechnic University, Humboldt, working with partners from Pacific Northwest National Laboratory, MARE Group, H. T. Harvey & Associates, and others, is exploring systems for detecting secondary entanglement hazards on offshore wind mooring lines with a combination of vibration sensors and underwater remotely operated vehicles. Early detection would enable removal of the hazards before animals become entangled.

Additional ongoing research, funded by the Bureau of Ocean Energy Management and led by Desray Reeb, is developing a three-dimensional entanglement simulation model to assess entanglement risk for two whale and one sea turtle species on the basis of animal movements, behavior, and types of ocean debris (BOEM 2023). Such assessments can contribute to evaluation of potential risks of different mooring designs and make improvements that minimize hazards to marine life.

## Electromagnetic Fields

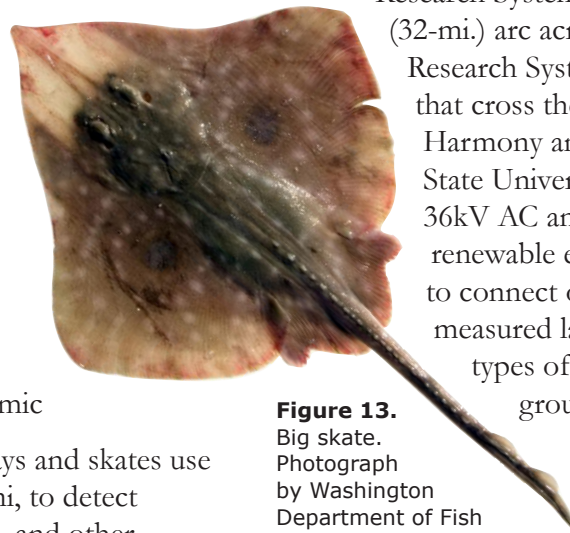Sarah Henkel, Kyle Newton, and Taylor Chapple

Ambient, natural electric and magnetic fields in the ocean come from three sources: Earth's geomagnetic field, electric fields induced by the movement of charged objects (e.g., currents, waves, organisms) through a magnetic field, and bioelectric fields produced by the exchange of ions across the gills and the movements of marine organisms during respiration (Normandeau et al. 2011, Bedore and Kajiura 2013, Gill et al. 2014). Marine organisms that are responsive to electric or magnetic fields include elasmobranchs (sharks, rays, and skates; Figure 13); some bony fishes, such as salmon, tuna, and sturgeon; crustaceans (e.g., crabs, shrimp, lobsters, and barnacles); and sea turtles (Normandeau et al. 2011, Putman 2018).

Offshore renewable installations harness the kinetic energy of offshore wind, waves, tides, or currents and convert the energy into electricity that is transported back to shore through high voltage cables (HVCs). The direct electrical signal from these cables is shielded by cable coatings or conduits and is often further reduced by burying the cable. However, as electricity is conducted through the HVCs, magnetic field artifacts of 0.05–150 µT are emitted radially from the cables. The strength of a magnetic field (or B-field) is measured as the magnetic flux density and is expressed in tesla units (T). At their maximum, the magnitudes of these magnetic fields may be up to three times that of the local geomagnetic field. The emitted magnetic fields induce electric field artifacts as currents, waves, or organisms move through them. The electric field artifacts (1–700 µVm[-1] or

microvolts per meter) can be detected at distances of tens of meters (Gill and Desender 2020). The intensity and characteristics of these fields depend on whether the current is alternating (AC) or direct (DC), the amount of power transmitted, and the cable characteristics. The relative detectability or influence of the emitted magnetic fields and the induced electric fields depends on the local geomagnetic field and other environmental factors.

In the United States, ecological studies have been conducted on the 69 kV cable that connects the San Juan Islands, Washington, to the mainland; the 200 kV DC Trans Bay Cable that runs from the East Bay to under San Francisco Bay; the Acoustic Thermometry of Ocean Climate/ Pioneer Seamount submarine cable (operational 1995–2002) that runs 95 km (59 mi.) from Pioneer Seamount to the Pillar Point Air Force Station in Half Moon Bay, California; the 10 kV DC Monterey Accelerated Research System power and data cable that follows a 52-km (32-mi.) arc across Monterey Bay to the Monterey Accelerated Research System observatory site; and 35 kV AC cables that cross the Santa Barbara Channel to power oil platforms Harmony and Heritage. In Oregon, the cables for Oregon State University's wave energy device test site (PacWave) are 36kV AC and have burial depths up to 1 m. Other offshore renewable energy installations may use DC cables, particularly to connect offshore wind facilities to shore. Below we highlight measured laboratory and field responses to different types of electromagnetic fields (described above) in taxonomic groups relevant to Oregon.



**Figure 13.** Big skate. Photograph by Washington Department of Fish and Wildlife.

**Elasmobranchs.** Sharks, rays and skates use their electroreceptors, or the ampullae of Lorenzini, to detect the bioelectric fields produced by prey, predators, and other individuals of their own species (Murray 1960, Dijkgraaf and Kalmijn 1962). These electroreceptors are best able to detect weak (about 20 nV/cm), low frequency (0.5–10 Hz), sinusoidal (AC) electric fields (reviewed in Newton et al. 2019) with behavioral thresholds at <1 nV/cm (Jordan et al. 2009, 2011). Elasmobranchs may also use their electroreceptors to detect the geomagnetic field as orientation and navigational cues during migration (Kalmijn 1982, Paulin 1995, Anderson et al. 2017, Newton and Kajiura 2017, Keller et al. 2021).

Laboratory experiments demonstrated that spotted catsharks (*Scyliorhinus canicula*), which occur in the northeastern Atlantic Ocean and Mediterranean Sea, were neither attracted to nor avoided electromagnetic fields. However, during DC trials they spent 20 percent less time moving among areas than during AC trials or control conditions, and their swimming speed increased (Hermans et al. 2024). In other laboratory experiments, juvenile thornback rays (*Raja clavata*) and New Zealand carpet sharks (*Cephaloscyllium isabellum*) were attracted to DC but not AC cables (Orr 2016, Albert et al. 2022). Two species native to the U.S. West Coast, big skates (*Beringraja binoculata*) (Figure 13) and longnose skates (*Caliraja rhina*), detected and responded to experimentally altered magnetic field conditions (41.0–54.6 µT constant) and the activation of a cable running either AC (±500 µT max) or DC (500 µT constant), but did not show measurable aversion to the cable. The average swimming velocity of big skates slightly increased during initial AC exposure and decreased during initial DC exposure, but after 10 minutes of electromagnetic field exposure, velocities became similar to those without such exposure. The generally less active longnose skates maintained decreased swimming velocity under both electromagnetic field conditions (Newton et al. unpublished data).

In the field, electroreceptive little skates (*Leucoraja erinacea*) spent significantly more time in the vicinity of HVCs emitting electromagnetic fields than in control areas (Hutchinson et al. 2020a). Within the zone of strong electromagnetic fields, the skates also traveled further and made large turns more often. There was no difference in the skates' average speed or height above the seabed.

**Bony Fishes.** Numerous species of teleosts (bony fishes) have electroreceptive capabilities (Kramer 1996, Bullock 1999). Salmonids and scombrids (e.g., tuna) have a magnetite receptor system and respond to magnetic fields in the 10–12 µT range (Normandeau et al. 2011). Geomagnetic field-based navigation behavior has been documented in salmon species (Putman et al. 2014, Minkoff et al. 2020, Naisbett-Jones et al. 2020).

In the laboratory, magnetic fields had no effects on embryonic or larval mortality, growth, or hatching success of Atlantic halibut (*Hippoglossus hippoglossus*), California flounder (*Paralichthys californicus*), northern pike (*Esox lucius*), or rainbow trout (*Oncorhynchus mykiss*), although magnetic fields shortened the time to hatching in northern pike embryos (Woodruff et al. 2013, Fey et al. 2019, 2020). The direction of swimming by naïve juvenile salmon exposed to magnetic field intensity and inclination angles similar to those at the northern and southern extremes of their

ocean distribution changed, indicating that salmon can detect and respond to both of those environmental attributes (Putman et al. 2014).

Field studies on teleost fishes revealed no evidence that magnetic fields act as permanent barriers to long-distance migrations of Chinook salmon (*Oncorhynchus tshawytscha*), green sturgeon (*Acipenser medirostris*) (Figure 14), or European eel (*Anguilla anguilla*) (Ohman et al. 2007, Westerberg and Lagenfeldt 2008, Wyman et al. 2018, 2023, Klimley et al. 2021). However,



**Figure 14.** Green sturgeon. Photograph by Mike Healy, California Department of Fish and Wildlife.

juvenile Chinook salmon and green sturgeon moved more slowly in an area in San Francisco Bay with an energized DC cable (Wyman et al. 2018, 2023). Similarly, juvenile lake sturgeon (*Acipenser fulvescens*) spent more time near AC cables (Bevelhimer et al. 2013).

**Crustaceans.** Western Atlantic spiny lobster (*Panulirus argus*) sense Earth's magnetic field, which aids in orientation and navigation (Lohmann et al. 1995, Lohmann and Ernst 2014, Boles and Lohman 2003). Some West Coast crab fishermen have suggested that Dungeness crab (*Metacarcinus magister*) are deterred by electrical charges emitted by corrosion of the metals used in crab pots.

In the laboratory, spinycheek crayfish (*Orconectes limosu*) preferred shelter with artificial magnetic fields over those without charge (Tanski 2005). During experimental exposure to relatively large increases in magnetic field strength, from ~0.05 mT background to 1.0–1.2 mT from direct current (DC), Dungeness crabs were slightly more attracted to zones with stronger electromagnetic fields and slightly more active in areas with weaker fields (Woodruff et al. 2013). The physiological and

behavioral response of brown crabs (*Cancer pagurus*) in the United Kingdom to 250 μT was limited, but the crabs clearly were attracted to shelters exposed to 500 and 1000 μT (Scott et al. 2021) and 2.8 mT (Scott et al. 2018), with a significant reduction in time spent roaming. At 500 and 1000 μT, the crabs' circadian rhythm was disrupted. The animals had higher d-Glucose concentrations and total haemocyte (blood cell) count after four or eight hours of exposure than with no exposure, but d-Glucose and blood cell count returned to baseline after 24 hours of exposure to the elevated electromagnetic field. The positions within a tank of Dungeness crab and red rock crab (*Cancer productus*) exposed to geomagnetic field displacement (41.0–54.6 μT constant), AC (±500 μT max), and DC (500 μT constant) changed, indicating that both crab species could detect and respond to the stimuli. Dungeness crabs were more evenly distributed in the tanks in electromagnetic field treatments, whereas red rock crabs appeared to be attracted to cable; DC slowed Dungeness crabs, whereas both AC and DC slowed red rock crabs (Newton et al. unpublished data).

In the field, abundances of crustaceans near the Acoustic Thermometry of Ocean Climate /Pioneer Seamount submarine cable off Half Moon Bay, California, were higher than in control areas (Kogan et al. 2006). Crustacean abundance also increased following installation of the Monterey Accelerated Research System cable (Kuhnz et al. 2015). Abundances of yellow rock (*Metacarcinus anthonyi*) and red rock crabs along an energized cable in the Santa Barbara Channel were higher than along an exposed pipe or in natural habitat, indicating that attraction to the cable was not limited to its structure (Love et al. 2017a, b). Similarly, American lobsters (*Homarus americanus*) spent more time in the vicinity of HVCs emitting electromagnetic fields than in control areas (Hutchison et al. 2020a). Despite these apparently attractive properties of cables, the positions of red rock and Dungeness crabs in arenas placed next to energized (0.046–0.08 mT) or unenergized submarine power cables did not differ (Love et al. 2015). Pursuit of bait by red rock or Dungeness crabs did not change when they had to walk over or away from energized cables (Love et al. 2017a, b; Williams et al. 2023).

**Sea Turtles.** Leatherback (*Dermochelys coriacea*), loggerhead (*Caretta caretta*), and green (*Chelonia mydas*) turtles may be capable of detecting magnetic fields as low as 0.005 to 29 μT (Normandeau et al. 2011) and may use magnetic fields for migration (Putman et al. 2011). However, loggerhead turtles did not differentiate magnetic displacements in laboratory experiments (Fuxjager et al. 2014).

These field and laboratory studies indicate that many marine species respond to electromagnetic fields from underwater cables or magnetic fields applied directly. In some cases, they are attracted to the fields. However, there is no evidence of harm associated with proximity to electromagnetic fields at the wide range of intensities that have been tested. Furthermore, marine species have been documented crossing high voltage subsea cables to continue on migratory pathways and pursue bait. At their present densities, high voltage subsea cables do not appear to hinder migration or feeding of marine species. As increasing numbers of cables are installed for offshore energy projects, migratory species of concern should be monitored for potential impacts due to repeated encounters.

## Effects on Fishes

Scott Heppell and Selina Heppell

Effects of floating offshore wind (FOSW) development on fishes are poorly studied. Therefore, potential effects are largely inferred from studies on fishes' responses to other physical structures in their environment, including offshore oil platforms, fixed wind structures, and artificial reefs. FOSW structures will likely affect fish habitat and will themselves become habitat for some species and their prey, so the location of the site affects biological responses (Maxwell et al. 2022). Transient effects

associated with FOSW installation, including placement of anchors and moorings, and laying and trenching of cables for power to reach shore-based facilities, can have negative impacts on fishes and their habitats through alteration of the physical and biological environment, sound, and pollution. Permanent effects associated with maintenance and operation of an FOSW site include the physical presence of structures, associated changes in oceanographic features and species' habitats, sound, and biofouling mitigation (Miller et al. 2013). Some transient effects could be long-lasting, especially if laying of cables or placement of anchors interacts with Essential Fish Habitat or Habitat Areas of Particular Concern as defined by the Pacific Fishery Management Council (PFMC 2021).

Many fishes are attracted to structures in the ocean; this is the fundamental basis for the placement of fish aggregation devices for fisheries and artificial reefs. Some fishes are attracted to offshore energy structures, including oil platforms (Snodgrass et al. 2020) and fixed wind energy structures (Miller et al. 2013). Depending on the location of the FOSW site, the fishes that are most likely to be attracted to turbine platforms and counterweights are water column (pelagic) species, such as small schooling fishes and their predators, and the pelagic juveniles of fishes that are associated with the ocean floor, such as rockfishes. Anchors and cables may create structure on the seafloor that can be attractive to fishes that are associated with rocks and reefs, including rockfishes and lingcod (*Ophiodon elongatus*) (Figure 15).



**Figure 15.** Lingcod. Photograph from Alaska Department of Fish and Game.

Installation processes, including placement of anchors for the moored device and routing of cables to onshore power transfer locations, may cause both transient and permanent habitat disturbance. Placement of anchors in Essential Fish Habitat or Habitat Areas of Particular Concern will likely affect species that rely on those areas. The Pacific Fishery Management Council warned the Bureau of Ocean Energy Management about these impacts in letters written under the authority of the Magnuson-Stevens Fisheries Conservation and Management Reauthorization Act (Pettinger 2024).

The renewable power from the FOSW arrays must come onshore at some location. This means interactions with nearshore environments that are also potential Essential Fish Habitat or Habitat Areas of Particular Concern and are designated as key habitats in the Oregon Nearshore Strategy (kelp, rocky reef) (ODFW 2016). Scouring of the seafloor by altered hydrodynamic flow and the physical movement of cables laid for power transmission and anchoring has been noted in some installations (Copping et al. 2021). In 2024, the Pacific Fisheries Management Council addressed concerns about transmission line and infrastructure interactions with Essential Fish Habitat and Habitat Areas of Particular Concern in a letter to the U.S. Department of Energy.

Three-dimensional hard structures placed in an otherwise open environment create both the potential for vertical habitat throughout the water column and a potential point of aggregation. Hard structures allow for the settlement of encrusting algae and invertebrates, which in turn attract

mobile invertebrates and fishes. This artificial reef effect can either increase or decrease growth rates of fish populations (Claisse et al. 2014, Fortune et al. 2024). Proximity to natural habitats may affect fish concentrations around the offshore wind structures and anchors, and the animals' natural tendency to aggregate around structures could have negative effects if the site is in an area of poor quality, such as a site in which hypoxia is frequent (Yu et al. 2023). FOSW placement in areas with good circulation and nutrient flow could increase the chances of creating new fish habitat that increases rather than decreases regional population size (Smith et al. 2016, Paxton et al. 2022). Similarly, including fine-grained structure that provides shelter for juvenile fishes could reduce predation and increase the quantity of habitat for some species or life stages of fishes. However, industry mitigation for biofouling (anti-fouling paint, cleaning) could reduce the potentially beneficial growth of algae and invertebrates that provide food and shelter for fishes on the structures. Furthermore, the potential for fishing restrictions near FOSW structures could enhance the role of the structures in increasing population size.

Underwater sounds created by FOSW during construction, maintenance, and operation will affect some fishes, particularly those that are sensitive to vibration (Popper et al. 2022). Sound produced by FOSW platforms at frequencies to which fishes are sensitive can affect fishes in a variety of ways (see *Underwater Sound*, this chapter). Some fishes produce a considerable amount of sound to communicate with one another. The calls of fishes near FOSW structures may be masked, or if the physiological capacity exists, fishes may shift the sonic frequency at which they call. The behavior of acoustically sensitive species may change as they either avoid or are attracted to the sound-producing device. Sound does not attenuate quickly in water, and low-frequency sounds produced by FOSW could affect fishes over a large area surrounding the site.

As detailed above, some fishes are sensitive to electromagnetic fields over short distances. However, electromagnetic fields attenuate quickly in water, so their effects are likely to be localized, and most studies have shown minimal effects on fish behavior (Hutchison et al. 2020b).

FOSW sites have the potential to negatively or positively impact fish habitat, and the effects vary by species, facility design, and spatial extent. Evaluating potential effects of FOSW on fishes will require detailed monitoring with a statistically rigorous design, such as before-after-control-impact (Bailey et al. 2014). Peer-reviewed data on observed effects are limited, and many of the impacts are speculative. Effects on fish presence, behavior, and life history functions must be measured locally, but also considered with respect to their potential impacts on local and regional populations.

## Submerged Cultural and Archaeological Resources off the Oregon Coast

Loren G. Davis

During the Pleistocene epoch, global sea levels were about 130 m (425 ft.) lower than at present because ice sheets covered much of the Northern Hemisphere. As a result, Oregon's coastline extended about 56 km (35 mi.) beyond its current boundaries. Offshore development is required to avoid disturbing archaeological sites that are now submerged.

Following the Pleistocene, rising sea levels undoubtedly caused ancestral coastal peoples to relocate repeatedly. The archaeological record of Oregon's coastal tribes is known from recorded sites that demonstrate ancestral settlements along shorelines that approximated the modern coastline. Archaeologists expect that additional evidence of Oregon's coastal tribes may be held in archaeological sites that are now submerged on Oregon's continental shelf.

Evaluating these submerged cultural resources is essential for understanding the region's complete human history and occupation. Submerged archaeological sites may provide evidence of early human habitation, migration routes, and adaptation strategies that are not captured in the terrestrial archaeological record. Federal law mandates the protection of archaeological resources on federal lands, including submerged sites. Oregon state law protects archaeological sites on public lands, which include the state waters of Oregon's continental shelf. Geophysical surveys of the seabed surface and below are used to identify potential archaeological features or ancient landforms. Marine coring then extracts sediment samples and can reveal evidence of ancestral human occupation on the now-submerged landforms.

Preservation of submerged archaeological and cultural heritage sites during development of offshore renewable energy facilities most effectively can be achieved by focusing construction and other disruptive activities within non-archaeological deposits, such as sediment layers that accumulated after the Pleistocene, and avoiding disturbance of older, deeper layers in which significant archaeological sites are more likely. Implementing such measures not only complies with legal protections, such as those mandated by Section 106 of the National Historic Preservation Act of 1966, but also ensures the preservation of archeological and tribal cultural resources and submerged heritage.

## Societal Responses to Offshore Wind Infrastructure

Shawn Hazboun and Hilary Boudet

Floating offshore wind infrastructure, including floating turbines, cable landings, substations, and port facilities, may affect coastal Oregon communities and ocean user groups. To ensure that planning and deployment bring the least harm to these people and places, several considerations are paramount, including prioritizing energy justice, ensuring adequate public engagement on siting, and implementing fair and inclusive community benefit plans.

In this section, we review public perceptions of offshore wind energy technologies and examine social concerns about potential impacts from floating offshore wind infrastructure in Oregon. We then examine floating offshore wind development through the lens of energy and environmental justice and offer points for thought, including the relevance and challenges of community benefit plans in mediating adverse impacts and distributing benefits.

### *Public Perceptions of Floating Offshore Wind Development*

Public support for floating offshore wind development off Oregon's coast is necessary for it to succeed as an energy technology and mode of decarbonization. Across the United States, there is broad public support for renewable energy technologies, such as onshore wind and solar photovoltaics (Ansolabehere and Koninsky 2014, Bergquist et al. 2020, Hazboun and Boudet 2020). However, the public has limited familiarity with marine renewable energies (Stelmach et al. 2023), including floating offshore wind, because their deployment is new. This is especially true on the West Coast, where no offshore wind facilities have been deployed. Despite public support for renewable energy, decades of public opinion research have revealed a social gap in renewable energy siting (Bell et al. 2005, 2013), or a mismatch between the high level of support for renewable energy in public opinion polls and the local opposition that can arise as a project begins siting. It may be tempting to frame the opposition as NIMBYism (not in my backyard), which is usually meant to represent local opponents as selfish, shortsighted, or not committed to decarbonization (Dear 1992, Schively

2007). However, scholars have discouraged use of the NIMBY label and encouraged developers and policymakers to instead validate and address local concerns (Devine-Wright 2005, 2011; Rand and Hoen 2017). The reasons why host communities may be concerned about or opposed to nearby renewable energy development include but are not limited to potential impacts on their environment, traditional economic drivers, culture, community character, or places that hold special value. Furthermore, scholars have recognized that local communities are often left out of planning processes for renewable energy siting, or are provided minimal opportunity to engage, which can shape how much they trust the developer and planning officials (Dwyer and Bidwell 2019).

An early motivation for developing offshore wind energy technology was the perception that it would not be opposed locally because the turbines were at sea and not in close physical proximity to communities (Haggett 2011). This assumption has proven incorrect. As with many cases of onshore wind energy development, offshore wind energy development can encounter both public support and public opposition (Firestone and Kempton 2007, Haggett 2011, Wiersma and Devine-Wright 2014, de Groot and Bailey 2016, Firestone et al. 2020, Fleming et al. 2022). Public concern or opposition stems from perceived potential adverse effects on coastal communities and ocean users, fishing and tourist economies, the visual landscape, and recreational and cultural resources (Haggett et al. 2020, Russell et al. 2020, Ferguson et al. 2021). Additional public concerns include the relative cost of offshore wind compared with other energy sources, perceptions of risks given the newness of the technology, the fact that wind energy developers are often outsiders and in many cases large corporations, the transmission of generated electricity to distant cities, and the belief that the resources needed to build and deploy a floating offshore wind array will cause more harm than benefit to the environment (Bidwell et al. 2022, Nytte et al. 2024).

The amount, timing, and quality of engagement with communities and the broader public before a facility is sited greatly affect public perception of the project, its developers, and regulators (Firestone and Kempton 2007, Haggett 2011, Dwyer and Bidwell 2019, Firestone et al. 2020). Early, meaningful, frequent, and two-way engagement with the public and impacted communities is central to whether the regulatory process is perceived as transparent and fair, or closed and partial. The main forms of public participation in that process, public comment periods and hearings, collect sentiments but do not require a change of action or even a direct response (Brown and Eckold 2020, De'Arman 2020). In analyzing the process surrounding the development of Block Island, the United States's first offshore wind array, and the high level of local support for the project, Dwyer and Bidwell (2019) suggested that regulatory process leaders built trust with affected and interested parties through diverse informal actions and by meeting their expectations for two-way engagement. Other studies also suggest that two-way deliberation is essential to successful public engagement for energy development, including offshore wind (McAdam and Boudet 2012, Klain et al. 2017).

Defining the public and the community impacted by floating offshore wind infrastructure is complex, perhaps even more so than for onshore development. One community might be closest to the coastal turbines, another might accommodate the cable landing, and a different district might host port infrastructure or turbine manufacturing. Additionally, many Oregonians may view the Oregon coast and marine environment as special places and therefore be concerned about what they perceive as the industrialization of the ocean for energy generation (Perry et al. 2014, Stelmach et al. 2023). Ocean economies, such as fisheries and whale watching, often use large areas of the ocean. Moreover, several tribal nations have direct interests in and rights to Oregon's coastal areas. With so many affected parties and such new technology, attending to community, tribal, and public concerns will be paramount to the future of floating offshore wind development in Oregon.

Despite its environmental benefits, the social impacts and equity considerations of renewable energy siting and deployment are often similar to those of traditional energy development (Ottinger et al. 2014, Dunlap 2018, Bacchiocchi et al. 2022, Walker et al. 2023). Development of floating offshore wind in Oregon and along the West Coast offers an opportunity for regulators, developers, and communities to learn from the past and work toward an inclusive, collaborative, and equitable development outcome. This goal of more-equitable development of new energy facilities is increasingly important to communities and at various levels of government.

The framework of energy justice has risen to prominence in academic, policy, and activist agendas on energy (Sovacool et al. 2017). Energy justice uses principles of justice to understand how energy production, energy policy, and energy consumption create unequal benefits and burdens for different members of society and leave out or ignore some groups (Jenkins et al. 2016).

The Biden administration had a central focus on energy justice. Promoting environmental justice was a key part of the Inflation Reduction Act, and Biden's Justice40 Initiative set a target for 40 percent of federal investments in clean energy and climate change to reach disadvantaged communities (DOE n.d.). Furthermore, Biden appointed an energy justice advocate and former professor, Shalanda Baker, as Director of the Office of Energy Justice and Equity at the U.S. Department of Energy. Under Biden, this office and the department had an exacting focus on energy justice.

Oregon and other state governments also designed and implemented policies that focus on a so-called clean energy transition for all, where all includes diverse racial, ethnic, geographic, and economic statuses— policies that foster a so-called just transition (Baker 2020). In Oregon, House Bill 2021, passed in 2021, not only set the ambitious goal of 100 percent clean electricity for Oregon's largest utilities by 2040 but placed a high priority on benefiting communities of color and rural, coastal, and low-income towns and workers.

Justice and equity are important considerations throughout the energy development process, and there are multiple dimensions of justice. Recognition justice acknowledges host communities and other affected groups and focuses on ensuring that no group is excluded from the process or misrepresented (Schlosberg 2007, Jenkins et al. 2016). Procedural justice refers to a fair and transparent process in which affected parties are participants; it is invoked most commonly during public engagement exercises but also in siting decisions, permitting, and negotiation of community benefits (Bell and Carrick 2017). Distributive justice relates to the equitable distribution of the benefits and harms of an energy facility and how the adverse impacts are mitigated.

Each dimension of justice may be most relevant at different points in the offshore wind energy development timeline. The timeline begins prior to project conception with a basic assumption that every person has human rights. Recognitional justice can be considered when envisioning the project by including and valuing divergent perspectives and recognizing intersectionality (compounding disadvantage from multiple marginalized identities). Existing meaningful areas, such as marine protected areas and cultural areas, must also be considered at this stage. Formal environmental assessments provide an opportunity for (and usually require) public participation. Procedural justice is most critical during the planning and siting process and must include engagement and meaningful participation by affected publics. Distributive justice is salient during implementation, and developers must negotiate with communities to understand what types of benefits, such as economic development, energy access, or education, are perceived as most important.

An additional two dimensions of justice, capability justice and future justice, are relevant to the operation and decommissioning process despite the long lag time before those stages. The capability approach to justice (Nussbaum and Sen 1993) suggests that the impact of an operating offshore wind array should be evaluated in terms of how it affects everyone's ability to live a safe, fulfilling, and dignified life. This evaluation includes factors such as economic impacts on fishers, effects of the supply chain on the workforce, and pricing implications for consumers (especially those living with lower incomes). Future justice refers to how offshore wind infrastructure might impact future generations that will be responsible for decommissioning. Future justice also includes consideration of wind energy development in the context of global climate change.

These concepts provide a framework for thinking about how development of floating offshore wind in Oregon can be equitable in its recognition of host communities and other impacted groups, fair and transparent in its decision-making processes, and just in the distribution of benefits and burdens. An emerging policy option with the potential to advance energy justice is the implementation of community benefit plans, which typically are negotiated between the developer and impacted communities and sometimes are overseen by regulators.

*Community Benefit Plans*

Negotiation of community benefit plans is increasingly common in offshore wind development. Community benefit plans are also required in some policy contexts. For example, the U.S. Department of Energy requires community benefit plans as part of all Bipartisan Infrastructure Law and Inflation Reduction Act funding opportunity announcements. Community benefit plans are not a new concept: they have been used during construction of some onshore renewable energy facilities and stadiums, and in development of European offshore wind energy. Other models of benefit-sharing from these types of development include community ownership. Here, we focus on community benefit plans because of their increasing use in the offshore wind energy sector in the United States.

Community benefit plans can help empower communities to negotiate terms of development and can lead to greater public acceptance of a project. For example, community benefits of the Block Island wind array were collaboratively negotiated by the island community and the developer, Deepwater Wind (Klain et al. 2017), and were vital for the project's success. The negotiated benefits were mainly non-monetary and included provision of an electrical grid connection from the mainland to the island (which previously had to transport diesel for generators), inclusion of fiber optic cables in the underwater cable bundle to increase the community's internet speed, several infrastructure improvements on the island, and local jobs (Klain et al. 2017).

Community benefit plans may be voluntary, legally binding Community Benefit Agreements (or Host Community Agreements or Good Neighbor Agreements) and may include Community Workforce or Project Labor Agreements. The negotiated suite of benefits may include direct payment to the community, tax incentives, restoration of public space, educational partnerships, infrastructure improvement, and other types of indirect benefits (Bedsworth and Hoff 2024).

In its California offshore wind leases of 2023, the Bureau of Ocean Energy Management offered a five percent bidding credit to developers if they demonstrated a commitment to entering into a General Community Benefit Agreement, and another five percent for committing to a Lease Area Use Community Benefit Agreement. The same provision was offered in the Oregon auction in 2024 (Federal Register 2024).

Because every community has different needs, and not all impacted groups are within the community closest to the infrastructure, there is no single model of community benefits for offshore wind development. Rudolph et al. (2018) proposed that negotiation of community benefits begin with a mutually agreed-on definition of the community, a collective understanding of who should benefit, agreement on the types of benefits that will be provided, and shared understanding of how the parties perceive the impacts of the project.

Although community benefit plans may lead to recognitional, procedural, and distributive equity in offshore wind development, they have challenges and pitfalls. For example, community benefit plans can be perceived by host communities as bribes offered by the developer to buy social acceptance. Additionally, a community's capacity to negotiate on its own behalf is often limited by staffing and funding; in some cases, the developer may agree to pay consultant or legal fees. Ensuring that all impacted parties participate in the negotiation can be a challenge, and there may be disagreement on who should be represented. Opinions on who should be represented depend partly on the definition of community and also on the actors' level of commitment to recognitional justice.

Floating offshore wind development in Oregon bears promise as a decarbonization technology, but it is not intrinsically different from traditional energy development in its potential to disproportionately burden communities and ocean user groups. Furthermore, a substantial proportion of Oregon coastal communities are rural, low-income, include Indigenous peoples and tribal governments, and are classified as disadvantaged communities (CEQ 2024). As development proceeds, regulators, developers and community leaders must ensure justice, gauge public perceptions of development, and manage expectations if trust and support for offshore wind are to grow and ultimately lead to more successful and accepted outcomes. If these factors are not addressed, development proposals are likely to stall and fail due to public mistrust and resistance.

## Adaptive Management Principles

Andrea Copping and Hayley Farr

Adaptive management is a systematic process intended to improve policies and practices by learning from the outcomes of management decisions and reducing scientific uncertainty. The concept of adaptive management originated to address the extent to which scientific uncertainty complicates natural resource management and development (Holling 1978, Walters and Hilborn 1978, Walters 1986). Recognizing the limitations of numerical modeling to represent complex natural systems and to predict outcomes of perturbations, early proponents of adaptive management proposed linking experiments with hypothesis testing and systems assessments and recommended that affected and interested parties participate in the process (Holling and Meffe 1996). In contemporary Oregon, adaptive management begins with the participation of tribal nations, coastal communities, and other interested and affected parties.

Adaptive management is often referred to as learning by doing, leading to iteration of management actions on the basis of new information (Walters and Holling 1990, Williams and Brown 2012). In the United States, adaptive management has been adopted by the Department of the Interior (Williams et al. 2009).

Adaptive management is most effective when the objectives of management are clear and measurable, there is an opportunity to learn, uncertainty impedes a decision or hinders the effectiveness of management, real choices among alternatives exist, institutions are committed

to and capable of measuring outcomes and acting in response to that information, and there is a mandate to act despite uncertainty. The development of floating offshore wind (FOSW) allows for learning that is intrinsic to adaptive management. However, if development may threaten legally protected species or other resources, it may be necessary to follow the more-conservative mitigation hierarchy: avoid, minimize, rectify, reduce, offset (Copping et al. 2019). If it becomes apparent at any step in the mitigation hierarchy that uncertainty is inhibiting actions or effectiveness, adaptive management can be implemented again.

Adaptive management has been used to facilitate permitting of land-based wind energy infrastructure (Köppel et al. 2014, May et al. 2017, Copping et al. 2019). The most common applications of adaptive management to land-based wind include curtailing energy production to avoid harm to protected species and consulting with groups of affected and relevant parties that examine monitoring data periodically to gauge whether changes in operations may be needed (Copping et al. 2019).

Many of the land-based mechanisms for avoiding conflicts between renewable energy development and protected species are not fit for offshore wind energy development. Adaptive management has been favored for marine energy permitting in the United Kingdom (Savidge et al. 2014) and United States (Oram and Marriott 2010, Jansujwicz et al. 2015, Marafino et al. 2023). As fixed-bottom offshore wind development has become a reality on the U.S. Atlantic Coast, adaptive management processes are being considered as viable given scientific uncertainty and the need to involve interested and affected parties in decision-making and management processes (Williams et al. 2009).

Adaptive management has not yet been applied to FOSW in the United States or other countries despite substantial uncertainty and limited evidence about the potential effects of the technology. We suggest that consideration of adaptive management for FOSW include four components. The first is determination of the level of uncertainty about potential effects and whether the proposed wind array is located away from areas with protected species or other resources. This determination is most useful at the start of planning for siting a wind array. Second, before installation, assess whether it is feasible to establish a robust, site-specific monitoring program. Third, before development permits are approved, evaluate the potential for convening an adaptive management team that is active for the life of the project. The team should include those with an immediate need for information about the project, such as the developers, regulatory agency staff, owners of the shore-based landing, and perhaps representatives of major user groups. The members of the team must be able to commit to meeting periodically, perhaps twice per year in the early stages of operation and annually thereafter, to review monitoring data and make informed recommendations for adjusting data collection and analysis. Fourth, during scoping of potential effects before permitting, ensure that other strategies, such as the mitigation hierarchy (Dempsey et al. 2023) and marine spatial planning (Douvere 2008, NCOOS n.d.), complement adaptive management.

## Conclusion

### Bryson Robertson and Karina Nielsen

The West Coast states of Oregon, Washington, and California have 2050 goals for economy-wide decarbonization and 100 percent clean electricity. Meeting these economy-wide and electricity-focused goals is imperative to mitigate the worst impacts of climate change. In 2022, more than 85 percent of carbon dioxide emissions in the United States were a result of energy generation, storage, transportation and combustion.

To meet these goals, each state will be grappling with the tripartite challenge of concurrently retiring significant fossil fuel-fired electricity generation capacity, meeting increasing electrical load or demand, and developing and managing a new suite of clean renewable energy generation, all while maintaining reliability and affordability for consumers. In assessing the possible pathways and actions that can be taken to achieve these goals, each state is examining its renewable energy resources and opportunities. Land-based wind and solar power will play a major role in the future electricity system, but they are insufficient to meet the triple challenge alone.

The offshore winds on the U.S. West Coast represent one of the most energetic and consistent renewable energy resources in the nation, and a possibly viable technological pathway to mitigate climate change and meet decarbonization goals. The technology to harness offshore winds is in a period of rapid global research, development, and deployment.

The lease areas in California and the proposed lease areas in Oregon are in far deeper ocean waters than previously attempted for offshore wind, which leads to uncertainty for many government, community, tribal, and industry parties. The development of floating offshore wind energy along the West Coast also has significant technological and supply chain uncertainty due to a limited trained workforce, aging electrical transmission, and a lack of the port infrastructure necessary to support deployments and delivery. However, the regulatory and permitting process is long, data intensive, and requires considerable public input. There is potential that this slow process will allow for clarification of many technological and economic concerns prior to deployment. Any deployments in Oregon will benefit from many years of experience, data collection, and knowledge of development from California and other regions worldwide.

Acknowledging Oregon's diverse and valued natural environment, existing ocean users, tribes, and Oregonians' attachment to the state's coast, any potential development is far more likely to succeed with authentic, collaborative, and capacity-generating engagement among a wide range of tribes, community groups, commercial operations, and the public.

## Acknowledgments

## Literature Cited

ACP (American Clean Power). 2023. Offshore wind vessel needs. cleanpower.org/wp-content/uploads/2021/09/OffshoreWind_Vessel_Needs_230104.pdf.

Albert, L., F. Olivier, A. Jolivet, L. Chauvaud, and S. Chauvaud. 2022. Insights into the behavioural responses of juvenile thornback ray *Raja clavata* to alternating and direct current magnetic fields. Journal of Fish Biology 100:645–659.

Anderson, J.M., T.M. Clegg, L.V.M.V.Q. Véras, and K.N. Holland. 2017. Insight into shark magnetic

field perception from empirical observations. Scientific Reports 7:11042. https://doi.org/10.1038/s41598-017-11459-8.

Ansolabehere, S., and D.M. Konisky. 2014. Cheap and clean: how Americans think about energy in the age of global warming. The MIT Press, Cambridge, Massachusetts.

Bacchiocchi, E., I. Sant, and A. Bates. 2022. Energy justice and the co-opting of indigenous narratives in U.S. offshore wind development. Renewable Energy Focus 41:133–142.

Bailey, H., K.L. Brookes, and P.M. Thompson. 2014. Assessing environmental impacts of offshore wind farms: lessons learned and recommendations for the future. Aquatic Biosystems 10:8. https://doi.org/10.1186/2046-9063-10-8.

Baker, S.H. 2020. Fighting for a just transition. NACLA Report on the Americas 52:144–151. https://doi.org/10.1080/10714839.2020.1768732.

Bakun, A. 1990. Global climate change and intensification of coastal ocean upwelling. Science 247:198–201.

Barth, J.A., B.A. Menge, J. Lubchenco, F. Chan, J.M. Bane, A.R. Kirincich, M.A. McManus, K.J. Nielsen, S.D. Pierce, and L. Washburn. 2007. Delayed upwelling alters nearshore coastal ocean ecosystems in the northern California Current. Proceedings of the National Academy of Sciences 104:3719–3724.

Barth, J.A., S.D. Pierce, and R.W. Castelao. 2005. Time-dependent, wind-driven flow over a shallow midshelf submarine bank. Journal of Geophysical Research: Oceans 110 (C10). https://doi.org/10.1029/2004JC002761.

Barth, J., S.D. Pierce, and R.L. Smith. 2000. A separating coastal upwelling jet at Cape Blanco, Oregon and its connection to the California Current System. Deep Sea Research Part II: Topical Studies in Oceanography 47:783–810.

Barth, J.A., et al. 2024. Widespread and increasing near-bottom hypoxia in the coastal ocean off the United States Pacific Northwest. Nature Scientific Reports 14:3798. https://doi.org/10.1038/s41598-024-54476-0.

Bedore, C.N., and S.M. Kajiura. 2013. Bioelectric fields of marine organisms: voltage and frequency contributions to detectability by electroreceptive predators. Physiological and Biochemical Zoology 86:298–311. https://doi.org/10.1086/669973.

Bedsworth, L., and K. Hoff. 2024. Offshore wind & community benefits agreements in California: CBA Examples. Center for Law, Energy, & the Environment, University of California, Berkeley, California. www.law.berkeley.edu/wp-content/uploads/2024/06/Offshore-Wind-CBAs-in-CA_Final.pdf.

Beiter, P., et al. 2016. A spatial-economic cost-reduction pathway analysis for U.S. Offshore Wind Energy Development from 2015–2030. NREL/TP-6A20-66579. National Renewable Energy Lab, Golden, Colorado. https://doi.org/10.2172/1324526.

Bell, D., and J. Carrick. 2017. Procedural environmental ,ustice. In The Routledge handbook of environmental justice. Routledge, London. https://doi.org/10.4324/9781315678986-9.

Bell, D., T. Gray, and C. Haggett. 2005. The "social gap" in wind farm siting decisions: explanations and policy responses. Environmental Politics 14:460–477.

Bell, D., T. Gray, C. Haggett, and J. Swaffield. 2013. Re-visiting the "social gap": public opinion and relations of power in the local politics of wind energy. Environmental Politics 22:115–135.

Bellmann, M.A., A. May, T. Wendt, S. Gerlach, P. Remmers, and J. Brinkmann. 2020. Underwater noise during percussive pile driving: influencing factors on pile-driving noise and technical possibilities to comply with noise mitigation values. ITAP Institut fur technische und angewandte Physik GmbH, Oldenburg, Germany. www.itap.de/media/experience_report_

underwater_era-report.pdf.

Benjamins, S., V. Harnois, H. Smith, L. Johanning, L. Greenhill, C. Carter, and B. Wilson. 2014. Understanding the potential for marine megafauna entanglement risk from marine renewable energy developments. Report No. 791. Scottish Natural Heritage. tethys.pnnl. gov/publications/understanding-potential-marine-megafauna-entanglement-risk-marine-renewable-energy-0.

Bergquist, P., D.M. Konisky, and J. Kotcher. 2020. Energy policy and public opinion: patterns, trends and future directions. Progress in Energy 2:032003. https://doi.org/10.1088/2516-1083/ ab9592.

Bevelhimer, M.S., G.F. Cada, A.M. Fortner, P.E. Schweizer, and K. Riemer. 2013. Behavioral responses of representative freshwater fish species to electromagnetic fields. Transactions of the American Fisheries Society 142:802–813.

Biden, J.R. 2023. Executive Order 14096. Revitalizing our nation's commitment to environmental justice for all. Federal Register 88(80):25251–25261.

Bidwell, D., J. Firestone, and M.D. Ferguson. 2022. Love thy neighbor (or not): regionalism and support for the use of offshore wind energy by others. Energy Research & Social Science 90:102599. https://doi.org/10.1016/j.erss.2022.102599.

Boehlert, G.W., and A.B. Gill. 2015. Environmental and ecological effects of ocean renewable energy development: a current synthesis. Oceanography 23:68–81.

BOEM (U.S. Bureau of Ocean Energy Management). 2023. Ongoing study plan: development of computer simulations to assess entanglement risk to whales and leatherback sea turtles in offshore floating wind turbine moorings, cables, and associated derelict fishing gear offshore California. Environmental Studies Program Ongoing Study PC-19-x07. espis.boem.gov/ study%20profiles/BOEM-ESP-PC-19-x07.pdf.

BOEM (U.S. Bureau of Ocean Energy Management). 27 September 2024. BOEM postpones Oregon offshore wind energy auction. www.boem.gov/newsroom/press-releases/boem-postpones-oregon-offshore-wind-energy-auction.

BOEM (U.S. Bureau of Ocean Energy Management). n.d. a. California activities. www.boem.gov/ renewable-energy/state-activities/california. Accessed 3 December 2024.

BOEM (U.S. Bureau of Ocean Energy Management). n.d. b. Oregon activities. www.boem.gov/ renewable-energy/state-activities/Oregon. Accessed 3 December 2024.

Boles, L.C., and K.J. Lohmann. 2003. True navigation and magnetic maps in spiny lobsters. Nature 421:60–63.

Brady, J. 8 June 2021. 'Energy justice' nominee brings activist voice to Biden's climate plans. National Public Radio. www.npr.org/2021/06/08/1004059950/energy-justice-nominee-brings-activist-voice-to-bidens-climate-plans.

Broström, G. 2008. On the influence of large wind farms on the upper ocean circulation. Journal of Marine Systems 74:585–591.

Brown, G., and H. Eckold. 2020. An evaluation of public participation information for land use decisions: public comment, surveys, and participatory mapping. Local Environment 25:85–100.

Buljan, A. 3 May 2024. Transformers for first US HVDC offshore wind grid connection arrive in New York. offshoreWIND.biz. www.offshorewind.biz/2024/05/03/transformers-for-first-us-hvdc-offshore-wind-grid-connection-arrive-in-new-york/.

Bullock, T.H. 1999. The future of research on electroreception and electrocommunication. Journal of Experimental Biology 202:1455–1458.

Burns, R., S. Martin, M. Wood, C. Wilson, C. Lumsden, and F. Pace. 2022. Hywind Scotland floating offshore wind farm: sound source characterisation of operational floating turbines. Report No. 02521. JASCO Applied Sciences. tethys.pnnl.gov/publications/hywind-scotland-floating-offshore-wind-farm-sound-source-characterisation-operational.

Castelao, R.M., and J.A. Barth. 2006. The relative importance of wind strength and along-shelf bathymetric variations on the separation of a coastal upwelling jet. Journal of Physical Oceanography 36:412–425.

Cawthorn, M.W. 1985. Entanglement in, and ingestion of, plastic litter in marine mammals, sharks, and turtles in New Zealand waters. Pages 336–343 in R.S. Shomura and H.O. Yoshida, editors. Proceedings of the Workshop on the Fate and Impact of Marine Debris, 27–29 November 1984, Honolulu, Hawaii.

CEQ (Council on Environmental Quality). 2024. Climate and economic justice screening tool. screeningtool.geoplatform.gov.

Chadderdon, J. 7 October 2022. Floating offshore wind can achieve cost parity with fixed-bottom solutions by early 2023: Equinor. Quest Floating Wind Energy. questfwe.com/saipem-and-siemens-energy-to-develop-500mw-floating-electrical-substation/.

Claisse, J.T., D.J. Pondella, M. Love, L.A. Zahn, C.M. Williams, J.P. Williams, and A.S. Bull. 2014. Oil platforms off California are among the most productive marine fish habitats globally. Proceedings of the National Academy of Sciences 111:15462–15467.

Copping, A., V. Gartman, R. May, and F. Bennet. 2019. The role of adaptive management in the wind energy industry. Pages 1–25 in R. Bispo, J. Bernardino, H. Coelho, and J. Lino Costa, editors. Wind energy and wildlife impacts: balancing energy sustainability with wildlife conservation. Springer, Cham, Switzerland. https://doi.org/10.1007/978-3-030-05520-2_1.

Copping, A.E., and L.G. Hemery, editors. 2020. 2020 state of the science report: environmental effects of marine renewable energy development around the world. https://doi.org/10.2172/1632878.

Copping, A.E., L.G. Hemery, H. Viehman, A.C. Seitz, G.J. Staines, and D.J. Hasselman. 2021. Are fish in danger? A review of environmental effects of marine renewable energy on fishes. Biological Conservation 262:109297. https://doi.org/10.1016/j.biocon.2021.109297.

CRS (Congressional Research Service). 2022. Offshore wind provisions in the Inflation Reduction Act. IN11980. Congressional Research Service, Washington, D.C. crsreports.congress.gov/product/pdf/IN/IN11980.

Daewel, U., N. Akhtar, N. Christiansen, and C. Schrum. 2022. Offshore wind farms are projected to impact primary production and bottom water deoxygenation in the North Sea. Communications Earth & Environment 3:1–8.

De'Arman, K.J. 2020. Is public participation public inclusion? The role of comments in US Forest Service decision-making. Environmental Management 66:91–104.

Dear, M. 1992. Understanding and overcoming the NIMBY syndrome. Journal of the American Planning Association 58:288–300.

de Groot, J. and I. Bailey. 2016. What drives attitudes towards marine renewable energy development in island communities in the UK? International Journal of Marine Energy 13:80–95.

Dempsey, L., C. Hein, and L. Münter. 2023. The mitigation hierarchy. tethys.pnnl.gov/sites/default/files/summaries/WREN-Short-Science-Story-Mitigation-Hierachy.pdf.

Devine-Wright, P. 2005. Beyond NIMBYism: towards an integrated framework for understanding public perceptions of wind energy. Wind Energy 8:125–139.

Devine-Wright, P. 2011. Public engagement with large-scale renewable energy technologies: breaking

the cycle of NIMBYism. WIREs Climate Change 2:19–26.

Dijkgraaf, S., and A.J. Kalmijn. 1962. Verhaltensversuche zur Funktion der Lorenzinischen Ampullen. Naturwissenschaften 49:400. https://doi.org/10.1007/BF00632257.

DLCD (Oregon Department of Land Conservation and Development). n.d. Where federal consistency applies. www.oregon.gov/lcd/OCMP/Pages/Where-FC-Applies.aspx. Accessed 3 December 2024.

DNV. 2022. Offshore wind transmission technical review—initial report. www.maine.gov/energy/ sites/maine.gov.energy/files/inline-files/Maine%20OSW%20DNV%20Offshore%20 Wind%20Transmission%20Technical%20Review%20Initial%20Report.pdf.

DOE (U.S. Department of Energy). n.d. Justice40 Initiative. www.energy.gov/justice/justice40-initiative. Accessed August 2024.

Douvere, F. 2008. The importance of marine spatial planning in advancing ecosystem-based sea use management. Marine Policy 32:762–771.

Duncan, E.M., Z.L.R. Botterell, A.C. Broderick, T.S. Galloway, P.K. Lindeque, A. Nuno, and B.J. Godley. 2017. A global review of marine turtle entanglement in anthropogenic debris: a baseline for further action. Endangered Species Research 34:431–448.

Dunlap, A. 2018. Counterinsurgency for wind energy: the Bii Hioxo Wind Park in Juchitán, Mexico. The Journal of Peasant Studies 45:630–652.

Dwyer, J., and D. Bidwell. 2019. Chains of trust: energy justice, public engagement, and the first offshore wind farm in the United States. Energy Research & Social Science 47:166–176.

EIA (U.S. Energy Information Administration). 29 November 2023. Coal generation decreased in 2022, but overall U.S. emissions increased. www.eia.gov/todayinenergy/detail.php?id=61022.

Equinor. n.d. a. Hywind Scotland. www.equinor.com/energy/hywind-scotland. Accessed 3 December 2024.

Equinor. n.d. b. Hywind Scotland. www.equinor.com/content/dam/statoil/documents/newsroom-additional-documents/news-attachments/brochure-hywind-a4.pdf.

Equinor. n.d. c. Hywind Tampen. www.equinor.com/energy/hywind-tampen. Accessed 3 December 2024.

Farr, H., B. Ruttenberg, R.K. Walter, Y.-H. Wang, and C. White. 2021. Potential environmental effects of deepwater floating offshore wind energy facilities. Ocean & Coastal Management 207:105611. https://doi.org/10.1016/j.ocecoaman.2021.105611.

Ferguson, M.D., D. Evensen, L.A. Ferguson, D. Bidwell, J. Firestone, T.L. Dooley, and C.R. Mitchell. 2021. Uncharted waters: exploring coastal recreation impacts, coping behaviors, and attitudes towards offshore wind energy development in the United States. Energy Research & Social Science 75:102029. https://doi.org/10.1016/j.erss.2021.102029.

Fey, D.P., M. Greszkiewicz, M. Jakubowska, A.M. Lejk, Z. Otremba, E. Andrulewicz, and B. Urban-Malinga. 2020. Otolith fluctuating asymmetry in larval trout, *Oncorhynchus mykiss walbaum*, as an indication of organism bilateral instability affected by static and alternating magnetic fields. Science of The Total Environment 707:135489. https://doi.org/10.1016/j. scitotenv.2019.135489.

Fey, D.P., M. Jakubowska, M. Greszkiewicz, E. Andrulewicz, Z. Otremba, and B. Urban-Malinga. 2019. Are magnetic and electromagnetic fields of anthropogenic origin potential threats to early life stages of fish? Aquatic Toxicology 209:150–158.

Firestone, J., C. Hirt, D. Bidwell, M. Gardner, and J. Dwyer. 2020. Faring well in offshore wind power siting? Trust, engagement and process fairness in the United States. Energy Research & Social Science 62:101393. https://doi.org/10.1016/j.erss.2019.101393.

Firestone, J., and W. Kempton. 2007. Public opinion about large offshore wind power: underlying factors. Energy Policy 35:1584–1598.

Fleming, C.S., S.B. Gonyo, A. Freitag, and T.L. Goedeke. 2022. Engaged minority or quiet majority? Social intentions and actions related to offshore wind energy development in the United States. Energy Research & Social Science 84:102440. https://doi.org/10.1016/j.erss.2021.102440.

Floeter, J., T. Pohlmann, A. Harmer, and C. Möllmann. 2022. Chasing the offshore wind farm wind-wake-induced upwelling/downwelling dipole. Frontiers in Marine Science 9:884943. https://doi.org/10.3389/fmars.2022.884943.

Fortune, I.S., A.S. Madgett, A.S. Bull, N. Hicks, M.S. Love, and D.M. Paterson. 2024. Haven or hell? A perspective on the ecology of offshore oil and gas platforms. PLoS Sustainability and Transformation 3:e0000104. https://doi.org/10.1371/journal.pstr.0000104.

Fuxjager, M.J., K.R. Davidoff, L.A. Mangiamele, and K.J. Lohmann. 2014. The geomagnetic environment in which sea turtle eggs incubate affects subsequent magnetic navigation behaviour of hatchlings. Proceedings of the Royal Society B: Biological Sciences 281:20141218. https://doi.org/10.1098/rspb.2014.1218.

Garavelli, L. 2020. Encounters of marine animals with marine renewable energy device mooring systems and subsea cables. Pages 146–153 in A.E. Copping and L.G. Hemery, editors. 2020 State of the science report: environmental effects of marine renewable energy development around the world. https://doi.org/10.2172/1633184.

García-Reyes, M., and J. Largier. 2010. Observations of increased wind-driven coastal upwelling off Central California. Journal of Geophysical Research: Oceans 115:2009JC005576. https://doi.org/10.1029/2009JC005576.

GE Vernova. 20 April 2024. Floating offshore substation solutions, part 1. resources.grid.gevernova.com/product-overviews/floating-offshore-substation-solutions.

Gilbert, B., B. Hoen, and H. Gagarin. 2024. Distributional equity in the employment and wage impacts of energy transitions. Journal of the Association of Environmental and Resource Economists 11:S1–S298. https://doi.org/10.1086/732186.

Gill, A., and M. Desender. 2020. Risk to animals from electromagnetic fields emitted by electric cables and marine renewable energy devices. Pages 86–103 in A.E. Copping and L.G. Hemery, editors. 2020 State of the science report: environmental effects of marine renewable energy development around the world. https://doi.org/10.2172/1633088.

Gill, A.B., I. Gloyne-Philips, J. Kimber, and P. Sigray. 2014. Marine renewable energy, electromagnetic (EM) fields and EM-sensitive animals. Pages 61–79 in M.A. Shields and A.I.L. Payne, editors. Marine renewable energy technology and environmental interactions. Springer, Dordrecht, Netherlands.

Gill, A., Z. Hutchison, and M. Desender. 2023. Electromagnetic fields (EMFs) from subsea power cables in the natural marine environment. tethys.pnnl.gov/publications/electromagnetic-fields-emfs-subsea-power-cables-natural-marine-environment.

Glasson, J., B. Durning, K. Welch, and T. Olorundami. 2022. The local socio-economic impacts of offshore wind farms. Environmental Impact Assessment Review 95:106783. https://doi.org/10.1016/j.eiar.2022.106783.

GWEC (Global Wind Energy Council). 2024. Global offshore wind report 2023. gwec.net/gwecs-global-offshore-wind-report-2023/.

Haggett, C. 2011. Understanding public responses to offshore wind power. Energy Policy 39:503–510.

Haggett, C., T. ten Brink, A. Russell, M. Roach, J. Firestone, T. Dalton, and B.J. McCay. 2020. Offshore wind projects and fisheries. Oceanography 33(4):38–47.

Hazboun, S.O., and H.S. Boudet. 2020. Public preferences in a shifting energy future: comparing public views of eight energy sources in North America's Pacific Northwest. Energies 13:1940. https://doi.org/10.3390/en13081940.

Hemery, L. 2020. 2020 State of the science report, chapter 6: changes in benthic and pelagic habitats caused by marine renewable energy devices. PNNL-29976CHPT6. https://doi.org/10.2172/1633182.

Hermans, A., T. Maris, J. Hubert, C. Rochas, K. Scott, A.J. Murk, and H.V. Winter. 2024. From subsea power cable to small-spotted catshark: behavioural effects of electromagnetic fields in tank experiments. SSRN abstract 4878891. https://doi.org/10.2139/ssrn.4878891.

Holling, C.S. 1978. Adaptive environmental assessment and management. John Wiley & Sons, Chichester, United Kingdom.

Holling, C.S., and G.K. Meffe. 1996. Command and control and the pathology of natural resource management. Conservation Biology 10: 328–337.

Huang, C., L. Busse, and R. Baker. 2023. Offshore wind transmission technologies assessment: overview of existing and emerging transmission technologies. Guidehouse reference no. 223437. efiling.energy.ca.gov/GetDocument.aspx?tn=250520.

Hutchison, Z.L., A.B. Gill, P. Sigray, H. He, and J.W. King. 2020a. Anthropogenic electromagnetic fields (EMF) influence the behaviour of bottom-dwelling marine species. Scientific Reports 10:4219. https://doi.org/10.1038/s41598-020-60793-x.

Hutchison, Z.L., D.H. Secor, and A.B. Gill. 2020b. The interaction between resource species and electromagnetic fields associated with electricity production by offshore wind farms. Oceanography 33(4):96–107.

Huyer, A. 1983. Coastal upwelling in the California Current system. Progress in Oceanography 12:259–284.

IEA (International Energy Agency). 2021. Net zero by 2050–a roadmap for the global energy sector. www.iea.org/reports/net-zero-by-2050.

Informal Offshore Wind Work Group. 2024. Oregon floating offshore wind energy roadmap with exit ramps: considerations. Oregon Consensus. oregonconsensus.org/projects/oregon-offshore-wind-work-group/.

Jansujwicz, J.S., and T.R. Johnson. 2015. Understanding and informing permitting decisions for tidal energy development using an adaptive management framework. Estuaries and Coasts 38:253–265.

Jenkins, K., D. McCauley, R. Heffron, H. Stephan, and R. Rehner. 2016. Energy justice: a conceptual review. Energy Research & Social Science 11:174–182.

Jordan, L.K., S.M. Kajiura, and M.S. Gordon. 2009. Functional consequences of structural differences in stingray sensory systems. Part II: electrosensory system. Journal of Experimental Biology 212: 3044–3050.

Jordan, L.K., J.W. Mandelman, and S.M. Kajiura. 2011. Behavioral responses to weak electric fields and a lanthanide metal in two shark species. Journal of Experimental Marine Biology and Ecology 409:345–350.

Kalmijn, A.J. 1982. Electric and magnetic field detection in elasmobranch fishes. Science 218:916–918.

Kao, S.-C., et al. 2022. The third assessment of the effects of climate change on federal hydropower. ORNL/TM-2021/2278. Oak Ridge National Laboratory, Oak Ridge, Tennessee. info.ornl.

gov/sites/publications/Files/Pub168510.pdf.

Keller, B.A., N.F. Putman, R.D. Grubbs, D.S. Portnoy, and T.P. Murphy. 2021. Map-like use of Earth's magnetic field in sharks. Current Biology 31:2881–2886.

Klain, S.C., T. Satterfield, S. MacDonald, N. Battista, and K.M.A. Chan. 2017. Will communities "open-up" to offshore wind? Lessons learned from New England islands in the United States. Energy Research & Social Science 34:13–26.

Klimley, A.P., N.F. Putman, A. Keller Bryan, and D. Noakes. 2021. A call to assess the impacts of electromagnetic fields from subsea cables on the movement ecology of marine migrants. Conservation Science and Practice 3:e436. https://doi.org/10.1111/csp2.436.

Kogan, I., C.K. Paull, L.A. Kuhnz, E.J. Burton, S. Von Thun, H.G. Greene, and J.P. Barry. 2006. ATOC/Pioneer seamount cable after 8 years on the seafloor: observations, environmental impact. Continental Shelf Research 26:771–787.

Köppel, J., M. Dahmen, J. Helfrich, E. Schuster, and L. Bulling. 2014. Cautious but committed: moving toward adaptive planning and operation strategies for renewable energy's wildlife implications. Environmental Management 54:744–755.

Kotek, T. 27 September 2024. Letter to the Honorable Elizabeth Klein, Director, Bureau of Ocean Energy Management. www.opb.org/pdf/GovernorKoteklettertoBOEMDirectorKlein_1727455319170.pdf. Accessed 3 December 2024.

Kramer, B. 1996. Electroreception and communication in fishes. Progress in Zoology 42. Gustav Fischer, Stuttgart, Germany. https://doi.org/10.5283/epub.2108.

Kuhnz, L., K. Buck, C. Lovera, P. Whaling, and J. Barry. 2015. Potential impacts of the Monterey Accelerated Research System (MARS) cable on the seabed and benthic faunal assemblages. tethys.pnnl.gov/publications/potential-impacts-monterey-accelerated-research-system-mars-cable-seabed-benthic.

Large, W.G., and S. Pond. 1981. Open ocean momentum flux measurements in moderate to strong winds. Journal of Physical Oceanography 11:324–336.

Larsson, J. 2021. Transmission systems for grid connection of offshore wind farms: HVAC vs HVDC breaking point. Thesis, Uppsala University, Sweden. urn.kb.se/resolve?urn=urn:nbn:se:uu:diva-444333.

Lim, J., and M. Trowbridge. 2023. AB 525 port readiness plan. Moffat & Nichol, Oakland, California. www.slc.ca.gov/renewable-energy/port-readiness-plan/.

Lohmann, K., and D. Ernst. 2014. The geomagnetic sense of crustaceans and its use in orientation and navigation. Pages 321–336 in C. Derby and M. Thiel, editors. Nervous systems and control of behavior. Oxford University Press, Oxford, England.

Lohmann, K., N. Pentcheff, G. Nevitt, G. Stetten, R. Zimmer-Faust, H. Jarrard, and L. Boles. 1995. Magnetic orientation of spiny lobsters in the ocean: experiments with undersea coil systems. The Journal of Experimental Biology 198:2041–2048.

Love, M., M. Nishimoto, S. Clark, and A. Bull. 2015. Identical response of caged rock crabs (genera *Metacarcinus* and *Cancer*) to energized and unenergized undersea power cables in southern California, USA. Bulletin, Southern California Academy of Sciences 114(1):33–41.

Love, M.S., M.M. Nishimoto, S. Clark, M. McCrea, and A.S. Bull. 2017a. Assessing potential impacts of energized submarine power cables on crab harvests. Continental Shelf Research 151:23–29.

Love, M.S., M.M. Nishimoto, S. Clark, M. McCrea, and A.S. Bull. 2017b. The organisms living around energized submarine power cables, pipe, and natural sea floor in the inshore waters

of Southern California. Bulletin, Southern California Academy of Sciences 116(2):61–87.

Macfadyen, G., T. Huntington, and R. Cappell. 2009. Abandoned, lost or otherwise discarded fishing gear. Technical Paper No. 523. Food and Agriculture Organization of the United Nations, Rome, Italy. openknowledge.fao.org/server/api/core/bitstreams/0c49669a-bc33-4792-ae8c-b24d985c79ad/content.

Madsen, J.D., P.A. Chambers, W.F. James, E.W. Koch, and D.F. Westlake. 2001. The interaction between water movement, sediment dynamics and submersed macrophytes. Hydrobiologia 444:71–84. https://doi.org/10.1023/A:1017520800568.

Mandler, C. 20 September 2024. Three Mile Island nuclear plant will reopen to power Microsoft data centers. National Public Radio. www.npr.org/2024/09/20/nx-s1-5120581/three-mile-island-nuclear-power-plant-microsoft-ai.

Marafino, G.A., G.B. Zydlewski, and J.S. Jansujwicz. 2023. Knowledge co-production to improve information uptake: a case study in Downeast Maine. Maine Policy Review 32:129–136.

Maxwell, S.M., F. Kershaw, C.C. Locke, M.G. Conners, C. Dawson, S. Aylesworth, R. Loomis, and A.F. Johnson. 2022. Potential impacts of floating wind turbine technology for marine species and habitats. Journal of Environmental Management 307:114577. https://doi.org/10.1016/j.jenvman.2022.114577.

May, R., A.B. Gill, J. Köppel, R.H.W. Langston, M. Reichenbach, M. Scheidat, S. Smallwood, C.C. Voigt, O. Hüppop, and M. Portman. 2017. Future research directions to reconcile wind turbine–wildlife interactions. Pages 255–276 in J. Köppel, editor. Wind energy and wildlife interactions: presentations from the CWW2015 conference. Springer, Cham, Switzerland.

McAdam, D., and H. Boudet. 2012. Putting social movements in their place: explaining opposition to energy projects in the United States, 2000-2005. Cambridge University Press, Cambridge, United Kingdom. https://doi.org/10.1017/CBO9781139105811.

Miller, R.G., Z.L. Hutchison, A.K. Macleod, M.T. Burrows, E.J. Cook, K.S. Last, and B. Wilson. 2013. Marine renewable energy development: assessing the benthic footprint at multiple scales. Frontiers in Ecology and the Environment 11:433–440.

Minkoff, D., N. Putman, J. Atema, and W. Ardren. 2020. Nonanadromous and anadromous atlantic salmon differ in orientation responses to magnetic displacements. Canadian Journal of Fisheries and Aquatic Sciences 77:1846–1852.

Mooney, T.A., M.H. Andersson, and J. Stanley. 2020. Acoustic impacts of offshore wind energy on fishery resources: an evolving source and varied effects across a wind farm's lifetime. Oceanography 33:82–95.

Murray, R.W. 1960. Electrical sensitivity of the ampullæ of Lorenzini. Nature 187:957.

Naisbett-Jones, L.C., N.F. Putman, M.M. Scanlan, D.L.G. Noakes, and K.J. Lohmann. 2020. Magnetoreception in fishes: the effect of magnetic pulses on orientation of juvenile Pacific salmon. Journal of Experimental Biology 223:jeb222091. https://doi.org/10.1242/jeb.222091.

NASEM (National Academies of Sciences, Engineering, and Medicine). 2021. Accelerating decarbonization of the U.S. energy system. The National Academies Press, Washington, D.C. https://doi.org/10.17226/25932.

National Research Council. 2004. Adaptive management for water resources project planning. The National Academies Press, Washington, D.C. https://doi.org/10.17226/10972.

NCCOS (National Center for Coastal Ocean Science). n.d. Coastal and marine planning. coastalscience.noaa.gov/science-areas/coastal-and-marine-planning/. Accessed 3 December 2024.

NMFS (National Marine Fisheries Service). 2018. 2018 revisions to technical guidance for assessing the effects of anthropogenic sound on marine mammal hearing (version 2.0): underwater thresholds for onset of permanent and temporary threshold shifts. NOAA Technical Memorandum NMFS-OPR-59. U.S. Department of Commerce, National Oceanic and Atmospheric Administration. www.fisheries.noaa.gov/resource/document/technical-guidance-assessing-effects-anthropogenic-sound-marine-mammal-hearing.

NRC (National Research Council0. 2003. Ocean noise and marine mammals. The National Academies Press, Washington, D.C.

Newton, K.C., A.B. Gill, and S.M. Kajiura. 2019. Electroreception in marine fishes: Chondrichthyans. Journal of Fish Biology 95:135–154.

Newton, K.C., and S.M. Kajiura. 2017. Magnetic field discrimination, learning, and memory in the yellow stingray (*Urobatis jamaicensis*). Animal Cognition 20:603–614.

Normandeau, E., T. Tricas, and A. Gill. 2011. Effects of EMFs from undersea power cables on elasmobranchs and other marine species. OCS Study OEMRE 2011-09. U.S. Department of the Interior, Bureau of Ocean Energy Management, Regulation, and Enforcement, Camarillo, California. espis.boem.gov/final%20reports/5115.pdf.

Nussbaum, M., and A. Sen. 1993. The quality of life. Clarendon Press, Oxford, United Kingdom.

Nytte, S., F. Alfnes, and S. Korhonen-Sande. 2024. Public support and opposition toward floating offshore wind power development in Norway. The Electricity Journal 37:107336. https://doi.org/10.1016/j.tej.2023.107336.

Ocean Policy Committee. 2023. Ocean climate action plan. www.whitehouse.gov/wp-content/uploads/2023/03/Ocean-Climate-Action-Plan_Final.pdf.

Ocean Winds. n.d. Korea floating wind. www.oceanwinds.com/projects/korea-floating-wind-farm/.

ODFW (Oregon Department of Fish and Wildlife). 2016. Oregon nearshore strategy. In Oregon conservation strategy. Salem, Oregon. www.oregonconservationstrategy.org/oregon-nearshore-strategy/.

OEMB (Ocean Energy Management Bureau). 2024. Pacific Wind lease sale 2 for commercial leasing for wind power development on the Oregon outer continental shelf–proposed sale notice. Federal Register 89(85):35210–35220.

Offshore. 2024. France reveals winner of offshore Brittany floating wind tender. www.offshore-mag.com/renewable-energy/article/55041767/france-reveals-winner-of-offshore-brittany-floating-wind-tender.

Ohman, M.C., P. Sigray, and H. Westerberg. 2007. Offshore windmills and the effects of electromagnetic fields on fish. Ambio 36:630–633.

Oram, C., and C. Marriott. 2010. Using adaptive management to resolve uncertainties for wave and tidal energy projects. Oceanography 23:92–97.

Orr, M. 2016. The potential impacts of submarine power cables on benthic elasmobranchs. Ph.D. dissertation, University of Auckland, Auckland, New Zealand.

Ottinger, G., T.J. Hargrave, and E. Hopson. 2014. Procedural justice in wind facility siting: recommendations for state-led siting processes. Energy Policy 65:662–669.

Paulin, M.G. 1995. Electroreception and the compass sense of sharks. Journal of Theoretical Biology 174:325–339.

Paxton, A.B., D.N. Steward, Z.H. Harrison, and J.C. Taylor. 2022. Fitting ecological principles of artificial reefs into the ocean planning puzzle. Ecosphere 13: e3924. https://doi.org/10.1002/ecs2.3924.

Perry, E.E., M.D. Needham, L.A. Cramer, and R.S. Rosenberger. 2014. Coastal resident knowledge

of new marine reserves in Oregon: the impact of proximity and attachment. Ocean & Coastal Management 95:107–116. https://doi.org/10.1016/j.ocecoaman.2014.04.011.

Pettinger, B. 3 October 2024. Letter from the Pacific Marine Fishery Management Council to Katharine Segal, Grid Deployment Office, U.S. Department of Energy.

PFMC (Pacific Fishery Management Council. n.d. Offshore wind on the Pacific coast. www.pcouncil.org/managed_fishery/offshore-wind/. Accessed 3 December 2024.

PFMC (Pacific Fishery Management Council). 18 October 2021. Fact sheet: habitat and essential fish habitat. www.pcouncil.org/fact-sheet-habitat-and-essential-fish-habitat/. Accessed 3 December 2024.

Pickett, M.H., and J.D. Paduan. 2003. Ekman transport and pumping in the California Current based on the U.S. Navy's high-resolution atmospheric model (COAMPS). Journal of Geophysical Research: Oceans 108:3327. https://doi.org/10.1029/2003JC001902.

Plumer, B. 30 September 2024. U.S. Approves billions in aid to restart Michigan nuclear plant. The New York Times. www.nytimes.com/2024/09/30/climate/michigan-nuclear-plant-palisades.html.

Popper, A.N., et al. 2022. Offshore wind energy development: research priorities for sound and vibration effects on fishes and aquatic invertebrates. The Journal of the Acoustical Society of America 151:205–215.

Porter, A., and S. Phillips. 2016. Determining the infrastructure needs to support offshore floating wind and marine hydrokinetic facilities on the Pacific West Coast and Hawaii. OCS Study BOEM 2016-011. U.S. Department of the Interior, Bureau of Ocean Energy Management, Camarillo, California. www.boem.gov/sites/default/files/environmental-stewardship/Environmental-Studies/Pacific-Region/Studies/BOEM-2016-011.pdf.

Principle Power. n.d. Kincardine offshore wind farm. www.principlepower.com/projects/kincardine-offshore-wind-farm Accessed 3 December 2024.

Putman, N. 2018. Marine migrations. Current Biology 28:R972–976.

Putman, N.F., C.S. Endres, C.M.F. Lohmann, and K.J. Lohmann. 2011. Longitude perception and bicoordinate magnetic maps in sea turtles. Current Biology 21:463–466.

Putman, N.F., M.M. Scanlan, E.J. Billman, J.P. O'Neil, R.B. Couture, T.P. Quinn, K.J. Lohmann, and D.L.G. Noakes. 2014. An inherited magnetic map guides ocean navigation in juvenile Pacific salmon. Current Biology 24:446–450.

Raghukumar, K., C. Chartrand, G. Chang, L. Cheung, and J. Roberts. 2022. Effect of floating offshore wind turbines on atmospheric circulation in California. Frontiers in Energy Research 10:863995. https://doi.org/10.3389/fenrg.2022.863995.

Raghukumar, K., T. Nelson, M. Jacox, C. Chartrand, J. Fiechter, G. Chang, L. Cheung, and J. Roberts. 2023. Projected cross-shore changes in upwelling induced by offshore wind farm development along the California Coast. Communications Earth & Environment 4:116. https://doi.org/10.1038/s43247-023-00780-y.

Rand, J., and B. Hoen. 2017. Thirty years of North American wind energy acceptance research: what have we learned? Energy Research & Social Science 29:135–148.

Rezaei, F., P. Contestabile, D. Vicinanza, and A. Azzellino. 2023. Towards understanding environmental and cumulative impacts of floating wind farms: lessons learned from the fixed-bottom offshore wind farms. Ocean & Coastal Management 243:106772. https://doi.org/10.1016/j.ocecoaman.2023.106772.

Richard, C. 4 June 2019. Ideol and Atlantique Offshore Energy unveil floating substation. Windpower Monthly. www.windpowermonthly.com/article/1586499/ideol-atlantique-

offshore-energy-unveil-floating-substation.

Risch, D., G. Favill, B. Marmo, N. van Geel, S. Benjamins, P. Thompson, A. Wittich, and B. Wilson. 2023. Characterisation of underwater operational noise of two types of floating offshore wind turbines. tethys.pnnl.gov/publications/characterisation-underwater-operational-noise-two-types-floating-offshore-wind.

Rudolph, D., C. Haggett, and M. Aitken. 2018. Community benefits from offshore renewables: the relationship between different understandings of impact, community, and benefit. Environment and Planning C: Politics and Space 36:92–117.

Russell, A., J. Firestone, D. Bidwell, and M. Gardner. 2020. Place meaning and consistency with offshore wind: an island and coastal tale. Renewable and Sustainable Energy Reviews 132:110044. https://doi.org/10.1016/j.rser.2020.110044.

Samelson, R., P. Barbour, J.A. Barth, S. Bielli, T. Boyd, D. Chelton, P. Kosro, M. Levine, E. Skyllingstad, and J. Wlczak. 2002. Wind stress forcing of the oregon coastal ocean during the 1999 upwelling season. Journal of Geophysical Research: Oceans 107:2-1, 2-8.

Savidge, G., et al. 2014. Strangford Lough and the SeaGen Tidal Turbine. Pages 153–172 in M.A. Shields and A.I.L. Payne, editors. Marine renewable energy technology and environmental interactions. Springer, Dordrecht, Netherlands.

Schively, C. 2007. Understanding the NIMBY and LULU phenomena: reassessing our knowledge base and informing future research. Journal of Planning Literature 21:255–266.

Schlosberg, D. 2007. Defining environmental justice: theories, movements, and nature. Oxford University Press, Oxford, United Kingdom.

Scott, K., P. Harsanyi, B. Easton, A. Piper, C. Rochas, A. Lyndon, and K. Chu. 2021. Exposure to electromagnetic fields (EMF) from submarine power cables can trigger strength-dependent behavioural and physiological responses in edible crab, *Cancer pagurus* (L.). Journal of Marine Science and Engineering 9:776. https://doi.org/10.3390/jmse9070776.

Scott, K., P. Harsanyi, and A.R. Lyndon. 2018. Understanding the effects of electromagnetic field emissions from Marine Renewable Energy Devices (MREDs) on the commercially important edible crab, *Cancer pagurus* (L.). Marine Pollution Bulletin 131 (Part A):580–588.

SEER (U.S. Offshore Wind Synthesis of Environmental Effects Research). 2022. Environmental effects of U.S. offshore wind energy development: compilation of educational research briefs. tethys.pnnl.gov/summaries/seer-educational-research-briefs.

Semco Maritime. 22 September 2022. Semco Maritime, Inocean and ISC Consulting Engineers join forces. www.semcomaritime.com/news/floating-offshore-wind. Accessed 3 December 2024.

Shields, M., et al. 2023. The impacts of developing a port network for floating offshore wind energy on the west coast of the United States. NREL/TP-5000-86864. National Renewable Energy Laboratory, Golden, Colorado. https://doi.org/10.2172/2005543.

Sierman, J., A. Bates, E. Euen, E. Hertzsch, S. Heuberger, L. Ross, R. Sadhir, and C. Splitt. 2022. Floating offshore wind: benefits & challenges for Oregon. Oregon Department of Energy, Salem, Oregon. www.oregon.gov/energy/Data-and-Reports/Documents/2022-Floating-Offshore-Wind-Report.pdf.

Sierra, A. 23 October 2024. Amazon plans to power Eastern Oregon data centers with nuclear reactors. Oregon Public Broadcasting. www.opb.org/article/2024/10/23/amazon-power-eastern-oregon-data-centers-nuclear-reactors/.

Smith, J.A., M.B. Lowry, C. Champion, and I.M. Suthers. 2016. A designed artificial reef is among the most productive marine fish habitats: new metrics to address "production versus attraction." Marine Biology 163:188. https://doi.org/10.1007/s00227-016-2967-y.

Snodgrass, D., E. Orbesen, J. Walter, J. Hoolihan, and C. Brown. 2020. Potential impacts of oil production platforms and their function as fish aggregating devices on the biology of highly migratory fish species. Reviews in Fish Biology and Fisheries 30:405-422.

Song, D., Y. Yang, S. Zheng, X. Deng, J. Yang, M. Su, W. Tang, X. Yang, L. Huang, and Y.H. Joo. 2020. New perspectives on maximum wind energy extraction of variable-speed wind turbines using previewed wind speeds. Energy Conversion and Management 206:112496. https://doi.org/10.1016/j.enconman.2020.112496.

Sovacool, B.K., M. Burke, L. Baker, C.K. Kotikalapudi, and H. Wlokas. 2017. New frontiers and conceptual frameworks for energy justice. Energy Policy 105:677–691.

Steinberg, D., M. Brown, R. Wiser, P. Donohoo-Vallett, P. Gagnon, A. Hamilton, M. Mowers, C. Murphy, and A. Prasanna. 2023. Evaluating impacts of the Inflation Reduction Act and Bipartisan Infrastructure Law on the U.S. Power System. NREL/TP-6A20-85242. National Renewable Energy Laboratory, Golden, Colorado. https://doi.org/10.2172/1962552.

Stelfox, M., J. Hudgins, and M. Sweet. 2016. A review of ghost gear entanglement amongst marine mammals, reptiles and elasmobranchs. Marine Pollution Bulletin 111:6–17.

Stelmach, G., S. Hazboun, D. Brandt, and H. Boudet. 2023. Public perceptions of wave energy development on the West Coast of North America: risks, benefits, and coastal attachment. Ocean & Coastal Management 241:106666. https://doi.org/10.1016/j.ocecoaman.2023.106666.

Sunrise Wind. 2021. Sunrise Wind will be first offshore wind project in United States to Use HVDC transmission technology. 2021. sunrisewindny.com/news/2021/10/sunrise-wind-will-be-first-offshore-wind-project-in-united-states--to-use-hvdc-transmission-technology.

Tanski, A., K. Formicki, P. Smietana, M. Sadowski, and A. Winnicki. 2005. Sheltering behaviour of spinycheek crayfish (*Orconectes limosus*) in the presence of an artificial magnetic field. Bulletin Francais De La Peche Et De La Pisciculture 376-377:787–793.

Tennet. n.d. The 2GW program. www.tennet.eu/about-tennet/innovations/2gw-program. Accessed 3 December 2024.

The White House. 29 March 2021. Fact sheet: Biden Administration jumpstarts offshore wind energy projects to create jobs. www.whitehouse.gov/briefing-room/statements-releases/2021/03/29/fact-sheet-biden-administration-jumpstarts-offshore-wind-energy-projects-to-create-jobs/.

The White House. 15 September 2022. Fact sheet: Biden-Harris Administration announces new actions to expand U.S. offshore wind energy. www.whitehouse.gov/briefing-room/statements-releases/2022/09/15/fact-sheet-biden-harris-administration-announces-new-actions-to-expand-u-s-offshore-wind-energy/.

Thompson, P.M., D. Lusseau, T. Barton, D. Simmons, J. Rusin, and H. Bailey. 2010. Assessing the responses of coastal cetaceans to the construction of offshore wind turbines. Marine Pollution Bulletin 60:1200–1208.

Trowbridge, M., J. Lim, and S. Phillips. 2022. Port of Coos Bay port infrastructure assessment for offshore wind development. OCS Study BOEM 2022-073. U.S. Department of the Interior, Bureau of Ocean Energy Management. www.boem.gov/sites/default/files/documents/renewable-energy/studies/BOEM-2022-073.pdf.

UNFCCC (United Nations Framework Convention on Climate Change). n.d. a. Nationally determined contributions. unfccc.int/process-and-meetings/the-paris-agreement/nationally-determined-contributions-ndcs. Accessed 3 December 2024.

UNFCCC (United Nations Framework Convention on Climate Change). n.d. b. What is the Paris

Agreement? unfccc.int/process-and-meetings/the-paris-agreement.

United States. 2021. The United States' nationally determined contribution. unfccc.int/sites/default/files/NDC/2022-06/United%20States%20NDC%20April%202021%202021%20Final.pdf.

Vestas. 30 August 2024. V236-15.0 MWTM. www.vestas.com/en/energy-solutions/offshore-wind-turbines/V236-15MW.

Walker, C., S. Ryder, J.-P. Roux, Z. Chateau, and P. Devine-Wright. 2023. Contested scales of democratic decision-making and procedural justice in energy transitions. Pages 317–326 in M. Nadesan, M.J. Pasqualetti, and J. Keahey, editors. Energy democracies for sustainable futures. Academic Press, Cambridge, Massachusetts.

Walters, C.J. 1986. Adaptive management of renewable resources. Macmillan, New York. Walters, C.J., and R. Hilborn. 1978. Ecological optimization and adaptive management. Annual Review of Ecology, Evolution, and Systematics 9:157–188.

Walters, C.J., and C.S. Holling. 1990. Large-scale management experiments and learning by doing. Ecology 71:2060–2068.

Westerberg, H., and I. Lagenfelt. 2008. Sub-sea power cables and migration behaviour of the european eel. Fisheries Management and Ecology 15:369–375.

Wiersma, B., and P. Devine-Wright. 2014. Public engagement with offshore renewable energy: a critical review. WIREs Climate Change 5:493–507.

Williams, B.K., and E.D. Brown. 2012. Adaptive management: the U.S. Department of the Interior applications guide. Adaptive Management Working Group. U.S. Department of the Interior, Washington, D.C.

Williams, B.K., R. Szaro C., and C.D. Shapiro. 2009. Adaptive management: the U.S. Department of the Interior technical guide. Adaptive Management Working Group. U.S. Department of the Interior, Washington, D.C.

Williams, J.P., E.M. Jaco, Z. Scholz, C.M. Williams, D.J. Pondella, M.K. Rasser, and D.M. Schroeder. 2023. Red rock crab (*Cancer productus*) movement is not influenced by electromagnetic fields produced by a submarine power transmission cable. Continental Shelf Research 269:105145. https://doi.org/10.1016/j.csr.2023.105145.

Wilson, J.D., and Z. Zimmerman. 2023. The era of flat power demand is over. Grid strategies. gridstrategiesllc.com/wp-content/uploads/2023/12/National-Load-Growth-Report-2023.pdf.

Windfloat Atlantic. n.d. World's first semi-submersible floating offshore wind farm. www.windfloat-atlantic.com. Accessed 3 December 2024.

Woodruff, D.L., V.I. Cullinan, A.E. Copping, and K.E. Marshall. 2013. Effects of electromagnetic fields on fish and invertebrates. Progress report, contract DE-AC05-76RL01830. Environmental effects of marine and hydrokinetic energy. U.S. Department of Energy, Pacific Northwest National Laboratory, Richland, Washington.

Wyman, M.T., R. Kavet, R.D Battleson, T.V. Agosta, E.D. Chapman, P.J. Haverkamp, M.D. Pagel, and A.P. Klimley. 2023. Assessment of potential impact of magnetic fields from a subsea high-voltage dc power cable on migrating green sturgeon, *Acipenser medirostri*s. Marine Biology 170:164. https://doi.org/10.1007/s00227-023-04302-4.

Wyman, M.T., A.P. Klimley, R.D. Battleson, T.V. Agosta, E.D. Chapman, P.J. Haverkamp, M.D. Pagel, and R. Kavet. 2018. Behavioral responses by migrating juvenile salmonids to a subsea high-voltage DC power cable. Marine Biology 165:134. https://doi.org/10.1007/s00227-018-3385-0.

Yoshida, K. and N. Baba. 1985. A survey of drifting stray fishing net fragments in the northern Sea of Japan (western Pacific Ocean). Document Submitted to 28th Meeting of the Standing

Scientific Committee of the North Pacific Fur Seal Commission, Tokyo, Japan.

Yu, H., G. Fang, K.A. Rose, J. Lin, J. Feng, H. Wang, Q. Cao, Y. Tang, and T. Zhang. 2023. Effects of habitat usage on hypoxia avoidance behavior and exposure in reef-dependent marine coastal species. Frontiers in Marine Science 10:1109523. https://doi.org/10.3389/fmars.2023.1109523.

# Trade-offs in Planting Trees in Urban and Suburban Areas

Dominique Bachelet

## Reduction of Urban Heat by Trees

An urban heat island is an urban area in which temperatures are higher than in nearby rural areas (e.g., Mentashi et al. 2022). Urban heat islands develop as natural vegetation is replaced by asphalt and concrete in roads, sidewalks, parking lots, buildings, and other structures typical of population centers. These materials absorb the sun's heat, causing ambient temperatures to rise (Akbari et al. 1992). Air temperatures in many U.S. cities are up to 10°F (5.6°C) warmer than the surrounding areas (EPA 2008). Differences in temperature are more pronounced at night, when wind speeds decrease, and in winter, when temperatures in the surrounding areas drop. The greatest difference occurs during summer, when relatively short nights inhibit full release of the excess heat absorbed during the day. Temperatures in urban heat islands in 65 major cities in the United States are an average of 8°F (4.4°C) higher than those in the surrounding areas (Climate Central 2024). Nearly 34 million people live in these urban heat islands.

In the United States, urban heat islands account for 5–10 percent of maximum urban electric demand for air conditioning, and up to 20 percent of population-weighted smog concentrations in urban areas (Akbari 2005). More than 50 percent of residential electricity use in the United States is dedicated to heating and cooling homes (USEIA 2020). An increase of 2.7°F (1.5°C) in global mean temperature is expected to cause an increase in air-conditioning use of up to 8 percent per household across the conterminous United States (Obringer et al. 2022), especially in southern states. In the Pacific Northwest, the use of air conditioning was projected to increase by 1–2 percent (Maia-Silva et al. 2020).

People in low-income communities and people of color are disproportionally affected by urban heat. These groups statistically are more likely to live in older housing with limited cooling capacity and, when they reside in cities, in areas with low tree cover (Jesdale et al. 2013, Leng et al. 2024). The urban heat burden is linked to a history of racially biased housing policy: summer temperatures are hotter in historically redlined areas (areas in which housing or housing loans were denied on the basis of race) than in non-redlined areas in 150 (84 percent) of 179 major U.S. cities (Hsu et al. 2021, Jung et al. 2024). Urban heat is caused not only by changes in land cover (e.g., Guo et al. 2020) but by waste heat generated by use of air conditioners in summer and furnaces and other heating devices in winter. As global temperatures rise and the frequency of extreme heat events increases, the compounded effects of urban heat and regional warming increasingly are becoming a hazard for human health. By creating shade (Akbari et al. 1997) (Figure 1) and decreasing ambient heat through evapotranspiration (Winbourne et al. 2020), urban trees can reduce the heat island effect by 2–14°F (1–8°C) (Rahman et al. 2020, Park et al. 2021). Trees such as mature oaks can transpire about 100 gallons of water a day (Akbari et al. 1992), which represents a cooling power equivalent of 70 kWh, enough to power two average household central air-conditioning units for one day.

Heat causes a greater number of human deaths than any other weather extreme. In 2023, 75,104 weather events in the United States resulted in an estimated 877 deaths and 3,857 injuries (NSC 2024). Heat, wildfires, and tornadoes were responsible for the greatest number of deaths: 294, 105, and 91, respectively (NSC 2024). Worldwide from 2012 through 2021, adults aged 65 and older were exposed to 3.2 more days of extreme heat per person than the annual average from 1986 through 2005, while children under 1 year of age were exposed to 4.4 more days per person (Romanello et

al. 2022, WMO 2023). Furthermore, sustained exposure to extreme temperatures can prove deadly even for healthy people (de Guzman et al. 2023).



**Figure 1.** Shade along the pedestrian walkway adjacent to the Garonne River, Lyon, France. Photograph by Dominique Bachelet.

Trees planted strategically around buildings can substantially reduce indoor air temperature by, for example, shading windows to prevent direct sunlight from entering a building. Dense and tall tree canopies can affect the temperature of the surrounding air and entire wall, reduce heat transfer through walls, and increase humidity, allowing for higher levels of evaporative cooling. However, for tree canopies to provide effective shade, traditional selection of species and placement of trees along streets must be adjusted. Street orientation, characteristics of surrounding buildings (e.g., window sizes and locations, building orientation, level of insulation), season, and geographic location affect shading and cooling potential (Sanusiet al. 2016, Rantzoudi and Georgi 2017).

Shading by trees also reduces temperatures inside vehicles. The temperature inside cars parked in a shaded parking lot in summer in Davis, California, a city near Sacramento in the Central Valley, was 45°F (25°C) cooler than the temperature inside cars parked in direct sunlight (Scott et al. 1999). The larger the area covered by tree canopies, the greater the cooling effect. Large trees can provide up to 70 percent shade during spring and autumn, thus saving the homeowner or renter a large amount of energy costs (Gómez-Muñoz et al. 2010).

While a row of trees can block cooling breezes in summer, continuous dense tree canopies—such as in urban parks—can increase local air circulation, generating breezes that have a neighborhood-wide cooling effect (Ca et al. 1998, Spronken-Smith and Oke 1999). A review of 202 peer-reviewed articles about cities worldwide indicated that during heat waves, city air can be cooled by up to 5.0° ± 3.5°C (9.0° ± 6.3°F) by botanical gardens, 4.1° ± 4.2°C (7.4° ± 7.6°F) by vegetated walls, 3.8°C ± 3.1°C (6.8° ± 5.6°F) by street trees (Figure 1), and 3.8°C ± 2.7°C (6.8° ± 4.9°F) by vegetated balconies (Kumar et al. 2024).

Beyond mitigating urban heat island effects, urban trees can provide psychological benefits by increasing species richness, particularly of birds (Fuller et al. 2007, Cameron et al. 2020, Methorst et al. 2021). Urban trees also can reduce levels of particulate matter less than 10 microns in diameter ($PM_{10}$) and of other pollutants, such as sulfur dioxide, carbon monoxide, nitrogen dioxide, and ozone (Freer-Smith et al. 2004, Nowak et al. 2006, Escobedo et al. 2008, 2009), further contributing to urban population health. On the basis of estimates of parameters such as leaf area index, Nowak et al. (2006) estimated that urban trees in Portland, Oregon, which covered 42 percent of the city, improved air quality by reducing levels of $PM_{10}$ by 0.3 to 3.5 percent, ozone by 0.1 to 3.7 percent, nitrous oxide by 0.1 to 2.7 percent, and sulfur dioxide by 0.1 to 4 percent. Although the percentage change in air pollutants is small, the estimates likely were conservative (Nowak et al. 2006). From 2008 through 2014, the percentage of tree cover in Oregon's urban areas was reported to decline by 0.38 percent per year (Nowak and Greenfield 2018).

## Challenges to Maintaining Urban Trees

Although trees ameliorate urban heat and have other public health benefits, establishing and maintaining trees in cities is challenging. Three of the primary challenges are difficult growing conditions, the partnerships necessary to sustain urban trees, and perceptions that the disadvantages of trees outweigh the benefits.

Beyond their exposure to the same climate variability and extremes that affect natural vegetation, urban trees are exposed to high levels of pollutants and high temperatures and have limited above ground and below ground space in which to grow (Figure 2), all which inhibits root and crown formation and increases susceptibility to insects and disease (Tubby and Webber 2010). If urban trees become weak or die, they can become inconveniences or hazards.

The water demands of trees are a consideration in urban environments. Large and older street trees that provide considerable shade (Figure 3) need large amounts of water for transpiration. Soil compaction, often combined with a high proportion of impervious surface surrounding street trees,



**Figure 2.** Portland, Oregon, is among the many cities that provide guidance on which trees to plant in areas with different amounts of space. Source: www.portland.gov/trees/tree-planting/street-tree-planting-lists.

reduces water infiltration and storage. Compaction and impervious surfaces also increase runoff to the street or gutter, thereby reducing the trees' access to water. Supplementation of irrigation water by rain or snow needs to be effective and timely, which can cause maintenance challenges. Over time, sprinklers directed at the base of a tree lead to rot and fungus growth. Overhanging structures along the street and sidewalk tend to intercept precipitation, as does the tree canopy, preventing the precipitation from entering the limited permeable area around the tree trunk. A water-stressed tree is generally more vulnerable to other stressors, such as pollution or diseases, and may require treatment to survive. In the United States, landscape irrigation is estimated to account for about one-third of all residential water use, and in dry climates, such as the Southwest, it amounts to nearly 60 percent (EPA 2017), raising issues of water availability and distribution (Park et al. 2023).

The effects of climate change on insects and pathogens that affect urban trees have not been studied extensively despite recognition of potential risks (Tubby and Webber 2010, Frank and Just 2020, Khan and Conway 2020, Tabassum et al. 2024). For example, given their generally short reproductive cycles, high reproductive potential, ability to adapt rapidly to environmental change, and capacity for dispersal, the distribution and abundance of many insects and pathogens that affect urban trees may be responsive to even moderate changes in climate (Tubby and Webber 2010). Trees, in comparison, are long-lived and adapt more slowly to environmental change, particularly in urban settings where natural recruitment is rare and limits evolution. Therefore, urban trees may become more vulnerable to endemic or introduced insects and pathogens. The damage to trees from insects and pathogens may become more serious than in the past because warmer temperatures reduce generation times and because the ranges of insects and pathogens with which the trees have not coevolved are expanding. Introduced non-native tree species also may introduce novel insects and diseases that are well-adapted to warmer and, depending on the region, more arid or humid conditions (Turbelin et al. 2022, Tabassum et al. 2024).



**Figure 3.** Integration of shade trees along sidewalks and roads in Lyon, France. Photograph by Dominique Bachelet.

Early detection of emerging insects and pathogens can halt or slow the rate at which they colonize newly planted urban trees (Fagan et al. 2008). Increased monitoring and knowledge transfer among plant health specialists, the arboriculture and horticulture trade, local authorities, and the public may counter the risks of new insects and pathogens.

Changes in climate are affecting tree phenology. Warmer winters that do not meet the chilling requirements of certain tree species reduce the trees' growth and render the trees more vulnerable to insects and pathogens, in part because some species of insects may emerge earlier and cold-induced mortality of disease agents declines. Furthermore, it can be difficult to address trade-offs between planting species that can survive the changing local climate while respecting cultural sensitivities. For example, mortality of endemic western redcedar (*Thuja plicata*), often following several years of decline, has been increasing in the Pacific Northwest (Andrus et al. 2023) and was high in Portland following the June 2021 heat wave and subsequent drought (Goodrich et al. 2023). However, because the species has high cultural value to some tribes, replacement with other species was not considered. Instead, new plantings were recommended in the areas with the greatest water availability with the intent of maintaining the species in Portland (Hautala 2024).

Limited resources often hinder maintenance of urban trees, whether along streets or in parks, gardens, or industrial areas. Long-term maintenance requires participation of and collaboration among private and public entities. Extreme weather such as ice storms, high winds, and lightning strikes can cause trees or limbs to fall, blocking roads or damaging residences, vehicles, or power lines. In autumn, leaves can block storm drains. During and following extreme weather, city services can be strained and may not be able to respond rapidly to all fallen trees or branches. Selecting locations for planting new trees that will minimize potential damages and reduce the associated financial burden therefore is a high priority (Czaja et al. 2020). The costs of urban tree maintenance and management are not well understood, and trees generally are a lower priority than police and fire departments, road improvements, schools, and other public services (Vogt et al. 2015).

Urban trees are often considered to be a financial burden or risk. Trees can be a substantial source of pollen in spring and summer, exacerbating seasonal allergies. Droppings from birds that use the trees can become obstacles to movement, especially for those dependent on mobility-assistance devices, and the birds can carry viruses such as H1N1 avian influenza. The negative effects of trees may be more visible to some urban residents than the benefits. Roots that penetrate houses' foundations, buckle sidewalks, or damage sewer pipes can place financial burdens on homeowners and city managers.

Certain trees emit terpenes, contributing to the formation of secondary particles (Khediv et al. 2017). Most trees, such as American oaks, emit isoprene, a common, nontoxic volatile organic compound. When isoprene contacts nitrogen oxides, which are emitted by burning fossil fuels, the resulting chemical reaction creates ground-level ozone, a pollutant that can cause respiratory illness (Wei et al. 2024). As temperatures increase, trees produce more isoprene, often during the period of peak use of fossil-fuel powered air conditioners. As a result, local levels of air pollution may be greatest during heat waves. Furthermore, tree maintenance incurs some environmental costs, such as the use of power saws that burn fossil fuels or pesticides to prevent outbreaks of pests and pathogens. Hudgins et al. (2022) estimated that 1.4 million street trees in the United States would be killed by invasive insects from 2020 through 2050, and Novak and Greenfield (2018) documented the decline of urban forests in the United States from 2009 through 2014. Consequently, recommendations have been issued to reduce the threat of dead trees near houses,

including removal of the trees or treatment with pesticides (e.g., Fahrner et al. 2017). The use of pesticides in cities might affect both human and ecological health (Raupp et al. 2001, Meftaul et al. 2020). Collaboration between health and environmental professionals on guidelines for planting trees with benefits for human health may increase the likelihood that urban trees thrive and provide diverse societal goods and services (Wolf et al. 2020).

## Literature Cited

Akbari, H. 2005. Energy saving potentials and air quality benefits of urban heat island mitigation. Lawrence Berkeley National Laboratory, Berkeley, California. www.osti.gov/servlets/purl/860475.

Akbari, H., S. Davis, J. Huang, S. Dorsano, and S. Winnett. 1992. Cooling our communities: a guidebook on tree planting and light-colored surfacing. U.S. Environmental Protection Agency and Lawrence Berkeley National Laboratory. https://doi.org/ 10.2172/5032229.

Akbari, H., D.M. Kurn, S.E. Bretz, and J.W. Hanford. 1997. Peak power and cooling energy savings of shade trees. Energy and Buildings 25:139–148.

Andrus, R.A., et al. 2024. Canary in the forest? Tree mortality and canopy dieback of western redcedar linked to drier and warmer summer conditions. 2024. Journal of Biogeography 51:103–119.

Ca, V.T., T. Aseada, and E.M. Abu. 1998. Reduction in air conditioning energy caused by a nearby park. Energy and Buildings 29:83–92.

Cameron, R.W.F., P. Brindley, and M. Mears. 2020. Where the wild things are! Do urban green spaces with greater avian biodiversity promote more positive emotions in humans? Urban Ecosystems 23:301–317.

Chatterjee, A., and M. Lenart. 2007. Water-energy trade-offs between swamp coolers and air conditioners. Southwest Hydrology September–October:28–32. climas.arizona.edu/sites/climas.arizona.edu/files/migrated_media/pdfwater-energy-trade-offs-between-swamp-coolers-and-air-conditioners_5.pdf.

Climate Central. 2024. Urban heat hot spots in 65 cities. www.climatecentral.org/climate-matters/urban-heat-islands-2024.

Czaja, M., A. Kolton, and P. Muras. 2020. The complex issue of urban trees—stress factor accumulation and ecological service possibilities. Forests 11:932. https://doi.org/10.3390/f11090932.

EPA (U.S. Environmental Protection Agency). 1992. Cooling our communities: a guidebook on tree planting and light-colored surfacing. GPO document 055-000-00371-8. U.S. Environmental Protection Agency, Office of Policy Analysis, Climate Change Division.

EPA (U.S. Environmental Protection Agency). 2008. Trees and vegetation. In Reducing urban heat islands: compendium of strategies. www.epa.gov/sites/default/files/2017-05/documents/reducing_urban_heat_islands_ch_2.pdf.

Escobedo, F.J., and D.J. Nowak. 2009. Spatial heterogeneity and air pollution removal by an urban forest. Landscape and Urban Planning 90:102–110.

Escobedo, F.J., J.E. Wager, D.J. Nowak, C. Luz de la Maza, M. Rodriguez, and D.E. Crane. 2008. Analyzing the cost effectiveness of Santiago, Chile's policy of using urban forests to improve air quality. Journal of Environmental Management 86:148–157.

Fagan, L., S. Bithell, M. Dick, K.J. Fourd, A.I. Popay, and S.M. Zydenbos. 2008. Systems for identifying invasive threats to New Zealand flora by using overseas plantings of New Zealand plants. Pages 51–62 in K.J. Froud, A.I. Popay, and S.M. Zydenbos, editors.

Surveillance for biosecurity: pre-border to pest management. New Zealand Plant Protection Society, Hastings, New Zealand. nzpps.org/book/surveillance-for-biosecurity-pre-border-to-pest-management/.

Fahrner, S.J., M. Abrahamson, R.C. Venette, and B.H. Aukema. 2017. Strategic removal of host trees in isolated, satellite infestations of emerald ash borer can reduce population growth. Urban Forestry & Urban Greening 24:184–194.

Frank, S.D., and M.G. Just. 2020. Can cities activate sleeper species and predict future forest pests? A case study of scale insects. Insects 11:142. https://doi.org/10.3390/insects11030142.

Freer-Smith, P.H., A.A. El-Khatib, and G. Taylor. 2004. Capture of particulate pollution by trees: a comparison of species typical of semi-arid areas (*Ficus nitida* and *Eucalyptus globulus*) with European and North American species. Water, Air, and Soil Pollution 155:173–187.

Fuller, R.A., K.N. Irvine, P. Devine-Wright, P.H. Warren, and K.J. Gaston. 2007. Psychological benefits of greenspace increase with biodiversity. Biology Letters 3:390–394.

Gómez-Muñoz, V.M., M.A. Porta-Gándara, and J.L. Fernández. 2010. Effect of tree shades in urban planning in hot-arid climatic regions. Landscape and Urban Planning 94:149–157.

Goodrich, B., M. Fischer, and C. Buhl. 2023. Western redcedar dieback. tinyurl.com/WRCStorymap.

Guo, A., J. Yang, X. Xiao, J. Xia, C. Jin, and X. Li. 2020. Influences of urban spatial form on urban heat island effects at the community level in China. Sustainable Cities and Society 53:101972. https://doi.org/10.1016/j.scs.2019.101972.

Hautala, L. 2024. As the climate changes, cities scramble to find trees that will survive. Grist. grist.org/agriculture/climate-change-tree-urban-city-arborists-heat-drought-native-species/.

Heisler, G.M., S. Grimmond, R.H. Grant, and C. Souch. 1994. Investigation of the influence of Chicago's urban forests on wind and air temperature within residential neighborhoods. Pages 19–40 in E.G. McPherson, D.J. Nowak, and R.A. Rowntree, editors. Chicago's urban forest ecosystem: results of the Chicago urban forest climate project. General Technical Report NE-186. U.S. Department of Agriculture, Forest Service, Northeastern Forest Experiment Station, Radnor, Pennsylvania. www.fs.usda.gov/psw/topics/urban_forestry/products/cufr_188_gtr186a.pdf.

Hibbard, K.A., F.M. Hoffman, D. Huntzinger, and T.O. West. 2017. Changes in land cover and terrestrial biogeochemistry. Pages 277–302 in D.J. Wuebbles, D.W. Fahey, K.A. Hibbard, D.J. Dokken, B.C. Stewart, and T.K. Maycock, editors. Climate science special report: Fourth National Climate Assessment, volume I. U.S. Global Change Research Program, Washington, D.C. https://doi.org/10.7930/J0416V6X.

Hsu, A., G. Sheriff, T. Chakraborty, and D. Manya. 2021. Disproportionate exposure to urban heat island intensity across major US cities. Nature Communications 12:2721. https://doi.org/10.1038/s41467-021-22799-5.

Hudgins, E.J., F.H. Koch, M.J. Ambrose, and B. Leung. 2022. Hotspots of pest-induced US urban tree death, 2020–2050. Journal of Applied Ecology 59:1302–1312.

Jesdale, B.M., R. Morello-Frosch, and L. Cushing. 2013. The racial/ethnic distribution of heat risk-related land cover in relation to residential segregation. Environmental Health Perspectives 121:811–817.

Jung, M.C., M.G. Yost, A.L. Dannenberg, K. Dyson, and M. Alberti. 2024. Legacies of redlining lead to unequal cooling effects of urban tree canopy. Landscape and Urban Planning 246:105028. https://doi.org/10.1016/j.landurbplan.2024.105028.

Khan, T., and M. Conway. 2020. Vulnerability of common urban forest species to projected climate change and practitioners perceptions and responses. Environmental Management 65:534–

547.

Khedive, E., A. Shirvany, M.H. Assareh, and T.D. Sharkey. 2017. In situ emission of BVOCs by three urban woody species. Urban Forestry & Urban Greening 21:153–157.

Kumar, P., et al. 2024. Urban heat mitigation by green and blue infrastructure: drivers, effectiveness, and future needs. The Innovation 5:100588. https://doi.org/10.1016/j.xinn.2024.100588.

Leng, S., R. Sun, X. Yang, and L. Chen. 2023. Global inequities in population exposure to urban greenspaces increased amidst tree and nontree vegetation cover expansion. Communications Earth & Environment 4:464. https://doi.org/10.1038/s43247-023-01141-5.

Maia-Silva, D., R. Kumar, and R. Nateghi. 2020. The critical role of humidity in modeling summer electricity demand across the United States. Nature Communications 11:1686. https://doi.org/10.1038/s41467-020-15393-8.

Meftaul, I.M., K. Venkateswarlu, R. Dharmarajan, P. Annamalai, and M. Megharaj. 2020. Pesticides in the urban environment: a potential threat that knocks at the door. Science of the Total Environment 711:134612. https://doi.org/10.1016/j.scitotenv.2019.134612.

Mentaschi, L., G. Duveiller, G. Zulian, C. Corbane, M. Pesaresi, J. Maes, A. Stocchino, and L. Feyen. 2022. Global long-term mapping of surface temperature shows intensified intra-city urban heat island extremes. Global Environmental Change 72:102441. https://doi.org/10.1016/j.gloenvcha.2021.102441.

Methorst, J., A. Bonn, M. Marselle, K. Böhning-Gaese, and K. Rehdanz. 2021. Species richness is positively related to mental health—a study for Germany. Landscape and Urban Planning 211:104084. https://doi.org/10.1016/j.ecolecon.2020.106917.

Nowak, D.J., D.E. Crane, and J.C. Stevens. 2006. Air pollution removal by urban trees and shrubs in the United States. Urban Forestry and Urban Greening 4:115–123.

Nowak, D.J., and E.J. Greenfield. 2018. Declining urban and community tree cover in the United States. Urban Forestry & Urban Greening 32:32–55.

NSC (National Safety Council). 2024. Weather-related deaths and injuries. injuryfacts.nsc.org/home-and-community/safety-topics/weather-related-deaths-and-injuries/.

Obringer, R., R. Nateghi, D. Maia-Silva, S. Mukherjee, V. CR, D.B. McRoberts, and R. Kumar. 2022. Implications of increasing household air conditioning use across the United States under a warming climate. Earth's Future 10:e2021EF002434. https://doi.org/10.1029/2021EF002434.

Park, Y., J. Guldmann, and D. Liu. 2021. Impacts of tree and building shades on the urban heat island: combining remote sensing, 3D digital city and spatial regression approaches. Computers, Environment and Urban Systems 88:101655. https://doi.org/10.1016/j.compenvurbsys.2021.101655.

Park, Y., Z. Qunshan, J.M. Guldmann, and E.A. Wentz. 2023. Quantifying the cumulative cooling effects of 3D building and tree shade with high resolution thermal imagery in a hot arid urban climate. Landscape and Urban Planning 240:104874. https://doi.org/10.1016/j.landurbplan.2023.104874.

Powe, N.A., and K.G. Willis. 2004. Mortality and morbidity benefits of air pollution ($SO_2$ and $PM_{10}$) absorption attributable to woodland in Britain. Journal of Environmental Management 70:119–128.

Rahman, M.A., L.M. Stratopoulos, A. Moser-Reischl, T. Zölch, K.H. Häberle, T. Rötzer, H. Pretzsch, and S. Pauleit. 2020. Traits of trees for cooling urban heat islands: a meta-analysis. Building and Environment 170:106606. https://doi.org/10.1016/j.buildenv.2019.106606.

Rantzoudi, E.C., and J.N. Georgi. 2017. Correlation between the geometrical characteristics of

streets and morphological features of trees for the formation of tree lines in the urban design of the city of Orestiada, Greece. Urban Ecosystems 20:1081–1093.

Raupp, M.J., J.J. Holmes, C. Sadof, P. Shrewsbury, and J.A. Davidson. 2001. Effects of cover sprays and residual pesticides on scale insects and natural enemies in urban forests. Journal of Arboriculture 27:203–214.

Romanello, M., et al. 2022. The 2022 report of the Lancet countdown on health and climate change: health at the mercy of fossil fuels. The Lancet 400:1619–1654.

Sanusi, R., D. Johnstone, P. May, and S.J. Livesley. 2016. Street orientation and side of the street greatly influence the microclimatic benefits street trees can provide in summer. Journal of Environmental Quality 45:167–174.

Scott, K., J. Simpson, and E. McPherson. 1999. Effects of tree cover on parking lot microclimate and vehicle emissions. Journal of Arboriculture 25:129–142.

Spronken-Smith, R.A., and T.R. Oke. 1999. Scale modeling of nocturnal cooling in urban parks. Boundary-Layer Meteorology 93:287–312.

Tabassum, S., A. Manea, and M.R. Leishman. 2024. Limiting the impact of insect pests on urban trees under climate change. Urban Forestry & Urban Greening 94:128246. https://doi.org/10.1016/j.ufug.2024.128246.

Townsend, J.B., T.W. Ilvento, and S.S. Barton. 2016. Exploring the relationship between trees and human stress in the urban environment. Arboriculture & Urban Forestry 42:146–159.

Tubby, K.V., and J.F. Webber. 2010. Pests and diseases threatening urban trees under a changing climate. Forestry 83:451–459.

Turbelin, A.J., et al. 2022. Introduction pathways of economically costly invasive alien species. Biological Invasions 24:2061–2079.

Vogt, J., R.J. Hauer, and B.C. Fischer. 2015. The costs of maintaining and not maintaining the urban forest: a review of the urban forestry and arboriculture literature. Arboriculture & Urban Forestry 41:293–323.

Wei, D., C. Cao, A. Karambelas, J. Mak, A. Reinmann, and R. Commane. 2024. High-resolution modeling of summertime biogenic isoprene emissions in New York City. Environmental Science & Technology 58:13783–13794.

Winbourne, J.B., T.S Jones, S.M Garvey, J.L Harrison, L. Wang, D. Li, P.H Templer, and L.R. Hutyra. 2020. Tree transpiration and urban temperatures: current understanding, implications, and future research directions. BioScience 70:576–588.

WMO (World Meteorological Organization). 2023. State of climate services for health. WMO-No. 1335. library.wmo.int/idurl/4/68500.

Wolf, K.L., S.T. Lam, J.K. McKeen, G.R.A. Richardson, M. van den Bosch, and A.C. Bardekjian. 2020. Urban trees and human health: a scoping review. Internation Journal of Environmental Resources and Public Health 17:4371. https://doi.org/10.3390/ijerph17124371.

# Public Health

Climate change increasingly affects the health of humans and other animals and the capacity of health care systems. The resulting economic burden to individuals and society can be considerable. Furthermore, exposure to health hazards and potential to prepare for and recover from adverse health outcomes is unequally and inequitably distributed (Romanello et al. 2022).

The three contributions in this section explore the range of responses of animal and human health to climate change and climate-related extreme events. Williams and Beechler concentrate on infectious disease in animals and potential transmission of disease from animals to humans. As they explain, compounded changes in climate and land use and growth of the human population increase the risk that novel pathogens will be transmitted into humans from species that did not evolve in close proximity to people (Barr-Massada et al. 2014, Plowright et al. 2017) and that human exposure to endemic pathogens will increase (García-Peña and Rubio 2024).

Hommel et al. present an innovative evaluation of connections among accelerating climate change, effects of wildfire smoke on population health, and the associated economic and quality-of-life costs in Oregon. They address a range of short-term health outcomes emblematic of a holistic understanding of human health, from mortality to asthma to depressive symptoms. Their estimates consider projected changes not only in the frequency of smoke days, but in the number and age distribution of people across Oregon. Population estimates drove significant differences in the projected number of health events between the early and mid-twenty-first century.

Although droughts are not generally perceived as health threats, the associations between droughts and negative health outcomes are established. As Lookadoo notes in the third contribution in this section, over the last century, drought events have caused more deaths worldwide than floods, hurricanes, or any other climate-related extreme event (WMO 2021). Furthermore, agricultural and migrant workers in particular have increased rates of mental health stress during and after drought events. Lookadoo offers evidence-based suggestions for effective drought preparedness and mitigation efforts that can reduce the negative health impacts to individuals and communities.

## Literature Cited

Barr-Massada, A., V.C. Radeloff, and S.I. Stewart. 2014. Biotic and abiotic effects of human settlements in the wildland-urban interface. BioScience 64:429–437.

García-Peña, G.E., and A.V. Rubio. 2024. Unveiling the impacts of land use on the phylogeography of zoonotic New World Hantaviruses. Ecography 10:e06996. https://doi.org/10.1111/ecog.06996.

Plowright, R.K., et al. 2024. Ecological countermeasures to prevent pathogen spillover and subsequent pandemics. Nature Communications 15:2577. https://doi.org/10.1038/s41467-024-46151-9.

Romanello, M., et al. 2022. The 2022 report of the Lancet Countdown on health and climate change: health at the mercy of fossil fuels. The Lancet 400:1619–1654.

WMO (World Medical Organization). 2021. WMO atlas of mortality and economic losses from weather, climate and water extremes 1970–2019. library.wmo.int/doc_num.php?explnum_id=10902.

# Effects of Climate Change on Transmission of Infectious Disease from Animals to Humans

Kurt Williams and Brianna Beechler

## Introduction

Discussion of the impacts of major climate-related natural hazards in Oregon usually emphasizes their effects on humans, particularly on human health, social and cultural well-being, and the economy. Less well appreciated is the impact of climate change on Oregon's animals, particularly with respect to infectious diseases. Not only do infectious diseases threaten conservation of wild animals, but diseases can spill over from wild animals into people, causing outbreaks or pandemics. The concept of One Health and the disease triad (Figure 1) recognizes that disease expression in individual organisms reflects connections among the host, the infectious disease agent, and the environment (Shaheen 2022).

Climate change likely will impact all taxonomic groups of animals. Their responses to diseases that are affected by climate change will be equally diverse, reflecting their biology and the biology of their pathogens. Humans' dependence on other species for health and well-being is often invisible, and sometimes forgotten. The effects of climate change on other animals and their diseases can directly impact human health, well-being, and livelihoods. Climate change also can create or increase social, economic, and environmental stressors that can make humans more susceptible to disease (Guégan et al. 2024).
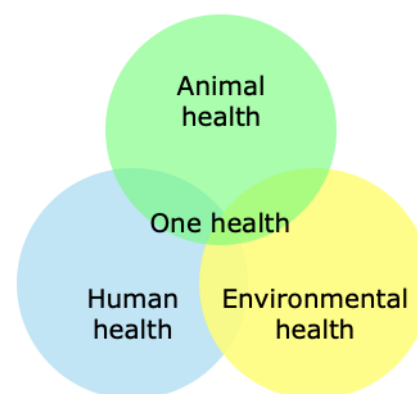


**Figure 1.** The One Health disease triad.

## Climate Change and Zoonotic Disease

Zoonotic diseases, infectious diseases transmitted to humans from other animal species, have been a feature of humans' existence throughout their evolution (Karesh et al. 2012). The COVID-19 pandemic exemplifies the intersection among animals, infectious disease, and climate change (Gupta et al. 2021). Although the animal species that transmitted SARS-CoV-2 (the virus that causes COVID-19) to humans has not been definitively established, there is wide agreement that this coronavirus originated in bats (Andersen et al. 2020).

Is COVID-19 simply another member of the large set of zoonotic diseases that have arisen over millennia, or does its emergence reflect anthropogenic climate change, human population growth, and changes in land use patterns in the twenty-first century? Changes in the environment linked to climate change, such as deforestation, industrialization, changes in humidity, air and water pollution, and increasing temperatures, contribute to spillover in general (Pfenning-Butterworth et al. 2024, Plowright et al. 2024) and may have contributed to the spillover of the progenitor of SARS-CoV-2 from bats into the wildlife trade (Gupta et al. 2021, Rulli et al. 2021).

A community of microbes (bacteria, viruses, and parasites) lives in and on the bodies of animals. Most microbes do not cause disease, and many are essential for maintaining the health of their animal hosts (Hou et al. 2022). Although an estimated 10,000 extant virus species theoretically may be able to infect humans (Carlson et al. 2019), about 270 are known to have done so. In the rare

cases in which these microbes move from the host species into humans, as did SARS-CoV-2 in 2019, they can have deleterious effects (Plowright et al. 2017, Hao et al. 2022). If global climate was relatively stable and human-caused fragmentation of wildlands minimal, opportunities for spillover into humans might remain uncommon. Worldwide, however, growth of the human population and expansion of the wildland-urban interface increases the risk that novel pathogens will be transmitted into humans from species that did not evolve in close proximity to people (Barr-Massada et al. 2014), or that human exposure to endemic pathogens will increase (García-Peña and Rubio 2024).

Additionally, animals may be threatened by diseases as a consequence of their exposure to novel pathogens from other species (Carlson et al. 2022). For example, in Oregon and many other western states, bighorn sheep (*Ovis canadensis*) acquired the pathogen *Mycoplasma ovipneumoniae* from domestic ruminants, such as sheep and goats. The pathogen causes respiratory disease in bighorn sheep, leading to extensive illness and death in that species (Rudolph et al. 2007, Besser et al. 2021).

Climate change may affect bighorn sheep through changes in water availability, forage quality, and migration patterns (Creech et al. 2016, 2020), increasing their susceptibility to diseases such as *M. ovipneumoniae*. For instance, the survival of bighorn sheep in southeastern Oregon is linked to decreases in their immune function and increased susceptibility to *M. ovipneumoniae* in selenium-deficient individuals (Spaan et al. 2021, Tsuchida et al. 2024). The selenium content of plants on which bighorn sheep forage is likely to decrease as climate changes and the distribution and density of non-native invasive plants increases (Jones et al. 2017). The severity of disease in bighorn sheep challenges Oregon's efforts to reestablish the species in the state after its extirpation in the twentieth century (USFWS 2021).

Most animal species are mobile for at least part of their life, and some species migrate seasonally to access food, avoid predation, and reproduce. Climate change is altering the timing and occurrence of migration in many species (Seebacher and Post 2015). Migration and climate-induced movements of animals may facilitate novel zoonotic diseases through virus sharing between species (Carlson et al. 2022). Increases in local density of animals as a result of resource scarcity or habitat loss also can facilitate outbreaks of disease (Plowright et al. 2024). Movement of viruses from other species into humans is expected to be most prevalent in regions of high species richness and high human population density, such as some areas in tropical Africa and Asia. But, as COVID-19 and previous pathogens demonstrated, novel diseases can rapidly spread worldwide, regardless of their geographic origin, after infecting people. Novel zoonotic viruses are not restricted to the tropics. In 2015, a resident of Alaska was diagnosed with a new poxvirus, a virus distantly related to smallpox, the host species of which are rodents and shrews (Gigante et al. 2019). The first human fatality associated with this virus occurred in February 2024, after the person acquired the virus from being scratched by a cat that apparently carried the virus on its claws following predation of an infected host species (Dyer 2024).

As climate changes, it is likely that the ranges or behavior of hosts will change, increasing the risk of spillover of diseases to which human exposure previously was limited and that were more geographically constrained. For instance, Ebola virus likely was restricted to wild animals until changes in land use and vegetation cover, such as fragmentation of tropical forests, increased contact between its animal hosts and humans (Ruli et al. 2017). Although not a risk to humans, a novel blood-borne parasite recently was identified in a population of Marbled Murrelet (*Brachyramphus marmoratus*), a seabird listed as endangered under the U.S. Endangered Species Act, off the Oregon Coast. Emergence of the parasite, which may inhibit recovery of the species, may be emerging as

a consequence of regional forest fragmentation (Michlanski and Beechler unpublished data). It is unknown whether other infectious diseases that pose risks to humans are present in Oregon's wildlife species or are likely to emerge in these species as changes in climate and land use lead to changes in species' distributions and interactions.
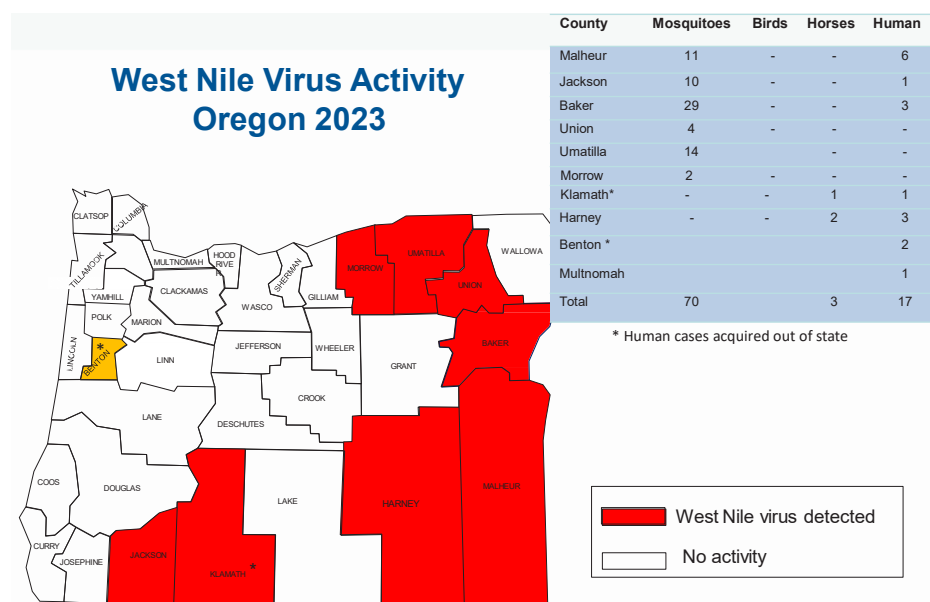
## Climate Change and Vector-Borne Disease

Terrestrial vector-borne diseases—viral, bacterial and parasitic diseases transmitted through an infected, blood-feeding tick, flea, louse, mosquito, midge, sandfly, black fly, tsetse fly, or triatomine bug—are a major global public health threat. More than six billion people, including people in Oregon, are at risk of vector-borne diseases. Over 300 million cases of vector-borne disease occur every year, with more than 700,000 people dying from such diseases annually (World Health Organization 2020). The Intergovernmental Panel on Climate Change concluded with high confidence that vector-borne diseases have become more prevalent because of higher global temperatures and changes in land use and land cover (IPCC 2022).

Vectors of infectious disease are ectothermic (sometimes called cold-blooded) animals, unable to regulate their body temperatures. Therefore, vector-borne diseases are most common in the tropics and warmer regions where environmental conditions favor the propagation and blood-feeding activity of vectors (de Souza and Weaver 2024). But the concept that a warmer planet inextricably leads to greater incidence of vector-borne diseases is overly simplistic and does not recognize the considerable variation in physiology of vectors and pathogens (Thompson and Stanberry 2022). For example, the relatively low optimal temperature for transmission of malaria means that the distribution of malaria may shift rather than expand (Mordecai et al. 2013). By contrast, the relatively high optimal temperature for transmission of dengue may lead to widespread expansion of this disease (Mordecai et al. 2017). Indeed, depending on their capacity to adapt, some vectors may lose the ability to carry certain pathogens or acquire new pathogens along with new reservoir species (animals or plants in which the vector-borne disease pathogen survives and from which it can be transmitted to other organisms) (Casadevall 2020). The Intergovernmental Panel on Climate Change assigned medium to high confidence to the likelihood that dengue, West Nile and chikunguya viruses, and lyme disease will become more of a threat in North America (IPCC 2022).

West Nile virus has been present in Oregon for



### West Nile Virus Activity Oregon 2023

| County | Mosquitoes | Birds | Horses | Human |
|---|---|---|---|---|
| Malheur | 11 | - | - | 6 |
| Jackson | 10 | - | - | 1 |
| Baker | 29 | - | - | 3 |
| Union | 4 | - | - | - |
| Umatilla | 14 | - | - | - |
| Morrow | 2 | - | - | - |
| Klamath* | - | - | 1 | 1 |
| Harney | - | - | 2 | 3 |
| Benton * | | | | 2 |
| Multnomah | | | | 1 |
| Total | 70 | | 3 | 17 |

\* Human cases acquired out of state

West Nile virus detected

No activity

**Figure 2.** Counties in Oregon in which West Nile virus was detected in 2023 and the number of detections of the virus in four taxonomic groups. Source: Oregon Health Authority.

decades. Surveillance efforts by the Oregon Health Authority in partnership with local public health agencies, mosquito control districts, and the Oregon Veterinary Diagnostic Laboratory at Oregon State University track and report the incidence of the virus in the state. In 2023, West Nile virus was detected in 70 groups of mosquitoes, three horses, and ten humans (Figure 2) (OHA 2024). Increases in seasonal temperatures associated with climate change and increases in the size of the human population were implicated in the expansion of West Nile virus across Europe (Erazo et al. 2024). Ongoing and projected changes in temperature, precipitation, relative humidity, and wind affect replication of the virus within mosquitoes; interactions among pathogens, vectors, and hosts; and the population dynamics and distributions of mosquitoes (Paz 2015).

Dengue is caused by several viruses in the Flaviviridae family (Kahn et al. 2023). The disease is not currently established in the United States. The Pan American Health Organization noted that the number of dengue cases in the first half of 2024 was greater than the maximum number of cases previously recorded in a full year (Pan American Health Organization 2024). This reality led the Centers for Disease Control and Prevention to issue a dengue health advisory to public health officials in the United States in 2024 (CDC 2024). The primary vectors of dengue transmission to humans are the mosquitos *Aedes aegypti* and, to a much lesser extent, *Aedes albopictus* (Kahn et al. 2023). *Aedes aegypti* is not native to the United States. However, following its inadvertent introduction to the country, it is now established in at least 23 states, including California.

Modeling by the Centers for Disease Control and Prevention characterized the establishment of *A. aegypti* and *A. albopictus* as unlikely to very unlikely in Oregon and unlikely to very likely in far northern California (CDC 2017)
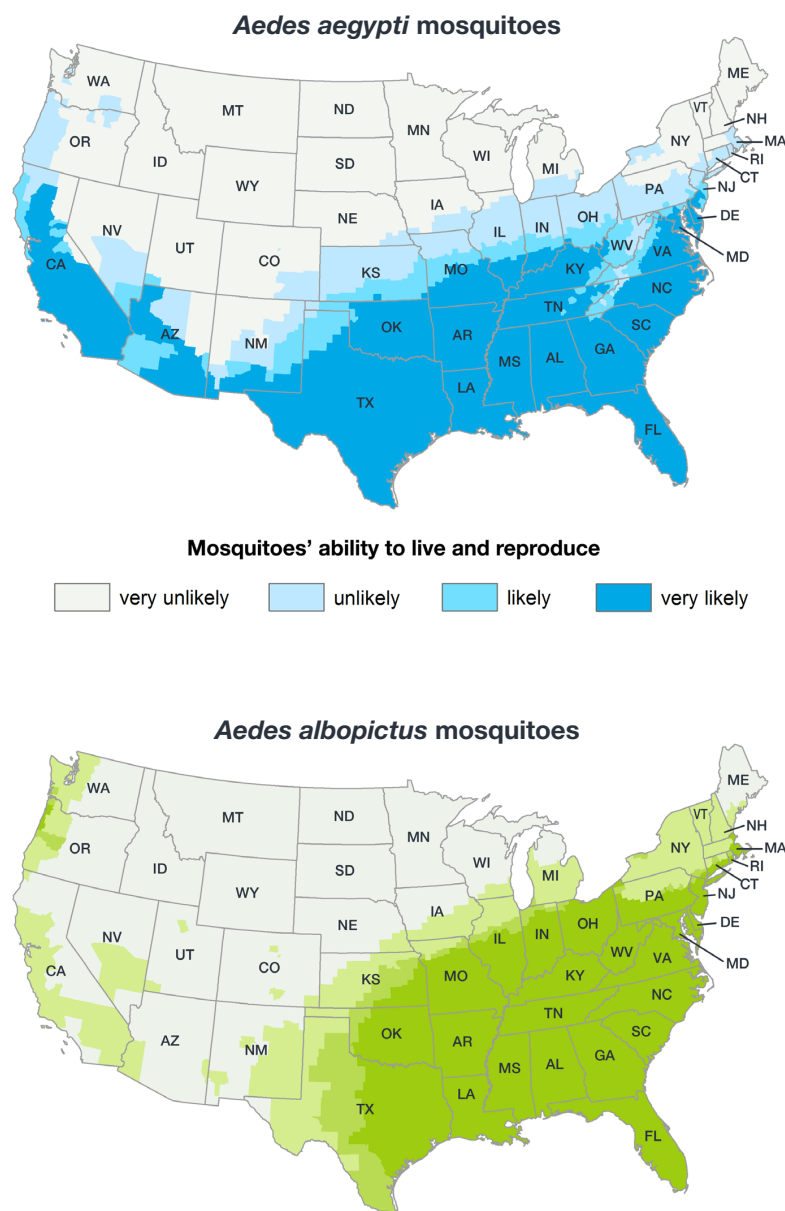


**Figure 3.** Potential ranges of *Aedes aegypti* and *A. albopictus* in the United States as of 2017. Source: U.S. Centers for Disease Control and Prevention

236

(Figure 3). However, *A. aegypti* was discovered on 23 July 2024 in Talent, Oregon (JCVC 2024). As Oregon's climate continues to warm, it's reasonable to expect continued and wider establishment in the state of mosquitoes capable of serving as vectors for viruses that cause dengue, yellow fever, chikungunya, and zika (although see Aliaga-Samanez et al. 2024).

## Climate Change and Highly Pathogenic Avian Influenza Virus

The highly pathogenic avian influenza (HPAI) virus that reemerged in 2021 in wild birds and is spilling over into mammals, including marine species, domestic livestock, and humans, may in part be exacerbated by the effects of climate change (Charostad et al. 2023, Prosser et al. 2023). The genes for pathogenicity of this virus likely evolved in domestic poultry and were transmitted globally by migratory birds (Xie et al. 2023), which were exposed to the virus in the feces of poultry (Charostad et al. 2023). Since February 2022, nearly 100 million domestic poultry have been affected by HPAI, causing severe economic impacts to farmers and consumers in the United States (USDA 2024c). In contrast, the same virus causes no or mild disease when living in the intestines of its natural hosts, primarily waterfowl and especially dabbling ducks, such as American Wigeons (*Mareca americana*), Mallards (*Anas platyrhynchos*), and Northern Pintails (*Anas acuta*).

In the past, HPAI was not known to affect wild bird species. Significant mortality in wild species not historically affected by HPAI, such as colonially nesting seabirds and waterbirds, has been documented in the current epizootic (epidemic in animals) (Ramey et al. 2021). HPAI may also jeopardize conservation of the highly endangered California Condor (*Gymnogyps californianus*), which has experienced significant mortality from HPAI. The threat of the virus led the U.S. Fish and Wildlife Service to attempt vaccination of California Condors (USFWS 2024). The Yurok Tribe is coordinating ongoing efforts to reintroduce the culturally significant species (prey-go-neesh in the Yurok language) into Redwood National and State Parks, which are Yurok lands, in northern California (The Yurok Tribe 2023). The potential effect of HPAI on the reintroduction effort is unclear.

Climate change has been implicated in the movement of HPAI into domestic poultry and wild birds (Ramey et al. 2021, Prosser et al. 2023). Climate-

| Species | Suspect cases | Positive |
|---|---|---|
| Cow (*Bos taurus*) | | |
|     Beef cow | 2 | 0 |
|     Dairy cow (milk sample) | 211* | 0 |
|     Dairy cow (tissue sample) | 3 | 0 |
| Domestic goat (*Capra hircus*) | 5 | 0 |
| Llama (*Lama glama*) | 1 | 0 |
| Mule deer (*Odocoileus hemionus*) | 1 | 0 |
| Domestic pig (*Sus scrofa domesticus*) | 7 | 0 |
| Domestic dog (*Canis lupus familiaris*) | 3 | 0 |
| Gray wolf (*Canis lupus*) | 1 | 0 |
| Coyote (*Canis latrans*) | 1 | 0 |
| Gray fox (*Urocyon cinereoargenteus*) | 8 | 0 |
| Red fox (*Vulpes vulpes*) | 3 | 1 |
| Domestic cat (*Felis catus*) | 21 | 3 |
| Striped skunk (*Mephitis mephitis*) | 17 | 12 |
| Sea otter (*Enhydra lutris*) | 1 | 0 |
| North American river otter (*Lontra canadensis*) | 1 | 0 |
| American marten (*Martes americana*) | 2 | 1 |
| Domestic ferret (*Mustela putorius furo*) | 1 | 0 |
| Steller sea lion (*Eumetopias jubatus*) | 10 | 0 |
| California sea lion (*Zalophus californianus*) | 44 | 0 |
| Raccoon (*Procyon lotor*) | 6 | 1 |
| Virginia opossum (*Didelphis virginiana*) | 1 | 0 |
| Brown rat (*Rattus norvegicus*) | 2 | 0 |
| Western gray squirrel (*Sciurus griseus*) | 1 | 0 |

**Table 1.** Number of mammal species tested for highly pathogenic avian influenza (HPAI) in Oregon as of 30 September 2024 and number of individuals that were positive for the virus. Source: Oregon Veterinary Diagnostic Laboratory, Oregon State University.

induced changes in bird migration, and human-caused destruction of wetlands globally, has been linked to its current worldwide spread (Prosser et al. 2023). Extreme climate change-related events such as drought, heat, and wildfires are associated with behavioral and physiological responses in animals conducive to increased risk from infectious diseases such as HPAI (Altizer et al. 2013).

Influenza viruses have an ignominious reputation for their propensity to evolve into pandemic pathogens. The most globally lethal influenza pandemic, which occurred in 1918, killed an estimated 50 million people (National Archives and Records Administration 2024). HPAI has infected and occasionally killed many species of mammals in the United States. To date more than 20 species have been infected, including dairy cattle (USDA 2024a,b).

Mammals in Oregon have been infected with and died from HPAI. As of late September 2024, the Oregon Veterinary Diagnostic Laboratory at Oregon State University had performed 353 tests for HPAI on samples from 22 species of mammals (Table 1). At that time, 18 mammals representing four wild species (red fox, marten, racoon, skunk) and three domestic cats died from infection with the HPAI virus in Oregon.

There is speculation that climate change will become the primary anthropogenic driver of cross-species transmission of viruses, including zoonotics (Carlson et al. 2022). While HPAI is not considered an imminent pandemic risk, scientists continue to monitor its spread into mammals, including humans. Infectious diseases in Oregon's animals will continue to evolve in the face of climate change. There's every reason to believe such diseases will significantly impact animals, human health, social and cultural values, and the economy.

## Literature Cited

Aliaga-Samanez, A., D. Romero, K. Murray, M. Cobos-Mayo, M. Segura, R. Real, and J. Olivero. 2024. Climate change is aggravating dengue and yellow fever transmission risk. Ecography 10:e06942. https://doi.org/10.1111/ecog.06942.

Altizer, S., R.S. Ostfeld, P.T.J. Johnson, S. Kutz, and C.D. Harvell. 2013. Climate change and infectious diseases: from evidence to a predictive framework. Science 341:514–519.

Andersen, K.G., A. Rambaut, W.I. Lipkin, E.C. Holmes, and R.F. Garry. 2020. The proximal origin of SARS-CoV-2. Nature Medicine 26:450–452.

Barr-Massada, A., V.C. Radeloff, and S.I. Stewart. 2014. Biotic and abiotic effects of human settlements in the wildland-urban interface. BioScience 64:429–437.

Besser, T.E., E.F. Cassirer, A. Lisk, D. Nelson, K.R. Manlove, P.C. Cross, and J.T. Hogg. 2021. Natural history of a bighorn sheep pneumonia epizootic: source of infection, course of disease, and pathogen clearance. Ecology and Evolution 11:14366–14382.

Carlson, C.J., G.F. Albery, C. Merow, C.H. Trisos, C.M. Zipfel, E.A. Eskew, K.J. Olival, N. Ross, and S. Bansal. 2022. Climate change increases cross-species viral transmission risk. Nature 607:555–562.

Carlson, C.J., C.M. Zipfel, R. Garnier, and S. Bansal. 2019. Global estimates of mammalian viral biodiversity accounting for host sharing. Nature Ecology and Evolution 3:1070–1075.

Casadevall, A. 2020. Climate change brings the specter of new infectious diseases. The Journal of Clinical Investigation 130:553–555.

CDC (Centers for Disease Control and Prevention). 2017. Estimated potential range of *Aedes aegypti* and *Aedes albopictus* in the United States, 2017. www.cdc.gov/mosquitoes/pdfs/Aedes-mosquito-maps.pdf.

CDC (U.S. Centers for Disease Control and Prevention). 2024. Increased risk of dengue virus infections in the United States. emergency.cdc.gov/han/2024/han00511.asp.

Charostad, J., J.R.Z. Rukerd, S. Mahmoudvand, D. Bashash, S.M.A. Hashemi, M. Nakhaie, and K. Zandi. 2023. A comprehensive review of highly pathogenic avian influenza (HPAI) H5N1: an imminent threat at doorstep. Travel Medicine and Infectious Disease 55:102638. https://doi.org/10:1016/j.tmaid.2023.102638.

Creech, T.G., C.W. Epps, R.J. Monello, and J.D. Wehausen. 2016. Predicting diet quality and genetic diversity of a desert-adapted ungulate with NDVI. Journal of Arid Environments 127:160–170.

Creech, T.G., C.W. Epps, J.D. Wehausen, R.S. Crowhurst, J.R. Jaeger, K. Longshore, B. Holton, W.B. Sloan, and R.J. Monello. 2020. Genetic and environmental indicators of climate change vulnerability for desert bighorn sheep. Frontiers in Ecology and Evolution 8:279. https://doi.org/10.3389/fevo.2020.00279.

de Souza, W.M., and S.C. Weaver. 2024. Effects of climate change and human activities on vector-borne diseases. Nature Reviews Microbiology 22:476–491.

Dyer, O. 2024. Alaskapox: first human death from zoonotic virus is announced. The BMJ 384:q415. https://doi.org/10.1136/bmj.q415.

Erazo, D., et al. 2024. Contribution of climate change to the spatial expansion of West Nile virus in Europe. Nature Communications 15:1196. https://doi.org/10.1038/s41467-024-45290-3.

Fleishman, E., editor. 2023. Sixth Oregon climate assessment. Oregon Climate Change Research Institute, Oregon State University, Corvallis, Oregon. https://doi.org/10.5399/osu/1161.

García-Peña, G.E., and A.V. Rubio. 2024. Unveiling the impacts of land use on the phylogeography of zoonotic New World Hantaviruses. Ecography 10:e06996. https://doi.org/10.1111/ecog.06996.

Gigante, C.M., J. Gao, S. Tang, A.M. McCollum, K. Wilkins, M.G. Reynolds, W. Davidson, J. McLaughlin, V.A. Olson, and Y. Li. 2019. Genome of Alaskapox virus, a novel orthopoxvirus isolated from Alaska. Viruses 11:708. https://doi.org/10.3390/v11080708.

Guégan, J.-F., T. Poisot, B.A. Han, and J. Olivero. 2024. Disease ecology and pathogeography: changing the focus to better interpret and anticipate complex environment-host-pathogen interactions. Ecography 10:e07684. https://doi.org/10.1111/ecog.07684.

Gupta, S., B.T. Rouse, and P.P. Sarangi. 2021. Did climate change influence the emergence, transmission, and expression of the COVID-19 pandemic? Frontiers in Medicine 8:769208. https://doi.org/10.3389/fmed.2021.769208.

Hao, Y., Y. Wang, M. Wang, L. Zhou, J. Shi, J. Cao, and D. Wang. 2022. The orgins of COVID-19 pandemic: a brief overview. Transboundary and Emerging Diseases 69:3181–3197.

Hou, K. et al. 2022. Microbiota in health and disease. Signal Transduction and Targeted Therapy 7:135. https://doi.org/10.1038/s41392-022-00974-4.

IPCC (Intergovernmental Panel on Climate Change). Climate change 2022: impacts, adaptation and vulnerability. www.ipcc.ch/report/ar6/wg2/.

JCVC (Jackson County Vector Control). 2024. Public health advisory: *Aedes aegypti* mosquito. jcvcd.org/mosquito/aedes-aegypti/.

Jones, G.D., B. Droz, P. Greve, P. Gottschalk, D. Poffet, S.P. McGrath, S.I. Seneviratne, P. Smith, and L.H.E. Winkel. 2017. Selenium deficiency risk predicted to increase under future climate change. Proceedings of the National Academy of Sciences 114:2848–2853.

Kahn, M.B., Z. Yang, C. Lin, M. Hsu, A.N. Urbina, W. Assavalapsakul, W. Wang, Y. Chen, and S. Wang. 2023. Dengue overview: an updated systemic review. Journal of Infection and Public

Health 16:1625–1642.

Karesh, W.B., et al. 2012. Ecology of zoonoses: natural and unnatural histories. Lancet 380:1936–1945.

Mordecai, E.A., et al. 2013. Optimal temperature for malaria transmission is dramatically lower than previously predicted. Ecology Letters 16:22–30.

Mordecai, E.A., et al. 2017. Detecting the impact of temperature on transmission of Zika, dengue, and chikungunya using mechanistic models. PLoS Neglected Tropical Diseases 11:e0005568. https://doi.org/10.1371/journal.pntd.0005568.

National Archives and Records Administration. 2024. The deadly virus: the influenza epidemic of 1918. www.archives.gov/exhibits/influenza-epidemic/.

OHA (Oregon Health Authority) 2024. West Nile virus activity Oregon 2024. www.oregon.gov/oha/PH/DISEASESCONDITIONS/DISEASESAZ/WESTNILEVIRUS/Documents/countymap-current-year.pdf.

Pan American Health Organization. 2024. Epidemiological update—increase in dengue cases in the region of the Americas—18 June 2024. www.paho.org/en/documents/epidemiological-update-increase-dengue-cases-region-americas-18-june-2024.

Paz, S. 2015. Climate change impacts on West Nile virus transmission in a global context. Philosophical Transactions of the Royal Society of London B: Biological Sciences 370:1665. https://doi.org/10.1098/rstb.2013.0561.

Pfenning-Butterworth, A., L.B. Buckley, J.M. Drake, J.E. Farner, M.J. Farrell, A.M. Gehman, E.A. Mordecai, P.R. Stephens, J.L. Gittleman, and T.J. Davies. 2024. Interconnecting global threats: climate change, biodiversity loss, and infectious diseases. The Lancet Planetary Health 8:E270–E283. https://doi.org/10.1016/S2542-5196(24)0002104.

Plowright, R.K., C.R. Parrish, H. McCallum, P.J. Hudson, A.I. Ko, A.L. Graham, and J.O. Lloyd-Smith. 2017. Pathways to zoonotic spillover. Nature Reviews Microbiology 15:502–510.

Plowright, R.K., et al. 2024. Ecological countermeasures to prevent pathogen spillover and subsequent pandemics. Nature Communications 15:2577. https://doi.org/10.1038/s41467-024-46151-9.

Prosser, D.J., C.S. Teitelbaum, S. Yin, N.J. Hill, and X. Xiao. 2023. Climate change impacts on bird migration and highly pathogenic avian influenza. Nature Microbiology 8:2223–2225.

Ramey, A.M. et a. 2021. Highly pathogenic avian influenza is an emerging disease threat to wild birds in North America. Journal of Wildlife Management 86:e22171. https://doi.org/10.1002/jwmg.22171.

Rudolph, K.M., D.L. Hunter, R.B. Rimler, E.F. Cassirer, W.J. Foreyt, W.J. DeLong, G.C. Weiser, and A.C.S. Ward. 2007. Microorganism associated with a pneumonic epizootic in Rocky Mountain bighorn sheep (*Ovis canadensis canadensis*). Journal of Zoo and Wildlife Medicine 38:548–558.

Rulli, M.C., P. D'Odorico, N. Galli, and D.T.S. Hayman. 2021. Land-use change and the livestock revolution increase the risk of zoonotic coronavirus transmission from rhinolophid bats. Nature Food 2:409–416.

Rulli, M.C., M. Santini, D.T.S. Hayman, and P. D'Odorico. 2017. The nexus between forest fragmentation in Africa and Ebola virus disease outbreaks. Scientific Reports 7:41613. https://doi.org/10.1038/srep41613.

Seebacher, F., and E. Post. 2015. Climate change impacts on animal migration. Climate Change Responses 2:5. https://doi.org/10.1186/s40665-015-0013-9.

Shaheen, M.N.F. 2022. The concept of one health applied to the problem of zoonotic diseases.

Reviews in Medical Virology 32:e2326. https://doi.org/10.1002/rmv.2326.

Spaan, R.S., C.W. Epps, R. Crowhurst, D. Whittaker, M. Cox, and A. Duarte. 2021. Impact of *Mycoplasma ovipneumoniae* on juvenile bighorn sheep (*Ovis canadensis*) survival in the northern Basin and Range ecosystem. PeerJ 9:e10710. https://doi.org/10.7717/peerj.10710.

The Yurok Tribe. 2023. Date set for possible release of three condors. www.yuroktribe.org/post/date-set-for-possible-release-of-three-condors.

Thompson, M.C., and L.R. Stanberry. 2022. Climate change and vectorborne diseases. New England Journal of Medicine 387:1969–1978.

Tsuchida, D.Y., M.F. Gentzkow, R.S. Spaan, J. Burco, C.E. Couch, J.M. Spaan, C.W. Epps, and B.R. Beechler. 2024. Bighorn sheep (*Ovis canadensis*) with higher whole blood selenium levels have improved survival and altered immune responses. Journal of Wildlife Diseases 60:721–726.

USDA (United States Department of Agriculture). 2024a. Detections of highly pathogenic avian influenza (HPAI) in livestock. www.aphis.usda.gov/livestock-poultry-disease/avian/avian-influenza/hpai-detections/livestock.

USDA (United States Department of Agriculture). 2024b. Detections of highly pathogenic avian influenza in mammals. www.aphis.usda.gov/livestock-poultry-disease/avian/avian-influenza/hpai-detections/mammals.

USDA (United States Department of Agriculture). 2024c. Confirmations of highly pathogenic avian influenza in commercial and backyard flocks. www.aphis.usda.gov/livestock-poultry-disease/avian/avian-influenza/hpai-detections/commercial-backyard-flocks.

USFWS (United States Fish and Wildlife Service). 2021. Hart Mountain National Antelope Refuge final bighorn sheep management plan and environmental impact statement. www.fws.gov/media/hart-mountain-national-antelope-refuge-final-bighorn-sheep-management-plan-and-eispdf.

USFWS (United States Fish and Wildlife Service). 2024. California Condor recovery program. www.fws.gov/program/california-condor-recovery/southwest-california-condor-flock-hpai-information-updates-2023.

World Health Organization. 2020. Vector-borne diseases. www.who.int/news-room/fact-sheets/detail/vector-borne-diseases.

Xie, R., et al. 2023. The episodic resurgence of highly pathogenic avian influenza H5 virus. Nature 622:810–817.

# Scenarios of Wildfire Smoke Exposure, Health Impacts, and Associated Costs in Oregon during the Early and Mid-Twenty-First Century

Annie Hommel, Collin Peterson, Mariah O'Brien, and Nancy Hiner

## Introduction

The relation between anthropogenic climate change and growth in the frequency and sizes of wildfires in the western United States is increasingly evident. Warmer temperatures, altered precipitation patterns, and prolonged droughts contribute to drier landscapes and extended fire-weather seasons, increasing the likelihood of wildfires (Abatzoglou and Williams 2016, Westerling 2016). The surge in wildfire activity has elevated the risk of human exposure to airborne particles 2.5 micrometers or microns (μm) in diameter or smaller ($PM_{2.5}$, or fine particulate matter), which poses substantial human health risks (Liu et al. 2021, Rohlman et al. 2023). Exposure to wildfire smoke has been causally linked to exacerbation of respiratory illnesses and an increase in the number of cardiovascular emergencies, particularly among vulnerable populations and those with pre-existing health conditions (EPA 2021). Over the last decade, research on wildfire smoke exposure expanded to address diverse health outcomes.

This exploratory research aims to improve understanding of the connections among accelerating climate change, effects of wildfire smoke on population health, and the associated economic costs in Oregon. Our goal was to identify the best evidence available and construct state- and county-level scenarios for the early and mid-twenty-first century. Our analyses relied on the peer-reviewed literature and publicly available secondary data that we compiled through an extensive literature review. We sought to include a range of short-term outcomes emblematic of a holistic understanding of human health that accounts for wildfire-attributable smoke as both a proximal and a distal factor, quantifying impacts in economic terms and as quality-of-life loss.

## Concepts and Definitions

### Smoke Exposure

We relied on publicly available data from Liu et al. (2016) to model smoke exposure. Liu et al. (2016) simulated wildfire smoke with the GEOS-Chem chemical transport model, a global, three-dimensional atmospheric chemistry model driven by meteorological input from the Goddard Earth Observing System (GEOS) of the National Aeronautics and Space Administration (NASA). The authors validated surface $PM_{2.5}$ results from the GEOS-Chem simulations against particulate matter observed from the ground or aircraft (Liu et al. 2016). Climate models assumed the A1B emissions scenario: rapid economic growth, a peak in global population around the middle of the twenty-first century, considerable improvements in technology, and a fairly even mix of fossil fuels and other energy sources (IPCC 2000). In the early 2010s, the A1B scenario commonly was used in impact assessments in the U.S. Pacific Northwest (Snover et al. 2013). Air quality was expressed as the number of smoke wave days during two six-year time periods, one in the early twenty-first century (2004–2009) and one in the mid-twenty-first century (2046–2051) (Liu et al. 2016).

### Human Health Outcomes

We projected the cumulative number of health events over the two six-year periods across a range of short-term health outcomes attributable to wildfire smoke. We developed three scenarios.

Scenario A assumed early twenty-first century smoke wave days and population estimates. Scenario B assumed mid-twenty-first century smoke wave day projections and early twenty-first century population estimates. Scenario C assumed mid-twenty-first century smoke wave day projections and population estimates.

These three scenarios allowed us to evaluate how projected changes in wildfire smoke and population growth affect health outcomes. We used published values of cost and quality-of-life loss per health event to estimate economic loss and quality of life reduction. Scenario A serves as a baseline for the twenty-first century. Scenario B isolates the effects of climate change by keeping estimated population size constant. Scenario C may be more realistic given that it accounts for both climate change and shifts in state-level population size and age distribution. Collectively, the scenarios illustrate the range of potential effects of wildfire smoke on human health and associated costs over the next 25 years.

*Economic Costs*

We expressed economic loss as total charges and as costs related to a health event with data from the Healthcare Cost and Utilization Project (HCUP; www.ahrq.gov/data/hcup/index.html) and published values of cost per health event. We reported economic losses for emergency department visits with data from HCUP's 2019 Nationwide Emergency Department Sample (NEDS). Total charges are the amount that a hospital bills for a case. Costs are the expenses associated with providing care, such as wages, supplies, and utilities. Neither total charges nor costs are equal to the amount that a hospital receives in payment or that a patient pays (HCUP 2022). Costs better indicate the resources needed to provide care associated with a health event, whereas total charges may better reflect the cumulative expenses incurred by all parties, such as costs to healthcare providers, third-party payors, and patients, albeit in unknown proportions.

We used the U.S. Environmental Protection Agency's definition of the value of a statistical life to report the economic cost related to mortality. Value of a statistical life represents the amount an individual is willing to pay to reduce their risk of death from adverse health conditions. The value is derived from value-of-life studies that directly report willingness to pay by subjects of different ages. The Environmental Protection Agency advises against adjusting value of a statistical life on the basis of age (EPA 2023), so we used the same value for all adults (19 years of age and older) and older adults (65 years of age and older).

*Quality-of-Life Loss*

We expressed lost quality-of-life for each health event as lost quality-adjusted life years (QALYs). A QALY is a life year adjusted by utility values assigned to a given health state, where 1 is a year of life in perfect health and 0 is death (Prieto and Sacristán 2003). We used QALY loss values that were based on studies that measured differences in quality of life between healthy and disease states over a specified period of time. Because we focused on short-term outcomes of varying severity and relied on values in the literature rather than primary data collection, we could not calculate all QALY loss values over the same duration. Some less-severe health outcomes accounted for QALY loss during the first eight weeks, whereas more-severe health outcomes accounted for QALY loss over the remainder of a predicted lifespan.

## Methods

*Scope and Data Selection*

We recognize that systematic data collection is essential for generating accurate and reliable scientific results. Our decision to use heterogeneous data from diverse sources, even if not systematically collected, is rooted in the principle of maximizing use of available information to advance understanding of complex population health phenomena. We believe that our integration of heterogeneous data is justified given that our research was an exploration to gain insight into the complicated nexus of wildfire smoke exposure and potential human health consequences. However, use of heterogeneous data may introduce variability or uncertainty in the results.

We drew from methods commonly used for short-term health impact assessment (Liu et al. 2021) to calculate wildfire-attributable risk for each health outcome. We limited our outcomes to acute, short-duration events and episodes. Chronic health impacts associated with wildfire smoke (Grant and Runkle 2022) were largely outside the scope of our research. We selected studies that measured exposure in terms of the number of days that the study population was exposed to smoke, roughly matching the U.S. Environmental Protection Agency's threshold for air quality that is unhealthy for sensitive groups (an air quality index value of 101 for $PM_{2.5}$).

To address wildfire smoke-attributable risk, we prioritized epidemiological results from studies conducted in Oregon. When Oregon-specific studies were unavailable, we drew from studies conducted in Washington or California. In one case, we used nationally derived data that were restricted to areas with substantial wildfire events. Many outcomes are expressed in terms of health care utilization, a common proxy for the occurrence of health events (HCUP 2021).

Although ample evidence indicates that wildfire smoke disproportionally affects vulnerable or traditionally marginalized groups (Burke et al. 2021, EPA 2021, D'Evelyn et al. 2022, Grant and Runkle 2022), data on aggregate effects that matched binary smoke days were limited, with the exception of data on older adult populations. Where possible, we estimated wildfire smoke-attributable risk for older adults in addition to risk for all adults.

Consistent with best practices for the design of health impact assessments (Hubbell et al. 2009), we relied on the most geographically discrete values we could obtain, whether state, regional, or national, to estimate baseline incidence of health outcomes among Oregonians. We used county-level birth and death rate data for all-cause mortality and pre-term birth analyses. For a given health outcome, where possible, we matched the period of baseline estimates to that of the selected epidemiological study.

*Data Sources*

### Estimated Smoke Exposure

Liu et al. (2016) defined a smoke wave as two or more consecutive days with high levels of wildfire-specific $PM_{2.5}$. They expressed risk of poor air quality as the number of smoke wave days during two six-year time periods, one in the early twenty-first century (2004–2009) and one in the mid-twenty-first century (2046–2051). Each day was classified as a smoke wave day or a non-smoke wave day. Smoke wave days were those on which wildfire-specific $PM_{2.5}$ exceeded the 98th percentile of the distribution of values from 2004–2009 across the 561 counties in the western United States. Liu et al. (2017) classified days during the same time period and in the same region with wildfire-specific $PM_{2.5}$ >20 μg/m$^3$ as smoke wave days.

Use of U.S. Environmental Protection Agency Air Quality Index (AQI) values of $PM_{2.5}$ (Table 1) is common in the epidemiological literature [some AQI category breakpoints changed on 7 February 2024; values here predate those changes]. However, these values are not wildfire-specific. Liu et al. (2016) reported that 71.3 percent of the $PM_{2.5}$ on days with total $PM_{2.5}$ >35 μg/m³ can be attributed to wildfire smoke. Wildfire-specific $PM_{2.5}$ appears to be a primary contributor to exceedance of the Environmental Protection Agency's daily $PM_{2.5}$ National Ambient Air Quality Standard, a threshold of 35 μg/m³ (Li et al. 2021).

| Level | Color | AQI value | $PM_{2.5}$ (μg/m³) range | $PM_{2.5}$ (μg/m³) midpoint |
|---|---|---|---|---|
| Good | Green | 0–50 | 0–12.0 | 6 |
| Moderate | Yellow | 51–100 | 12.1–35.4 | 24 |
| Unhealthy for sensitive groups | Orange | 101–150 | 35.5–55.4 | 45 |
| Unhealthy | Red | 151–200 | 55.5–150.4 | 103 |
| Very unhealthy | Purple | 201–300 | 150.5–250.4 | 201 |
| Hazardous | Maroon | ≥ 301 | ≥ 250.5 | |

**Table 1.** Values of the U.S. Environmental Protection Agency's Air Quality Index (AQI) prior to 7 February 2024.

We believe it is reasonable to assume that Liu et al.'s (2017) smoke wave day threshold (wildfire-specific $PM_{2.5}$ >20 μg/m³) is comparable to, or higher than, the National Ambient Air Quality Standard's daily total $PM_{2.5}$ 35 μg/m³ threshold, which is equivalent to the Air Quality Index threshold between moderate and unhealthy for sensitive groups (101). This assumption is necessary to associate a range of short-term human health outcomes attributed to wildfire smoke exposure, corresponding to total $PM_{2.5}$, with our binary smoke wave day variable (Liu et al. 2016). As noted above, our methods for estimating smoke exposure are not standardized and are heterogeneous (Table 2).

**Population Estimates**

Publicly available data from Liu et al. (2016) include population estimates for both the early and mid-twenty-first century that were based on the U.S. Environmental Protection Agency's Integrated Climate and Land Use Scenarios population projections given the A1B emissions scenario (EPA 2011). Early twenty-first century values were derived from county-level estimates for 2005, and mid-twenty-first century values were derived from county-level projections from the Integrated Climate and Land Use Scenarios for 2050 (iclus.epa.gov/). U.S. Census data from 2005 were used to estimate the size of the early twenty-first century older-adult subpopulation, and growth rates from 2012 U.S. Census estimates were used to estimate the size of the mid-twenty-first century older-adult subpopulation. Liu et al.'s (2016) subpopulation data are not publicly available.

We retained the Liu et al. (2016) 2005– and 2050–year targets for early and mid-twenty-first century population estimates, but used reported values from the 2005 Oregon Vital Statistics county data (Center for Health Statistics 2008) to calculate early twenty-first century population size, county-level birth and death totals, and older-adult subpopulation data. We based our mid-century population estimates on publicly available data from Portland State University's Population Research Center in support of the statewide Oregon housing needs analysis mandated by Oregon's legislature (Marquez et al. 2023). These data include county-level population forecasts for 2050 and are aggregated to enable analyses of the older-adult subpopulation (see Table 3). The Population Research Center shared their county-level birth and death forecasts for 2050, which are not public. We applied observed population size in 2005, and projected size in 2050, to the subsequent five years.

| Response metric | Reference | Method for estimating smoke exposure | Smoke day threshold | Air Quality Index category |
|---|---|---|---|---|
| Smoke wave days | Liu et al. 2016 | Simulated with the GEOS-Chem chemical transport model, a global, three-dimensional atmospheric chemistry model driven by meteorological input from the National Aeronautics and Space Administration's Goddard Earth Observing System (GEOS). Modeled values of surface $PM_{2.5}$ were validated against measurements made from the ground or aircraft. | ≥2 consecutive days with wildfire-specific $PM_{2.5}$ exceeding the 98th percentile of values from 2004–2009 across 561 counties in the western United States | Similar to the threshold between moderate and unhealthy for sensitive groups. Close to the midpoint |
| Smoke wave days | Liu et al. 2017 | | ≥2 consecutive days with wildfire-specific $PM_{2.5}$ >20 µg/m³, near the 98th percentile of values from 2004–2009 across 561 counties in the western United States | groups. Close to the midpoint for sensitive groups. |
| All-cause mortality | Doubleday et al. 2020 | AIRPACT (Air Indicator Report for Public Awareness and Community Tracking). AIRPACT predicts air quality on the basis of the chemistry and physics of air pollutants given emissions, regional air chemistry, and predicted meteorology. | 24-hour average $PM_{2.5}$ >20.4 µg/m³ | Similar to midpoint between moderate and unhealthy for sensitive groups |
| All-cause respiratory (emergency department visits) | Wettstein et al. 2018 | Data from National Oceanic and Atmospheric Administration (NOAA) Hazard Mapping System Fire and Smoke product. Spatial smoke plume boundaries were measured with satellite imagery. Each smoke plume was accompanied by an estimated concentration of $PM_{2.5}$ attributed to wildfire smoke, generated with atmospheric models. | Dense smoke: same-day total $PM_{2.5}$ >22 µg/m³ | Similar to midpoint between moderate and unhealthy for sensitive groups |
| All-cause cardiovascular (emergency department visits) | Wettstein et al. 2018 | | | |
| Asthma (office visits) | Gan et al. 2020 | Integrated data from Kriged surface site monitors, satellite-based aerosol optical depth, and modeled $PM_{2.5}$ from the Weather Research and Forecasting with Chemistry (WRF-Chem) chemical transport model | Wildfire smoke impact day: same-day $PM_{2.5}$ >15/m³ | Above threshold between good and moderate, but not close to midpoint of moderate |
| Asthma (emergency department visits) | Doubleday et al. 2023 | Matched simulated and observed $PM_{2.5}$. Simulation relied on AIRPACT. Observed $PM_{2.5}$ was daily concentration measured by nearest regulatory air quality monitor. | 24-hour average total $PM_{2.5}$ >20.4 µg/m³ | Similar to midpoint between moderate and unhealthy for sensitive groups |
| Stroke (emergency department visits) | Wettstein et al. 2018 | See all-cause respiratory and cardiovascular | | |
| Pre-term birth | Heft-Neal et al. 2022 | Data from NOAA Hazard Mapping System Fire and Smoke product. Plume boundaries were hand-drawn by analysts. Each smoke plume was accompanied by estimated surface concentrations of $PM_{2.5}$. | Same-day total $PM_{2.5}$ >0 µg/m³ | Similar to midpoint of good and threshold between good and moderate |
| Mental health (depression) | Mirabelli et al. 2022 | Data from NOAA Hazard Mapping System. Smoke plume density was based on visual classification of smoke plumes by expert analysts. | Same-day total $PM_{2.5}$ >22 µg/m³, measured as number of weeks of smoke day exposure | Similar to midpoint between moderate and unhealthy for sensitive groups |
| Injury (long-bone fracture emergency department visits) | Wettstein et al. 2018 | See all-cause respiratory and cardiovascular | | |

**Table 2.** Methods for estimation of wildfire smoke exposure across health outcomes. Air Quality Index categories reflect breakpoints prior to 7 February 2024.

## Human Health Outcomes

We selected human health outcomes that represented the spectrum affected by wildfire smoke exposure and for which values were available in the literature (Table 4). For each health

| | Adults | Older adults |
|---|---|---|
| Early twenty-first century (2005) | 2,765,863 | 455,973 |
| Mid-twenty-first century (2050) | 4,456,975 | 1,280,723 |

**Table 3.** Estimated population of Oregon. Adults are ages 19 and older. Older adults are ages 65 and older.

outcome, we located baseline annual incidence rates and the increase in risk given exposure to a smoke wave day. We used separate baseline incidence and increase in risk values for the adult and older adult populations. Where possible, we selected data sources in which populations most closely resembled the Oregon population. Because incidence rate projections for our mid-twenty-first century period were not available (with the exception of all-cause mortality), baseline incidence rates for the early and mid-twenty-first century scenarios were the same.

**All-cause mortality.** All-cause mortality includes all non-traumatic mortality from cardiovascular, respiratory, and cerebrovascular causes. We estimated baseline incidence rates of all-cause mortality among the adult and older adult populations for the early twenty-first century from the 2005 Oregon

| Health outcome | Baseline incidence rate per 1000 people | Spatial resolution | Years | Data sources |
|---|---|---|---|---|
| All-cause mortality (non-traumatic) | 8.38 (2005) (all adults) 10.75 (2050) (all adults) | County | 2006–2017 (mean) | Oregon Health Authority Vital Statistics Annual Reports |
| | 50.4 (2005) (older adults) 38.0 (2050) (older adults) | | | Oregon Trauma Registry Annual Reports |
| All-cause respiratory (emergency department visits) | 43.4 (all adults) 58.3 (older adults) | National | 2019 | NEDS |
| All-cause cardiovascular (emergency department visits) | 10.3 (all adults) 28.1 (older adults) | National | 2019 | NEDS |
| Asthma (office visits) | 24.2 (all adults) | Regional | 2013 | CDC 2023 |
| Asthma (emergency department visits) | 3.6 (all adults) | Regional | 2017–2019 (mean) | NAMCS |
| Stroke (emergency department visits) | 2.5 (all adults) 7.5 (older adults) | National | 2019 | NEDS |
| Pre-term birth (<37 weeks) | 8% risk (state level) | County | 2006–2012 (mean) | Linked Birth and Infant Death Data (National Vital Statistics System) |
| Mental health (depressive symptoms) | 3% risk | National | 2000 | Measuring Healthy Days: Population Assessment of Health-Related Quality of Life |
| Injury (long-bone fracture emergency department visits) | 0.6 (all adults) 13.5 (older adults) | National | 2019 | NEDS |

**Table 4.** Baseline incidence rate estimates across health outcomes. We held the baseline incidence rate constant across analyses of all health outcomes except all-cause mortality, which we calculated for both 2005 and 2050. We estimated state-level rates of all-cause mortality of all adults, adjusted for non-traumatic deaths. We used county-level death rates, adjusted for non-traumatic deaths with state-level data, to estimate all-cause mortality of older adults. We did not include 2020 data for emergency department visits for asthma because data may be confounded with COVID-19 outcomes. We used county-level birth rate data to estimate pre-term births. Regional values refer to the U.S. Census Bureau's west region: Alaska, Arizona, California, Colorado, Hawaii, Idaho, Montana, Nevada, New Mexico, Oregon, Utah, Washington, and Wyoming. NEDS, Nationwide Emergency Department Sample; NAMCS, National Ambulatory Medical Care Survey (U.S. Centers for Disease Control and Prevention and National Center for Health Statistics).

Vital Statistics county-level data. We estimated mid-twenty-first century baseline incidence with projections from the Population Research Center at Portland State University. We adopted odds ratios for the increased risk of mortality given smoke wave day exposure from a study of non-traumatic mortality during Washington's peak fire seasons from 2006–2017 (Doubleday et al. 2020). The latter study incorporated a one-day lag between smoke wave day exposure and health outcomes.

**All-cause respiratory.** All-cause respiratory includes emergency department visits for asthma, chronic obstructive pulmonary disease, pneumonia, and other chest or respiratory syndromes. We used the 2019 Nationwide Emergency Department Sample to calculate national-level incidence rates of emergency department visits for all respiratory causes among the adult and older adult populations. We obtained relative risk values, which compared the risk of an emergency department visit given same-day smoke exposure or no smoke exposure, from a study of California emergency department visits during the 2015 wildfire season (Wettstein et al. 2018).

**All-cause cardiovascular.** All-cause cardiovascular includes emergency department visits for hypertension, ischemic heart disease, myocardial infarction, pulmonary embolism, dysrhythmia and conduction disorders, heart failure, and peripheral arterial disease. We used the 2019 Nationwide Emergency Department Sample to calculate national-level incidence rates of emergency department visits for all cardiovascular causes among the adult and older adult populations. We derived values for the relative risk of a cardiovascular emergency department visit given smoke exposure from Wettstein et al. (2018).

**Asthma.** We measured the health burden of asthma in adults in two ways, asthma-related office visits and asthma-related emergency department visits. We estimated the population at risk for an asthma-related event on the basis of county-specific estimates of asthma prevalence from 2004–2007 (Garland 2010). We used data from the National Ambulatory Medical Care Survey (www.cdc.gov/nchs) to estimate baseline incidence rates of asthma-related physician office visits and emergency department visits for adults in 2013 in the West region (Alaska, Arizona, California, Colorado, Hawaii, Idaho, Montana, Nevada, New Mexico, Oregon, Utah, Washington, and Wyoming). We obtained relative risk of an asthma-related office visit given same-day smoke exposure from an Oregon-based study of the 2013 wildfire season (Gan et al. 2020), and odds ratios for increased risk of an asthma-related emergency department visit given same-day smoke exposure from a study of wildfire smoke events in Washington from 2017–2020 (Doubleday et al. 2023).

**Stroke.** We measured stroke burden as emergency department visits for ischemic stroke in the populations of adults and older adults. We used the 2019 Nationwide Emergency Department Sample to estimate national incidence rates of stroke-related emergency department visits in both populations. We obtained values for the relative risk of a stroke-related emergency department visit given smoke exposure from Wettstein et al. (2018). The difference in relative risk of a stroke-related emergency department visit given smoke exposure or no smoke exposure was not statistically significant (Wettstein et al. 2018). It is uncertain whether the difference in Oregon also is not statistically significant.

**Pre-term births.** We defined pre-term births as any births before a gestational age of 37 weeks. We estimated the exposed population in the early twenty-first century with 2005 Oregon Vital Statistics data on county-level births, and the exposed population in the mid-twenty-first century with projections from the Population Research Center at Portland State University. To obtain a baseline incidence of pre-term births, we used state-level Linked Birth and Infant Death Data from the National Center for Health Statistics (n.d.; www.cdc.gov/nchs/nvss/linked-birth.htm). We obtained

a relative risk value from a study that compared the effects of any wildfire smoke exposure and no wildfire smoke exposure on the risk of birth before 37 gestational weeks (Heft-Neal et al. 2022).

**Mental health.** We defined a mental health event as an adult experiencing depressive symptoms such as feeling down, depressed, hopeless, nervous, anxious, on edge, or unable to stop or control worrying. We estimated the exposed population as adults who previously reported depressive symptoms and derived the incidence rate of adults who reported depressive symptoms from the U.S. Centers for Disease Control and Prevention's Population Assessment of Health-related Quality of Life (Taylor 2000). We adjusted prevalence ratios that compared exposure to heavy smoke over four or more weeks to exposure to heavy smoke over less than two weeks (Mirabelli et al. 2022) to daily values. This interpretation of increased risk as a result of smoke exposure may be inappropriate. Although the prevalence ratio in Mirabelli et al. (2022) was not statistically significant, we included it to highlight the range of potential health outcomes affected by wildfire smoke. Therefore, our estimates of mental health events have high uncertainty.

**Injury.** We used an injury outcome of emergency department visits for long-bone fractures for both adult and older adult populations. Although long-bone fractures are an unusual outcome to link to acute smoke exposure, an association between wildfire smoke and long-bone fractures was observed. The authors hypothesized that fractures could result from falls or motor vehicle accidents during evacuations as a result of wildfire smoke (Wettstein et al. 2018). We estimated baseline incidence rates of emergency department visits for long-bone fractures from the 2019 Nationwide Emergency Department Sample. We obtained values of the relative risk of an emergency department visit for long-bone fracture given smoke exposure from Wettstein et al. (2018).

*Analyses*

In our health impact assessment, we used attributable fraction (AF) methods similar to those of Liu et al. (2021) to calculate wildfire-attributable risk for each health outcome:

$$\Delta Y = AF \times Y0 \times Pop_{county} \times W_{days},$$

where $\Delta Y$ is the estimated number of health events attributable to wildfire smoke over the six-year time period of interest in each county; $AF$ is the fraction of health events attributable to $PM_{2.5}$ exposure; $Y0$ is a baseline incidence rate for the health outcome (see Table 4) that we adjusted to reflect daily incidence rates; $Pop_{county}$ is the population within the county at risk of exposure, derived from Liu et al. (2016) and the 2005 Oregon Vital Statistics; and $W_{days}$ is the total number of wildfire smoke days for the time period of interest. We adjusted the population at risk of exposure to reflect the number of people at risk for specific health outcomes that only are applicable to subpopulations with certain conditions (e.g., asthma office and emergency department visits, pre-term births, and older adult outcomes) (Table 5). Values of $Pop_{county}$ and $W_{days}$ in our analyses depended on the scenario of smoke wave days and population estimates (see *Human Health Outcomes* above).

We calculated the attributable fraction for each health outcome with adjusted odds ratio (*OR*) or relative risk (*RR*) values for wildfire smoke days compared to non-smoke days from available health impact assessment research (see Table 6):
$AF = (OR - 1) / OR$
$AF = (RR - 1) / RR$

We used Wilcoxon sign-rank tests, which accounted for our non-normally distributed data and small sample size, to test whether differences between early twenty-first-century and mid-twenty-first

century estimates were statistically significant. We estimated economic and quality-of-life loss for each health outcome by multiplying the number of health events by the per-health event cost and QALY loss. We obtained per-health event costs and QALY loss values from the literature (Table 7), and adjusted economic costs to 2022 U.S. dollars with the Consumer Price Index (BLS 2024).

| Oregon state-level population estimates | Adults | Older adults | Pregnancies | Adults with asthma | Adults experiencing depressive symptoms |
|---|---|---|---|---|---|
| Early twenty-first century (2005) | 2,765,863 | 455,973 | 45,905 | 362,230 | 829,759 |
| Mid-twenty-first century (2050) | 4,456,975 | 1,280,723 | 43,833 | 522,372 | 1,337,093 |

**Table 5.** Prevalence of health events for condition-specific subpopulations. Adults are ages 19 and older. Older adults are ages 65 and older. Pregnancies are not exclusive to the adult population.

| Health outcome | Wildfire smoke day risk, all adults | Wildfire smoke day risk, older adults | Location | Period or year | Reference |
|---|---|---|---|---|---|
| All-cause mortality (non-traumatic) | OR 1.02 (1.00, 1.05) | OR 1.03 (0.99, 1.07) | Washington | 2006–2017 | Doubleday et al. 2020 |
| All-cause respiratory (emergency department visits) | RR 1.09 (1.03, 1.15) | RR 1.14 (1.05, 1.24) | Air basins in northern and central California | 2015 | Wettstein et al. 2018 |
| All-cause cardiovascular (emergency department visits) | RR 1.08 (1.03, 1.12) | RR 1.15 (1.09, 1.22) | Air basins in northern and central California | 2015 | Wettstein et al. 2018 |
| Asthma (office visits) | RR 1.37 (1.11, 1.69) | | Medford metropolitan statistical area, Oregon | 2013 | Gan et al. 2020 |
| Asthma (emergency department visits) | OR 1.13 (1.10, 1.17) | | Washington | 2017–2020 | Doubleday et al. 2023 |
| Stroke (emergency department visits) | RR 1.11 (0.86, 1.45) | RR 1.25 (0.91, 1.71) | Air basins in northern and central California | 2015 | Wettstein et al. 2018 |
| Pre-term birth (<37 weeks) | 0.49% (0.41, 0.59) RR increase | | California | 2006–2012 | Heft-Neal et al. 2022 |
| Mental health (depressive symptoms) | PR 1.08 (0.96, 1.21) | | Oregon | 2018 | Mirabelli et al. 2022 |
| Injury (long-bone fracture emergency department visits) | RR 1.31 (1.09, 1.56) | RR 1.46 (1.12, 1.90) | Air basins in northern and central California | 2015 | Wettstein et al. 2018 |

**Table 6.** Wildfire smoke day risk across health outcomes. OR, odds ratio; RR, Relative risk; PR, prevalence ratio. Numbers in parentheses are 95 percent confidence intervals. Mental health was measured over four weeks (Mirabelli et al. 2022); we divided those cumulative measures by 28 to estimate the wildfire smoke day effect size. All odds ratios and relative risk values are same-day with the exception of all-cause mortality, which we estimated for the day following exposure.

## Results

We report state-level results for each wildfire-attributable health outcome and associated quality-of-life and economic loss (Tables 8–16). Visualizations of the estimated number of health events for all adults and older adults at the county level are in Appendix C1. Maps of the estimated number of all-cause mortalities, emergency department visits for respiratory events, and emergency department visits for cardiovascular events per county, across smoke wave day and population scenarios, for adult and older adult populations are in Appendix C2.

When we held population size constant but allowed the number of smoke wave days to vary, the difference in the number of health events between the early twenty-first century and mid-twenty-

| Health outcome | Economic cost | Reference | QALY loss per health event | Timespan for QALY loss measurement | Reference |
|---|---|---|---|---|---|
| All-cause mortality (non-traumatic) | Value of a statistical life: $10.8 million | BenMAP (2023) | | | |
| All-cause respiratory (emergency department visits) | Costs: $1077 Total charges: $8688 | NEDS | | | |
| All-cause cardiovascular (emergency department visits) | Costs: $1662 Total charges: $11,608 | NEDS | | | |
| Asthma (office visits) | $201 (average listed price of an office visit in Oregon) | Batra et al. 2022 | 0.010 | First eight weeks after an asthma-related event | Crossman-Barnes et al. 2019 |
| Asthma (emergency department visits) | Costs: $611 Total charges: $4800 | NEDS | 0.010 | First eight weeks after an asthma-related event | Crossman-Barnes et al. 2019 |
| Stroke (emergency department visits) | Costs: $2590 Total charges: $17,801 | NEDS | 6.1 (adults in South Korea) | Predicted rest of life | Jia and Lubetkin 2016, Cheon et al. 2023 |
| | | | 7.8 (older adults) | | |
| Pre-term birth (<37 weeks) | $38,244 (converted from Euros) | Korvenranta et al. 2010 | 0.486 QALYs (older adults in Finland) | First four years after pre-term birth | Korvenranta et al. 2010 |
| Mental health (depressive symptoms) | | | | | |
| Injury (long-bone fracture emergency department visits) | Costs: $1200 Total charges: $7669 | NEDS | 0.0356 (all adults) | First year after fracture | Raich et al. 2022 |
| | | | 0.094 (older adults in Canada) | First three years after fracture event (does not account for mortalities) | Tarride et al. 2016 |

**Table 7.** Economic costs and quality-adjusted life year (QALYs) loss. BenMAP Community Edition, U.S. Environmental Protection Agency Environmental Benefits Mapping and Analysis Program. NEDS, Nationwide Emergency Department Sample (2019).

first century was not statistically significant. However, when we allowed both population size and the number of smoke wave days to vary, the difference in the number of health events between the early twenty-first century and mid-twenty-first century was statistically significant for all health outcomes ($p<0.001$) except pre-term births. Differences were statistically significant for both the adult and older adult populations. Estimates of economic loss and quality of life loss were greatest for all-cause mortality and emergency department visits for ischemic stroke, respectively.

Our adult population included older adults, but when we assumed that only older adults are at risk of exposure to wildfire smoke, the estimated number of wildfire-attributable health events among older adults was greater than among all adults for all-cause mortality and emergency department visits for all cardiovascular causes, ischemic stroke, and long-bone fracture (Tables 8, 10, 13, 16).

Despite statistically significant results, the absolute differences between the early and mid-twenty-first century in the numbers of health events for many health outcomes were quite small. For example, the estimated number of asthma-related office visits was about 150 office visits over six years. Nevertheless, given the wide range in the severity of health outcomes included in our models,

| Scenario | | Early twenty-first century smoke wave and population estimates | Mid-twenty-first century smoke wave and early twenty-first century population estimates | | Mid-twenty-first century smoke wave and population estimates | |
|---|---|---|---|---|---|---|
| Population | | Total | Total | p-value | Total | p-value |
| Adults | Health events | 78.4 (41.2, 115.6) | 81.8 (44.3, 119.3) | 0.09 | 150.7 (81.8, 219.6) | <0.001 |
| | Economic loss | 847 million | 884 million | | 1.63 billion | |
| Older adults | Health events | 88.3 (46.7, 123.0) | 92.1 (50.3, 134.0) | 0.09 | 192.4 (105.8, 279.0) | <0.001 |
| | Economic loss | 954 million | 995 million | | 2.08 billion | |

**Table 8.** Estimates of burden of smoke wave day-related all-cause mortality in Oregon. Population estimates derived from 2005 reporting and 2050 forecasts. Adults are aged 19 and older; older adults are aged 65 and older. Number of health events estimated over six-year periods. Economic loss values assume a value of statistical life of $10.8 million per mortality (EPA 2023) and are reported in 2022 U.S. dollars. Values in parentheses are 95 percent confidence intervals.

some differences, such as those for all-cause mortality (Table 8), may have a considerable impact on population health and economic loss even if differences are relatively small.

We estimated that the number of smoke wave day-related all-cause mortality events, per six years, could exceed 151 adults and 192 older adults by the year 2050, with a total economic loss of 1.63 billion for all adults and 2.08 billion for older adults (Table 8).

The number of smoke wave day-related emergency department visits for all respiratory causes among the adult population in Oregon, per six years, by the mid-twenty-first century could reach 2130—an increase of about 66 percent compared to 2005 (Table 9).

| Scenario | | Early twenty-first century smoke wave and population estimates | Mid-twenty-first century smoke wave and early twenty-first century population estimates | | Mid-twenty-first century smoke wave and population estimates | |
|---|---|---|---|---|---|---|
| Population | | Total | Total | p-value | Total | p-value |
| Adults | Health events | 1282.0 (622.5, 1941.6) | 1344.3 (672.1, 2016.5) | 0.09 | 2130.0 (1006.9, 3253.2) | <0.001 |
| | Economic loss: cost | 1.38 million | 1.45 million | | 2.29 million | |
| | Economic loss: total charges | 11.1 million | 11.7 million | | 18.5 million | |
| Older adults | Health events | 432.02 (236.18, 627.86) | 448.94 (253.96, 643.92) | 0.10 | 1233.9 (651.9, 1815.8) | <0.001 |
| | Economic loss: cost | 0.47 million | 0.48 million | | 1.33 million | |
| | Economic loss: total charges | 3.75 million | 3.90 million | | 10.7 million | |

**Table 9.** Estimates of burden of smoke wave day-related emergency department visits for all respiratory causes in Oregon. Population estimates derived from 2005 reporting and 2050 forecasts. Number of health events estimated over six-year periods. Costs are the cost of providing treatment. Total charges are the amount billed by the hospital. Reported in 2022 U.S. dollars.

The number of smoke wave day-related emergency department visits for all cardiovascular causes by older adults in Oregon, per six years, could nearly triple between 2005 and 2050 (Table 10). As noted above, the absolute difference in number of smoke wave day-related office visits (Table 11) and emergency department visits (Table 12) for asthma between the early and mid-twenty-first century was relatively small. Available data were insufficient to estimate inequities in exposure and health outcomes for older adults or for some other groups at high risk, such as outdoor workers.

| Scenario | | Early twenty-first century smoke wave and population estimates | Mid-twenty-first century smoke wave and early twenty-first century population estimates | | Mid-twenty-first century smoke wave and population estimates | |
|---|---|---|---|---|---|---|
| Population | | Total | Total | *p*-value | Total | *p*-value |
| Adults | Health events | 272.4 (132.3, 412.6) | 285.7 (142.8, 428.5) | 0.09 | 452.7 (214.0, 691.3) | <0.001 |
| | Economic loss: cost | 0.45 million | 0.47 million | | 0.75 million | |
| | Economic loss: total charges | 3.16 million | 3.32 million | | 5.25 million | |
| Older adults | Health events | 220.6 (120.6, 320.6) | 229.3 (129.7, 328.8) | 0.10 | 630.1 (332.9, 927.3) | <0.001 |
| | Economic loss: cost | 0.37 million | 0.38 million | | 1.05 million | |
| | Economic loss: total charges | 2.56 million | 2.66 million | | 7.31 million | |

**Table 10.** Estimates of burden of smoke wave day-related emergency department visits for all cardiovascular causes in Oregon. Population estimates derived from 2005 reporting and 2050 forecasts. Adults are aged 19 and older; older adults are aged 65 and older. Number of health events estimated over six-year periods. Costs are the cost of providing treatment. Total charges are the amount billed by the hospital. Costs are reported in 2022 U.S. dollars. Values in parentheses are 95 percent confidence intervals.

| Scenario | | Early twenty-first century smoke wave and population estimates | Mid-twenty-first century smoke wave and early twenty-first century population estimates | | Mid-twenty-first century smoke wave and population estimates | |
|---|---|---|---|---|---|---|
| Population | | Total | Total | *p*-value | Total | *p*-value |
| Adults with asthma | Health events | 306.9 (154.2, 459.6) | 322.01 (165.6, 478.4) | 0.11 | 456.3 (221.9, 690.7) | <0.001 |
| | QALY loss | 3.07 | 3.22 | | 4.56 | |
| | Economic loss | 61,635 | 64,668 | | 91,641 | |

**Table 11.** Estimates of burden of smoke wave day-related office visits for asthma in Oregon. Population estimates derived from 2005 reporting and 2050 forecasts. Adults are aged 19 and older. Number of health events estimated over six-year periods. QALY, quality adjusted life years. QALY loss was measured for the first eight weeks after an asthma-related event (Crossman-Barnes et al. 2019). Economic loss was measured as the average price of an Oregon primary care office per health event (Batra and Candon 2022). Costs are reported in 2022 U.S. dollars. Values in parentheses are 95 percent confidence intervals.

The difference in the percentage increase in smoke wave day-related emergency department visits for ischemic stroke between all adults and older adults was considerable (Table 13). The number of visits among all adults increased by 66 percent, whereas the number of visits among older adults increased by 286 percent.

The estimated difference in pre-term births between the early and mid-twenty-first century was not statistically significant (Table 14). As noted in the sixth Oregon Climate Assessment (Rohlman et al. 2023), a review of prenatal smoke exposure, pre-term birth, and low birth weight globally found significant, positive associations (Amjad et al. 2021). The timing of exposure to wildfire smoke also appears to be associated with the magnitude of incidence of pre-term birth: the risk may be greatest when exposure occurs during the second trimester (Abdo et al. 2019, Heft-Neal et al. 2022, Requia et al. 2022, Rohlman et al. 2023).

As is often the case when investigating more complex, distal relationships, mental health impacts remain difficult to measure, largely due to lack of operational understanding. People also may be

| Scenario | Early twenty-first century smoke wave and population estimates | Mid-twenty-first century smoke wave and early twenty-first century population estimates | | Mid-twenty-first century smoke wave and population estimates | |
|---|---|---|---|---|---|
| Population | Total | Total | p-value | Total | p-value |
| Adults with asthma — Health events | 19.7 (9.9, 29.5) | 20.7 (10.6, 30.7) | 0.11 | 29.3 (14.2, 44.3) | <0.001 |
| Adults with asthma — QALY loss | 0.20 | 0.21 | | 0.29 | |
| Adults with asthma — Economic loss: cost | 12,022 | 12,613 | | 17,874 | |
| Adults with asthma — Economic loss: total charges | 94,481 | 99,131 | | 140,478 | |

**Table 12.** Estimates of burden of smoke wave day-related emergency department visits for asthma by all adults in Oregon. Population estimates derived from 2005 reporting and 2050 forecasts. Number of health events estimated over six-year periods. QALY, quality adjusted life years. QALY loss was measured for the first eight weeks after an asthma-related event (Crossman-Barnes et al. 2019). Costs are the cost of providing treatment. Total charges are the amount billed by the hospital. Costs are reported in 2022 U.S. dollars. Values in parentheses are 95 percent confidence intervals.

less likely to seek medical attention for mental health episodes than for physical health episodes. Nevertheless, we estimated a significant increase in smoke wave day-related depressive symptom episodes between the early and mid-twenty-first century (Table 15).

| Scenario | Early twenty-first century smoke wave and population estimates | Mid-twenty-first century smoke wave and early twenty-first century population estimates | | Mid-twenty-first century smoke wave and population estimates | |
|---|---|---|---|---|---|
| Population | Total | Total | p-value | Total | p-value |
| Adults — Health events | 87.5 (42.5, 132.5) | 91.7 (45.9, 137.6) | 0.09 | 145.4 (68.7, 222.0) | <0.001 |
| Adults — QALY loss | 533.69 | 559.61 | | 886.7 | |
| Adults — Economic loss: cost | 0.23 million | 0.24 million | | 0.38 million | |
| Adults — Economic loss: total charges | 1.56 million | 163 million | | 2.59 million | |
| Older adults — Health events | 90.8 (49.7,132.0) | 94.4 (53.4, 135.4) | 0.10 | 259.4 (137.0, 381.7) | <0.001 |
| Older adults — Economic loss: cost | 708.3 | 736.1 | | 2,023.0 | |
| Older adults — QALY loss | 0.24 million | 0.24 million | | 0.67 million | |
| Older adults — Economic loss: total charges | 1.62 million | 1.68 million | | 4.62 million | |

**Table 13.** Estimates of burden of smoke wave day-related emergency department visits for ischemic stroke in Oregon. Population estimates derived from 2005 reporting and 2050 forecasts. Adults are aged 19 and older; older adults are aged 65 and older. Number of health events estimated over six-year periods. QALY, quality adjusted life years. QALY loss was predicted for the rest of life ((Jia and Lubetkin 2016, Cheon et al. 2023). Costs are the cost of providing treatment. Total charges are the amount billed by the hospital. Costs are reported in 2022 U.S. dollars. Values in parentheses are 95 percent confidence intervals.

Emergency department visits for long-bone fractures may be linked to falls or motor vehicle accidents related to wildfire-related evacuations (Wettstein et al. 2018). This relation is speculative, but underscores the possibility that many economic and societal costs of wildfire smoke impacts are hidden and unaccounted for. We estimated that the number of smoke wave day-related emergency

department visits for long-bone fractures may increase by two-thirds among all adults, and nearly three times among older adults, between the early and mid-twenty-first century (Table 16).

| Scenario | | Early twenty-first century smoke wave and population estimates | Mid-twenty-first century smoke wave and early twenty-first century population estimates | | Mid-twenty-first century smoke wave and population estimates | |
|---|---|---|---|---|---|---|
| Population | | Total | Total | p-value | Total | p-value |
| Pregnancies | Health events | 2.3 (1.0, 3.5) | 2.4 (1.1, 3.7) | 0.07 | 2.2 (0.9, 3.6) | 0.97 |
| | QALY loss | 1.09 | 1.15 | | 1.09 | |
| | Economic loss | 41,840 | 44,142 | | 41,708 | |

**Table 14.** Estimates of burden of smoke wave day-related pre-term births (less than 37 gestation weeks) in Oregon. Population estimates derived from 2005 reporting and 2050 forecasts. Number of health events estimated over six-year periods. Values in parentheses are 95 percent confidence intervals. QALY, quality adjusted life years. QALY loss was measured for the first four years after pre-term birth. Costs are reported in 2022 U.S. dollars. Economic loss accounts for emergency and non-emergency costs.

| Scenario | | Early twenty-first century smoke wave and population estimates | Mid-twenty-first century smoke wave and early twenty-first century population estimates | | Mid-twenty-first century smoke wave and population estimates | |
|---|---|---|---|---|---|---|
| Population | | Total | Total | p-value | Total | p-value |
| Adults experiencing depressive symptoms | Health events | 182.4 (88.6, 276.2) | 191.3 (95.6, 286.9) | 0.08 | 303.0 (143.2, 462.8) | <0.001 |

**Table 15.** Estimates of burden of smoke wave day-related episodes of depressive symptoms in Oregon. Population estimates derived from 2005 reporting and 2050 forecasts. Adults are aged 19 and older. Number of health events estimated over six-year periods.

## Discussion

Across analyses, effect sizes for the isolated effects of increased wildfire smoke given early twenty-first century smoke wave and population estimates compared with mid-twenty-first century smoke wave estimates, or both smoke wave and population estimates, were modest. Population estimates clearly drove statistically significant differences. Estimates of the number of health events for mortality, ischemic stroke, and long-bone fracture among older adults regularly were greater than those among all adults across scenarios, even given that older adults accounted for roughly 16 percent and 29 percent of the projected adult population in the early and mid-twenty-first-century, respectively. The difference in estimates reflected our health impact assessment methods, which accounted for increases in baseline incidence rates and attributable fraction values for older adult populations. Although the difference highlights some limitations in accurately measuring wildfire-attributable events with heterogeneous model values, it also suggests the relevance of accounting for increases in vulnerability of particular populations. Over the next 25 years, the proportion of older adults in Oregon is expected to increase, with an associated increase in vulnerability to smoke.

Our inclusion of asthma and ischemic stroke allowed us to isolate conditions within the broader categories of all-cause respiratory and cardiovascular outcomes. As a result, we were able to investigate not only the economic cost of these discrete outcomes but quality-of-life loss, an indication of the burden on overall population well-being.

We sought to include a range of short-term health outcomes in addition to causally established respiratory and cardiovascular events to capture a more holistic understanding of the impact of

| Scenario | | Early twenty-first century smoke wave and population estimates | Mid-twenty-first century smoke wave and early twenty-first century population estimates | | Mid-twenty-first century smoke wave and population estimates | |
|---|---|---|---|---|---|---|
| Population | | Total | Total | $p$-value | Total | $p$-value |
| Adults | Health events | 49.9 (24.2, 75.6) | 52.3 (26.2, 78.5) | 0.09 | 82.9 (39.2, 126.6) | <0.001 |
| | QALY loss | 1.78 | 1.86 | | 2.95 | |
| | Economic loss: cost | 0.06 million | 0.06 million | | 0.10 million | |
| | Economic loss: total charges | 0.38 million | 0.40 million | | 0.64 million | |
| Older adults | Health events | 257.2 (140.6, 373.9) | 267.3 (151.2, 383.4) | 0.10 | 734.7 (388.2, 1081.2) | <0.001 |
| | Economic loss: cost | 24.18 | 25.13 | | 69.06 | |
| | QALY loss | 0.31 million | 0.32 million | | 0.88 million | |
| | Economic loss: total charges | 1.97 million | 2.05 million | | 5.63 million | |

**Table 16.** Estimates of burden of smoke wave day-related emergency department visits for long-bone fracture in Oregon. Population estimates derived from 2005 reporting and 2050 forecasts. Adults are aged 19 and older; older adults are aged 65 and older. Number of health events estimated over six-year periods. QALY, quality adjusted life years. QALY loss was measured for the first year after fracture in adults and first three years after fracture, not accounting for mortality events, in older adults. Costs are reported in 2022 U.S. dollars. Values in parentheses are 95 percent confidence intervals.

wildfire-attributable smoke on human health outcomes. For example, both pre-term births (Amjad et al. 2021, Ha et al. 2024) and mental health impacts (Eisenman and Galway 2022, Humphreys et al. 2022) are gaining the attention of researchers.

*Limitations*

**Smoke Exposure**

Across epidemiological studies, wildfire smoke exposure is measured and simulated with diverse methods that vary with respect to accuracy, spatial extent, and temporal resolution. Fixed-location monitoring of $PM_{2.5}$ concentrations is widely used to estimate exposure near those locations. Satellite remote sensing provides estimates over large areas, but the estimates are less precise. Air quality simulation models, including dispersion and chemical transport models, can provide detailed exposure estimates over time and space. These and other methods inevitably lead to differences in how wildfire smoke exposure is quantified and linked to human health outcomes. Methods for estimating smoke exposure across our selected studies are not standardized, and only approximately matched the Liu et al. (2016) simulations of smoke wave days (Table 2). Moreover, in the studies we selected, methods that controlled for heat exposure and other factors in estimating increased risk of adverse health outcomes from smoke exposure also were heterogeneous.

Attributable fraction methods that use air quality thresholds to define a wildfire day likely underestimate the impact of wildfire smoke on health outcomes because they treat all wildfire days as equivalent, rather than considering that higher values of $PM_{2.5}$ may cause additional health events (Liu et al. 2021). Use of a single $PM_{2.5}$ threshold for identifying a wildfire day may also underestimate health impacts at lower levels of $PM_{2.5}$ exposure. The rate of health outcomes such as emergency department visits for asthma may be higher at low levels of $PM_{2.5}$ than at high levels of $PM_{2.5}$

(Henderson et al. 2024). Our calculations of attributable fraction applied odds ratios and relative risk values from studies with generally similar $PM_{2.5}$ thresholds and definitions of a smoke wave day, but some thresholds differed. For example, estimates of asthma-related office visits and pre-term births applied $PM_{2.5}$ thresholds of $>15$ μg/m³ and $>0$ μg/m³, respectively. The latter thresholds are much lower than the $PM_{2.5}$ $>20$ μg/m³ used to define a smoke wave day in our model. By contrast, all-cause respiratory, all-cause cardiovascular, and ischemic stroke used a higher threshold, $PM_{2.5}$ $>22$ μg/m³. The differences in definitions of thresholds for a smoke wave day may lead to underestimates or overestimates of the number of health events.

The Liu et al. (2016) data included a smoke wave day intensity rating, which we did not use. Although the mean difference in values of the binary smoke wave day variable between the early and mid-twenty-first century periods was modest, values of the smoke wave day intensity variable nearly doubled (Table 17). By focusing solely on the frequency of smoke events and not accounting for changes in intensity across time periods, we may have underestimated effect sizes. A comparison of attributable fraction methods found a greater number of wildfire smoke-attributable health events with methods that accounted for daily changes in smoke intensity than with a binary smoke day variable (Liu et al. 2021). Moreover, our omission of potential compounding health impacts due to the duration of exposure events may further bias our results (Johnson and Garcia-Menendez 2022). We suggest that future research on health impacts account for multiple climate hazards, such as the interacting effects of wildfire smoke and extreme heat (Chen et al. 2024).

|  | Mean number of smoke wave days by county | Mean wildfire-specific daily PM$_{2.5}$ intensity rating by county |
|---|---|---|
| Early twenty-first century (2004–2009) | 39.2 (32.3, 46.1) | 14.4 (13.5, 15.3) |
| Mid-twenty-first century (2046–2051) | 45.4 (40.0, 50.9) | 27.7 (25.3, 30.2) |
| Mean difference | 6 days | 13.3 units |
| p-value | <0.01 | <0.001 |

**Table 17.** Comparison of smoke wave days and daily intensity ratings in the data of Liu et al. (2016). Confidence intervals in parentheses.

## Health Outcomes

We derived baseline incidence rates of health outcomes from diverse sources, including national and regional estimates that were not specific to Oregon. The values we used did not adjust for changes in baseline incidence rates across years and did not always match the years of our smoke data.

A focus on short-term health impacts of wildfire smoke exposure excludes many longer-term health outcomes that may represent a larger health burden. Wildfire smoke has been linked to long-term morbidity and mortality from increases in chronic respiratory illness, cardiovascular disease, cancer, and premature mortality. Estimates of the annual economic impact of long-term health effects from wildfire smoke exposure in the United States range from \$15–90 billion (Grant and Runkle 2022). Consideration of both short-term and long-term health and economic costs is necessary to fully estimate the burden of increases in exposure to wildfire smoke.

We sought to include a variety of short-term health outcomes linked to wildfire smoke, but doing so was not always possible given our use of attributable fraction methods. Furthermore, outcomes such as ischemic stroke and mental health were dependent on published values that were not statistically significant, creating an additional source of uncertainty in our results. We did not attempt to estimate several other short-term health outcomes emblematic of a holistic understanding of

human health because available values did not fit our measure of smoke exposure and our analysis model. Examples include headache (Elser et al. 2023), influenza (Landguth et al. 2020), and violence (Burkhardt et al. 2020).

## Vulnerable Populations

Epidemiological studies consistently have shown that exposure to wildfire smoke is associated with exacerbation of asthma, an increase in the number of hospital admissions for respiratory illnesses, and impaired lung function in children (EPA 2021). We were unable to include estimates of the early and mid-twenty-first century size of the population aged 18 and younger in Oregon due to limitations in literature match with our smoke exposure measure and analysis model. Similarly, other recognized factors in the complex relationship between wildfire smoke and human health consequences fall outside of the scope of our study. Although the likelihood increases with age, we do not explicitly account for pre-existing conditions. Moreover, we were unable to account for estimates of social vulnerability other than older age. Oregon's low-income communities, historically marginalized racial and ethnic groups, and rural residents experience disproportionate impacts from wildfire smoke (Oregon Climate and Health Program 2023). These populations often have higher incidence of pre-existing health conditions, limited access to healthcare, and live in areas with greater exposure to environmental hazards, exacerbating their vulnerability to wildfire smoke (Burke et al. 2021, D'Evelyn et al. 2022). Outdoor workers and unhoused populations are at particular risk (EPA 2021, Grant and Runkle 2022). The notable difference in magnitude of risk of mortality, ischemic stroke, and long-bone fracture among older adults in our results suggests the relevance of accounting for differential incidence rates among vulnerable populations.

## Conclusion

The primary contribution of our research at the intersection of climate change, wildfire smoke exposure, and human health outcomes is conceptual. We emphasize the potential benefits of standardized research that integrates contemporary, fine-resolution climate projections with estimates of the impacts of smoke exposure across health outcomes and associated costs, both monetary and in terms of quality-of-life lost. Systems thinking approaches will be necessary to accurately estimate the true burden of wildfire-specific smoke exposure and tailor mitigation and adaptation efforts to protect public health in Oregon and across the western United States.

## Appendix

Visualizations of the estimated number of health events for all adults and older adults at the county level are in Appendix C1. Maps of the estimated number of all-cause mortalities, emergency department visits for respiratory events, and emergency department visits for cardiovascular events per county, across smoke wave day and population scenarios, for adult and older adult populations are in Appendix C2.

## Literature Cited

Abatzoglou, J.T., and A.P. Williams. 2016. Impact of anthropogenic climate change on wildfire across western US forests. Proceedings of the National Academy of Sciences 113:11770–11775.

Abdo, M., I. Ward, K. O'Dell, B. Ford, J.R. Pierce, E.V. Fischer, and J.L. Crooks. 2019. Impact of

wildfire smoke on adverse pregnancy outcomes in Colorado, 2007–2015. International Journal of Environmental Research and Public Health 16:3720. https://doi.org/10.3390/ijerph16193720.

Amjad, S., D. Chojecki, A. Osornio-Vargas, and M.B. Ospina. 2021. Wildfire exposure during pregnancy and the risk of adverse birth outcomes: a systematic review. Environment International 156:106644. https://doi.org/10.1016/j.envint.2021.106644.

Batra, A., and M. Candon. 2022. Price transparency for primary care office visits and routine tests: results from a 2016 audit study. INQUIRY 59:00469580221092122. https://doi.org/10.1177/00469580221092122.

BLS (U.S. Bureau of Labor Statistics). 2024. Consumer Price Index. www.bls.gov/cpi/.

Burke, M., A. Driscoll, S. Heft-Neal, J. Xue, J. Burney, and M. Wara. 2021. The changing risk and burden of wildfire in the United States. Proceedings of the National Academy of Sciences 118:e2011048118. https://doi.org/10.1073/pnas.2011048118.

Burkhardt, J., J. Bayham, A. Wilson, J.D. Berman, K. O'Dell, B. Ford, E.V. Fischer, and J.R. Pierce. 2020. The relationship between monthly air pollution and violent crime across the United States. Journal of Environmental Economics and Policy 9:188–205.

CDC (U.S. Centers for Disease Control and Prevention). 2023. 2013 Healthcare use data: asthma-related physician office visits. www.cdc.gov/asthma/healthcare-use/2013/table_c.html#print.

Center for Health Statistics. 2008. Oregon Vital Statistics county data 2005. Oregon Department of Human Services. www.oregon.gov/oha/PH/BIRTHDEATHCERTIFICATES/VITALSTATISTICS/ANNUALREPORTS/COUNTYDATABOOK/Documents/2005/cdb2005.pdf.

Chen, C., L. Schwarz, N. Rosenthal, M. Marlier, and T. Benmarhnia. 2024. Exploring spatial heterogeneity in synergistic effects of compound climate hazards: extreme heat and wildfire smoke on cardiorespiratory hospitalizations in California. Science Advances 10:eadj7264. https://doi.org/10.1126/sciadv.adj7264.

Cheon, S., C.-Y. Li, J.-S. Jeng, J.-D. Wang, and L.-J.E. Ku. 2023. The lifetime burden following stroke: long term impact of stroke on survival and quality of life. International Journal of Stroke 18:795–803.

Crossman-Barnes, C.-J., T. Sach, A. Wilson, and G. Barton. 2019. Estimating loss in quality of life associated with asthma-related crisis events (ESQUARE): a cohort, observational study. Health and Quality of Life Outcomes 17:58. https://doi.org/10.1186/s12955-019-1138-5.

D'Evelyn, S.M., et al. 2022. Wildfire, smoke exposure, human health, and environmental justice need to be integrated into forest restoration and management. Current Environmental Health Reports 9:366–385.

Doubleday, A., J. Schulte, L. Sheppard, M. Kadlec, R. Dhammapala, J. Fox, and T. Busch Isaksen. 2020. Mortality associated with wildfire smoke exposure in Washington state, 2006–2017: a case-crossover study. Environmental Health 19:4. https://doi.org/10.1186/s12940-020-0559-2.

Doubleday, A., L. Sheppard, E. Austin, and T.B. Isaksen. 2023. Wildfire smoke exposure and emergency department visits in Washington state. Environmental Research: Health 1:025006. https://doi.org/10.1088/2752-5309/acd3a1.

Eisenman, D.P., and L.P. Galway. 2022. The mental health and well-being effects of wildfire smoke: a scoping review. BMC Public Health 22:2274. https://doi.org/10.1186/s12889-022-14662-z.

Elser, H., S.T. Rowland, M.S. Marek, M.V. Kiang, B. Shea, V. Do, T. Benmarhnia, A.L.C. Schneider, and J.A. Casey. 2023. Wildfire smoke exposure and emergency department visits for headache: a case-crossover analysis in California, 2006–2020. Headache 63:94–103.

EPA (U.S. Environmental Protection Agency). 2011. Integrated climate and land use scenarios (ICLUS) tools and datasets (Version 1.3 & 1.3.1). cfpub.epa.gov/ncea/risk/recordisplay. cfm?deid=257306.

EPA (U.S. Environmental Protection Agency). 2021. Wildfire smoke: a guide for public health officials. www.airnow.gov/publications/wildfire-smoke-guide/wildfire-smoke-a-guide-for-public-health-officials/.

EPA (U.S. Environmental Protection Agency). 2023. Environmental Benefits Mapping and Analysis Program – community edition user's manual. www.epa.gov/benmap/benmap-ce-manual-and-appendices.

Gan, R.W., et al. 2020. The association between wildfire smoke exposure and asthma-specific medical care utilization in Oregon during the 2013 wildfire season. Journal of Exposure Science & Environmental Epidemiology 30:618–628.

Garland, R. 2010. The burden of asthma in Oregon. Oregon Health Authority, Public Health Division. www.oregon.gov/oha/ph/HealthyEnvironments/WorkplaceHealth/Documents/Burden%20Asthma%202010%20linked_1.pdf.

Grant, E., and J.D. Runkle. 2022. Long-term health effects of wildfire exposure: a scoping review. The Journal of Climate Change and Health 6:100110. https://doi.org/10.1016/j.joclim.2021.100110.

Ha, S., J.T. Abatzoglou, A. Adebiyi, S. Ghimire, V. Martinez, M. Wang, and R. Basu. 2024. Impacts of heat and wildfire on preterm birth. Environmental Research 252:119094. https://doi.org/10.1016/j.envres.2024.119094.

HCUP (Healthcare Cost and Utilization Project). 2021. Introduction to the HCUP Nationwide Emergency Department Sample (NEDS) 2019. Agency for Healthcare Research and Quality. hcup-us.ahrq.gov/db/nation/neds/NEDS2019Introduction.pdf.

HCUP (Healthcare Cost and Utilization Project). 2022. Cost-to-charge ratios for emergency department files. Agency for Healthcare Research and Quality. hcup-us.ahrq.gov/db/ccr/ed-ccr/ed-ccr.jsp.

Heft-Neal, S., A. Driscoll, W. Yang, G. Shaw, and M. Burke. 2022. Associations between wildfire smoke exposure during pregnancy and risk of preterm birth in California. Environmental Research 203:111872. https://doi.org/10.1016/j.envres.2021.111872.

Henderson, S., P. Nguyen, J. Yao, and M. Lee. 2024. The public health paradox of wildfire smoke. British Columbia Medical Journal 66:93,95.

Hubbell, B., N. Fann, and J.I. Levy. 2009. Methodological considerations in developing local-scale health impact assessments: balancing national, regional, and local data. Air Quality, Atmosphere & Health 2:99–110.

Humphreys, A., E.G. Walker, G.N. Bratman, and N.A. Errett. 2022. What can we do when the smoke rolls in? An exploratory qualitative analysis of the impacts of rural wildfire smoke on mental health and wellbeing, and opportunities for adaptation. BMC Public Health 22:41. https://doi.org/10.1186/s12889-021-12411-2.

IPCC (Intergovernmental Panel on Climate Change). 2000. Emissions scenarios: summary for policymakers. https://archive.ipcc.ch/pdf/special-reports/spm/sres-en.pdf.

Jia, H., and E.I. Lubetkin. 2016. Impact of nine chronic conditions for US adults aged 65 years and older: an application of a hybrid estimator of quality-adjusted life years throughout

remainder of lifetime. Quality of Life Research 25:1921–1929.

Johnson, M.M., and F. Garcia-Menendez. 2022. Uncertainty in health impact assessments of smoke from a wildfire event. GeoHealth 6:e2021GH000526. https://doi.org/10.1029/2021GH000526.

Korvenranta, E., et al. 2010. Hospital costs and quality of life during 4 years after very preterm birth. Archives of Pediatrics & Adolescent Medicine 164:657–663.

Landguth, E.L., et al. 2020. The delayed effect of wildfire season particulate matter on subsequent influenza season in a mountain west region of the USA. Environment International 139:105668. https://doi.org/10.1016/j.envint.2020.105668.

Li, Y., D. Tong, S. Ma, X. Zhang, S. Kondragunta, F. Li, and R. Saylor. 2021. Dominance of wildfires impact on air quality exceedances during the 2020 record-breaking wildfire season in the United States. Geophysical Research Letters 48:e2021GL094908. https://doi.org/10.1029/2021GL094908.

Liu, J.C., et al. 2016. Particulate air pollution from wildfires in the western US under climate change. Climatic Change 138:655–666.

Liu, J.C., et al. 2017. Wildfire-specific fine particulate matter and risk of hospital admissions in urban and rural counties. Epidemiology 28:77–85. https://doi.org/10.1097/EDE.0000000000000556.

Liu, Y., E. Austin, J. Xiang, T. Gould, T. Larson, and E. Seto. 2021. Health impact assessment of the 2020 Washington state wildfire smoke episode: excess health burden attributable to increased $PM_{2.5}$ exposures and potential exposure reductions. GeoHealth 5:e2020GH000359. https://doi.org/10.1029/2020GH000359.

Marquez, N., E. Sharygin, D. Loftus, H. Alkitkat, G. Montcho, D. Swanson, and J. Wilde. 2023. Oregon AIAN area & county population projections by race/ethnicity. Population Research Center, Portland State University.

Mirabelli, M.C., A. Vaidyanathan, A.F. Pennington, D. Ye, and C.A. Trenga. 2022. Wildfire smoke and symptoms affecting mental health among adults in the U.S. state of Oregon. Preventive Medicine 164:107333. https://doi.org/10.1016/j.ypmed.2022.107333.

National Center for Health Statistics. (n.d.). Linked birth and infant death data. National Vital Statistics System, U.S. Centers for Disease Control and Prevention. www.cdc.gov/nchs/nvss/linked-birth.htm.

Oregon Climate and Health Program. 2023. Climate and health in Oregon 2023 report. Oregon Health Authority Public Health Division. www.oregon.gov/oha/PH/HEALTHYENVIRONMENTS/CLIMATECHANGE/Documents/FINAL%20Climate%20Health%20in%20Oregon%202023%20v071124%20(1).pdf.

Prieto, L., and J.A. Sacristán. 2003. Problems and solutions in calculating quality-adjusted life years (QALYs). Health and Quality of Life Outcomes 1:80. https://doi.org/10.1186/1477-7525-1-80.

Raich, W., J. Baxter, M. Sheahan, J. Goldhaber-Fiebert, P. Sullivan, and J. Hanmer. 2022. Estimates of quality-adjusted life-year loss for injuries in the United States. Medical Decision Making 43:288–298.

Requia, W.J., H. Amini, M.D. Adams, and J.D. Schwartz. 2022. Birth weight following pregnancy wildfire smoke exposure in more than 1.5 million newborns in Brazil: a nationwide case-control study. The Lancet Regional Health–Americas 11:100229. https://doi.org/10.1016/j.lana.2022.100229.

Rohlman, D., S. Attridge, K. O'Malley, and K.A. Anderson. 2023. Composition of wildfire smoke

and health risks. Pages 192–206 in E. Fleishman, editor. Sixth Oregon climate assessment. Oregon Climate Change Research Institute, Oregon State University, Corvallis, Oregon. https://doi.org/10.5399/osu/1161.

Snover, A., G. Mauger, M. Whitely Binder, M. Krosby, and I. Tohver. 2013. Climate change impacts and adaptation in Washington State: technical summaries for decision makers. cig.uw.edu/projects/climate-change-impacts-and-adaptation-in-washington-state-technical-summaries-for-decision-makers/.

Tarride, J.E., et al. 2016. Loss of health related quality of life following low-trauma fractures in the elderly. BMC Geriatrics 16:84. https://doi.org/10.1186/s12877-016-0259-5.

Taylor, V.R. 2000. Measuring healthy days: population assessment of health-related quality of life. U.S. Centers for Disease Control and Prevention, Atlanta, Georgia. stacks.cdc.gov/view/cdc/6406.

Westerling, A.L. 2016. Increasing western US forest wildfire activity: sensitivity to changes in the timing of spring. Philosophical Transactions of the Royal Society B: Biological Sciences 371:20150178. https://doi.org/10.1098/rstb.2015.0178.

Wettstein, Z.S., S. Hoshiko, J. Fahimi, R.J. Harrison, W.E. Cascio, and A.G. Rappold. 2018. Cardiovascular and cerebrovascular emergency department visits associated with wildfire smoke exposure in California in 2015. Journal of the American Heart Association 7. https://doi.org/10.1161/JAHA.117.007492.

# Drought and Health in Oregon

Rachel Lookadoo

Over the last century, drought events have caused more deaths worldwide than floods, hurricanes, or any other climate-related extreme event (WMO 2021). Droughts, however, are not generally thought of as health threats, although the associations between droughts and negative health outcomes are established. As the intensity, frequency, and duration of droughts increases, the health impacts of these events will only grow (Bell et al. 2016). This chapter explores the health impacts of drought and how those impacts affect the overall well-being of Oregon residents.

Drought is a complex, multifaceted natural hazard that can have detrimental impacts on diverse enterprises or values, such as health, agriculture, water supply, wildlife, energy, and tourism. The American Meteorological Society (2019) defines drought as "a period of abnormally dry weather sufficiently long enough [sic] to cause a serious hydrological imbalance." Different types of drought are distinguished on the basis of their effects on particular components of human and natural systems. For example, meteorological drought is defined as lack of precipitation or evaporative demand that exceeds precipitation for a prolonged period of time. Prolonged meteorological drought that affects surface or subsurface water supply is characterized as hydrological drought. Agricultural drought occurs when meteorological and hydrological drought adversely impacts agricultural production. Socioeconomic drought is characterized by the impacts of meteorological, hydrological, and agricultural drought on the supply and demand of economic goods (NWS n.d.).

In an effort to better delineate and characterize the stages of drought, the U.S. Drought Monitor uses five severity-based classes: abnormally dry (D0) (not a formal drought designation), moderate drought (D1), severe drought (D2), extreme drought (D3), and exceptional drought (D4). Different regions may experience each stage of drought in different ways.

## Drought in Oregon

Since the 1950s, the frequency, duration, and intensity of drought events across the western United States has increased as a result of rising temperatures and, to some extent, changing precipitation patterns. Rising temperatures can contribute to snow droughts due to reduced or earlier water runoff from spring snowpack, which sustains snow-fed rivers (Fosu et al. 2016). Additionally, as the population grows, demand for freshwater increases, straining water availability and increasing the likelihood of drought conditions (Barros et al. 2014).

Although droughts often develop more slowly than other types of natural hazards, they can still have catastrophic effects. Of the 41 weather or climate events in Oregon since 1980 with an economic loss exceeding $1 billion, 16 were droughts, representing 32.4 percent of the total costs of billion-dollar disasters in the state (NOAA n.d.). The most recent billion-dollar drought that affected Oregon occurred from April through September 2023, resulted in $14.8 billion in costs, and led to 247 documented deaths (NOAA n.d.). From 2020 through 2022, the cumulative economic costs and mortality caused by droughts in Oregon were similar to those in 2023 (NOAA n.d.).

## Health Impacts of Drought

Drought is associated with numerous negative health outcomes (Figure 1). Many of the most fundamental characteristics of drought can directly lead to health effects. For example, water
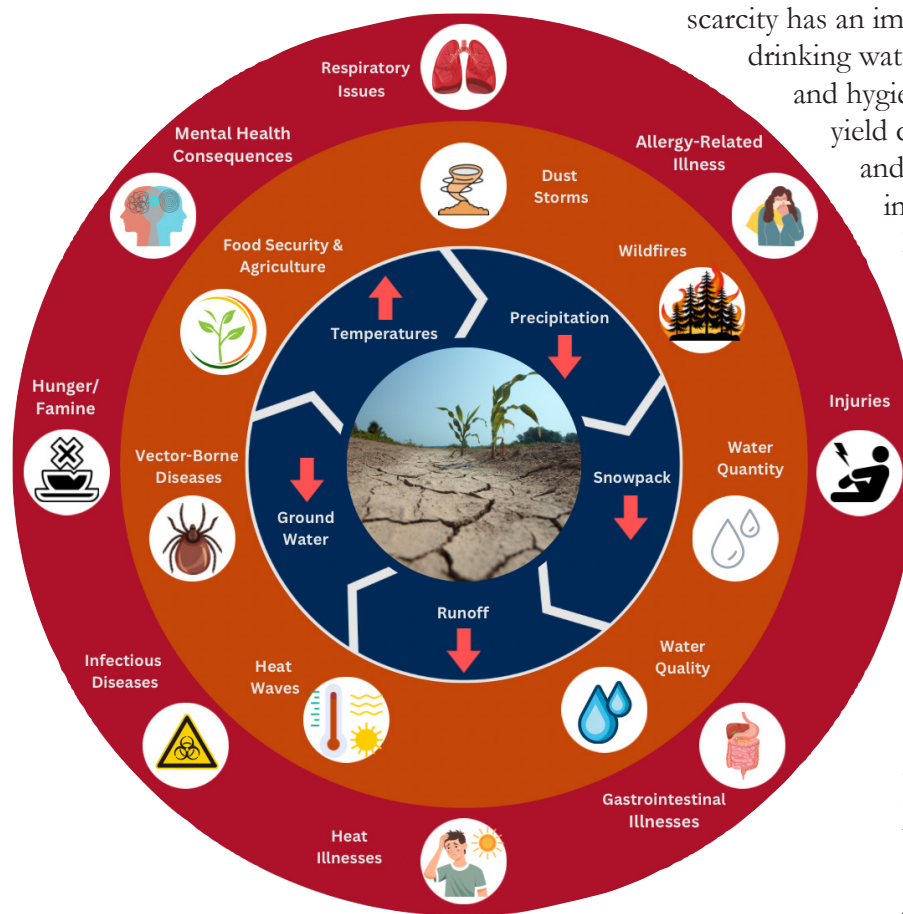
**Figure 1.** Relation between drought and health. Courtesy of Azar Abadi; Lookadoo and Bell 2020.

scarcity has an immediate impact on drinking water supplies, sanitation, and hygiene. Reduction in crop yield can lead to food insecurity and nutritional deficits in impacted communities. Drought conditions contribute to poor air quality due to increased concentrations of dust and particulate matter, thus exacerbating respiratory conditions such as asthma and chronic obstructive pulmonary disease (COPD) (Stanke et al. 2013). Older adults and residents of rural areas can face higher risks of respiratory morality due to drought (Gwon et al. 2023). Wildfires, which are often more frequent and severe during droughts, release large amounts of smoke and pollutants, leading to increased hospital admissions and mortality rates due to respiratory and cardiovascular issues (OHA 2020, Dalton and Fleishman 2021). Drought-related impacts to air quality have also been linked to premature mortality and cardiovascular disease (Berman et al. 2017).

*Drought and Mental Health*

Drought conditions and increased rates of mental health issues, including anxiety, depression, and suicide, are correlated (Vins et al. 2015). Economic pressures from agricultural losses, coupled with the stress of water scarcity, contribute to higher rates of depression and anxiety. In Oregon, rural areas with high agricultural dependency are more likely to experience significant mental health impacts during prolonged drought periods. The reduced crop yield associated with drought can lead to economic strain as food costs increase and farmers and other agricultural producers face income reduction and potential job loss (Berman et al. 2021). Access to mental health services in rural areas is often limited or stigmatized, which can compound the problem (Berman et al. 2021). To address some of these concerns and improve the resiliency of those working in the agriculture industry, Oregon State University Extension has created an online module on climate-related stress for food producers (OSU Extension n.d.).

*Drought and Vector-Borne Diseases*

Because drought can improve habitat quality for certain disease vectors, the incidence of Valley Fever and other vector-borne diseases may increase (Stanke et al. 2013). Within Oregon, there has been an increase in confirmed cases per capita of Lyme disease, West Nile virus, cryptococcal infections, and Valley Fever in recent years (OHA 2020; also see *Effects of Climate Change on Infectious Disease in Animals and Humans*, this volume). Valley Fever (coccidioidomycosis), a fungal infection prevalent in arid regions, is caused by *Coccidioides* fungi in soil. During droughts, soil disturbances from wind and human activities can release fungal spores into the air, increasing the risk of inhalation (OHA 2017).

## Vulnerability to Drought Impacts

As with any natural hazard, some populations may be disproportionately susceptible to and experience disproportional impacts of drought. Children, older adults, and individuals living in long-term care facilities are more susceptible to common health effects associated with drought, such as dehydration and respiratory issues, and to heat-related illnesses, which may arise in co-occurring drought and heat events (Berman et al. 2017). Rural populations often experience greater burdens from drought than populations in non-rural locations. Additionally, rural communities may rely on small or poorly maintained water systems, and thus may be at risk of illnesses associated with poor water quality or contaminant exposure resulting from insufficient water resources for hand hygiene and food safety (Lookadoo and Bell 2020). Approximately 20 percent of Oregon residents use private domestic wells as their primary source of drinking water, and thus are particularly vulnerable to the water quality risks associated with under-maintained wells or wells that are not regularly tested for known contaminants such as nitrates, dissolved solids, coliform bacteria, uranium, and arsenic. (Schimpf and Cude 2020). Unhoused populations or individuals facing housing insecurity also experience disparate impacts from the water insecurity risks associated with drought (Schimpf and Cude 2020). As previously noted, agricultural and migrant workers have increased rates of mental health stress during and after drought events, and often face direct health impacts from heat that can be associated with drought (Berman et al. 2021). Recreational water users may also be at increased risk of exposure to waterborne diseases as a result of lower surface water volumes (CDC 2010).

*Impacts to Tribal Communities*

Tribal and Indigenous communities in Oregon are disproportionately affected by drought due to their dependence on water for cultural, subsistence, and economic practices (OHA 2020). Tribes in Oregon have faced significant challenges due to warming water temperatures and increases in the incidence of harmful algal blooms that affect salmon and other fish populations, which are central to their diet and cultural traditions (OHA 2020).

## Preparedness and Mitigation Efforts for Drought

As drought events continue to occur across Oregon, effective drought preparedness and mitigation efforts can reduce the negative health impacts to individuals and communities. These efforts require partnerships and collaborations across academic and practitioner communities that engage in drought and health-related work (Bell et al. 2023). The following five specific, whole-community mitigation practices are among those applicable to Oregon. First, implementation of water conservation programs may encourage efficient water use in individual homes, agriculture, and other

industries. Second, creation of emergency drinking water access plans can ensure continuity of water supply during shortages. Third, established public health surveillance programs can be used to monitor and respond to drought-related health issues, such as respiratory conditions and vector-borne diseases. Fourth, some effects of drought can be mitigated by promoting accessible mental health care and support services for impacted populations, particularly in rural and agricultural communities. The fifth practice is building community awareness about the negative health impacts of drought.

Engaging partners from across state agencies, local governments, tribal governments, and community organizations is critical to developing inclusive solutions to the negative health impacts of drought. Because one of the most crucial elements of drought preparedness and mitigation is community awareness, it can be particularly effective to train established, trusted messengers such as public health and healthcare providers on appropriate messaging to use with patients and community members during the various stages of drought (Lookadoo et al. 2024).

## Literature Cited

American Meteorological Society. 18 November 2019. AMS Glossary: drought. glossary.ametsoc. org/wiki/Drought.

Barros, V.R., et al., editors. 2014. Climate change 2014–impacts, adaptation and vulnerability: part B: regional aspects. Working Group II contribution to the Fifth Assessment Report of the Intergovernmental Panel on Climate Change. Cambridge University Press, Cambridge, United Kingdom. https://doi.org/10.1017/CBO9781107415386.

Bell, J.E., R.E. Lookadoo, K. Hansen, A. Sheffield, M. Woloszyn, S. Reeves, and B. Parker. 2023. Drought and public health: a roadmap for advancing engagement and preparedness. National Integrated Drought Information System. www.drought.gov/sites/default/ files/2023-06/NIDIS-Drought-Public-Health-Strategy-May2023.pdf.

Bell, J.E., et al. 2016. Impacts of extreme events on human health. Pages 99–128 in A. Crimmins et al., editors. The impacts of climate change on human health in the United States: a scientific assessment. U.S. Global Change Research Program, Washington, D.C.

Berman, J.D., K. Ebisu, R.D. Peng, F. Dominici, and M.L. Bell. 2017. Drought and the risk of hospital admissions and mortality in older adults in western USA from 2000 to 2013: a retrospective study. The Lancet Planetary Health 1:E17–E25. https://doi.org/10.1016/ S2542-5196(17)30002-5.

Berman, J.D., M.R. Ramirez, J.E. Bell, R. Bilotta, F. Gerr, and N.B. Fethke. 2021. The association between drought conditions and increased occupational psychosocial stress among U.S. farmers: an occupational cohort study. Science of the Total Environment 798:149245. https://doi.org/10.1016/j.scitotenv.2021.149245.

CDC (U.S. Centers for Disease Control and Prevention). 2010. When every drop counts: protecting public health during drought conditions—a guide for public health professionals. National Center for Environmental Health (U.S.). Division of Environmental Hazards and Health Effects. stacks.cdc.gov/view/cdc/40520.

Dalton, M., and E. Fleishman, editors. 2021. Fifth Oregon climate assessment. Oregon Climate Change Research Institute, Oregon State University, Corvallis, Oregon. https://doi. org/10.5399/osu/1160.

Fosu, B.O., S.Y.S. Wang, and J.H. Yoon. 2016. The 2014/15 snowpack drought in Washington state and its climate forcing. Bulletin of the American Meteorological Society 97:S19–S24.

https://doi.org/10.1175/BAMS-D-16-0154.1.

Gwon, Y., Y. Ji, J.E. Bell, A.M. Abadi, J.D. Berman, A. Rau, R.D. Leeper, and J. Rennie. 2023. The association between drought exposure and respiratory-related mortality in the United States from 2000 to 2018. International Journal of Environmental Research and Public Health 20:6076. https://doi.org/10.3390/ijerph20126076.

Lookadoo, R.E., and J.E. Bell. 2020. Public health policy actions to address health issues associated with drought in a changing climate. The Journal of Law, Medicine & Ethics 48:653–663.

Lookadoo, R.E., J.E. Bell, and S.L. Woolsey. 2024. Drought and health: a messaging framework for public health professionals & healthcare providers. www.drought.gov/sites/default/files/2024-04/drought__health.pdf.

NIDIS (National Integrated Drought Information System) n.d. U.S. Drought Monitor: Oregon. www.drought.gov/states/Oregon.

NOAA (National Oceanic and Atmospheric Administration). n.d. Billion-Dollar Weather and Climate Disasters: Oregon Summary. www.ncei.noaa.gov/access/billions/state-summary/OR.

NWS (National Weather Service). n.d. www.weather.gov/safety/drought-types.

OHA (Oregon Health Authority). 2017. Coccidioidomycosis fact sheet. www.oregon.gov/oha/PH/DISEASESCONDITIONS/COMMUNICABLEDISEASE/DISEASESURVEILLANCEDATA/ANNUALREPORTS/Documents/2017/2017-Cocci.pdf.

OHA (Oregon Health Authority). 2020. Climate and health in Oregon: 2020 report. www.oregon.gov/oha/PH/HEALTHYENVIRONMENTS/CLIMATECHANGE/Documents/2020/Climate and Health in Oregon 2020 - Full Report.pdf.

OSU (Oregon State University) Extension. n.d. Climate stress and grief: building resilience in farmers and ranchers. extension.oregonstate.edu/climate-stress-grief-building-resilience-farmers-ranchers.

OWRD (Oregon Water Resources Department). n.d. Oregon drought. www.oregon.gov/owrd/programs/climate/droughtwatch/pages/default.aspx.

Schimpf, C., and C. Cude. 2020. A systematic literature review on water insecurity from an Oregon public health perspective. International Journal of Environmental Research and Public Health 17:1122. https://doi.org/10.3390/ijerph17031122.

Stanke, C., M. Kerac, C. Prudhomme, J. Medlock, and V. Murray. 2013. Health effects of drought: a systematic review of the evidence. PLoS CURRENTS 5. www.ncbi.nlm.nih.gov/pmc/articles/PMC3682759/.

Vins, H., J. Bell, S. Saha, and J.J. Hess. 2015. The mental health outcomes of drought: a systematic review and causal process diagram. International Journal of Environmental Research and Public Health 12:13251–13275.

WMO (World Medical Organization). 2021. WMO atlas of mortality and economic losses from weather, climate and water extremes 1970–2019. library.wmo.int/doc_num.php?explnum_id=10902.

# Social Systems

Among the goals of Oregon's Climate Change Adaptation Framework is to create equitable, livable, and engaged Oregon communities in response to the impacts of climate change. As the contributions in this section illustrate, Oregonians are leveraging the legal system, storytelling, and data and models as shifts in climate and their effects become increasingly evident. Creativity and experience are enabling mitigation and adaptation, and in some cases climate change is facilitating economic opportunity.

Austin details the proliferation of climate-related litigation at state and national levels. The courts are considering cases related to reducing greenhouse gas emissions into the atmosphere, responding to the present or anticipated effects of climate change, and remedying climate change harms after they have occurred. The most far-reaching constitutional climate case, brought by youth plaintiffs against the federal government, was filed in Oregon. Moreover, Multnomah County filed the first legal claim centered on the impacts of extreme heat. As the chapter emphasizes, even where there is relevant legislation or government policy, people often turn to the courts to compel action.

In the second chapter in this section, Bloemers relates insights from wildfire survivors, researchers, and practitioners who are featured in the 2022 film *Elemental: Reimagine Wildfire*, for which he served as Executive Producer. Although scientific and emotional debates about the effects of pre-fire and post-fire vegetation management on wildfire behavior continue, ample evidence indicates that the design and maintenance of a structure and the five feet around it are critical for reducing the chance that the structure will ignite. Investments in home hardening also may stabilize insurance markets in Oregon and throughout the western United States.

Earth system models often may seem arcane or far removed from practical relevance. To the contrary, Emard et al. found that long-term climate projections and soil data from the Community Earth System Model version 2 (CESM2) might support adaptation to climate change by farmers in Oregon's Willamette Valley. Moreover, farmers' feedback on relations between modeled data and their observations and the usability of data and data formats is informing the next steps of CESM development by the National Center for Atmospheric Research.

Bachelet and Tomasino explain how trends toward warmer and drier summers and improvements in viticulture practices have contributed to making Oregon a world-class wine production state. As Panwar and Barnett note in *Business and Climate Change* (this volume), Oregon also has a greater number of B Corporation-certified wineries than any other state or country. B Corporations are certified as upholding high standards of social and environmental performance, accountability, and transparency. Nevertheless, wine grape and wine production in Oregon is contending with climate-related extreme events, such as early season heat waves and late season frosts; wildfire smoke that can taint fruit and wine quality; and changes in the identity and intensity of pests and pathogens.

# The Emergence of Climate Litigation

Jay Austin

As the impacts of climate change are increasingly felt across Oregon and nationwide, demands on the legal system have also increased. Disputes can arise wherever human health, well-being, livelihoods, property, natural resources, or ecosystems are at stake. Even where there is relevant legislation or government policy, people often turn to the courts to resolve those disputes or to compel action. Not only has climate-related litigation become its own rapidly growing field, but climate change has begun driving and amplifying other forms of litigation.

## Scope of Climate Litigation

Climate change cases can be grouped into three broad categories on the basis of the factual issues that give rise to them (Thiam and Page 2023). Mitigation cases relate to reducing greenhouse gas emissions into the atmosphere. Adaptation cases generally involve responding to the present or anticipated effects of climate change. Impacts cases are retrospective, attempting to remedy climate change harms after they have occurred. These three concepts are fluid—useful labels, but not legal terms—and a single lawsuit may encompass more than one.

*Mitigation* cases include attempts to stop or slow fossil fuel-based projects, such as environmental review of or challenges to permits for coal-fired power plants, oil and natural gas development, refineries, pipelines, and associated infrastructure. Also in this category are cases about carbon sequestration, whether by retaining capacity to absorb greenhouse gases in ecosystems such as forests and wetlands, or through technological means such as carbon dioxide capture and storage. Additionally, mitigation includes disputes related to the transition to renewable energy, such as siting and land use, environmental impact assessments, and approvals of wind and solar projects or transmission lines.

Examples of *adaptation* include responses to or preparation for sea level rise, storm events, flooding, wildfires, and other climate-related hazards. The legal cases may entail requests to force adaptive actions, claims of inadequate adaptation efforts, or claims seeking funding for adaptation (Waisman 2024). Conceptually, adaptation goes beyond government policy and regulatory law to encompass almost any activity that individuals, markets, or society undertake to anticipate and reduce vulnerability to climate change.

Perhaps the broadest range of cases relate to *climate impacts* on public health and to public and private property and natural resources, again from phenomena such as heat waves, sea-level rise, drought, wildfires, and extreme storms. Some of these impacts inevitably will result in legal disputes, and will require courts to determine who, if anyone, bears responsibility for the damages and which remedies are available. Whether overtly labeled climate litigation or not, these cases are already numerous, as the cost and frequency of climate-related natural disasters continues to rise (NOAA 2024).

## Trends in Number of Cases

Columbia Law School's Sabin Center for Climate Change Law maintains an online database of climate change cases, searchable by topic or jurisdiction (Sabin Center 2024). Their database defines "climate change litigation" as cases that are before a judicial body and feature climate science, policy, or law as a material issue of fact or law: in short, cases where these issues are central to plaintiffs'

claims. It does not include many other cases that touch on those topics in passing, nor where climate effects are in the background of more traditional legal claims, such as insurance or bankruptcy.

Even within these constraints, the Sabin Center data show a sharp increase in the number of climate cases over the past 20 years, both within the United States and in other countries (Figure 1). As of mid-November 2024, the Center's database documented over 2800 cases, with the majority arising in U.S. courts. Of the more than 1800 cases filed in the United States, about 45 percent have been filed in state courts and 55 percent in federal courts. The Fifth National Climate Assessment notes that litigation is already playing a role in U.S. climate governance (USGCRP 2023). The current trajectory, coupled with advances in climate science, suggests that the number of cases will only increase.
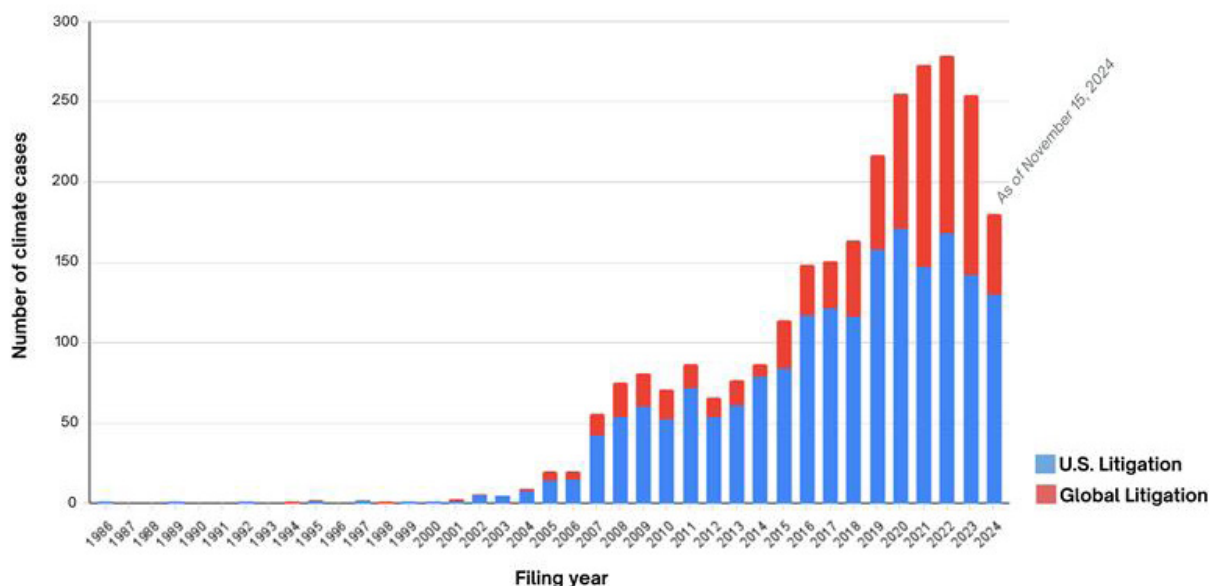


**Figure 1.** Number of climate cases by filing year as of 15 November 2024. Compiled by the Climate Judiciary Project from data in the Sabin Center for Climate Change Law's U.S. Climate Litigation and Global Climate Litigation databases.

The state with the greatest number of climate cases by far is California (Figure 2), which perhaps is unsurprising given its population (nearly 40 million, almost 25 percent greater than any other state), its strong environmental laws, and the scope of its recent natural disasters. Washington, D.C., also attracts numerous lawsuits against the federal agencies headquartered there. But multiple cases have been filed in almost every state, with more than 50 in Oregon even by the Sabin Center's relatively narrow definition. Wildfire, heat and drought, and coastal flooding and erosion have increased awareness of climate change across the West, which in turn is being reflected on court dockets.

**Parties**

Climate litigation involves parties at all levels of government (federal, state, tribal, and local), nongovernmental organizations, industry and trade associations, and individuals. In general, litigants seeking to hold governments or companies accountable for action (or inaction) on climate change or seeking compensation for climate-related damages outnumber those suing to undermine climate protections (Thiam and Page 2023), but there are significant examples of each. Nongovernmental organizations, state and local governments, and industry have been the most frequent plaintiffs in climate lawsuits, and governments and government agencies are the most frequent defendants.
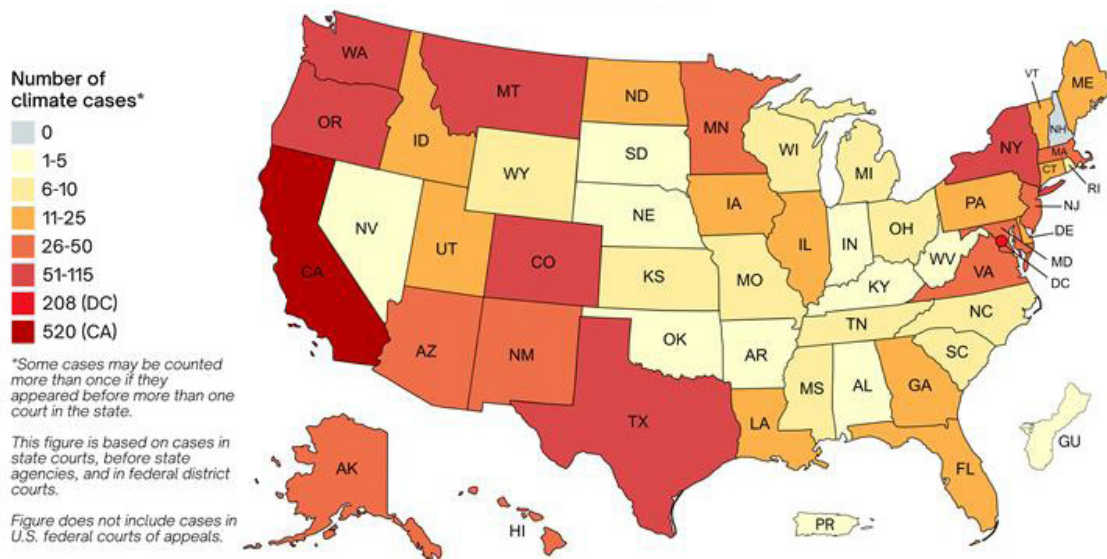
**Figure 2.** Number of climate cases by state and territory as of 15 November 2024. Compiled by the Climate Judiciary Project from data in the Sabin Center for Climate Change Law's U.S. Climate Litigation database.

The *federal government*, typically through its administrative agencies, has often been in court defending climate-related cases. The U.S. Environmental Protection Agency and Department of the Interior are among the most frequent federal defendants. In a widely publicized case filed in Eugene, Oregon, youth plaintiffs essentially sued the entire federal government, including officials from the Council on Environmental Quality, Office of Management and Budget, Office of Science and Technology Policy, and Environmental Protection Agency and the Secretaries of Energy, Interior, Transportation, Agriculture, Commerce, Defense, and State (*Juliana* 2015).

*State governments* have been plaintiffs in climate change cases. Climate-related litigation brought by Connecticut against utility companies was an early example (*Connecticut* 2005). Since then, California, Delaware, Minnesota, New Jersey, and Rhode Island have filed suits against fossil fuel companies. Local governments, including Multnomah County, Oregon, and municipalities in California, Puerto Rico, and Hawaii, have brought similar cases.

Other states have sued to slow or halt climate action, for example by challenging federal regulation of greenhouse gases (e.g., *West Virginia* 2022). States also have been defendants: Washington was sued by youth plaintiffs who alleged that the state created and supported a "fossil fuel-based energy and transportation system" that violated the state constitution and the public trust (*Aji P.* 2021). Hawaii recently reached a settlement in a similar youth lawsuit (*Navahine F.* 2022).

*Nongovernmental organizations* are involved in a large number of climate cases, at times representing a local client or clients. These include both environmental groups and industry trade groups, although environmental nongovernmental organizations appear far more often (Thiam and Page 2023). Corporations also appear in climate cases, almost always as defendants. Many of these companies are defending against claims that they should be held liable for their role in production, transportation, and refining of fossil fuels. Although none of these cases has been fully adjudicated, the claims have been compared to tobacco-related litigation in the 1990s (Geiling 2019) and litigation over exposure to toxicants (McCormick et al. 2017).

*Individuals* also appear in climate litigation, often in cases against government entities. In the United States, many suits have been brought by community groups over project siting, and by youth

271

plaintiffs who assert that government actions and directives related to fossil fuel extraction and consumption violated their constitutional rights or the public trust. One of the latter cases went to trial in Montana, resulting in a judgment for plaintiffs that was affirmed by the Montana Supreme Court on 18 December 2024 (*Held* 2023).

## Types of Legal Claims

As noted above, the legal theories pursued by plaintiffs vary widely. They include federal and state constitutional, statutory, regulatory, and common-law claims, often several in a single suit. The Sabin Center data suggest that federal claims tend to cluster around a handful of environmental statutes, whereas the state-law claims are more diffuse (Table 1).

| Claim | Number of cases | Percentge of cases |
|---|---|---|
| National Environmental Policy Act | 425 | 17.3 |
| State environmental review statutes | 294 | 12.0 |
| Clean Air Act | 291 | 8.9 |
| Other federal statutes | 255 | 10.4 |
| Other state law case categories | 252 | 10.3 |
| Endangered Species Act and other species protection statutes | 231 | 9.4 |
| Adaptation | 167 | 6.8 |
| Constitutional | 154 | 6.3 |
| Freedom of Information Act | 95 | 3.9 |
| Clean Water Act | 68 | 2.8 |
| Cases filed by climate change protesters and scientists | 62 | 2.5 |
| State utility regulations | 61 | 2.5 |
| Carbon offsets and credits | 59 | 2.4 |
| Securities and financial regulation | 41 | 1.7 |
| Common law claims | 38 | 1.5 |
| Public trust | 30 | 1.2 |
| Trade agreements | 3 | 0.1 |

**Table 1.** U.S. climate cases by claim as of 15 November 2024. Compiled by the Climate Judiciary Project from data in the Sabin Center for Climate Change Law's U.S. Climate Ligitation database.

The greatest number of climate-related claims are challenging environmental review procedures under the National Environmental Policy Act or its state-law equivalents. Federal and state constitutional and environmental rights cases receive a great deal of attention from the news media, litigants, and legal scholars, but represent only 6.3 percent of the total number. Tort liability claims, typically based in state common law or statute, are fewer in number but potentially major in impact. These include the cases filed by state and local governments arguing that companies have created a public nuisance or deceived consumers through their sale and promotion of fossil fuels. State utility regulation has also been the subject of climate-related cases.

Most climate cases can be sorted into six categories that reflect the parties, legal claims, and relief being sought. The breadth of categories is likely to expand in the future, particularly in light of increased government commitments to address climate change and accelerating economic drivers of a transition to renewable energy (Thiam and Page 2023).

*Suits to compel government to consider the climate impacts of government or private actions.* These include lawsuits brought under the National Environmental Policy Act and state environmental review laws, which have become a vehicle for parties to argue for consideration of climate change effects in government decision-making and permitting, and that agencies must analyze and disclose the impacts of a wide array of actions, especially actions related to fossil fuel leasing or transport.

The federal Endangered Species Act and state wildlife laws likewise have been invoked to argue that agencies must consider climate change when making decisions about individual species, their habitats, and the impacts of government or private actions on species (Thiam and Page 2023).

*Suits to compel government to take action to prevent climate change, or to prevent government from rolling back climate action.* These include cases claiming that the impacts of climate change are interfering with constitutional or fundamental rights, such as the rights to life, liberty, property, equal protection, or due process; the public trust; and in some states (although not in Oregon), an express right to a clean and healthy environment. They also include statutory and regulatory cases, such as the landmark U.S. Supreme Court decision holding that greenhouse gases qualify as "pollutants" under the federal Clean Air Act (*Massachusetts* 2007), or challenges to subsequent deregulatory actions taken under the same statute (*American Lung Association* 2021).

*Suits against government to challenge climate action.* Conversely, industry and some states have sued the federal government or state governments to challenge regulations and actions that aim to reduce greenhouse gas emissions or adapt to climate impacts. A number of states and industry groups halted implementation of the federal Clean Power Plan for electricity generation (*West Virginia* 2022), and have challenged a successor plan. Many of the same states have also sued to prevent California from continuing to enact its own higher standards for vehicle emissions.

*Suits against fossil fuel companies seeking damages to pay for harms caused by climate change.* These include the climate liability suits mentioned above, brought by various state and local governments and usually grounded in state common law. The most frequently asserted common-law claims rely on tort theories, notably negligence and nuisance, and strict liability claims of trespass, product liability, and failure to warn. Many suits also allege deception or fraud, sometimes overlapping with state consumer protection laws.

*Other suits raising climate-related legal issues.* Climate change is also shaping the law and legal concepts in more traditional litigation. Tort and contract cases often raise issues of foreseeability, such as whether impacts in a specific location were reasonably foreseeable, when they may have become so, and who bears the risk of financial loss. For example, are impacts from an unprecedented wildfire or storm simply unforeseeable, or does climate science suggest that even unprecedented events have become foreseeable? Negligence cases implicate governments' or private parties' standard of care, in terms of both climate adaptation planning (Rizzardi 2024) and the appropriate responses to climate-induced emergencies.

*Suits about events made more frequent and severe because of climate change.* As climate-driven impacts become more common and increasingly costly, litigation will follow. *Utility liability cases* have proliferated in proportion to wildfires allegedly sparked by negligent maintenance or operation of the power grid and exacerbated by extended heat, drought, and high winds. *Insurance litigation* is more prominent as claims and payouts rise (Flavelle and Rojanasakul 2024), and insurers have responded by reducing or withdrawing coverage in high-risk zones in Florida, California, and Oregon (Baumhardt 2024). Legislation and regulations are only beginning to address these issues (Ellfeldt 2024). *Climate migration* may trigger a wave of litigation associated with disaster recovery, resettlement, or access to resources as people are temporarily or permanently displaced due to climate change and related natural hazards (Abate and Choksi 2024, Lara 2024).

## Legal Defenses

*Jurisdiction and preemption.* In most climate cases, jurisdiction is not contested (Thiam and Page 2023). For example, most claims against federal agencies undeniably arise under a federal statute and thus can be filed in federal court. Challenges to state permitting or siting procedures fall squarely within state court jurisdiction. But several high-profile cases, initially filed by state and local governments in state courts on the basis of state law, have led fossil-fuel company defendants to attempt to remove the suits to federal court or to assert that the claims are preempted by federal law. Federal appellate courts have consistently sent these cases back to state court, and the U.S. Supreme Court has so far declined to weigh in.

As one such case proceeded in Hawaii, the state trial court denied the defendant companies' motion to dismiss the City and County of Honolulu's claims that defendants had failed to disclose climate harms and deceptively promoted fossil fuels. The court ruled that the case was grounded in state tort law, and thus not preempted by the federal Clean Air Act (*City and County of Honolulu* 2022). Hawaii's Supreme Court affirmed, and the defendants have petitioned the U.S. Supreme Court for review of that decision; as of November 2024, the Court had not yet ruled on that petition. In contrast to the Hawaii decision, a similar suit brought by the City of Baltimore was dismissed by a Maryland judge, who ruled that federal law controlled the claims made there (*Mayor and City Council of Baltimore* 2024).

*Standing.* The right to bring a lawsuit, or "standing," has been a principal issue in climate litigation. In federal courts, plaintiffs must demonstrate that three criteria are met: they have suffered a concrete and particularized injury, the injury was caused by the defendant, and the court is capable of redressing the injury (*Massachusetts* 2007). Most state courts follow a similar formula, but not all: for example, Connecticut law provides even broader standing for nearly anyone to bring a claim about environmental issues in state court (Ct. Gen. Stat. §22a-16).

The outcome of standing analysis varies among cases depending on what the plaintiff is challenging, what harms they allege, and what remedy they request. Cases seeking injunctive relief to compel government defendants to address climate change may fail on grounds that the claims are too general or are not capable of redress by the court (e.g., *Juliana* 2020). Tort plaintiffs seeking monetary damages, however, have so far faced fewer obstacles to standing.

*Separation of powers and political question.* Constitutional separation-of-powers principles and the so-called political question doctrine have likewise played a role in determining the viability of climate cases. As outlined by the U.S. Supreme Court, the political question defense is implicated when a court determines that aspects of an issue are reserved to a governmental branch other than the judiciary. Some federal trial courts have ruled that climate-related claims present such non-justiciable political questions, although appellate courts have tended to reverse those decisions (*Comer* 2009, *Connecticut* 2009). Some state courts have invoked analogous doctrines to dismiss part or all of the youth climate suits (*Held* Order 2021, *Reynolds* 2021, *Sagoonick* 2022); other courts have rejected this defense and allowed the claims to proceed (*Navahine F.* 2022).

## Remedies

Reflecting the diverse plaintiffs, defendants, and legal theories related to climate change, the remedies requested are diverse (Thiam and Page 2023). Many are fairly conventional, including *monetary damages* for climate-related harms, with substantially different amounts sought in different

suits; various forms of *injunctive relief* to compel government or private-sector action, both remedial and prospective; *declaratory judgments* as to whether a particular government action or inaction is legal; and requests for *vacatur* (voiding a previous decision) of administrative or regulatory actions (Dernbach and Parenteau 2023).

Some plaintiffs are seeking less conventional, sometimes sweeping remedies directed at changing foundational elements of energy and transportation policy. For example, the Montana youth climate case commenced with plaintiffs requesting equitable relief, including enjoining the state from carrying out its official energy policy, an accounting of Montana's emissions, and a court order requiring the state "to develop a remedial plan or policies to effectuate reductions of greenhouse gas emissions in Montana consistent with the best available science" (*Held* Complaint 2020).

The judge eventually ruled out broad injunctive relief, but after trial issued a declaratory judgement that Montana officials had violated state constitutional guarantees, and enjoined them from enforcing a provision of a statute (*Held* 2024). In Hawaii, plaintiffs' similar demands resulted in a settlement where the state government agreed to phase out all greenhouse gas emissions from the state transportation system by 2045 (*Navahine F.* Settlement 2024).

## Western Topics and Examples

Recent examples of litigation in Oregon and its neighboring states illustrate several of the climate change impacts and legal theories outlined above. The most prominent cases thus far have been traditional tort lawsuits against electric utilities for wildfires, the magnitude of which is associated with climate change (NOAA 2023) even if that driver is not directly at issue. But various suits in the state and region also have addressed the root causes of climate change.

During 2023 and 2024, PacifiCorp was found liable for and settled hundreds of claims totaling hundreds of millions of dollars from Oregon homeowners affected by the Labor Day 2020 fires (Haas 2023, AP June 2024). The company faces a separate $100 million suit from Willamette Valley wineries and vineyards whose products were tainted by soot and smoke (AP May 2024). Similar litigation in California sent Pacific Gas and Electric into bankruptcy in 2019 (California PUC 2024), and plaintiffs in the deadly 2023 Lahaina wildfire announced they had reached a $4 billion settlement with Hawaiian Electric, Maui County, and the State of Hawaii (PBS News 2024).

Oregon also is the locus of the most far-reaching constitutional climate case, brought by youth plaintiffs against the federal government. Their suit was rejected by the Ninth Circuit (*Juliana* 2020), and the U.S. Supreme Court has declined to intervene (Clark 2024). Similar claims against state governments have been more successful. For example, a Montana trial judge determined that a state law that barred state agency officials from considering climate impacts and greenhouse gas emissions when carrying out environmental reviews violated youth plaintiffs' state constitutional right to a "clean and healthful environment" (*Held* 2023). That decision was upheld by the Montana Supreme Court. Hawaii settled a similar lawsuit brought by youth plaintiffs there (*Navahine F.* 2022).

State and local governments in western jurisdictions have brought a number of tort suits against fossil-fuel companies in which they sought monetary damages for diverse climate impacts. In California, such suits began in 2017 with several counties and municipalities (e.g., *County of San Mateo* 2017) and culminated in the state itself filing suit (*People v. Exxon Mobil* 2023); under state procedural rules, these cases are now being jointly coordinated in a San Francisco trial court (Drugmand 2024). Similar suits are pending in Colorado and Hawaii (*Boulder County* 2018, *City and County of Honolulu*

2020, *County of Maui* 2020), with a petition for review of a Hawaii Supreme Court decision in the Honolulu case currently being considered by the U.S. Supreme Court.

In Oregon, following the June 2021 Pacific Northwest heat wave (Gardner 2021), Multnomah County filed the first legal claim centered on the impacts of extreme heat (*County of Multnomah* 2023, St. Martin 2024); that case is pending in state court. An earlier industry-led lawsuit brought by Oregon and California fishermen for climate harm to the Pacific Dungeness crab (*Metacarcinus magister*) fishery stalled on procedural grounds (*Pacific Coast Federation* 2023).

Plaintiffs have also challenged state and local governments' regulatory actions to mitigate or adapt to climate change. For example, when the California Coastal Commission established a setback requirement for new residences in Encinitas, property owners challenged the Commission's projections of sea-level rise and coastal erosion. An appellate court found for the state, noting that it "used well-accepted scientific methodology to support its setback recommendation," and employed more recent data than did the plaintiffs' expert witness (*Martin* 2021). The California Court of Appeals also rejected a takings claim after the state prohibited a property owner from constructing a seawall to forestall coastal erosion (*Lindstrom* 2019).

The State of Montana has challenged the City of Portland's zoning code amendments that block the bulk transportation or storage of fossil fuels within city borders, alleging that Portland is interfering with interstate commerce (*Montana* 2023). An earlier challenge to those amendments by local builders initially was successful before the Oregon Land Use Board of Appeals, but the Board's decision was reversed by the Oregon Court of Appeals (*Columbia Pacific Building Trades Council* 2018). Oregon's land-use planning system, with statewide goals that encourage dense housing and mass transit, local implementation, and adjudication by the Land Use Board of Appeals, is itself a potentially useful framework for adapting to climate change and resolving disputes (Adams-Schoen and Smith 2023, *City of Cornelius* 2024).

For Oregon and the West as for the rest of the country, the number of pending cases moving through the courts and the increase in climate-related impacts suggest that climate litigation across the region will continue to grow.

## Literature Cited

Abate, R.S., and A. Choksi. 2024. Coastal migration with dignity: safeguards for vulnerable communities. Environmental Law Reporter 54:10744–10754.

Adams-Schoen, S.J., and M. Smith. 2023. Land-use law and climate change. Pages 171–189 in E. Fleishman, editor. Sixth Oregon climate assessment. Oregon Climate Change Research Institute, Oregon State University, Corvallis, Oregon. https://doi.org/10.5399/osu/1161.

*Aji P. v. State of Washington*, No. 80007-8-I (Washington Court of Appeals, 8 February 2021), certiorari denied, No. 99564-8 (Washington Supreme Court, 6 October 2021).

*American Lung Association v. EPA*, 985 F.3d 914 (U.S. Court of Appeals for the District of Columbia Circuit, 2021)

AP (Associated Press). May 2024. Oregon wine industry seeks $100M from PacifiCorp for wildfire smoke damage. Greenwire. subscriber.politicopro.com/article/eenews/2024/05/30/oregon-wine-industry-seeks-100m-from-pacificorp-for-wildfire-smoke-damage-00160410.

AP (Associated Press). June 2024. PacifiCorp to pay $178M to victims of deadly 2020 Oregon blazes. Greenwire. subscriber.politicopro.com/article/eenews/2024/06/04/pacificorp-to-pay-178m-to-victims-of-deadly-2020-oregon-blazes-00161408.

Baumhardt, A. 2024. Oregon homeowners face soaring premiums, few property insurance options over wildfires. Oregon Public Broadcasting. www.opb.org/article/2024/02/26/wildfire-protection-insurance-premium-oregon-wildfires-homeowners-fire-policies/

*Boulder County v. Suncor Energy*, No. 2018CV030349 (Colorado District Court, 17 April 2018).

California PUC (California Public Utilities Commission). 2024. PG&E bankruptcy. www.cpuc.ca.gov/industries-and-topics/pge/pge-bankruptcy.

*City and County of Honolulu v. Sunoco LP*, 1CCV-20-0000380 (Hawaii Circuit Court, 9 March 2020); denial of motion to dismiss affirmed, SCAP-22-0000429 (Hawaii Supreme Court, 31 October 2023); petition for writ of certiorari filed, 23-952 (U.S. Supreme Court, 28 February 2024).

*City of Cornelius v. Department of Land Conservation & Development*, No. A180037 (Oregon Court of Appeals, 2024).

Clark, L. 2024. Supreme Court nixes bid to revive *Juliana*. Youth say they'll try again. Climatewire. subscriber.politicopro.com/article/eenews/2024/11/13/supreme-court-nixes-bid-to-revive-juliana-youth-say-theyll-try-again-00189089.

*Columbia Pacific Building Trades Council v. City of Portland*, 289 Or. App. 739 (Oregon Court of Appeals, 2018).

*Comer v. Murphy Oil USA*, 585 F.3d 855, 869-76 (U.S. Court of Appeals for the Fifth Circuit, 2009).

*Connecticut v. American Electric Power (AEP), Inc.*, 406 F. Supp. 2d 265 (U.S. District Court for the Southern District of New York, 2005); vacated and remanded, 582 F.3d 309 (U.S. Court of Appeals for the Second Circuit, 2009); reversed and remanded, 564 U.S. 410 (U.S. Supreme Court, 2011).

*County of Maui v. Sunoco LP*, No. 2CCV-20-0000283 (Hawaii Circuit Court, 12 October 2020).

*County of Multnomah v. Exxon Mobil Corporation*, No. 23CV25264 (Oregon Circuit Court, 22 June 2023).

*County of San Mateo v. Chevron Corporation*, No. 17CIV03222 (California Superior Court, 17 July 2017).

Dernbach, J.C., and P.A. Parenteau. 2023. Climate science and law for judges curriculum — judicial remedies for climate disruption: a preliminary analysis. Climate Judiciary Project. cjp.eli.org/curriculum/overview-climate-litigation.

Drugmand, D. 2024. Judge ok's coordination for multiple California climate cases against big oil. DeSmog. www.desmog.com/2024/02/20/bonta-california-climate-lawsuits-merging-chevron-exxon-shell-oil/.

Ellfeldt, A. 2024. California bill would force insurers to consider wildfire mitigation. Climatewire. subscriber.politicopro.com/article/eenews/2024/04/19/calif-bill-would-force-insurers-to-consider-wildfire-mitigation-00153172.

Flavelle, C., and M. Rojanasakul. 2024. As insurers around the U.S. bleed cash from climate shocks, homeowners lose. The New York Times. www.nytimes.com/interactive/2024/05/13/climate/insurance-homes-climate-change-weather.html.

Gardner, J.R. 2021. Seventy-two hours under the heat dome. The New Yorker. www.newyorker.com/magazine/2021/10/18/seventy-two-hours-under-the-heat-dome.

Geiling, N. 2019. *City of Oakland v. BP*: testing the limits of climate science in climate litigation. Ecology Law Quarterly 46:683.

Haas, R. 2023. Oregon jury finds electric utility PacifiCorp liable in devastating wildfires. National Public Radio. www.npr.org/2023/06/15/1182377213/oregon-jury-finds-electric-utility-pacificorp-liable-in-devastating-wildfires.

*Held v. Montana*, No. CDV-2020-307 103 (Montana First Judicial District Court, 13 March 2020);

judgment for plaintiffs (14 August 2023); affirmed DA 23-0575 (Montana Supreme Court, 18 December 2024).

*Juliana v. United States*, No. 15-01517 (U.S. District Court of Oregon, 10 September 2015); motion to dismiss denied (10 November 2016); reversed, 947 F.3d 1159, 1170-71 (U.S. Court of Appeals for the Ninth Circuit, 2020).

Lara, N. 2024. Climate migration as climate resilience: a case study of Orlando, Florida. Environmental Law Reporter 54:10736–10743.

*Lindstrom v. California Coastal Commission*, 40 Cal.App.5th 73 (California Court of Appeals, 2019).

*Martin v. California Coastal Commission*, 66 Cal.App.5th 622 (California Court of Appeals, 2021).

*Massachusetts v. U.S. Environmental Protection Agency*, 549 U.S. 497 (United States Supreme Court, 2007).

*Mayor and City Council of Baltimore v. BP*, 24-C-18-004219 (Maryland Circuit Court, 10 July 2024).

McCormick, S., et al. 2017. Science in litigation: the third branch of U.S. climate policy. Science 357:979–980.

*Montana v. City of Portland*, No. 3:23-cv-00219 (U.S. District Court of Oregon, 14 February 2023).

*Navahine F. v. Hawai'i Department of Transportation*, 1CCV-22-0000631 (Hawaii Circuit Court, 2022), settled (20 June 2024).

NOAA (National Oceanic and Atmospheric Administration). 2023. Wildfire climate connection. www.noaa.gov/noaa-wildfire/wildfire-climate-connection.

NOAA (National Oceanic and Atmospheric Administration). 2024. Billion-dollar weather and climate disasters. www.ncei.noaa.gov/access/billions/.

*Pacific Coast Federation of Fishermen's Associations, Inc. v. Chevron Corporation*, No. CGC-18-571285 (California Superior Court, 2018), removed No. 3:18-cv-07477 (U.S. District Court for the Northern District of California, 2018), voluntarily dismissed (14 December 2023).

PBS. 2024. Parties in lawsuits seeking damages for Maui wildfires reach $4 billion global settlement. www.pbs.org/newshour/nation/parties-in-lawsuits-seeking-damages-for-maui-wildfires-reach-4-billion-global-settlement.

*People v. Exxon Mobil Corporation*, No. CGC23609134 (California Superior Court, 2023).

*Reynolds v. State of Florida*, No. 1D20-2036 (Florida Supreme Court, 18 May 2021).

Rizzardi, K. 2024. Rising seas and the property professions: have ethics and best practices adapted? George Washington Journal of Energy and Environmental Law 61: in press.

Sabin Center for Climate Change Law. 2024. Climate change litigation databases. climatecasechart.com.

*Sagoonick v. State*, 503 P.3d 777 (Alaska Supreme Court, 2022).

St. Martin, V. 2024. 'Not caused by an act of God': in a rare court action, an Oregon county seeks to hold fossil fuel companies accountable for extreme temperatures. Inside Climate News. insideclimatenews.org/news/08072024/multnomah-county-oregon-lawsuit-against-fossil-fuel-industry-for-heat-dome/.

Thiam, S.N., and J.C. Page. 2023. Climate science and law for judges curriculum — overview of climate litigation. Climate Judiciary Project. cjp.eli.org/curriculum/overview-climate-litigation.

USGCRP (U.S. Global Change Research Program). 2023. The fifth National Climate Assessment. nca2023.globalchange.gov.

Waisman, D. 2024. Failure-to-adapt climate litigation: an underused tool? Environmental Law Reporter 54:10960–10986.

*West Virginia v. EPA*, 597 U.S. 697 (U.S. Supreme Court, 2022).

# Reimagining the Wildfire Challenge and Local Solutions

Ralph Bloemers

As the climate of the western United States becomes warmer and drier, both the area burned and the number of homes lost to wildfires are increasing. The greatest losses occur when dry winds spread fire and burning embers into communities and ignite combustible materials, vegetation, and structures. Burning structures then ignite other nearby structures, causing conflagrations in which hundreds of homes burn in several hours. These urban fires are occurring more often, and in places not previously identified as high risk.

The most destructive wildfires are best understood as "wind events with fire in them" (Donato and Halofsky 2019, Balch et al. 2024). These fires can grow by hundreds of acres per hour, and thousands to tens of thousands of acres per day, overwhelming suppression efforts. For example, the 2018 Camp Fire burned over 18,000 structures in and around the town of Paradise, California, and took 85 lives. The 2020 Labor Day fires in Oregon burned over 1 million acres (4,050 km²) and destroyed communities believed to be at low risk for wildfire. In 2021, the Dixie Fire became California's largest on record (Branson-Potts 2021), and the Marshall Fire, while small, grew rapidly and destroyed more structures than any other fire on record in Colorado (Branson-Potts 2021, Holmstrom et al. 2022). In July 2024, the Park Fire outside Chico, California, grew to over 400,000 acres (1,618 km²) at a rate of about 4,000 acres (16 km²) per hour.

Between the decades of 1999–2009 and 2010–2020, the number of structures lost to wildfires in the western United States increased by 246 percent (Higuera et. al. 2023). For several decades, wildfire prevention efforts in the United States have focused on vegetation clearing and other forms of land management (USFS 2023). Yet during periods of extreme fire behavior with high winds, thinned forest plantations, areas treated with prescribed burns, fuel breaks, dirt roads, city streets, multiple-lane highways, and natural barriers such as the crest of the Sierra Nevada did not prevent fire from spotting over great distances or igniting fuels (Syphard 2011, Boxall 2019, Siegler 2021).

Destructive fires ignite and spread in all vegetation types. For example, two ignitions leading to the burning of dry grasses and shrubs in Boulder County, Colorado, generated enough embers to ignite and then burn 1,057 homes in the Marshall Fire in six hours. In August 2023, wind drove fire into Lahaina, Hawaii, and caused structure-to-structure ignitions, leaving at least 102 people dead and two missing. Over 70 percent of the more than 1.8 million acres burned in Oregon in 2024 as of 28 October, when the Oregon Department of Forestry ended fire restrictions, were grasslands and shrublands (Wildland Mapping Institute 2024).

More than four years after the 2020 Labor Day fires, many of the Oregonians who survived these fires, but lost their homes, are still struggling, and most of the communities are only partially rebuilt. A number of survivors died before receiving compensation for their economic and emotional losses. These survivors and all Oregonians need a clear-eyed understanding of the threat that wildfire poses to communities and scalable ways to prevent homes from burning.

I have worked on forest and wildfire issues in the Pacific Northwest for over 20 years. I have spent time with firefighters, fire scientists, and fire survivors. For over seven years, I have taken extensive time-lapse and wildlife photographs in burned landscapes (Figure 1), and worked with journalists to report on fires across the West. My focus is on stories that distill the best science, identify the dominant factors that lead to home and community losses, and motivate people to take actions

to protect life and property and make their homes savable in the most extreme conditions. From 2017 to 2022, I worked with a team to produce *Elemental: Reimagine Wildfire*. I then traveled across the United States and Canada to screen the film in hundreds of theaters and at community events, conferences, K-12 schools, and universities. Time and again, I found that people are eager for solutions that are based on a proper problem definition and actions they can take on their own home and property.

Ample research demonstrates how to prevent losses of life and property via actions that largely are adjacent



**Figure 1**. Black bear (*Ursus americanus*) in 2022 within an area that burned at high severity during the 2017 Eagle Creek Fire, Columbia River Gorge, Oregon. Photograph by Ralph Bloemers.

to homes, and durable. The question is whether society can shift from investing in fire suppression and vegetation management that defines the inevitable wildfire as the problem and instead mitigate the risk of home ignition, even in the most extreme fire weather (Calkin et al. 2023). Making this shift requires reimagining humans' relationship with fire, which in turn necessitates acceptance of the natural reality of fire and preparation of homes and communities well before fires ignite.

## Dominant Cultural Narratives About Wildfire

In the twenty-first century, technology and media influence many aspects of people's thoughts, perceptions, and social constructs, and have affected the way that society in the United States views natural events. Wildfire is an emotional topic, and news coverage is filled with stories about devastating losses of lives, homes, and other property. Stories about fires in natural areas such as Yellowstone and Yosemite National Parks, the Columbia River Gorge, and the Cascade Range have often represented fires as catastrophes instead of as natural processes that renew, restore, and maintain ecosystems.

In his book *Media and Apocalypse*, Conrad Smith (1992) examined the media coverage of the Yellowstone fires of 1988. Conrad Smith loved Yellowstone, and was distraught when he learned from news reports that it had burned. Then he visited the burned area in 1990 and discovered that the regrowth in burned areas was prolific. He interviewed hundreds of people, and identified three dominant perceptions about fire: fire destroys forests and other vegetation, fire kills all wildlife, and people can and should be in control of fire. The narrative that fire is big, bad, and must be put out is powerful and widespread. These beliefs reinforce the message that wildfire is the problem and that the problem is solved by management of forests: that people can reduce smoke, protect communities, or limit the expense of wildfire suppression by reducing the volume of vegetation or altering the canopy in forests, and then maintaining the reduction of vegetation over time and space.

Forests and other ecosystems burn, and then regrow (Figure 2). Homes that burn, of course, do not regrow. Yet this significant distinction sometimes is blurred by the media, and an urban view of fire is superimposed on wildlands. Wildfires are often depicted in terms of disaster, damages, and victims, with stories that center on how, where, and what they burn. A forest is "destroyed" or "nuked" by "catastrophic" "megafire" (Stoof et al. 2024). Although there are high-quality aspects of wildfire coverage, reporting on wildfires routinely personifies harm, emphasizes the graphic effects of the events, and relies on generalizations about cause and effect that are inconsistent with scientific understanding (Fire Learning Network 2024). This rhetoric affects the public's conception of wildfires. Media outlets and government officials are challenged in portraying events accurately, with context, nuance, and paradox, rather than presenting a stereotype of a disaster. They are also hampered by the fact that hyperbolic headlines often boost readership and views. Limited reporting on the social, political, and scientific contexts of wildfires creates a disconnect between public perception of wildfires, an understanding of the reality of and reasons for their occurrence, and viable, scalable ways to reduce losses.
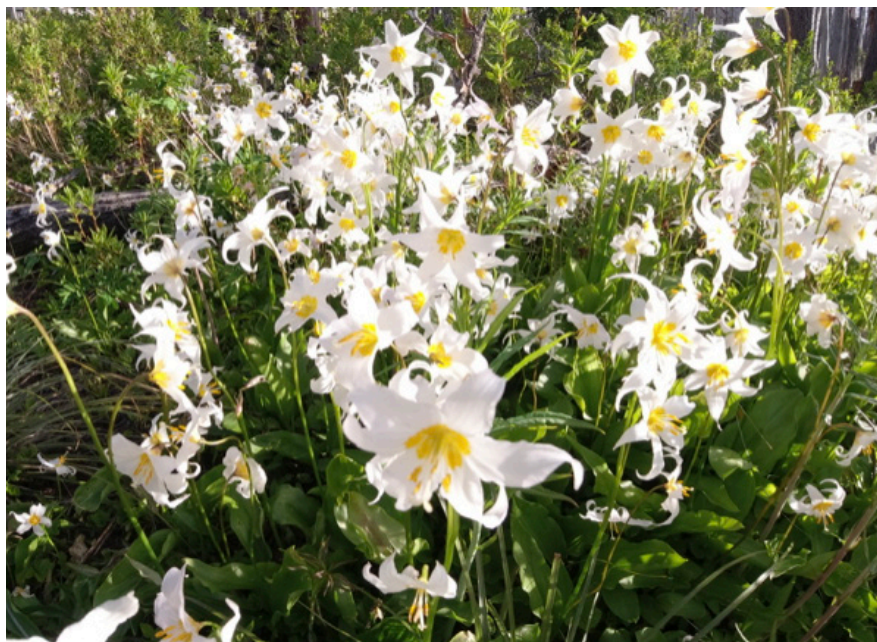


**Figure 2**. Avalanche lilies (*Erythronium montanum*) in an area recovering from the 2011 Dollar Lake Fire, Mt. Hood, Oregon. Photograph by Ralph Bloemers.

Coverage of fire in forests is full of references to acres consumed or destroyed without an examination of what is happening within the fire perimeters (Ingalsbee 2007). The entirety of Yellowstone National Park did not burn in 1988, although some Americans concluded it had after reading press accounts of the fires or watching the nightly news (Smith 1992). Similarly, the Columbia River Gorge was not destroyed by the Eagle Creek Fire. Although the fire perimeter enclosed around 50,000 acres (202 km²), only 8,000 acres (32 km²) burned at high severity (killed most of the vegetation). The remainder of the area burned at low or moderate severity or was unburned (USFS 2017). Eight years later, the high severity patches are full of new growth, and wildlife is abundant. Fires do not ordinarily destroy forests or cause animals to flee in terror, as suggested by some media networks and Walt Disney Productions' movie *Bambi*.

## Public Perceptions of Wildfire Control and Responsibility

The most immediate, major concern when a wildfire ignites is protecting human life and property. When communities burn, blame often is placed on officials and agencies who attempted but failed to suppress wildfire regardless of whether suppression is realistic. For decades, the dominant belief that wildfires can be controlled or stopped has led society to prepare for fire ineffectively.

Media coverage of wildfires generally is similar to that of other disasters in that it highlights the damages and the vivid impacts. The public's preconception that wildfire can be controlled determines how stories about fires and their causes and solutions are reported and received. Earthquakes and hurricanes are considered to be uncontrollable, whereas fires are considered to be controllable, leading to unrealistic public expectations during extreme fire weather conditions. Most fires are controllable, but extreme fire behavior is not. When societal expectations of control are not met, the public's perception of institutional ineptitude is reinforced.

## Stories to Protect Oregonians

In 2017, in the wake of the Eagle Creek Fire, I worked with Trip Jennings, a filmmaker based in Oregon, to document the extent of the burn. We produced numerous short films about ecological recovery in the Columbia River Gorge. For example, we flew over the burned area with John Bailey, a professor at Oregon State University, and *Oregonian* reporter Kale Williams. Lisa Ellsworth, an Oregon State University scientist, took us to forests in the Clackamas River drainage that had burned in a fire several years before and explained how quickly the forest grows back after fire. *The Oregonian* picked up the film, communities throughout the Columbia River Gorge played it at forums, and media outlets shared our photographs to help Oregonians make sense of the fire.

Over the last seven years, Trip and I deployed time-lapse and wildlife cameras in areas that burned at high severity throughout the Columbia River Gorge; in the Clackamas, Santiam, and McKenzie river corridors following more recent fires; and in areas in the Klamath-Siskiyou Mountains and on Mt. Hood that burned in the past. With these cameras, we documented the return of life to burned areas, and our images have been featured in the Oregon Public Broadcasting Field Guide (Profita 2021), KOIN (Arden 2023), KGW News (2024), *The Statesman Journal*, *The Register Guard*, and numerous films.

With support from National Geographic, Film Action Oregon, the Oregon Community Foundation, Meyer Memorial Trust, and the Lazar Foundation, I worked with Trip's team at Balance Media Productions to produce *Elemental: Reimagine Wildfire*. I shot photographs, examined fire science, interviewed scientists, secured the film's narrator, and worked with a fact-checking team to produce the film. The film helps viewers understand the dominant factors in structure loss in extreme fires, the benefits of fire in forests in the western United States, and actions to prevent the losses of homes. After two years on tour and hundreds of theatrical screenings, special events, and professional conferences, most with a public question-and-answer session afterward, I have seen how stories can help people live with fire and adapt to more extreme weather in a changing climate. The following are ten major insights from the fire survivors, fire and home safety researchers, meteorologists, Indigenous fire lighters, and firefighters who are featured in the film.

## Firefighting has Limits

The opening scenes of *Elemental: Reimagine Wildfire* are narrated by a young couple, a nurse, and a firefighter who survived the Camp Fire. Survivors' stories help people understand the conditions that lead to the greatest losses: a wind-driven ember storm entering a community that ignites homes, which in turn become the fuel that ignites other homes (Cohen 2000, Joyce 2018).

After-action reports on destructive fires reveal that these fires were not controlled until the weather conditions changed. Although investments in wildfire suppression and vegetation management have significantly increased, the number of homes lost to wildfires has increased exponentially. Urban

conflagrations in Santa Rosa, Malibu, Ventura, and Paradise, California; Superior, Colorado; Talent and Phoenix, Oregon; and Lahaina, Hawaii; have exceeded the limits of firefighting capacity. A small number of fires cause most of the life and property loss (Balch et al. 2024). These are wind-driven fires that escape suppression and either skip over or burn through vegetation treatments. Stemming the losses from these fires require people to focus on preparing homes to resist ignition instead of expecting that a fire can be controlled.

During the film's production and on our nationwide tour, firefighters shared how important it is for the public to understand the limits of firefighting and shift perceptions away from the dominant narratives of heroes in a firefight and megafires (usually defined as fires larger than 100,000 acres [405 km²]) that can and must be suppressed at all costs. To bring the limits into sharp focus, firefighters who responded to the Camp Fire explained that five or six fire engines are needed to defend a single structure in a wind-driven fire, and many more are needed to douse the fire if the structure ignites. To put this in perspective, for firefighters to have had a chance of saving one-third of the more than 18,000 structures that were lost in the Camp Fire, every fire truck in California would have needed to arrive in Paradise in less than an hour. During wind-driven fires, aircraft may be grounded, and even if they can fly, the water or retardant they drop barely reaches the ground. Sharing the limits of fire suppression informs reasonable public expectations, and in turn motivates action before fires ignite.

**Most Destructive Fires Are Wind-Driven and in Grasslands and Shrublands**

Considerable attention and resources are directed at fire in forests, yet fires burn in grasslands and shrublands, too. From 1990–2020, wildfires in grasslands and shrublands burned 80 percent of the homes and structures lost to wildfire in the conterminous United States (Radeloff et al. 2023). The vegetation types that tend to burn in fast fires, defined as fires that grow by over 4,000 acres (1619 hectares) per hour, are mostly grasses and shrubs. Fast fires led to 88 percent of the home and structure losses across the conterminous United States from 2001–2020 (Balch et al. 2024).

Sixty percent of homes lost to wildfires in the western United States from 1999–2020 occurred during wildfires driven by downslope winds (Abatzoglou et al. 2023). All types of vegetation can produce embers that ignite receptive fuels in and around homes. For example, embers can ignite bark mulch next to the structure, fine plant material in gutters, and fences against which the embers accumulate (Joyce 2018). The burning bark mulch, fine plant materials, or fences become the pathways to home ignition. The greatest risk is not from a wall of flames in the tree canopy bearing down on a community. Experiments and after-action reports from numerous fires demonstrate that the intensity of a wildfire is not directly related to ignition of homes and other structures (Cohen 1999, 2000, 2004; Cohen and Westhaver 2022).

Wildfires ignited by human causes accounted for 76 percent of structure losses in the western United States from 1999–2009 (Higuera et al. 2023). Over that period, the median number of structures lost per unit area burned by human-ignited fires was ten times greater than that burned by lightning-ignited fires (Higuera et al. 2023). Across the conterminous United States from 1992–2012, human-caused wildfires accounted for 84 percent of all wildfires and accounted for nearly half of the cumulative area burned (Balch et al. 2017). Human-caused ignitions have tripled the length of the fire season, extending it into months when lightning is rare (Balch et al. 2017, Coop et al. 2022).

## Weather and Climate Drive Large Fires

Among the factors contributing to increases in the area burned and the duration of the fire season across the western United States are decreases in vegetation and soil moisture as a result of higher temperatures. The resulting drier vegetation enables rapid fire growth, particularly when it coincides with strong winds (Abatzgolou and Williams 2016, Abatzgolou et al. 2023). Ecosystem modifications, including expansion of non-native invasive grasses and conversion of native forests to tree plantations, also contribute to fire risk. The frequency of extreme fire weather is increasing, nights are becoming more conducive to burning, and fires are burning at higher elevations (Bowman et al. 2020, Alizadeh et al. 2021, Balch et al. 2022). For example, limited late summer, autumn, and early winter precipitation in Colorado's Front Range left grasses dry and flammable, which facilitated the spread of the wind-driven Marshall Fire. Reduction in wind speeds and heavy snow on the following day led to containment (Colorado Division of Fire Prevention and Control 2021).
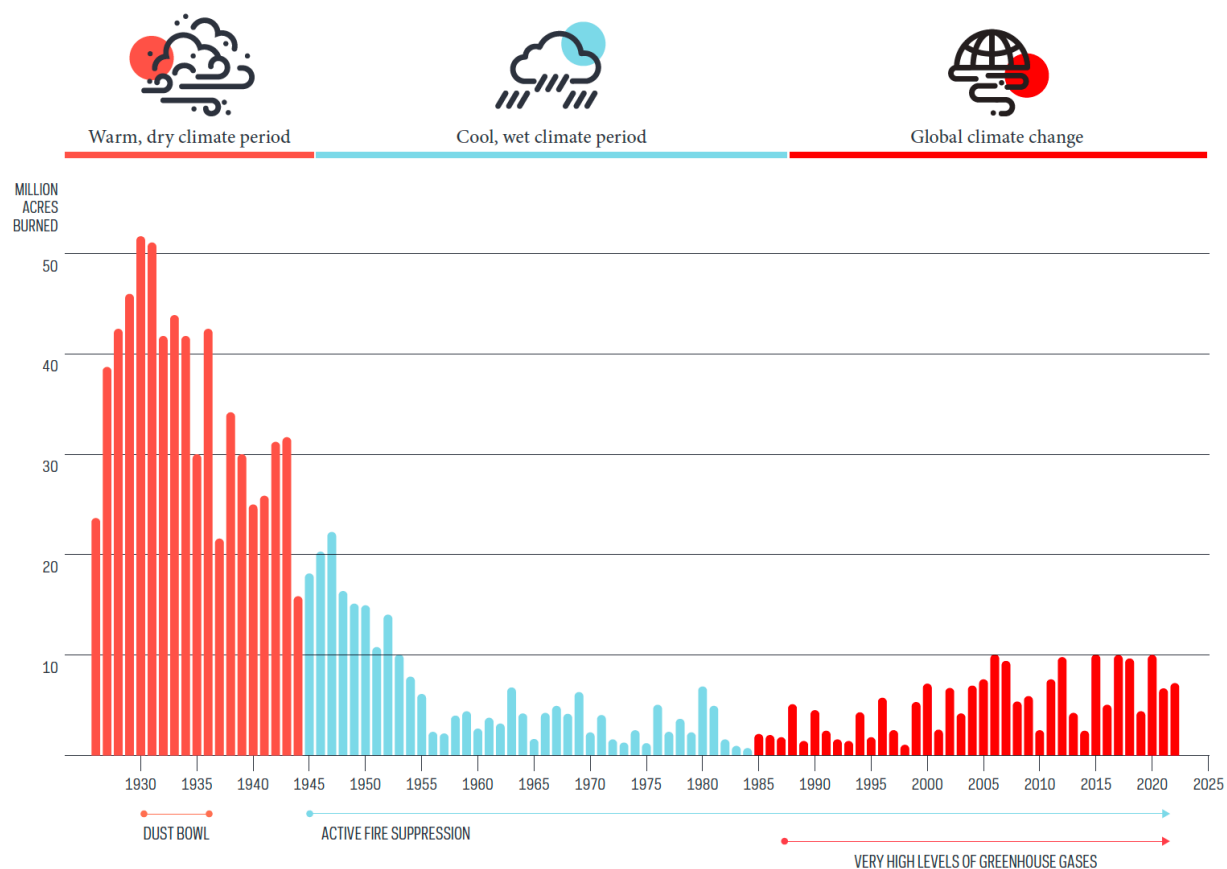


**Figure 3**. Variability in climate, trends in land management, and human-driven climate change contribute to variability in area burned in the conterminous United States.

Human-induced climate change contributed to a doubling of the area burned in western forests from 1984 through 2015 (Abatzgolou and Williams 2016). Large fires, such as the Lionshead (Oregon, 2020), Camp (California, 2018), Woolsey (California, 2018), Glass (California, 2020), and North Complex (California, 2020), often co-occur with low fuel moisture, high downslope winds,

and high temperatures (Abatzgolou et al. 2023). Although the annual area burned in Oregon and the western United States since the 1980s has increased considerably, creating the impression that the extent of fire is unprecedented, the area burned is similar to that during earlier decades with relatively warm and dry conditions (Figure 3). (Littell et al. 2009, ODF 2022). Aridity of the atmosphere and vegetation were significant contributors to the annual average area burned in the western United States in the last decades of the twentieth century and first two decades of the twenty-first century (Abatzgolou and Williams 2016, Coop et al. 2022).

As climate change increases the odds of large fires and extreme fire behavior in the western United States, fire suppression is becoming less viable as a way to mitigate wildfire risk than it was from the 1940s through the 1980s. Although fire size attracts considerable attention, speed has a stronger effect on the potential for destruction of homes and communities. Downslope wind events, such as the easterly winds that are common in late summer and autumn in Oregon, are associated with significant losses (Abatzgolou et al. 2021, Evers et al. 2022).

## Focus Investments From the Home Outward

As home losses increase, numerous insurance providers are not writing new homeowners policies in any or large parts of the California market because the financial risk is too high. Insurance retreat, which also is occurring in Oregon (Baumhardt 2024), is prompting a reexamination of which strategies for preventing home loss are most effective. For several decades, the U.S. Forest Service's Missoula Fire Sciences Laboratory, National Fire Protection Association, Insurance Institute for Business and Home Safety, Underwriters Laboratory's Fire Safety Research Institute, and National Institute for Standards & Technology have studied causes of home losses and how the losses can be prevented. Their experiments and analyses consistently suggest that the design and maintenance of a home and the five feet around it, or the home ignition zone, are critical for reducing the chance that the home will ignite (Figure 4) (Cohen 2004, Cohen and Westhaver 2022, Hedayati et al. 2023, Kerber and Alkonis 2024). Although structures can ignite from intense radiant heat within 30 ft. (9 m), the most effective actions are close to the structure. In contrast, attempts to control fire intensity by altering vegetation over large areas have a limited probability of success (Schoenagel et al. 2017).

The Wildfire Prepared Home, a new certification by the Insurance Institute for Business and Home Safety, focuses on that home ignition zone. The distance between many homes and the property boundary is no more than 5 ft. (1.5 m), and the distance between neighboring homes is often not more than 10 ft. (3 m). Therefore, recommendations to address defensible space beyond those distances—often 30, 60, or 100 ft. (9, 18, or 30 m) from the home—can be confusing and discourage action. The top five recommendations provided to homeowners in over 100,000 fire preparedness assessments conducted in 2023 and 2024 with the Fire Aside application focus on actions in the immediate area around the home (Figure 5) (Fire Aside 2024).

Showing people videos of home-ignition experiments (Figure 4) and homes that have survived extreme fire illustrates the dominant influences on home loss and underscores that they have the power to prepare their homes for fire. Insurance companies are also telling homeowners that these preparations are needed to make the companies' risk acceptable and stabilize insurance markets (PBS 2023). Although a full retrofit may cost $100,000, the cost of retrofits such as installing ember-resistant vents or metal flashing along a deck, or replacing combustible mulch next to the house with pavers or stone, is $2,000–15,000 (Barrett and Quarles 2024). The cost of building new homes that are resistant to wildfires is equal to that of traditional construction (Quarles and Pohl 2018).

**Figure 4**. Testing resistance of home building and landscaping materials to ignition from wind-blown embers. Photograph courtesy of ElementalFilm.com.

## Effects of Vegetation Management on Fire Behavior are Uncertain

Many contemporary forests in the western United States are fragmented, and in the Pacific Northwest, numerous older forests have been cut and replaced with younger plantations. Forests cover about 30 million acres (121,400 km²) in Oregon, and nearly 19 million acres (76,890 km²) are publicly owned. The remainder of Oregon's landscapes are dominated by grasslands and shrublands. Of the 11 million acres (44,510 km²) of privately owned forest, around 6.8 million acres (27,520 km²) are managed as tree plantations. Tree removal has the greatest effect on fire behavior if the managed area burns before forest regenerates.

Heavily managed tree plantations that are logged on short rotations tend to burn faster and at higher severity than naturally regenerated forests (Zald and Dunn 2018, Levine et. al. 2022). In a subset of fires that burned in California from 1985 through 2019, the incidence of high-severity fire was greater in areas closer to private industrial land than in areas further away (Levine et al. 2022). Nearly 70 percent of the area burned within the 2020 Holiday Farm Fire in Oregon was in timber plantations (Gavin 2020) (Figure 6). Many of the forests in the western United States have been cut over and replanted, and therefore their structure and the species present are not the same as those during the sixteenth through eighteenth centuries.

The Pacific Northwest's mesic, cool forests, which include about 60 percent of the forests in Oregon, historically burned infrequently. Wildfire dynamics in these systems are characterized as climate-limited rather than fuel-limited. Large fires have occurred in forests west of Oregon's Cascade Range since at least the year 1500 (Spies et al. 2018, Donato and Halofsky 2019). The 2017 Eagle Creek Fire and several of the 2020 Labor Day fires are emblematic of the fires that occur in this region. These events are driven by downslope winds that, when combined with an ignition, result in large fires with rapid rates of spread. Suppression is often not feasible during wind events, and tree thinning with the aim of changing fire behavior is largely ineffective and cost prohibitive in

systems in which trees regenerate rapidly and fires tend to be wind-driven (Evers et al. 2022, Reilly et al. 2022).

While thinning and reintroducing fire in a small patch of forest can serve human values, such as reducing risk to infrastructure, the area thinned across extensive public forests has little relation to area burned (Schoennagel et al. 2017). Across the western United States from 2005–2014, roughly one percent of U.S. Forest Service fuels treatments burned each year (Schoennagel et al. 2017). Dry forest types that may be candidates for intervention cover less than one-third of forested area nationwide (Schmidt et al. 2002), and about 40 percent of forests in Oregon (Spies et al. 2018). Furthermore, in ponderosa pine (*Pinus ponderosa*) forests, thinning, prescribed burning, and other maintenance generally must be repeated every 10 to 20 years to be effective (Wasserman et al. 2022).

Statements to the effect that dry forests are unnaturally dense or have burned infrequently and therefore are likely to burn severely evince a focus on low-intensity surface fire. However, efforts to influence outcomes in dry forests are complicated by many factors. For example, mixed intensity and stand-replacing fires (crown fires) historically were common in most dry forests in the western United States (Schmidt et al. 2002), and it is challenging to thin vast areas of trees to reduce the likelihood of these fires over space and time (Rhodes and Baker 2014, Schoenagel et al. 2017). Among 60,000 fires that burned in the conterminous United States from 2001 through 2000, the ten with the fastest single-day growth rates occurred in areas with more than 50 percent grass cover (Balch et al. 2024). Grasses tend to dry quickly, and grasslands provide little friction to slow wind speeds (Balch et al. 2024). To manage wildland fire as a natural disturbance, society needs to accept that fires across a gradient of size and intensity are inevitable, essential ecological processes.

**Reduce the Incidence of Human-Caused Ignitions**

Since humans discovered fire, deliberate and inadvertent human-caused ignitions have expanded the season during which ignitions occur and the number of ignitions. The U.S. Forest Service's Fire Program Analysis Fire-Occurrence Database, which currently includes more than 2 million wildfires that occurred in the United States

**Top 5 Recommendations**

Based on over 100,000 home evaluations across the Western U.S. in 2023 & 2024

1. Remove Vegetation in Zone 0

2. Replace Vents to Prevent Ember Entry

3. Remove Attached Combustible Fence/Gate

4. Limb or Cut Back Overhanging Trees

5. Remove Combustible Mulch

Source: fire aside

**Figure 5**. Fire Aside's top five recommendations for reducing the risk of home ignition.

from 1992 through 2020, recognizes 13 ignition causes. The ten classes of human-caused ignitions range from debris and open burning to fireworks to misuse of fire by a minor. Across the western United States, debris and open burning accounted for the greatest percentage of wildfires during downslope wind events (about 30 percent). During periods of downslope winds, wildfires attributed to recreation and ceremony became 116 percent more likely (Abatzoglou et al. 2023). Likewise, those attributed to power generation, transmission, or distribution were 75 percent more likely during downslope winds. From 1992–2015, 97 percent of wildfires ignited in the wildland-urban interface across the conterminous United States were human-caused (Mietkiwiecz et al. 2020). Across the United States, the number of ignitions caused by fireworks spikes on and around 4 July (Mietkiewicz et al. 2020, Vachula et al. 2023). In Oregon, cities increasingly are banning fireworks (De Dios 2024), while federal jurisdictions such as the U.S. Forest Service and National Park Service commonly ban camp fires and other open fires during hot, dry, or windy conditions (e.g., NPS 2024, USFS 2024).
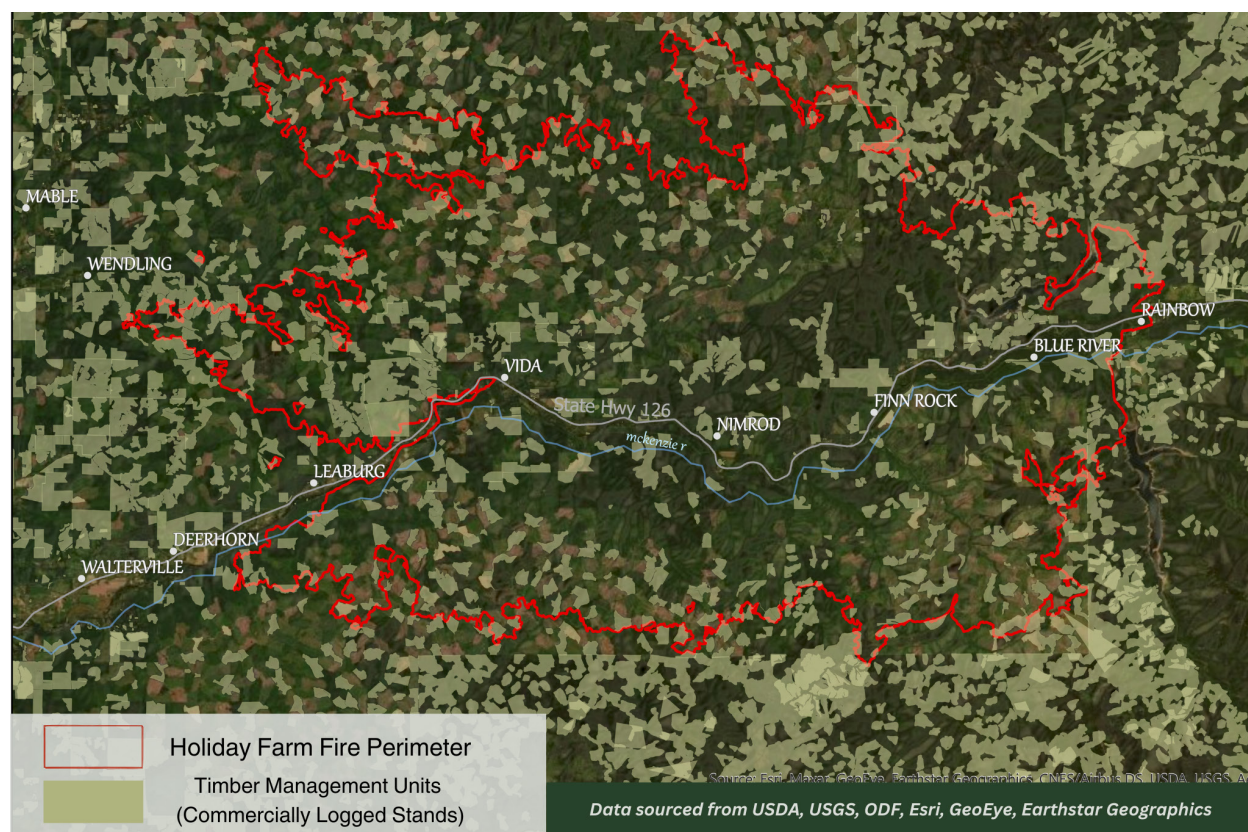


**Figure 6**. Almost 70 percent of the area within the perimeter of the Holiday Farm Fire, Oregon (8 September–3 October 2020) was in timber plantations. Figure courtesy of Firefighters United for Safety, Ethics, and Ecology.

The Fire Program Analysis Fire-Occurrence Database indicates that debris and open burning caused the greatest percentage of human-ignited wildfires in Oregon from 1992–2020 (14 percent), and equipment and vehicle use led to greatest percentage of area burned (5 percent). Ignitions caused by power generation, transmission, or distribution accounted for two percent of the total number of fires >1 acre, and 0.3 percent of the area burned. Nevertheless, the role of power systems is attracting increasing attention given that they ignited or contributed to ignition of some of the recent wildfires that caused the greatest losses of life and structures. These include the Tubbs (2017, Santa Rosa, California), Camp (2018, Paradise, California), Almeda (2020, Talent and Phoenix, Oregon), Marshall (2021, Boulder County, Colorado), and Lahaina (2023, Maui, Hawaii) fires. From

2015 through 2020, energized power lines ignited six of 20 of California's most destructive fires (California State Auditor 2021). Wildfires ignited by power systems rapidly can become large because they generally begin during periods of high wind.

Public safety power shutoffs increasingly are being implemented with the aim of preventing ignitions from power generation, transmission, or distribution. Use of such shutoffs was approved in California in 2012, and Portland General Electric implemented one in Oregon in 2020. Although shutoffs widely are believed to be effective, few data are available given how recently they were adopted. Utilities in Oregon are encouraging individuals whose medical care requires power to contact their utility provider to ensure that their health is not compromised during a shutoff. Vegetation management along power line corridors, modifications to equipment, and monitoring technologies also are strategies for reducing the number of ignitions from electricity infrastructure.

## Most Forest Fires Release Relatively Small Amounts of Carbon

Forest carbon is in a constant state of flux. Vegetation regrows and sequesters carbon after fires, and carbon emissions from forests and other ecosystems often occur in pulses. *Elemental: Reimagine Wildfire* explores the impacts of wildfires on carbon stocks in forests, and viewers are often surprised. Although moderate to high intensity fire can kill trees, most of the carbon remains in the ecosystem as dead wood that decomposes over decades to centuries. From 2009–2018, carbon emissions from timber harvest and burning of fossil fuels in the western United States were 16 times greater than emissions from forest fires (Bartowitz et al. 2022), albeit state-level or regional carbon emissions from wildfires can be considerable in years in which the area burned is high. Emissions of carbon per unit area were 1.5 to 8 times greater in harvested areas than in burned areas because harvest killed a greater proportion of trees (Bartowitz et al. 2022). In part because 1–20 percent of areas in which fuels were reduced are likely to burn within 10–25 years after treatment, it may be necessary to treat an average of 25 acres (10 hectares) of forest to appreciably reduce wildfire potential in a given 2.5 acres (1 hectare) (Campbell et al. 2012). Field-based studies of combustion rates in two large fires in California found that carbon emissions across the entire area burned were equivalent to 0.6 to 1.8 percent of the vegetative biomass (Harmon et al. 2022). In mixed conifer and ponderosa pine forests that burned in fires in 2013 and 2020 in the central and southern Sierra Nevada, California, the majority of biomass was large trees with low combustion rates, and less than half of the area within the fire perimeter burned at high intensity (Harmon et al. 2022). These findings are consistent with field studies from the 500,000-acre (2023 km$^2$) Biscuit Fire that burned in southern Oregon in 2002 (Campbell et al. 2007).

Oregon's rainforests are among the most carbon-rich forests in the world. When trees are harvested, some of the carbon they stored is released into the atmosphere (Law et al. 2022). Although carbon estimates depend on available data, and average values mask variation among stands, a significant amount of the tree remains on site to decompose or be burned as logging residue (Smith et al. 2006). At the mill, an additional component of the harvested wood becomes residue from producing the end product. In addition, transportation of the wood to the mill and market uses carbon. Therefore, the carbon stored in wood products over their lifetime, and potentially for some time after in a landfill, is a fraction of the carbon in living trees. Over the last several decades, carbon losses from logging outpaced carbon losses by fire on a per unit area basis in the western United States. For example, in the western United States from 1984 through 2020, carbon emissions from harvest of mature trees were 2 to 8 times greater per unit area than from wildfires larger than 1,000 acres (405 hectares) with at least 50 percent forest cover within the perimeter (Bartowitz et al. 2022).

Mature and older trees and forests generally store more carbon than younger forests. Models suggest that 120 years following harvest, a harvested mature forest and its associated wood products contain less carbon than a comparable, unharvested mature forest (Law et al. 2022). On public forests in Oregon, projected increases in the harvest rotation from 40 to 80 years, in conjunction with projected halving of harvest levels, would store considerably more carbon than planting trees in previously forested or unforested areas (Law et al. 2022). Averaged among 48 plots in undisturbed primary or older secondary forests worldwide, half of the aboveground biomass was in the one percent of trees with the largest diameter (Lutz et al. 2018). In six National Forests in the eastern Cascade Range and Blue Mountains in Oregon, Washington, and Idaho, an average of three percent of five species of trees had diameters of 21 in. (0.5 m) or greater, and stored about 42 percent of the aboveground carbon (Mildrexler et al. 2020).

## Invest in the Fire Workforce of the Future

Many of the European-American settlers who colonized the western United States viewed fire as a destructive force to be controlled and eliminated. In the 1850s, state and federal governments outlawed Indigenous fire practices that had been used for thousands of years. After World War II, surplus military equipment was deployed to augment fire suppression. This increased investment coincided with a cool, wet period from the 1940s to the 1980s (Figure 3) and contributed to the belief that fire could be controlled if enough people and money were dedicated to doing so.

Thinning of shrubs, saplings, and the lower limbs of large trees can help prepare the ground surface of dry forests for the controlled reintroduction of fire by Indigenous, cultural, and prescribed-fire practitioners. This kind of understory thinning more often resembles pruning than removal of trees, and is generally followed by pile and broadcast burning where dead limbs and needles accumulate. The combustion of the surface and understory fuels provides nutrients for new plant growth (WFMMC 2023). The use of intentionally ignited fire is growing in Oregon. For example, Indigenous fire practitioners are reintroducing fire to the Willamette Valley, Southern Oregon, and the Klamath Basin. Oregon Senate Bill 762 (2021) required the Oregon Department of Forestry to establish a Certified Burn Manager Program that includes certification requirements, standards, and procedures and reduces individual liability for certified personnel who start prescribed burns consistent with legal and program criteria.

A number of organizations in Oregon offer workforce training. For example, the Lomakatsi Restoration Project works with tribes and agencies to implement ecosystem restoration projects and build a tribal workforce in the process. The Northwest Youth Corps established the Community Wildfire Protection Corps, which trains and employs people to reduce fire risk in high priority areas in and around communities. The Northwest Youth Corps crews focus on clearing vegetation in a buffer zone around infrastructure and homes. The organization works in coordination with local fire departments, Oregon Department of Forestry, and Office of State Fire Marshal.

## Protect Aquatic Systems and Soils After Fire

Fires of all severities are natural ecosystem processes (Lindenmayer et al. 2004). Species richness and abundance of some taxa, including the abundances of some species of birds, often increases in the first few years after a wildfire (Smucker et al. 2005). Whether to log fire-damaged and fire-killed trees (Figure 7) has been debated for decades. Post-fire logging, especially in systems with sustained human activity and near streams, creeks, and rivers, can increase soil compaction and erosion

**Figure 7**. Logging following a wildfire. Photograph courtesy of ElementalFilm.com.

(McIver and McNeil 2006, Slesak et al. 2015, Wagenbrenner et al. 2015, 2016), increase sediment loads in waterways (Emelko et al. 2011, Silins et al. 2014), adversely affect habitat for some aquatic species, and hinder regeneration of some plant species (Karr et al. 2004). These effects result from both removal of trees and the infrastructure necessary for timber harvest, such as road building, vehicle traffic, and use of heavy machinery.

Effects of post-fire logging on soil nutrients, soil microbial and fungal communities, and carbon exchange capacity are difficult to distinguish from effects of the wildfire, which often are greater. However, in mixed-conifer forests in central Oregon, nutrients that contribute to soil productivity decreased in response to mechanical, post-fire timber harvest (Jennings et al. 2012). In mixed-conifer forests in the Sierra Nevada, post-fire logging reduced carbon storage, and carbon storage in mineral soil was particularly low in tree plantations that were logged following fire (Powers 2013).

Post-fire logging usually is a short-term economic decision, but can have long-term ecological impacts. Retaining dead, dying, and living trees in burned areas can contribute to conservation of water quality, commercially harvested fishes, and other aquatic species. Converting burned forests to tree plantations without dead wood increases the extent of a homogenous vegetation type that is well-represented in western Oregon, and the potential for high-severity fire (Zald and Dunn 2018). Furthermore, forests with diverse tree species are expected to tolerate climate extremes and other disturbances more effectively than monocultures, and to store carbon for longer (Osuri et al. 2020).

**Harness Technology to Support Situational Awareness and Action**

Community-level preparation for wildfire can benefit from technologies that provide accurate, timely, and actionable data. For example, real-time data on fire ignitions, spread, weather, and evacuation orders inform people about rapidly developing events. A growing number of companies and nonprofit organizations have devoted significant resources to predicting, detecting, mitigating, adapting to, and communicating about fire. These entities are capitalizing on satellite remote sensing data, drones, and artificial intelligence. Some of the tools and technologies are reliable and are being rapidly adopted, whereas others require further scrutiny.

Users of remote sensing data relevant to wildfires include the general public, media, federal and state agencies, and insurance and utility sectors. Satellite remote sensing provides information on the environmental characteristics that affect fire probability, wildfire behavior, the extent and recovery of burn areas, post-fire erosion, and impacts on air and water quality. Satellites deployed by the National Aeronautics and Space Administration and operated by the National Oceanic and Atmospheric Administration provide real-time weather and fire weather forecasting capabilities.

To facilitate parcel-level mitigation and ideally reduce the risk of insuring homes, entrepreneurs have developed tools that allow fire departments to directly assess home flammability and provide homeowners with clear, actionable recommendations. For example, Fire Aside developed software to enable firefighters to efficiently assess a home's preparedness for fire. The software allows an expert assessor to quickly provide a homeowner with a prioritized list of potential actions, grant opportunities, and a simple mechanism for reporting steps taken. Fire Aside has been adopted in Ashland and Eugene, Oregon, and is under consideration by other jurisdictions in the state. The Fire Aside defensible space report also is being used by about 70 percent of homeowners in Truckee, California, to identify defensible space and home-hardening actions and to qualify for discounts on insurance premiums.

For the last two decades, the public and the media have relied on Inciweb, an interagency, all-risk incident information management system that provides data on active fires. In recent years, people also have turned to social media. In some cases, the information from social media is outdated, inaccurate, and rife with conspiracy theories. To illustrate constructive responses to this reality, in 2022, Watch Duty launched a mobile application to provide real-time, accurate information on fires, including alerts, fire perimeters, and images from live cameras. Watch Duty's information comes from a team of firefighters, dispatchers, and reporters who monitor radio scanners around the clock. Watch Duty Pro, which is available to firefighters and first responders, includes information on land ownership, evacuation zones, radio repeaters, critical infrastructure, and utility service territories.

As another innovative example, with the aim of reducing the risk of ignitions from power generation, transmission, or distribution, Gridware has engineered a sensing system that monitors overhead power infrastructure. The system detects and identifies disturbances such as vegetation strikes on power lines, fallen lines, broken poles, and conductor clashes and reports them to the utilities. The tool is intended to increase safety and reduce outage durations by providing information even when the electrical system is down.

**A Vision for the Future**

Shifting from a societal perspective that all fires are harmful to fire-resilient communities requires understanding of the dominant influences on wildfire ignition and behavior and strategic investment

in wildfire mitigation. To make this shift, scientists and firefighters are encouraging the public to make homes and communities resistant to fire rather than attempting to control the flammability of vegetation across vast areas. Home mitigation specialists, landscapers, architects, and builders are supporting homeowners to prepare structures to resist ignition. Public agencies, firefighters, and legislators are supporting prescribed burn associations. Companies are harnessing existing technology and developing new tools that provide people with situational awareness and analysis before, during, and after fires.

*Elemental: Reimagine Wildfire* was produced to help people learn to live within the natural realities of fire. During our nationwide tour, teachers, students and firefighters asked our film team if we were aware of any curricula on wildfire-prepared homes. We were not, and therefore hired an experienced curriculum developer to prepare the peer-reviewed *We Live With Fire* curriculum. The curriculum is adaptable for grades 6–12, undergraduates, and the general public. It focuses on what people can do to design, build, retrofit, and maintain homes and communities to be fire-ready and fire-safe.

The *We Live with Fire* curriculum and *Elemental: Reimagine Wildfire* are part of a larger, collective effort by firefighters, fire survivors, tribes, utilities, businesses, legislators, non-profit organizations, philanthropists, and others to set Oregon on a new path. In this envisioned future, Oregonians understand that fire is inevitable and can be beneficial, and are prepared for fire and smoke.

## Literature Cited

Abatzoglou, J.T., C.A. Kolden, A.P. Williams, M. Sadegh, J.K. Balch, and A. Hall. 2023. Downslope wind-driven fires in the western United States. Earth's Future 11:e2022EF003471. https://doi.org/10.1029/2022EF003471.

Abatzoglou, J.T., C.S. Juang, A.P. Williams, C.A. Kolden, and A.L. Westerling. 2021. Increasing synchronous fire danger in forests of the western United States. Geophysical Research Letters 48:e2020GL091377. https://doi.org/10.1029/2020GL091377.

Abatzoglou, J.T., and A.P. Williams. 2016. Impact of anthropogenic climate change on wildfire across western US forests. Proceedings of the National Academy of Sciences 113:11770–11775.

Alizadeh, M.R., J.T. Abatzoglou, C.H. Luce, J.F. Adamowski, A. Farid, and M. Sadegh. 2021. Warming enabled upslope advance in western US forest fires. Proceedings of the National Academy of Sciences 118:e2009717118. https://doi.org/10.1073/pnas.2009717118.

Arden, A. 27 June 2023. 6 years later: photographer documents Columbia Gorge 'reset' after Eagle Creek Fire. KOIN 6. www.koin.com/local/6-years-later-photographer-documents-columbia-gorge-reset-after-eagle-creek-fire/.

Balch, J.K., J.T. Abatzoglou, M.B. Joseph, M.J. Koontz, A.L. Mahood, J. McGlinchy, M.E. Cattau, and A.P. Williams. 2022. Warming weakens the night-time barrier to global fire. Nature 602:442–448.

Balch, J.K., B.A. Bradley, J.T. Abatzoglou, R.C. Nagy, E.J. Fusco, and A.L. Mahood. 2017. Human-started wildfires expand the fire niche across the United States. Proceedings of the National Academy of Sciences 114:2946–2951.

Balch, J.K., et al. 2024. The fastest growing and most destructive fires in the US (2001 to 2020). Science 386:425–431.

Barrett, K., and S.L. Quarles. 2024. Retrofitting a home for wildfire resistance: costs and considerations. Headwaters Economics, Bozeman, Montana. headwaterseconomics.org/natural-hazards/retrofitting-home-wildfire-resistance/.

Bartowitz, K.J., E.S. Walsh, J.E. Stenzel, C.A. Kolden, and T.W. Hudiburg. 2022. Forest carbon emission sources are not equal: putting fire, harvest, and fossil fuel emissions in context. Frontiers in Forests and Global Change 5:867112. https://doi.org/10.3389/ffgc.2022.867112/.

Baumhardt, A. 26 February 2024. Oregon homeowners face soaring premiums, few property insurance options over wildfires. Oregon Capital Chronicle. oregoncapitalchronicle.com/2024/02/26/oregon-homeowners-face-soaring-premiums-few-property-insurance-options-over-wildfires/.

Bowman, D.M.J.S., C.A. Kolden, J.T. Abatzoglou, F.H. Johnston, G.R. van der Werf, and M. Flannigan. 2020. Vegetation fires in the Anthropocene. Nature Reviews Earth and Environment 1:500–515.

Boxall, B. 11 September 2019. California is spending $32 million on a fire prevention strategy that doesn't work in high winds. Los Angeles Times. www.latimes.com/projects/wildfire-california-fuel-breaks-newsom-paradise/.

Branson-Potts, H. 18 August 2021. Dixie Fire races toward Susanville, forcing some residents to evacuate. The San Diego Union-Tribune. www.sandiegouniontribune.com/news/california/story/2021-08-18/dixie-fire-races-toward-susanville-forcing-some-residents-to-evacuate.

California State Auditor. 2021. Electrical system safety. auditor.ca.gov/reports/2021-117/index.html. Accessed 10 October 2023.

Calkin, D.E., K. Barrett, J.D. Cohen, M.A. Finney, S.J. Pyne, and S.L. Quarles. 2023. Wildland-urban fire disasters aren't actually a wildfire problem, Proceedings of the National Academy of Sciences 120:e2315797120. https://doi.org/10.1073/pnas.2315797120.

Campbell, J.L., D.C. Donato, D.A. Azuma, and B.E. Law. 2007. Pyrogenic carbon emission from a large wildfire in Oregon, USA. Journal of Geophysical Research 112(G4):G04014. https://doi.org/ l0.1029/2007JG00045.

Campbell, J.L., M.E. Harmon, and S.R. Mitchell. 2012. Can fuel-reduction treatments really increase forest carbon storage in the western US by reducing future fire emissions? Frontiers in Ecology and the Environment 10:83–90.

Cohen, J.D. 1999. Reducing the wildland fire threat to homes: where and how much? Pages 189–195 in A. Gonzales-Caban and P.N. Omi, technical coordinators. Proceedings of the Symposium on Fire Economics, Planning, and Policy: bottom lines. General Technical Report PSW-GTR-173. U.S. Department of Agriculture, Forest Service, Pacific Southwest Research Station, Albany, California.

Cohen, J.D. 2000. Preventing disaster: home ignitability in the wildland-urban interface. Journal of Forestry 98:15–21.

Cohen, J.D. 2004. Relating flame radiation to home ignition using modeling and experimental crown fires. Canadian Journal of Forest Research 34:1616–1626.

Cohen, J.D., and A. Westhaver. 2022. An examination of the Lytton, British Columbia wildland urban-fire destruction. ICLR research paper 73. Institute for Catastrophic Loss Reduction, Toronto, Ontario. firesmartbc.ca/wp-content/uploads/2022/05/An-examination-of-the-Lytton-BC-wildland-urban-fire-destruction.pdf.

Coop, J.D., S.A. Parks, C.S. Stevens-Rumann, S.M. Ritter, and C.M. Hoffman. 2022. Extreme fire spread events and area burned under recent and future climate in the western USA. Global Ecology and Biogeography 31:1949–1959.

De Dios, A. 2 July 2024. See fireworks bans, restrictions in Portland, Milwaukie, Eugene, Beaverton, Vancouver, Oregon beaches, campgrounds. The Oregonian. www.oregonlive.com/

crime/2024/07/see-fireworks-bans-restrictions-in-portland-milwaukie-eugene-beaverton-vancouver-oregon-beaches-campgrounds.html.

Donato, D., and J. Halofsky. 2019. Western Washington wildfires: managing the risk. www.nnrg.org/wp-content/uploads/2019/12/Donato_Halofsky_20191105-1.pdf.

Emelko, M.B., U. Silins, K.D. Bladon and M. Stone. Implications of land disturbance on drinking water treatability in a changing climate: demonstrating the need for "source water supply and protection" strategies, Water Research 45:461–472.

Evers, C., A. Holz, S. Busby, and M. Nielsen-Pincus. 2022. Extreme winds alter influence of fuels and topography on megafire burn severity in seasonal temperate rainforests under record fuel aridity. Fire 5:41. https://doi.org/10.3390/fire5020041.

Fire Aside. n.d. Our impact. www.fireaside.com/impact. Accessed 20 November 2024.

Fire Learning Network. 2024. Learning from the media: a conversation with journalists. youtu.be/C0FqAycw9wc?si=m4qsJFNNoIe3cGVp. Accessed 20 November 2024.

Gavin, D. 2020. In Oregon's 2020 fires, highly managed forests burned the most. Firefighters United for Safety, Ethics & Ecology. fusee.org/fusee/oregons-2020-fires-highly-managed-forests-burned-the-most.

Harmon, M.E., C.J. Hanson, and D.A. DellaSalla. 2022. Combustion of aboveground wood from live trees in megafires, CA, USA. Forests 13:391. https://doi.org/10.3390/f13030391.

Hedayati, F., S. Quarles, and S. Hawks. 2023. Wildland fire embers and flames: home mitigations that matter. Insurance Institute for Business & Home Safety. ibhs1.wpenginepowered.com/wp-content/uploads/Home-Mitigations-that-Matter-FINAL.pdf.

Higuera, P.E., M.C. Cook, J.K. Balch, E.N. Stavros, A.L. Mahood, and L.A. St. Denis. 2023. Shifting social- ecological fire regimes explain increasing structure loss from Western wildfires. PNAS Nexus 2:pgad005. https://doi.org/10.1093/pnasnexus/pgad005.

Holmstrom, M., S. Orient, J. Gordon, R. Johnson, S. Rodeffer, L. Money, I. Rickert, B. Pietruszka, and P. Duarte. 2021. Marshall Fire: facilitated learning analysis. storymaps.arcgis.com/stories/83af63bd549b4b8ea7d42661531de512.

Ingalsbee, T. 2007. A reporter's guide to wildland fire, second edition. Firefighters United for Safety, Ethics & Ecology, Eugene, Oregon. static1.squarespace.com/static/5e2c7d5a807d5d13389c0db6/t/5ea0b87637136b7a9591fb52/1587591292299/RptrsGuide2007_web.pdf.

Jennings, T.N., J.E. Smith, K. Cromack, Jr., E.W. Sulzman, D. McKay, B.A. Caldwell, and S.I. Beldin. 2012. Impact of postfire logging on soil bacterial and fungal communities and soil biogeochemistry in a mixed-conifer forest in central Oregon. Plant and Soil 350:393–411.

Joyce, S. 2018. Built to burn. 99% Invisible. Episode 317. 99percentinvisible.org/episode/built-to-burn/.

Karr, J.R., J.J. Rhodes, G.W. Minshall, F.R. Hauer, R.L.. Beschta, C.A. Frissell, and D.A. Perry. 2004. The effects of post-fire salvage logging on aquatic ecosystems in the American West. BioScience 54:1029–1033.

Kerber, S., and D. Alkonis. 2024. Lahaina fire incident analysis report. UL Research Institutes, Fire Safety Research Institute. https://doi.org/10.60752/102376.26858962.

KGW News. 2024. Nature rebounds in the Columbia River Gorge, 6 years after Eagle Creek Fire. www.youtube.com/watch?v=mG5JtR7XmhQ.

Law, B.E., W.R. Moomaw, T.W. Hudiburg, W.H. Schlesinger, J.D. Sterman, and G.M. Woodwell. 2022. Creating strategic reserves to protect forest carbon and reduce biodiversity losses in the United States. Land 11:721. https://doi.org/10.3390/land11050721.

Levine, J.I., B.M. Collins, Z.L. Steel, P. de Valpine, and S.L. Stephens. 2022. Higher incidence of high-severity fire in and near industrially managed forests. Frontiers in Ecology and the Environment 20:397–404.

Lindenmayer, D.B., D.R. Foster, J.F. Franklin, M.L. Hunter, R. Noss, F.A. Schmiegelow, and D. Perry. Salvage harvesting policies after natural disturbance. Science 303:1303.

Littell, J.S., D. McKenzie, D.L. Peterson, and A.L. Westerling. 2009. Climate and wildfire area burned in western U.S. ecoprovinces, 1916–2003. Ecological Applications 19:1003–1021.

Lutz, J.A., et al. 2018. Global importance of large-diameter trees. Global Ecology and Biogeography 27:849–864.

McIver, J.D., and R. McNeil. 2006. Soil disturbance and hill-slope sediment transport after logging of a severely burned site in northeastern Oregon. Western Journal of Applied Forestry 21:123–133.

Mietkiewicz, N., J.K. Balch, T. Schoennagel, S. Leyk, L.A. St. Denis, and B.A. Bradley. 2020. In the line of fire: consequences of human-ignited wildfires to homes in the U.S. (1992–2015). Fire 3:50. https://doi.org/10.3390/fire3030050.

Mildrexler, D.J., L.T. Berner, B.E. Law, R.A. Birdsey, and W.R. Moomaw. 2020. Large trees dominate carbon storage east of the Cascade crest in the United States Pacific Northwest. Frontiers in Forests and Global Change 3:594274. https://doi.org/10.3389/ffgc.2020.594274.

NPS (National Park Service). 24 July 2024. Crater Lake National Park fire ban 2024. www.nps.gov/crla/learn/news/crater-lake-national-park-fire-ban-2024.htm. Accessed 20 November 2024.

ODF (Oregon Department of Forestry). 2022. ODF fire history 1911–2022. www.oregon.gov/odf/fire/documents/odf-century-fire-history-chart.pdf

Osuri, A.M., A. Gopal, T.R.S. Raman, R.S. DeFries, S.C. Cook-Patton. and S. Naeem. 2020. Greater stability of carbon capture in species-rich natural forests compared to species-poor plantations. Environmental Research Letters 15:034011. https://doi.org/10.1088/1748-9326/ab5f75.

PBS. 1 August 2023. The insurance industry can't weather another wildfire season. Weathered season 3, episode 17. www.pbs.org/video/the-insurance-industry-cant-weather-another-wildfire-season-5q4yvw.

Powers, E.M., J.D. Marshall, J. Zhang, and L. Wei. 2013. Post-fire management regimes affect carbon sequestration and storage in a Sierra Nevada Mixed conifer forest. Forest Ecology and Management 291:268–277.

Profita, C. 10 September 2021. Remote cameras capture life returning to Oregon forests after wildfire. Oregon Public Broadcasting. www.opb.org/article/2021/09/10/remote-cameras-capture-life-returning-to-oregon-forests-after-wildfire/.

Quarles, S.L., and K. Pohl. 2018. Building a wildfire-resistant home: codes and costs. Headwaters Economics, Bozeman, Montana. headwaterseconomics.org/wildfire/homes-risk/building-costs-codes.

Radeloff, V.C., M.H. Mockrin, D. Helmers, A. Carlson, T.J. Hawbaker, S. Martinuzzi, F. Schug, P.M. Alexandre, H.A. Kramer, and A.M. Pidgeon. 2023. Rising wildfire risk to houses in the United States, especially in grasslands and shrublands. Science 382:702–707.

Reilly, M.J., et al. 2022. Cascadia burning: the historic, but not historically unprecedented, 2020 wildfires in the Pacific Northwest, USA. Ecosphere 13:e4070. https://doi.org/10.1002/ecs2.4070.

Rhodes, J.J., and W.L. Baker. 2009. Fire probability, fuel treatment effectiveness and ecological tradeoffs in western U.S. public forests. The Open Forest Science Journal 1:1–7.

Schmidt, K.M., J.P. Menakis, C.C. Hardy, W.J. Hann, and D.L. Bunnell. 2002. Development of coarse-scale spatial data for wildland fire and fuel management. General Technical Report RMRS-GTR-87. U.S. Department of Agriculture, Forest Service, Rocky Mountain Research Station, Fort Collins, Colorado.

Schoennagel, T., et al. 2017. Adapt to more wildfire in western North American forests as climate changes. Proceedings of the National Academy of Sciences 114:4582–4590.

Siegler, K. 31 August 2021. Winds have been high as the Caldor Fire threatens California's South Lake Tahoe. National Public Radio. www.npr.org/2021/08/31/1033002680/winds-have-been-high-as-the-caldor-fire-threatens-californias-south-lake-tahoe.

Silins, U., et al. 2014. Five-year legacy of wildfire and salvage logging impacts on nutrient runoff and aquatic plant, invertebrate, and fish productivity. Ecohydrology 7:1508–1523.

Slesak, R.A., S.H. Schoenholtz, and D. Evans. 2015. Hillslope erosion two and three years after wildfire, skyline salvage logging, and site preparation in southern Oregon, USA. Forest Ecology and Management 342:1–7.

Smith, C. 1992. Media and apocalypse: news coverage of the Yellowstone forest fires, Exxon Valdez oil spill, and Loma Prieta earthquake. Greenwood Press, Westport, Connecticut.

Smith, J.E., L.S. Heath, K.E. Skog, and R.A. Birdsey. 2005. Methods for calculating forest ecosystem and harvested carbon with standard estimates for forest types of the United States. General Technical Report NE-343. U.S. Department of Agriculture, Forest Service, Northeast Research Station.

Smucker, K.M., R.L. Hutto, and B.M. Steele. 2005. Changes in bird abundance after wildfire: importance of fire severity and time since fire. Ecological Applications 15:1535–1549.

Spies, T.A., P.A. Stine, R. Gravenmier, J.W. Long, and M.J. Reilly, technical coordinators. 2018. Synthesis of science to inform land management within the Northwest Forest Plan area, volume 1. General Technical Report PNW-GTR-966 Vol. 1. U.S. Department of Agriculture, Forest Service, Pacific Northwest Research Station.

Stoof, C.R., et al. 2024. Megafire: an ambiguous and emotive term best avoided by science. Global Ecology and Biogeography 33:341–351.

Syphard, A.D., J.E. Keeley, and T.J. Brennan. Factors affecting fuel break effectiveness in the control of large fires on the Los Padres National Forest, California. International Journal of Wildland Fire 6:764–775.

USFS (U.S. Forest Service). 2017. Eagle Creek BAER soil burn severity map. www.fs.usda.gov/Internet/FSE_DOCUMENTS/fseprd600997.pdf. Accessed 20 November 2024.

USFS (U.S. Forest Service). 2023. Confronting the wildfire crisis. www.fs.usda.gov/managing-land/wildfire-crisis. Accessed 20 November 2024.

USFS (U.S. Forest Service). 10 July 2024. Fire restrictions on Mt. Hood National Forest. www.fs.usda.gov/detail/mthood/news-events/?cid=FSEPRD1188609. Accessed 20 November 2024.

Vachula, R.S., J.R. Nelson, and A.G. Hall. 2023. The timing of fireworks-caused wildfire ignitions during the 4th of July holiday season. PLoS ONE 18:e0291026. https://doi.org/10.1371/journal.pone.0291026.

Wagenbrenner, J.W., L.H. MacDonald, R.N. Coats, P.R. Robichaud, and R.E. Brown. 2015. Effects of post-fire salvage logging and a skid trail treatment on ground cover, soils, and sediment production in the interior western United States. Forest Ecology and Management 335:176–193.

Wagenbrenner, J.W., P.R. Robichaud, and R.E. Brown. 2016. Rill erosion in burned and salvage

logged western montane forests: effects of logging equipment type, traffic level, and slash treatment. Journal of Hydrology 541:889-901.

Wasserman, T.N., A.E.M. Waltz, J.P. Roccaforte, J.D. Springer, and J.E. Crouse. 2022. Natural regeneration responses to thinning and burning treatments in ponderosa pine forests and implications for restoration. Journal of Forestry Research 33:741–753.

WFMMC (Wildland Fire Mitigation and Management Commission). 2023. On fire. www.usda.gov/sites/default/files/documents/wfmmc-final-report-092023-508.pdf.

Wildland Mapping Institute. 2024. What's burning this year? wildlandmaps.users.earthengine.app/view/fires24. Accessed 23 November 2024.

Zald, H.S.J., and C.J. Dunn. 2018. Severe fire weather and intensive forest management increase fire severity in a multi-ownership landscape. Ecological Applications 28:1068–1080.

# Integrating Farmers' Perspectives into Climate Modeling

Kelsey A. Emard, Olivia Z. Cameron, Elizabeth G. Hyde, Danica L. Lombardozzi, and Will R. Wieder

Farmers in western Oregon are adapting to the effects of climate change, including extreme heat, changes in precipitation patterns, increased water stress, and shifts in season length (Parks and Garrett 2021). The needs of 123 producers on small farms in the southern Willamette Valley were assessed in 2017 (Roesch-McNally et al. 2020). Seventy percent of respondents believed climate change is occurring, and 58 percent strongly agreed that adaptation is necessary. Yet only 32 percent felt they had sufficient information and best practices to cope with the effects of climate change on their operations (Roesch-McNally et al. 2020). Respondents wanted more detailed and localized climate projections and more information on adaptive farm practices, including new crop varieties and techniques to cope with weather extremes. Although the study's small sample size limits the generalizability of the results, the responses suggest data needs for at least some producers in the region. Responding to these identified needs for accessible and actionable data, we examined how long-term climate projections and soil data from the Community Earth System Model version 2 (CESM2) might support adaptation to climate change by farmers in the Willamette Valley.

CESM2, developed and maintained at the U.S. National Science Foundation's National Center for Atmospheric Research, is a global, fully coupled atmosphere, land, ocean, and ice model that simulates Earth's climate processes and physical dynamics over long periods of time (Danabasoglu et al. 2020). CESM2 is one of the Earth system models used in the Coupled Model Intercomparison Project (CMIP6), the climate modeling foundation for the most recent assessment report of the Intergovernmental Panel on Climate Change (Dalton and Bachelet 2023). CESM2 is among the CMIP6 models that most skillfully represent climate and physical processes in the northwest United States (Srivastava et al. 2020). We used climate projections for the region that were generated with the CESM2 Large Ensemble (CESM2-LE; Rodgers et al. 2021). This 100-member ensemble allows us to quantify uncertainty in the Earth system response to climate change projections under the SSP3–7.0 scenario (a doubling of carbon dioxide emissions by 2100, conflicts among regions, and substantial challenges to mitigation and adaptation), which we believed would be meaningful to farmers. Additionally, the Community Land Model, the terrestrial component of CESM2, represents crops, irrigation systems, and soil characteristics better than most Earth system models (Lombardozzi et al. 2020).

Despite their usefulness for analyzing regional and global phenomena, the coarse spatial resolution and long temporal extents of Earth system models such as CESM2 rarely are conducive to local, daily decision making. The base resolution of CESM2 is a nominal grid cell size of 100 km (Danabasoglu 2019), far larger than the size of fields for which most farmers make their decisions (Figure 1). Although CESM2 outputs have been downscaled to 6 km grid cells, we opted to display the coarser-resolution projections to reduce the uncertainty that is introduced into projections through downscaling (van den Hurk et al. 2018, Jacobs and Street 2020).

During 2022 and 2023, we conducted individual, on-farm interviews (Figure 2) with 31 farmers in the Willamette Valley, from the Portland region south to Eugene. During each interview, we gave the farmer a set of figures of simulated climate and soil conditions in the valley from 1850–2100 (Figure 3). Models such as CESM2 do not replicate observations, but simulate past states or plausible future changes in climate and interactions among physical, hydrological, and biogeochemical processes.
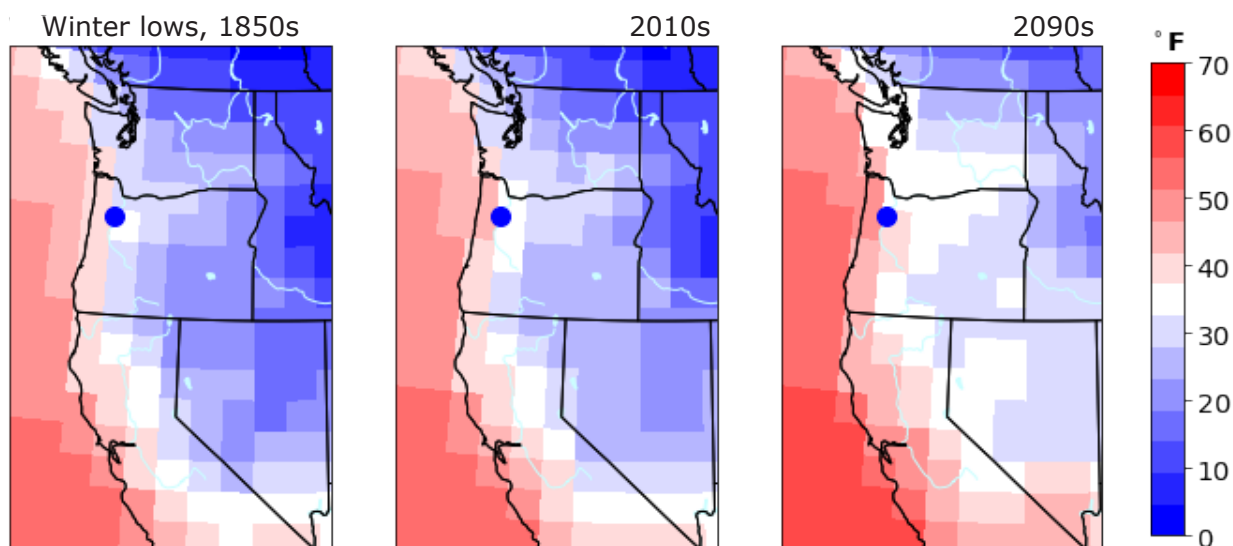
**Figure 1.** Mean minimum January temperatures per decade as projected by CESM2 at the base resolution of 100 km. Blue dot indicates the location of Salem, Oregon.

During interviews, we asked farmers how the modeled data compared to their observations, the ways in which they might use the data, which variables and formats were most usable, what limited the data's usability, and what other data or data formats would be more useful for their decision-making. Interviews were semi-structured and allowed farmers to raise issues or concerns pertinent to climate data and their farming experience that were not originally part of our interview guide.

Following the interviews, we held three focus-group meetings with subsets of the same group of 31 farmers. All interviewees were invited to select one of the focus groups in which to participate, and 18 accepted the invitation. We convened the focus groups in Corvallis, Oregon (seven attendees), in Newberg, Oregon (four attendees), and on Zoom (seven attendees). During the meetings, we shared additional CESM2-LE data that the farmers requested during their interviews. We also shared an online, interactive platform with access to CESM2-LE data that allowed participants to select variables and time periods of interest. We facilitated small group discussions among the participants on the usability of these data for adaptive decision making and on perceptions of climate change risks, adaptation needs, and barriers to adaptation. One of the benefits of the focus groups was the opportunity to observe dialogue not only between researchers and individual farmers, but among farmers (Emard et al. 2024).



**Figure 2.** An on-farm interview.

We audio recorded, transcribed, and thematically coded the transcripts from all interviews and focus group meetings. Our coding identified themes emphasized and points made by multiple farmers in response to our questions regarding the usability of CESM2 and other Earth system models' data for supporting farm management and decision making. Below, we include quotations from the interviews to illustrate themes that emerged in the qualitative analysis.

Despite the coarse spatial resolution and long temporal extent (250 years) of the data, farmers were adept at applying their understanding of the data to the microclimate of their farm and timing
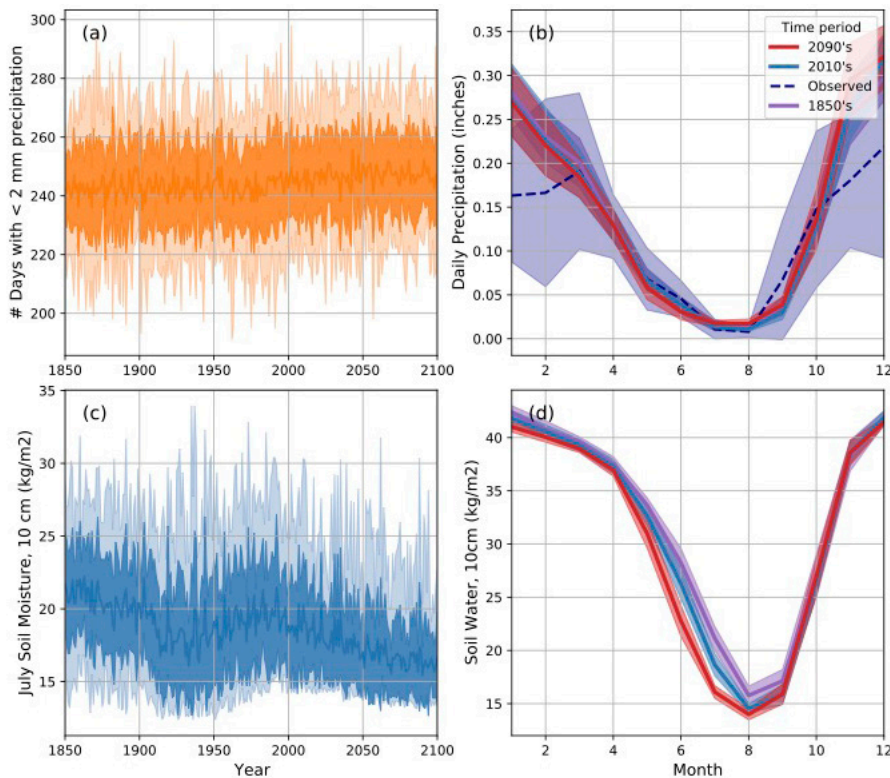
**Figure 3.** Modeled precipitation presented as (a) number of dry days (<2 mm precipitation) per year from 1850 through 2100 and (b) mean monthly precipitation over three past and future decades. Soil moisture presented as (c) July soil moisture at 10-cm depth and (d) mean soil moisture (10-cm depth) over the same three decades. Lighter colors represent the full range of results from 100 ensemble members, and darker colors represent means and standard deviations. In (b) and (d), month numbers correspond to the calendar year (e.g., February is the second month). Light purple shading in (b) represents the variability in weather observations from 2010–2019. Source: Emard et al. 2024. © Copyright 2024 American Meteorological Society; republication allowed.

of their decisions. For example, one farmer explained that by comparing the time series of modeled changes in soil moisture and precipitation in the Willamette Valley, he identified a need to change certain soil management practices:

*"Yeah. I mean, it's good to see that the rainfall will be more or less [the same] . . . you can count on it not being super dry, maybe not super wet as well. And in terms of soil moisture [declining, as shown here] . . . to me, it would mean I've got to do more to preserve, get more organic matter into the soil or do more no-tilling. And so yeah, it would make a difference to know that there's going to be less [soil moisture] . . . Yeah, I could think, 'Well, we're getting an average amount of rain. Why are things drying out so quickly?' Other than saying, 'Well, things are drying out so quickly because I'm disking the grass down instead of mowing it,' and different things like that, that I could do better to help with retaining the moisture that's there."*

Another farmer was similarly clear about their ability to apply regional projections to their farm: *"I'm not sure if having it more granular [would be] more valuable. This shows a trend… And farmers tend to know their microclimate. I know that when I look at the weather forecast, we're likely to be two to three degrees colder than whatever the weather forecast is. So, we have a kind of a, not a sixth sense, but a general idea of how our particular very small microclimate will relate to a broader forecast."*

Farmers highlighted many ways that data from CESM2 could be used for long-term decision making, such as when deciding whether, where, and when to plant a multiyear crop such as hazelnuts or blueberries, selecting crop varieties (e.g., some peach varieties require a minimum number of chill hours each year to fruit), preparing for potential changes in species' ranges or population sizes of pests or pollinators, and planning for water catchment or irrigation. Furthermore, farmers expressed hope that these data could inform state policy on water rights and funding for drought relief and pest mitigation.

Despite the opportunities for use of data such as these to inform their adaptation actions, farmers highlighted barriers to usability of the data and recommended ways to improve the usability of

data generated by CESM2. One major barrier is simply that data from Earth system models such as CESM are intended to study climate and other physical processes over large spatial and long temporal extents. Downscaled models may be more relevant to local decision makers, and, as noted above, CESM2 has been downscaled, but uncertainty in projections at the finest resolutions is relatively high (van den Hurk et al. 2018, Jacobs and Street 2020). Our interviews suggested that farmers effectively interpret the data relevant to local conditions and can therefore obtain data relevant to their decision making from global models such as CESM2. Nevertheless, the farmers with whom we engaged also agreed that shorter time periods and finer-resolution data generally would be more relevant to their daily decision making. For example, they suggested creation of interactive data platforms that would allow them to tailor model projections to their own farm conditions, such as by selecting the soil type or vegetation cover of a given field as an input for projecting soil moisture or by selecting temperature thresholds (e.g., 27°F for blueberries) to assess potential for maintaining certain crops. They emphasized that



**Figure 4.** Farmer interest in practices that could assist in adapting to climate change. Responses gathered through a question with a Likert scale from very uninterested to very interested.

their climate data needs vary among crops; slope, aspect, and soils; and many other local factors that climate models, even downscaled models, are unlikely to accurately represent.

Farmers also would like their practices represented in the model so they can explore the impacts of actions such as low and no tilling, cover cropping, and mulching on soil conditions, including moisture, temperature, nitrogen and organic matter content, and microbial activity (Figure 4).

We asked farmers about the level of importance they attributed to variables that either are or could be included in the CESM2 outputs. They ranked extreme weather and precipitation as the most important, followed by soil characteristics such as moisture, temperature, and microbial activity (Figure 5). Although it was not included in the survey questions, several participants requested representations of air quality given the impact of wildfire smoke on crops such as wine grapes and blueberries (see *Responses of Oregon's Wine Industry to Climate Change*, this volume).

The farmers' feedback is informing the next steps of CESM development. For example, in part as a result of our collaboration, scientists at the National Center for Atmospheric Research are developing or expanding representations of tillage, use of cover crops, impacts of air quality, and soil microbial activity in the land model of the CESM2 (Lombardozzi et al. 2018, Graham et al. 2021, Fung et al. 2022, Ran et al. 2023). These data could supplement local or regional models (Gilliam et al. 2021) to increase understanding of the effects of agricultural practices on climate.
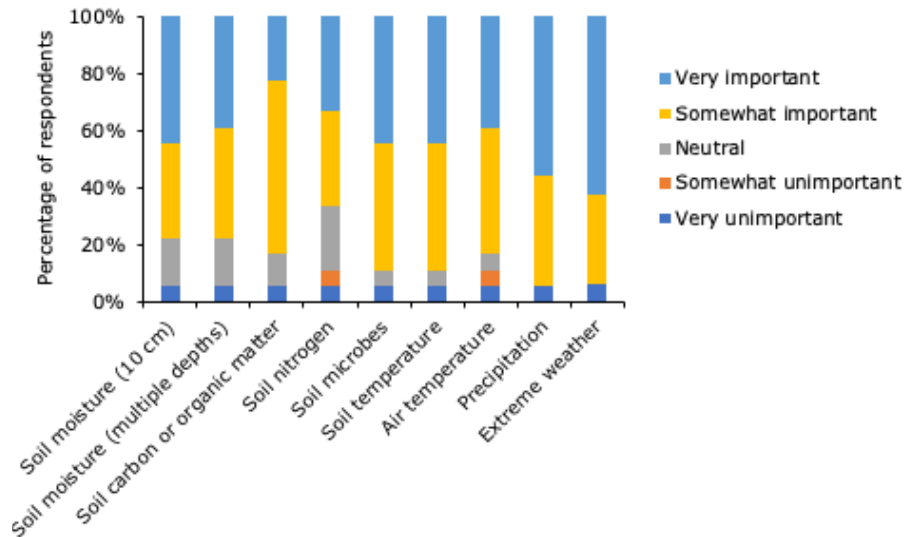
**Figure 5.** Farmer interest in variables that are or could be included in the CESM2 outputs to inform adaptive decision-making. Responses gathered through a question with a Likert scale from very uninterested to very interested.

As explored here, connecting climate models with those who are adapting to climate change has multiple potential benefits. The interactions themselves can highlight ways that scientists can make climate models and tools more useful, and encourage observations of local climate that may improve model design and performance. Climate models can provide end users with data that inform decisions, and policy makers with data to support legislation for climate change adaptation. Our work not only provided data to farmers that may inform their future decisions, but produced insights that are leading to the next steps of CESM development.

## Literature Cited

Dalton, M., and D. Bachelet. 2023. Understanding the most current climate projections. Pages 21–39 in E. Fleishman, editor. Sixth Oregon climate assessment. Oregon Climate Change Research Institute, Oregon State University, Corvallis, Oregon. https://doi.org/10.5399/osu/1161.

Danabasoglu, G. 2019. NCAR CESM2 model output prepared for CMIP6 CMIP historical. Version 20241113. Earth System Grid Federation. https://doi.org/10.22033/ESGF/CMIP6.7627.

Danabasoglu, G., et al. 2020. The Community Earth System Model version 2 (CESM2). Journal of Advances in Modeling Earth Systems 12:e2019MS001916. https://doi.org/10.1029/2019MS001916.

Emard, K., O. Cameron, W.R. Wieder, D.L. Lombardozzi, R. Morss, and N. Sobhani. 2024. Integrating farmers' perspectives into Earth system model development: interviews with end users in the Willamette Valley, Oregon, to guide actionable science. Weather, Climate, and Society 16:453–465.

Fung, K.M., M. Val Martin, and A.P. Tai. 2022. Modeling the interinfluence of fertilizer-induced $NH_3$ emission, nitrogen deposition, and aerosol radiative effects using modified CESM2. Biogeosciences 19:1635–1655.

Gilliam, R.C., J.A. Herwehe, O.R. Bullock, Jr., J.E. Pleim, L. Ran, P.C. Campbell, and H. Foroutan. 2021. Establishing the suitability of the model for prediction across scales for global retrospective air quality modeling. Journal of Geophysical Research: Atmospheres 126:e2020JD033588. https://doi.org/10.1029/2020JD033588.

Graham, M.W., R.Q. Thomas, D.L. Lombardozzi, and M.E. O'Rourke. 2021. Modest capacity of no-till farming to offset emissions over the 21st century. Environmental Research Letters 16:054055. https://doi.org/10.1088/1748-9326/abe6c6.

Jacobs, K.L., and R.B. Street. 2020. The next generation of climate services. Climate Services

20:100199. https://doi.org/10.1016/j.cliser.2020.100199.

Lombardozzi, D.L., G.B. Bonan, W. Wieder, A.S. Grandy, C. Morris, and D. L. Lawrence. 2018. Cover crops may cause winter warming in snow-covered regions. Geophysical Research Letters 45:9889–9897.

Lombardozzi, D.L., Y. Lu, P.J. Lawrence, D.M. Lawrence, S. Swenson, K.W. Oleson, W.R. Wieder, and E.A. Ainsworth. 2020. Simulating agriculture in the Community Land Model version 5. Journal of Geophysical Research: Biogeosciences 125:e2019JG005529. https://doi.org/10.1029/2019JG005529.

Parks, M., and A. Garrett. 2021. Small farmers' climate change beliefs and experiences with weather challenges in Oregon. Oregon State University Extension. smallfarms.oregonstate.edu/system/files/parks_garrett_small_farmers_weather_challenges42.pdf.

Ran, Q., J. Moore, T. Dong, S.Y. Lee, and W. Dong. 2023. Statistical bias correction for CESM-simulated $PM_{2.5}$. Environmental Research Communications 5:101001. https://doi.org/10.1088/2515-7620/acf917.

Rodgers, K.B., et al. 2021. Ubiquity of human-induced changes in climate variability. Earth System Dynamics 12:1393–1411.

Roesch-McNally, G., A. Garrett, and M. Fery. 2020. Assessing perceptions of climate risk and adaptation among small farmers in Oregon's Willamette Valley. Renewable Agriculture and Food Systems 35:626–630.

Srivastava, A., R. Grotjahn, and P.A. Ullrich. 2020. Evaluation of historical CMIP6 model simulations of extreme precipitation over contiguous US regions. Weather and Climate Extremes 29:100268. https://doi.org/10.1016/j.wace.2020.100268.

van den Hurk, B., C. Hewitt, D. Jacob, J. Bassembinder, F. Doblas-Reyes, and R. Döscher. 2018. The match between climate services demands and Earth system models supplies. Climate Services 12:59–63.

# Responses of Oregon's Wine Industry to Climate Change

Dominique Bachelet and Elizabeth Tomasino

## Introduction

Oregon's climate was largely unsuitable for growing traditional wine grape cultivars prior to the 1950s and 1960s. From the 1970s through the 1990s, Oregon's early vineyards struggled to ripen fruit. However, trends toward warmer and drier summers and improvements in viticulture practices have made Oregon a world-class wine production state. As of 2024, Oregon has 23 American Viticultural Areas from Walla Walla and the Columbia Gorge in the northeast to the Southern Rogue and Applegate Valleys in the southwest. The American Viticultural Areas include 1512 vineyards with about 46,000 planted acres (18,600 ha).

Many farmers in western Oregon, where the majority of vineyards are located, report that the weather has become less predictable (Jones and Goodrich 2008). Warming is projected to continue, with increases in the magnitude and frequency of heat waves (Dahl et al. 2019, O'Neill et al. 2023) and later dates of first frost (Climate Central 2024). Increases in the intensity and frequency of extreme precipitation and drought (Kossin et al. 2017, Schoof et al. 2019, Dalton et al. 2021) may pose additional challenges for Oregon wine grape production. Climate's impact on wine characteristics can be substantial enough to cause the flavor and quality of different vintages from the same vineyard to vary dramatically. As Tom Fitzpatrick of Elevee Vineyards (Dundee, Oregon) said, "Vintage is actually an element of terroir . . . it's the environmental conditions Mother Nature gives us during a given year."

Terroir, a combination of soil type and nutrient content, climate, and other environmental factors, determines the chemical composition of wine and thus its quality. Photosynthesis drives the accumulation of sugars in the fruits, and yeasts consume those sugars during fermentation to form alcohol. Hotter years that result in high sugar content in grapes may lead to undesirably high alcohol content. As grapes ripen, their acidity declines, and warmer temperatures hasten the drop of acidity (Sadras et al. 2013). Acidity of wine may need to be adjusted in warmer climates, whereas this practice is uncommon in cooler climates (De Orduna 2010). Other quality components responsible for aroma, flavor, and mouthfeel also accumulate during the growing season. Anthocyanins protect grapes from sunburn (Teisseidre and Jourdes 2016) and give red wines their color, but degrade when exposed to high temperatures, affecting the appearance of the wine. Tannins provide bitterness and astringency and serve as defenses against herbivores and other pests (Ma et al. 2014). Although natural annual variability persists, the greatest challenge of climate change to farming in general and winemaking in particular is unpredictability.

## Responses of Wine Grapes to Climate Trends in Oregon

The increase in maximum and minimum temperatures in Oregon over the past 125 years (Figure 1) benefited wine grape production in the state, where seasonally cool temperatures previously limited ripening (Jones and Webb 2010). Oregon's annual average temperature increased by around 2.2°C over the past century and is projected to increase by 5°C by mid-century (Fleishman 2023, O'Neill et al. 2023). Temperature increases in Oregon are expected to be most pronounced in summer and minimum (overnight) temperatures are increasing more rapidly than maximum (daytime) temperatures. Both of these changes can increase plant respiration and insect development rates.
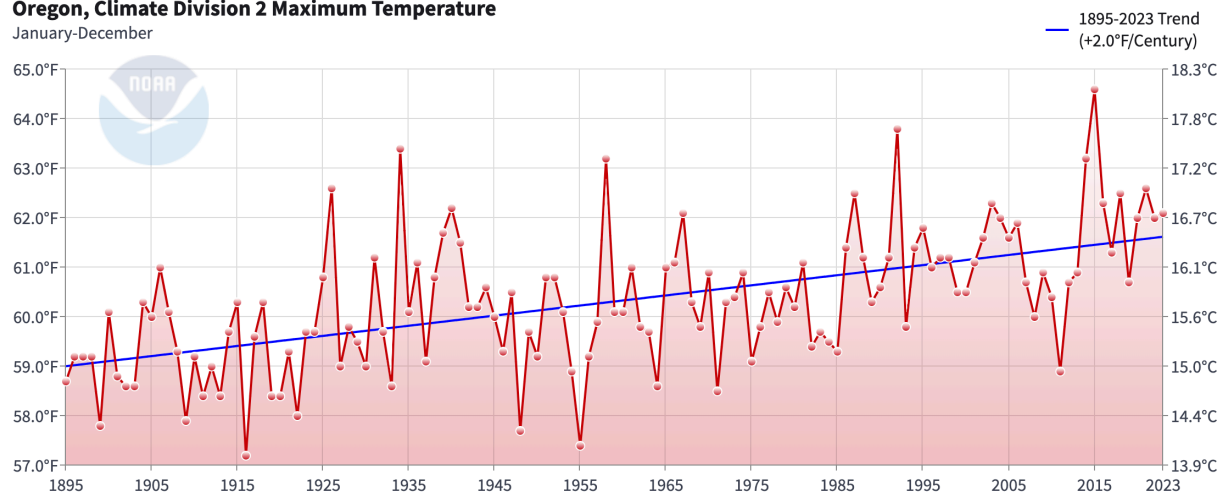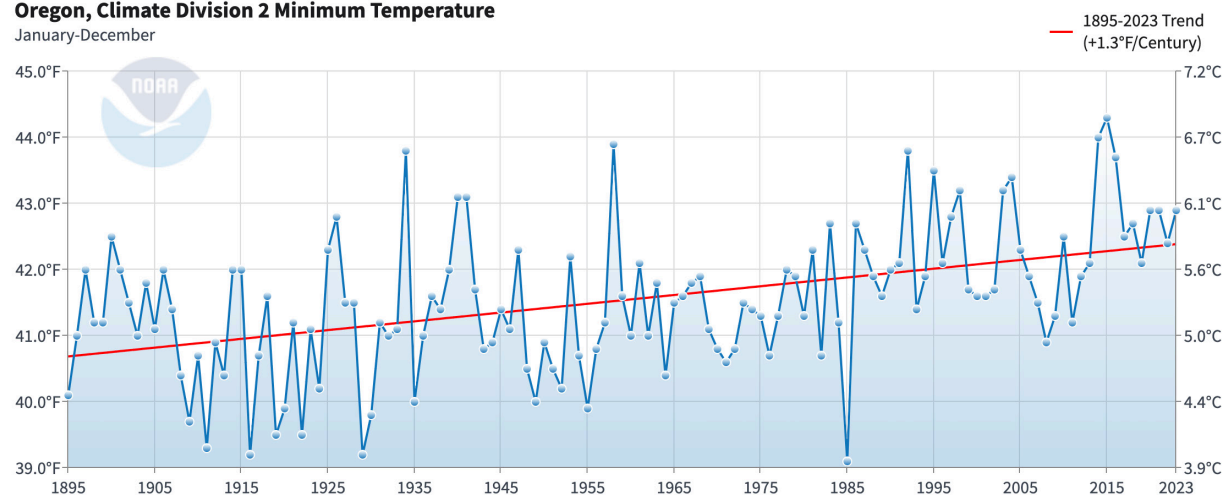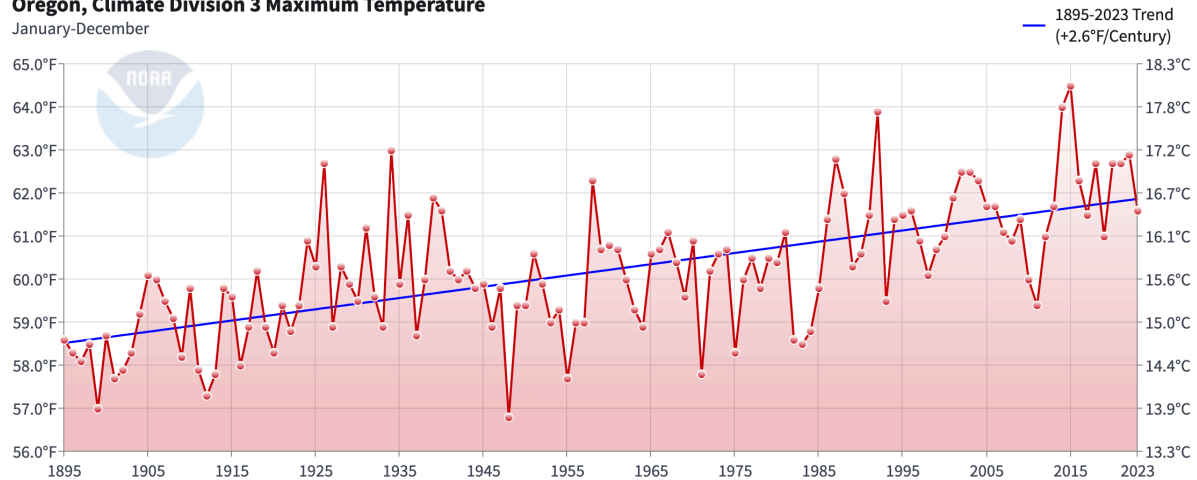
**Figure 1.** Trends in maximum (top panel) and minimum (bottom panel) temperature in the Willamette Valley (Climate Division 2), Oregon. Source: National Centers for Environmental Information, National Oceanic and Atmospheric Administration.

Increases in temperature also have been greater in southern Oregon (Figure 2), where vineyard owners have already switched to grape cultivars that are better adapted to warm temperatures, than in northern Oregon.

The average minimum temperatures for budbreak and leaf production of many cultivars are 3.5 and 7°C, respectively (Jackson 2014). Flowering does not occur until air temperature reaches 20°C. Temperature also affects the development time of grapes. The period between budbreak and harvest shortens by about 8 days for each 1°C warming (Tomasi et al. 2011). The optimum temperature range for grape maturation is 20–25°C. At higher temperatures, heating suppresses photosynthesis. For example, at 35°C, depending on the cultivar and radiation intensity, the photosynthetic rate is about 15 percent of its rate at 25°C (Jackson 2014). Sun exposure is usually beneficial for grapevines, but excess exposure causes sunburn and dehydration, in turn altering the fragrance of the wine.

Annual average precipitation in western Oregon is variable, and no trend is apparent to date (Figure 3). However, drought conditions are projected to become more frequent, widespread, and severe across the state (Fleishman 2023).
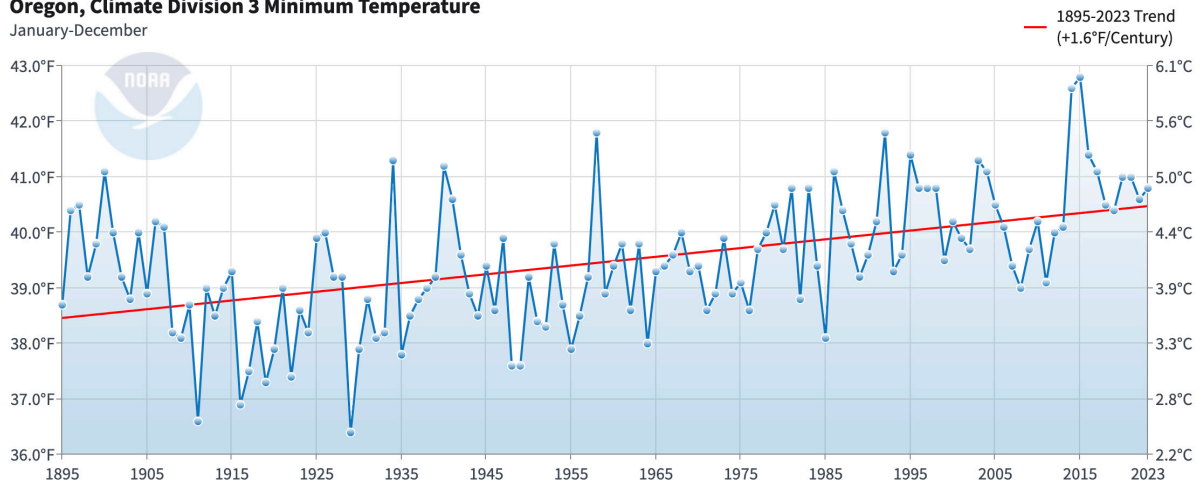
**Figure 2.** Trends in maximum (top panel) and minimum (bottom panel) temperature in the Southwestern Valleys (Climate Division 3), Oregon. Source: National Centers for Environmental Information, National Oceanic and Atmospheric Administration.

## Impact of Extreme Weather Events and Wildfires

Oregon vineyards have been affected by weather events such as the extreme June 2021 heat wave across the Pacific Northwest, a late frost in 2022, and a spring heat wave in 2023. Widespread foliar damage followed the June 2021 heat wave (Still et al. 2023), and extensive seedling mortality was reported in local tree plantations. Because the heat wave occurred early in summer, when grape berries were still small and green, damages were minimal and yield reduction moderate (White et al. 2023). However, the frequency of heat waves that coincide with extended droughts is expected to increase (Alizadeh et al. 2020) and, depending on the timing of future heat waves, damages to grapes could be more severe. Extreme heat also affects the health and capacity of field workers.

A late frost in the Willamette Valley in April 2022 affected some vineyards in which budbreak of Chardonnay vines had just started. The cold period was short and damages were limited. However, frosts can cause major losses in vineyards (e.g., Poling 2008, Yilmaz 2024). Prolonged exposure to cold temperatures can cause chilling injuries to grapes, with irreversible physiological damage that retards ripening. The effect of short-duration frost exposure is reversible (Jackson 2014).

In May 2023, high temperatures in the Willamette Valley (e.g., 34°C [94°F] in Eugene and 33°C [92°F] in Portland) led to rapid bud break and bloom, although the heat was too early in the growing season to substantially affect grape development. Reduced production that year was due to extreme August heat, with sunburned vines and drought conditions in many wine grape-growing areas (Oregon Wine Board 2024).

Extensive wildfire smoke exposure in September 2020 caused significant losses to vineyards and wineries from the Willamette Valley south to the Rogue River American Viticultural Area. When smoke concentrations are high during grape ripening, volatile phenols bind to the grape berry's waxy cuticle (skin) and are absorbed into the grape. These phenols bind with grape sugars to form odorless glycosides. During fermentation, the phenols are released from their sugars, giving the resulting wine an undesirable ashy taste and smoky smell (e.g., Tran et al. 2023). Because the phenols accumulate in grape skins, smoke taint mainly threatens red wines that are fermented with the grape skins. Activated carbon and reverse osmosis can help remove smoky compounds from wine, but also can remove desirable aromas. Strongly smoke-tainted fruit may not be harvested, or wine produced from that fruit may be discarded. Both happened in 2020. Many Pinot Noir producers in
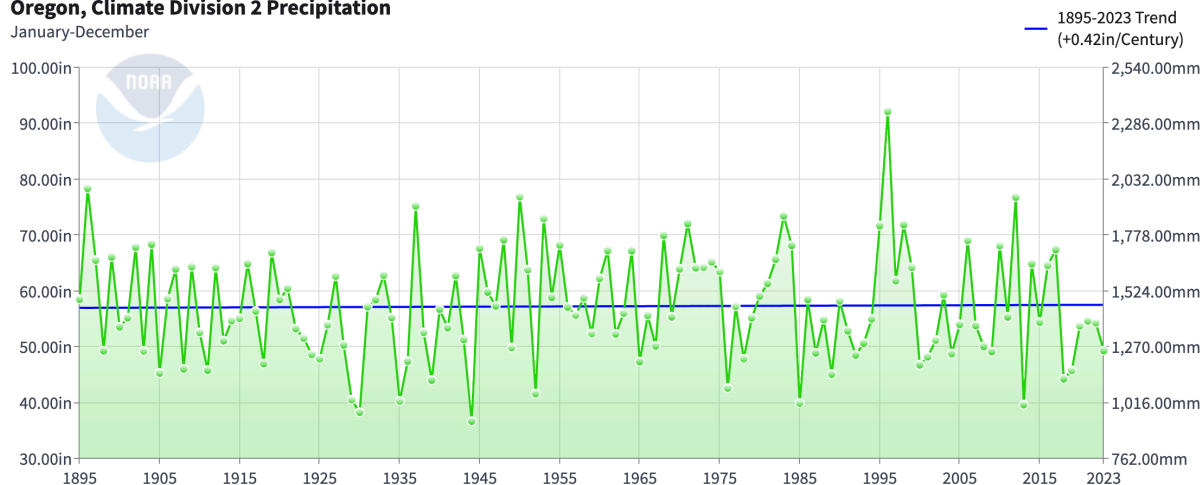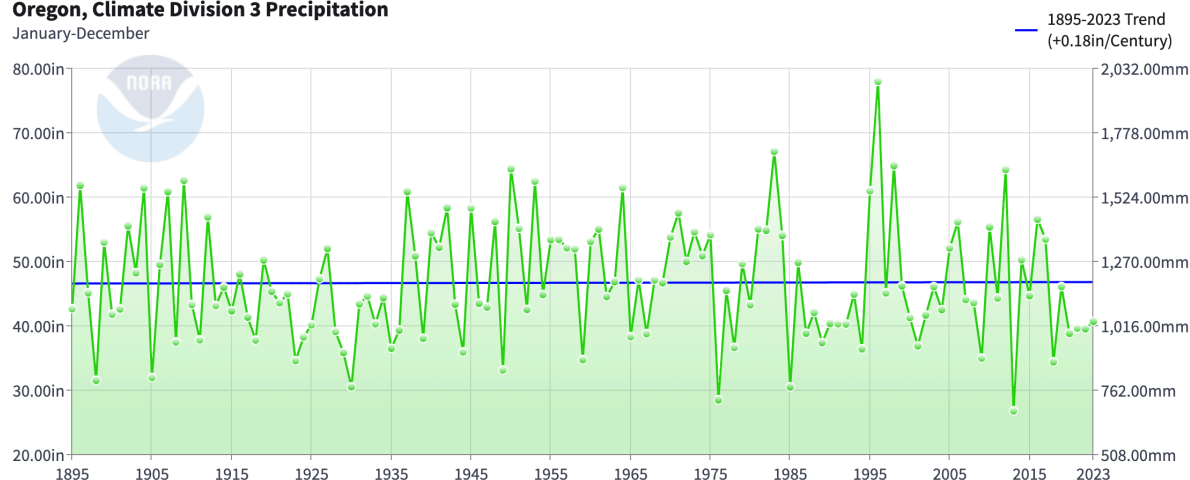


**Figure 3.** Annual average precipitation in the Willamette Valley (Climate Division 2; top panel) and Southwestern Valleys (Climate Division 3; bottom panel), Oregon. Source: National Centers for Environmental Information, National Oceanic and Atmospheric Administration.

the Willamette Valley could not risk producing and selling poor-quality products, and therefore did not make wine in 2020. Given the regularity of wildfires in northern California, southern Oregon wineries increasingly are affected by wildfire smoke (Williams et al. 2019). Projected increases in the frequency of wildfires (Sheehan et al. 2019) are causing concern among vineyard owners throughout Oregon. Coatings to prevent wine grapes from absorbing aromatic compounds after extended exposure to wildfire smoke are being tested (Tran et al. 2023).

## Impacts of Precipitation and Drought

Grape vines are often deeply rooted, which allows them to avoid serious water deficit during summer drought. In fact, excess soil moisture is a challenge for vineyard owners in the northern Willamette Valley. Soil moisture favors vegetative growth, whereas drought stress causes the vines to concentrate sugars in grapes and increases the fruits' polyphenol content, which affects color, aroma, flavor, and overall quality of the wine. Winter precipitation in Oregon's vineyards recharges ground water and prevents water stress in spring and early summer, before grapes ripen.

To date, summer irrigation has not been necessary in northern Oregon. Drip irrigation has been used more regularly in vineyards in southern and eastern Oregon and parts of the Columbia River Gorge, where soil is shallow and precipitation is limited. In areas with greater cumulative precipitation but progressive aquifer depletion, such as the Willamette Valley, vineyards are exploring dryland farming, which requires no irrigation. Vintage quality has been correlated positively with mild water deficit stress before harvest independent of mean annual precipitation (Jackson 2014).

Mildews are a major threat in most of the world's wine growing regions. Their effects depend on the amount and frequency of precipitation or irrigation. Variable projections of the quantity and timing of future precipitation make adaptation of mildew control strategies difficult. Rose bushes are often planted at the ends of rows in vineyards because roses are highly sensitive to powdery mildew and serve as an early warning of the mildew's presence before it spreads to the grapes (Figure 4). The challenge is to find vines that require less fungicide to fight the mildew that may afflict harvests after extreme rainfall.



**Figure 4.** Rose bushes planted at the end of a row of wine grapes. Photograph by Dominique Bachelet.

## Challenges and Adaptive Capacity

During the last few decades, winemakers have begun growing grapes in locations once considered too cold but where soil

conditions are adequate (e.g., Hewer and Brunette 2020, Hewer and Gough 2024). For example, growers are experimenting at elevations above 460 m (1,500 ft.), once considered inhospitable due to potential frost damage. In Washington's Walla Walla Valley, vines are being tested at 920 m (3,000 ft.). High elevation soils are often low in nutrients and moisture, but grapevines can thrive in such environments: yields are relatively low, yet phenolic ripeness high (Asimov 2019). Moreover, the pronounced diurnal shift in temperature at high elevations helps grapes to ripen at a more even pace and over a longer period of time than at low elevations. However, frosts and hailstorms at high elevations remain a threat.

Traditionally, grapevines in the Northern Hemisphere were planted on warm south or southeast-facing slopes, allowing grapes to fully ripen. To prevent over-ripening, wine producers in California are now planting on north-facing slopes. Other recent plantings were oriented northeast-to-southwest to allow the grape leaves to shade the clusters. Shade cloths and anti-hail nets also are being used to protect grapes from intense heat and radiation. Some winemakers spray clay powder on vines to slow photosynthesis, preventing the grapes from over-ripening and becoming too high in alcohol content.

Pinot Noir, Oregon's signature varietal (about 60 percent of all planted area and 57 percent of wine grape production), is a cool climate variety that grows in areas with average growing season temperatures of 14–16°C (57–61°F). The Willamette Valley is currently in the middle of that range, and warming in recent decades benefitted Pinot Noir (Jones et al. 2012) and several other varieties (Gambetta et al. 2021). However, projected regional warming could exceed the threshold for growing Pinot Noir, and Oregon wine grape growers may have to shift to different varieties to remain profitable. Some vineyards have already planted grape varieties better adapted to warm temperatures, such as Gamay Noir, Tempranillo, and Syrah (Castillo 2022). Winemakers can also alter the vinification process by blending varieties or grapes grown in different years.

Many traditional practices are changing to adapt to the effects of warming (van Leeuwen et al. 2024). Grapes are being harvested earlier in the year to prevent over-ripening and, in fire-prone regions, to miss the usual peak of wildfire season and avoid smoke taint. In the Bordeaux region of France, berries are picked early in the morning when acidity is highest, dense grapevine canopies are thinned to curb sugar production, and shade cloths or films are used to filter near-infrared radiation to prevent sunburn. In larger vineyards, the cost of the shade material can be high, so trellises that shield the grapes are being used instead. Additionally, herbaceous vegetation is being planted between rows of grapevines with the aim of increasing soil carbon content and reducing surface evaporation while shading the low-growing clusters.

Research is exploring mitigation options in response to increases in the sugar content of grapes (Mira de Orduña 2010, Tilloy et al. 2015). For example, researchers in France have grown novel strains of yeast that producing less alcohol during fermentation. Scientists also have developed an electrodialysis process to remove potassium ions from grape juice (or grape must or wine), which enhances the wine's acidity and freshness. There may be a threshold of climate change beyond which growers are unable to adapt, but so far research is keeping pace with the effects of climate change on vineyards.

Many pest or disease agents of grape vines have been documented (Esmenjaud et al. 2008, Gessler et al. 2011, Gadoury et al. 2012, Chuche and Thiéry 2014, Reineke and Thiéry 2016), but their response to climate change is difficult to predict (Gregory et al. 2009). Furthermore, plants' sensitivity to pathogens may change as climate changes. At the same time, pathogens or their

vectors will be affected by changes in climate, potential new interactions among pests, and evolving cultivation practices. Plant protection is expected to evolve in step with pest or disease development in the vineyard (Salinari et al. 2006, Caffarra et al. 2012). However, public concerns about the use of chemicals that persist in the soil, and related new legislation, may affect allowable practices.

Agriculture is responsible for about 20 percent of global emissions of greenhouse gases (Jia et al. 2022) and about 10 percent of emissions in the United States (2022 data; EPA 2024). Emissions from viticulture, as from many other crops, are produced by application of fertilizers and pesticides, use of fossil fuels for maintenance and harvesting equipment, power use at the winery, and packaging and transportation of the finished product (Pinto da Silva and Esteves da Silva 2022). Public or policy demands are leading many growers to explore ways to reduce their carbon footprint. In 2009, 14 wineries, nearly 20 percent of Oregon wine production, joined forces with the Oregon Environmental Council to start the Carbon Neutral Challenge, the first carbon-reduction program initiated by the wine industry in the United States. As part of the program, wineries throughout Oregon installed solar panels. In 2009, Willamette Valley Vineyards co-founded the cork recycling program Cork ReHarvest. Commercial cork oak (*Quercus suber*) primarily are grown in Spain, Portugal, and other countries in Mediterranean Europe and North Africa. Use of recycled corks or screw-top bottles reduces the demand for harvesting cork oak trees and allows the trees to store carbon over their ~200-year lifespan (Dias and Aroja 2014). For every ton of cork produced, about 73 tons of $CO_2$ are captured (Corklink 2016). However, extreme heat, drought, and more frequent fires in the Mediterranean region are jeopardizing the future of cork oaks and, therefore, wine corks.

## Literature Cited

Alizadeh, M.R., J. Adamoski, M.R. Nikoo, A. AghaKouchak, and M. Sadegh. 2020. A century of observations reveals increasing likelihood of continental scale compound dry-hot extremes. Science Advances 6:eaaz4571. https://doi.org/10.1126/sciadv.aaz4571.

Asimov, E. 14 October 2019. How climate change impacts wine. The New York Times. www.nytimes.com/interactive/2019/10/14/dining/drinks/climate-change-wine.html.

Caffarra, A., M. Rinaldi, E. Eccel, V. Rossi, and I. Pertot. 2012. Modelling the impact of climate change on the interaction between grapevine and its pests and pathogens: European grapevine moth and powdery mildew. Agriculture, Ecosystems & Environment 148:89–101.

Castillo, E. 25 April 2022. How climate change affects Oregon wine. Oregon Public Broadcasting. www.opb.org/article/2022/04/25/how-climate-change-affects-oregon-wine/.

Chuche, J., and D. Thiéry. 2014. Biology and ecology of the Flavescence dorée vector *Scaphoideus titanus*: a review. Agronomy for Sustainable Development 34:381–403.

Climate Central. 16 October 2024. Warmer fall, later freeze. www.climatecentral.org/climate-matters/warmer-fall-later-freeze. Accessed 26 November 2024.

Corklink. 24 October 2016. How cork production sequesters $CO_2$. www.corklink.com/index.php/how-cork-production-sequesters-co2. Accessed 26 November 2024.

Dahl, K., R. Licker, J.T. Abatzoglou, and J. Declet-Barreto. 2019. Increased frequency of and population exposure to extreme heat index days in the United States during the 21st century. Environmental Research Communications 1:075002. https://doi.org/10.1088/2515-7620/ab27cf.

Dalton M, H. Chang, B. Hatchett, P.C. Loikith, P.W. Mote, L.E. Queen, and D.E. Rupp. 2021. State of climate science. Pages 11–30 in M. Dalton and E. Fleishman, editors. Fifth Oregon climate assessment. Oregon Climate Change Research Institute, Oregon State University,

Corvallis, Oregon. https://doi.org/10.5399/osu/1160.

De Orduna, R.M. 2010. Climate change associated effects on grape and wine quality and production. Food Research International 43:1844–1855.

Dias, A.C., and L. Aroja. 2014. A model for estimating carbon accumulation in cork products. Forest Systems 23:236–246.

EPA (U.S. Environmental Protection Agency). 2024. Inventory of U.S. greenhouse gas emissions and sinks: 1990–2022. EPA 430R-24004. www.epa.gov/ghgemissions/inventory-us-greenhouse-gas-emissions-and-sinks-1990-2022.

Esmenjaud, D., S. Kreiter, M. Martinez, R. Sforza, D. Thiéry, M. van Helden, and M. Yvon. 2008. Ravageurs de la vigne. Editions Féret, Bordeaux.

Fleishman, E., editor. 2023. Sixth Oregon climate assessment. Oregon Climate Change Research Institute, Oregon State University, Corvallis, Oregon. https://doi.org/10.5399/osu/1161.

Gadoury, D.M., L. Cadle-Davidson, W.F. Wilcox, I.B. Dry, R.C. Seem, and M.G. Milgroom. 2012. Grapevine powdery mildew (*Erysiphe necator*): a fascinating system for the study of the biology, ecology and epidemiology of an obligate biotroph. Molecular Plant Pathology 13:1–16.

Gambetta, G.A., and S.K. Kurtural. 2021. Global warming and wine quality: are we close to the tipping point? OENO One 55:353–361.

Gessler, C., I. Pertot, and M. Perazzolli. 2011. *Plasmopara viticola*: a review of knowledge on downy mildew of grapevine and effective disease management. Phytopathologia Mediterranea 50:3–44.

Gregory, P.J., S.N. Johnson, A.C. Newton, and J.S.I. Ingram. 2009. Integrating pests and pathogens into the climate change/food security debate. Journal of Experimental Botany 60:2827–2838.

Jackson, R.S. 2014. Wine science: principles and applications. Academic Press, Cambridge, Massachusetts.

Jia, G., et al. 2022. Land–climate interactions. Pages 131–248 in P.R. Shukla et al., editors. Climate change and land: an IPCC special report on climate change, desertification, land degradation, sustainable land management, food security, and greenhouse gas fluxes in terrestrial ecosystems. Cambridge University Press, Cambridge, United Kingdom. https://doi.org/10.1017/9781009157988.004.

Jones, G.V., and L.B. Webb. 2010. Climate change, viticulture, and wine: challenges and opportunities. Journal of Wine Research 21:103–105.

Jones, G.V., R. Reid, and A. Vilks. 2012. Climate, grapes, and wine: structure and suitability in a variable and changing climate. Pages 109–133 in P. Dougherty, editor. The geography of wine. Springer, Dordrecht. https://doi.org/10.1007/978-94-007-0464-0_7.

Kossin, J.P., T. Hall, T. Knutson, K.E. Kunkel, R.J. Trapp, D.E. Waliser, and M.F. Wehner. 2017. Extreme storms. Pages 257–276 in D.J. Wuebbles, D.W. Fahey, K.A. Hibbard, D.J. Dokken, B.C. Stewart, and T.K. Maycock, editors. Climate science special report: Fourth National Climate Assessment, Volume I. U.S. Global Change Research Program, Washington, D.C. science2017.globalchange.gov/chapter/9/.

Ma, W., A. Guo, Y. Zhang, H. Wang, Y. Liu, and H. Li. 2014. A review on astringency and bitterness perception of tannins in wine. Trends in Food Science and Technology 40:6–19.

Mira de Orduña, R. 2010. Climate change associated effects on grape and wine quality and production. Food Research International 43:1844–1855.

O'Neill, L., N. Siler, P. Loikith, and A. Arends. 2023. Extreme temperatures. Pages 40–61 in E.

Fleishman, editor. Sixth Oregon climate assessment. Oregon Climate Change Research Institute, Oregon State University, Corvallis, Oregon. https://doi.org/10.5399/osu/1161.

Oregon Wine Board. 26 September 2024. 2023 Oregon harvest report. industry.oregonwine.org/resources/reports-studies/2023-oregon-harvest-report/. Accessed 26 November 2024.

Poling, E.B. 2008. Spring cold injury to winegrapes and protection strategies and methods. HortScience 43:1652–1662.

Reineke, A., and D. Thiéry. 2016. Grapevine insect pests and their natural enemies in the age of global warming. Journal of Pest Science 89:313–328.

Sadras, V.O., P.R. Petrie, and M.A. Moran. 2013. Effects of elevated temperature in grapevine. II juice pH, titratable acidity and wine sensory attributes. Australian Journal of Grape and Wine Research 19:107–115.

Salinari, F., S. Giosuè, F.N. Tubiello, A. Rettori, V. Rossi, F. Spanna, C. Rosenzweig, and M.L. Gullino. 2006. Downy mildew (*Plasmopara viticola*) epidemics on grapevine under climate change. Global Change Biology 12:1299–1307.

Schoof, J.T., S.C. Pryor, and T.W. Ford. 2019. Projected changes in United States regional extreme heat days derived from bivariate quantile mapping of CMIP5 simulations. Journal of Geophysical Research: Atmospheres 124:5214–5232.

Sheehan, T., D. Bachelet, and K. Ferschweiler. 2019. Fire, $CO_2$, and climate effects on modeled vegetation and carbon dynamics in western Oregon and Washington. PLoS ONE 14:e0210989. https://doi.org/10.1371/journal. pone.0210989.

Still, C.J., et al. 2022. Causes of widespread foliar damage from the June 2021 Pacific Northwest heat dome: more heat than drought. Tree Physiology 43:203–209.

Teissedre, P.L., and M. Jourdes. 2013. Tannins and anthocyanins of wine: phytochemistry and organoleptic properties. Pages 2255–2274 in K. Ramawat and J.M. Mérillon, editors. Natural products. Springer, Berlin. https://doi.org/10.1007/978-3-642-22144-6_73.

Tilloy, V., A. Cadière, M. Ehsani, and S. Dequin. 2015. Reducing alcohol levels in wines through rational and evolutionary engineering of *Saccharomyces cerevisiae*. International Journal of Food Microbiology 213:49–58.

Tran, T.T., J. Jung, L. Garcia, J. Deshields, C. Cerrato, M.H. Penner, E. Tomasino, A. Levin, and Y. Zhao. 2023. Evaluation of functional spray coatings for mitigating the uptake of volatile phenols by Pinot Noir Wine grapes via blocking, absorption, and/or adsorption. Journal of Agricultural and Food Chemistry 71:20222–20230. https://doi.org/10.1021/acs. jafc.3c05621.

Universidade de Aveiro. 1 February 2016. UA revela que a indústria da cortica ajuda a atenuar alteracoes climáticas. www.ua.pt/pt/noticias/0/45245. Accessed 26 November 2024.

White, R.H., et al. 2023. The unprecedented Pacific Northwest heatwave of June 2021. Nature Communications 14:727. https://doi.org/10.1038/s41467-023-36289-3.

Williams, A.P., J.T. Abatzoglou, A. Gershunov, J. Guzman-Morales, D.A. Bishop, J.K. Balch, and D.P. Lettenmaier. 2019. Observed impacts of anthropogenic climate change on wildfire in California. Earth's Future 7:892–910.

Yilmaz, T. 2024. Understanding the influence of extreme cold on grapevine phenology in South Dakota's dormant season: implications for sustainable viticulture. Applied Fruit Science 66:1019–1026.